Source to sine relations between the Qaidam basin (Tibet) and the surrounding mountains

Feng Cheng

▶ **To cite this version:**

Feng Cheng. Source to sine relations between the Qaidam basin (Tibet) and the surrounding mountains. Earth Sciences. Université de Rennes; Université de Pékin, 2016. English. NNT : 2016REN1S017 . tel-01381651

HAL Id: tel-01381651

https://theses.hal.science/tel-01381651

Submitted on 14 Oct 2016

HAL is a multi-disciplinary open access archive for the deposit and dissemination of scientific research documents, whether they are published or not. The documents may come from teaching and research institutions in France or abroad, or from public or private research centers.

L'archive ouverte pluridisciplinaire **HAL**, est destinée au dépôt et à la diffusion de documents scientifiques de niveau recherche, publiés ou non, émanant des établissements d'enseignement et de recherche français ou étrangers, des laboratoires publics ou privés.

ANNÉE 2016

THÈSE / UNIVERSITÉ DE RENNES 1
sous le sceau de l'Université Européenne de Bretagne

En Cotutelle Internationale avec

L' Université de Pékin, Chine

pour le grade de

DOCTEUR DE L'UNIVERSITÉ DE RENNES 1

Mention : Sciences de la Terre

Ecole doctorale Sciences de la Matière

présentée par

Feng CHENG

Préparée à l'unité de recherche Géosciences Rennes
OSUR (Observatoire des Sciences de l'Univers) – UMR 6118
UFR Sciences et Propriétés de la Matière

Relations érosion – sédimentation entre le bassin du Qaidam (Tibet) et les chaines associées.

Source to sink relations between the Qaidam basin (Tibet) and the surrounding mountains.

Thèse soutenue à Rennes
le 25 Mai 2016
devant le jury composé de :

Johan De Grave
Professeur, Université de Ghent / *rapporteur*
Jacques Malavieille
Directeur de Recherche CNRS, Université de Montpellier / *rapporteur*
Cécile Robin
Maître de Conférence, Université de Rennes 1 / *examinateur*
Marc Poujol
Maître de Conférence, Université de Rennes 1 / *examinateur*
Marc Jolivet
Chargé de Recherche CNRS, Université de Rennes 1 / *directeur de thèse*
Zhaojie Guo
Professeur, Université de Pékin / *co-directeur de thèse.*

Résumé en français

Le basin du Qaidam, situé sur la bordure nord du Plateau Tibétain est unique au monde en ce qu'il représente le bassin intracontinental le plus profond bien que situé sur le plus haut plateau et la plus épaisse croute continentale actuels (figure R1). Comprendre le développement et l'évolution de ce bassin en lien avec la collision Inde-Asie a des implications multiples pour la géologie du Tibet en particulier et la tectonique continentale dans les zones de convergence en général. De nombreuses études incluant de la thermochronologie, de la paléobotanique, du paléomagnétisme, de la paléoaltimétrie, de la sédimentologie et de la géologie structurale se sont intéressées à l'histoire tectonique et topographique de cette région. Toutefois la topographie initiale de la région actuellement représentée par le Plateau Tibétain ainsi que les premiers stades de développement du plateau restent méconnus et très débattus. Afin de mieux comprendre l'évolution cénozoïque du bassin du Qaidam et des régions environnantes (la chaine des Eastern Kunlun au sud, la chaine de l'Altyn Tagh au nord-ouest et la chaine des Qilian Shan au nord-east), quatre questions principales ont été abordées dans ce travail : 1) l'évolution cénozoïque conjointe du bassin du Qaidam et de la chaine des Eastern Kunlun ; 2) les relations entre la sédimentation dans le bassin du Qaidam et la tectonique le long de la faille de l'Altyn Tagh ; 3) une estimation quantitative de l'extrusion latérale du nord Tibet les long du système Altyn Tagh – Qilian Shan ; 4) la nature et la typologie du bassin du Qaidam.

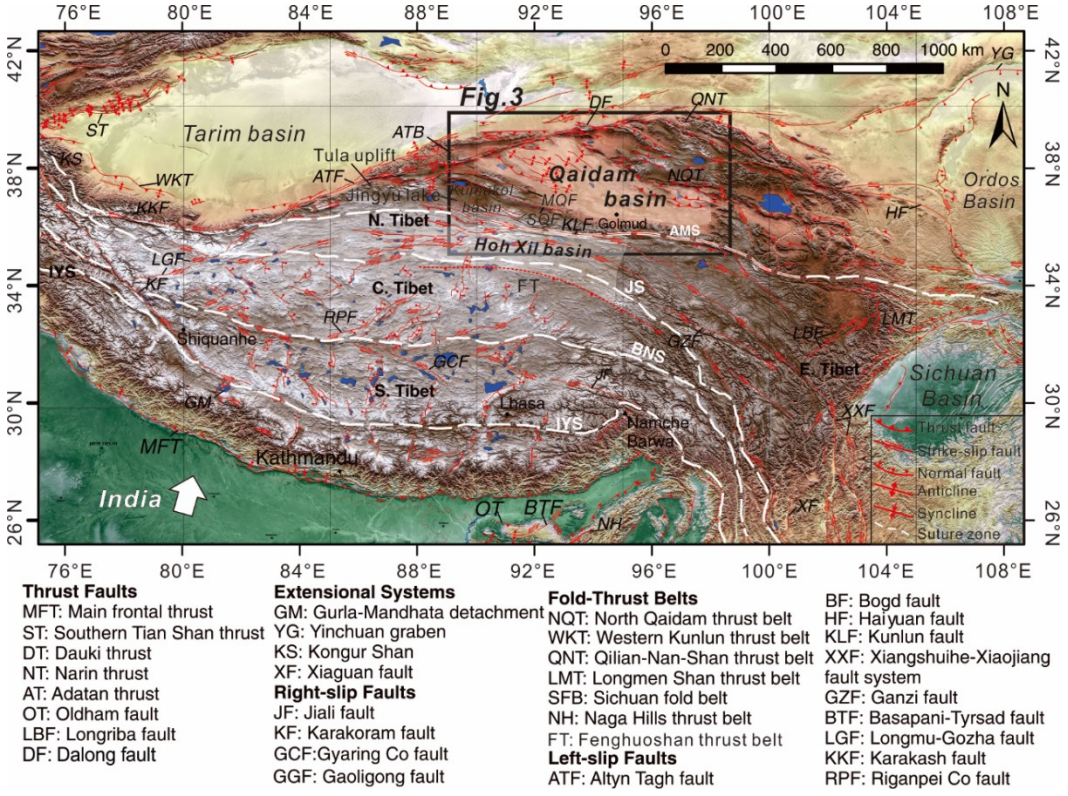

Figure R1 : Carte topographique du Plateau Tibétain montrant les principales structures tectoniques (d'après Yin et al. (2007), Taylor and Yin (2009) et Cheng et al. (2014, 2016).

Au cours des dernières décennies, de nombreux modèles ont été proposés pour rendre compte de l'évolution tectonique et sédimentaire du bassin du Qaidam. La majorité d'entre eux considèrent que la très forte subsidence du bassin au Cénozoïque est liée à la propagation vers le nord du prisme d'accrétion continental du Kunlun qui forme actuellement la bordure sud du bassin (figure R2). L'initiation de ce prisme est généralement datée de l'Oligocène ou du Miocène inférieur.

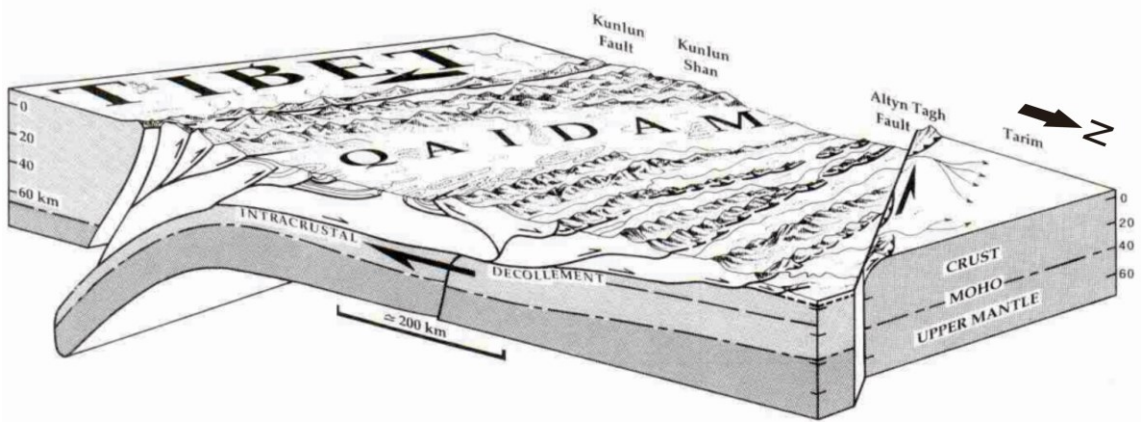

Figure R2 : Modèle de propagation vers le nord du prisme d'accrétion du Kunlun. D'après Meyer et al. (1998).

A partir de nouvelles observations et données de terrain, de l'interprétation de lignes sismiques nouvellement acquises dans le SO du bassin du Qaidam, d'images satellitaires et de données sismologiques, je suggère que le SO du bassin du Qaidam a été limité au sud par une série de failles décrochantes (constituant actuellement les chaînons du Qimantag) depuis le Miocène inférieur et non, comme initialement suggéré, par un système chevauchant vers le nord ou le sud. Les failles constituant ce système s'initient dans la continuité du système décrochant sénestre du Kunlun et sont progressivement déplacées vers le nord tout en subissant une rotation pour être enfin amenées dans leur position actuelle avec une cinématique transpressive. A ce titre le SO du bassin du Qaidam n'a pas été soumis à une compression et un raccourcissement important N-S avant le Miocène inférieur. D'autre part, à partir de l'analyse U-Pb par LA-ICP-MS de zircons détritiques obtenus dans 22 échantillons de grès (paléocène à holocène) provenant de 4 sections dans le SO du bassin du Qaidam, de l'analyse des provenances sédimentaires sur ces mêmes sections, et de profiles sismiques, je démontre que les sédiments paléocènes sont caractérisés par une source principale paléozoïque à protérozoïque supérieur. La présence de débris de carbonate à foraminifères paléozoïque dans les conglomérats paléocènes confirme ce résultat et suggère que la chaine des Esatern Kunlun était exhumée avant le Paléocène. De plus le recouvrement vers le sud des séries paléocènes à oligocènes, observé sur les profiles sismiques, et l'occurrence d'une composante mésozoïque dans les âges U-Pb sur zircon détritiques des séries éocènes à oligocène indiquent que le bassin du Qaidam s'élargissait vers le sud au début du Cénozoïque. Les strates de croissance post-oligocènes et l'augmentation des proportions des âges détritiques mésozoïques et paléozoïques à partir des séries du Néogène supérieur démontrent un accroissement du relief dans les Eastern Kunlun et l'Altyn Tagh, entrainant un isolement et un rétrécissement du bassin entre le Miocène et l'actuel (figure R3). Cette déformation par phases souligne la complexité de l'histoire tectonique du Plateau Tibétain.

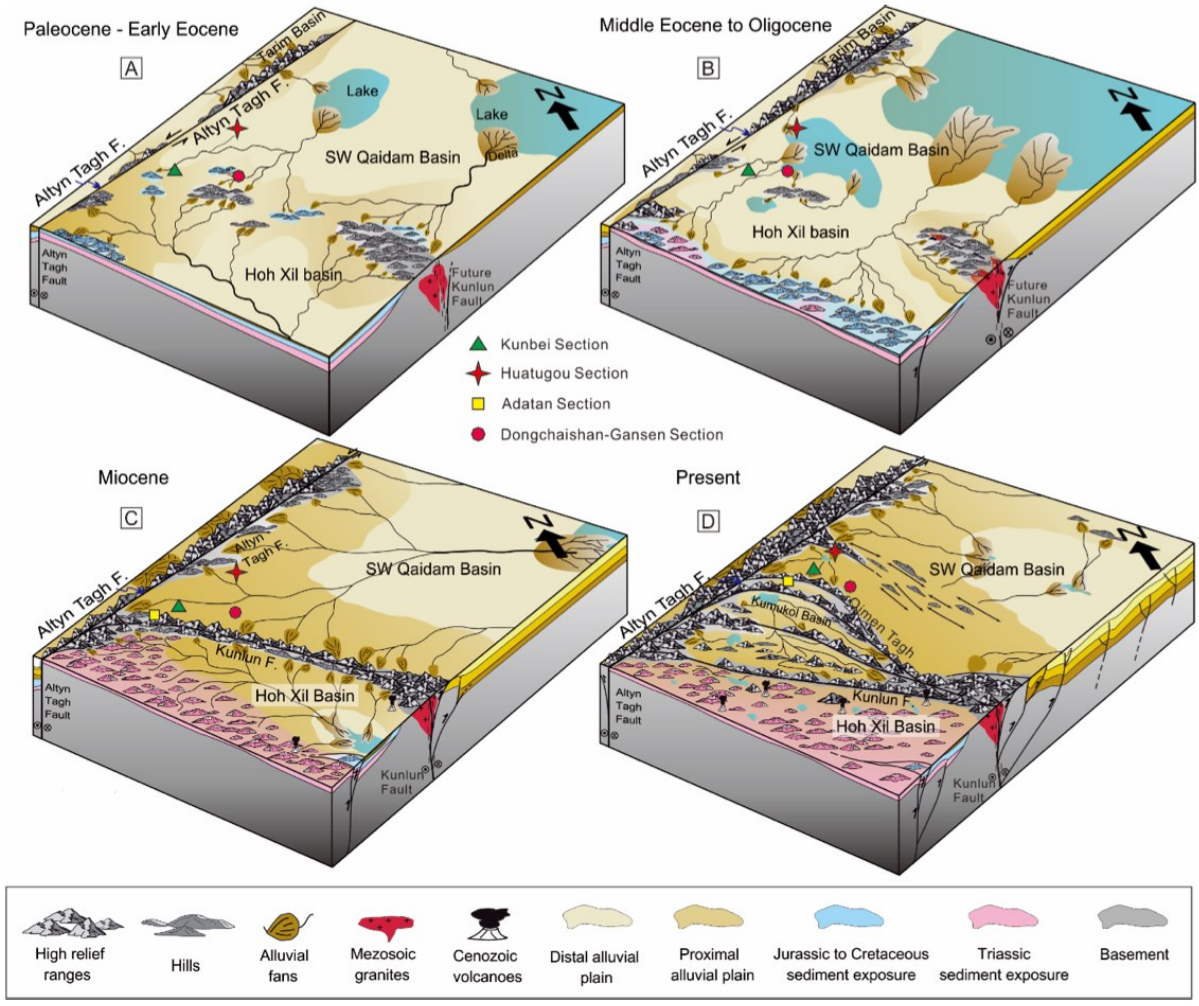

Figure R3 : Reconstitution de l'évolution tectonique et topographique de la bordure sud du bassin du Qaidam entre le Paleocene – Eocene inférieur (A) et le présent (D). Cheng et al., GSAB, 2015.

En combinant des données de sismique 3D, de stratigraphie et de géochronologie détritique sur les séries mésozoïques de l'ouest du bassin du Qaidam, j'ai identifié plusieurs sections comme étant des marqueurs du déplacement le long de la faille de l'Altyn Tagh. Ces données m'ont permis d'identifier les régions d'Anxi et de Tula à l'ouest du bassin, dans la zone où les systèmes tectoniques du Kunlun et de l'Altyn Tagh se rencontrent, comme faisant initialement partie intégrante du bassin du Qaidam (figure R4). Je suggère que la faille de l'Altyn Tagh a accommodé environs 360 km de déplacement depuis sont initiation au Miocène inférieur et que l'activité tectonique dans l'Altyn Tagh et le NO du Qaidam s'est accrue à partir du Miocène. Il est communément admis que le déplacement senestre le long de la faille de l'Altyn Tagh est accommodé pour une très faible partie par du raccourcissement dans le bloc lithosphérique du Qaidam mais surtout par le raccourcissement dans les systèmes d'accrétion contientale du Kunlun et des Qilian Shan. Je démontre toutefois que le bloc lithopshérique du Qaidam est très rigide et ne participe que d'une manière infime à l'accommodation de ce raccourcissement. En me basant sur les 360 km de migration vers le NE du bloc relativement rigide du Qaidam le long de la faille de l'Altyn Tagh, je démontre, à partir d'un bilan isovolumétrique 3D de la déformation crustale au sein du système Altyn Tagh – Qilian Shan,

l'existence d'un raccourcissement N20E de 250 ± 28 km (43.8 – 49.4 %) et de 250 à 370 km d'extrusion vers l'est de la croute des Qilian Shan. Cette déformation est prise en compte par du décrochement dans les Qilian Shan, de l'épaississement crustal dans les Qinling et de l'extension dans le système de grabens de Chine du Nord. Ce résultat remet en cause les calculs de vitesse et de taux de déformation au sein du système Kunlun – Altyn Tagh – Qilian Shan.

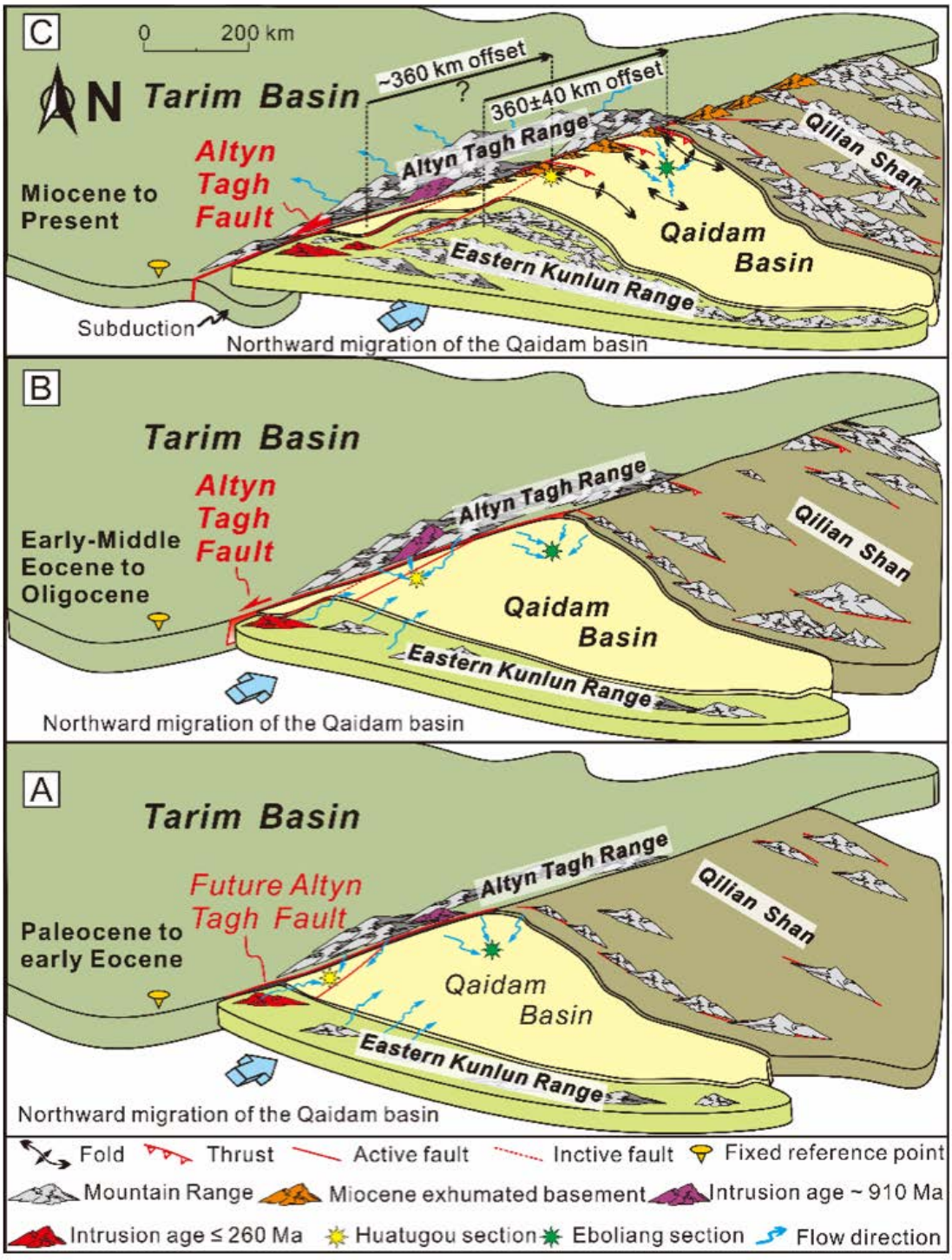

Figure R4 : Modèle cinématique de l'évolution cénozoïque de la faille de l'Altyn Tagh avec indication de l'évolution des principales zones d'apport de matériel sédimentaire dans le bassin du Qaidam. Cheng et al., Tectonophysics, 2016, accepté.

Enfin, à partir d'une analyse intégrée des données sur l'évolution cénozoïque du Qaidam, associée à des données récentes de géologie pétrolière (par exemple la distribution des roches mères dans le Qaidam), je conclu que le bassin du Qaidam est de type décrochant, contrôlé conjointement par les failles décrochantes de l'Altyn Tagh et du Kunlun Est. La faille de l'Altyn Tagh, au nord du bassin, contrôle l'essentiel de la structure sédimentaire du bassin, la faille du Kunlun au sud n'agissant que localement sur la bordure sud-ouest du bassin. La superposition dans le temps et l'espace des effets de ces deux décrochements majeurs durant le Cénozoïque a contrôlé l'évolution du bassin et la répartition des réserves d'huile et de gaz. Au cours du Paléogène, l'essentiel des roches mères se déposent dans des sous-bassins « sag » extensifs le long de la bordure sud-ouest du Qaidam. Les systèmes transpressif qui se met en place dans la région du Qimantag à partir du Miocène inférieur constitue des pièges majeurs pour les hydrocarbures (huile et gaz) (figure R5).

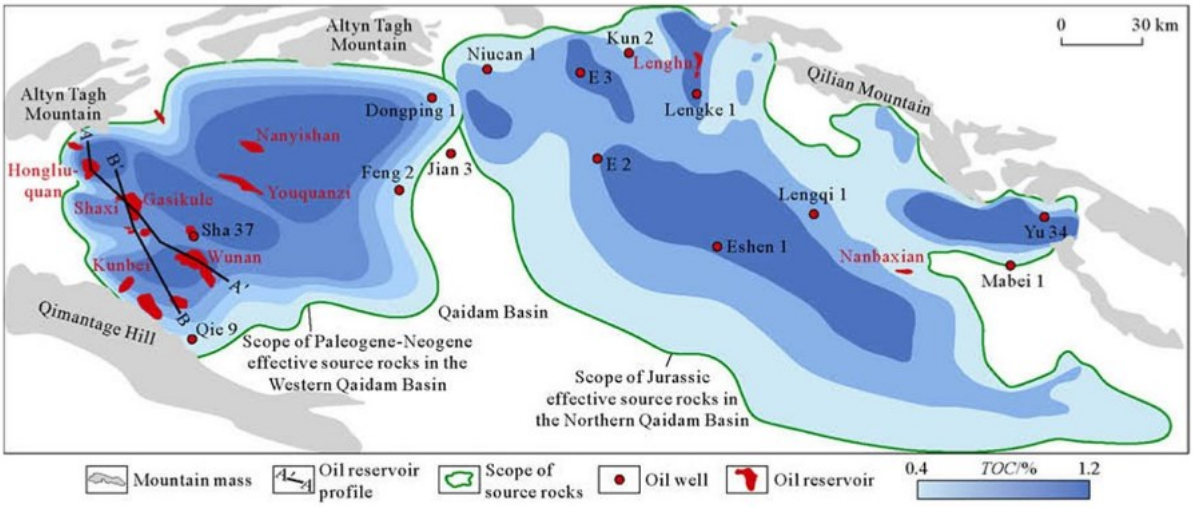

Figure R5 : Distribution des roches mères et des réservoir d'huile et de gaz dans le bassin du Qaidam. D'après Fu et al., Petroleum Exploration and Development, 2015.

MOTS CLÉS : Le basin du Qaidam, Plateau Tibétain, Détritique zircon géochronologie, l'interprétation de lignes sismiques, Relations érosion – sédimentation, décrochement, raccourcissement, extrusion

.

Abstract

The Qaidam basin, located within the northern Tibetan plateau, is unique in the world in that it is the deepest intracontinental basin, yet located in the highest plateau with the thickest continental crust. Understanding how this peculiar basin developed during the India-Asia collision has broad implications for the Tibetan geology in particular and for continental tectonics in general. Though many approaches, including thermochronology, paleobotany, paleomagnetism, paleoaltimetry coupled with stratigraphic and tectonic analyses, have been used to decipher the tectonic and topographic history of that region, the initial topography of the area now represented by the northern Tibetan plateau, as well as the early stages of development of the present day topography remain poorly constrained and highly debated. In order to better understand the Cenozoic evolution of the Qaidam basin and its surrounding regions (including Eastern Kunlun Range to the south, Altyn Tagh Range to the northwest, and Qilian Shan to the northeast), four critical issues are addressed in this thesis: 1) the Cenozoic joint tectonic evolution of the Qaidam basin and the Eastern Kunlun Range; 2) the interplay between the sedimentation within the Qaidam basin and the active tectonics within the Altyn Tagh Range; 3) a quantitative estimate of the lateral extrusion along the Altyn Tagh Fault-Qilian Shan tectonic system; 4) the nature and classification of the Qaidam basin.

Based on new field observation and data, interpretation of newly acquired seismic reflection profiles within the southwestern Qaidam basin, remote sensing images, and earthquake focal mechanisms and epicenter distribution, I suggest that the SW Qaidam basin has been bordered by a series of strike-slip faults to the south since the Early Miocene, rather than, as previously suggested by a continuous northward or southward thrusting system. The SW Qaidam basin did not suffer major N–S compression and shortening before the Early Miocene. On the other hand, by conducting U-Pb dating (LA-ICP-MS) of detrital zircons from 22 sandstone samples (Paleocene to Holocene) collected from 4 sections within the southwestern Qaidam basin combined with provenance analysis and new seismic profile interpretation, I demonstrated that the U-Pb age distribution of detrital grains from Paleocene strata are characterized by a major component of Paleozoic to late Proterozoic ages, and recognized carbonate debris containing foraminifera in the Paleocene conglomerate sequences. These data suggest that the Eastern Kunlun Range was already exhumed prior to the Paleocene. In addition, the southward onlaps of Paleocene to Oligocene strata observed on seismic profiles and the appearance of a Mesozoic component in the detrital zircon age spectra of Eocene to Oligocene strata indicate that the Qaidam basin was widening southward during

that early Cenozoic period. Well-developed post-Oligocene growth strata and the increasing proportion of Mesozoic and Paleozoic U-Pb ages in detrital zircon grains from late Neogene strata demonstrate that the relief of the Eastern Kunlun and Altyn Tagh ranges had increased, leading to isolation and narrowing of the Qaidam basin from Miocene to the present. The inferred pulsed deformation in the Eastern Kunlun Range highlights the complex growth history of the Tibetan plateau.

By correlating stratigraphic contacts and lithologies, U-Pb age spectra of Mesozoic samples within the western Qaidam basin, and newly acquired 3D seismic reflection profiles interpretation, I identified the Tula-Huatugou and Anxi-Eboliang sections as piercing points along the western segment of Altyn Tagh Fault. I further defined the Tula and Anxi regions as residual parts of the original Qaidam basin. I thus suggest that the Altyn Tagh Fault has experienced a total of ~360 km of displacement since its Early Eocene initiation, whereas tectonic activity largely increased within the Altyn Tagh Range and northwestern Qaidam basin from Miocene time.

In addition, based on the ~360 km northeastward migration of the relatively rigid Qaidam block along the Altyn Tagh Fault and 3D isovolumetric balance of the crustal deformation within the Altyn Tagh Fault – Qilian Shan system, I demonstrate that 250 ± 28 km (43.8~49.4 %) of N20E directed crustal shortening and an additional ~250 to ~370 km of eastward motion of the Qilian Shan crust must be accounted for by strike-slip faulting in the Qilian Shan and crustal thickening in the Qinling area, as well as extension in the adjoining North China block graben systems.

Finally, based on a comprehensive analysis of the Cenozoic evolution of the Qaidam basin combined with recent petroleum exploration geological results (e.g. distribution of source rocks in the Qaidam basin), I conclude that the Qaidam Basin is a strike-slip superimposed basin jointly controlled by the left-lateral strike-slip Altyn Tagh and East Kunlun faults. The temporal and spatial superimposition of these two strike-slip faults during the Cenozoic controlled the evolution of the basin as well as the oil and gas accumulation.

KEY WORDS: Qaidam basin, Tibetan plateau, Detrital zircon geochronology, Seismic profile interpretation, Source to sink relation, Strike-slip tectonics, Compression, Extrusion.

Acknowledgements

I would like to extend thanks to the many people, in many countries, who so generously contributed to the work presented in this thesis.

First and foremost I want to thank my two doctorial tutors Marc Jolivet, Université de Rennes 1 and Zhaojie Guo, Peking University. I thank Zhaojie wholeheartedly, not only for his tremendous academic guidance, but also for nurturing my enthusiasm for Tibetan geology and many wonderful opportunities. Not many PhDs involve field investigation throughout western China (including the Qaidam basin, Altyn Tagh and Eastern Kunlun ranges and Tian Shan) and a French-Chinese bilateral programme. His innovated ideas and fantastic geological thinking that linking the local geological information to regional or global scale tectonics inspired me to acquire critical thinking and overall four- dimensional perspective when doing Earth Science research. My gratitude is also extended to Marc, for his scientific advice and knowledge and many insightful discussions and advices during my PhD research. I cannot complete all the designed research in the framework of my PhD plan and pursue geologic research on the Tibetan plateau without his encouragement and suggestions. He not only taught me how the conduct the apatite fission track analysis, but also let me to know how to give the reasonable interpretation on the basic of scientific data in the rigorous and precise way. I am particularly indebted to Marc for his support when so generously hosting me in Rennes. I have very fond memories of my time in France and hope to revisit this land of exceptional beauty in the near future.

Heartfelt and special thanks are given to Chaodong Wu, Marc Jolivet and Guillaume Dupont-Nivet for their kindly assistance in applying the French-Chinese bilateral programme (Egide Cai Yuanpei program 2014). Special mention goes to China Scholarship Council who offered me the shcolarship these years. I would never have had a chance to enjoy the romantic and peaceful French life without the support of this international project.

I am grateful to members of my middle dissertation evaluation committee, Michel Ballevre, Sylvie Bourquin, Hervé Régnauld. Their kind jugement and valuable comments are greatly appreciated. Similarly, Zhicheng Zhang, JinjiangZhang, Baofu Han, Chaodong Wu, Bo Zhang, who provide logical and forethoughtful suggestions that strongly facilitated the scientific integrity of my dissertation, are acknowledged.

I am also hugely appreciative to Guillaume Dupont-Nivet, Hillary S. Jenkins, Kerry Gallagher for the excellent cooperation. Their insightful suggestions and polishing largely improved the quality of my manuscripts and helped me to develop my scientific analytical and

writing skills. I also thank Erwan Hallot and Wenzhe Fa for valuable discussion and generous help during data interpretation and drafting.

Profound gratitude goes to An Yin, Jean-Philippe Avouac, Jason Phipps Morgan, Shanaka de Silva, Christian Koeberl, Mian Liu, James A. Spotila, Todd A. LaMaskin, Franz Neubauer, and all the other anonymous referees, for their carefully reviewing my manuscripts and providing the constructive and insightful comments. The modification during the manuscript submitting process have left an indelible mark on my memory and will push me to present much higher quality contributions in my geology career.

I am very grateful to Suotang Fu, Dade Ma, Shuwei Guan, Yan Chen, Chuanwu Wang, Qiquan Zhang for giving me the opportunities to get involved to the incredible Qaidam basin. I would also like to commemorate Shihu Fang who gave me tremendous help during the first two years since I entered the Zhaojie's group. I must acknowledge with deep thanks Suping Zhou, Ruiying Chen, Qingyang Meng, Chuanming Zhou, Changhao Zhang, Yiquan Jiang, Wenjun Zhu, Peizhi Du, Anping Hou, Mingde Liu, Tailiang Jiang, Jihong Wang, and Xiangfeng Dai from Dunhuang, China, for their contribution to the field investigation and data collection.

Special mention also goes to those doctor and master students in Zhaojie's group, namely Yuanyuan Zhang, Shi Chen, Shufang Wang, Dongdong Liu, Wentao Huang, Wei Yang, Meng Li, Bei Zhu, Xiangjiang Yu, Ziya Zhang, Hanwen Hu, Xiang Cheng, Tuo Zhang, Runchao Liu, Wei Du, Xiaoru Tian, Zhendong Wang, Yang Zhang and Qing Bian.

Bo Zhang and Xiaoxian Wang are highly appreciated, for their help with cathodoluminescence (CL) imaging at Peking University, Beijing, while. Moreover, Li Su, Hongyu Zhang, Jiao Li, Linxi Zhong and Tong Liu are acknowledged for their help with detrital zircon U-Pb geochronology testing at China University of Geoscience, Beijing.

I also thank geologists from Université de Rennes 1, Marc Poujol, Cécile Robin, Thierry Nalpas, Jean-Noël Proust, for giving the outstanding lessons that highly impove my basic geologic skills. Dominique Bavay, Isabelle Dubigeon, Eddie Gaudin, Christian Le Carlier de Veslud, Michel Ballevre, Philippe Boulvais, François Guillocheau, Olivier Dauteuil, Aline Dia, Laura le Barzic and Marie-Anne Zeghers are highly appreciably for providing convenience for my daily life at Geoscience Rennes, Université de Rennes 1. In particular, I would like to appreciate those PhD. students, namely Christophe Ballouard, Youssef Nohra, Olivier Bochet, Benoît Quesnel, Duprat-Oualid Sylvia, De la Bernardie Jérôme Bondet, Roman Chelalou, Benjamin Corre, Gemma De Vicente I Bosch, Antoine Delaunay, Daniel Jara Heredia, Tamara Kolbe, Caroline Lotout. Thanks for their great assistance and accompany during my campus

life at Université de Rennes 1.

In addition, these acknowledgements would not be complete if I did not mention my forever friends, Qian Yuan, Yi Wei, Zhao Zhou, Sen Gu, and Pengfei Fan. Their assistance, patience, encouragement and enthusiastic help me pass through the hardship during my doctor study and shed a new light in my life. It is my honor to be your friend.

Through my PhD study, I have met many nice and compassionate individuals who did not hesitate to devote their valuable time to me when it was needed. I dare not risk missing to mention anyone's names, so I will simply say "Thank you ALL for being there for me.

Finally, but by no means least, I dedicate this thesis to my mum, dad, and my beloved fiancée for their unbelievable support and unconditional love. My parents have instilled many admirable qualities in me and given me a good foundation with which to meet life. My fiancée went through every excruciating step and mood change with me, and I could not have completed this journey without her by my side. I love you all dearly.

Curriculum Vitae

Feng Cheng
Laboratoire Géosciences Rennes, Université de Rennes 1, Rennes, 35042, France
Phone: +33 (0)652766226; +86 18810523726
cfcf.chengfeng@gmail.com
https://www.researchgate.net/profile/Feng_Cheng10

EDUCATION

Ph. D., Sciences de la Terre, Université de Rennes 1, **Advisor: Marc Jolivet,** 2013-2016 (expected)
Thesis: Source to sink relations between the Qaidam basin and the surrounding mountains
Ph. D., Structure geology, Peking University, **Advisor: Zhaojie Guo**, 2011-2016 (expected)
Thesis: Cenozoic evolution of Qaidam basin, northern Tibetan Plateau: Implications for the plateau growth
B. SC., Geology (Advance class), China University of Geoscience, Wuhan, **Advisor: Dewei Li** 2007-2011
Thesis: Surface ruptures of the Eastern Kunlun, Wenchuan and Yushu earthquakes and their tectonic implications

PROFESSIONAL EXPERIENCE

Laboratory Assistant, SEM-EBSD-EDS-CL laboratory in the Key lab of Orogenic belts and crust evolution, Ministry of Education, Peking University, 2012-2013.

FELLOWSHIPS & AWARDS

Chinese-French Egide Cai Yuanpei program scholarship, China Scholarship Council, 2014-2016
Dingdong Geology Scholarship, School of Earth and Space Science, Peking University, 2016
National Scholarship, Chinese Ministry of Education (Top prize for PhD candidates in China), 2015
National Scholarship, Chinese Ministry of Education (Top prize for PhD candidates in China), 2014
Innovation Award (Academic), Peking University, 2014
Excellent Learning Student of the Peking University, Peking University, 2013
Major and Minor Academic Scholarship, Peking University, 2011, 2012
Top Ten Pacesetter Students, China University of Geosciences (Wuhan)
Won the May 4th Youth Medal (Top prize for undergraduates in China University of Geosciences), 2011
First prize of the Science and Technology Papers Contest, China University of Geoscience (Wuhan), 2011
National Scholarship for Encouragement, Chinese Ministry of Education, 2009

RESEARCH INTERESTS

Tectonics, Provenance analysis, Low-temperature thermochronology
My current research focuses on the Cenozoic kinematic evolution of the Tibetan Plateau. I am now targeting the Qaidam basin and seek to reconstruct the source to sink relations between the Qaidam basin and the surrounding regions, North Tibet (including Eastern Kunlun Range, Altyn Tagh Range as well as the Qilian Shan Range), and finally provide some constraints on the plateau growth process.
I conduct multi-faceted approach in my research, including field investigation, provenance analysis (detrital zircon U-Pb geochronology), thermochronology (AFT), seismic profile interpretation, remote sensing interpretation, ect.

RESEARCH EXPERIENCE

Identifying the nature of the basement of the Qaidam basin, northern Tibetan Plateau, 2014-Present

I collected granitoid basement rocks of the Qaidam basin from drill wells (Qinghai Petroleum Research Institute of PetroChina). I am conducting petrology, geochronology and geochemistry analysis to understand the origin of the Qaidam basin basement. In addition, Apatite Fission Track analysis is also used to constrain the Late Mesozoic to Cenozoic tectonics evolution of the basin.

Quantitative estimation of the lateral extrusion along the Altyn Tagh Fault-Qilian Shan system, northern Tibetan Plateau, 2014-Present

I propose a quantitative evaluation of the Cenozoic crustal shortening and lateral extrusion budget in the northern Tibetan Plateau, derived by both considering the northeastward migration of the relatively rigid Qaidam block along the ATF and restoring the 3D crustal deformation in the Qilian Shan.

Source to sink relation between the Qaidam basin and the Eastern Kunlun Mountains, northern Tibetan Plateau, 2011-Present

I conducted field investigation on several sections in the Qaidam basin and collected plenty of Cenozoic samples (outcrop and drill well samples). Then, U-Pb dating (LA-ICP-MS) of detrital zircons from 22 sandstone samples (Paleocene to Holocene) collected from four sections within the southwestern Qaidam basin is combined with provenance analysis and new seismic profile interpretation to investigate the mountain building of the Eastern Kunlun Range.
In addition, based on a new field observation and data, interpretation of newly acquired seismic reflection profiles within the SW Qaidam basin, remote sensing images, and earthquake focal mechanisms and epicenter distribution, I re-evaluated the tectonic pattern along the western portion of the Kunlun fault to decipher the Late Cenozoic interaction between the Eastern Kunlun Range and the SW Qaidam basin.

Initial rupture and displacement on the Altyn Tagh Fault, northern Tibetan Plateau, 2011-Present

I conducted an integrated analysis on several Mesozoic to Cenozoic stratigraphic sections in the western Qaidam basin, adjacent to the Altyn Tagh Fault. Detrital zircon U-Pb

geochronology data (outcrop and drill core samples) obtained from these sections are associated to high-quality newly acquired seismic profiles to better understand the kinematic history of the Altyn Tagh Fault.

Surface rupture of the Eastern Kunlun, Wenchuan and Yushu earthquakes and their tectonic implications, 2008-2011

After the Yushu earthquake (2010), I conducted fieldtrip in Yushu, Wenchuan and the Kunlun Mountains to investigate the surface rupture of these earthquakes to identify their features and explore potential connections among them in the context of the plateau growth.

RECENT FIELD EXPERIENCE

Northern Tibet: *Qaidam basin, Eastern Kunlun Range, Yushu*

Seismic profile interpretation and drill core samples collection (Mesozoic-Cenozoic and basement samples) in the PetroChina, Dunhuang, Gansu Province, China. Totaling 3 months 2012 to 2014.

Field investigation in the Qaidam basin and Eastern Kunlun Range to collect paleomagnetism and detrital zircon samples throughout the basin. Four weeks, 2011.

Field mapping in the Eastern Kunlun Range (to the west of Golmud). Six weeks, 2010.

Investigate the surface ruptures of the Kunlun earthquake. One week, 2010.

Investigate the surface ruptures of the Yushu earthquake. One week, 2010.

Eastern Tibet: *Wenchuan*

Investigate the surface ruptures of the Eastern Kunlun earthquake, One week, 2010.

Central Asian Orogenic Belt: *Tian Shan*

Investigate several Mesozoic sections along the northern and southern flanks of Tian Shan (Kuche, Shawan, Heiyingshan, etc.) and collect paleomagnetism and detrital zircon samples. Three weeks, 2010.

ANALYTICAL TECHNIQUES UTILIZED

Structural mapping, Geochronology (U-Pb zircon LA-ICP-MS), Low-temperature thermochronology (Apatite Fission Track), Seismic profile interpretation (SMT), Remote sensing interpretation (ENVI, ArcGIS), Geochemistry (Major and trace elements, Sr-Nd isotope).

PEER-REVIEWED PUBLICATIONS

Papers in preparation:

Cheng F., Jolivet M., Fu S., Zhang C., Zhang, Q., Guo Z., Reconstructing the Cenozoic tectonics in the northern Tibetan plateau: insight from apatite fission track study of deep-drill-core samples from the basement of Qaidam basin. In Prep for Tectonics.

Cheng F., Han B., Jolivet M., Fu S., Zhang C., Guo Z., Tectono-magmatic transformed Qaidam craton insight from the borehole core samples geochronological and geochemical constraints. In Prep for EPSL.

Papers in review and revision:

Cheng F., Jolivet M., Fu S., Zhang C., Zhang, Q., Guo Z., Large-scale displacement along the Altyn Tagh Fault (North Tibet) since its Eocene initiation: insight from detrital zircon U-Pb

geochronology and subsurface data: ***Tectonophysics***, accepted with minor revision.

Published, in press and accepted papers:

2016

Cheng, F., Fu, S., Jolivet, M., Zhang, C., and Guo, Z., 2016, Source to sink relation between the Eastern Kunlun Range and the Qaidam Basin, northern Tibetan Plateau, during the Cenozoic: ***Geological Society of America Bulletin***, v. 128, no. 1-2, p. 258-283, doi: 10.1130/B31260.1.

2015

Cheng F., Jolivet M., Dupont-Nivet G., Wang L., Yu X., Guo Z., Lateral extrusion along the Altyn Tagh Fault, Qilian Shan (NE Tibet): insight from a 3D crustal budget: ***Terra Nova***, v. 27, no. 6, p. 416-425, doi: 10.1111/ter.12173.

Fu S., Ma D., Guo Z., **Cheng F.**, 2015. Strike-slip superimposed Qaidam basin and control on oil and gas accumulation: ***Petroleum Exploration and Development***, v. 42, no. 6, 712-722, doi: 10.11698/PED.2015.06.03.

Cheng, F., Guo Z., Jenkins, H., Fu S., and Cheng X., 2015.Initial Rupture and Displacement on the strike-slip Altyn Tagh Fault, Northern Tibetan Plateau: Constraints based on residual Mesozoic to Cenozoic deposits in the western Qaidam Basin: ***Geosphere***, v. 11, no. 3, 921-942, doi: 10.1130/GES01070.1.

Liu, D., **Cheng, F.**, Guo, Z., Jolivet, M., Song, Y., 2015. Lahar facies of the Latest Paleozoic Arbasay Formation: Geomorphological characters and paleoenvironment reconstruction of Northern Tian Shan, NW China. ***Journal of Asian Earth Sciences***, v. 113, Part 1, p. 282-292, doi: 10.1016/j.jseaes.2015.01.024.

Wang L. and **Cheng F.**, 2015. DEM and GIS analysis of the stream gradient index for evaluating effects of active tectonics: Tula basin, north Tibet, China, Geoscience and Remote Sensing Symposium (IGARSS), 2015 IEEE International, Milan, 2015, 4680-4683, doi: 10.1109/IGARSS.2015.7326873.

Cheng, X., Fu, S., Wang, H., Yu, X., **Cheng, F.**, Liu, R., Du, W., Guo, Z., 2015. Geometry and kinematics of the Arlar strike-slip fault, SW Qaidam basin, China: New insights from 3-D seismic data. ***Journal of Asian Earth Sciences*** v. 98, 198-208, doi: 10.1016/j.jseaes.2014.09.039.

2014

Cheng, F., Jolivet, M., Fu, S., Zhang, Q., Guan, S., Yu, X., and Guo, Z., 2014, Northward growth of the Qimen Tagh Range: A new model accounting for the Late Neogene strike-slip deformation of the SW Qaidam Basin: ***Tectonophysics***, v. 632, p. 32-47, doi: 10.1016/j.tecto.2014.05.034.

Liu, D., Guo, Z., Jolivet, M., **Cheng, F.**, Song, Y., Zhang, Z., 2014. Petrology and geochemistry of Early Permian volcanic rocks in South Tian Shan, NW China: implications for the tectonic evolution and Phanerozoic continental growth. ***International Journal of Earth Sciences*** 103, 737-756, doi: 10.1007/s00531-013-0994-1.

Zhu, B., Guo, Z., Zhang, Z., **Cheng, F.**, 2014. Peperites in the Permian Tarim large igneous province in Northwest China and their constraints on the local eruption environments. ***Science China Earth Sciences*** 57, 2914-2921. doi: 10.1007/s11430-014-4966-5.

Yu, X.J., Fu, S.T., Guan, S.W., Huang, B., **Cheng, F.**, Cheng, X., Zhang, T., Guo, Z.J., 2014. Paleomagnetism of Eocene and Miocene sediments from the Qaidam basin: Implication for

no integral rotation since the Eocene and a rigid Qaidam block. ***Geochemistry, Geophysics, Geosystems*** 15, 2109-2127., doi: 10.1002/2014GC005230.

Yu, X., Huang, B., Guan, S., Fu, S., **Cheng, F.**, Cheng, X., Zhang, T., Guo, Z., 2014. Anisotropy of magnetic susceptibility of Eocene and Miocene sediments in the Qaidam Basin, Northwest China: Implication for Cenozoic tectonic transition and depocenter migration. ***Geochemistry, Geophysics, Geosystems*** 15, 2095-2108, doi: 10.1002/2014GC005231.

2013

Cheng F., and Guo Z., 2013. Northward Migration of the Western Segment of Eastern Kunlun Strike-slip Fault: Implications for Late Cenozoic Evolution of the Qimen Tagh Range and Southwestern Qaidam Basin, North Tibet, China. ***Acta Geologica Sinica (English Edition)***, v. 87(supp.), p. 205.

Zhang C., **Cheng F.**, Huang G., Huang Y., Xing C., Guan B., Zhang Q., Xu G.,. 2013. Sediment and reservoir characteristics with reservoir evaluation of Lunlehe Formation in Qie16 block of Kunlun oilfield in Qaidam Basin: ***Acta Petrologica Sinica***, v. 29, no. 8, p. 2883-2894 (in Chinese with English abstract).

Liu, D., Jolivet, M., Yang, W., Zhang, Z., **Cheng, F.**, Zhu, B., Guo, Z., 2013. Latest Paleozoic–Early Mesozoic basin–range interactions in South Tian Shan (northwest China) and their tectonic significance: Constraints from detrital zircon U–Pb ages. ***Tectonophysics*** 599, 197-213, doi: 10.1016/j.tecto.2013.04.018.

2012

Cheng F., Li D., Luo W., Bartholomew J., 2012. Characteristics and Patterns of Surface Ruptures Caused by the Yushu Earthquake: ***Geotectonica Et Metallogenia***, v. 36, no.1, p. 69-75 (in Chinese with English abstract).

CONFERENCES (1ST author only)

Cheng F., Jolivet M., Guo Z. 2016. Eastward extrusion of the North Tibetan plateau: insight from the Altyn Tagh fault offset and a 3D crustal budget in North Tibet. **The 5th International Geologica Belgica Meeting (GB2016), Oral**, Mons, Belgium.

Cheng F., Jolivet M., Guo Z., 2015. Reconstruction of Cenozoic growth process in North Tibet: Source to sink relation between the Qaidam Basin and East Kunlun Mountains. **EGU General Assembly** 2015, **Poster**, Vienna, Austria.

Cheng F., Guo Z., 2014, Initial rupture and displacement on the strike-slip Altyn Tagh fault, northern Tibetan plateau. **Seventh session of national tectonic geology and geodynamics academic seminar**, **Oral report**, Qingdao, China.

Cheng F., Guo Z., 2013. Northward Migration of the Western Segment of Eastern Kunlun Strike-slip Fault: Implications for Late Cenozoic Evolution of the Qimen Tagh Range and Southwestern Qaidam Basin, North Tibet, China. **Roof of the World --- the First Joint Meeting of GSC and GSA, Oral report**, Chengdu, China.

Cheng F., Li D., Bartholomew M., Luo W., 2011. Characteristics and mechanism of surface ruptures associated with the East Kunlun, Wenchuan and Yushu Earthquakes. **Fourth session of national tectonic geology and geodynamics academic seminar, Poster,** Nanjing, China.

RESEARCH GRANTS

China University of Geoscience Student Research Grant, 2009-2011 (1571 $)

Table of contents

Résumé en français I

Abstract VI

Acknowledgements VIII

Curriculum Vitae XI

Table of contents XVI

Chapter 1 Preface 1

1.1 Introduction, Reginal Geology and Problems 1

1.2 Research plan and framework of the dissertation 8

Chapter 2 Cenozoic tectonic evolution between the Qaidam basin and the Eastern Kunlun Range 11

2.1 Tectonic relationship between the Eastern Kunlun Range and the Qaidam basin 11

Abstract 11

2.1.1 Introduction 12

2.1.2 Regional Geology 14

2.1.2.1 Eastern Kunlun Mountains 14

2.1.2.2 SW Qaidam Basin and Kumukol Basin 15

2.1.3 Active tectonic pattern in the western segment of the East Kunlun Range 17

2.1.4 Splay Fault System of the Kunlun Fault Zone 19

2.1.4.1 Strike-slip faulting in the Qimen Tagh Range 19

2.1.4.2 Pleistocene series within the Adatan valley 22

2.1.5 Strike-slip faulting in the SW Qaidam Basin 23

2.1.5.1 Seismic Section C-C' 25

2.1.5.2 Seismic Section D-D' 26

2.1.5.3 Seismic Section E-E' 27

2.1.6 Discussion 28

2.1.6.1 Available models for the Cenozoic evolution of the SW Qaidam Basin 28

2.1.6.2 Strike-slip tectonics and northward growth of western segment of Kunlun Fault 31

2.1.7 Conclusions 34

Acknowlegements 34

Reference 35

2.2 Cenozoic source to sink relation between the Qaidam basin and the Eastern Kunlun Mountains 42

Abstract 42

2.2.1 Introduction....43
2.2.2 Geological Setting....46
2.2.2.1 Eastern Kunlun Range....46
2.2.2.2 Qaidam basin....48
2.2.3 Synthesis of existing zircon U-Pb ages from basement....50
2.2.4 Stratigraphy and sedimentary characteristics of the sections....56
2.2.5 Sampling and analytical methods....61
2.2.6 Results....63
2.2.6.1 Huatugou section....63
2.2.6.2 Dongchaishan-Gansen section....65
2.2.6.3 Kunbei section....68
2.2.6.4 Adatan section....70
2.2.6.5 Summary....71
2.2.7 Discussion....72
2.2.7.1 Pre-Paleocene exhumation of the Eastern Kunlun Range....72
2.2.7.2 Cenozoic source to sink relationship between the South Qaidam basin and the Eastern Kunlun Range....75
2.2.8 Conclusions....81
Acknolegdements....82
References Cited....82
Chapter 3 The interplay between the sediments within Qaidam basin and the active tectonic within Altyn Tagh Range....101
3.1 Initial rupture and displacement on the Altyn Tagh fault, northern Tibetan plateau: constraints based on residual Mesozoic to Cenozoic strata in the western Qaidam basin....101
Abstract....101
3.1.1 Introduction....102
3.1.2 Regional geology....104
3.1.2.1 Altyn Tagh Range....104
3.1.2.2 Qaidam basin....105
3.1.3 Residual Mesozoic-Cenozoic stratigraphy along the Altyn Tagh Fault....107
3.1.3.1 Mesozoic to Eocene strata in the Tula section....107
3.1.3.2 Cenozoic strata in the Anxi section....110
3.1.4 Methods....112
3.1.4.1 Field investigation and seismic profile interpretation....112
3.1.4.2 Sampling and analytical process....113
3.1.5 Results....115
3.1.5.1 U–Pb geochronology of detrital zircons....115

3.1.6 Discussion 118
3.1.6.1 New piercing points 118
3.1.6.2 Provenance analysis of Jurassic to Cretaceous strata 121
3.1.6.3 Implications for the initial timing and total offset of the ATF 124
3.1.7 Conclusions 128
Acknolegdements 129
References Cited 129
3.2 Large-scale displacement along the Altyn Tagh Fault (North Tibet) since its Eocene initiation: insight from detrital zircon U-Pb geochronology and subsurface data 142
Abstract 142
3.2.1 Introduction 143
3.2.2 Geological Background 145
3.2.2.1 Altyn Tagh Range 145
3.2.2.2 Qaidam basin 146
3.2.3 Stratigraphy and sedimentary characteristics of the studied sections 147
3.2.3.1 Eboliang section 147
3.2.3.2 Huatugou section 150
3.2.4 Methods and analytical procedures 153
3.2.4.1 Detrital zircon geochronology 153
3.2.4.2 Seismic profile 154
3.2.5 U–Pb geochronology results of detrital zircons 154
3.2.5.1 Eboliang section 157
3.2.5.2 Huatugou section 160
3.2.6 Discussion 163
3.2.6.1 Geochronological characteristics of potential sources for the sedimentary rocks in the western Qaidam basin 163
3.2.6.2 Provenance analyses of the Mesozoic-Cenozoic strata in the western Qaidam basin 165
3.2.6.3 Tectonics implications 173
3.2.7 Conclusions 176
Acknolegdements 176
References 177
Chapter 4 Quantitative estimate of the lateral extrusion along the Altyn Tagh Fault-Qilian Shan tectonic system 191
Abstract 191
4.1 Introduction 192
4.2 Geological setting 193
4.3 Methods 194

4.4 Results 198
4.5 Discussion and Conclusions 199
Acknowledgements 202
Reference 202
4.6 Chapter summary 209
Chapter 5 Strike-slip superimposed Qaidam Basin and its control on oil and gas accumulation 210
Abstract 210
5.1 Introduction 211
5.2 Similarities, differences and key points of the cognition 212
5.3 Structural features of peripheral Qaidam Basin 214
5.3.1 Altyn Tagh left-lateral strike-slip fault – North Qaidam thrust system 214
5.3.2 Left-lateral strike-slip of East Kunlun fault and its superimposed regulation on the basin since the Miocene 218
5.4 Structural control of the strike-slip superimposed Qaidam Basin on oil and gas accumulation 219
5.4.1 Distribution of sourcerocks in the Qaidam Basin 219
5.4.2 Control of strike-slip superimposed basin on oil and gas accumulation 222
Reference 223
Chapter 6 Conclusions and Follow-up research 230
6.1 General Conclusions 230
6.2 Follow-up research 231
Reference 232
Appendix 240
Appendix to Chapter 2.2 240
Appendix to Chapter 3.1 327
Appendix to Chapter 3.2 356
Appendix to Chapter 4 398
List of Figures and Tables 408
Figures to Chapter 1 408
Figures to Chapter 2.1 409
Figures and tables to Chapter 2.2 412
Figures and tables to Chapter 3.1 416
Figures and tables to Chapter 3.2 418

Figures and tables to Chapter 4 422
Figures and tables to Chapter 5 424

List of publications during the PhD. thesis work 426

Chapter 1 Preface

1.1 Introduction, Reginal Geology and Problems

Understanding the kinematics of the Asian tectonic system that contains one of the most diverse and complex patterns of active deformation on Earth not only has significant implications for deciphering the mechanisms of continental crust evolution or the interplay between lithospheric deformation and atmospheric circulation, but also contributes to exploring the crustal growth process of other planets within the solar system (Fig. 1; Molnar and Tapponnier, 1975; Tapponnier et al., 1982; England and Houseman,1986; Tapponnier et al., 1986; Cobbold and Davy, 1988; Davy and Cobbold, 1988; Molnar et al., 1993; Métivier et al., 1998; Meyer et al., 1998; Yin and Harrison, 2000; Tapponnier et al., 2001; Basilevsky and Head, 2007; Dupont-Nivet et al., 2007; Yin, 2010; Jolivet et al., 2015).

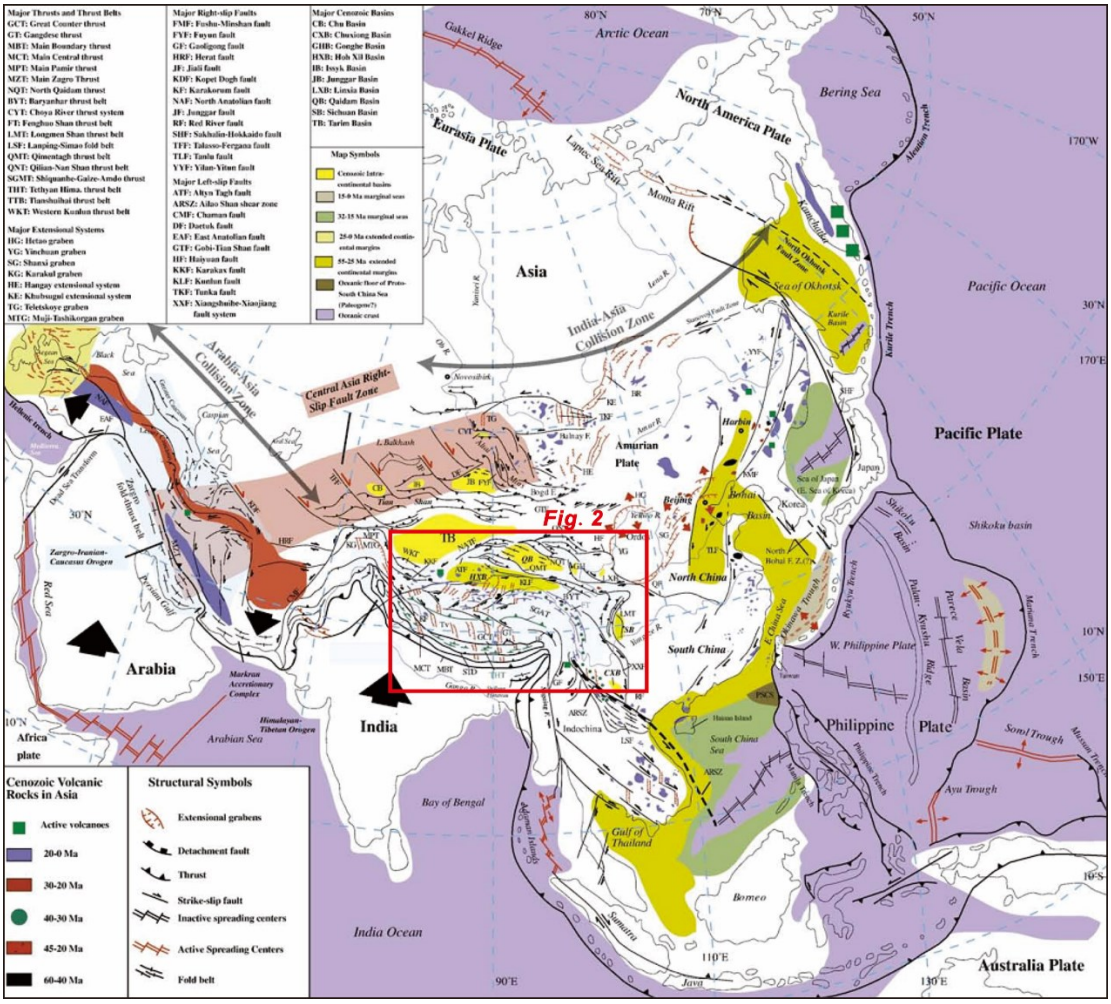

Fig.1 Cenozoic structures and distribution of volcanic rocks in Asia, modified from Yin, 2010.

Though it is widely acknowledged that the Cenozoic deformation of East Asia was associated with the India-Asia continental collision and the subsequent post-collision convergence, how this extensive area developed has long been a puzzling question. Resolving that question has implications on the understanding of the mechanical behavior of the continental lithosphere in convergent zones as well as climate evolution on regional and global scale (Molnar and Tapponnier, 1975; Métivier et al., 1998; Yin and Harrison, 2000; Tapponnier et al., 2001; Garzione et al., 2005; Dupont-Nivet et al., 2007; Yin, 2010; Jolivet et al., 2015). In particular, the initial topography of the area now represented by the Tibetan plateau and the early stages of development of the present-day topography remain poorly constrained and highly debated (e.g. England and Houseman,1986; Yin and Harrison, 2000; Tapponnier et al., 2001; Wang et al., 2006; Kapp et al., 2007; Yin et al., 2007, 2008a, 2008b; Wang et al., 2008; Wang et al., 2014).

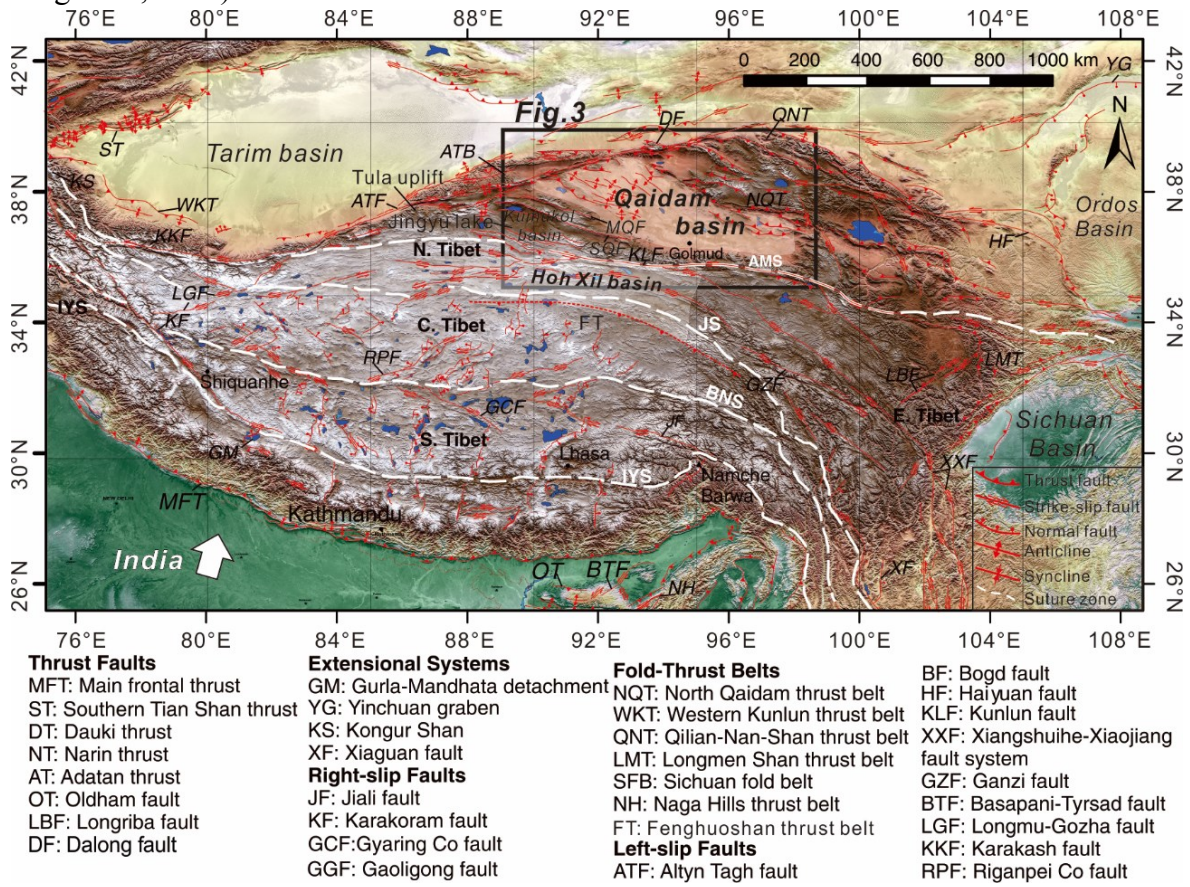

Fig.2 Digital topographic map of the Tibetan Plateau. Active fault kinematics and suture zones are mainly based on Yin et al. (2007), Taylor and Yin (2009), and Cheng et al. (2014, 2016).

The Qaidam basin is unique in the world in that it is the deepest intracontinental basin (>16 km thick of Cenozoic sediments alone), yet located in the highest plateau with the thickest continental crust. As the largest petroliferous basin on the Tibetan plateau, the triangular-shaped endorheic Qaidam basin is surrounded by the Altyn Tagh, the Qilian Shan,

and the Eastern Kunlun ranges, with ~2000 m of relief from the basin to the ranges (Figs. 2 and 3). The complete sequence of Cenozoic non-marine sedimentary rocks within the Qaidam basin as well as geological transects across the basin and ranges allow unraveling the formation mechanism and growth history of the Tibetan plateau, as well as the interplay between tectonics and climate. However, the Cenozoic evolution of the Qaidam basin and the Cenozoic kinematic evolution of the surrounding regions are highly debated, as briefly described below.

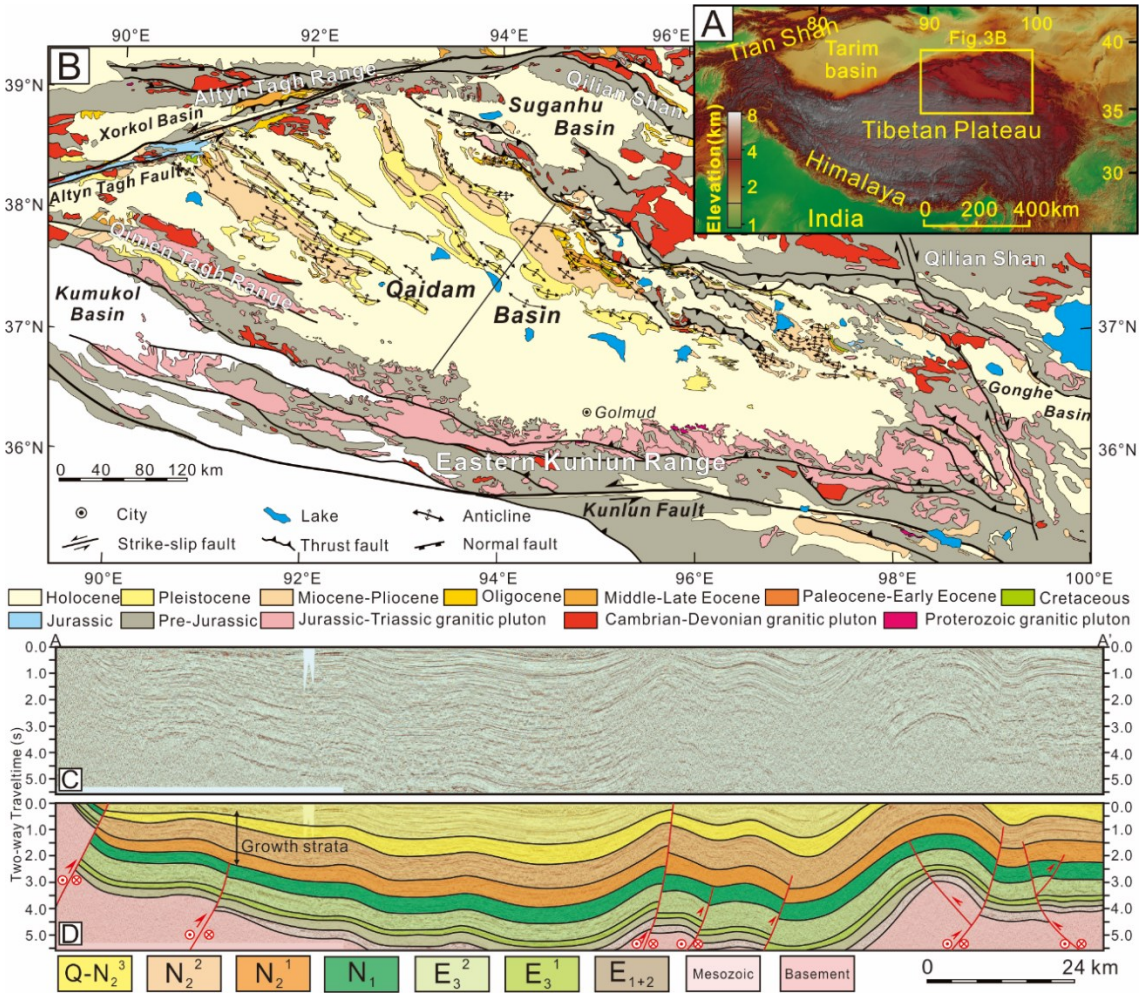

Fig.3 Geological map of the Qaidam basin, northern Tibetan plateau, modified from Chen et al. (2015). Seismic profile interpretations on the dip of the basement faults in the southwestern Qaidam basin are in dispute. Yin et al. (2007) proposed a series of south thrusting faults, whereas Cheng et al. (2014) and Wu et al. (2014) suggested those are south-dipping faults which are adopted in this study. Q-N_2^3—Quaternary to Late Miocene strata; N_2^2—Middle Miocene strata; N_2^1—Early Miocene strata; N_1—Oligocene strata; E_3^2—Late Eocene strata; E_3^1—Middle Eocene strata; E_{1+2}—Paleocene to Early Eocene strata.

In the past decades, several models have been proposed to explain the Cenozoic tectonic and sedimentary evolution of the Qaidam Basin. Most of those simply defined the tectonic pattern between the Eastern Kunlun Mountains and the Qaidam Basin through a northward or

southward thrusting model (Burchfiel et al., 1989; Meyer et al., 1998; Chen et al., 1999; Mock et al., 1999; Yin and Harrison, 2000; Jolivet et al., 2001; Tapponnier et al., 2001; Jolivet et al., 2003; Wang et al., 2006; Yin et al., 2007; Shi et al., 2009; Wang et al., 2011). The northward thrusting model prevailed during the last two decades, explaining the subsidence of the Qaidam Basin as a result of the basinward propagation of successive thrust sheets along the southern edge of the basin. Burchfiel et al. (1989) proposed that the southern edge of the Qaidam Basin is limited by a south-dipping thrust fault. Based on a synthesis of focal mechanisms and focal depth distribution combined with geological features, Chen et al. (1999) again speculated the existence of this south-dipping North Kunlun thrust fault along the northern margin of the East Kunlun belt. In addition, many authors indicated that northward basement thrusting across the Eastern Kunlun Mountains was associated to the northward propagation of a crustal-scale accretionary wedge initiating around ca. 30–20 Ma. (Fig. 4; Meyer et al., 1998; Mock et al., 1999; Jolivet et al., 2001; Tapponnier et al., 2001; Jolivet et al., 2003; Wang et al., 2006). These ideas suggest that the Eastern Kunlun Mountains consists in a large transpressional system limited to the south by the left-lateral strike slip Kunlun fault and to the north by a series of south-verging basement thrusts affecting the southern edge of the Qaidam Basin.

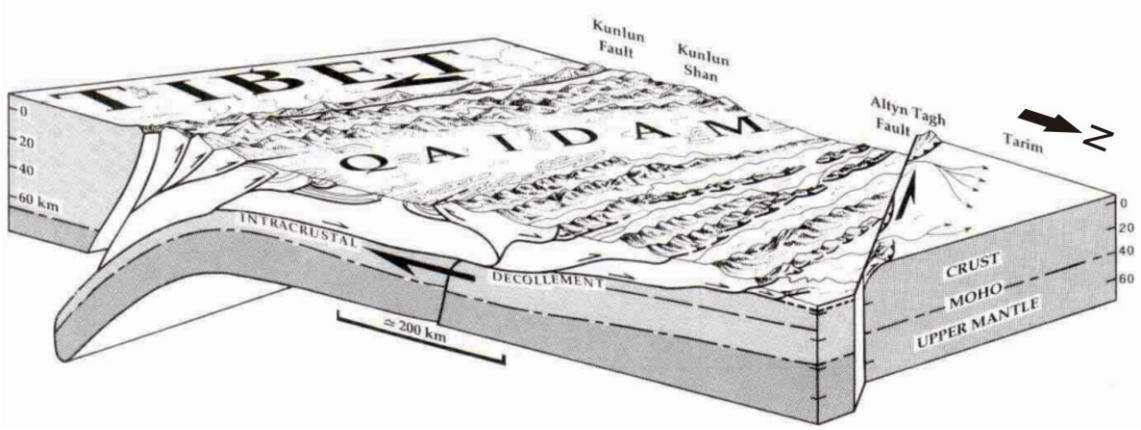

Fig.4 Northward propagation model, modified from Meyer et al. (1998). Note the south-dipping fault in the southern Qaidam basin.

The southward thrusting model has drawn much attention in recent years (Fig. 5; Yin et al., 2007; 2008; Shi et al., 2009; Wang et al., 2011). Yin and Harrison (2000) suggested that two major thrusts, the Qimen Tagh Thrust and the North Kunlun Thrust mark the southern boundary of the Qaidam Basin. Using seismic profiles within the Qaidam Basin as well as field observations, Yin et al. (2007) then proposed that the low altitude Qaidam Basin has been thrust onto the Eastern Kunlun Mountains along a major north dipping Cenozoic thrusts. Wang et al. (2011) later expanded this model based on a high-resolution deep seismic reflection

profile across this area. This model indicates that the Eastern Kunlun Mountains should not thrust northward onto the Qaidam Basin and that the initiation of compressive deformation along the southern margin of the Qaidam Basin is much younger than along the northern margin of the basin.

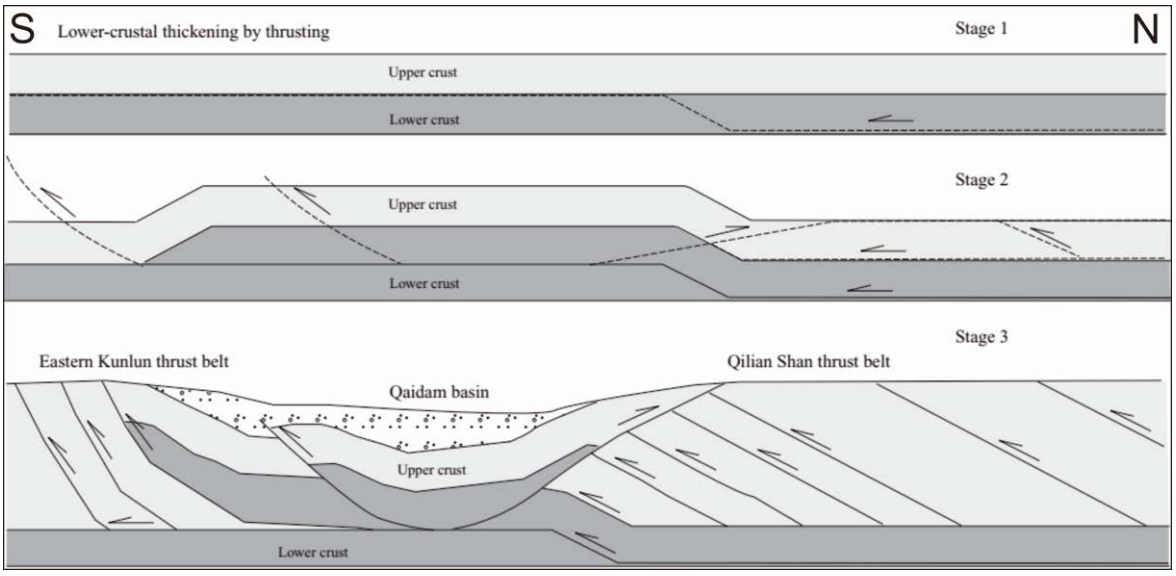

Fig.5 Southward propagation model, modified from Yin et al. (2008a). Note the south-thrusting fault in the southern Qaidam basin.

Other tectonic models have been proposed aside from the two main ones described above. Xia et al. (2001) proposed that the Qaidam Basin experienced a two stages evolution: an initial extension phase during the Early Tertiary was followed by a compressive phase leading to basin inversion. However, few seismic profiles in the western Qaidam Basin have revealed any extensional faults during the Early Tertiary. Meng and Fang (2008) suggested that the Cenozoic tectonic subsidence of the Qaidam Basin resulted from crustal folding or buckling in response to regional horizontal compression. However, the seismic profiles across the whole Qaidam Basin imply that the magnitude of Cenozoic upper crustal shortening decreases eastward across the basin from >48% in the west to <1% in the east (Yin et al., 2008a). In particular, the proposed onset time of uplift of the Eastern Kunlun Range mainly varies from Eocene to Miocene, depending on the approach used to estimate the onset of deformation (Mock et al., 1999; Jolivet et al., 2001; Yuan et al., 2006; Yin et al., 2007, 2008a; C. Wang et al., 2008; Clark et al., 2010; Dai et al., 2013; Duvall et al., 2013). Based on regional stratigraphic correlation between the Qaidam Basin and the Hoh Xil Basin to the south, Yin et al. (2008a) argued that they represented a single basin during the Paleogene, bounded to the north by the Altyn Tagh Range and the Qilian Shan, and to the south by the proto–Tibetan Plateau. This large structure was then partitioned by the tectonic uplift of the Eastern Kunlun

Range during the Neogene. This model questions the assumption of a progressive northward growth of the plateau through in-sequence propagation of thrust systems associated with filling of the intermediate basins (e.g., Métivier et al., 1998; Meyer et al., 1998; Tapponnier et al., 2001). This idea has motivated several attempts to reassess the tectonic processes affecting the northern edge of the Tibetan Plateau (e.g., Shi et al., 2009; Wang et al., 2011; Mao et al., 2014; Yu et al., 2014).

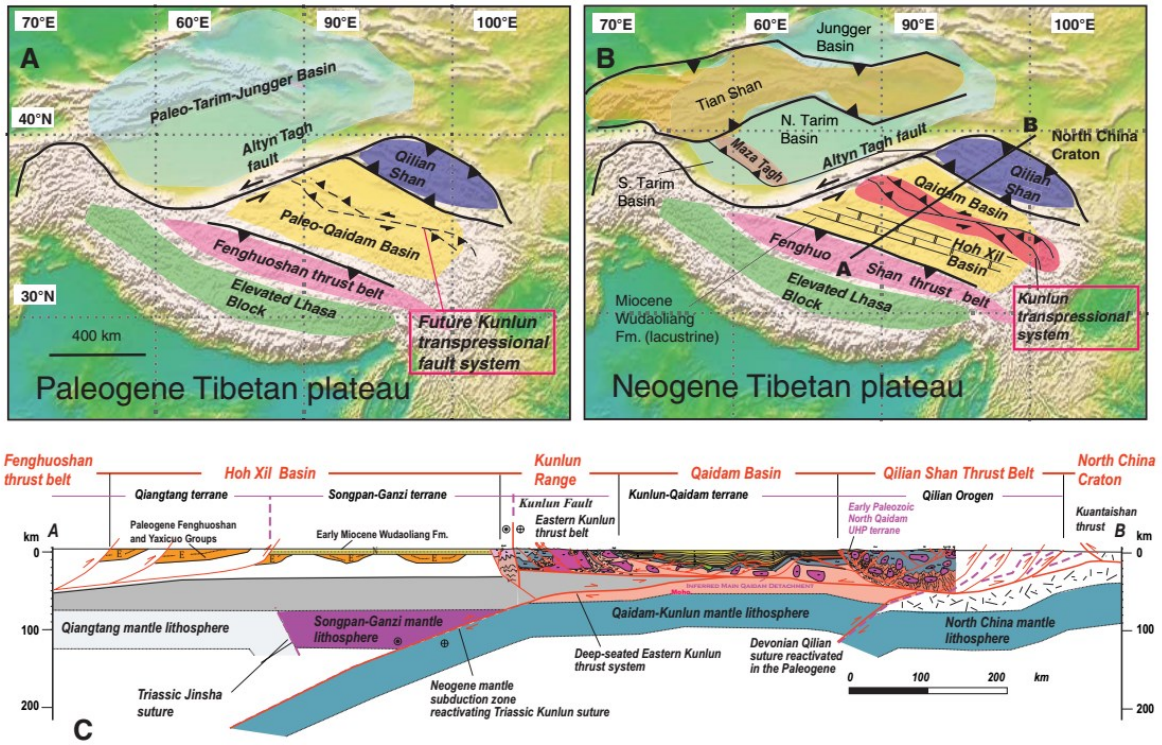

Fig.6 Paleo-Qaidam basin model, cited from Yin et al. (2008a). Note that during the Paleogene, the Paleo-Qaidam basin lies between the elevated Lhasa block and the Fenghuo Shan thrust belt in the south and the elevated Qilian Shan in the north. The region north of the Tibetan plateau was a large topographic depression that links Tarim and Junggar basins across the Tian Shan, as the Tian Shan was not uplifted until the early Miocene. The initiation of the Eastern Kunlun left-slip transpressional system caused the uplift of the Eastern Kunlun Range, which has partitioned the PaleoQaidam basin into the Hoh Xil basin to the south and the Qaidam basin to the north.

As the northwestern boundary of the Qaidam basin, the sinistral strike-slip Altyn Tagh fault plays a significant role in the Cenozoic deformation of northern Tibet (Fig. 7). Understanding the Cenozoic kinematic pattern of the Altyn Tagh fault holds important implications for unraveling the evolution of northern Tibet, deciphering the growth history of the entire Tibetan Plateau, and contributing to oil and gas exploration in the surrounding region (Fig. 2; Yue and Liou, 1999; Yin and Harrison, 2000; Tapponnier et al., 2001; Yin et al., 2002; Wang et al., 2014). Recent studies have revealed much about the large-scale geology of the Altyn Tagh Range and the surrounding region (Wang, 1997; Yue et al., 2001; Yin et al., 2002;

Chen et al., 2003; Cowgill et al., 2003; Dupont-Nivet et al., 2003, 2004; Ritts et al., 2004; Wu et al., 2012a, 2012b; Lu et al., 2014; Zhang et al., 2014). However, the immense size and extent of the Altyn Tagh Range make it difficult to locate ideal piercing points with which to estimate the initial timing of left-slip movement and total displacement along the Altyn Tagh fault. As a result, both the timing and amount of slip along the fault are vigorously debated (e.g., Yin et al., 2002; Cowgill et al., 2003; Gehrels et al., 2003a, 2003b; Ritts et al., 2004; Wu et al., 2012a, 2012b). Although some studies reference Mesozoic shearing in the Altyn Tagh Range (Arnaud et al., 2003; Wang et al., 2005; Li et al., 2006; Liu et al., 2007), the growth of the Tibetan Plateau is largely related to Cenozoic faulting along the Altyn Tagh fault rather than to any pre-Cenozoic shearing in the Altyn Tagh Range (Tapponnier et al., 2001). Various approaches have been used to constrain the initial timing of left-lateral slip movement along the Altyn Tagh fault, and the estimates vary greatly. Initial movement along the Altyn Tagh fault is estimated to have occurred broadly between the Eocene and Miocene epochs (Chen et al., 2001; Jolivet et al., 2001; Meng et al., 2001; Wan et al., 2001; Yue et al., 2001; Yin et al., 2002; Robinson et al., 2003; Wu et al., 2012a, 2012b), and estimates of the total displacement along the Altyn Tagh fault vary anywhere from ~1200 km to less than 90 km (Tapponnier et al., 1986; Wang, 1997; Yin and Harrison, 2000; Yang et al., 2001; Yin et al., 2002; Cowgill et al., 2003; Gehrels et al., 2003a, 2003b; Ritts et al., 2004). The wide variety of estimates regarding the initial timing and offset of the Altyn Tagh fault highlight the incomplete understanding of this remote region.

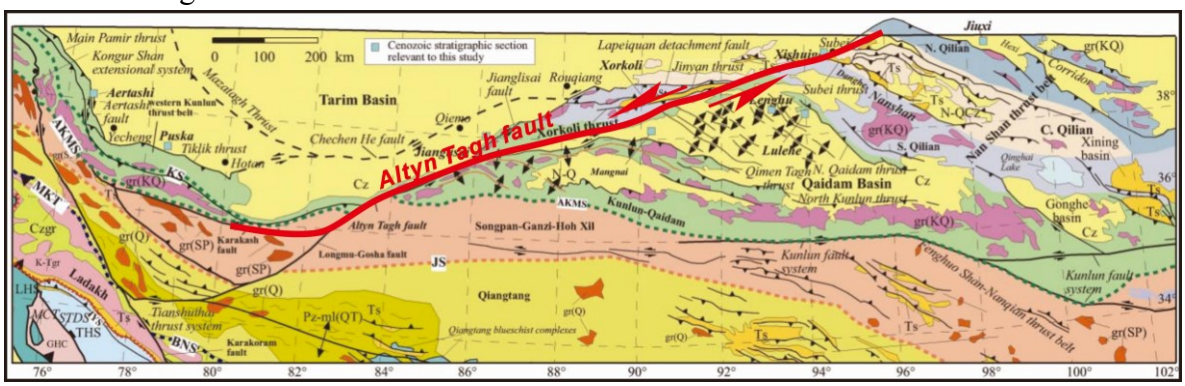

Fig.7 Simplified tectonic map of northern Tibet showing major tectonic terranes, sutures, and faults (modified from Yin et al., 2002). Cenozoic stratigraphic sections (locations shown by turquoise blue squares) were measured by this study at Aertashi, Puska, Jianglisai, and Xishuigou in the southern Tarim Basin. Other relevant stratigraphic sections are Mangnai, Lenghu, Lulehe, Xorkoli, and Jiuxi (Hexi Corridor). Map symbols: N-Q—Neogene–Quaternary sediments, Ts—Tert iary sedimentary rocks, THS—Tethyan Himalayan sequences (Proterozoic to Upper Cretaceous passive-continental-margin strata of northern India), GHC—Greater High Himalayan Crystalline Complex, LHS—Lesser Himalayan metasedimentary series. Major plutonic rocks: Czgr—Cenozoic granites, K-Tgr—plutonic rocks belongi ng to the Gangdese batholith, Ladakh batholith, and Kohistan arc, gr(Q)—plutonic rocks

in the Qiangtang terrane (mostly Jurassic–Cretaceous), gr(SP)—plutonic roc ks in the Songpan–Ganzi–Hoh Xil terrane (mostly Late Triassic), gr(KQ)—Ordovician–Silurian and Permian–Triassic plutonic rocks in the Kunlun and Qilian terranes. Major sutures: IYS—Indus-Yalu suture, BNS—Bangong-Nujiang suture, JS—Jinsha suture, AKMS—Ayimaqin-Kunlun-Mutztagh suture, KS—Kudi suture, MCT—Main Centra l thrust, MKT—Main Karakoram thrust, STDS—South Tibet detachment system.

Finally, with regard to the northeastern boundary of the Qaidam basin, the Qilian Shan separates the plateau from the Gobi-Alxa block to the northeast (Fig. 8). This crustal-scale wedge consists of massive NW-SE striking mountain ranges growing on folds, thrusts or strike-slip faults accommodating the northward motion and eastward extrusion of the Tibetan Plateau (Meyer et al., 1998; Yin and Harrison, 2000; Tapponnier et al., 2001; Bovet et al., 2009). The proposed Palaeocene to early Eocene initiation of the Cenozoic deformation and crustal shortening in the Qilian Shan (Jolivet et al. 2001; Yin et al., 2008; Clark et al., 2010; Duvall et al., 2011; Zhuang et al., 2011; Yuan et al., 2013) challenges the model of post-Pliocene initial deformation in the northern Tibetan plateau inferred from the hypothesis of northward progressive plateau growth (Métivier et al., 1998; Meyer et al., 1998; Tapponnier et al., 2001). Although large amounts of NE-SW directed shortening and eastward motion of the northern Tibetan crust have long been observed (e.g. Tapponnier and Molnar, 1977; Burchfiel et al., 1991; Dupont-Nivet et al., 2004; Zhang et al., 2004), the proposed amounts of Cenozoic crustal shortening vary widely from ~20% to ~60% (Bally et al., 1986; Meyer, et al., 1998; Yin et al., 2008a, 2008b; Zhang et al., 2014) and quantitative estimation of the amount of lateral extrusion in the northeastern Tibetan Plateau is deficient.

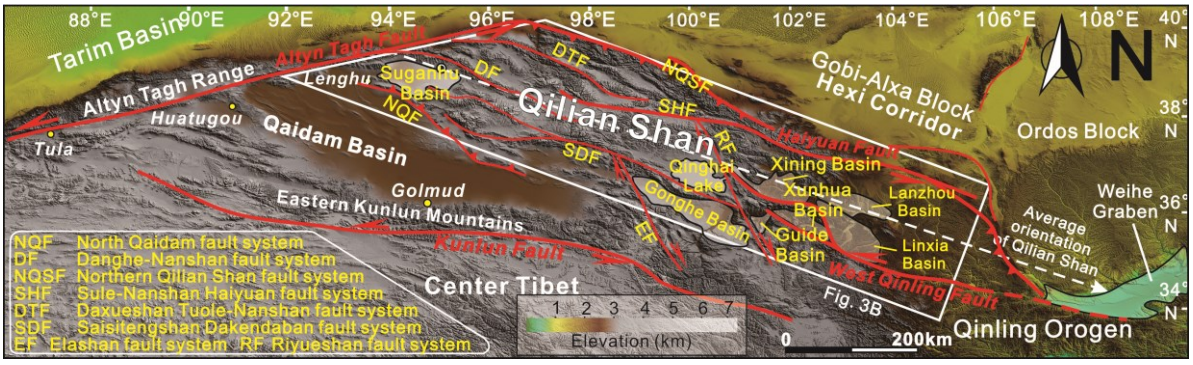

Fig.8 Topographic map of northern Tibet showing major tectonic terranes and faults within the Qilian Shan.

1.2 Research plan and framework of the dissertation

My PhD dissertation focuses on four key issues that contribute to understand the evolution of the Qaidam basin itself and kinematic history of the entire Tibetan plateau since the onset of the India-Asia collision: ***1) The Cenozoic tectonic evolution between the Qaidam***

basin and the Eastern Kunlun Range; 2) The interplay between the sediments within the Qaidam basin and the active tectonic within the Altyn Tagh Range; 3) The quantitative estimate of the lateral extrusion along the Altyn Tagh Fault-Qilian Shan tectonic system; 4) The classification of the Qaidam basin: Foreland basin or Strike-slip superimposed basin**?***

Firstly, I discuss the Cenozoic tectonic evolution between the Qaidam basin and the Eastern Kunlun Range in Chapter 2. I subdivided this issue into two parts: ***Chapter 2.1 Tectonic relationship between the Eastern Kunlun Range and the Qaidam basin***, and ***Chapter 2.2 Cenozoic source to sink relation between the Qaidam basin and the Eastern Kunlun Mountains***. In the first part, I analyze newly acquired 3D seismic-reflection profiles within the SW Qaidam basin, isopach maps of the Cenozoic strata in the SW Qaidam basin, remote sensing images in the Qimen Tagh Range, and earthquake focal mechanisms and epicenter distribution within the Qaidam basin, in order to re-evaluate the tectonic pattern along the western portion of the Kunlun fault and to decipher the Late Cenozoic interaction between the Eastern Kunlun Range and the SW Qaidam basin. I published this work in ***Tectonophysics*** as first author. Concerning the Cenozoic source to sink relation between the Qaidam basin and the Eastern Kunlun Mountains, I conducted field investigation, detrital zircon geochronology analysis combined with the seismic profile interpretation, in order to characterize the nature of the relation between the Eastern Kunlun Range and the Qaidam Basin, and present a clear image on the source to sink relation between these two regions. I published this contribution in ***Geological Society of American Bulletin*** as first author.

Secondly, in order to constrain ***the initial timing and kinematic pattern of movement along the Altyn Tagh fault***, I present a detailed analysis of the stratigraphy, sediment types, and detrital zircon U-Pb ages combined with seismic profile data along three sections (Tula, Anxi, and Caishiling sections) of the western segment of the Altyn Tagh fault in ***Chapter 3.1***. I also carried out a detailed analysis of the stratigraphy and detrital zircon geochronology of four key lithologic sections (Tula, Anxi, Caishiling and Eboliang) along the Altyn Tagh fault, presented in ***Chapter 3.2***. I published part of this work in ***Geosphere*** as first author (see ***Chapter 3.1***), while submitted the other part to ***Tectonophysics*** again as first author (see ***Chapter 3.2***). This last manuscript as been accepted with minor revision.

Thirdly, my work on ***the quantitative estimate of the lateral extrusion along the Altyn Tagh Fault-Qilian Shan system which*** is a follow-up research of issue 2 (i.e. ***the initial timing and kinematic patterns of movement along the Altyn Tagh fault***). The lithospheric strike-slip Altyn Tagh fault has accommodated hundreds of kilometers of displacement (~360 km) between the Qaidam and Tarim blocks since its Eocene reactivation. However, the way the

deformation is accommodated in the Qilian Shan and further east remains uncertain. I propose a new quantitative evaluation of the Cenozoic crustal shortening and lateral extrusion budget in the northern Tibetan plateau, based on my 360 km estimation of north-eastward migration of the relatively rigid Qaidam block along the Altyn Tagh fault, and 3D isovolumetric balancing of the crustal deformation within the Altyn Tagh fault–Qilian Shan system. I published this work in ***Terra Nova*** as first author, and present it in ***Chapter 4***.

Finally, in order to ***classify the peculiar Qaidam basin (Foreland basin or Strike-slip superimposed basin)***, I review the recent arguments on the Cenozoic evolution of the Qaidam baisn and summarize the kinematic features within the Qaidam basin and surrounding regions based on the abovementioned findings combined with recent petroleum exploration achievements in recent years (e.g. distribution of source rocks in the Qaidam basin). I conclude that the Qaidam basin is a strike-slip superimposed basin jointly controlled by the left-lateral strike-slip Altyn Tagh and East Kunlun faults. The temporal and spatial superimposition of these two strike-slip faults during the Cenozoic controlled the evolution of the basin as well as the oil and gas accumulation. This work is presented in ***Chapter 5***. I have published this contribution in ***Petroleum Exploration and Development*** as co-author.

Chapter 2 Cenozoic tectonic evolution between the Qaidam basin and the Eastern Kunlun Range

2.1 Tectonic relationship between the Eastern Kunlun Range and the Qaidam basin

Paper published in Tectonophysics, 2014, vol. 632, pp. 32-47

Northward growth of the Qimen Tagh Range: a new model accounting for the Late Neogene strike-slip deformation of the SW Qaidam Basin

Feng Cheng [a], Marc Jolivet [b], Suotang Fu [c], Qiquan Zhang [c], Shuwei Guan [d], Xiangjiang Yu [a], Zhaojie Guo [a, *]

[a] Key Laboratory of Orogenic Belts and Crustal Evolution, Ministry of Education, School of Earth and Space Sciences, Peking University, Beijing, 100871, China

[b] Laboratoire Géosciences Rennes, CNRS-UMR6118, Université Rennes 1 - Observatoire des Sciences de L'Univers de Rennes, Rennes, France

[c] Qinghai Oilfield Company, PetroChina, Dunhuang, Gansu, 736202, China

[d] Research Institute of Petroleum Exploration and Development, PetroChina, Beijing, 100083, China

[*] Corresponding author. Tel.: + 86-10-62753545; fax: + 86-10-62758610. E-mail address: zjguo@pku.edu.cn

Note: The online version of this contribution can be found as: ***Cheng, F., Jolivet, M., Fu, S., Zhang, Q., Guan, S., Yu, X., Guo, Z., 2014. Northward growth of the Qimen Tagh Range: A new model accounting for the Late Neogene strike-slip deformation of the SW Qaidam Basin. Tectonophysics 632, 32-47, doi: 10.1016/j.tecto.2014.05.034***

Abstract

Situated along the western termination of the Eastern Kunlun Mountains, the Qimen Tagh Range represents a key area to understand the Cenozoic basin-range interactions between the northeastern Tibetan Plateau and the Qaidam Basin. Within that region, several huge bow-like

fault systems such as the Kunbei and Qimen Tagh fault systems accommodate the transpressive deformation but their kinematic evolution is still highly debated. Newly acquired seismic profiles and isopach maps of the Late Eocene sediments strongly suggest that the Kunbei fault system (consisting of the Kunbei, Arlar and Hongliuquan faults) in the southwestern Qadaim Basin was initially a left-lateral strike-slip fault system rather than a thrusting system. Growth strata indicate an Early Miocene onset age for this strike-slip deformation. However, earthquakes focal mechanisms show that the present-day tectonic pattern of this fault system is dominated by NE-SW transpression. As for the Qimen Tagh fault system, numerous linear geomorphic features and fault scarps indicate that it was again a strike-slip fault system. Deformed sediments within the Adatan Valley prove that strike-slip motion prevailed during the Pleistocene, yet the present day deformation is marked by NE-SW transpression. Collectively, the Kunbei and Qimen Tagh fault systems were initially left-lateral strike-slip fault systems that formed during Early Miocene and Pleistocene respectively. Colligating with these southward younging left-lateral strike-slip faulting ages and the fact that these convex-northward structures converge to the center segment of active Kunlun Fault in the east, we thus considered the Kunbei and Qimen Tagh fault systems as former western segments of the Kunlun Fault once located further south in the present-day location of that fault. These faults gradually migrated northward since the Early Miocene while their kinematics changed from left-lateral strike-slip motion to NE-SW transpression.
Keywords: Cenozoic tectonics, North Tibet, Kunlun Fault, Qimen Tagh Range, southwestern Qaidam Basin.

2.1.1 Introduction

The Eastern Kunlun Mountains and adjacent Qaidam Basin present one of the strongest topographic gradients in Eurasia, similar to that of the Longmen Shan Range in East Tibet (Fig. 1). Within that region, the left-lateral strike-slip Kunlun Fault Zone represents one of the key tectonic features controlling the active deformation along the northern margin of the Tibetan Plateau (e.g. Avouac and Tapponnier, 1993; Meyer et al., 1998; Jolivet et al., 2001; Tapponnier et al., 2001; Xia et al., 2001 ;Yin et al., 2007). Most of the previous studies that dealt with the Tertiary deformation in the East Kunlun ranges focused on the central and eastern segment of the Kunlun Fault (Kirby et al., 2007; Harkins and Kirby, 2008) where the deformation is mostly localized along the major, unique strike-slip fault zone. However, only a limited number of studies describe the more structurally complex western termination of the

Kunlun Fault system (Jolivet et al., 2001, 2003).

Although the Cenozoic tectonic evolution of North Tibet has been largely studied, the relationship between the Qaidam Basin and the East Kunlun Range, as well as the tectonic pattern of the Kunlun Fault itself, remains controversial. For example, several contradicting models have been proposed to describe the tectonic structure of the southern edge of the Qaidam Basin: a crustal-scale south-dipping thrust system (Burchfiel et al., 1989); a large transpressional system including the left-lateral strike - slip Kunlun Fault to the south and a north - directed thrust system along the northern flank of the Eastern Kunlun Mountains (Meyer et al., 1998; Tapponnier et al., 2001; Jolivet et al., 2003); or a series of north - dipping thrusts carrying the Qaidam Basin southward onto the Qimen Tagh Range (Yin et al., 2007; Shi et al., 2009; Wang et al., 2011). Within most of those models, the large amount of Cenozoic strike-slip motion along the Kunlun Fault (Fu and Awata, 2007) is generally considered as secondary in controlling the overall structural setting of the SW Qaidam Basin and East Kunlun Range. However, if the boundary fault between the Qaidam Basin and the East Kunlun Range was indeed accommodating a large amount of lateral displacement, the southern Qaidam Basin should be largely decoupled from the Tibetan Plateau to the south and should not be affected by major N-S compression and shortening since the initiation of the strike-slip Kunlun Fault. Nonetheless, the Qimen Tagh Range, bordering the SW Qaidam Basin to the south forms a convex-northward bow-like tectonic prism clearly accommodating shortening along the southern margin of the basin while strike-slip motion occurs along the Kunlun Fault to the south.

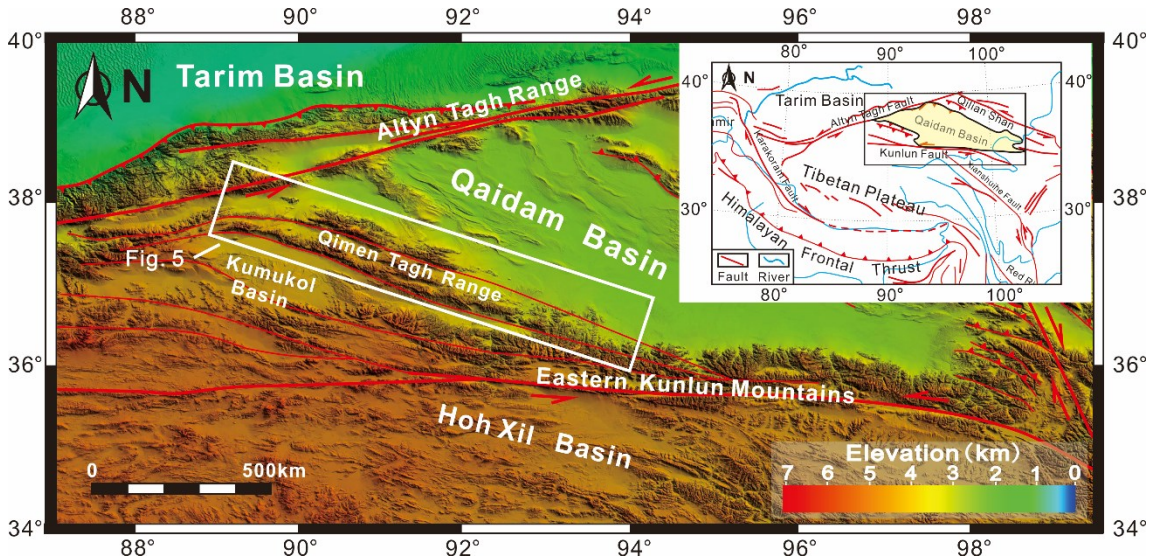

Fig.1 Digital topographic map of the western Qaidam Basin and surrounding area. Topography from SRTM data.

This paper aims to re-evaluate the tectonic pattern along the western portion of the Kunlun Fault and to decipher the Late Cenozoic interaction between the East Kunlun Range and the SW Qaidam Basin in the Qimen Tagh Range. This work is based on new field observation and data, interpretation of newly acquired seismic reflection profiles within the SW Qaidam Basin, remote sensing images, and earthquake focal mechanisms and epicenters distribution. Based on those data we propose that the Late Neogene northward growth of the convex-northward structures in the Qimen Tagh Range and SW Qaidam Basin is driven by left-lateral strike-slip motion along the Kunlun Fault. While migrating northward, the western segment of the Kunlun Fault gradually rotates through time. This northward rotation induces a progressive change from left-lateral strike-slip to NE-SW compressional motion. Continuous activity along the Kunlun Fault finally initiates a new strike-slip segment.

2.1.2 Regional Geology

2.1.2.1 Eastern Kunlun Mountains

The Eastern Kunlun Mountains, with an average altitude of ~4500m, separates the relatively low-relief Qaidam Basin to the north from the Hoh Xil Basin to the south. The Kunlun Fault Zone itself represents a major tectonic boundary between the Bayan Har-Songpan Garze terrane and the Kunlun-Qaidam basement (e.g. Meyer et al., 1996). The fault extends about 1600 km along-strike, initiating on the eastern margin of the Tibetan Plateau (Kirby et al., 2007; Lin and Guo, 2008) and ending in a splay structure with several curved faults in the west (Xu et al., 2002; Fu and Awata, 2007) (Fig. 1). Intense seismicity attests of the activity of this left-lateral strike-slip fault system (e.g., M_w 7.8 Kunlunshan earthquake in 2001(Lin et al., 2002; Xu et al., 2002); M_w 7.6 Manyi earthquake in 1997 (Peltzer et al., 1999); M_w 7.5 Manyi earthquake in 1973 (Velasco et al., 2000); M_w 7.5 Tuosu Lake earthquake in 1937 (Guo et al., 2007); M_s 7.0 Alake Lake earthquake in 1963(Guo et al., 2007)). Both GPS and geological data suggest that the central segment of the Kunlun Fault has a uniform slip rate of ca.10 mm/yr (Kidd and Molnar, 1988; Van Der Woerd et al., 1998; Wang et al., 2001; Zhang et al., 2004; Fu et al., 2005; Kirby et al., 2007). This rate decreases to ~5 mm/yr along its eastern segment and finally dies out toward the eastern fault tip (Kirby et al., 2007; Harkins and Kirby, 2008). The total displacement along the fault since its initiation is approximately 100 ± 20 km according to the largest cumulative offset of basement rocks along the tectonic lineament (Fu and Awata, 2007).

The Cenozoic deformation and exhumation history of the Eastern Kunlun Mountains is

complex and still largely debated. For instance, the onset age of the Cenozoic cooling event in this area range from 35 to 10 Ma depending on the authors (Mock et al., 1999; Jolivet et al., 2001; Wang et al., 2004a; Liu et al., 2005; Yuan et al., 2006; Clark et al., 2010; Duvall et al., 2013). However, the onset age of left-lateral strike-slip motion along the Kunlun Fault has been estimated to be 15 Ma or earlier (Jolivet et al., 2003). Similarly, based on the growth strata records in the seismic profiles across the SW Qaidam Basin, Yin et al. (2008) asserted that the Cenozoic deformation across the Qimen Tagh Range and in the SW Qaidam Basin, directly related to the tectonic development of the Kunlun Fault Zone, initiated during or after Late Oligocene to Early Miocene times.

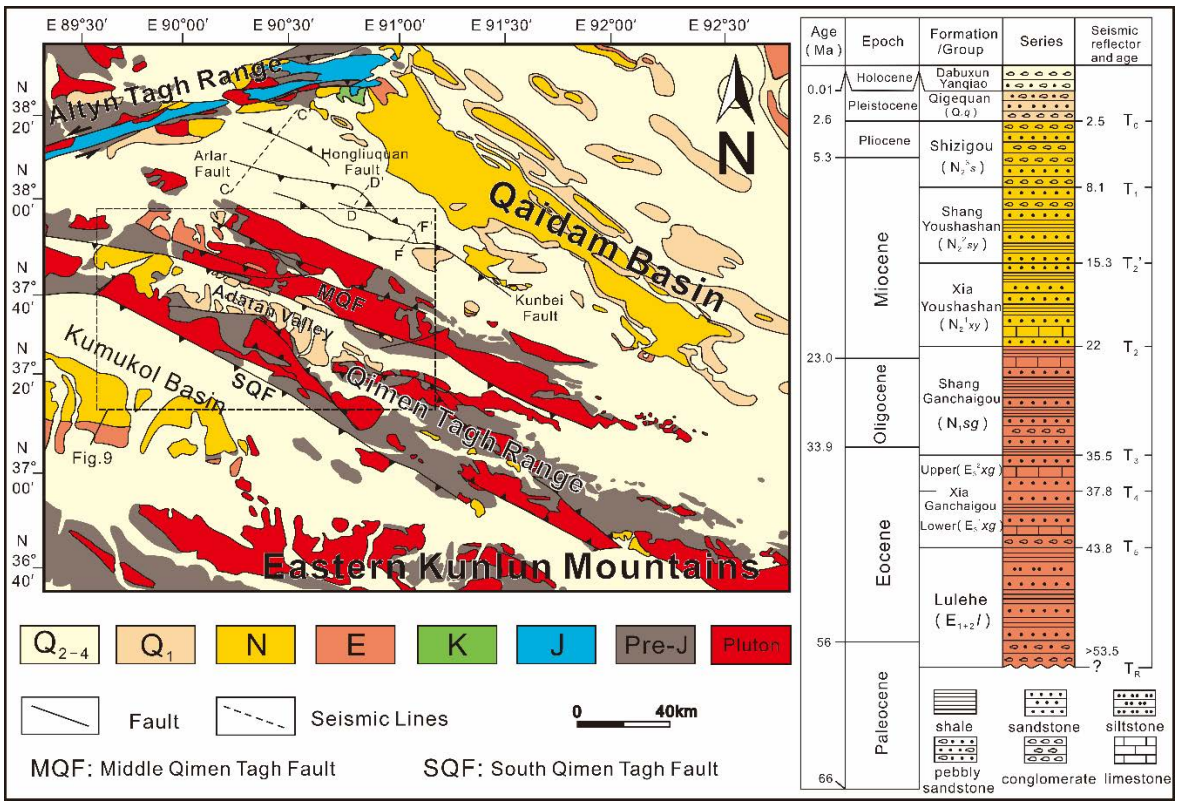

Fig.2 Geological map of the Qimen Tagh Range and SW Qaidam Basin. See Fig. 1 for location and the text for discussion. Modified after the Kulangmiqiti J46C003001 1:250,000 geological map (IGSQP, 2004).

2.1.2.2 SW Qaidam Basin and Kumukol Basin

The ~3500 m high (on average), low relief triangular Qaidam Basin is bounded by the Altyn Tagh Range to the northwest, the Eastern Kunlun Mountains to the south, and the Qilian Shan to the northeast (Fig. 1). Recent geological cross sections within the Qaidam Basin, mostly based on seismic profiles and drill cores data, demonstrate that the upper Cretaceous and Tertiary sediments rest unconformably on the Jurassic to Cretaceous strata. This

unconformity indicates that some deformation already took place within the basin during the Cretaceous (Xia et al., 2001; Fang et al., 2007). The Cenozoic sequences mainly consist of a series of continental clastic deposits (Fig. 2). The successive depocenters were consistently located along the long axis of the basin and gradually migrated eastward since the Eocene (Balley, 1986; Song and Wang, 1993; Qiu, 2002; Xia et al., 2001; Sun et al., 2005; Yin et al., 2008).

The chronology of the Cenozoic stratigraphic units has been precisely defined (Fig. 2) mostly using magnetostratigraphy, but also based on palynology and paleontology studies within the entire basin (QBGMR, 1991; Yang et al., 1992; Deng et al., 2004a, 2004b; Sun et al., 2005; Song et al., 2006; Zhang et al., 2006; Fang et al., 2007; Sun et al., 2007; Wang et al., 2007; Lu and Xiong, 2009; Ke et al., 2013). The series include: (1) the Lulehe Formation, $E_{1+2}l$, >53.5 - 43.8 Ma (Yang et al., 1992; Song et al., 2006; Zhang, 2006; Ke et al., 2013); (2) the lower Xiaganchaigou Formation, E_3^1xg, 43.8 - 37.8 Ma (Song et al., 2006; Zhang, 2006; Sun et al., 2007; Pei et al., 2009); (3) the upper Xiaganchaigou Formation, E_3^2xg, 37.8 - 35.5 Ma (Sun et al., 2005; Sun et al., 2007; Pei et al., 2009); (4) the Shangganchaigou Formation, N_1sg, 35.5 - 22.0 Ma (Sun et al., 2005; Lu and Xiong, 2009); (5) the lower Youshashan Formation, N21xy, 22.0 - 15.3 Ma (Fang et al., 2007; Lu and Xiong, 2009); (6) the upper Youshashan Formation, N_2^2sy, 15.3 - 8.1 Ma (Fang et al., 2007); (7) the Shizigou Formation, N_2^3s, 8.1 - 2.5 Ma (Fang et al., 2007); and finally, (8) the Quaternary sediments, including the Qigequan Formation (Q1q) and the Dabuxun - Yanqiao Formation, 2.5 - 0 Ma (Fang et al., 2007; Yin et al., 2008). The boundaries between these formations have been labeled T_R, T_5, T_4, T_3, T_2', T_2, T_1 and T_0 (from bottom to top) by petroleum geologists and will be used as it below (Fig. 2).

The Kumukol Basin (Figs. 1 and 2), with an average elevation of ~4000m, is located between the Qimen Tagh Range to the north and the western branches of the Eastern Kunlun Range to the south. Remote sensing image and field evidence indicate that the northern part of the Kumukol Basin is bordered by an active fault which controls the distribution of the present drainage system (IGSSP, 2003). The basin contains an Eocene to Pliocene sequence which has been deformed into a NW-SE oriented syncline (Meng and Fang, 2008). Based on fossils and stratigraphic correlation (Zhang et al., 1996), these Tertiary sequences can be divided into four units (from bottom to top) (Meng and Fang, 2008): the Huatiaoshan Formation (Eocene to Oligocene), the Hongshiliang Formation (Early Miocene), the Fengchenkou Formation (Middle Miocene), and the Jiantuliang Formation (Pliocene to Pleistocene). The Eocene to Oligocene series in the Kumukol Basin are dominated by

lacustrine deposits (IGSSP, 2003) displaying similar facies and depositional environments as the Eocene to Oligocene deposits in the SW Qaidam Basin and Hoh Xil Basin. This similarity of the deposits within the three basins suggests that they were largely connected during the Paleogene (Yin et al., 2008).

2.1.3 Active tectonic pattern in the western segment of the East Kunlun Range

The distribution and focal mechanisms of earthquakes reflect the occurrence and kinematics of active faults and allow describing the active tectonic pattern of the study area (e.g. Taylor and Yin, 2009; Jolivet et al., 2013). We analyzed the parameters of all earthquakes in an area between 89°E to 98°E and 35°N to 39°N, for which precisely determined hypocenter depths and focal mechanisms are available. The epicenters and depth - frequency distribution of seismicity used in this study are issued from the China Earthquakes Network Center (CENC). Only events with magnitude M > 3 that occurred between 1970 and 2011 have been considered (Fig. 3). Focal mechanisms were obtained from the U.S. Geological Survey and the Global Centroid Moment Tensor Project. The depth - frequency distribution of seismicity is presented along two profiles, A - A' (Fig. 4a) and B - B' (Fig. 4b) (See Fig. 3 for the location of the profiles). The epicenters of earthquakes situated between 89°E to 92°E and 35°N to 39°N are projected on profile A-A'; Those of the earthquakes situated between 90°E to 98°E and 35°N to 37°N are projected on profile B-B' .

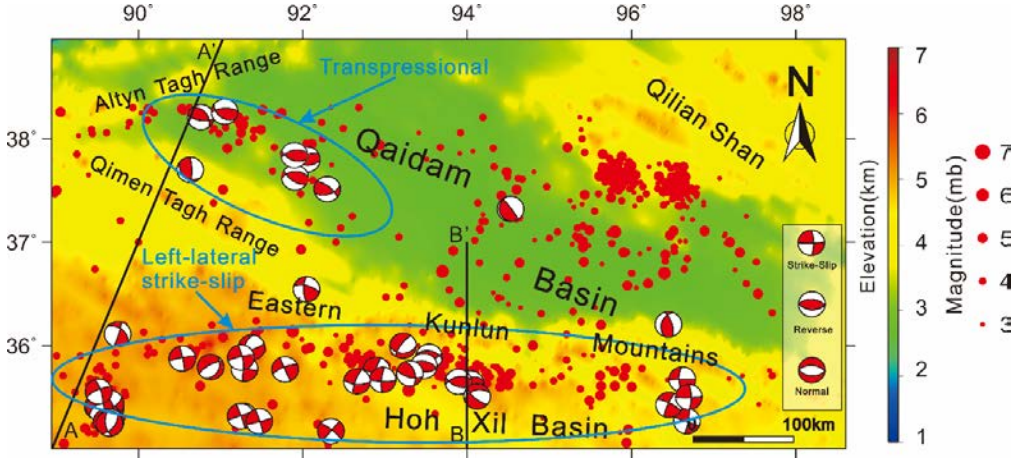

Fig.3. General topographic map of the Qaidam Basin and Eastern Kunlun Mountains with background seismicity from the China Earthquake Networks Center (CENC) from 1st January 1970 to 1st January 2011 (M>3).

Earthquakes magnitude ranges from M = 3 (the selected cut-off value) to M = 7. Strong tectonic activities (mean M between 5 and 6) are recorded along the Eastern Kunlun Mountains, on the southern edge of the Qaidam Basin. However, diffuse seismicity (mean M between 4 and 5) also occurs inside the basin (Fig. 3 and 4). Surprisingly, the Qimen Tagh

Range displays a relative lack of seismicity. Within the Eastern Kunlun Mountains, the distribution and focal mechanisms of the earthquakes are coherent with left-lateral, transpressive strike-slip movement on the Kunlun Fault. The existing few transtensive focal mechanisms can be explained by the occurrence of extensional relay-zones along the main Kunlun Fault (Jolivet et al., 2003). The focal mechanisms available inside the Qimen Tagh Range and the SW Qaidam Basin all correspond to reverse faults activity indicative of a general compressive stress field with no or extremely limited strike-slip motion.

The depth-frequency distribution of the earthquakes indicates that both in the Eastern Kunlun Mountains and in the Qaidam Basin, seismicity affects the upper 30 to 35 km of the crust (that is thought to be at least 50 km thick in that region (e.g. Jolivet et al., 2003; Zhang et al., 2011)) with most events occurring in the upper 10 to 15 km. This distribution pattern is similar to the depth-frequency distribution of seismicity over the entire Tibetan Plateau (Taylor and Yin, 2009), with exceptions where earthquakes might have occurred within the lower crust or upper lithospheric mantle (Chu et al., 2009). The observed seismicity is thus mostly indicative of the deformation of the upper to middle crust and can be reasonably compared to the fault pattern observed on the surface.

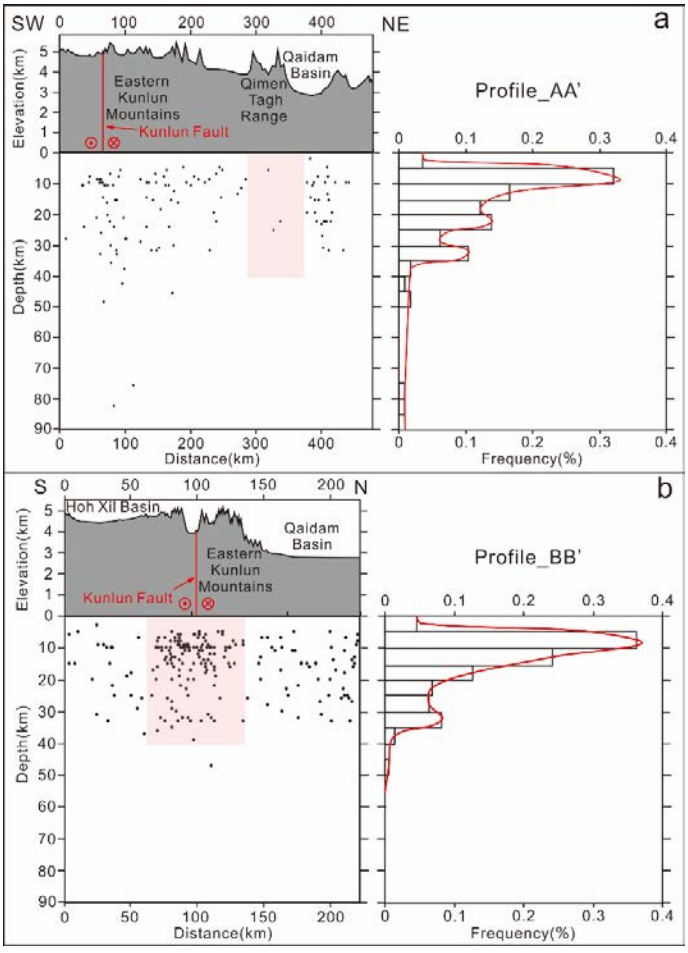

Fig.4. Depth-frequency distribution of earthquakes within the study area. Data from the China Earthquakes Networks Center (CENC), 1st January 1970 to 1st January 2011 with M>3. Two seismic profiles (AA' (a) and BB'. (b) (see location on Fig. 3)) are investigated with (left) depth distribution of earthquakes and (right) depth – frequency distribution of seismic events. See text for discussion.

2.1.4 Splay Fault System of the Kunlun Fault Zone

Different from the typical horse-tail structure, the western segment of the Kunlun Fault develops several asymmetric northward curved structures topographically characterized by a series of ridges and valleys (Fig. 1). These elongated linear geomorphic landforms are similar to those of the central segment of the Kunlun Fault, such as the Xidatan and Dongdatan valleys (Xu et al., 2002), and indicate the occurrence of left-lateral strike-slip faulting. Meanwhile, the valleys are largely filled with Cenozoic deposits that recorded the history of the strike-slip faulting and especially its onset time. In this study, taking the Qimen Tagh Range as an example, we aim at clarifying the tectonic pattern of the western segment of the Kunlun Fault through time.

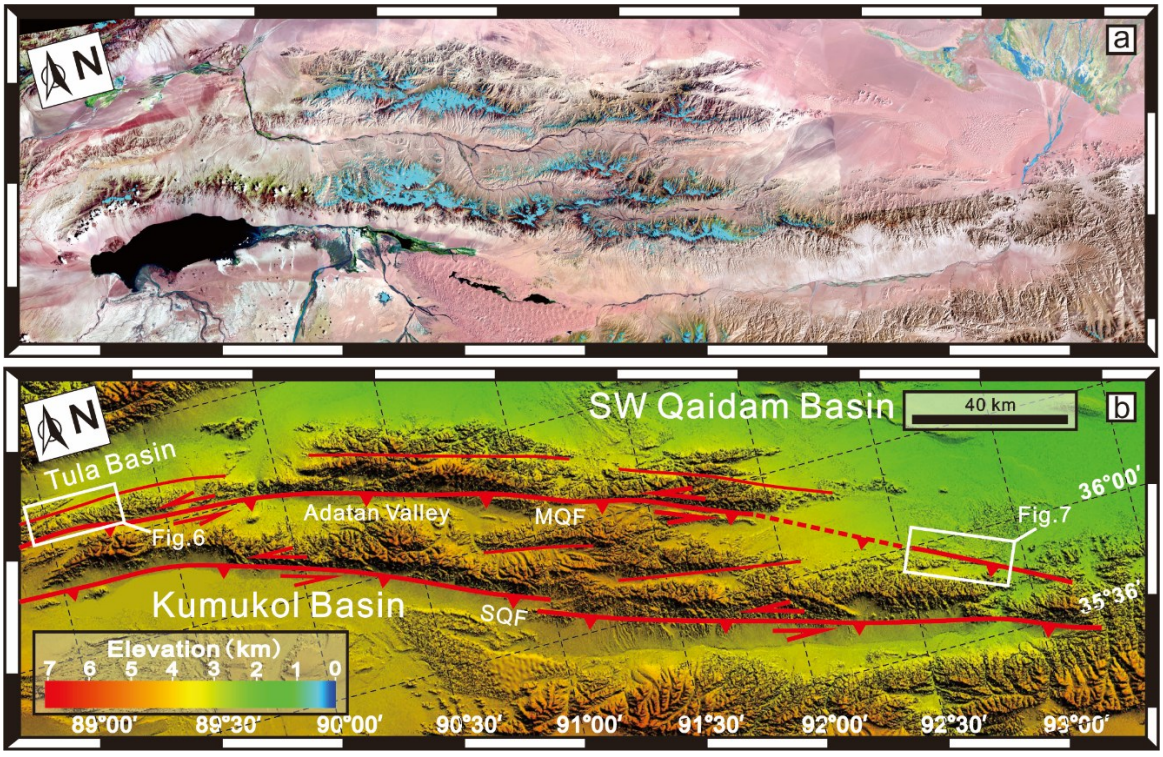

Fig.5. Remote sensing image from Landsat 5 on December 5, 2008 (USGS) (a) and SRTM digital topography map (b) of the Qimen Tagh Range. The red solid lines show the main tectonic structures. See the location in Fig. 1.

2.1.4.1 Strike-slip faulting in the Qimen Tagh Range

The Qimen Tagh Range, located in the western part of the Eastern Kunlun Mountains, is

over ~4500 m high on average and marks the boundary between the Kumukol Basin to the south and the Qaidam Basin to the north (Fig. 1). The range has a general WNW-ESE elongated shape. To the NW, it bends sharply to a southwestward trend sub-parallel to the Altyn Tagh Range that lies directly to the north. To the SE, the Qimen Tagh Range converges with the Eastern Kunlun Mountains (Fig. 1 and 5). It is separated into two parallel NW-SE oriented sub-ranges by the Adatan Valley (Fig. 2).

To the north, the sharp contact between the Qaidam Basin and the Qimen Tagh Range has been interpreted as evidence for active north-directed thrusting (e.g., Meyer et al., 1998; Jolivet et al., 2003), whereas field examination suggests that this is a steeply north-dipping unconformity between bedrock in the south and north-dipping Cenozoic strata in the north (Yin et al., 2007). Detailed analysis of both SRTM digital elevation models (DEM) and Landsat 5 satellite images across the Qimen Tagh Range reveals abundant tectonic lineaments (Fig. 5). The extensive Qimen Tagh fault system consists of two major, sub-parallel tectonic lineaments: the Middle Qimen Tagh Fault (MQF) and the South Qimen Tagh Fault (SQF) (Fig. 5).

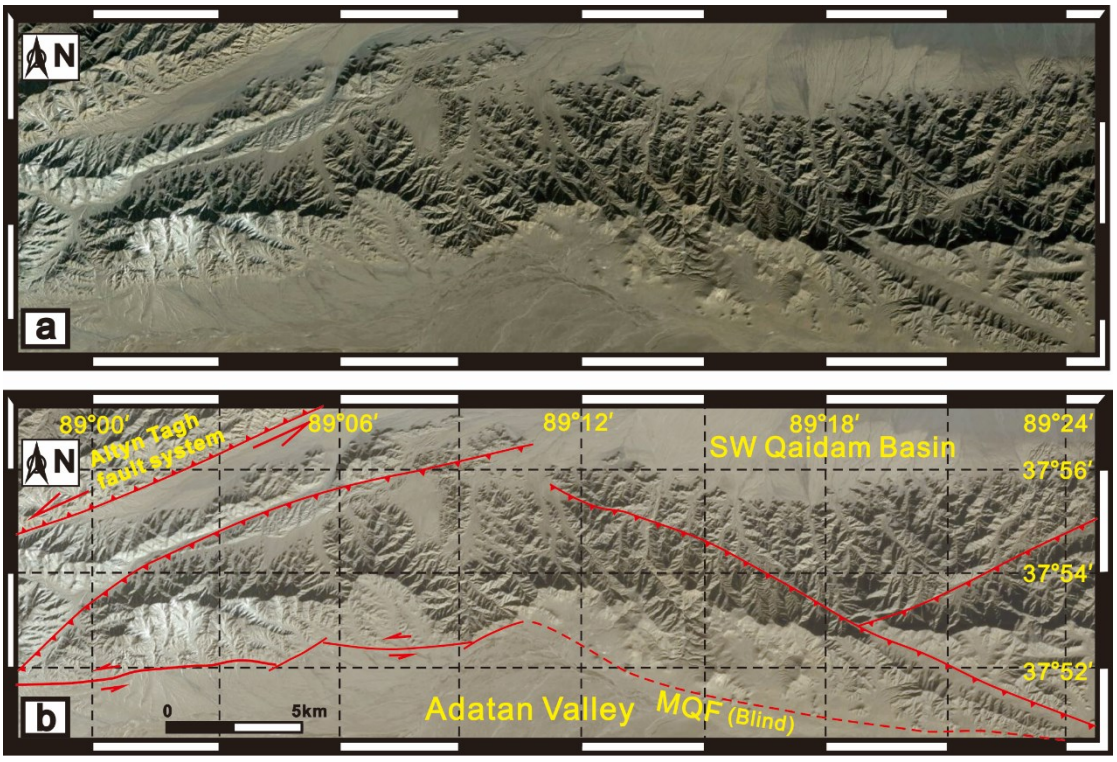

Fig.6. Un-interpreted (a) and interpreted SPOT-5 image (b) (Google Earth) centered on the western part of the Middle Qimen Tagh fault (MQF). See the location in Fig. 5. The red solid lines indicate the fault segments imaged by fault scarps on the surface. The dashed line represents the blind fault covered by the Quaternary sediments. The fault scarps in en-échelon arrangement indicates a left-lateral strike-slip movement on the MQF.

The MQF affects the northern edge of the Adatan Valley. Based on field measurements and on previous studies (Wang et al., 2007), the MQF dips about 55° to the south. The strike of the MQF changes from ENE in the western part of the range to WNW in the eastern part. The western segment shows a reverse motion associated to a slight left-lateral strike-slip component. Some of the scarps and branched faults are arranged in echelons (Fig. 6). In the eastern part of the MQF the main active fault is obliterated by Quaternary deposits. However, some linear structures are visible on the eastern end of the MQF and in the convergence zone with the Kunlun Fault system (Figs. 5 and 7). This however poorly exposed tectonic pattern suggests a very probable connection between the Qimen Tagh Fault system in the west and the Kunlun Fault system in the east.

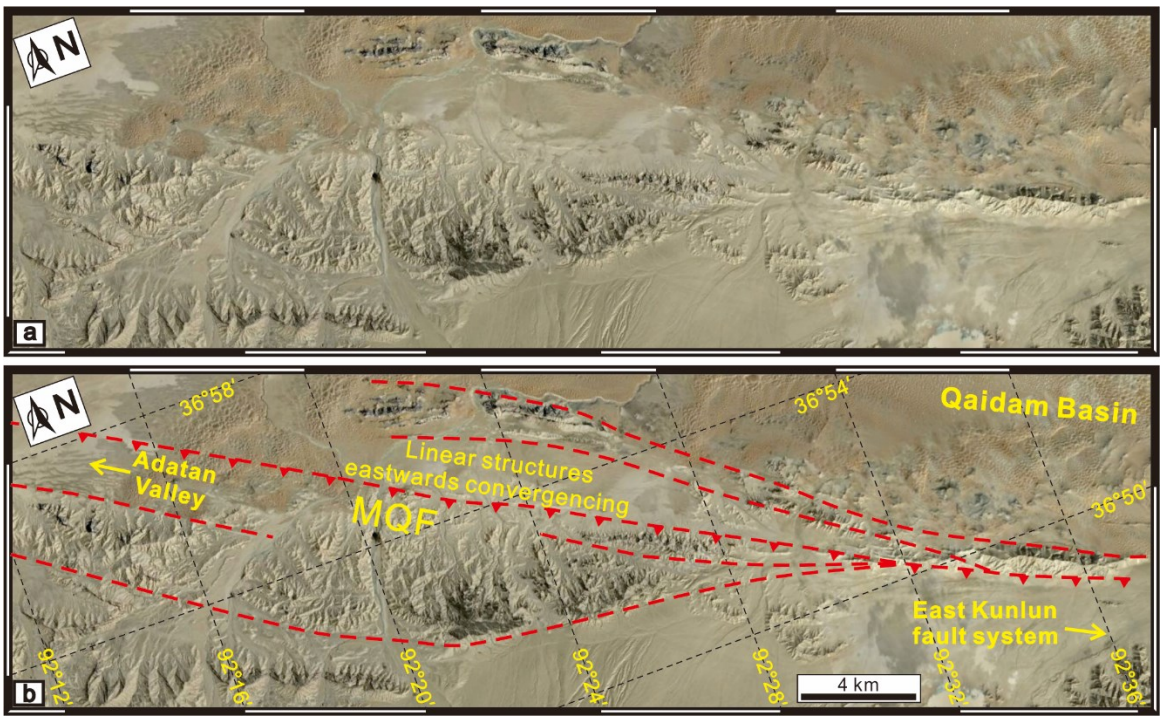

Fig.7. Un-interpreted (a) and interpreted SPOT-5 image (b) (Google Earth) centered on the eastern part of the Middle Qimen Tagh fault. See the location in Fig. 5. The red dashline indicates the linear fault linking the Qimen Tagh fault system in the west with the Eastern Kunlun fault system in the east.

The SQF separates the southern sub-range of the Qimen Tagh Range from the Kumukol Basin to the south (Fig. 5). The fault zone is marked by a series of distinctive fault scarps and structural lineaments which are inferred to be reverse faults striking approximately NE120° (Fig. 5). Furthermore, several evidences of recent activity such as river offsets and alluvial fan displacements indicate a left-lateral reverse movement on the fault.

Although the offset channels and geomorphic surfaces indicate a recent, probably still active general left-lateral shearing within the range, the focal mechanism solution mentioned

above suggest that this recent left-lateral strike-slip faulting is relatively slight compared to the NE-SW compressive component.

2.1.4.2 Pleistocene series within the Adatan valley

Fieldwork in the Adatan Valley was conducted to determine the timing of the strike-slip faulting in the south Qimen Tagh sub-range. Detailed analysis of the Cenozoic syntectonic deposits was conducted to provide a better understanding of the deformation in the Qimen Tagh Range (Fig. 8).

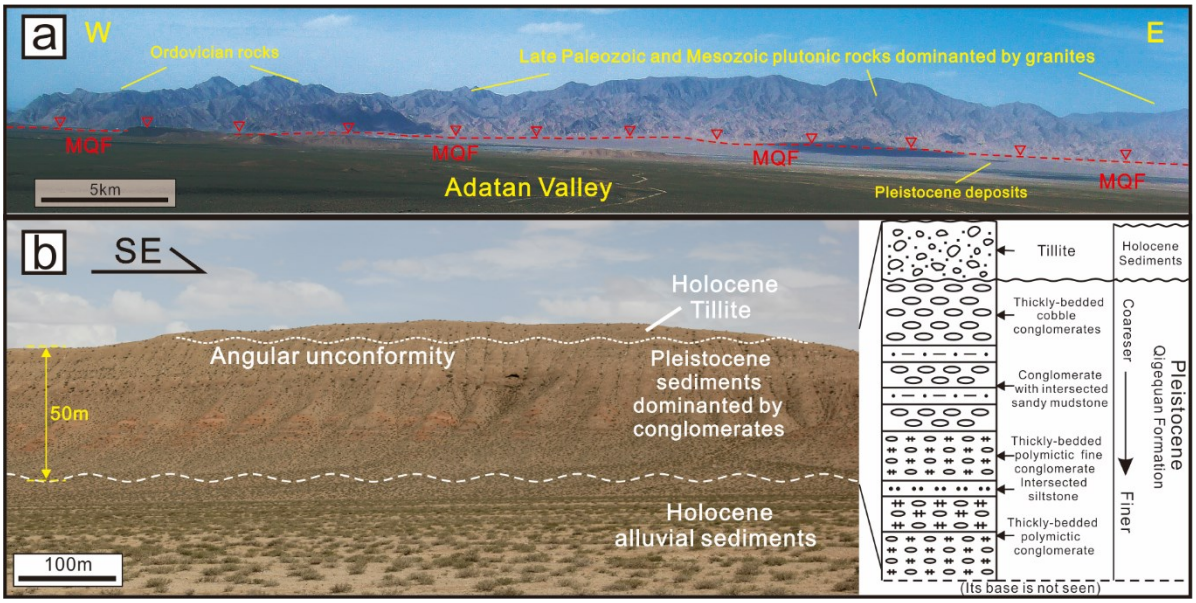

Fig.8. Cenozoic formations within the Adatan Valley. (a) General view of the Qimen Tagh Range. The picture, taken from ~10 km south of the Atantihan River checkpoint, shows the strong relief between the Adatan Valley and the mountains bordered by a series of triangular facets and fault scarps belonging to the MQF. The foothill domain is represented by Cenozoic strata which are deformed and pushed into gentle folds. See the location in Fig. 9. (b) Uplifted Pleistocene series covered by Holocene tillites (left) and general stratigraphic column (right). See the photographs' location in Fig. 9.

The morphology of the Adatan Valley is marked by a strong topographic relief between the valley and the mountains (Fig. 8a). Within the two sub-ranges, the series are mainly composed of Precambrian basement, Paleozoic metasediments and Paleozoic and Mesozoic igneous rocks. The Cenozoic series exposed within the Adatan Valley was assigned a Pleistocene age based on previous geology mapping and regional stratigraphic correlation (IGSSP, 2003; IGSQP, 2004; Wang et al., 2004b; Wang et al., 2007; Fu et al., 2008).

The deposits are deformed into several anticlines cut by modern rivers within the valley (Figs. 8a and 9). Along the northern edge of the valley, the Cenozoic series overlap northward on the Ordovician basement and are dominated by a sequence of conglomerates and sandstones. Along the southern edge of the valley, the Cenozoic series are deformed and

uncomformably covered by Holocene tillites and alluvial sediments. As in the north, these deposits are composed of coarse-grained conglomerates and sandstones in alluvial fans facies. The petrological composition of the conglomerates corresponds to the whole range of basement rocks exposed in the Qimen Tagh Range, including igneous, metamorphic rocks and marine limestones. Poor sphericity and poor sorting of the grains indicate very proximal deposits. The grain size generally increases upward (Fig. 8b). Similarly to the Quaternary sedimentary within the Xidatan Valley further east (Xu et al., 2002) that record the present active feature of the Kunlun Fault, the Pleistocene sequences exposed in the Adatan Valley record the topographic growth of both the north and south Qimen Tagh sub-ranges. They indicate a Pleistocene age for the onset of strike-slip faulting in the Qimen Tagh Range.

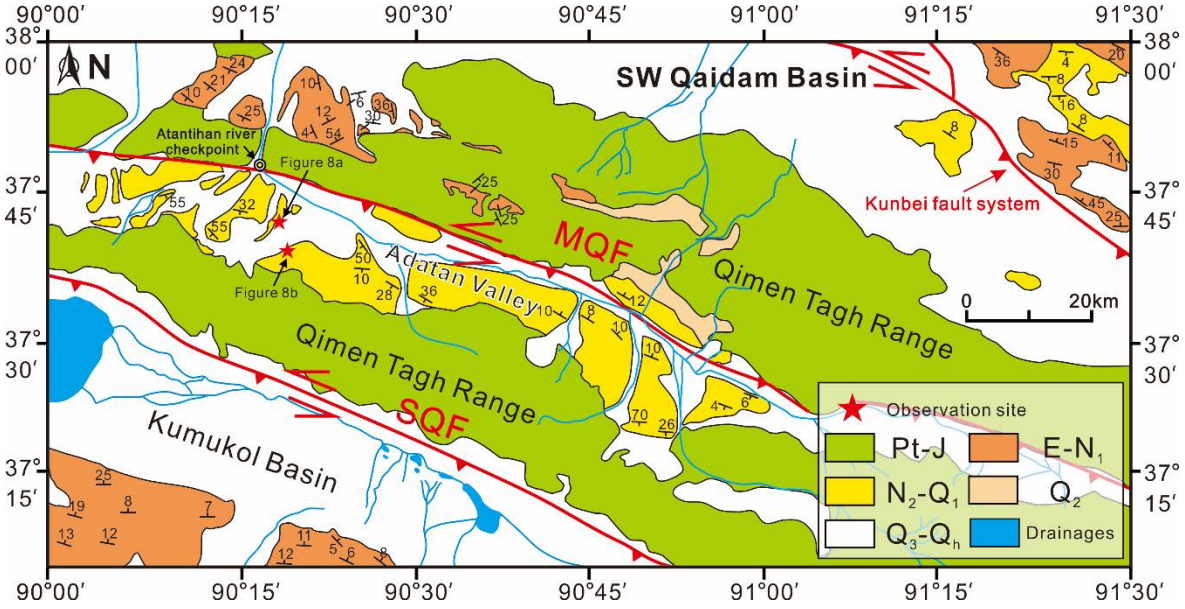

Fig.9. Geological sketch of the Qimen Tagh Range showing the distribution of the Cenozoic series. Modified after the Kulangmiqiti J46C003001 1:250,000 geological map (IGSQP, 2004) and the Ayakekumu J45C003004 1:250,000 geological map (IGSSP, 2003). See the location in Fig. 2.

As a consequence, the linear geomorphic features, occurrence of faults scarps in the Qimen Tagh Range as well as the deformed Pleistocene deposits in the Adatan Valley indicate that the reverse strike-slip deformation in the region has been active since the Pleistocene.

2.1.5 Strike-slip faulting in the SW Qaidam Basin

In order to decipher the Cenozoic strike-slip faulting pattern in the SW Qaidam Basin, we choose the isopach map of the upper Xiaganchaigou Fm. (E_3^2xg) as an example to analyze the impact of fault motion on the sediment distribution within the basin (Fig. 10). Data were obtained from the Qinghai Oilfield Company (China) who recently compiled information from thousands of drill holes and a dense network of seismic profiles.

The Kunbei fault system was composed of three major WNW trending faults, including the Kunbei Fault, the Arlar Fault and the Hongliuquan Fault. As reported on the isopach map based on seismic data, these three faults controls the general tectonic pattern of the SW Qaidam Basin. The Kunbei Fault and Arlar Fault have been previously interpreted as reverse faults active since the Paleogene (Wang et al., 2010). However, the three major faults mentioned above are arranged into a left-lateral right-step en-échelon pattern (Fig. 10), that does not correspond to the usual imbricated pattern of purely compressive thrust systems such as, for example, in the Appalachian thrust belt (Macedo and Marshak, 1999; Thomas, 2001) or in the Zagros fold and thrust belt (McQuarrie, 2004; Sepehr and Cosgrove, 2004). Meanwhile, the isopach lines of the Late Eocene Upper Xiaganchaigou Fm. are obviously offset across the faults reflecting a left-lateral strike-slip movement along these three faults. According to the well-expressed offset of the 400 meters isopach line, the left-lateral displacement of the Honglingquan Fault, the Arlar Fault and the Kunbei Fault increases from a few kilometers to tens of kilometers (Fig. 10). Therefore, the variations in thickness of the Late Eocene series across these three faults, as well as the en-échelon pattern of the faults, clearly demonstrates the occurrence of left-lateral strike-slip faulting in the SW Qaidam Basin after the Late Eocene.

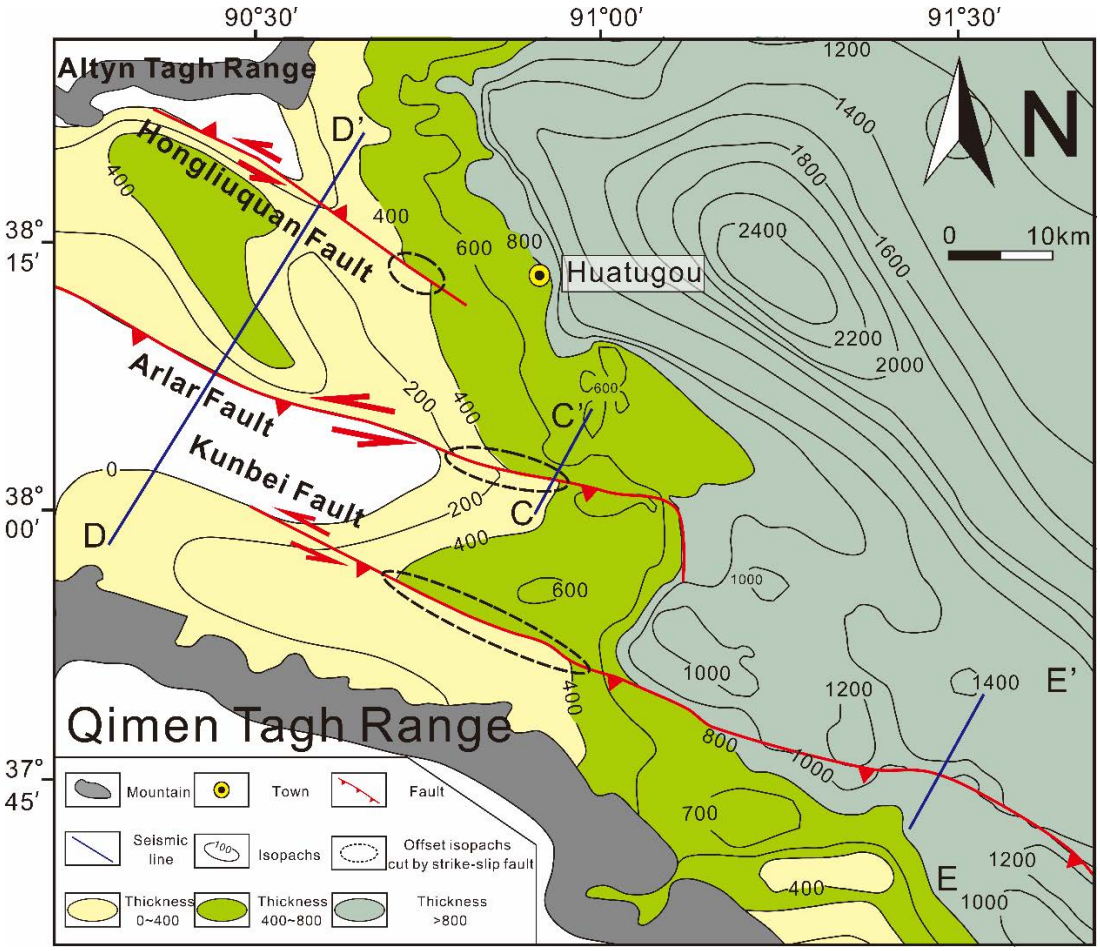

Fig.10. Isopach map of the Upper Xiaganchaigou Formation (E_3^2xg). Three major faults (the Kunbei fault, the Arlar fault and the Hongliuquan fault) are also marked on the isopach mapbased on seismic data. These data were acquired by the Qinghai Oilfield Company (China) who compiled information from thousands of drill holes and a dense network of seismic profiles in recent years. Note the offset of the 400 isopach line controlled by the faults and indicating the left-lateral strike-slip faulting of these faults.

To further explore the tectonic pattern of the SW Qadaim Basin and the timing of faulting, three seismic reflection profiles (C-C', D-D', E-E') recently acquired by the Qinghai Oilfield Company have been selected. These three NE-trending seismic lines extend from the northern front of the Qimen Tagh Range towards the center of the SW Qaidam Basin (See location on Figs. 2 and 10).

2.1.5.1 Seismic Section C-C'

The seismic section C-C' situated in the central part of the SW Qaidam Basin, intersects the Arlar Fault (Fig. 10 and 11). On that section the Arlar Fault is a south dipping high angle fault associated to a few branched faults. The Mesozoic series are not preserved on both sides of the Arlar Fault where only Cenozoic deposits can be identified. Although the strata on each side of the fault consist in the same Cenozoic series, the thickness of each formation is quite different showing obvious stratigraphic throw. This major stratigraphic throw corresponds to the offset

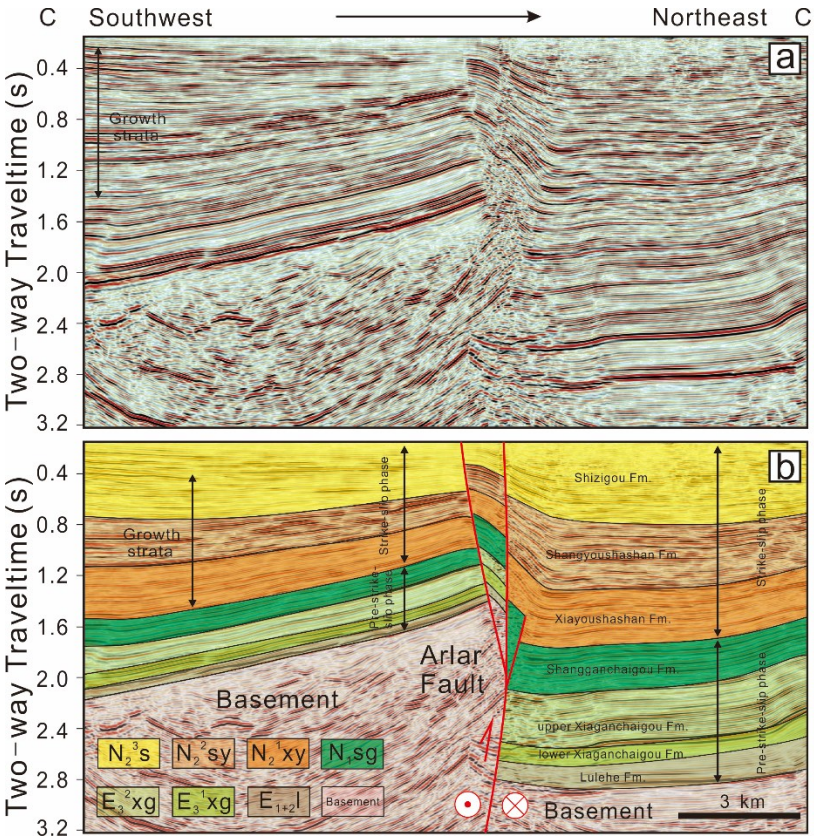

Fig.11. Seismic profile C-C'in the SW Qaidam Basin. See the location in Figs. 2 and 10. Note that the thickness of the Paleocene to Eocene strata shows a sharp difference between both sides of the Arlar fault. The growth strata associated to the positiveflower structure started to develop during the initial deposition of the Early Miocene unit (N_2^1xy), which suggests that the strike-slip movement on the Arlar fault initiated during the deposition of this unit.

observed in the isopach lines of the Late Eocene Upper Xiaganchaigou Fm. on both side of the Arlar Fault (Fig. 10). Combined together, these two sets of data demonstrate a left-lateral reverse motion along the Arlar Fault during the Tertiary.

The thickness of the strata younger than Neogene Xiayoushashan Fm. (N_2^1xy) decreases towards the Arlar Fault and growth strata develop on both sides of the fault. Based on these features, previous studies interpreted the Arlar Fault as a purely reverse fault that accommodated rapid uplift in the Eastern Kunlun Mountains since the Late Oligocene - Early Miocene (Song and Wang, 1993; Yin et al., 2007; Wang et al., 2010). Since it is very difficult to identify strike-slip faults on seismic profiles (Durand-Riard et al., 2012), these studies did not take into consideration the strike-slip component along the major faults within the SW Qaidam Basin. Growth strata are generally used to reveal the initiation time of a reverse fault (e.g. Suppe et al., 1992; Vergés et al., 2002), but strike-slip motion may also induce vertical offset of strata, such as in positive flower structure (e.g. Christophoul et al., 2002). Such motion can also generate growth strata which will then provide an accurate initiation time for the strike-slip faulting (e.g. Hinsch et al., 2005). Consequently, the growth strata associated to the positive flower structure in seismic profile C-C' presented above, as well as the northward thinning of the Early Miocene and younger series in the footwall of the Arlar Fault date the onset time of left-lateral strike-slip faulting along that fault (Fig. 10 and 11).

2.1.5.2 Seismic Section D-D'

The tectonic pattern of section D-D' is characterized by several high angle faults defining a block-like structure (Fig. 12). The major faults are the Arlar Fault and the Hongliuquan Fault. The sediments within the section are Mesozoic to Cenozoic in age. The cover sequence in the hanging wall of the Arlar Fault is composed of Cenozoic sediments whereas the footwall is dominated by Late Mesozoic, Paleogene and Early Neogene deposits. The Mesozoic sediments are relatively thick within the footwall where the Tertiary series are also obviously thicker than that of the hanging wall. The basement and Cenozoic strata on both sides of the Arlar Fault display obvious stratigraphic throw. Further to the north, the Early to Middle Cenozoic and Late Mesozoic strata are cut by the north dipping high angle Hongliuquan Fault. In the hangingwall of the Hongliuquan Fault, the pre-Early Miocene strata were deformed in an anticline later cut and sealed by the Early Miocene sediments clearly indicating Early Miocene motion of this fault. Like in profile C-C', the thickness of the Cenozoic units is constant within each tectonic compartment but varies sharply between two adjacent blocks. Combined with the offset isopach lines of the Late Eocene deposits (Fig. 10), this pattern can

also be explained by lateral movements along the faults during the Tertiary. Again like in seismic profile C-C', the occurrence of growth strata initiating in the Early Miocene series north of the Arlar and Hongliuquan faults implies that left-lateral strike-slip deformation initiated during the Early Miocene in the SW Qaidam Basin.

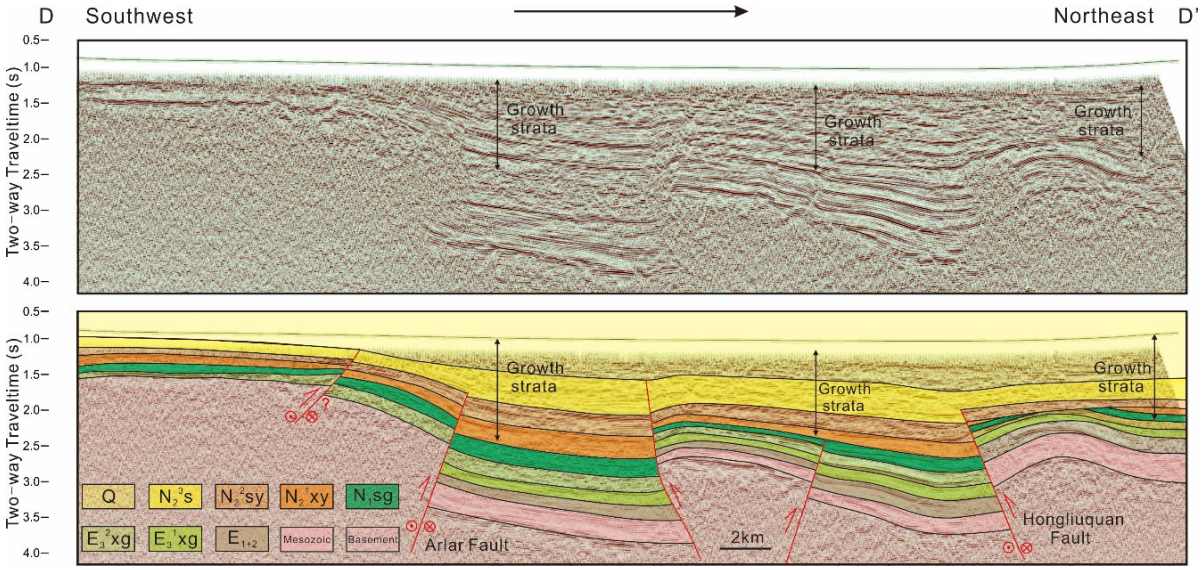

Fig.12. Seismic section D-D'in the SW Qaidam Basin. See Figs. 2 and 10 for location. Note that the strata below the Shangyoushashan Fm. (N_2^1xy) keep a constant thickness in the section, while the strata above it are thinning northward. The thickness of the Paleocene to Eocene strata shows a sharp difference between both sides of the Arlar fault. Meanwhile, Early Miocene growth strata above the Arlar and Hongliuquan faults indicate the onset of left-lateral strike-slip faulting during the Early Miocene.

2.1.5.3 Seismic Section E-E'

Seismic section E-E' is located about 20 km east of seismic section C-C' and again runs from the northern front of the Qimen Tagh Range to the western part of the central Qaidam Basin (Figs. 10 and 13). As in section D-D', the tectonic pattern is characterized by several high angle faults but the cover-sequence only consists in Cenozoic strata. To the south, the activity along the Kunbei Fault is marked in the hanging wall by the erosion of the Late Eocene and younger strata and probably by the non-deposition of some of the upper Tertiary and Quaternary series. This erosion also affects the footwall of the Kunbei Fault, though the Early Tertiary series are better preserved with some Late Eocene sediments still present. Like in section C-C' and D-D', the thickness of the Early Tertiary series vary across the fault showing obvious stratigraphic throw. To the north, the XIII fault dips to the north and cuts the Early to Middle Cenozoic sequence, while the large stratigraphic throw on both sides of the fault decreases from basement to Quaternary series. Like in the previous sections, the thickness of the Paleocene to Eocene strata varies sharply from both sides of the Kunbei and XIII faults,

again attesting of lateral movements on those structures during the Tertiary. Furthermore, the thickness of the strata younger than the Xiayoushashan Fm. (N_2^1xy) within the footwall of the Kunbei and XIII faults decreases towards the faults. Growth strata are again initiating in the footwall of both faults during Early Miocene times dating again the onset of deformation in that region.

From what has been discussed above, we conclude that the tectonic attribute of the Kunbei Fault during the Early Miocene is featured by a left-lateral transpressive system mainly composed of the Kunbei Fault, the Arlar Fault and the Hongliuquan Fault. Among these faults, the Kunbei and Arlar faults are the two major boundary faults separating the Cenozoic series within the SW Qaidam Basin from the Kunlun basement to the south.

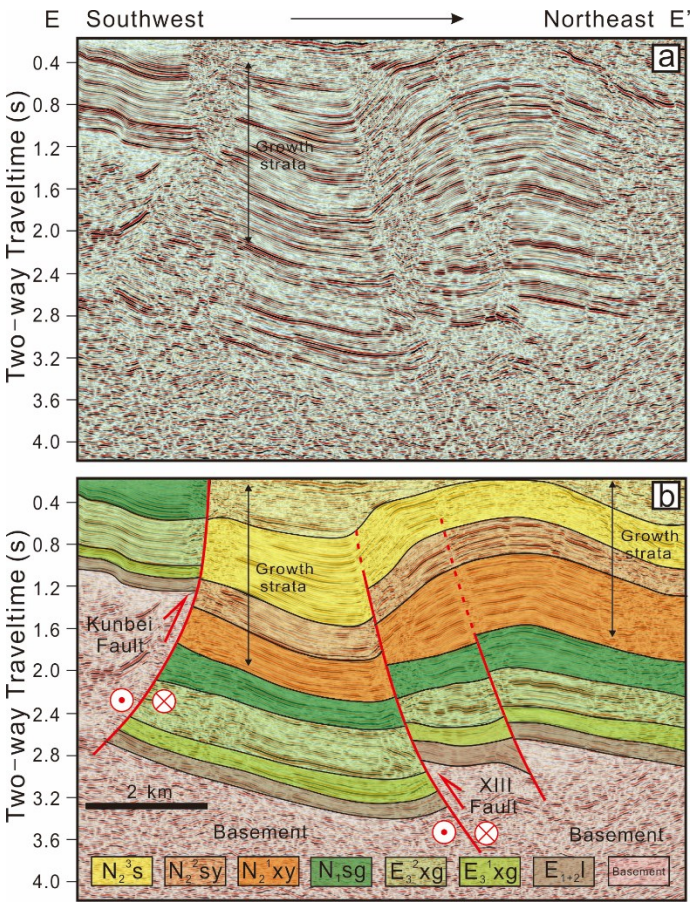

Fig.13. Seismic profile E-E' in the SW Qaidam Basin. See the location in Figs. 2 and 10. Note that the thickness of the Paleocene to Eocene strata shows a sharp difference between both sides of the Kunbei fault. Meanwhile, Early Miocene growth strata again indicate an onset of left-lateral strike-slip faulting during the Early Miocene.

2.1.6 Discussion

2.1.6.1 Available models for the Cenozoic evolution of the SW Qaidam Basin

In the past decades, several models have been proposed to explain the Cenozoic tectonic and sedimentary evolution of the Qaidam Basin. Most of those concentrated on the tectonic pattern displayed in the Qimen Tagh Range and SW Qaidam Basin, and simply defined the tectonic pattern between the Eastern Kunlun Mountains and the Qaidam Basin through a northward thrusting or southward thrusting model.

The northward thrusting model prevailed in the last two decades, explaining the subsidence of the Qaidam Basin as a result of the basinward propagation of successive thrust sheets along the southern edge of the basin. Burchfiel et al. (1989) proposed that the southern

edge of the Qaidam Basin is limited by a south-dipping thrust fault. However, field observation revealed that the contact between the Eastern Kunlun Mountains and the Qaidam Basin is defined by gentle north-dipping Pliocene strata overlapping north-dipping Carboniferous beds (Yin et al., 2007). Based on a synthesis of focal mechanisms and focal-depth distribution combined with geological features, Chen et al. (1999) again speculated the existence of this south-dipping North Kunlun thrust fault along the northern margin of the East Kunlun belt. However, their data projected on the single cross section were collected along the over 1000 km long Eastern Kunlun Mountains and Yin et al. (2007) showed that it was not possible to differentiate between the two possible fault planes solutions (N dipping or S dipping). In addition, many authors indicated that northward basement thrusting across the Eastern Kunlun Mountains was associated to the northward propagation of a crustal-scale accretionary wedge initiating around ca. 30-20 Ma. (Meyer et al., 1998; Mock et al., 1999; Jolivet et al., 2001; Tapponnier et al., 2001; Jolivet et al., 2003; Wang et al., 2006). These ideas suggest that the Eastern Kunlun Mountains consists in a large transpressional system limited to the south by the left-lateral strike-slip Kunlun Fault and to the north by a series of south-verging basement thrusts affecting the southern edge of the Qaidam Basin. Yet, the observed thickness pattern of the Cenozoic strata across the Qaidam Basin (Yin et al., 2008) seems poorly compatible with a major south-dipping range-bounding thrust along the northern margin of the Eastern Kunlun Mountains. All the individual Cenozoic units in the basin consistently thicken from the margins towards the center of the basin (Bally, 1986; Huang et al., 1996; Sobel et al., 2003; Wang et al., 2006; Yin et al., 2007, 2008). This isopach pattern contradicts the classic tectonically subsiding foreland-basin model that requires the maximum sediment thickness to be localized near the bounding thrust system (Jordan, 1981).

The southward thrusting model has drawn much attention in recent years (Yin et al., 2007; Shi et al., 2009; Wang et al., 2011). Yin and Harrison (2000) suggested that two major thrusts, the Qimen Tagh Thrust and the North Kunlun Thrust mark the southern boundary of the Qaidam Basin. Using seismic profiles within the Qaidam Basin and field observations, Yin et al. (2007) then proposed that the low altitude Qaidam Basin has been thrust onto the Eastern Kunlun Mountains along major north dipping Cenozoic thrusts. This model was later expanded by Wang et al., (2011) based on a high-resolution deep seismic reflection profile across this area. This model indicates that the Eastern Kunlun Mountains should not thrust northward onto the Qaidam Basin and that the initiation of compressive deformation along the southern margin of the Qaidam Basin is much younger than along the northern margin of basin. However, this model does not take any strike-slip component in the Qimen Tagh Range and

SW Qaidam Basin into account. In addition, the convex-northward bow-like tectonic structures in the Qimen Tagh Range are not consistent with southward thrusting of the basin onto the range. Such a deformation pattern would rather generate a southward inflexion of the structures.

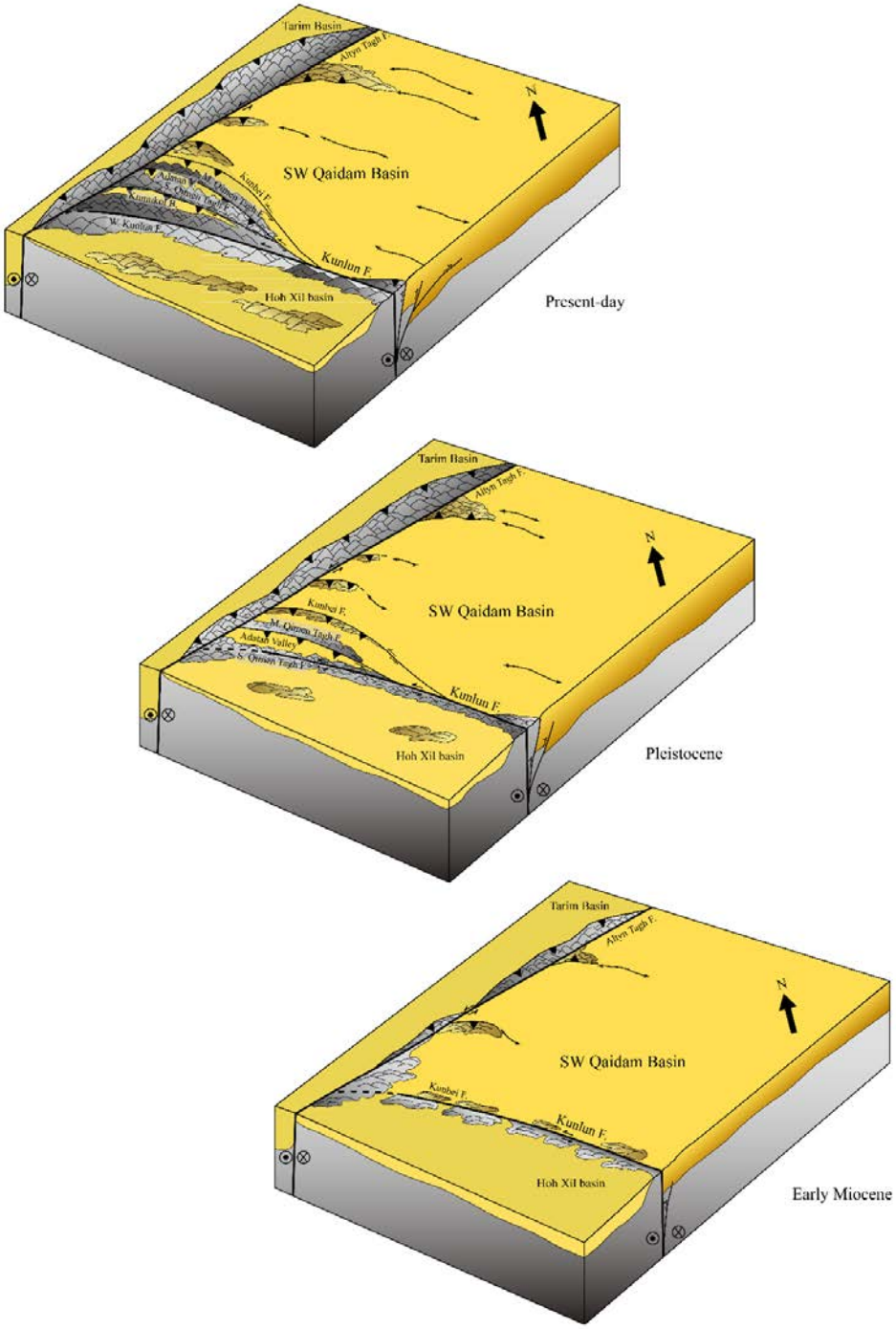

Fig.14. Tectonic evolution of the Qimen Tagh Range and the SW Qaidam Basin since the Early Neogene. See the text for discussion

Other tectonic models have been proposed aside from the two main ones described above. Xia et al. (2001) proposed that the Qaidam Basin experienced a two stages evolution: an initial extension phase during the Early Tertiary was followed by a compressive phase leading to basin inversion. However, few seismic profiles in the western Qaidam Basin have revealed any extensional faults during the Early Tertiary. Meng and Fang (2008) suggested that the Cenozoic tectonic subsidence of the Qaidam Basin resulted from crustal folding or buckling in response to regional horizontal compression. However, the seismic profiles across the whole Qaidam Basin imply that the magnitude of Cenozoic upper crustal shortening decreases eastward across the basin from >48% in the west to <1% in the east (Yin et al., 2008), whereas the present day basin is wider to the west and relatively narrow to the east. This phenomenon is difficult to explain only by crustal folding or buckling.

To summarize, despite the large number of models that have been proposed, few studies took the left-lateral strike-slip factor into account when considering the relationship between the Qaidam Basin and the Eastern Kunlun Mountains.

2.1.6.2 Strike-slip tectonics and northward growth of western segment of Kunlun Fault

The Qaidam Basin is bordered to the northwest by the Altyn Tagh Fault which has been active since the Early or Middle Eocene (Jolivet et al., 1999, 2001; Yin et al., 2002). In addition, despite that Chen et al. (2002) concluded that the Qaidam Basin experienced an over 20° clockwise rotation during the Neogene resulting in differential shortening in the Nan Shan fold and thrust belt (Fig. 1), Dupont-Nivet et al. (2003, 2004) suggested that the Nan Shan fold and thrust belt and the Qaidam Basin did not experience any vertical axis rotation during the Neogene. As the limit between the thick, rigid Tarim block and the more deformable Qaidam Basin, the Altyn Tagh Fault is considered stable in time. Consequently, the deformation in the SW Qaidam Basin and the western segment of the Kunlun Fault should be bordered and limited to the NW by the Altyn Tagh Fault. When considering the geometric relation between the Altyn Tagh Fault and Kunlun Fault, the western Kunlun fault segment has to rotate northward: the left-lateral movement on the Altyn Tagh is progressively driving the connection point between that fault and the Kunlun fault towards the east. For the Kunlun Fault to be able to continuously act as a strike-slip fault, it would jump backwards towards its initial position creating a new strike-slip segment. As mentioned above, the distribution and focal mechanisms of earthquakes indicate that the active tectonic pattern along the Kunlun Fault is characterized by left-lateral strike-slip motion. However, in the SW Qaidam Basin and the Qimen Tagh Range the deformation is accommodated by NW-SE directed thrust faults

associated to a limited left-lateral strike-slip component (Fig. 3). In addition, the geomorphological WNW trending linear structures in the Qimen Tagh Range (Fig. 5) and deformed Pleistocene sequences in the Adatan Valley (Figs. 8 and 9) record the left-lateral strike-slip movements within the Qimen Tagh Range since the Pleistocene. Finally, the overall tectonic and structural architecture within the SW Qaidam Basin is dominated by a series of high angle faults. The sudden variation in sediment thickness marked by the offset of the isopachs on both side of the faults (Fig. 10) associated to the growth strata and the positive flower structures generated by movements on those faults (Figs. 11, 12 and 13), indicate Early Miocene left-lateral strike-slip faulting in SW Qaidam Basin. Synthesizes the above analysis, we thus propose that the Late Neogene northward growth of the convex-northward structures in the Qimen Tagh Range and SW Qaidam Basin (northern margin of the Tibetan Plateau) is driven by progressive northward migration of the left-lateral strike-slip Kunlun Fault (Fig. 14).

Around the Early Miocene, the left-lateral strike-slip faulting in the Kunlun Fault Zone initiated. This motion lead to E-W extension along the northern margin of the Tibetan Plateau and the deeply rooted strike-slip faults were acting as pathways for the shoshonitic magmas (Jolivet et al., 2003), leucogranites and rhyolites (Zhang et al., 2012) to reach the surface. During that period, the parallel Kunbei, Arlar and Hongliuquan faults (designated below as the Kunbei fault system) were forming the western segment of the Kunlun Fault, located in the same position as the present-day Kunlun Fault with a nearly E-W striking trend. The left-lateral movement between the Qiangtang-Bayan Har and Qaidam blocks caused the en-échelon arrangement of the faults and generated the growth strata recording the onset time (Early Miocene) of fault activation. Following this initial phase, the Kunbei fault system, progressively rotated clockwise and migrated northwards, forming the successive high-angle left-lateral compressional faults now observed in the SW Qaidam Basin. In order to maintain the strike-slip motion along the western segment of the Kunlun Fault, a new strike-slip fault system, the Qimen Tagh fault system (including the MQF and SQF) developed during the Pleistocene in place of the older western Kunlun Fault segment that migrated northward. This second phase is recorded by the deformed coarse-grain Pleistocene deposits in the Adatan Valley. This newly formed Qimen Tagh strike-slip fault segment again migrated northwards and progressively rotated clockwise forming the present-day Qimen Tagh prism. Another new strike-slip fault segment developed on the western end of the Kunlun Fault, replacing the previous one. During the process of northward migration of these left-lateral strike-slip faults (the Kunbei Fault, the Arlar Fault, the Hongliuquan Fault, the MQF and the SQF), their motion changed from left-lateral strike-slip to nearly NE-SW compressional motion. The

characteristic northward-convex bow-like shape of the Kubei fault system and of the Qimen Tagh prism is governed by the strike-slip motion along the Altyn Tagh Fault to the northwest. The northward migration of the western segment of the Kunlun Fault explains the lack of Early Miocene sediment records at the present day location of this western segment that would relate to the initiation of the Kunlun Fault.

The model proposed above is an evolution of the previously proposed transpressional model (Meyer et al., 1998; Jolivet et al., 2001; Tapponnier et al., 2001). It identifies the Kunbei fault system and Qimen Tagh fault systems as the western segment of the Kunlun Fault Zone and describes their progressive northward migration since Early Miocene. Their initiation as strike-slip faults explains the present-day steepness of the fault planes.

Based on the analysis of geological features in the Jingyu Basin (North Tibet) and the intrusion of Tertiary to Quaternary shoshonites along the western segment of the Eastern Kunlun Mountains, Meyer et al. (1998) and Jolivet et al. (2003) suggested that the strike-slip Kunlun Fault initated during the Early Neogene. Recently, after detailed geochemistry and geochronology studies on the Miocene leucogranites and rhyolites found in the Hoh Xil Lake area (north of the Kunlun Fault) (Fig. 1), Zhang et al. (2012) suggested that the dehydration melting in this area was probably triggered by localized E - W stretching decompression within the left-lateral strike-slip Kunlun Fault system around 15 Ma. Meanwhile, Duvall et al. (2013) and Yin (2010) also considered that the left-lateral East Kunlun transpressional system initiated around 30 to 20 Ma as a response to the collision between India and Asia. These ages of initial faulting in the Eastern Kunlun Mountains are roughly consistent with our results.

In addition, from the data described above, the boundary between the SW Qaidam Basin and the Eastern Kunlun Mountains is characterized, since the Early Miocene by a series of northward migrating and eastward rotating left-lateral strike-slip faults rather than by a continuous northward thrusting (e.g. Burchfiel et al., 1989; Meyer et al., 1998) or southward thrusting system (e.g. Yin et al., 2007; Wang et al., 2011). Consequently, the SW Qaidam Basin did not suffer a large amount of N-S compression and shortening before the Early Miocene. This observation is compatible with the Paleo-Qaidam model of Yin et al., (2008) which suggests the existence, during the Paleogene, of a large topographic depression encompassing the Hoh Xil Basin to the south and the Qaidam Basin to the north. This wide basin was partitioned by the uplift of the Eastern Kunlun Mountains during Late Oligocene - Early Miocene times.

2.1.7 Conclusions

The Eastern Kunlun Mountains and adjacent Qaidam Basin present one of the largest topographic gradients in the Tibetan Plateau. In that respect, determining the tectonic relations between the Qaidam Basin and the Eastern Kunlun Mountains and deciphering the complex tectonic architecture of the western segment of the Kunlun Fault has major implications in understanding the tectonic, sedimentary and geomorphic Cenozoic history of North Tibet.

The distribution and focal mechanisms of earthquakes presented in this study indicate that the active tectonic pattern in the SW Qaidam Basin and the Qimen Tagh Range is dominated by transpressional structures while that of the Eastern Kunlun Mountains is characterized by left-lateral strike-slip faulting. Geomorphological interpretation of remote sensing images shows that the Qimen Tagh Range is affected by obvious WNW trending linear structures which relate to left-lateral strike-slip motion. The deformed Pleistocene sediments within the Adatan Valley strongly suggest strike-slip faulting along those WNW trending faults during the Pleistocene. To the north, in the SW Qaidam Basin, the offset isopachs of the Late Eocene sediments and the en-échelon arrangement of Kunbei, Arlar and Hongliuquan faults again indicate left-lateral strike-slip faulting. This, associated to growth strata, implies an Early Miocene onset age for the left-lateral strike-slip deformation of the Kunbei fault system in the SW Qaidam Basin. This tectonic pattern and the southwards younging of the left-lateral strike-slip phases lead us to identify the Kunbei Fault system and the Qimen Tagh faults system as former western segments of the Kunlun Fault once located further south in the present-day location of that fault. These faults gradually migrated northward since the Early Miocene while their kinematics changed from left-lateral strike-slip motion to NE-SW compression.

We conclude that the SW Qaidam Basin has been bordered by a series of strike-slip faults to the south since the Early Miocene, rather than by a continuous northward thrusting or southward thrusting system. The SW Qaidam Basin did not suffer major N-S compression and shortening before the Early Miocene.

Acknowlegements

This study was financially supported by grants from the National Science and Technology Major Project (2011E-03). Marc Jolivet was supported by the Darius Program, the French - Chinese Egide Cai Yuanpei Program and the French Centre National de la Recherche Scientifique (CNRS), Institut National des Sciences de l'Univers (INSU) Syster Program. We would like to thank Editor Mian Liu and anonymous reviewers who provided constructive and

thoughtful comments that helped improving the manuscript.

Reference

Bally, A.W., Chou, I.-M., Clayton, R., Eugster, H.P., Kidwell, S., Meckel, L.D., Ryder, R.T., Watts, A.B., and Wilson, A.A., 1986. Notes on Sedimentary Basins in China-Report of the American Sedimentary Basins delegationto the People's Republic of China. U.S. Geological Survey Open-File Report, 108 pp. 86-327.

Burchfiel, B.C., Quidong, D., Molnar, P., Royden, L., Yipeng, W., Peizhen, Z., Weiqi, Z., 1989. Intracrustal detachment within zones of continental deformation. Geology 17, 748-752. doi: 10.1130/0091-7613(1989) 017<0448:IDWZOC>2.3.CO;2.

Chen, W., Chen, C., L Nábelek, J., 1999. Present-day deformation of the Qaidam basin with implications for intra-continental tectonics. Tectonophysics 305, 165-181, doi: 10.1016/S0040-1951(99)00006-2.

Christophoul, F., Baby, P., Dávila, C., 2002. Stratigraphic responses to a major tectonic event in a foreland basin: the Ecuadorian Oriente Basin from Eocene to Oligocene times. Tectonophysics 345, 281-298.

Chu, R., Zhu, L., Helmberger, D.V., 2009. Determination of earthquake focal depths and source time functions in central Asia using teleseismicPwaveforms. Geophysical Research Letters 36, doi: 10.1029/2009GL039494.

Clark, M.K., Farley, K.A., Zheng, D., Wang, Z., Duvall, A.R., 2010. Early Cenozoic faulting of the northern Tibetan Plateau margin from apatite (U–Th)/He ages. Earth and Planetary Science Letters 296, 78-88, doi:10.1016/j.epsl.2010.04.051.

Deng, T., Wang, X. M., 2004a. New material of the Neogene rhinocerotids from the Qaidam Basin in Qinghai, China, Vertebr. PalAsiat 42(3), 216-229.

Deng, T., Wang, X. M., 2004b. Late Miocene Hipparion (Equidae, Mammalia) of eastern Qaidam Basin in Qinghai, China, Vertebr. PalAsiat 42 (4), 316-333.

Dupont-Nivet, G., Butler, R.F., Yin, A., Chen, X., 2003. Paleomagnetism indicates no Neogene vertical axis rotations of the northeastern Tibetan Plateau. J. geophys. Res 108, 2386, doi: 10.1029/2003JB002399.

Dupont-Nivet, G., Robinson, D., Butler, R.F., Yin, A., Melosh, H.J., 2004. Concentration of crustal displacement along a weak Altyn Tagh fault: Evidence from paleomagnetism of the northern Tibetan Plateau. Tectonics 23, TC1020, doi: 10.1029/2002TC001397, 2004.

Durand-Riard, P., Shaw, J.H., Plesch, A., Lufadeju, G., 2013. Enabling 3D geomechanical restoration of strike-and oblique-slip faults using geological constraints, with applications to

the deep-water Niger Delta. Journal of Structural Geology, 48: 33-44, doi: 10.1016/j.jsg.2012.12.009.

Duvall, A.R., Clark, M.K., Kirby, E., Farley, K.A., Craddock, W.H., Li, C., Yuan, D.-Y., 2013. Low-temperature thermochronometry along the Kunlun and Haiyuan Faults, NE Tibetan Plateau: Evidence for kinematic change during late-stage orogenesis. Tectonics 32, 1190-1211, doi:10.1002/tect.20072.

Fang, X., Zhang, W., Meng, Q., Gao, J., Wang, X., King, J., Song, C., Dai, S., Miao, Y., 2007. High-resolution magnetostratigraphy of the Neogene Huaitoutala section in the eastern Qaidam Basin on the NE Tibetan Plateau, Qinghai Province, China and its implication on tectonic uplift of the NE Tibetan Plateau. Earth and Planetary Science Letters 258, 293-306, doi:10.1016/j.epsl.2007.03.042.

Fu, B.H., Awata, Y., Du, J.G., He, W.G., 2005. Late Quaternary systematic stream offsets caused by repeated large seismic events along the Kunlun fault, northern Tibet. Geomorphology 71, 278-292, doi:10.1016/j.geomorph.2005.03.001.

Fu, B. H., Awata, Y., 2007. Displacement and timing of left-lateral faulting in the Kunlun Fault Zone, northern Tibet, inferred from geologic and geomorphic features. Journal of Asian Earth Sciences 29, 253-265, doi:10.1016/j.jseaes.2006.03.004.

Fu J., 2008. Division of Quaternary sedimentary types in Adatan area, Xinjiang. World Nuclear Geoscience 25(2), 94-97(in Chinese with English abstract).

Gao, J., Li, S., Dai, S., Li, A., Peng, Y., 2009. Constraints of tectonic evolution in provenance from detrital zircon fission-track data of Cenozoic strata of Xichagou district in western Qaidam basin: Journal of Lanzhou University (Natural Sciences), 45 (3), 1-7, doi: 0455-2059(2009)03-0001-07 (in Chinese with English abstract).

Guo, J., Lin, A., Sun, G., Zheng, J., 2007. Surface ruptures associated with the 1937 M 7.5 Tuosuo Lake and the 1963 M 7.0 Alake Lake earthquakes and the paleoseismicity along the Tuosuo Lake Segment of the Kunlun Fault, Northern Tibet. Bulletin of the Seismological Society of America 97, 474-496, doi: 10.1785/0120050103.

Harkins, N., Kirby, E., 2008. Fluvial terrace riser degradation and determination of slip rates on strike-slip faults: An example from the Kunlun fault, China. Geophysical Research Letters 35, doi: 10.1029/2007GL033073.

Hinsch, R., Decker, K., Peresson, H., 2005. 3-D seismic interpretation and structural modeling in the Vienna Basin: implications for Miocene to recent kinematics. Austrian J. Earth Sci 97, 38-50.

Huang, H., Huang, Q., Ma, Y., 1996. Geology of Qaidam Basin and its petroleum prediction.

Geological Publishing House, Beijing pp. 1-257 (in Chinese with English abstract).
Huo, G.M., 1990. Petroleum geology of China: Oil fields in Qianghai and Xizang. Chinese Petroleum Industry Press, Beijing 14, pp. 1-483 (in Chinese with English abstract).
IGSSP (Insititute of Geological Survey of Shanxi Province), 2003. The Report of Regional Geological Survey at Scale 1:250000. P.R.C. China Industry Press, pp. 1-274 (in Chinese).
IGSQP (Insititute of Geological Survey of Qinhai Province), 2004. The Report of Regional Geological Survey at Scale 1:250000. P.R.C. China Industry Press, pp. 1-386 (in Chinese).
Jolivet, M., Roger, F., Arnaud, N., Brunel, M., Tapponnier, P., Seward, D., 1999. Histoire de l'exhumation de l'Altun Shan: indications sur l'âge de la subduction du bloc du Tarim sous le système de l'Altyn Tagh (Nord Tibet). C.R. Acad. Sci. Paris 329, 749-755, doi: 10.1016/S1251-8050(00)88495-5
Jolivet, M., Brunel, M., Seward, D., Xu, Z., Yang, J., Roger, F., Tapponnier, P., Malavieille, J., Arnaud, N., Wu, C., 2001. Mesozoic and Cenozoic tectonics of the northern edge of the Tibetan plateau: fission-track constraints. Tectonophysics 343, 111-134, doi: 10.1016/S0040-1951(01)00196-2.
Jolivet, M., Brunel, M., Seward, D., Xu, Z., Yang, J., Malavieille, J., Roger, F., Leyreloup, A., Arnaud, N., Wu, C., 2003. Neogene extension and volcanism in the Kunlun Fault Zone, northern Tibet: New constraints on the age of the Kunlun Fault. Tectonics 22, 1052, doi: 10.1029/2002TC001428.
Jolivet, M., Arzhannikov, S., Chauvet, A., Arzhannikova, A., Vassallo, R., Kulagina, N., Akulova, V., 2013. Accomodating large-scale intracontinental extension and compression in a single stress-field: A key example from the Baikal Rift System. Gondwana Research, 24(3), 918-935, doi:10.1016/j.gr.2012.07.017.
Jordan, T.E., 1981. Thrust loads and foreland basin evolution, Cretaceous, western United States. AAPG bulletin 65, 2506-2520.
Ke, X., Ji, J., Zhang, K., Kou, X., Song, B., Wang, C., 2013. Magnetostratigraphy and Anisotropy of Magnetic Susceptibility of the Lulehe Formation in the Northeastern Qaidam Basin. Acta Geologica Sinica-English Edition 87, 576-587, doi: 10.1111/1755-6724.12069.
Kidd, W.S.F., Molnar, P., 1988. Quaternary and active faulting observed on the 1985 Academia Sinica--Royal society geotraverse of Tibet. Philosophical Transactions of the Royal Society of London. Series A, Mathematical and Physical Sciences 327(1594), 337-363, doi: 10.1098/rsta.1988.0133.
Kirby, E., Harkins, N., Wang, E., Shi, X., Fan, C., Burbank, D., 2007. Slip rate gradients along the eastern Kunlun fault. Tectonics 26, doi: 10.1029/2006TC002033.

Lin, A., Fu, B., Guo, J., Zeng, Q., Dang, G., He, W., Zhao, Y., 2002. Co-seismic strike-slip and rupture length produced by the 2001 Ms 8.1 Central Kunlun earthquake. Science 296, 2015-2017, doi: 10.1126/science.107087.

Lin, A., Guo, J., 2008. Nonuniform Slip Rate and Millennial Recurrence Interval of Large Earthquakes along the Eastern Segment of the Kunlun Fault, Northern Tibet. Bulletin of the Seismological Society of America 98, 2866-2878, doi: 10.1785/0120070193.

Liu, Y.J., Genser, J., Neubauer, F., Jin, W., Ge, X.H., Handler, R., Takasu, A., 2005. $^{40}Ar/^{39}Ar$ mineral ages from basement rocks in the Eastern Kunlun Mountains, NW China, and their tectonic implications. Tectonophysics 398, 199-224, doi: 10.1016/j.tecto.2005.02.007.

Lu, H., Xiong, S., 2009. Magnetostratigraphy of the Dahonggou section, northern Qaidam Basin and its bearing on Cenozoic tectonic evolution of the Qilian Shan and Altyn Tagh Fault. Earth and Planetary Science Letters 288, 539-550, doi:10.1016/j.epsl.2009.10.016.

Macedo, J., Marshak, S., 1999. Controls on the geometry of fold-thrust belt salients. Geological Society of America Bulletin 111, 1808-1822, doi: 10.1130/0016-7606(1999)111<1808:COTGOF>2.3.CO;2.

McQuarrie, N., 2004. Crustal scale geometry of the Zagros fold–thrust belt, Iran. Journal of Structural Geology 26, 519-535, doi:10.1016/j.jsg.2003.08.009.

Meng, Q.R., Fang, X., 2008. Cenozoic tectonic development of the Qaidam Basin in the northeastern Tibetan Plateau. Geological Society of America Special Papers 444, 1-24, doi: 10.1130/2008.2444(01).

Meyer, B., Tapponnier, P., Bourjot, L., Metivier, F., Gaudemer, Y., Peltzer, G., Shunmin, G., Zhitai, C., 1998. Crustal thickening in Gansu-Qinghai, lithospheric mantle subduction, and oblique, strike‐slip controlled growth of the Tibet plateau. Geophysical Journal International 135, 1-47, doi: 10.1046/j.1365-246X.1998.00567.x.

Mock, C., Arnaud, N.O., Cantagrel, J.M., 1999. An early unroofing in northeastern Tibet? Constraints from $^{40}Ar/^{39}Ar$ thermochronology on granitoids from the Eastern Kunlun Mountains (Qianghai, NW China). Earth and Planetary Science Letters 171, 107-122, doi: 10.1016/S0012-821X(99)00133-8.

Pei, J., Sun, Z., Wang, X., Zhao, Y., Ge, X., Guo, X., Li, H., Si, J., 2009. Evidence for Tibetan plateau uplift in Qaidam Basin before Eocene-Oligocene boundary and its climatic implications. Journal of Earth Science 20, 430-437, doi: 10.1007/s12583-009-0035-y.

Peltzer, G., Crampé, F., King, G., 1999. Evidence of nonlinear elasticity of the crust from the Mw7. 6 Manyi (Tibet) earthquake. Science 286, 272-276, doi:10.1126/science.286.5438.272.

QBGMR (Qinhai Bureau of Geology Mineral Resources), 1991. Regional Geology of Qinghai

Province. Geological Publishing House, Beijing, pp. 1-662 (in Chinese).

Qiu, N., 2002. Tectono-thermal evolution of the Qaidam Basin, China: evidence from Ro and apatite fission track data. Petroleum Geoscience 8, 279-285, doi: 10.1144/petgeo.8.3.279.

Sepehr, M., Cosgrove, J., 2004. Structural framework of the Zagros fold–thrust belt, Iran. Marine and Petroleum Geology 21, 829-843, doi:10.1016/j.marpetgeo.2003.07.006.

Sobel, E.R., Hilley, G.E., Strecker, M.R., 2003. Formation of internally drained contractional basins by aridity-limited bedrock incision. J. Geophys. Res 108, 25, doi: 10.1029/2002JB001883.

Song, T., Wang, X., 1993. Structural styles and stratigraphic patterns of syndepositional faults in a contractional setting: Examples from Quaidam basin, northwestern China. AAPG bulletin 77, 102-117.

Song, C. H. 2006. Tectonic uplift and Cenozoic sedimentary evolution in the northern margin of the Tibetan Plateau. [Dissertation]. Lanzhou University, Lanzhou. 85-123 (in Chinese with English abstract).

Sun, Z.M., Yang, Z.Y., Pei, J.L., Ge, X.H., Wang, X.S., Yang, T.S., Li, W.M., Yuan, S.H., 2005. Magnetostratigraphy of Paleogene sediments from northern Qaidam Basin, China: implications for tectonic uplift and block rotation in northern Tibetan plateau. Earth and Planetary Science Letters 237, 635-646, doi: 10.1016/j.epsl.2005.07.007.

Sun, Z. C., Jing M. C., Sun, N. D., Lu Y.L., Cao, L., 2007. Discussion on boundary between the upper and lower members of Xiaganchaigou Formation of Paleogene in Well Kun-2, Qaidam Basin. Journal of Palaeogeography, 9(6), 611-618 (in Chinese with English abstract).

Suppe, J., Chou, G.T., Hook, S.C., 1992. Rates of folding and faulting determined from growth strata, Thrust tectonics. Springer, pp. 105-121.

Tapponnier, P., Zhiqin, X., Roger, F., Meyer, B., Arnaud, N., Wittlinger, G., Jingsui, Y., 2001. Oblique stepwise rise and growth of the Tibet Plateau. Science 294, 1671-1677, doi: 10.1126/science.105978.

Taylor, M., Yin, A., 2009. Active structures of the Himalayan-Tibetan orogen and their relationships to earthquake distribution, contemporary strain field, and Cenozoic volcanism. Geosphere 5, 199-214, doi: 10.1130/GES00217.1.

Van Der Woerd, J., Ryerson, F.J., Tapponnier, P., Gaudemer, Y., Finkel, R., Mériaux, A.S., Caffee, M., Guoguang, Z., Qunlu, H., 1998. Holocene left-slip rate determined by cosmogenic surface dating on the Xidatan segment of the Kunlun fault (Qinghai, China). Geology 26, 695-698, doi: 10.1130/GES00217.1.

Velasco, A.A., Ammon, C.J., Beck, S.L., 2000. Broadband source modeling of the November

8, 1997, Tibet (Mw=7.5) earthquake and its tectonic implications. Journal of Geophysical Research: Solid Earth (1978–2012) 105 (B12), 28065-28080, doi: 10.1029/2000JB900282.

Vergés, J., Marzo, M., Muñoz, J., 2002. Growth strata in foreland settings. Sedimentary Geology 146, 1-9, doi: 10.1016/S0037-0738(01)00162-2.

Wang, Q., Zhang, P.Z., Freymueller, J.T., Bilham, R., Larson, K.M., Lai, X., You, X., Niu, Z., Wu, J., Li, Y., 2001. Present-day crustal deformation in China constrained by global positioning system measurements. Science 294, 574-577, doi: 10.1126/science.1063647.

Wang, F., L., C. H., Li, Q., Yeh, M. W., Wan, J., Zheng, D., Wang, E., 2004a. Onset timing of significant unroofing around Qaidam basin, northern Tibet, China: constraints from $^{40}Ar/^{39}Ar$ and FT thermochronology on granitoids. Journal of Asian Earth Sciences 24, 59-69, doi: 10.1016/j.jseaes.2003.07.004.

Wang, S. J., Bai, Y. S., Hao, P., Chang, G. H., Bao, G. P., 2004b. Discovery of fresh water Gastropoda fossils in Ancient Neoteric period and its geological significance in Adatan basin. Northwestern Geology 37(3), 21-23 (in Chinese with English abstract).

Wang, E., Xu, F.Y., Zhou, J.X., Wan, J., Burchfiel, B.C., 2006. Eastward migration of the Qaidam basin and its implications for Cenozoic evolution of the Altyn Tagh fault and associated river systems. Geological Society of America Bulletin 118, 349-365, doi: 10.1130/B25778.1.

Wang, S. J., Bai, Y. S., Xu, Y. F., Zhang, K. C., Chang, G. H., 2007. Tectonic Evolution of the Adatan Basin in Late Paleogene. Northwestern Geology 40(4), 53-57 (in Chinese with English abstract).

Wang, Y.D., Nie, J.S., Zhang, T., Sun, G.Q., Yang, X., Liu, Y.H., Liu, X.W., 2010. Cenozoic tectonic evolution in the western Qaidam Basin inferred from subsurface data. Geosciences Journal 14, 335-344, doi: 10.1007/s12303-010-0033-1.

Wang, C.S., Gao, R., Yin, A., Wang, H., Zhang, Y.X., Guo, T.L., Li, Q.S., Li, Y.L., 2011. A mid-crustal strain-transfer model for continental deformation: A new perspective from high-resolution deep seismic-reflection profiling across NE Tibet. Earth and Planetary Science Letters 306, 279-288, doi: 10.1016/j.epsl.2011.04.010.

Xia, W.C., Zhang, N., Yuan, X.P., Fan, L.S., Zhang, B.S., 2001. Cenozoic Qaidam basin, China: A stronger tectonic inversed, extensional rifted basin. AAPG bulletin 85, 715-736.

Xu, X.W., Chen, W.B., Ma, W.T., Yu, G.H., Chen, G.H., 2002. Surface rupture of the Kunlunshan earthquake (Ms 8.1), northern Tibetan plateau, China. Seismological Research Letters 73, 884-892.

Yang, F., Ma, Z.Q., Xu, T.C., Ye, S.J., 1992. A Tertiary paleomagnetic stratigraphic profile in

Qaidam basin. Acta Petrolei Sinica 13(2), 97-101(in Chinese with English abstract).

Ye, D., 1997. Tertiary in Petroliferous Regions of China. Petroleum Inductry Press, Beijing, pp. 1-374 (in Chinese with English abstract).

Yin, A., Harrison, T.M., 2000. Geologic evolution of the Himalayan-Tibetan orogen. Annual Review of Earth and Planetary Sciences 28, 211-280, doi: 10.1146/annurev.earth.28.1.211.

Yin, A., Rumelhart, P.E., Cowgill, E., Butler, R., Harrison, T.M., Ingersoll, R.V., Cooper, K., Zhang, Q., and Wang, X. F., 2002. Tectonic history of the Altyn Tagh fault system in northern Tibet inferred from Cenozoic sedimentation. Geological Society of America Bulletin 114, 1257-1295, doi: 10.1130/0016-7606(2002)114<1257: THOTAT>2.0.CO;2.

Yin, A., Dang, Y.Q., Zhang, M., McRivette, M.W., Burgess, W.P., Chen, X.H., 2007. Cenozoic tectonic evolution of Qaidam basin and its surrounding regions (part 2): Wedge tectonics in southern Qaidam basin and the Eastern Kunlun Mountains. Geological Society of America Special Papers 433, 369-390, doi: 10.1130/2007.2433(18).

Yin, A., Dang, Y.Q., Zhang, M., Chen, X.H., McRivette, M.W., 2008. Cenozoic tectonic evolution of the Qaidam basin and its surrounding regions (Part 3): Structural geology, sedimentation, and regional tectonic reconstruction. Geological Society of America Bulletin 120, 847-876, doi: 10.1130/B26232.1.

Yin, A., 2010. Cenozoic tectonic evolution of Asia: A preliminary synthesis. Tectonophysics 488, 293-325, doi:10.1016/j.tecto.2009.06.002.

Yuan, W.M., Dong, J.Q., Wang, S.C., Carter, A., 2006. Apatite fission track evidence for Neogene uplift in the eastern Kunlun Mountains, northern Qinghai–Tibet Plateau, China. Journal of Asian Earth Sciences 27, 847-856, doi: 10.1016/j.jseaes.2005.09.002.

Zhang, Y.X., Che, Z.C., Liu, L., Luo, J.L., 1996. Tertiary in the Kumkol Basin, Xinjiang. Regional Geology of China 4, 311-316 (in Chinese with English abstract).

Zhang, P.Z., Shen, Z., Wang, M., Gan, W., Bürgmann, R., Molnar, P., Wang, Q., Niu, Z., Sun, J., Wu, J., 2004. Continuous deformation of the Tibetan Plateau from global positioning system data. Geology 32, 809-812, doi: 10.1130/G20554.1.

Zhang, W., 2006. The high precise Cenozoic magnetostratigraphy of the Qaidam Basin and uplift of the Northern Tibetan plateau. [Doctoral dissertation]. Lanzhou University, Lanzhou. 95-105 (in Chinese with English abstract).

Zhang, Z., Klemperer, S., Bai, Z., Chen, Y., Teng, J., 2011. Crustal structure of the Paleozoic Kunlun orogeny from an active-source seismic profile between Moba and Guide in East Tibet, China. Gondwana Research 19, 994-1007, doi: 10.1016/j.gr.2010.09.008.

Zhang, L.Y., Ding, L., Yang, D., Xu, Q., Cai, F.L., Liu, D.L., 2012. Origin of middle Miocene

leucogranites and rhyolites on the Tibetan Plateau: Constraints on the timing of crustal thickening and uplift of its northern boundary. Chinese Science Bulletin 57, 511-524, doi: 10.1007/s11434-011-4813-4.

Zhao, J., Mooney, W.D., Zhang, X., Li, Z., Jin, Z., Okaya, N., 2006. Crustal structure across the Altyn Tagh Range at the northern margin of the Tibetan plateau and tectonic implications. Earth and Planetary Science Letters 241, 804-814, doi:10.1016/j.epsl.2005.11.003.

2.2 Cenozoic source to sink relation between the Qaidam basin and the Eastern Kunlun Mountains

Paper published in Geological Society of America Bulletin, 2016, vol. 128, pp. 258-283

Source to sink relation between the Eastern Kunlun Range and the Qaidam Basin, northern Tibetan Plateau, during the Cenozoic

Feng Cheng [1, 2], Suotang Fu [3], Marc Jolivet [2], Changhao Zhang [3], Zhaojie Guo [1, *]

[1] Key Laboratory of Orogenic Belts and Crustal Evolution, Ministry of Education, School of Earth and Space Sciences, Peking University, Beijing, 100871, China

[2] Laboratoire Géosciences Rennes, CNRS-UMR6118, Université Rennes 1 - Observatoire des Sciences de l'Univers, Rennes, 35042, France

[3] Qinghai Oilfield Company, PetroChina, Dunhuang, Gansu, 736202, China

[*] Corresponding author. Tel.: + 86-10-62753545; fax: + 86-10-62758610. E-mail address: zjguo@pku.edu.cn

Note: The online version of this contribution can be found as: ***Cheng, F., Fu, S., Jolivet, M., Zhang, C., Guo, Z., 2016. Source to sink relation between the Eastern Kunlun Range and the Qaidam Basin, northern Tibetan Plateau, during the Cenozoic. Geological Society of America Bulletin 128, 258-283, doi: 10.1130/B31260.1.***

Abstract

Understanding the source to sink relationship through time between the Eastern Kunlun Range, one of the major mountain belts in the northern Tibetan Plateau, and the actively deforming Qaidam Basin to the north has important implications for unravelling the growth history of the Tibetan plateau. In this study, U-Pb dating (LA-ICP-MS) of detrital zircons from

22 sandstone samples (Paleocene to Holocene) collected from 4 sections within the southwestern Qaidam basin is combined with provenance analysis and new seismic profile interpretation to investigate the mountain building of the Eastern Kunlun Range and its effects on the development of the Qaidam basin. The U-Pb age distributions of detrital grains from Paleocene strata are characterised by a major component of Paleozoic to late Proterozoic ages. Furthermore, carbonate debris containing foraminifera have been recognized in the Paleocene conglomerate sequences. We thus suggest that the Eastern Kunlun Range was already exhumed prior to the Paleocene. The southward onlaps of Paleocene to Oligocene strata observed on seismic profiles and the appearance of a Mesozoic component in the detrital zircon age spectra of Eocene to Oligocene strata indicate that the Qaidam basin was widening southward during that early Cenozoic period. Well-developed post-Oligocene growth strata and the increasing proportion of Mesozoic and Paleozoic U-Pb ages in detrital zircon grains from late Neogene strata demonstrate that the relief of the Eastern Kunlun and Altyn Tagh ranges had increased, leading to isolation and narrowing of the Qaidam basin from Miocene to the present. The inferred pulsed deformation in the Eastern Kunlun Range highlights the complex growth history of the Tibetan plateau.

Keywords: Cenozoic, North Tibet, Qaidam basin, Eastern Kunlun Range, Detrital U-Pb zircon geochronology, Source to sink

2.2.1 Introduction

The Tibetan plateau is the widest area of elevated topography on Earth (Fig. 1). Many approaches have been used to decipher the tectonic and topographic history of that region. These include thermochronology (e.g. Jolivet et al., 1999, 2001, 2003; Kapp et al., 2005), paleobotany (e.g. Spicer et al., 2003), paleomagnetism (e.g. Dupont-Nivet et al., 2010), paleoaltimetry (e.g. Graham et al., 2005; Rowley et al., 2006; Kent-Corson et al., 2009; Rieser et al., 2009; Quade et al., 2011; Hough et al., 2011) coupled with stratigraphic and tectonic analyses (e.g. Yin et al., 2008a, 2008b; C.Wang et al., 2008a, 2014; C.S.Wang et al., 2011). However, the initial topography of the area now represented by the Tibetan plateau, as well as the early stages of development of the present day topography remain poorly constrained and highly debated. Two competing models suggest that either the Tibetan lithosphere thickened as a thin viscous layer, with buoyancy driven uplift of the plateau (e.g. England and Houseman, 1989) or that the plateau grew stepwise by successive addition of large crustal thrust-wedges (e.g. Tapponnier et al., 2001). This last model is partly supported, for example, by the progressive decrease of initial deformation age from the center of the plateau towards its edges

(e.g. Métivier et al., 1998; Wang et al., 2008a, 2014). However, it has been recently suggested that an already elevated proto-plateau (similar to the present-dayAndean margin) surrounded by low-level basins already existed prior to the India – Asia collision (e.g. Kapp et al., 2003; Ding et al., 2013, Xu et al., 2013; Ding et al., 2014). In addition, the recent suggestion that the northern Tibetan plateau began to undergo horizontal shortening in the early Eocene, shortly after the India – Asia collision, also challenges the northward progressive plateau growth hypothesis (Yin et al., 2008b; Duvall et al., 2011; Zhuang et al., 2011; F. Cheng et al., 2015a).

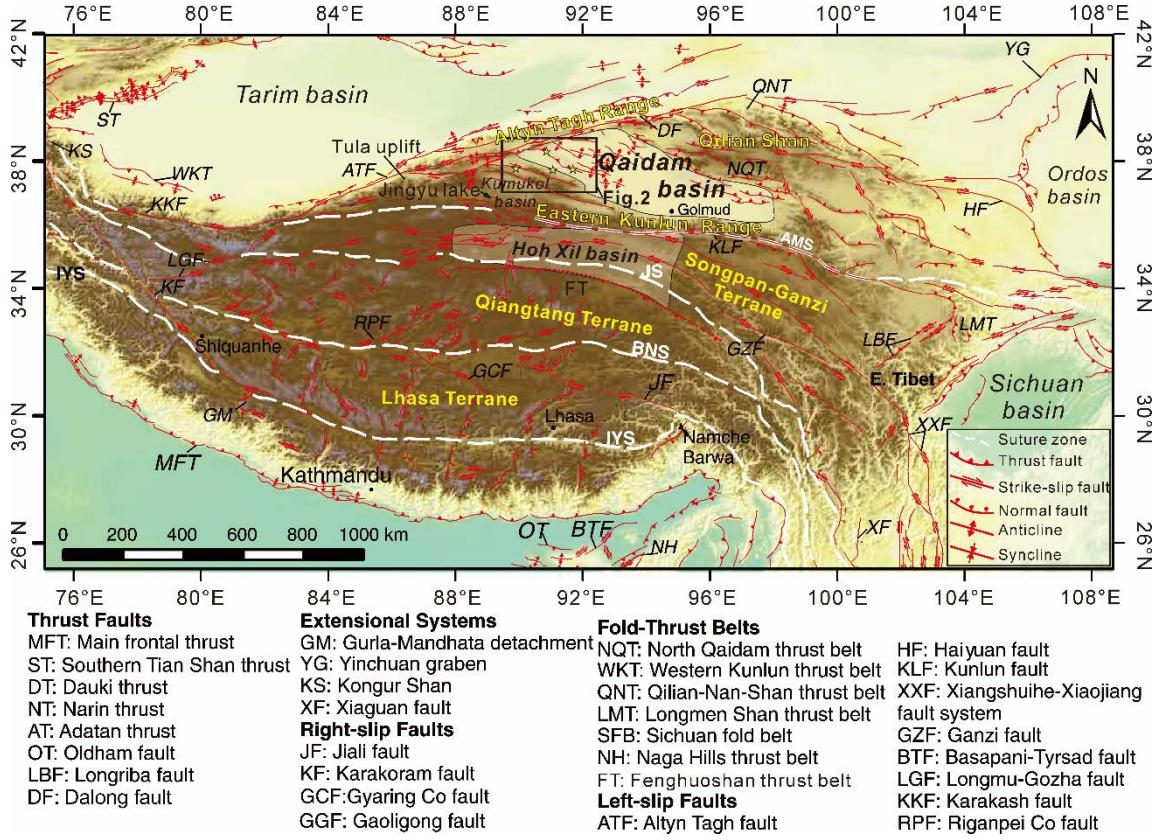

Thrust Faults
MFT: Main frontal thrust
ST: Southern Tian Shan thrust
DT: Dauki thrust
NT: Narin thrust
AT: Adatan thrust
OT: Oldham fault
LBF: Longriba fault
DF: Dalong fault

Extensional Systems
GM: Gurla-Mandhata detachment
YG: Yinchuan graben
KS: Kongur Shan
XF: Xiaguan fault

Right-slip Faults
JF: Jiali fault
KF: Karakoram fault
GCF:Gyaring Co fault
GGF: Gaoligong fault

Fold-Thrust Belts
NQT: North Qaidam thrust belt
WKT: Western Kunlun thrust belt
QNT: Qilian-Nan-Shan thrust belt
LMT: Longmen Shan thrust belt
SFB: Sichuan fold belt
NH: Naga Hills thrust belt
FT: Fenghuoshan thrust belt

Left-slip Faults
ATF: Altyn Tagh fault

HF: Haiyuan fault
KLF: Kunlun fault
XXF: Xiangshuihe-Xiaojiang fault system
GZF: Ganzi fault
BTF: Basapani-Tyrsad fault
LGF: Longmu-Gozha fault
KKF: Karakash fault
RPF: Riganpei Co fault

Figure 1. Digital topographic map of the Tibetan Plateau modified after Taylor and Yin (2009). Active fault kinematics and suture zones are based on Yin et al. (2007), Taylor and Yin (2009), and Cheng et al. (2014). Note that the Hoh Xil Basin has been diced up by the Neogene uplift phase. The yellow stars refer to the location of sampling sites. IYS—Indus Yalu suture zone; AMS—Anyimagen-Kunlun-Muztagh suture zone; JS—Jinsha suture zone; BNS—Bangong Nujiang suture zone.

The actively deforming northeastern and eastern edges of the Tibetan plateau are characterized by both a strong topographic gradient and a marked dichotomy between low relief basins (Qaidam and Sichuan basins) and highly dissected Alpine-style high ranges (Eastern Kunlun, Altyn Tagh, Qilian Shan and Longmen Shan ranges). Along the northeastern margin of the plateau, the ca. 3000 m high Qaidam basin is located between the ca. 5000 m high Eastern Kunlun Range, Altyn Tagh Range and Qilian Shan (Fig. 1). The late Mesozoic – Cenozoic evolution of the deformation pattern, sediment composition and depositional

environments in the basin are thus directly related to the tectonic and topographic growth of the surrounding ranges and represent key constraints on the tectonic and topographic evolution of the Tibetan plateau (e.g. Métivier et al., 1998; Rieser et al., 2006; Yin et al., 2007, 2008b; Fu et al., 2010; Zhuang et al., 2011; Song et al., 2013; F. Cheng et al., 2015a).

The proposed onset time of uplift of the Eastern Kunlun Range mainly varies from Eocene to Miocene depending on the approach used to estimate the onset of deformation (Mock et al., 1999; A. Wang et al., 2000; Jolivet et al., 2001; Yuan et al., 2003; Wang et al., 2006a; Yuan et al., 2006; Yin et al., 2007, 2008b; C. Wang et al., 2008a; Clark et al., 2010; Dai et al., 2013; Duvall et al., 2013). In particular, based on regional stratigraphic correlation between the Qaidam basin and the Hoh Xil basin to the south (Fig. 1), Yin et al. (2008b) argued that they represented a single basin during the Paleogene, bounded to the north by the Altyn Tagh Range and the Qilian Shan, and to the south by the proto-Tibetan plateau. This large structure was then partitioned by the tectonic uplift of the Eastern Kunlun Range during the Neogene. This model questions the assumption of a progressive northward growth of the plateau through in-sequence propagation of thrust systems associated with filling of the intermediate basins (e.g. Métivier et al., 1998, Meyer et al., 1998; Tapponnier et al., 2001). This idea has motivated several attempts to reassess the tectonic processes affecting the northern edge of the Tibetan plateau (e.g. Shi et al., 2009; Wang et al., 2011; Cheng et al., 2014; Mao et al., 2014; Yu et al., 2014).

In recent years, a number of studies have concentrated on the tectonic evolution of the southern margin of the Qaidam basin to describe the Cenozoic growth history of the Eastern Kunlun Range (Yin et al., 2007, 2008a, 2008b; Shi et al., 2009; Wang et al., 2011; Cheng et al., 2014). However, partially due to the remote, inaccessible geographical location of the late Mesozoic to Cenozoic sections in the South Qaidam basin (SQB) and northern flank of the Eastern Kunlun Range, little information is available on the temporal and spatial evolution of the sediment sources and depositional environments. Such source-sink information is of primary importance when trying to decipher the topographic growth of the Eastern Kunlun Range during the Cenozoic and to constrain the early Cenozoic topography of the northern edge of the Tibetan plateau (i.e. the pre-orogenic status).

In this study, twenty-two sandstone samples from Paleocene to Holocene strata (including six core samples from Paleogene strata) were collected along the Dongchaishan-Gansen, Kunbei, Huatugou and Adatan sections (Fig. 2) for U-Pb dating of detrital zircons using Laser Ablation Inductively Coupled-Plasma Mass Spectrometry (LA-ICP-MS). In order to characterize the nature of any relation between the Eastern Kunlun Range and the Qaidam

basin, this analysis was conducted together with sedimentology and petrography studies, as well as interpretation of newly-acquired seismic profiles in the SQB. Data are then interpreted in terms of Cenozoic topographic history of northern Tibet, and more precisely in terms of the influence of the Cenozoic topographic growth of the Eastern Kunlun Range on the sedimentary and topographic evolution of the SQB. Finally, this study provides a local framework for a better assessment of the Cenozoic spatial and temporal evolution of the entire Tibetan Plateau.

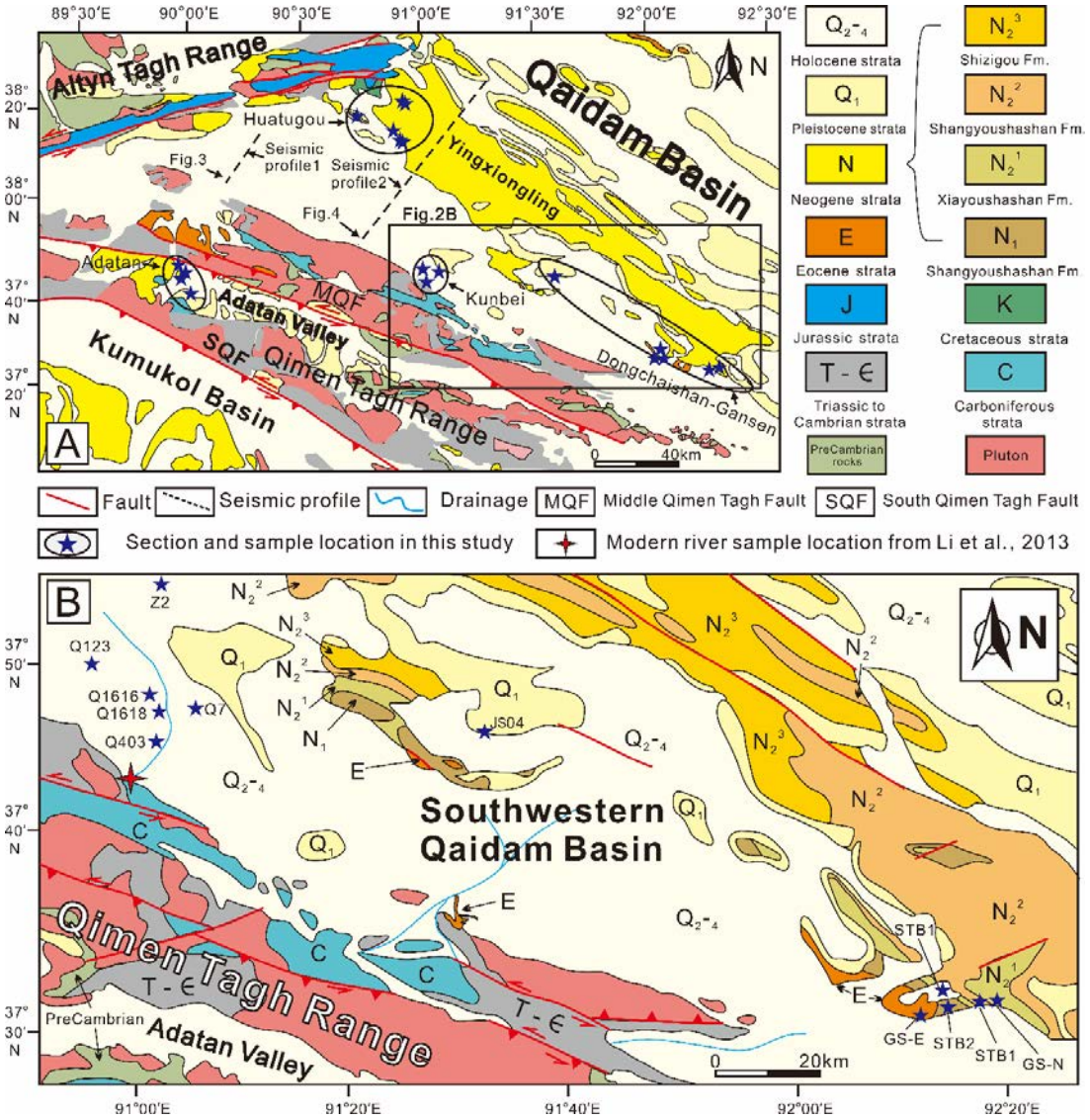

Figure 2. Geological map of the southwestern Qaidam Basin and surrounding area, modified after the 1:250,000 geologic map (SIGS, 2003; QIGS, 2004). See Figure 1 for location. Active fault kinematics are based on Cheng et al. (2014), SIGS (2003), and QIGS (2004).

2.2.2 Geological Setting

2.2.2.1 Eastern Kunlun Range

The Eastern Kunlun Range is oriented in a more or less east-west direction with an

average elevation of about 5000 m and has the largest topographic gradients within the Tibetan plateau. Both morphologically and tectonically, it separates the Hoh Xil basin to the south from the Qaidam basin to the north (Fig. 1). The sub-ranges that form the belt diverge westwards gradually forming a series of valleys and ranges such as the Qimen Tagh Range, the Adatan valley or the Kumukol basin (Figs.1 and 2). The basement of the Eastern Kunlun Range mainly consists of Proterozoic and Paleozoic metamorphic rocks overlaid by Paleozoic to Mesozoic strata. These were intruded by Paleozoic and Mesozoic (Permo – Triassic) igneous rocks and were then covered by Jurassic to Cenozoic continental deposits (Fig. 2; Mock et al., 1999; Cowgill et al., 2003; Robinson et al., 2003; Roger et al., 2003; QIGS, 2004; Yin et al., 2007). Finally, late Cenozoic to Quaternary volcanism crosscut the entire sequence (e.g. Jolivet et al., 2003).

Three ophiolite belts of Cambrian, Mississippian and Permo – Triassic ages are exposed within the Eastern Kunlun Range, indicating a long and complex history of oceanic closure within the area (Roger et al., 2008; Wang et al., 2011). Both the basement and sediment cover of the range are cut by a series of high angle faults, related to the major left-lateral strike-slip Kunlun Fault and forming ESE-WNW trending structures (e.g. Kirby et al., 2007; Duvall et al., 2013; Cheng et al., 2014). The Kunlun Fault initiates on the eastern margin of the Tibetan plateau (Lin and Guo, 2008), and terminates in the west with a splay structure composed of several curved thrust faults (Xu et al., 2002; Jolivet et al., 2003; Fu and Awata, 2007; Cheng et al., 2014). Initiation of the modern Kunlun Fault is dated around 30-20 Ma and the calculated total displacement is around 100 ± 20 km (Kidd and Molnar, 1988; Wang et al., 2001; van Der Woerd et al., 2002; Jolivet et al., 2003; Zhang et al., 2004; Yuan et al., 2006; Fu and Awata, 2007; Kirby et al., 2007; Duvall et al., 2013; Cheng et al., 2014). The Cenozoic deformation and exhumation patterns of the Eastern Kunlun Range are complex and remain controversial with estimated onset ages ranging from Eocene-Oligocene (Mock et al., 1999; Jolivet et al., 2001; Wang et al., 2004a; Clark et al., 2010; Duvall et al., 2013) to Miocene (Yuan et al., 2003; Yi et al., 2008) and even as young as Pliocene (A. Wang et al., 2006). Recent analyses of seismic profiles within the Qaidam basin also suggest that the Cenozoic deformation across the Eastern Kunlun Range and SQB initiated during or after the latest Oligocene – early Miocene (Yin et al., 2007; Y.D. Wang et al., 2010a). As the tectonic and topographic evolution of the Eastern Kunlun Range is assumed to control the northward growth of the Tibetan plateau (Yin et al., 2007; Wang et al., 2014), it is of primary importance to resolve the discrepancies in inferred timing.

2.2.2.2 Qaidam basin

As the largest petroliferous basin on the Tibetan plateau, the triangular shaped endorheic Qaidam basin is surrounded by the Altyn Tagh Range, the Qilian Shan and the Eastern Kunlun Range (Fig. 1), with about 2000 m of relief difference from the basin to the ranges. Numerous subsurface data (seismic profiles and drill cores) and sequence stratigraphy studies demonstrate that the Qaidam basin is filled with Jurassic, Cretaceous and Cenozoic continental clastic sediments (e.g. Xia et al., 2001; Fang et al., 2007; Yin et al., 2008b). The Cenozoic stratigraphy of the basin has been defined and dated in detail using magnetostratigraphy, and palynology data (Huo, 1990; QBGMR, 1991; Yang et al., 1992; Huang et al., 1996; Xia et al., 2001; Qiu, 2002; Z.M. Sun et al., 2005; Zhang, 2006; Zhao et al., 2006; Fang et al., 2007; Z.M. Sun et al., 2007; Yin et al., 2008b; Gao et al., 2009; Lu and Xiong, 2009; Pei et al., 2009; Ke et al., 2013). The Cenozoic sequences (Fig. 3) are composed of: 1) the Lulehe Formation, Paleocene to early Eocene, >53.5 - 43.8 Ma (Yang et al., 1992; Zhang, 2006; Ke et al., 2013); 2) the Lower Xiaganchaigou Formation, middle Eocene, 43.8 - 37.8 Ma (Zhang, 2006; Sun et al., 2007; Pei et al., 2009); 3) the Upper Xiaganchaigou Formation, late Eocene, 37.8 - 35.5 Ma (Z.M. Sun et al., 2005; Z.M. Sun, 2007; Pei et al., 2009); 4) the Shangganchaigou Formation, Oligocene, 35.5 - 22.0 Ma (Z.M. Sun et al., 2005; Lu and Xiong, 2009); 5) the Xiayoushashan Formation, early Miocene, 22.0 - 15.3 Ma (Fang et al., 2007; Lu and Xiong, 2009); 6) the Shangyoushashan Formation, middle to late Miocene, 15.3 - 8.1 Ma (Fang et al., 2007); 7) the Shizigou Formation, late Miocene to Pliocene, 8.1 - 2.5 Ma (Fang et al., 2007); and finally, 8) the Quaternary sediments, including the Qigequan Formation and the Dabuxun - Yanqiao Formation, Pleistocene to present, 2.5 - 0 Ma (Fang et al., 2007; Yin et al., 2008b).

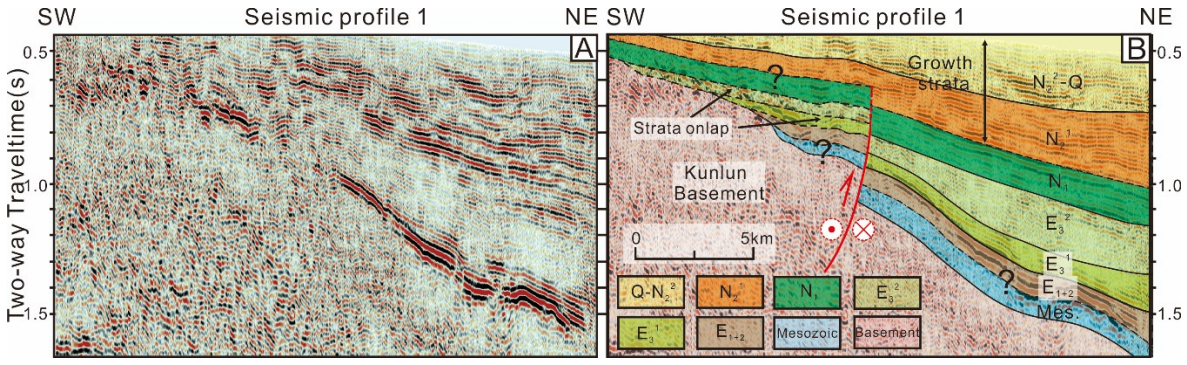

Figure 3. Original (A) and interpreted (B) NE-SW–oriented seismic profile 1 in SW Qaidam Basin. See the location in Figure 2. Note that stratigraphic overlaps between the Paleocene to early Eocene (E_{1+2}) and middle to late Eocene (E_3) strata, the middle to late Eocene (E_3) and Oligocene (N_1) strata, and the Oligocene (N_1) and early Miocene (N_2^1) strata, indicating the gradually enlarging basin from Paleocene to middle Miocene. The growth strata within the middle to late Miocene (N_2^2) strata, late Miocene to Pliocene (N_2^3) strata, and Pleistocene (Q_1) strata demonstrate the shrinking of the basin

since the Miocene.

Large-scale isopach maps, available for each Cenozoic stratigraphic unit in the Qaidam basin provide a clear image of the geometry of the Cenozoic strata (Meng and Fang, 2008; Yin et al., 2008b; Mao et al., 2014). From the Lulehe Formation up, all the formations are systematically thicker in the central part of the basin and thin toward the margins (Huang et al., 1996; E. Wang et al., 2006; Yin et al., 2008b). While the depocenter of the Qaidam basin migrated to the south and east during the Eocene (E. Wang et al., 2006; Yin et al., 2008b), the western Qaidam basin developed extensive saline oil accumulations dominated by two sets of major source rocks deposited in the early Eocene and Oligocene (Huang et al., 1996; Zhu et al., 2005). Newly acquired seismic profiles across the northern flank of the Qimen Tagh Range also show successive onlap of the Eocene and Oligocene Formations (Fig. 3). This geometry suggests a progressive widening of the Qaidam basin to the south from the Eocene to the Oligocene. Subsequently, from the early Miocene to Pliocene, the depocenter migrated northeastwards while the southern limit of the deposition area in the SQB gradually retreat northward, suggesting uplift along the southern edge of the basin (Yin et al., 2008a; Mao et al., 2014). Growth strata developed during this period (Figs. 3 and 4), which again implies tectonic activity (e.g. initiation of strike-slip faulting) in the Eastern Kunlun Range and the SQB (Clark et al., 2010; Duvall et al., 2013; Cheng et al., 2014).

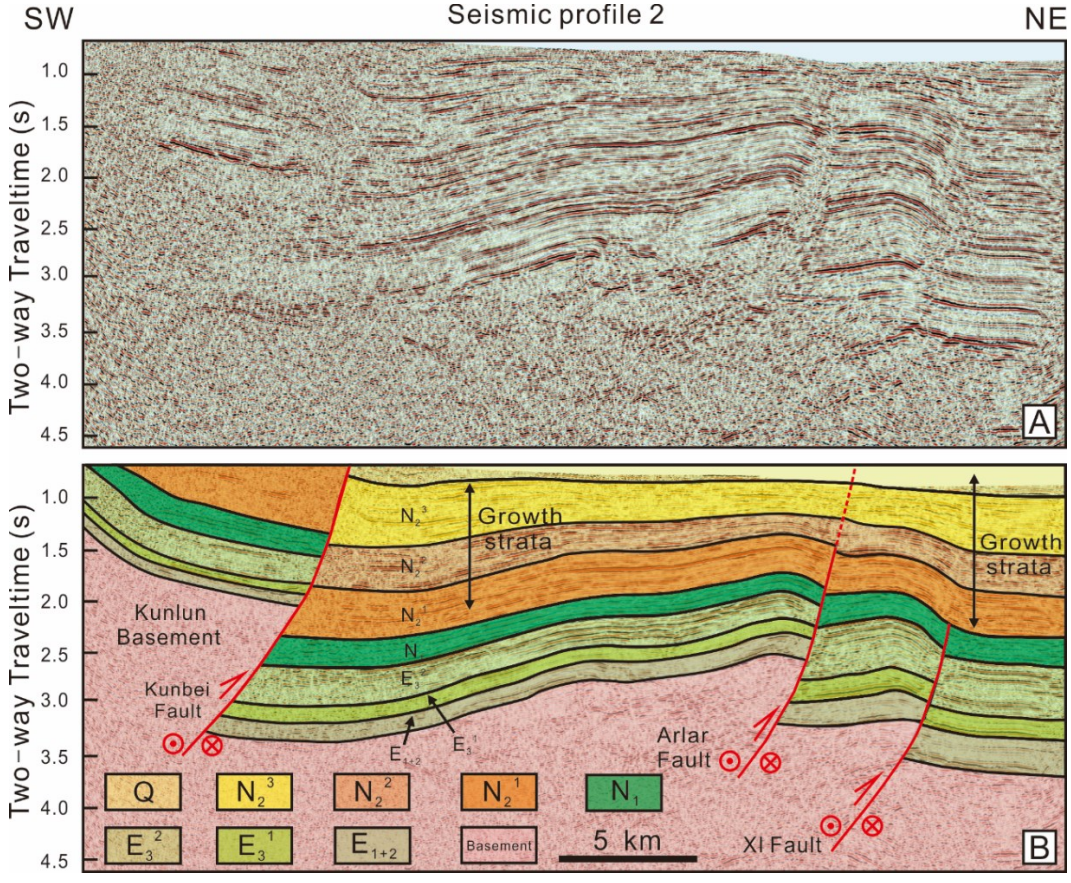

Figure 4. Original (A) and interpreted (B) NE-SW–oriented seismic profile 2 in the South Qaidam Basin. See the location in Figure 2. Note that growth strata near the Kunbei and Arlar faults indicate the uplifting of the Eastern Kunlun Range and shrinking of the basin since the Miocene.

The present-day structure of the SQB is dominated by a series of high angle north-dipping or south-dipping Cenozoic reverse faults accommodating the ongoing shortening generated by the India – Eurasia collision stress field (Wu et al., 2014). Some of these faults display an en echelon arrangement indicating transpressional deformation in local areas, such as the Kunbei and Arlar faults, (Fig. 4; F. Cheng et al., 2014, X. Cheng et al., 2015. Balanced cross-sections throughout the basin indicate that the Cenozoic shortening of the Qaidam Basin increased westward in response to several Eocene and younger shortening phases (Zhou et al., 2006; Yin et al., 2008b; Y.D. Wang et al., 2010).

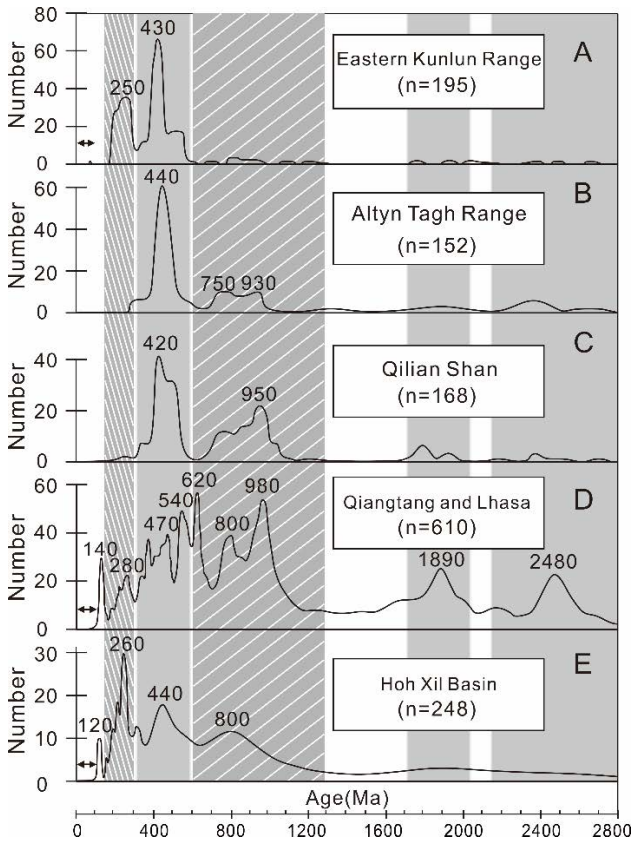

Figure 5. Relative probability plots of granitoid pluton ages in (A) the Eastern Kunlun Range, (B) the Altyn Tagh Range, (C) the Qilian Shan, and U-Pb ages of detrital zircons from (D) the Qiangtang and Lhasa blocks as well as (E) the Hoh Xil Basin. The age data were obtained from: J.S. Yang et al. (1996, 2002, 2006); J.X. Zhang et al. (1997, 2001, 2011); Chen et al. (2003); Gehrels et al. (2003a, 2003b); Yue et al. (2005); L. Liu et al. (2007, 2009); Lu et al. (2008); Chen et al. (2012); Dai et al. (2012); L. Liu et al. (2013b); C. Wang et al. (2013); Staisch et al. (2014); L.Y. Zhang et al. (2014). See also Figure DR1 and Table DR1 for more information on the data (see text footnote 1). Double-headed arrow within the figure refers to the few early Cenozoic and late Mesozoic $^{40}Ar/^{39}Ar$ and U-Pb zircon ages found with each range. Age distributions are marked by different shades according to age groups.

2.2.3 Synthesis of existing zircon U-Pb ages from basement

In order to identify the potential sediment source areas for the SQB, we compiled published zircon U-Pb ages on basement rocks from the surrounding Eastern Kunlun, Altyn Tagh and Qilian Shan ranges. A similar compilation was also made using the detrital zircon U-Pb ages available from the Qiangtang and Lhasa blocks as well as

from the Hoh Xil basin (Figs. 5 and DR1 [see footnote 1]; Table DR1 [see footnote 1[①]]).

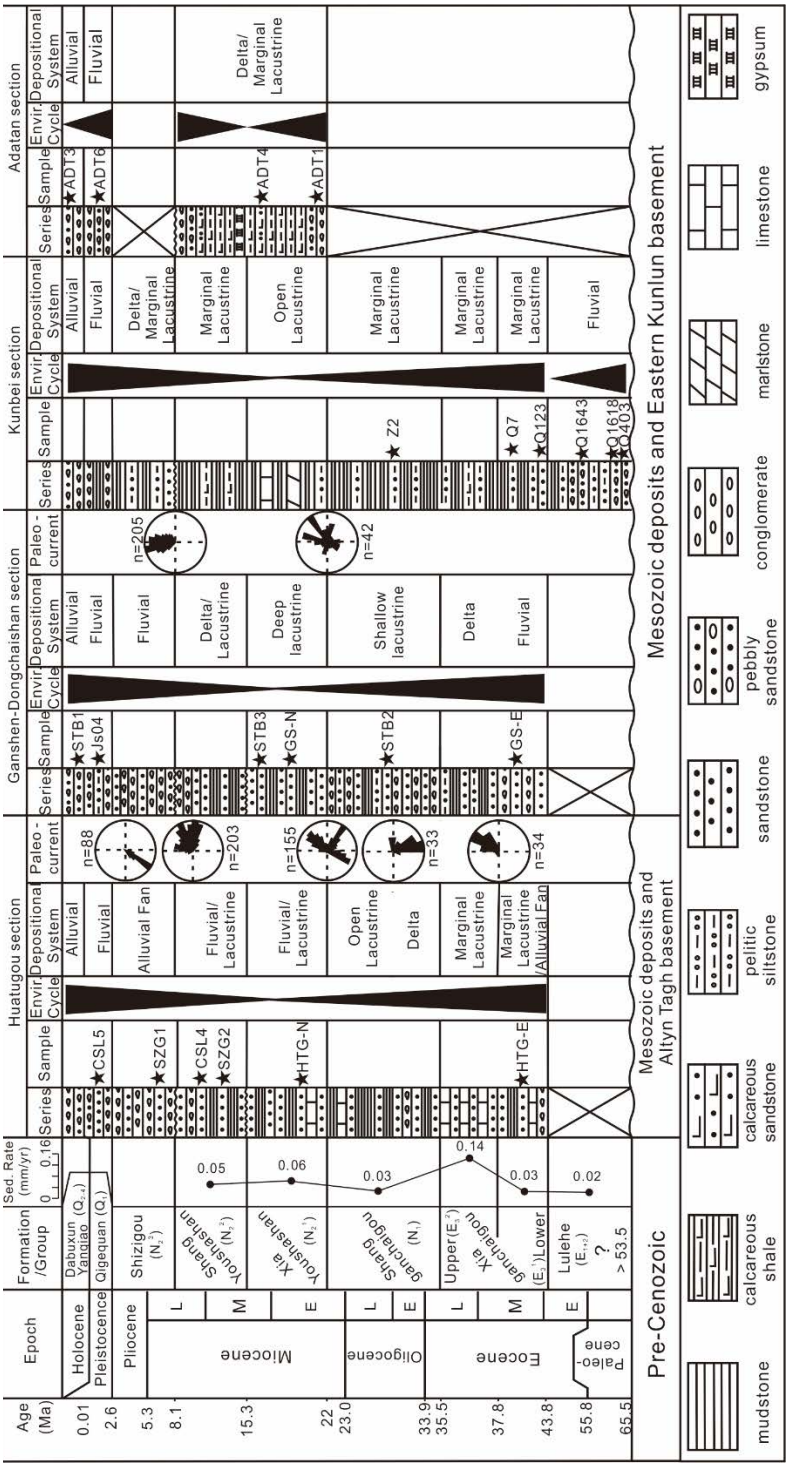

Figure 6. Generalized stratigraphic column of the studied Cenozoic series. Paleocurrent directions were obtained from Meng and Fang (2008) and Zhuang et al. (2011). Envir. Cycle and Sed. Rate in the figure refer to the environment cycle and average sedimentary rate in the South Qaidam Basin, respectively. The average sedimentary rate is generally calculated based on the Cenozoic sequence thickness data from three-dimensional seismic profiles (F. Cheng et al., 2014; X. Cheng et al., 2015) and the age ranges of each sequence (F. Yang et al., 1992; Fang et al., 2007; Zhang, 2006; Sun et al., 2005; Lu and Xiong, 2009; Pei et al., 2009; Ke et al., 2013).

Within the Eastern Kunlun Range, Archean and Proterozoic U-Pb zircon ages are very rare although three age groups can be inferred at 1300-600 Ma, 2100-1700 Ma and 2800-2200 Ma (Fig. 5A; QIGS, 2004; G.C. Wang et al., 2004). The late Proterozoic to Paleozoic age

[①] 1 GSA Data Repository item 2015256, Figure DR1 and Tables DR1–DR2, is available at http:// www.geosociety .org /pubs /ft2015 .htm or by request to editing@ geosociety .org.

group is well represented with a clear age peak around 430 Ma, derived from the early Paleozoic metamorphic rocks associated to the Ordovician – Silurian docking of the Kunlun and Tarim blocks (e.g. Cowgill et al., 2003; QIGS, 2004; Li et al. 2013). However, the Eastern Kunlun basement age distribution is mostly characterized by abundant late Paleozoic – early Mesozoic ages (ca. 300 Ma to ca. 200 Ma) (Fig. 5A). These ages correspond in timing to magmatism associated to the Permo – Triassic closure of the Paleo-Tethys Ocean and to the post-collision magmatism that followed the docking of the Qiangtang block (Roger et al., 2003; Liu et al., 2006; Roger et al., 2008, 2010; Li et al., 2013; Jolivet et al., 2015). Although a few similar Mesozoic ages are found in the Qilian Shan and Altyn Tagh Range, they do not represent such a well-defined component as in the Eastern Kunlun Range (Fig. 5). Finally, a few Cretaceous ages have been obtained from the Tula Uplift in the western reach of the Eastern Kunlun Range (Fig. 1; Robinson et al., 2003) and some Miocene to Quaternary volcanism is occurring in the southwestern part of the range (Jolivet et al., 2003).

The basement of the Altyn Tagh Range (Fig. 5B) displays a relatively large proportion of Archean and Proterozoic zircon U-Pb ages, with Archean ages ranging from ca. 3.6 Ga (Lu et al., 2008) to ca. 2.6 Ga (Lu and Yuan, 2003; Long et al., 2014) and Proterozoic ages ranging from ca. 2.4 Ga to ca. 650 Ma (Gehrels et al., 2003a, 2003b; C, Wang et al., 2006; Zhang et al., 2011). Among those Proterozoic ages, a clear age group can be inferred between ca. 1050 Ma and ca. 650 Ma (Fig. 5B; Wang et al., 2013). Large Paleozoic intrusions are mapped along the range with zircon U-Pb ages ranging from ca. 550 Ma to ca. 400 Ma, forming the major age group (~53 % of the total) within the age distribution pattern (Figs. 5B and DR1 [see footnote 1]; Sobel and Arnaud, 1999; Yue et al., 2004, 2005; J.X. Zhang et al., 2005; C. Wang et al., 2008; Liu et al., 2009; J. Zhang et al., 2014). Finally only a few isolated late Paleozoic igneous rocks are distributed along the central part of the range, with zircon U-Pb ages ranging between ca. 330 Ma and ca. 270 Ma (Cowgill et al., 2003; Gehrels et al., 2003a, 2003b). These ages only represent a small minority (~4% of the total) within the available data.

The age distribution observed in the Qilian Shan basement is largely similar to that of the Altyn Tagh Range (Fig. 5C). It consists of late Archean – early Proterozoic orthogneisses with zircon U-Pb ages ranging from ca. 2.6 Ga to 1.75 Ga (Lu et al., 2002); of late Proterozoic metamorphic rocks with zircon U-Pb ages of ca. 1.0 Ga (Guo and Li, 1999; Song, 2001; Wan et al., 2001); and finally of late Proterozoic ultramafic intrusions with zircon U-Pb ages of ca. 800 Ma (Li et al., 2005). Within the synthetic distribution of ages presented on Figure 5, the late Proterozoic ages form a distinct group between ca. 1050 Ma and 700 Ma. Early Paleozoic granitoid plutons, intruding the Proterozoic basement provide zircon U-Pb ages ranging

between 550 and 400 Ma (Yang et al., 2002; Cowgill et al., 2003; Gehrels et al., 2003a, 2003b; Shi et al., 2006; Bovet et al., 2009). Those ages represent a very distinctive component on the age spectrum (Fig. 5C). The northern part of the Qilian Shan was affected by an early to late Devonian (400 - 360 Ma) metamorphic phase (e.g. Wu et al.,1993; Zhang et al., 1997; Zuo and Wu, 1997), with peak metamorphism dated at 440 - 423 Ma within the north Qaidam ultrahigh pressure belt (Yang et al., 2001, 2002; Song et al., 2004, 2006; Yang et al., 2006). Finally Permian to Triassic igneous rocks are distributed sporadically within the range, with zircon U-Pb ages ranging between 270 Ma and 210 Ma (Fig. 5C; Menold, 2006; Wu et al., 2008). However, as in the Altyn Tagh Range, these Mesozoic ages are not a significant component of the Qilian Shan Range, which display predominantly Paleozoic and Precambrian ages.

The zircon U-Pb age spectrum of the Qiangtang and Lhasa terranes is extremely complex, with ages ranging from late Cenozoic to Archean and showing numerous distinctive peaks (Fig. 5D). In the Songpan – Ganzi and northern Qiangtang terranes, Mesozoic granitic intrusions cluster between 220 Ma and 200 Ma (e.g. Leier et al., 2007; Roger et al., 2010). In the southern part of the Qiangtang and to the south-east in Yidun, Mesozoic intrusion ages are

younger, between 150 Ma and 100 Ma (e.g. Reid et al., 2005). Finally, in the Lhasa terrane Mesozoic intrusions are dated between ~180 Ma and ~90 Ma (e.g. Kapp et al., 2005, 2007; Leier et al., 2007). In addition, sedimentary and meta-sedimentary rocks in both the Qiangtang and Lhasa terranes contain detrital zircons with U-Pb age populations of 2480 Ma, ~1890 Ma, ~980 Ma, ~800 Ma, ~620 Ma, ~540 Ma, and ~470 Ma (Fig. 5D; Kapp et al., 2005, Leier et al., 2007; Dai et al., 2012). Unlike in the other three areas mentioned above, the Paleoproterozoic and Archean populations are largely represented (over 75% of the total). Finally, Cenozoic volcanic activity is also widely distributed within those two blocks, with ages ranging between early Paleogene to late Miocene in the Lhasa block and early Paleocene to late Oligocene in the Qiangtang block (e.g. Ding et al., 2007; C. Wang et al., 2008; Xia et al., 2011).

The Hoh Xil basin contains a series of Mesozoic to Cenozoic stratigraphic sequences (Fig. 1; C. Wang et al., 2008a; Dai et al., 2012). Detrital zircon ages from the Cenozoic strata throughout the basin are dispersed between ~2800 Ma and ~60 Ma with major age peaks of ~800 Ma, ~440 Ma, ~260 Ma, and ~120 Ma (Dai et al., 2012). L. Y. Zhang et al. (2014) recently obtained eight sensitive high-resolution ion microprobe (SHRIMP) zircon U-Pb ages ranging from 225 Ma to 193 Ma from intrusives units. These are interpreted to be a consequence of the Mesozoic closure of the Paleo-Tethys Ocean. Late Oligocene to late Miocene volcanic rocks are also widespread in the central and eastern part of the Hoh Xil

basin and Pliocene ages have been reported from its western edge (e.g. Xia et al., 2011). Recently, Staisch et al. (2014) reported zircon U-Pb ages clustering around 60 Ma from a tuff layer interbedded within the sedimentary strata.

To summarize, the basement of the Eastern Kunlun Range displays a dominantly bimodal distribution of Mesozoic and Paleozoic ages, with some minor components (less than 10% of the total) of Proterozoic and Archean ages. The sediments of the Hoh Xil basin also contain those two age groups but they are associated to a much larger proportion of Proterozoic to Archean ages (over 30% of the total) and to late Mesozoic (mostly Cretaceous) ages, which are most probably derived from the Qiangtang and Lhasa terranes to the south. Finally, Cenozoic ages from volcanic rocks are widespread within the Lhasa and Qiangtang blocks, in the Hoh Xil basin, and to a more limited amount (less than 5% of the total) in the Eastern Kunlun Range.

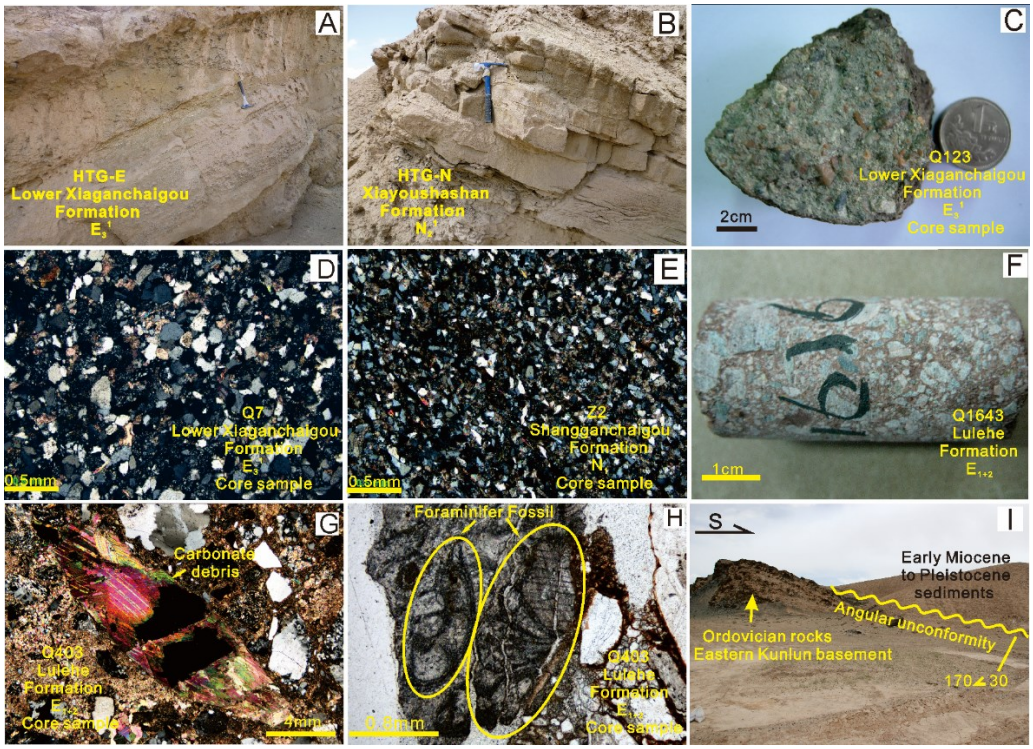

Figure 7. (A) Gray-yellow sandstones interbedded with conglomerates of the middle Eocene Lower Xiaganchaigou Formation (E_3^1) in the Huatugou section. (B) Gray-yellow sandstones interbedded with mudstones of the middle Miocene Xiayoushashan Formation (N21) in the Huatugou section. (C) Core sample of grayish white conglomerates of the middle Miocene Lower Xiaganchaigou Formation (E_3^1) in the Kunbei section. (D–E) Microscopic characteristics (crossed polarized light) of the middle Eocene to Oligocene sandstone core samples from the Kunbei section. Note the large number of lithic fragments, the fining of the grain size, and the increasing textural maturity from middle Eocene to Oligocene. (F) Core sample of conglomerates of the Paleocene Lulehe Formation (E_{1+2}) in the Kunbei section. (G) Carbonate debris included in conglomerates of the Paleocene Lulehe Formation (E_{1+2}) in the Kunbei section (core sample, crossed polarized light microphotograph). (H) Foraminifera in

carbonate debris within conglomerates of the Paleocene Lulehe Formation (E_{1+2}) in the Kunbei section (core sample, plane polarized light microphotograph). (I) Angular unconformity between the early Miocene to Pleistocene sediments and the Ordovician basement rocks of the Tanjianshan Group in the Adatan valley.

Table 1 Summary of major characteristics and the corresponding statistical data for of the samples

Epoch	Formation	Sample number	GPS data/well number	Description	Detrital zircon age range (Ma)	Detrital zircon peaks (Ma)	Number of effective data points	Th/U ratios
Huatugou Section								
Pleistocene	Qigequan Fm.	CSL5	38°20′40.5″ N; 90°41′20″ E	Gray-white fine-grained sandstones, well-sorted.	211~2430	~260 ~420 ~860	98	0.04, 0.07, 0.09, 0.15~ 1.48
Pliocene	Shizigou Fm.	SZG1	38°18′7″ N; 90°50′53.8″ E	Gray-yellow fine-grained sandstones, well-sorted.	211~2430	~240 ~430 ~890	93	0.03, 0.09, 0.14~2.15
Middle Miocene	Shangyou shashan Fm.	CSL4	38°22′5.4″ N; 90°48′10.6″ E	Brown fine-grained sandstones, well-sorted.	202~2378	~220 ~430 ~880	95	0.03, 0.06, 0.08, 0.09, 0.11~2.00
Middle Miocene	Shangyou shashan Fm.	SZG2	38°18′7″ N; 90°50′53.8″ E	Brown fine-grained sandstones, well-sorted.	234~2019	~250 ~440 ~876	90	0.03, 0.04, 0.08, 0.10-1.20
Early Miocene	Xiayousha shan Fm.	HTG-N	38°25′53″ N; 90°53′15″ E	Gray-white fine-grained sandstones, well-sorted.	235~2378	~260 ~400	95	0.12~1.56
Middlc Eocene	Lower Xiagancha igou Fm.	HTG-E	38°25′00″ N; 90°53′00″ E	Gray-white medium-grained sandstones, well-sorted.	181~2662	~260 ~430	98	0.22~1.59
Dongchaishan-Gansen Section								
Holocene	Dabuxun-Yanqiao Fm.	STB1	37°31.6′ N; 92°11.2′ E	Gray-yellow coarse-grained sandy conglomerate, poorly sorted.	109, 209~2573	~210 ~430 ~900	89	0.08, 0.10~2.15
Pleistocence	Qigequan Fm.	JS04	37°47.9′ N; 91°33′ E	Gray-white fine-grained sandstones, well-sorted.	56, 217~2430	~290 ~420 ~780	57	0.03, 0.07, 0.11~1.19
Middle Miocene	Xiayousha shan Fm.	STB3	37°28′48″ N; 92°18′32.8″ E	Gray-yellow fine-grained sandstones, well-sorted.	200~1350	~215 ~410 ~900	89	0.19~1.58
Early Miocene	Xiayousha shan Fm.	GS-N	37°28′53″ N; 92°19′27″ E	Brown medium-grained sandstones, well-sorted.	128~2091	~220 ~400 ~890	97	0.13~1.57
Oligocene	Shanggan chaigou	STB2	37°29′24.2″ N; 92°11′16.7″ E	Gray-yellow fine-grained	200~1900	~220 ~390	93	0.12~1.03

	Fm.			sandstones, well-sorted.		~890		
Middlc Eocene	Lower Xiagancha igou Fm.	GS-E	37°28′29.2″N; 92°8′39″ E	Gray- white fine-coarse-grained sandstones, well sorted.	240~300 0	~250 ~450 ~890	52	0.02~2.19
Kunbei Section								
Oligoc ene	Shanggan chaigou Fm.	Z2	Zha 2 well	Gray-white fine-grained sandstones, well-sorted.	173~108 6	~230 ~400 ~	69	0.10~1.30
Middlc Eocene	Lower Xiagancha igou Fm.	Q7	Qie 7 well	Gray-white fine-grained sandstones, well-sorted.	203~262 1	~250 ~410	88	0.08, 0.10~2.25
Middlc Eocene	Lower Xiagancha igou Fm.	Q123	Qie 123 well	Gray coarse-grained sandstones, poorly sorted.	276~472	~280 ~420	91	0.04, 0.32~1.51
Early Eocene	Lulehe Formation	Q1643	Qie 1616 well	Brownish red coarse-grained sandstone, poorly sorted.	224~202 6	~230 ~390	46	0.12~2.05
Early Eocene	Lulehe Formation	Q1618	Qie 1618 well	Brownish red coarse-grained sandstone, poorly sorted.	219~199 4	~430	96	0.17~0.99
Early Eocene	Lulehe Formation	Q403	Qie 403 well	Brownish red coarse-grained sandstone, poorly sorted.	272~245 9	~470	84	0.29~0.96
Adatan Section								
Holoce ne	Dabuxun-Yanqiao Fm.	ADT3	37°45′24.9″ N; 89°56′39.1″ E	Gray-white coarse-grained conglomerate, poorly sorted.	226, 340~387	~360	98	0.39~1.11
Pleisto cence	Qigequan Fm.	ADT6	37°41′19.9″ N; 89°55′10.5″ E	Brown fine-grained sandstones, well-sorted.	222~213 3	~230 ~380	83	0.14~1.00
Early Mioce ne	Xiayousha shan Fm.	ADT4	37°44′31.7″ N; 89°55′28.5″ E	Gray-yellow grained sandstones, well-sorted.	37, 177~185 7	~220 ~410 ~447 ~776 ~890	51	0.02, 0.07, 0.18~2.45
Early Mioce ne	Xiayousha shan Fm.	ADT1	37°47′50.9″ N; 89°55′19.9″ E	Gray-yellow coarse-grained sandy conglomerate, poorly sorted.	206~182 4	~220 ~380	73	0.06, 0.09, 0.22~2.09

2.2.4 Stratigraphy and sedimentary characteristics of the sections

The four selected sections are located in the southwestern Qaidam basin, close to the northern flank of the Qimen Tagh Range that belongs to the western part of the Eastern Kunlun Range (Figs. 1 and 2; Cheng et al., 2014). Within the Huatugou and Dongchaishan- Gansen

sections, all the Cenozoic formations described above in the geological setting are exposed except for the Lulehe Fm. The Kunbei section was constructed using well data that sample the complete Cenozoic sequences including the Lulehe Fm. Finally, the Adatan section from the Qimen Tagh Range is restricted to the late Upper Oligocene to present sequences (Fig. 4). A brief description of the lithologies, sediment facies and paleocurrents directions obtained from fieldwork and drill-core data in each section is given next.

The Huatugou section is located in the northernmost part of the prominent Yingxiongling uplift structure (Fig. 2). Except for the Lulehe Fm., the whole Cenozoic sequence is well exposed (Figs. 2 and 6). The over 180 m thick Lower Xiaganchaigou Fm. is composed mainly of grey green, green yellow sandstones and pebbly sandstones at the base, evolving upward towards brown red sandstones and siltstones. The sediment facies vary from fluvial to shallow lake deposits upward (Figs. 6 and 7A; Zhuang et al., 2011; Wu et al., 2012). The ~750 m thick Upper Xiaganchaigou Fm. rests conformably on the Lower Xiaganchaigou Fm. and consists mainly of earthy yellow, grey green sandstones, greyish-green silty mudstones and argillaceous siltstones intercalated with calcareous shales. The sediment facies vary upward from braided river to shallow lake deposits (Fig. 6; Wu et al., 2012). Paleocurrents are consistently directed towards the NE (Fig. 6; Meng and Fang, 2008). The over 800 m thick Shangganchaigou Fm. again rests conformably on the Upper Xiaganchaigou Fm. It is mainly composed of greyish-green carbonaceous mudstones and sandstones interbedded with grey-white mudstones. The sediment facies correspond to deltaic to shallow lake deposits (Fig. 6). Reported paleocurrent directions for this formation vary from SE (Fig. 6; Meng and Fang, 2008) to S-SSW (Wu et al., 2012) depending on the authors. The over 700 m thick Xiayoushashan Fm. conformable with the Shangganchaigou Fm., is mainly composed of yellowish-brown, purple red conglomerates, pebbly sandstones, sandstones and argillaceous siltstones with intercalations of thick-bedded limestones. The facies vary from shallow lake to fluvial deposits (Figs. 6 and 7B). Paleocurrent directions are variable but have three main orientations: towards the NE, SE and SW (Zhuang et al., 2011; Wu et al., 2012). The ~1000 m thick Shangyoushashan Fm. unconformably overlies the Xiayoushashan Fm. and consists of earthy yellow pebbly sandstones, sandstones and silty mudstones (Fig. 6). The sediment facies is characterized by shallow lake, alluvial plain and braided river deposits (Wu et al., 2012). Paleocurrents are mostly oriented towards the NE (Zhuang et al., 2011), although Wu et al. (2012) again report S to SSW paleocurrent directions probably due to local topography or to local effects of river meandering. The 190 m thick Shizigou Fm., again lying unconformably on the Shangyoushashan Fm., is mainly composed of earth-yellow sandstones and silty

mudstones corresponding to fluvial facies sediments (Fig. 6). Paleocurrent measurements indicate a S-SW flow direction (Fig. 6; Zhuang et al., 2011; Wu et al., 2012). The Qigequan and Dabuxun-Yanqiao Formations, resting unconformably on the Shizigou Fm., are mainly composed of grey and brown sandstones and conglomerates corresponding to flood plain and alluvial facies deposits (Fig. 6).

The Dongchaishan-Gansen section is situated within the southeastern part of the Yingxiongling structure (Fig. 2). The over 600 m thick Xiaganchaigou Fm. is composed of grey white conglomerates, grey brown sandstones and mudstones with intercalations of limestones and gypsum layers. The unit shows a distinct fining-upward sequence evolving from deltaic sediment facies at the base, to shore shallow lacustrine facies at the top (Fig. 6). The 700 m thick Shangganchaigou Fm., conformably resting on the Upper Xiaganchaigou Fm., consists of brownish green siltstones, grey sandstones, mudstones and limestones. This series is dominated by horizontally bedded deep lacustrine sediment facies (Fig. 6). The over 1000 m thick Xiayoushashan Fm., lying conformably on the Shangganchaigou Fm., is mainly composed of brownish red siltstones, brownish yellow mudstones and limestones successions corresponding to deep lacustrine facies deposits. The sedimentary sequence displays a generally retrograding cycle (Fig. 6) from its lower to its middle part (increasing frequency of limestone layers and horizontal beddings within the sandstones), followed by a prograding cycle from its middle to its upper part (increasing frequency of sandstones layers). Paleocurrent directions in that formation are N-NE (Fig. 6; Hertz et al., 2005; Zhuang et al., 2011). The 300 m thick Shangyoushashan Fm., lying unconformably on the Xiayoushashan Fm., is composed of grey mudstones, sandstones, siltstones with intercalations of limestones. The sedimentary sequence generally shows a progradation cycle characterized by shore to shallow lacustrine facies in the lower part and deltaic facies in the upper part of the section. The over 200 m thick Shizigou Fm., resting unconformably on the Shangyoushashan Fm., consists mainly of cross-bedded coarse grey white sandstones and grey brown conglomerates corresponding to fluvial deposits (Fig. 6). Paleocurrent directions in both the Shangyoushashan and Shizigou Formations are strongly unimodal towards N-NE (Fig. 6; Meng and Fang, 2008; Zhuang et al., 2011). As in the Huatugou section, the Qigequan and the Dabuxun-Yanqiao Formations (Yin et al., 2007) rest unconformably on the Shizigou Fm. They mainly consist of a succession of grey and brown sandstones and conglomerates corresponding to flood plains deposits (Fig. 6).

The Kunbei section, established on the basis of core data, is located along the northern flank of the Qimen Tagh Range (Fig. 2). Except for the occurrence of the Lulehe Fm., the

stratigraphy and sedimentary characteristics of both the Dongchaishan-Gansen and the Kunbei sections are similar (Figs. 6, 7C, 7D and 7E). In front of the Eastern Kunlun Range, the Altyn Tagh Range and the Qilian Shan, the Paleocene Lulehe Fm. is characterized by coarse-grained detrital sediments corresponding to braided river to deltaic sediment facies (Xia et al., 2001; Wu et al., 2012). The thickness of the formation generally increases towards the center of the Qaidam basin (Xia et al., 2001; Yin et al., 2008b). In the Kunbei section, the Mesozoic strata are missing and the Lulehe Fm. unconformably overlies the Eastern Kunlun crystalline basement (Paleozoic granitoid intrusions). Locally, the thickness of the formation may not exceed 200 m. The lithology is dominated by feldspathic litharenite and lithic arkoses. The strata show poor compositional and textural maturity, characterized by poorly sorted and poorly rounded clasts (Fig. 7F and 7G). The clasts are dominated by granitic grains, metamorphic fragments and some carbonate debris which are composed mainly of biosparite containing abundant foraminifera (Fig. 7G and 7H). The size of the carbonate debris is relatively large ranging from 5 to 30 mm. As carbonate is easily dissolved, it is assumed that carbonate fragments are generally not transported over long distances (Zuffa, 1980; Mack and Rasmussen, 1984), and thus the source area of the clasts preserved within the Lulehe Fm. must be relatively proximal. As a consequence of poor exposure, no paleocurrent data are available for the Paleocene series in the SQB. However, based on heavy mineral contents, calculated Zircon-Tourmaline-Rutile (ZTR) indices and the heavy mineral assemblages for the drill core samples from a large number of oil wells in the Kunbei section, Gong et al. (2012) and Fu et al. (2013) suggested that during the deposition of the Paleocene Lulehe Fm., the material deposited in the Kunbei area was derived from the south, probably from the Eastern Kunlun Range. In addition, the Carboniferous strata, largely exposed south of the Kunbei section (Fig. 2), consist mainly of biomicrite, biosparite, and bioclastic littoral to neritic limestones containing abundant brachiopods, coral, gastropods and foraminifera that could represent the source of the Lulehe Fm. carbonate clasts (QIGS, 2004).

The Adatan section is located within the Adatan valley between the two main sub-ranges forming the Qimen Tagh Range (Fig. 2). In this section, only the Xiayoushashan, Qigequan and Dabuxun-Yanqiao Formations are exposed, with the other formations being absent due to erosion. The Xiayoushashan Fm., unconformably resting on the Ordovician metamorphic basement (Fig. 7I), is composed of conglomerates, pebbly sandstones, siltstones and calcilutites. The sediment facies evolve upward from deltaic to shallow lake deposits (SIGS, 2003). The Qigequan Fm., unconformably overlying the Shizigou Fm., consists of conglomerates intercalated with sandstones and mudstones and mainly corresponds to alluvial

facies deposits (QIGS, 2004). Finally, the Dabuxun-Yanqiao Fm. is mainly composed of variegated gravels, erratic blocks, sandy soil and clay deposits of alluvial fan and fluvial facies (QIGS, 2004).

In general, from the Eocene to the Miocene, the sediments in the SQB are composed of lithic feldspar sandstones and lithic sandstones, with only a slight variation in composition (e.g. Fig. 7D). The lithic fragments are mainly of volcanic and magmatic origin, although a small proportion has a sedimentary origin, indicating that recycling of the Eocene to Miocene strata in the Qaidam basin is weak (Rieser et al., 2005, 2007; Xia et al., 2012). Material directly derived from the erosion of basement rocks in the source areas provides the largest contribution to the sediment deposited in the basin during that period.

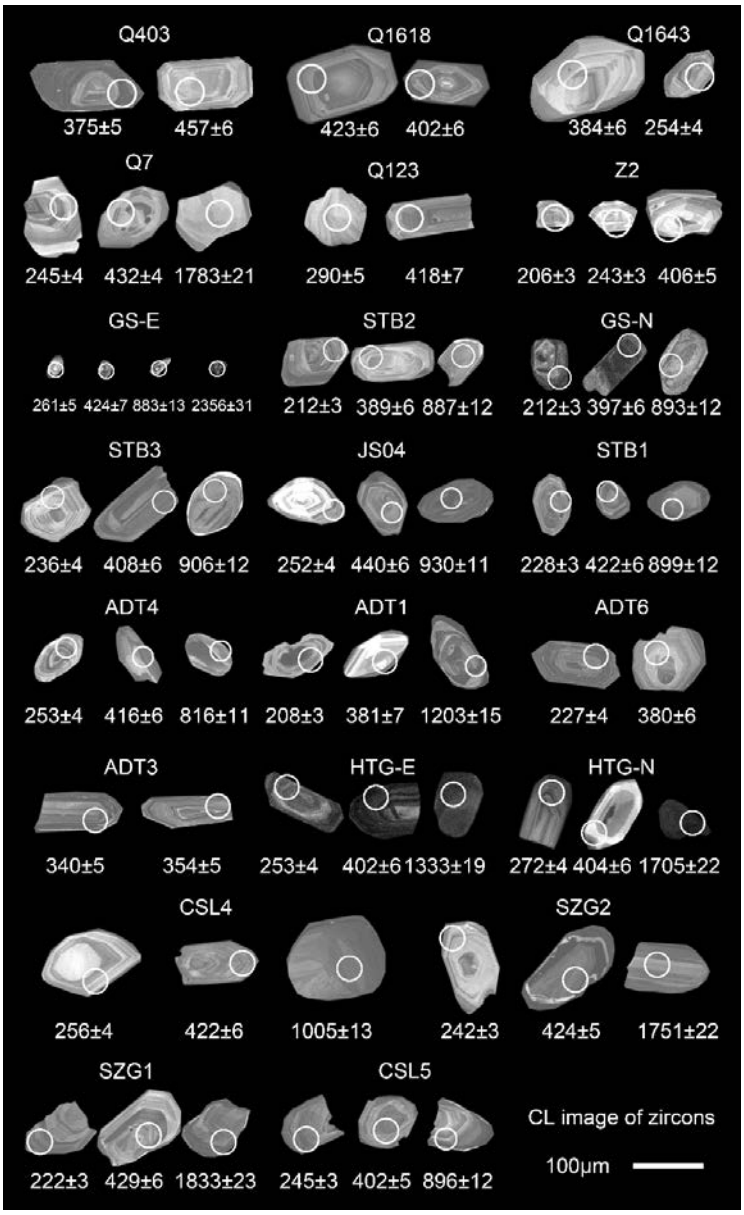

Figure 8. Representative cathodoluminescence (CL) images of detrital zircons from the 22 sandstone

samples. The white circles show the location of the U-Pb analysis spots. Numbers are U-Pb ages in Ma.

2.2.5 Sampling and analytical methods

Over the last decade or so, detrital zircon U-Pb geochronology has evolved into a very powerful provenance tool for reconstructing landscape evolution and tectonics. This is achieved by systematically relating detrital zircon age populations measured on sediments back to the potential source terranes ages (e.g., Fedo et al., 2003; Gehrels et al., 2011; D.D. Liu et al., 2013; Yang et al., 2013, 2014; Gehrels, 2014; F. Cheng et al., 2015). In this study, 22 samples, ranging in stratigraphic age from Paleocene to Quaternary, were collected from the four sections (Figs. 2, 6, and 7). Six samples from the Kunbei section were recovered from well cores. The major characteristics of the samples are briefly described in Table 1.Zircon grains were extracted from each sample following the standard procedures outlined in Yang et al. (2014). This work was conducted at the Chengxin Geology Service Co. Ltd., Langfang, Hebei Province, China. Individual zircon crystals (generally more than 200 grains) were mounted in epoxy resin without handpicking to avoid sampling bias. Samples were then polished to obtain a smooth flat internal surface. Reflected and transmitted light microscopy, as well as cathodoluminescence (CL) imagery, was undertaken to reveal internal heterogeneities and to select internal targets for isotopic dating. The U-Pb dating of zircon was performed on an Agilent 7500a ICP-MS connected to a 193 nm excimer laser-ablation system of an American New Wave UP 193 SS at the China University of Geosciences, Beijing, following the method described by Yang et al. (2014). All samples were analyzed using a laser spot size of 36 mm and a frequency of 10 Hz, except for GS-E, which was analyzed using a laser spot size of 25 mm and a frequency of 5 Hz due to the small grain size. To correct for instrument fluctuations and determine fractionation factors, two standards (Black et al., 2003; Qi et al., 2005) were analyzed every 10–20 grains. Zircons Qinghu and 91500 (Wiedenbeck et al., 1995) were the monitoring standards. For elemental concentration analysis, NIST610 was the external standard, and 29Si was the internal standard. NIST612 and NIST6 14 were used as monitoring standards. GLITTER 4.4 software was used to calculate the U-Pb isotope ratios and element contents (China University of Geosciences, laboratory of Y.S. Liu, Beijing, China). The U-Pb ages obtained were checked for discordance by plotting the analyses on concordia diagrams using the Isoplot 3.0 software (Ludwig, 2003). The common-Pb correction followed the method described by Andersen (2002). Ages younger than ca. 1000 Ma are based on common Pb–corrected $^{206}Pb/^{238}U$ ratios, whereas ages older than ca. 1000 Ma are based on

common Pb–corrected $^{207}Pb/^{206}Pb$ ratios. The U-Pb ages reported are those from analyses that range between 90% and 110% concordance, and reported errors are 1s. A more complete description of sample separation methods and analytical procedures is given in Yuan et al. (2004). Isotopic ages with errors and related raw data are listed in full in Table DR2 (see footnote 1). Representative CL images are provided in Figure 8.

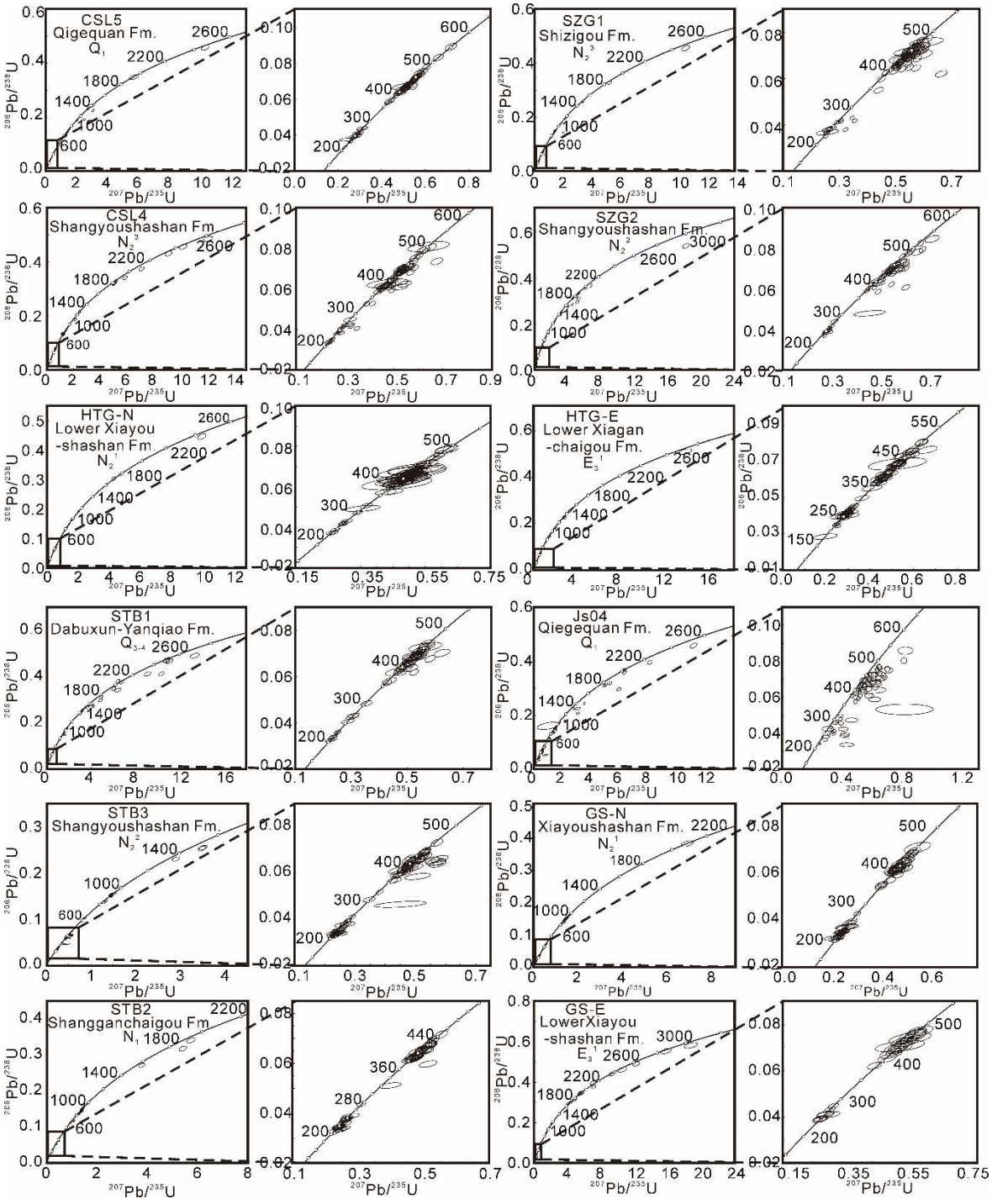

Figure 9. U-Pb concordia diagrams for zircon grains of the samples in the Huatugou and Dongchaishan-Gansen sections.

2.2.6 Results

The various zircon age ranges and the summary statistical data for each sample are shown in Table 1 (Figs. 9–15). Major age groups and their corresponding peak ages have been inferred by visual inspection of the detrital zircon U-Pb age probability plots for all 22 samples (Figs. 10, 11, 13, 14, and 15). A major peak refers to age populations including at least 50% of the total number of data, whereas a minor peak refers to those representing less than 20% of the total number of data.

2.2.6.1 Huatugou section

Sample: HTG-E (Xiaganchaigou Fm., 43.8-37.8 Ma)

The zircon grains are generally large (50 μm ~ 150 μm) with well-preserved euhedral shapes. While a few grains show only faint zoning in CL suggesting a metamorphic origin, more than 90% of the crystals are characterized by relatively distinct oscillatory zoning (Fig. 8) indicating a magmatic origin. The Th/U ratios vary from 0.22 to 1.59, also indicative of a magmatic origin (Corfu et al., 2003; Hanchar and Rudnick, 1995; Hoskin and Black, 2000). Of 100 zircons analyzed, 98 ages have been obtained with discordance degree <10% (Fig. 9). U-Pb ages range from ~2662 Ma to ~181 Ma, with two peaks at ~430 Ma and ~260 Ma. A number of ages are spread between 2662 Ma and 500 Ma with 18% of the data clustering between 1500 Ma and 500 Ma (Fig. 10).

Sample: HTG-N (Xiayoushashan Fm., 22-15.3 Ma)

In this sample, zircon grains show euhedral to abraded shapes with an average size ranging between 80 μm and 200 μm. A large majority of crystals (about 90%) display distinct oscillatory zoning on CL images indicating a magmatic origin (Fig. 8). The Th/U ratios vary from 0.12 to 1.56 again indicating a magmatic origin. Among 100 analyses, 95 yield concordant ages (Fig. 9). U-Pb ages range from ~2378 Ma to ~235 Ma, with a small peak at ~260 Ma, a major peak at ~400 Ma and a possible sub-peak at ~960 Ma (Fig. 10).

Samples: SZG2 and CSL4 (Shangyoushashan Fm., 15.3-8.1 Ma)

Both samples were collected from the Shangyoushashan Fm. Zircon grains show euhedral to abraded shapes with an average size ranging between 50 μm and 250 μm. Most of the crystals (more than 90%) display distinct oscillatory zoning on CL images implying a magmatic origin (Fig. 8). However, like in the previous samples a few grains (less than 10%) show only faint zoning in CL suggesting a metamorphic origin.

For sample SZG2, 100 analyses were performed, providing 90 zircon ages with a discordance degree <10% (Fig. 9) and the Th/U ratios vary from 0.10 to 1.20, with three

exceptions of 0.03 (1473 Ma), 0.04 (637 Ma) and 0.08 (493 Ma), confirming the magmatic origin. U-Pb ages range from ~2019 Ma to ~234 Ma with two peaks at ~440 Ma and ~250 Ma. Some additional ages (less than 20%) are spread between ~1992 Ma and ~523 Ma with a potential sub-peak at ~870 Ma. The number of ages belonging to this last age group appears higher than in the previous samples. In sample CSL4, 95 ages were obtained from 100 analyzed zircon grains (Fig. 9). The Th/U ratios of the detrital zircons mainly vary from 0.11 to 2.00, with four exceptions of 0.03 (413 Ma), 0.06 (906 Ma), 0.08 (960 Ma) and 0.09 (947 Ma), reflecting the largely magmatic origin of the zircons. U-Pb ages range from ~2378 Ma to ~235 Ma, with three peaks at ~880 Ma, ~430 Ma and ~220 Ma. Some ages are again spread from 800 Ma to 1020 Ma (Fig. 10).

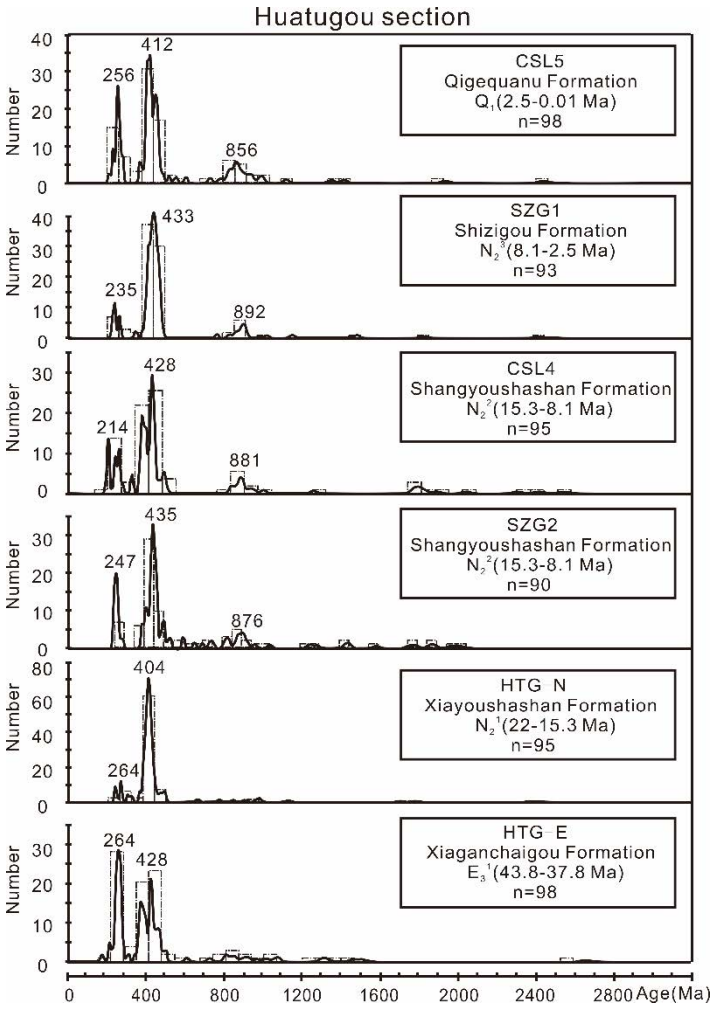

Figure 10. Relative probability plot histograms of U-Pb ages of detrital zircons from the Cenozoic samples in the Huatugou section. The number of zircons is given on the vertical axis (note the change in scale from one sample to the other); the ages, in Ma, are indicated on the horizontal axis.

Sample: SZG1 (Shizigou Fm., 8.1-2.5 Ma)

The zircon grains show euhedral to abraded shapes with an average size ranging between 80 μm and 200 μm. Again, most crystals (more than 90%) display a distinct oscillatory zoning on CL images indicating a magmatic origin. The Th/U ratios vary from 0.14 to 2.15, with two exceptions of 0.03 (440 Ma) and 0.09 (911 Ma), again suggesting a magmatic origin. 93 usable data points were obtained among 100 analyzed zircon grains (Fig. 9). U-Pb ages range from ~2421 Ma to ~222 Ma, with three peaks at ~890 Ma, ~430 Ma and ~240 Ma (Fig. 10).

Sample: CSL5 (Qigequan Fm., 2.5-0.01 Ma)

The zircon crystals are generally large (50 μm ~ 200 μm) with well-preserved euhedral shapes. Again, only a few grains (about 5%) show faint zoning in CL suggesting a metamorphic origin and most crystals display distinct oscillatory zoning characteristic of their magmatic origin (Fig. 8). The Th/U ratios vary from 0.15 to 1.48, with three exceptions of 0.04 (448 Ma), 0.07 (864 Ma) and 0.09 (462 Ma), confirming the predominant magmatic origin of the zircons. Among 100 analyzed zircons, 98 U-Pb ages with discordance degree <10% have been obtained (Fig. 9). U-Pb ages range from ~2430 Ma to ~211 Ma, with two major peaks at ~420 Ma and ~260 Ma and a minor peak at ~860 Ma (Fig. 10).

2.2.6.2 Dongchaishan-Gansen section

Sample: GS-E (Xiaganchaigou Fm., 43.8-37.8 Ma)

The zircon grains morphologies vary from euhedral to abraded with an average size (25 μm ~ 70 μm) distinctly smaller than in any of the other samples. CL images (Fig. 8) show that most of these crystals (more than 90%) are characterized by relatively distinct oscillatory zoning indicating a magmatic origin. Only a few (less than 5%) show faint zoning suggesting a metamorphic origin. This is confirmed by the Th/U ratios that vary between 0.12 and 2.19, with three exception of 0.02 (437 Ma), 0.02 (965 Ma), and 0.05 (985 Ma), and are predominantly higher than 0.10, reflecting that magmatic zircons are in majority (Hoskin and Black, 2000).

Due to the small number of available grains, only 56 zircon crystals were analyzed providing 52 concordant ages (Fig. 9). U-Pb ages range from ~3000 Ma to ~240 Ma, with four distinctive age populations. Two major peaks are at ~450 Ma and ~250 Ma, while a smaller peak at ~890 Ma could be equivalent to the ~850 Ma - ~890 Ma peaks observed in the Huatugou section described above. Finally a number of Proterozoic ages are distributed between 3000 Ma and 1600 Ma (Fig. 11).

Sample: STB2 (Shangganchaigou Fm., 35.2-22 Ma)

In this sample, zircon crystals are large (80 μm ~ 200 μm) with well-preserved euhedral shapes. Most of the crystals (more than 95%) are characterized by a relatively distinct oscillatory zoning in CL images (Fig. 8) implying a magmatic origin. The Th/U ratios vary from 0.12 to 1.03, and are mostly higher than 0.10, confirming the predominantly magmatic origin of the zircons.

Among 100 analyzed crystals, 93 effective ages were obtained (Fig. 9). U-Pb ages range between ~1900 Ma and ~200 Ma, with two major peaks at ~390 Ma and ~220 Ma and one minor peak at ~890 Ma. The proportion of ages older than 1000 Ma is much smaller than in

sample GS-E (Fig. 11).

Sample: GS-N and STB3 (Xiayoushashan Fm., 22-15.3 Ma)

Both samples were collected from the Xiayoushashan Fm. In sample GS-N, the zircon grains have euhedral to abraded shapes and an average size between 40 μm and 100 μm. A large majority of (more than 95%) crystals show a distinct oscillatory zoning in CL images (Fig. 8) indicating a magmatic origin. The Th/U ratios vary from 0.13 to 1.57, again indicating a magmatic source. 100 crystals were analyzed and 97 ages having discordance degree <10% were obtained (Fig. 9). The U-Pb ages range from ~2091 Ma to ~128 Ma (Fig. 11), and can be divided into three populations with two major peaks at ~400 Ma and ~220 Ma, and a minor peak at ~890 Ma. The number of ages older than 1000 Ma is low (less than 5%). A single age at 128 Ma indicates the possibility of a Cretaceous zircon source.

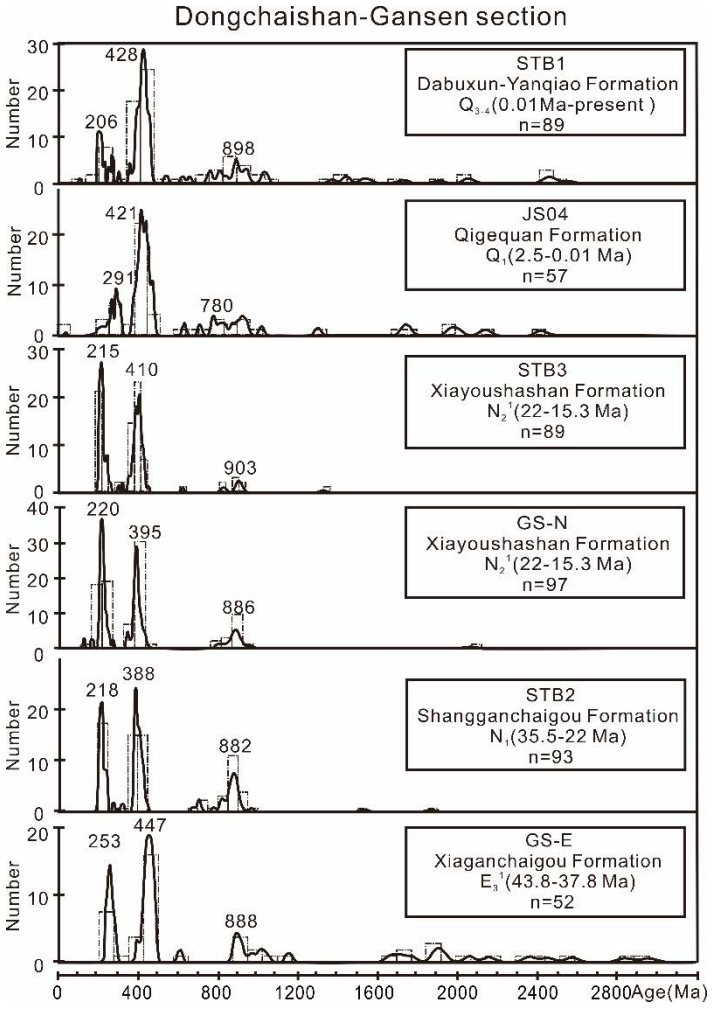

Figure 11. Relative probability plot histograms of U-Pb ages of detrital zircons from the Cenozoic samples in the DongchaishanGansen section (note the change in scale from one sample to the other); the ages, in Ma, are indicated on the horizontal axis.

In sample STB3, the zircon crystals again show euhedral to abraded shapes and an average size between 50 μm and 250 μm. Like in the previous samples most of the crystals (~95%) are of magmatic origin as indicated by distinct oscillatory zoning in CL images (Fig. 8). The Th/U ratios vary from 0.19 to 1.58, confirming the magmatic source. A hundred crystals have been analyzed and 89 yield concordant ages (Fig. 9). U-Pb ages range from ~1350 Ma to ~200 Ma (Fig. 11). The age populations are very similar to the ones observed in

the previous samples, with two major peaks at ~410 Ma and ~215 Ma and a possible minor peak at 900 Ma. Ages older than 1000 Ma are rare.

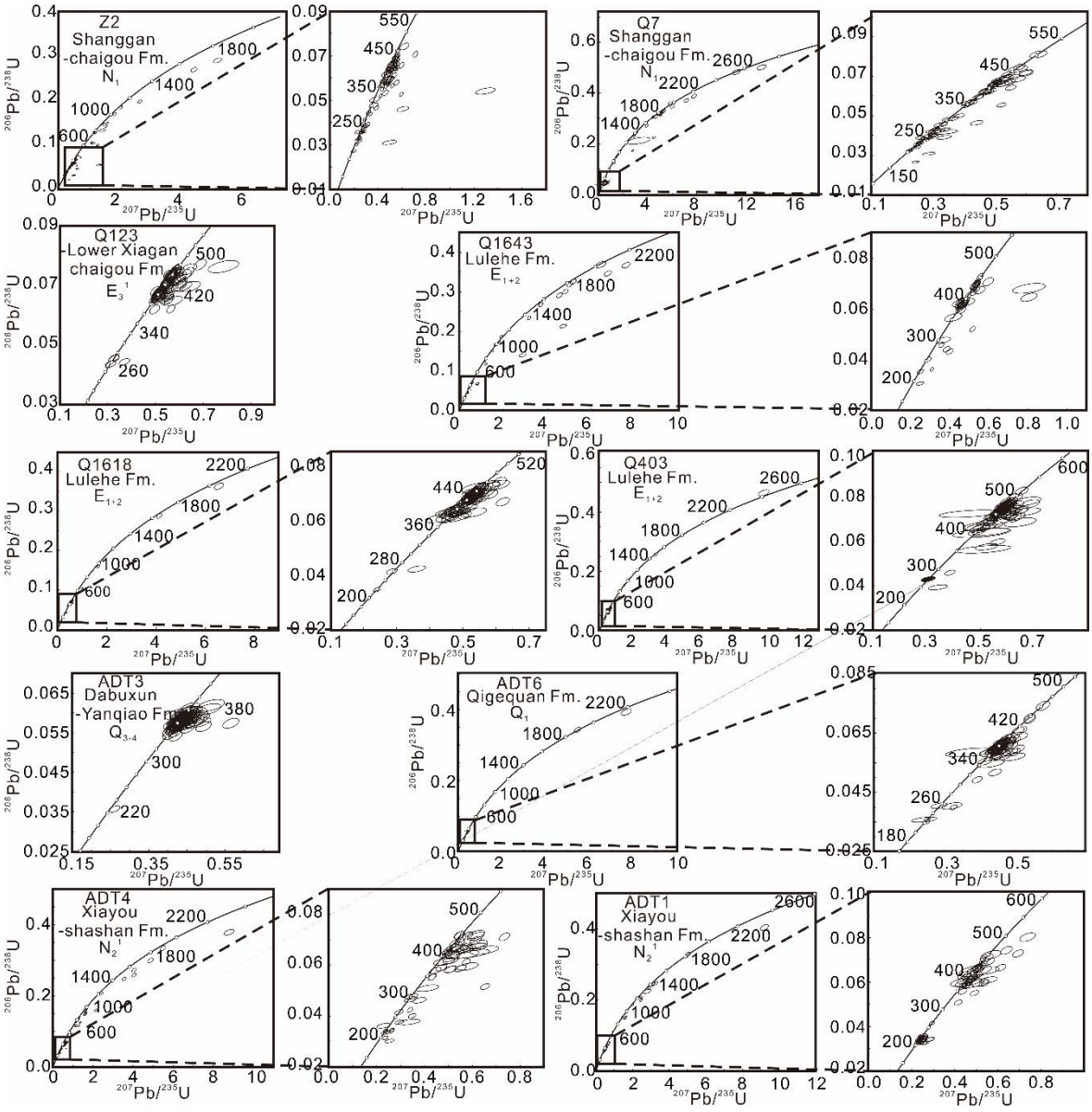

Figure 12. U-Pb concordia diagrams for zircon grains of the samples from the Kunbei and Adatan sections.

Sample: JS04 (Qigequan Fm., 2.5-0.01 Ma)

The zircon crystals display euhedral to abraded shapes for an average size ranging between 50 μm and 200 μm. The majority of the crystals (~95%) display distinct oscillatory zoning in CL images (Fig. 8) indicating a magmatic origin confirmed by Th/U ratios varying between 0.11 and 1.19, with two exceptions of 0.03 (385 Ma) and 0.07 (1828 Ma). Among 100 crystals analyzed, only 57 ages with discordance degree <10% were obtained (Fig. 9). The U-Pb ages range from ~2430 Ma to ~220 Ma (Fig. 11). The ages are distributed in four

groups with two major peaks at ~420 Ma and ~290 Ma, one more restricted peak at ~780 Ma corresponding to a more distributed population and finally a number of ages spread between 2430 Ma and 1200 Ma. A single age of 57 Ma indicates a possible Cenozoic source.

Sample: STB1 (Dabuxun-Yanqiao Fm., 0.01 Ma-present)

In this sample, zircon grains show euhedral to abraded shapes with an average size comprised between 50 μm and 200 μm. Most crystals (more than 90%) are again of magmatic origin as indicated by distinct oscillatory zoning in CL images (Fig. 8) and Th/U ratios varying from 0.10 to 2.15, with one exception of 0.08 (362 Ma). 100 grains were analyzed and 89 effective data points were obtained (Fig. 9). The U-Pb ages range from 2573 Ma to ~109 Ma (Fig. 11). The ages can be separated in four main populations with three peak ages at ~900 Ma, ~430Ma and ~210 Ma. Like in sample JS04 and GS-E a significant number of Proterozoic ages are distributed above 1000 Ma. Finally a single age at 109 Ma is obtained, probably reflecting recycling of a Cretaceous source.

2.2.6.3 Kunbei section

Samples: Q403, Q1618 and Q1643 (Lulehe Fm., 53.5-43.8 Ma)

Three samples were collected from the Lulehe Fm. The zircon grains show euhedral to abraded shapes and an average size between 50 μm and 250 μm. Within all three samples, the majority of the zircons (more than 95%) show distinct oscillatory zoning in CL images indicating a magmatic origin (Fig. 8). Th/U ratios range from 0.29 to 0.96 in samples Q403, from 0.17 to 0.99 in sample Q1618 and from 0.12 to 2.05 in sample Q1643 confirming the magmatic source.

In sample Q403, 84 ages were obtained from 100 analyzed zircon grains (Fig. 12). The U-Pb ages range from ~2459 Ma to ~272 Ma with a single peak at ~470 Ma the few remaining ages being widely distributed (Fig. 13).

In sample Q1618, 96 ages were obtained among 100 analyzed zircon grains (Fig. 12). The U-Pb ages range from ~1994 Ma to ~219 Ma with a single peak at ~430 Ma and some few, widely distributed ages (Fig. 13).

In sample Q1643, due to the small amount of available zircons, only 46 ages were obtained among 62 analyzed grains (Fig. 12). The U-Pb ages range from ~2026 Ma to ~224 Ma with a major peak at ~390 Ma and a potential sub-peak at ~230 Ma (Fig. 13).

Samples: Q123 and Q7 (Xiaganchaigou Fm., 43.8-37.8 Ma)

In these two samples from the Lower Xiaganchaigou Fm., the zircon grains show euhedral to abraded shapes and an average size between 50 μm and 250 μm. Distinct

oscillatory zoning observed in CL images in the majority of the zircons (more than 95%) indicates again a largely magmatic origin (Fig. 8). The Th/U ratios vary from 0.32 to 1.51, with one exception at 0.04 (418 Ma), in sample Q123 and 0.10 to 2.25, with one exception at 0.08 (907 Ma), in sample Q7 confirming the magmatic origin of the crystals.

In sample Q123, 91 ages were obtained among 100 analyzed zircon grains (Fig. 12). This sample displays a narrow range in ages between 472 Ma and 276 Ma (Fig. 13). A major age peak at ~420 Ma is associated to a small sub-peak at ~280 Ma. No Proterozoic ages are observed although we cannot rule out a possible analytical bias (the Proterozoic zircons could be too small or simply badly preserved within the sample).

In sample Q7, 88 ages were obtained from 100 analyzed zircon grains (Fig. 12). The U-Pb ages ranges from ~2621 Ma to ~203 Ma with two major age peaks at ~410 Ma and ~250 Ma (Fig. 13). A sub-peak at ~1780 Ma might be individualized from the widely spread, well-represented Proterozoic age population.

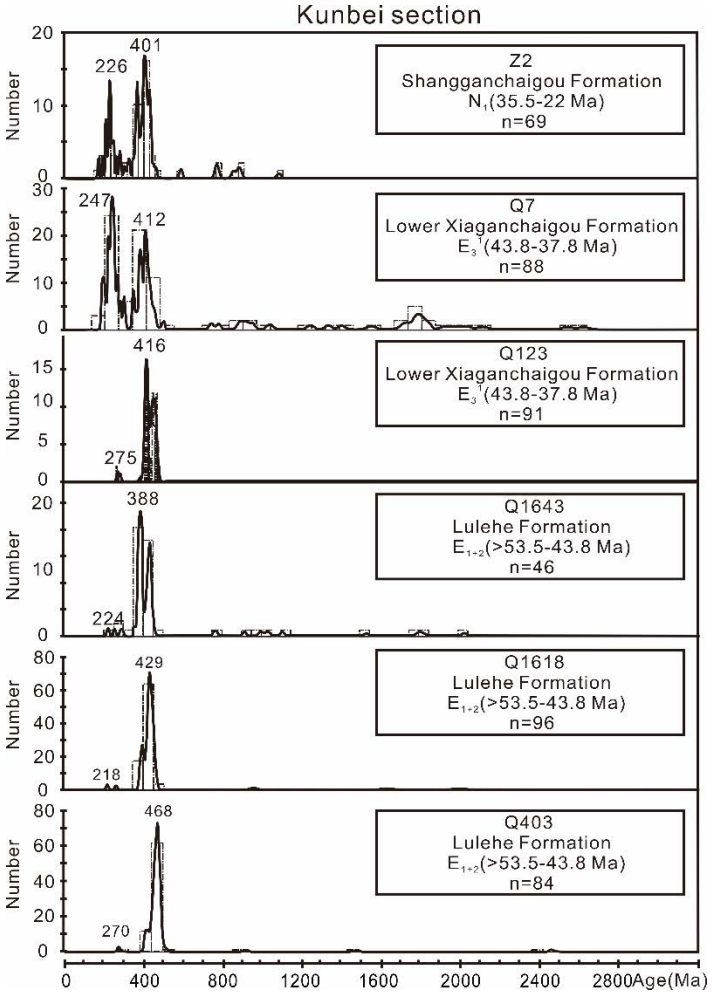

Figure 13. Relative probability plot histograms of U-Pb ages of detrital zircons from the Cenozoic samples in the Kunbei section. The number of zircons is given on the vertical axis (note the change in scale from one sample to the other); the ages, in Ma, are indicated on the horizontal axis

Sample: Z2 (Shangganchaigou Fm., 35.5-22 Ma)

In this sample, zircon grains show euhedral to abraded shapes and an average size between 50 μm and 150 μm. Distinct oscillatory zoning in CL images indicate a magmatic source for a large majority of (~95%) crystals (Fig. 8). The Th/U ratios vary from 0.10 to 1.30 confirming the magmatic source. Ninety-eight crystals have been analyzed and 69 yield

concordant ages (Fig. 12). The U-Pb ages range from ~1086 Ma to ~173 Ma with two major peaks at ~400 Ma and ~230 Ma associated to a potential minor age population around ~770 Ma (Fig. 13).

2.2.6.4 Adatan section

Samples: ADT1 and ADT4 (Xiayoushashan Fm., 22-15.3 Ma)

These two samples were collected from the Xiayoushashan Fm. The zircon grains show euhedral to abraded shapes and an average size between 50 μm and 150 μm. Again, distinct oscillatory zoning in CL images indicates the magmatic origin of most of the crystals (more than 90%) (Fig. 8). The Th/U ratios vary from 0.22 to 2.09, two exceptions of 0.06 (456 Ma) and 0.09 (397 Ma), in sample ADT1 and from 0.18 to 2.45, with two exceptions of 0.02 (442 Ma) and 0.07 (967 Ma), in sample ADT4 confirming the magmatic origin or the zircons.

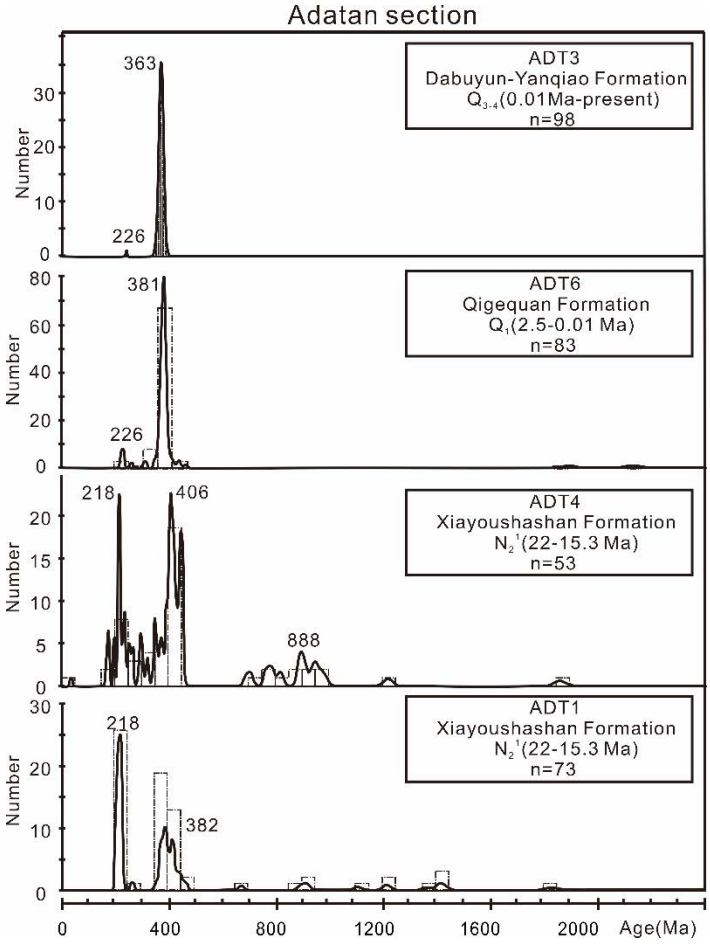

Figure 14. Relative probability plot histograms of U-Pb ages of detrital zircons from the Cenozoic samples in the Adatan section. The number of zircons is given on the vertical axis (note the change in scale from one sample to the other); the ages, in Ma, are indicated on the horizontal axis.

In sample ADT1, 100 crystals were analyzed and yield 73 concordant ages (Fig. 12). The U-Pb ages range from ~1824 Ma to ca. 206 Ma and two major age peaks are individualized at ~380 Ma and ~220 Ma (Fig. 14).

In sample ADT4, among 100 analyses, 51 yield concordant ages (Fig. 12). The U-Pb ages range between ~1857 Ma and ~37 Ma (Fig. 14). Two major peaks are displayed at ~410 Ma and ~220 Ma and a third distinctive small age population is centered around ~890 Ma. A single

age of 37 Ma seems to indicate a Cenozoic source similar to the one suggested by the 57 Ma age in sample JS04 (Dongchaishan-Gansen section).

Sample: ADT6 (Qigequan Fm., 2.5-0.01 Ma)

In this sample from the Qigequan Fm., zircon grains are large (80 μm ~ 250 μm) and show a well-preserved euhedral shape. The magmatic origin of most of the crystals (more than 95%) is indicated by distinct oscillatory zoning in CL images (Fig. 8) and Th/U ratios varying between 0.14 and 1.00. Among 100 analyzed zircons, 83 ages having discordance degree <10% were obtained (Fig. 12). The U-Pb ages ranges from 2133 Ma to 222 Ma, with a major age peak at ~380 Ma and a minor peak around 230 Ma (Fig. 14).

Sample: ADT3 (Dabuxun-Yanqiao Fm., 0.01 Ma-present)

In this sample, the zircon grains show euhedral to abraded shapes and an average size of 100 μm to 200 μm. As in all the other samples, the predominantly (more than 95%) magmatic origin of the crystals is attested by distinct oscillatory zoning in CL images (Fig. 8) and Th/U ratios varying between 0.39 and 1.11. Among 100 analyzed zircons, 98 ages showing discordance degree <10% were obtained (Fig. 12). The U-Pb ages vary from 387 Ma to 226 Ma with a major population around and age peak of ~360 Ma and a single age of 226 Ma (Fig. 14).

2.2.6.5 Summary

The data presented above show that the detrital zircons from the 22 sediment samples ranging in deposition age from Paleocene to Holocene are dominantly of magmatic origin (around 95%). On CL images, most of the Precambrian zircons are characterized by inner cores and outer rings or light zones on the surface (Fig. 8) indicating the occurrence of tectono-magmatic

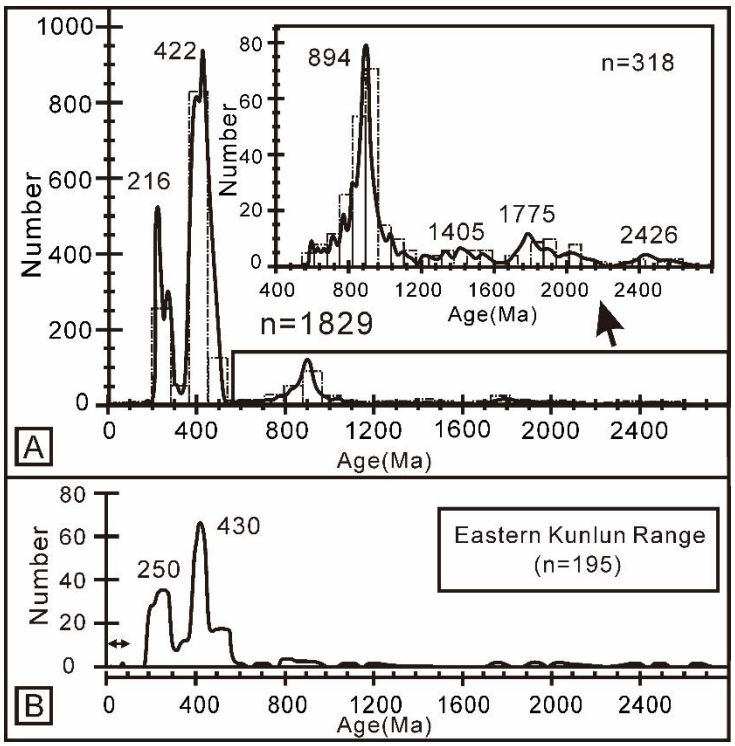

Figure 15. (A) Relative probability plot histograms of U-Pb ages of detrital zircons of the 22 samples. The insert diagram to the right corresponds to the black box in the first diagram. (B) Relative probability plots of granitoid pluton ages in the Eastern Kunlun Range.

hydrothermal events in their source areas. The U-Pb ages vary widely between 2956 Ma and 37 Ma (Fig. 15) and can be statistically divided into five main populations: a Cretaceous – Cenozoic group only represented by a few ages, a late Paleozoic – Mesozoic group, an early-middle Paleozoic group, a late Proterozoic group and finally an early Proterozoic – Archean group. Except for the occurrence of a few Cenozoic – Cretaceous ages and a distinctive late Proterozoic peak, the combined age distribution of the detrital zircons of the 22 samples appears similar to the basement age distribution of the Eastern Kunlun Range characterized by the late Paleozoic – Mesozoic and early-middle Paleozoic peaks (Figs. 3 and 15). However, the age distributions in each individual sample are variable. As the Eastern Kunlun Range, the Qilian Shan Range and the Altyn Tagh Range provided numerous Paleozoic basement zircon U-Pb ages, the early Paleozoic age peak observed in all the analyzed samples is not distinctive of a specific source area. In contrast, the Altyn Tagh and the Qilian Shan ranges display only a very small number of late Paleozoic – early Mesozoic ages that are characteristic of the Eastern Kunlun Range. Similarly, Cretaceous ages are only found in the Tula Uplift, in the western part of the Eastern Kunlun Range, in the Hoh Xil basin or further south in the Qiangtang and Lhasa terranes. Cenozoic and Quaternary volcanic rocks have been recognized and dated using $^{40}Ar/^{39}Ar$ and U-Pb zircon geochronology on rocks inside the Eastern Kunlun Range and to the south in the Hoh Xil basin and Qiangtang block (Pearce and Mei, 1988; Jolivet et al., 2003; Q. Wang et al., 2008; Xia et al., 2011; Staisch et al., 2014). However, no Cenozoic or Cretaceous zircon U-Pb ages have been reported from the Altyn Tagh Range or the Qilian Shan. Consequently, the distinctive late Paleozoic – early Mesozoic ages, as well as the limited number of Cretaceous and Cenozoic ages represented in the U-Pb age spectra can be used to fingerprint the source area of the Cenozoic sediments in order to explore the source to sink relations between the South Qaidam basin and the Eastern Kunlun Range.

2.2.7 Discussion

2.2.7.1 Pre-Paleocene exhumation of the Eastern Kunlun Range

Low temperature thermochronology studies suggested that the uplift of the Eastern Kunlun Range was initiated during late Eocene to early Oligocene times (Jolivet et al., 2001; Yuan et al., 2003, 2006; A. Wang et al., 2006; Clark et al., 2010; Dai et al., 2013; Duvall et al., 2013). This age is coeval with the age of initiation of crustal shortening along the southern margin of the Qaidam basin as inferred from published growth-strata analysis within the basin (Yin et al., 2008b; L. Wang et al., 2010). In addition, paleocurrent studies along the northern

margin of the Hoh Xil basin show that during the Eocene, paleorivers were flowing northward with a unidirectional dispersal pattern suggesting an absence of significant positive topography in the Eastern Kunlun Range area (Yi et al., 2008). This direction gradually switched eastwards during the Oligocene and Yi et al. (2008) interpreted this variation as due to the uplift of the Eastern Kunlun Range during the late Paleogene.

However, using detailed petrological analysis of core samples obtained from the Lulehe Fm. in the SQB, we have identified numerous angular carbonate fragments (containing abundant foraminifera) within the Paleocene strata (Fig. 7G and 7H). Foraminifera are generally found in marine environments (Rohling et al., 1998), although some have been found in salt lakes (Cann et al., 1981). However, while ostracoda, sporopollen and algae have been described in the Paleocene deposits of the Lulehe Fm., foraminifera have never been found within the Paleocene series of the southwestern Qaidam basin (QBGMR, 1991; QIGS, 2004; Xia et al., 2012; Ke et al., 2013). Paleocene strata in the southwestern Qaidam basin are characterized by coarse-grained detrital sediments corresponding to braided river to deltaic sediment facies (Xia et al., 2001; Meng and Fang, 2008; Yin et al., 2008b; Gong et al., 2012; Fu et al., 2013; C. Zhang et al., 2013) an environment that does not allow the development of foraminifera. These newly-identified foraminifera-bearing carbonate fragments found in the Paleocene Lulehe Fm. are therefore derived from a pre-Cenozoic source containing foraminifera. As they dissolve rapidly, carbonate fragments are generally not transported over long distances (Zuffa, 1980; Mack and Rasmussen, 1984). This then suggests a relatively proximal source area for the clasts preserved within the Lulehe Fm. In addition, the Carboniferous strata, exposed south of the Kunbei section (Fig. 2), consist mainly of biomicrite, biosparite, and bioclastic littoral to neritic limestones containing abundant brachiopods, coral, gastropods and foraminifera (QIGS, 2004). Thus, the carbonate fragments contained in the Paleocene Lulehe Fm. of the Kunbei section are most probably sourced from the foraminifera-rich Carboniferous sequences of the Qimen Tagh Range forming the western segment of the Eastern Kunlun Range (QIGS, 2004). This inference has the corollary that the basement of the Eastern Kunlun Range had already been exposed prior to the Paleocene, providing material for the Qaidam basin. Furthermore, a newly-acquired seismic profile in the northern flank of the Eastern Kunlun Range (Fig. 3) shows a discordance level separating the Mesozoic series from the Paleocene - Eocene deposits (Lulehe Fm.), possibly indicating a pre-Paleocene exhumation of the Eastern Kunlun Range as well.

Our new finding pushes back the onset time of the Eastern Kunlun Range uplift from Eocene/Oligocene (Jolivet et al., 2001; Yuan et al., 2003; A. Wang et al., 2006; Yuan et al.,

2006; Yin et al., 2007; Yin et al., 2008b; Clark et al., 2010; Dai et al., 2013; Duvall et al., 2013) to pre-Paleocene. With regard to the pre-Paleocene exhumation of the Eastern Kunlun Range, the northern Tibetan Plateau, over 1000 km away from the locus of the India – Eurasia collision front, had already been deformed or partially uplifted before the India – Eurasia collision occurred around ~50 Ma (e.g. Dupont-Nivet et al., 2010).

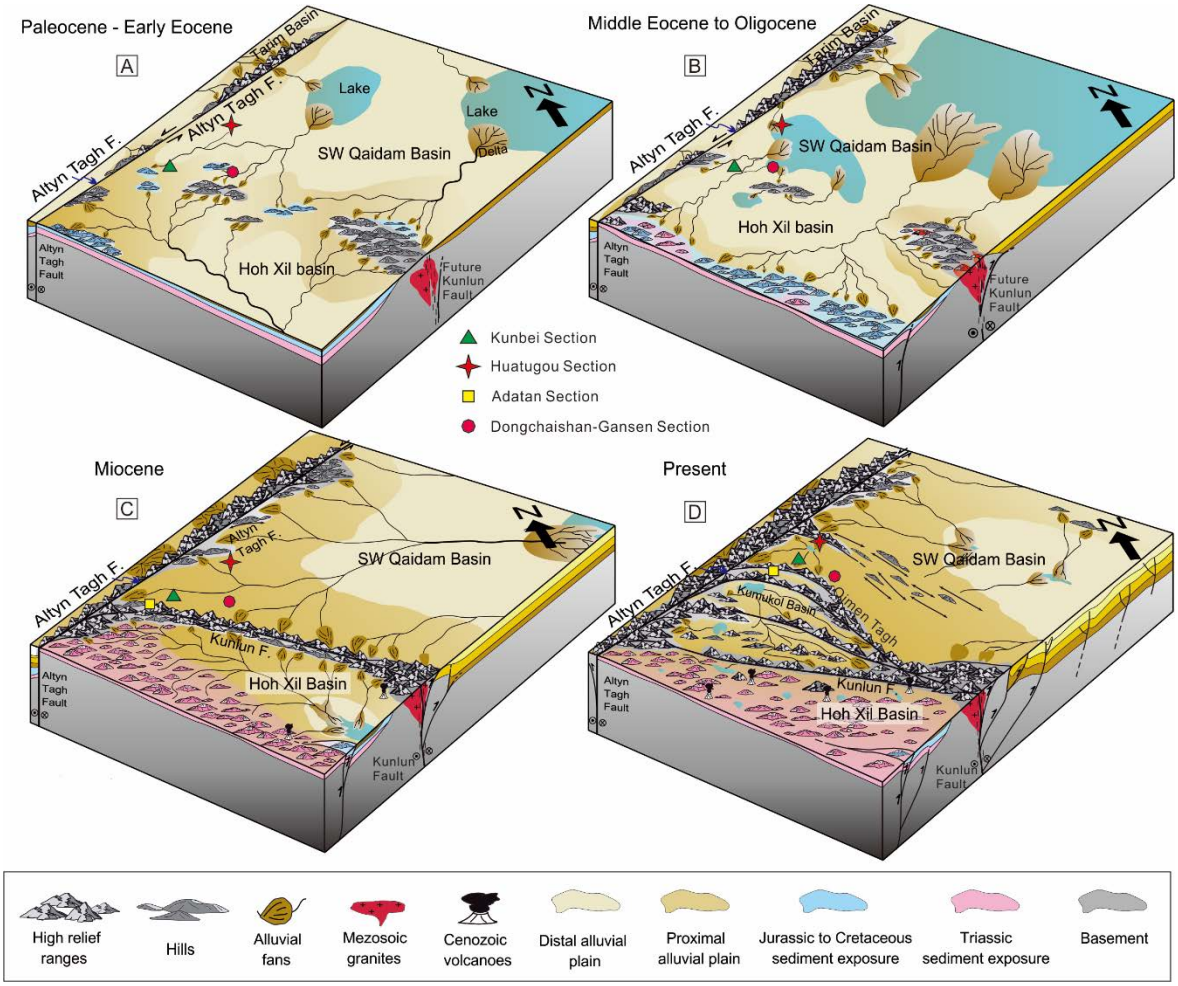

Figure 16. (A) Paleocene to early Eocene tectonic configuration of the Qaidam Basin. The Eastern Kunlun Range had already uplifted, separating the paleo–Qaidam Basin in the north from the North Qiangtang and Bayan Har terranes to the south. The Qaidam Basin is characterized by small lakes with limited extent during this period. (B) Middle Eocene to Oligocene tectonic configuration of the Qaidam Basin. During this period, the scope of the Qaidam Basin expanded southward with water getting deeper. The southward-expanding Qaidam Basin may have locally inundated the Eastern Kunlun Range and connected with the Kumukol Basin or even the Hoh Xil Basin to the south. (C–D) Miocene to present tectonic configuration of the Qaidam Basin. The scope of the basin narrowed, with water getting gradually shallower during this period. Note that intense Miocene uplifting of the Eastern Kunlun Range separated the Qaidam Basin and Hoh Xil Basin. The Eastern Kunlun Range and the Altyn Tagh Range had already been largely denudated, forming the major two provenance areas for the sediments deposited in the South Qaidam Basin.

2.2.7.2 Cenozoic source to sink relationship between the South Qaidam basin and the Eastern Kunlun Range

2.2.7.2.1 Paleocene - Early Eocene (Lulehe Fm.)

The fluvial deposits of the Lulehe Fm. are only exposed in the western Qaidam basin and pinch out eastward (Meng and Fang, 2008; Yin et al., 2008b). Sediment facies, sediment petrology and heavy minerals data obtained in the Kunbei area indicate that this formation most probably reflects rapid accumulation of clastic sediments along the front of a gradually uplifting topography in the Eastern Kunlun Range (this study; Xia et al., 2001; Gong et al., 2012; Wu et al., 2012; Fu et al., 2013). The zircon U-Pb age distributions in samples Q403, Q1618 and Q1643 are simple, mostly characterized by a major early Paleozoic age peak (Fig. 13). Only sample Q1643 shows a significant - although low - number (less than 5%) of Mesozoic and Proterozoic ages. The lack of Mesozoic ages in the spectra implies a source to the south either from the Mesozoic granites in the Eastern Kunlun and Qiangtang basement, or from recycled Mesozoic sediments in the Hoh Xil basin (Figs. 5 and DR1 [see footnote 1]). However, the effective absence of significant Proterozoic ages in the samples rules out a contribution from the Qiangtang – Lhasa and Hoh Xil sources. Similarly, no sediment seem to be derived from the Altyn Tagh or the Qilian Shan ranges, which is consistent with the occurrence of a depocenter in the central part of the basin (e.g. Meng and Fang, 2008; Yin et al., 2008b). Finally, the ZTR index variation from heavy mineral analysis (Gong et al., 2012; Fu et al., 2013), coupled with the occurrence of carbonate pebbles in the Lulehe Fm., suggests that the basement of the Eastern Kunlun Range was already acting as a significant sediment source feeding the SQB from the Paleocene (Fig. 16A). However, the lack of obvious growth strata in the Paleocene to early Eocene deposits of the SQB suggests that tectonic uplift in the Eastern Kunlun Range was limited at that time (Figs. 3, 4 and 16A).

Our new data contradict to some extent the Paleo-Qaidam model of Yin et al. (2008b) which suggests that, during the Paleocene, the Qaidam, Kumukol and Hoh Xil basins were forming a single, wide depression between the Qilian Shan to the north and the Fenghuo Shan to the south. This interpretation was based on the similarity of Paleocene to Eocene sedimentary features within these three basins (Fig. 1). This model prompted several attempts to reassess the tectonic processes affecting the northern edge of the Tibetan plateau (e.g. Jian et al., 2013; Cheng et al., 2014; Mao et al., 2014). However, the Paleo-Qaidam hypothesis is mostly based on the similarities between the Paleocene and Eocene depositional environments and sediment facies in the three basins. As proposed in Figure 16A, similar depositional

environments may have developed contemporaneously in the three basins without implying a unique drainage system between the SQB and the other two basins to the south. The slowly growing Eastern Kunlun Range was probably shedding sediments northward and southward but as suggested by the unimodal distribution of zircon ages in the Lulehe Fm. (Fig. 13), the SQB was not receiving sediments from the Qiangtang – Lhasa and Hoh Xil region.

2.2.7.2.2 Middle Eocene – Oligocene (Xiaganchaigou Fm. to Shangganchaigou Fm.)

Compared with the Paleocene – early Eocene Lulehe Fm., the middle Eocene Xiaganchaigou Fm. is largely distributed throughout the basin and source rocks are well-developed in the western Qaidam basin, indicating a general widening of the basin (Jin et al., 2002; Pang et al., 2004; Chen et al., 2008; Meng and Fang, 2008; Yin et al., 2008b; Mao et al., 2014). This is further attested by the southward migration of the depocenter in the SQB from the Paleocene to Oligocene (Meng and Fang, 2008; Yin et al., 2008b; Mao et al., 2014) and the southward successive onlaps of the Eocene and Oligocene deposits from our newly-acquired seismic profile (Fig. 3). A clear retrogradational trend is observed in the three sections (Kunbei, Huatugou and Dongchaishan-Gansen), from alluvial to shallow lake depositional environments in the middle Eocene Xiaganchaigou Fm. to the mostly lacustrine environments of the Oligocene Shangganchaigou Fm. (Fig. 6). Previous studies, using core and log analyses, revealed that the central part of the basin was occupied by widespread, probably deep lake environments characterized by dark mudstones and limestones (e.g. Xia et al., 2001).

In the Kunbei section, sample Q123 from the lowermost Xiaganchaigou Fm. (Fig. 13) shows a detrital zircon age distribution pattern identical to that of the lower part of the Lulehe Fm. (samples Q403 and Q1618). Proterozoic ages that were identified in sample Q1643 (upper Lulehe Fm.) are not found in sample Q123. Sample Q7 (Kunbei section), GS-E (Dongchaishan-Gansen section) and HTG-E (Huatugou section), collected slightly above sample Q123 in the Xiaganchaigou Fm. display a significant change in the age distribution pattern: the minor Mesozoic age peak that was nearly negligible in the previous samples becomes major and the proportion and number of Proterozoic to Archean ages increases significantly, especially in sample Q7 (Fig. 13). The appearance of a strong Mesozoic component (e.g. ~20% of the total amount of ages in sample Q7) in the sediments of the Lower Xiaganchaigou Fm. represents the main characteristic of the whole dataset. The occurrence of a large lake in the central part of the basin (e.g. Xia et al., 2001; Fig. 16B) most probably prevented sediments from coming from the Qilian Shan. Furthermore, the north-directed paleocurrents measured in the Eocene deposits of the Huatugou section implies that the source

region should be located south of the all four sections. The early Proterozoic and Archean zircons observed in the Eocene and Oligocene samples can then only be derived from the Eastern Kunlun Range, the Qiangtang – Lhasa region or the Hoh Xil basin. As recently shown by Dai et al. (2012), numerous potential sources for the early Proterozoic and Archean ages are exposed in the Qiangtang block to the south and were incorporated into the Mesozoic sediments (Fig. 5D). The southward progradation of the Eocene – Oligocene sediments (Fig. 3A) and the general widening of the Qaidam basin suggest that part of the slowly growing topography in the Eastern Kunlun Range was buried back during the Eocene. This sediment progradation might have allowed some connection between the Qaidam basin and the Hoh Xil and Kumukol basins to the south, providing routes for material eroded in the Qiangtang region to reach the SQB (Fig. 16B). Although limited early Proterozoic and Archean sources exist in the Eastern Kunlun Range, most of the Precambrian zircons observed in the Xiaganchaigou Fm. were thus probably derived from Triassic and Jurassic deposits eroded from the uplifting range or from the Hoh Xil basin to the south (Fig. 16B). Recycling of the Triassic series might explain the absence of the middle Mesozoic to early Cenozoic ages observed in the Qiangtang – Lhasa and Hoh Xil sediments.

Low temperature thermochronology studies suggested a late Eocene to Oligocene uplift and exhumation in the ranges surrounding the Qaidam basin. Paleocene – Eocene exhumation has been recorded by apatite fission track data and $^{40}Ar/^{39}Ar$ thermochronology data in the Altyn Tagh Range (e.g. Jolivet et al., 2001; Sobel et al., 2001) and in the Eastern Kunlun Range (e.g. Mock et al., 1999; Jolivet et al., 2001). On a larger scale, the uplift of the Tibetan plateau is assumed to have been initiated in the Eocene or late Paleocene (e.g. DeCelles et al., 2007; C. Wang et al., 2008; Dai et al., 2012). This is consistent with the Paleocene topographic barrier implied by our data between the Hoh Xil – Kumukol basins and the SQB during the Paleocene. However, the widening of the Qaidam basin and the re-establishment of connections between the three basins during the Eocene suggest that the relief in the Eastern Kunlun Range was still low enough to be occasionally buried back, possibly during periods of increased sedimentation rate (Fig. 16B).

The age distributions of samples Z2 (Kunbei section, Fig. 13) and STB2 (Dongchaishan-Gansen section, Fig. 11) from the Oligocene Shangganchaigou Fm. are similar to that of the Eocene Lower Xiaganchaigou Fm. However, the middle and early Proterozoic – Archean ages are absent, indicating a change in the source regions that most probably became restricted to the Eastern Kunlun Range basement (including the Mesozoic granites). This implies in turn that the Hoh Xil and Kumukol basins were again disconnected from the SQB during the

Oligocene. Uplift of the Eastern Kunlun Range during the Oligocene is also indicated by the clear increase in sedimentation rates observed on the seismic profiles (Figs. 3 and 4). In addition, published apatite (U-Th)/He and fission track basement ages in the Eastern Kunlun Range indicate rapid cooling and exhumation between 35 to 20 Ma (Jolivet et al., 2001, 2003; Liu et al., 2005; Clark et al., 2010; Duvall et al., 2013). Due to the poor exposure of the Shangganchaigou Fm. in the Kunbei and Dongchaishan-Gansen sections, no paleocurrent information is available for the southern sections. However, in the Huatugou section, the paleoflows direction from NNE to SSE, indicates relief building in the Altyn Tagh Range that became a significant sediment source at least for this northernmost section.

Our data thus confirm that the Oligocene is a key period in the tectonic evolution of North Tibet: the limited deformation that prevailed since at least the Paleocene, leading to a slowly growing topography in the Eastern Kunlun Range, was replaced by active exhumation and significant construction of topography. The connections that developed between the Qaidam, Kumukol and Hoh Xil basins during the Eocene had definitely ended in the late Oligocene.

2.2.7.2.3 Miocene to Present phase (Xiayoushashan Fm. to Dabuxun-Yanqiao Fm.)

As seen in the Miocene Xiayoushashan Fm., the sediment coarsened upward, gradually changing from shallow lacustrine facies to alluvial and fluvial facies (Fig. 6). Miocene active tectonic deformation has been demonstrated around the Qaidam basin, both in the Qilian Shan, Eastern Kunlun and Altyn Tagh ranges (e.g. Jolivet et al., 2001, 2003; Yuan et al., 2003; C. Wang et al., 2006; Fu and Awata, 2007; Yin et al., 2007, 2008a, 2008b; Zhang et al., 2012). The basin progressively shrunk, its depocenter shifting eastwards, and its southern edge migrating northward due to intense tectonic deformation in the Eastern Kunlun Range (Meng and Fang, 2008; Yin et al., 2008b; Mao et al., 2014). Rapid uplift of the Eastern Kunlun Range is implied by the development of growth strata in the early Miocene Xiayoushashan Fm. (Figs. 3 and 4). Throughout the Miocene and up to the present, these growth strata are associated with a series of unconformities along the northern flank of the Eastern Kunlun Range and the southern flank of the Altyn Tagh Range (e.g. Yin et al., 2007, 2008b; Y.D. Wang et al., 2010, L. Wang et al., 2010; Cheng et al., 2014; Wu et al., 2014).

In the Dongchaishan-Gansen section, the early Miocene (Xiayoushashan Fm., GS-N, STB3) zircon age population pattern remains similar to the Oligocene pattern except for the relative increase in Mesozoic ages (e.g., the percentage of Mesozoic grains increases from ~7.7% in sample GS-E to 42.7% in sample GS-N) and the corresponding decrease in Proterozoic ages (e.g., the percentage of Precambrian grains decreases from ~42.3% in sample

GS-E to 19.1% in sample GS-N) (Fig. 11). The similar signal seen in the Adatan section (samples ADT1 and ADT4, Fig. 14) seems to indicate that, by the early Miocene, the source area for the whole SQB was largely homogeneous and situated within the Eastern Kunlun Range. The Miocene uplift of the Eastern Kunlun Range is also registered by changes in the paleocurrent directions both in the SQB and in the Hoh Xil basin (e.g. Hertz et al., 2005; Yi et al., 2008). The generally northward paleoflow directions in the early Miocene deposits of the Dongshaishan-Gansen section indicate that the Eastern Kunlun Range formed a positive topography at this time (Fig. 6). The single Cretaceous age observed in sample GS-N (Fig. 11) is difficult to interpret. It could either represent material from the Tula Uplift (Fig. 1), west of the Qaidam basin (Robinson et al., 2003), or more probably from recycling of pre-Miocene sediments that contain some late Mesozoic volcanic zircons derived from the Lhasa or Qiangtang blocks. Similarly, the Eocene zircon age observed in sample ADT4 from the Adatan section (Fig. 14) is likely to be derived from the Cenozoic volcanics exposed further south on the northern edge of the Qiangtang block (e.g. Jolivet et al., 2003; Ding et al., 2007). This indicates that while the Eastern Kunlun Range were being actively uplifted, the wide drainage system prevailing during the Eocene – Oligocene was not yet completely destroyed and that some rivers still connected the SQB to the south and west across the range. In the Huatugou section, the proportion of Mesozoic zircon ages largely decreases (from 32.7% in Eocene sample HTG-E to 8.4% in sample Miocene HTG-N) compared to the Paleozoic ages. This is consistent with an increased denudation in the Altyn Tagh Range (Jolivet et al., 1999, 2001) and southward-directed paleocurrents (Fig. 6) which would bring a higher proportion of Paleozoic ages with respect to the Mesozoic ones derived from the Eastern Kunlun Range.

The middle and upper Miocene series (Shangyoushashan and Shizigou Formations) have only been sampled in the Huatugou section. The Shangyoushashan Fm. corresponds to a second major tectonically driven change in the sedimentary environment of the SQB with the disappearance of major deep lakes and the eastward migration of the depocenters (e.g. Wang et al., 2006c; Yin et al., 2008b). Detrital zircon age distributions in samples SZG2, CSL4 and SZG1, with a minor but consistent Mesozoic age peak, indicate a mixed source between the Eastern Kunlun Range (most probably the growing Qimen Tagh Range) and the Altyn Tagh Range.

The Pliocene to Holocene detrital zircon U-Pb ages distributions in both the Huatugou and Dongchaishan-Gansen sections are complex and correspond in part to a mixture between sources in the basement of the Eastern Kunlun Range and the Altyn Tagh Range, but also to recycling of earlier Cenozoic or even Mesozoic sediments exhumed in the surrounding ranges

and inside the basin (Figs. 2, 10 and 11). This is demonstrated by the occurrence of Cretaceous and Paleocene ages in the Pleistocene and Holocene deposits of the Dongchaishan-Gansen section (Fig. 11). By that time, this section was isolated both from the Tula Uplift to the west and from the northern Qiangtang margin to the south by the topographically prominent Eastern Kunlun Range. The Pliocene rapid uplift and exhumation is recorded by magnetostratigraphy and sedimentology studies in the western Qaidam basin (e.g. W. Zhang et al., 2013) and the detrital zircon U-Pb age distributions registered in the Dongchaishan-Gansen (see samples JS04 and STB1 in the Fig. 11) is similar to that of modern river sands (Li et al., 2013) suggesting are similar drainage pattern from Pliocene to the present day. The unimodal zircon age distributions from the Pleistocene and the Holocene strata in the Adatan valley (samples ADT6 and ADT3) suggest that the valley-range landform in the Qimen Tagh Range formed around the Pleistocene isolating the Adatan valley from the Mesozoic zircon sources to the south. By that time, the extension of the drainage system became limited and sediment sources were limited to the locally exposed Paleozoic basement. Since the Miocene, the Qaidam basin narrowed with lake-water depth becoming gradually shallower. The Eastern Kunlun Range and the Altyn Tagh Range were being exhumed, forming the major two provenance areas for the sediments deposited in the SQB (Fig. 16C and 16D). The Qaidam basin and the depressions to the south (Kumukol and Hoh Xil basins) were no longer connected.

To summarize, the Cenozoic topographic evolution of the southern edge of the Qaidam basin can generally be separated in three main phases: 1) a pre-Paleocene exhumed Eastern Kunlun Range served as the source area for the SQB and separated the SQB from the Hoh Xil basin to the south from the Paleocene to the early Eocene; 2) southward widening of the SQB locally buried the Eastern Kunlun Range and connected the basin with the Hoh Xil basin to the south from the late Eocene to Oligocene; 3) intense uplift of the Eastern Kunlun Range since the Miocene limited the connection between the SQB and the Hoh Xil basin. The multiple-pulse growth of the Eastern Kunlun Range reflects a complex deformation history of the Tibetan plateau rather than a monotonous northwards stepwise growth process as previously proposed (e.g. Métivier et al., 1998; Tapponnier et al., 2001). Furthermore, although detrital zircons chronology has been proven to be an important tool for provenance and geodynamic studies (e.g. Fedo et a., 2003; Gehrels, 2014), our new interpretation on the pulsed growth process (multiple denudation and burial phases) for the Eastern Kunlun Range and the subtle variation of drainage connections between the Qaidam basin and Hoh Xil basin alert us to be cautious when dealing with the detrital zircon ages alone. A comprehensive integration of the detrital zircon age spectra, subsurface seismic profiles, petrographical

features, strata isopach maps, paleocurrents direction, as well as thermochronology data from the potential sources (e.g. fission track ages, $^{40}Ar/^{39}Ar$ ages, and (U-Th)/He ages) is critical when trying to decipher the nature of source to sink relations in regions with a complex growth history.

2.2.8 Conclusions

The twenty two detrital zircon U-Pb ages population spectra (including six core samples from Paleogene strata), the newly identified foraminifera-bearing carbonate debris from the Paleocene strata, and the newly-acquired seismic profiles in the SQB presented in this work bring important new constraints on the onset of uplift in the Eastern Kunlun Range and on the source to sink relations between the Qaidam basin and the Eastern Kunlun Range.

The carbonate debris which contains foraminifera in the Paleocene conglomerate sequences, the appearance of a wide population of Paleozoic to late Proterozoic U-Pb ages on detrital zircon from Paleocene strata, and the discordance level separating the Mesozoic series from the Paleocene – early Eocene deposits observed in the seismic profile strongly suggest that the Eastern Kunlun Range basement was locally exhumed prior to the Paleocene and that the Mesozoic sediment cover had been at least partially removed.

The topographic evolution of the southern edge of the Qaidam basin can be separated in three main phases: 1) the onset of exhumation in the Eastern Kunlun Range initiated during or possibly before the deposition of the Paleocene Lulehe Fm. Erosion only affected the existing Mesozoic cover and the Paleozoic basement without eroding the Mesozoic granitoids and the Precambrian basement. The South Qaidam basin was already separated from the Hoh Xil basin to the south; 2) during the middle Eocene to Oligocene, the Qaidam basin widened towards the south and east. However, during the widening of the basin, uplift and erosion in the Eastern Kunlun Range were still active and probably increased over time leading to the exhumation of the Mesozoic granitoids. The occurrence of numerous early Proterozoic and Archean zircon U-Pb ages suggests that at least local connections remained between the Qaidam basin and the Hoh Xil and Kumukol basins through the growing Eastern Kunlun Range; 3) from the Miocene to present, the topography of the Eastern Kunlun Range and the Altyn Tagh Range increased, progressively enclosing the Qaidam basin. The Eastern Kunlun Range formed the main source for the sediments deposited in the SQB while in the Huatugou area, materials were derived from both the Altyn Tagh and Eastern Kunlun ranges. During the Pliocene to Present, an increasing amount of sediment recycling occurred, leading to complex detrital zircon U-Pb age distributions. The present-day valley-range landform in the Qimen Tagh

Range developed around the Pleistocene. This multiple-pulsed growth history of the Eastern Kunlun Range and the SQB in turn reminds us to be cautious when dealing with detrital zircon ages. It is important to integrate all the available detrital zircon age spectra, subsurface seismic profiles, petrographic features, strata isopach maps, paleocurrents direction, and thermochronology data of potential source to try and decipher the sources to sink relation in regions with complex growth history.

Acknolegdements

This work was supported by the National Science & Technology Major Project of China (Grant ZX05003) and the China Scholarship Council Chinese-French Egide Cai Yuanpei program (N° 32393WL, 2014). M. Jolivet was also supported by the Darius program, and the French Centre National de la Recherche Scientifique (CNRS), Institut National des Sciences de l'Univers (INSU) Syster program. We gratefully acknowledge the assistance of Dr. Ruiying Chen, Qinyang Meng, Suping Zhou, Xiangjiang Yu, Xiang Cheng and Tuo Zhang during field work. We particularly thank Li Su of the Geological Lab Center, China University of Geosciences (Beijing), for her help during detrital zircon analysis, and to Bo Zhang (Peking University) for his help with cathodoluminescence (CL) imaging. We gratefully acknowledge Yan Chen, Chuanwu Wang, Qiquan Zhang and Shihu Fang for their helpful suggestions on Cenozoic evolution of the Qaidam basin. Kerry Gallagher is thanked for his help with the English writing. We are grateful to the Science Editor Christian Koeberl, the Associate Editor An Yin, the referee Franz Neubauer and an anonymous reviewer, who provided constructive feedback that helped improving the manuscript.

References Cited

Andersen, T., 2002, Correction of common lead in U-Pb analyses that do not report 204Pb: Chemical Geology, v. 192, no. 1, p. 59-79, doi: 10.1016/S0009-2541(02)00195-X.

Black, L. P., Kamo, S. L., Allen, C. M., Aleinikoff, J. N., Davis, D. W., Korsch, R. J., and Foudoulis, C., 2003, TEMORA 1: a new zircon standard for Phanerozoic U-Pb geochronology: Chemical Geology, v. 200, no. 1, p. 155-170, doi: 10.1016/S0009-2541(03)00165-7.

Bovet, P. M., Ritts, B. D., Gehrels, G., Abbink, A. O., Darby, B., and Hourigan, J., 2009, Evidence of Miocene crustal shortening in the north Qilian Shan from Cenozoic stratigraphy of the western Hexi Corridor, Gansu Province, China: American Journal of Science, v. 309, no. 4, p. 290-329, doi: 10.2475/00.4009.02.

Cann, J. H., and De Deckker, P., 1981, Fossil Quaternary and living foraminifera from

athalassic (non-marine) saline lakes, southern Australia: Journal of Paleontology, p. 660-670.

Chen, X. H., Yin, A., Gehrels, G. E., Cowgill, E. S., Grove, M., Harrison, T. M., and Wang, X. F., 2003, Two phases of Mesozoic north-south extension in the eastern Altyn Tagh range, northern Tibetan Plateau: Tectonics, v. 22, no. 5, p. 1053, doi: 10.1029/2001TC001336.

Chen, Z. H., Hu, S. Y., Jin, Z. J., Pang, X. Q., Jiang, Z. X., and Kirk, O. G., 2008, Exploration risk evaluation using object-based modeling, an example from the Tertiary fractured play, western Qaidam Basin of China: Petroleum Science, v. 5, no. 3, p. 195-202, doi: 10.1007/s12182-008-0031-3.

Chen, X., Gehrels, G., Yin, A., Li, L., and Jiang, R. B., 2012, Paleozoic and Mesozoic Basement Magmatisms of Eastern Qaidam Basin, Northern Qinghai-Tibet Plateau: LA-ICP-MS Zircon U-Pb Geochronology and its Geological Significance: Acta Geologica Sinica - English Edition, v. 86, no. 2, p. 350-369, doi: 10.1111/j.1755-6724.2012.00665.x.

Cheng, F., Jolivet, M., Fu, S., Zhang, Q., Guan, S., Yu, X., and Guo, Z., 2014, Northward growth of the Qimen Tagh Range: A new model accounting for the Late Neogene strike-slip deformation of the SW Qaidam Basin: Tectonophysics, v. 632, p. 32-47, doi: 10.1016/j.tecto.2014.05.034.

Cheng, F., Guo, Z., Jenkins, H.S., Fu, S., and Cheng, X., 2015a, Initial rupture and displacement on the Altyn Tagh fault, northern Tibetan Plateau: Constraints based on residual Mesozoic to Cenozoic strata in the western Qaidam Basin: Geosphere, v. 11, no. 3, doi: 10.1130 /GES01070.1.

Cheng, X., Fu, S., Wang, H., Yu, X., Cheng, F., Liu, R., Du, W., and Guo, Z., 2015b, Geometry and kinematics of the Arlar strike-slip fault, SW Qaidam basin, China: New insights from 3-D seismic data: Journal of Asian Earth Sciences, v. 98, no. 0, p. 198-208, doi: 10.1016/j.jseaes.2014.09.039.

Clark, M. K., Farley, K. A., Zheng, D., Wang, Z., and Duvall, A. R., 2010, Early Cenozoic faulting of the northern Tibetan Plateau margin from apatite (U-Th)/He ages: Earth and Planetary Science Letters, v. 296, no. 1, p. 78-88, doi:10.1016/j.epsl.2010.04.051.

Corfu, F., Hanchar, J. M., Hoskin, P. W., and Kinny, P., 2003, Atlas of zircon textures: Reviews in mineralogy and geochemistry, v. 53, no. 1, p. 469-500, doi: 10.2113/0530469.

Cowgill, E., Yin, A., Harrison, T. M., and Wang, X., 2003, Reconstruction of the Altyn Tagh fault based on U-Pb geochronology: Role of back thrusts, mantle sutures, and heterogeneous crustal strength in forming the Tibetan Plateau: Journal of Geophysical Research, v. 108, no. B7, p. 2346, doi: 10.1029/2002JB002080.

Dai, J. G., Zhao, X. X., Wang, C. S., Zhu, L. D., Li, Y. L., and Finn, D., 2012, The vast proto-

Tibetan Plateau: New constraints from Paleogene Hoh Xil Basin: Gondwana Research, v. 22, no. 2, p. 434-446, doi:10.1016/j.gr.2011.08.019.

Dai, J., Wang, C., Hourigan, J., and Santosh, M., 2013, Multi-stage tectono-magmatic events of the Eastern Kunlun Range, northern Tibet: Insights from U–Pb geochronology and (U–Th)/He thermochronology: Tectonophysics, v. 599, p. 97-106, doi: 10.1016/j.tecto.2013.04.005.

DeCelles, P. G., Quade, J., Kapp, P., Fan, M., Dettman, D. L., and Ding, L., 2007, High and dry in central Tibet during the late Oligocene: Earth and Planetary Science Letters, v. 253, no. 3, p. 389-401, doi: 10.1016/j.epsl.2006.11.001.

Ding, L., Kapp, P., Yue, Y., and Lai, Q., 2007, Postcollisional calc-alkaline lavas and xenoliths from the southern Qiangtang terrane, central Tibet: Earth and Planetary Science Letters, v. 254, no. 1, p. 28-38, doi:10.1016/j.epsl.2006.11.019.

Ding, L., Yang, D., Cai, F. L., Pullen, A., Kapp, P., Gehrels, G. E., Zhang, L. Y., Zhang, Q. H., Lai, Q. Z., Yue, Y. H., and Shi, R. D., 2013, Provenance analysis of the Mesozoic Hoh-Xil-Songpan-Ganzi turbidites in northern Tibet: Implications for the tectonic evolution of the eastern Paleo-Tethys Ocean: Tectonics, v. 32, no. 1, p. 34-48, doi: 10.1002/tect.20013.

Ding, L., Xu, Q., Yue, Y., Wang, H., Cai, F., and Li, S., 2014, The Andean-type Gangdese Mountains: Paleoelevation record from the Paleocene-Eocene Linzhou Basin: Earth and Planetary Science Letters, v. 392, p. 250-264, doi: 10.1016/j.epsl.2014.01.045.

Dupont-Nivet, G., Lippert, P. C., Van Hinsbergen, D. J. J., Meijers, M. J. M., and Kapp, P., 2010, Palaeolatitude and age of the Indo–Asia collision: palaeomagnetic constraints: Geophysical Journal International, v. 182, no. 3, p. 1189-1198, doi: 10.1111/j.1365-246X.2010.04697.x.

Duvall, A. R., Clark, M. K., van der Pluijm, B. A., and Li, C., 2011, Direct dating of Eocene reverse faulting in northeastern Tibet using Ar-dating of fault clays and low-temperature thermochronometry: Earth and Planetary Science Letters, v. 304, no. 3-4, p. 520-526, doi: 10.1016/j.epsl.2011.02.028.

Duvall, A. R., Clark, M. K., Kirby, E., Farley, K. A., Craddock, W. H., Li, C., and Yuan, D.Y., 2013, Low-temperature thermochronometry along the Kunlun and Haiyuan Faults, NE Tibetan Plateau: Evidence for kinematic change during late-stage orogenesis: Tectonics, v. 32, no. 5, p. 1190-1211, doi:10.1002/tect.20072, 2013.

England, P., and Houseman, G., 1989, Extension during continental convergence, with application to the Tibetan Plateau: Journal of Geophysical Research: Solid Earth (1978–2012), v. 94, no. B12, p. 17561-17579, doi: 10.1029/JB094iB12p17561.

Fang, X., Zhang, W., Meng, Q., Gao, J., Wang, X., King, J., Song, C., Dai, S., and Miao, Y., 2007, High-resolution magnetostratigraphy of the Neogene Huaitoutala section in the eastern Qaidam Basin on the NE Tibetan Plateau, Qinghai Province, China and its implication on tectonic uplift of the NE Tibetan Plateau: Earth and Planetary Science Letters, v. 258, no. 1-2, p. 293-306, doi:10.1016/j.epsl.2007.03.042.

Fedo, C. M., Sircombe, K. N., and Rainbird, R. H., 2003, Detrital zircon analysis of the sedimentary record: Reviews in mineralogy and geochemistry, v. 53, no. 1, p. 277-303, doi: 10.2113/0530277.

Fu, B. H., and Awata, Y., 2007, Displacement and timing of left-lateral faulting in the Kunlun Fault Zone, northern Tibet, inferred from geologic and geomorphic features: Journal of Asian Earth Sciences, v. 29, no. 2, p. 253-265, doi:10.1016/j.jseaes.2006.03.004.

Fu, S. T., Xu, L. G., Gong, Q. L., and Lv, Y. S., 2010, Petroleum Geologic Characteristics of Southwestern Qaidam Basin and Recommendations for Further Exploration and Study: Petroleum Geology, v. 1, p. 6-10 (in Chinese with English abstract).

Fu, L., Guan, P., Zhao, W. Y., Wang, M., Zhang, Y., Lu, J. W., 2013, Heavy mineral feature and provenance analysis of Paleogene Lulehe Formation in Qaidam Basin: Acta Petrologica Sinica, v. 29, no. 8, p 2867-2875 (in Chinese with English abstract).

Graham, S. A., Chamberlain, C. P., Yue, Y., Ritts, B. D., Hanson, A. D., Horton, T. W., Waldbauer, J. R., Poage, M. A., and Feng, X., 2005, Stable isotope records of Cenozoic climate and topography, Tibetan plateau and Tarim basin: American Journal of Science, v. 305, no. 2, p. 101-118, doi: 10.2475/ajs.305.2.101.

Gao, J., Li, S., Dai, S., Li, A., and Peng, Y., 2009, Constraints of tectonic evolution in provenance from detrital zircon fission-track data of Cenozoic strata of Xichagou district in western Qaidam basin: Journal of Lanzhou University (Natural Sciences), v. 3, p. 1-7 (in Chinese with English abstract).

Gehrels, G. E., Yin, A., and Wang, X. F., 2003a, Detrital-zircon geochronology of the northeastern Tibetan plateau: Geological Society of America Bulletin, v. 115, no. 7, p. 881-896, doi: 10.1130/0016-7606(2003)115<0881:DGOTNT>2.0.CO;2 .

Gehrels, G. E., Yin, A., and Wang, X. F., 2003b, Magmatic history of the northeastern Tibetan Plateau: Journal of Geophysical Research, v. 108, no. B9, p. 2423, doi: 10.1029/2002JB001876.

Gehrels, G., Kapp, P., DeCelles, P., Pullen, A., Blakey, R., Weislogel, A., Ding, L., Guynn, J., Martin, A., and McQuarrie, N., 2011, Detrital zircon geochronology of pre-Tertiary strata in the Tibetan-Himalayan orogen: Tectonics, v. 30, no. 5, p. TC5016,

doi:10.1029/2011TC002868.

Gehrels, G., 2014, Detrital Zircon U-Pb Geochronology Applied to Tectonics: Annual Review of Earth and Planetary Sciences, v. 42, no. 1, p. 127-149, doi: 10.1146/annurev-earth-050212-124012.

Gong, Q. S., Shou, J. F., Huang, G. P., Li, S. M., and Wang, Y. Q., 2012, Sedimentary characteristic of braided delta in Lulehe Formation of Kunbei oilfield in Qaidam Basin: Chinese Journal of Geology, v. 47, no. 1, p. 116-128 (in Chinese with English abstract).

Guo, J. J., and Li, H. K., 1999, Angular Unconformity between the Huashishan Group and Huangzhong Group in the Eastern Mid-Qilian Massif: Identification and Implications: Progress In Precambrian Research, v. 22, no. 2, p. 47-52 (in Chinese with English abstract).

Hanchar, J., and Rudnick, R., 1995, Revealing hidden structures: the application of cathodoluminescence and back-scattered electron imaging to dating zircons from lower crustal xenoliths: Lithos, v. 36, no. 3, p. 289-303, doi: 10.1016/0024-4937(95)00022-4.

Hertz, M., Ritts, B., Bovet, P., and Kent-Corson, M., 2005, Qimen Tagh Uplift Constrained From Tectonostratigraphy of Southwest Qaidam Basin, Northern Tibet Plateau, China: Eos Trans. AGU, 86(52), Fall Meet. Suppl., Abstract T41A-1276.

Hoskin, P., and Black, L., 2000, Metamorphic zircon formation by solid-state recrystallization of protolith igneous zircon: Journal of metamorphic Geology, v. 18, no. 4, p. 423-439, doi:10.1046/j.1525-1314.2000.00266.x.

Hough, B. G., Garzione, C. N., Wang, Z., Lease, R. O., Burbank, D. W., and Yuan, D., 2011, Stable isotope evidence for topographic growth and basin segmentation: Implications for the evolution of the NE Tibetan Plateau: Geological Society of America Bulletin, v. 123, no. 1-2, p. 168-185, doi: 10.1130/B30090.1.

Huang, H., Huang, Q., and Ma, Y., 1996, Geology of Qaidam Basin and its petroleum prediction, Beijing, Geological Publishing House, 257 p (in Chinese).

Huo, G. M., 1990, Petroleum geology of China: Oil fields in Qianghai and Xizang, Chinese Petroleum Industry Press, Beijing, 483 p (in Chinese with English abstract).

Jian, X., Guan, P., Zhang, W., and Feng, F., 2013, Geochemistry of Mesozoic and Cenozoic sediments in the northern Qaidam basin, northeastern Tibetan Plateau: Implications for provenance and weathering: Chemical Geology, v. 360, p. 74-88, doi: 0.1016/j.chemgeo.2013.10.011.

Jin, Q., Zha, M., Liu, Z., Gao, X. Z., Peng, D. H., and Lin, L. M., 2002, Geology and Geochemistry of source rocks in the Qaidam Basin, NW CHina: Journal of Petroleum Geology, v. 25, no. 2, p. 219-238, doi: 10.1111/j.1747-5457.2002.tb00005.x.

Jolivet, M., Roger, F., Arnaud, N., Brunel, M., Tapponnier, P., and Seward, D., 1999, Histoire de l'exhumation de l'Altun Shan: indications sur l'âge de la subduction du bloc du Tarim sous le système de l'Altyn Tagh (Nord Tibet): Comptes Rendus de l'Académie des Sciences-Series IIA-Earth and Planetary Science, v. 329, no. 10, p. 749-755, doi: 10.1016/S1251-8050(00)88495-5.

Jolivet, M., Brunel, M., Seward, D., Xu, Z., Yang, J., Roger, F., Tapponnier, P., Malavieille, J., Arnaud, N., and Wu, C., 2001, Mesozoic and Cenozoic tectonics of the northern edge of the Tibetan plateau: fission-track constraints: Tectonophysics, v. 343, no. 1-2, p. 111-134, doi: 10.1016/S0040-1951(01)00196-2.

Jolivet, M., Brunel, M., Seward, D., Xu, Z., Yang, J., Malavieille, J., Roger, F., Leyreloup, A., Arnaud, N., and Wu, C., 2003, Neogene extension and volcanism in the Kunlun Fault Zone, northern Tibet: New constraints on the age of the Kunlun Fault: Tectonics, v. 22, no. 5, p. 1052, doi: 10.1029/2002TC001428.

Jolivet, M., Roger, F., Xu, Z. Q., Paquette, J. L., and Cao, H., 2015, Mesozoic–Cenozoic evolution of the Danba dome (Songpan Garzê, East Tibet) as inferred from LA-ICPMS U–Pb and fission-track data: Journal of Asian Earth Sciences, v. 102, p. 180-204, doi: 10.1016/j.jseaes.2015.02.009.

Kapp, P., Yin, A., Manning, C. E., Harrison, T. M., Taylor, M. H., and Ding, L., 2003, Tectonic evolution of the early Mesozoic blueschist-bearing Qiangtang metamorphic belt, central Tibet: TECTONICS, v. 22, no. 4, p. 1043, doi: 10.1029/2002TC001383.

Kapp, P., Yin, A., Harrison, T. M., and Ding, L., 2005, Cretaceous-Tertiary shortening, basin development, and volcanism in central Tibet: Geological Society of America Bulletin, v. 117, no. 7-8, p. 865-878, 10.1130/B25595.1.

Kapp, P., DeCelles, P. G., Gehrels, G. E., Heizler, M., and Ding, L., 2007, Geological records of the Lhasa-Qiangtang and Indo-Asian collisions in the Nima area of central Tibet: Geological Society of America Bulletin, v. 119, no. 7-8, p. 917-933, doi: 10.1130/B26033.1.

Ke, X., Ji, J., Zhang, K., Kou, X., Song, B., and Wang, C., 2013, Magnetostratigraphy and Anisotropy of Magnetic Susceptibility of the Lulehe Formation in the Northeastern Qaidam Basin: Acta Geologica Sinica-English Edition, v. 87, no. 2, p. 576-587, doi: 10.1111/1755-6724.12069.

Kent-Corson, M. L., Ritts, B. D., Zhuang, G., Bovet, P. M., Graham, S. A., and Chamberlain, C. P., 2009, Stable isotopic constraints on the tectonic, topographic, and climatic evolution of the northern margin of the Tibetan Plateau: Earth and Planetary Science Letters, v. 282, no. 1, p. 158-166, doi: 10.1016/j.epsl.2009.03.011.

Kidd, W. S. F., and Molnar, P., 1988, Quaternary and active faulting observed on the 1985 Academia Sinica--Royal society geotraverse of Tibet: Philosophical Transactions of the Royal Society of London. Series A, Mathematical and Physical Sciences, v. 327, p. 337-363, doi: 10.1098/rsta.1988.0133.

Kirby, E., Harkins, N., Wang, E., Shi, X., Fan, C., and Burbank, D., 2007, Slip rate gradients along the eastern Kunlun fault: Tectonics, v. 26, no. 2, TC2010, doi: 10.1029/2006TC002033.

Leier, A. L., Kapp, P., Gehrels, G. E., and DeCelles, P. G., 2007, Detrital zircon geochronology of Carboniferous–Cretaceous strata in the Lhasa terrane, Southern Tibet: Basin Research, v. 19, no. 3, p. 361-378, doi: 10.1111/j.1365-2117.2007.00330.x.

Li, X. H., Su, L., Chung, S. L., Li, Z. X., Liu, Y., Song, B., and Liu, D. Y., 2005, Formation of the Jinchuan ultramafic intrusion and the world's third largest Ni-Cu sulfide deposit: Associated with the~825 Ma south China mantle plume?: Geochemistry, Geophysics, Geosystems, v. 6, no. 11, p. Q11004, doi:10.1029/2005GC001006.

Li, W., Neubauer, F., Liu, Y. J., Genser, J., Ren, S. M., Han, G. Q., and Liang, C. Y., 2013, Paleozoic evolution of the Qimantagh magmatic arcs, Eastern Kunlun Mountains: constraints from zircon dating of granitoids and modern river sands: Journal of Asian Earth Sciences, v.77, 183-202, doi: 10.1016/j.jseaes.2013.08.030.

Lin, A., and Guo, J., 2008, Nonuniform Slip Rate and Millennial Recurrence Interval of Large Earthquakes along the Eastern Segment of the Kunlun Fault, Northern Tibet: Bulletin of the Seismological Society of America, v. 98, no. 6, p. 2866-2878, doi: 10.1785/0120070193.

Liu, Y. J., Genser, J., Neubauer, F., Jin, W., Ge, X. H., Handler, R., and Takasu, A., 2005, $^{40}Ar/^{39}Ar$ mineral ages from basement rocks in the Eastern Kunlun Mountains, NW China, and their tectonic implications: Tectonophysics, v. 398, no. 3-4, p. 199-224, doi: 10.1016/j.tecto.2005.02.007.

Liu, Y. H., Mo, X. X., Yu, X. H., Zhang, X. T. and Xu, G. W., 2006. Zircon SHRIMP U-Pb dating of the Jingren granite, Yemaquan region of the east Kunlun and its geological significance: Acta Petrologica Sinica, v. 22, no. 10, doi: 10.3321/j.issn:1000-0569.2006.10.006 (in Chinese with English abstract).

Liu, L., Zhang, A., Chen, D., Yang, J., Luo, J., and Wang, C., 2007, Implications Based on LA-ICP-MS Zircon U-Pb Ages of Eclogite and Its Country Rock from Jianggalesayi Area, Altyn Tagh, China: Earth Science Frontiers, v. 14, no. 1, p. 98-107, doi: 10.1016/S1872-5791(07)60004-9.

Liu, L., Wang, C., Chen, D., Zhang, A., and Liou, J., 2009, Petrology and geochronology of HP-UHP rocks from the South Altyn Tagh, northwestern China: Journal of Asian Earth

Sciences, v. 35, no. 3, p. 232-244, doi: 10.1016/j.jseaes.2008.10.007.

Liu, D. D., Jolivet, M., Yang, W., Zhang, Z. Y., Feng, C., Zhu, B., and Guo, Z. J., 2013a, Latest Palaeozoic-Early Mesozoic basin-range interactions in South Tian Shan (Northwest China) and their tectonic significance: Constraints from detrital zircon U-Pb ages: Tectonophysics, v. 599, no. 25, p. 197-213, doi: 10.1016/j.tecto.2013.04.018.

Liu, L., Cao, Y. Y., Chen, D. L., Zhang, C. L., Yang, W. Q., Kang, L., and Liao, X. Y., 2013b, New progresses on the HP-UHP metamorphism in the South Altyn Tagh and the North Qinling: Chin Sci Bull, v. 58, p. 2113-2123 (in Chinese).

Long, X., Yuan, C., Sun, M., Kröner, A., and Zhao, G., 2014, New geochemical and combined zircon U–Pb and Lu–Hf isotopic data of orthogneisses in the northern Altyn Tagh, northern margin of the Tibetan plateau: Implication for Archean evolution of the Dunhuang Block and crust formation in NW China: Lithos, v. 200–201, p. 418-431, doi: 10.1016/j.lithos.2014.05.008.

Lu, H., and Xiong, S., 2009, Magnetostratigraphy of the Dahonggou section, northern Qaidam Basin and its bearing on Cenozoic tectonic evolution of the Qilian Shan and Altyn Tagh Fault: Earth and Planetary Science Letters, v. 288, no. 3, p. 539-550, doi:10.1016/j.epsl.2009.10.016.

Lu, S. N., Wang, H. C., Li, H. K., Yuan, G. B., Xin, H. T., and Zhen, J. K., 2002, Redefinition of the "Dakendaban Group" on the northern margin of the Qaidam Basin: Geological Bulletin of China, v. 21, no. 1, p. 19-23 (in Chinese with English abstract).

Lu, S. N., and Yuan, G. B., 2003, Geochronology of early Precambrian magmatic activities in Aketasdhtage, east Altyn Tagh: Journal of Acta Geologica Sinica, v. 77, no. 1, p. 61-68 (in Chinese with English abstract).

Lu, S. N., Li, H. K., Zhang, C. L., and Niu, G. H., 2008, Geological and geochronological evidence for the Precambrian evolution of the Tarim Craton and surrounding continental fragments: Precambrian Research, v. 160, no. 1, p. 94-107, doi:10.1016/j.precamres.2007.04.025.

Ludwig, K. R., 2003, User's manual for Isoplot 3.0: a geochronological toolkit for Microsoft Excel: Berkeley, California, Berkeley Geochronology Center. Center Special Publication no. 4, 70 p.

Mack, G. H., and Rasmussen, K. A., 1984, Alluvial-fan sedimentation of the Cutler Formation (Permo-Pennsylvanian) near Gateway, Colorado: Geological Society of America Bulletin, v. 95, no. 1, p. 109-116, doi: 10.1130/0016-7606(1984)95<109:ASOTCF>2.0.CO;2.

Mao, L. G., Xiao, A. C., Wu, L., Li, B. L., Wang, L. Q., Lou, Q. Q., Dong, Y. P., and Qin, S. H., 2014, Cenozoic tectonic and sedimentary evolution of southern Qaidam Basin, NE Tibetan

Plateau and its implication for the rejuvenation of Eastern Kunlun Mountains: Science China Earth Sciences, v.57, p.2726-2739, doi: 10.1007/s11430-014-4951-z.

Meng, Q. R., and Fang, X., 2008, Cenozoic tectonic development of the Qaidam Basin in the northeastern Tibetan Plateau: Geological Society of America Special Papers, v. 444, p. 1-24, doi: 10.1130/2008.2444(01).

Métivier, F., Gaudemer, Y., Tapponnier, P., and Meyer, B., 1998, Northeastward growth of the Tibet plateau deduced from balanced reconstruction of two depositional areas: The Qaidam and Hexi Corridor basins, China: Tectonics, v. 17, no. 6, p. 823-842, doi: 10.1029/98TC02764.

Menold, C. A., 2006, Tectonic and metamorphic evolution of the North Qaidam ultrahigh-pressure metamorphic terrane, Western China [Ph.D. thesis]: University of California, Los Angeles, 261 p.

Meyer, B., Tapponnier, P., Bourjot, L., Metivier, F., Gaudemer, Y., Peltzer, G., Shunmin, G., and Zhitai, C., 1998, Crustal thickening in Gansu‐Qinghai, lithospheric mantle subduction, and oblique, strike‐slip controlled growth of the Tibet plateau: Geophysical Journal International, v. 135, no. 1, p. 1-47, doi: 10.1046/j.1365-246X.1998.00567.x.

Mock, C., Arnaud, N. O., and Cantagrel, J. M., 1999, An early unroofing in northeastern Tibet? Constraints from 40 Ar/39 Ar thermochronology on granitoids from the eastern Kunlun range (Qianghai, NW China): Earth and Planetary Science Letters, v. 171, no. 1, p. 107-122, doi: 10.1016/S0012-821X(99)00133-8.

Pang, X. Q., Li, Y. X., and Jiang, Z. X., 2004, Key geological controls on migration and accumulation for hydrocarbons derived from mature source rocks in Qaidam Basin: Journal of Petroleum Science and Engineering, v. 41, no. 1–3, p. 79-95, doi: 10.1016/S0920-4105(03)00145-1.

Pearce, J. A., and Mei, H. J., 1988, Volcanic rocks of the 1985 Tibet geotraverse: Lhasa to Golmud: Philosophical Transactions of the Royal Society of London. Series A, Mathematical and Physical Sciences, v. 327, no. 1594, p. 169-201, doi: 10.1098/rsta.1988.0125.

Pei, J., Sun, Z., Wang, X., Zhao, Y., Ge, X., Guo, X., Li, H., and Si, J., 2009, Evidence for Tibetan plateau uplift in Qaidam basin before Eocene-Oligocene boundary and its climatic implications: Journal of Earth Science, v. 20, p. 430-437, doi: 10.1007/s12583-009-0035-y.

QBGMR, 1991, Regional Geology of Qinghai Province, Beijing, Geological Publishing House, 662 p (in Chinese).

Qi, C., Li, X., Liang, X., Liu, Y., and Tu, X., 2005, High-precision measurement of Hf isotopic reference values for the U-Pb geochronology standard zircons by multi-collector inductively coupled plasma-mass spectrometry: Journal of Chinese Mass Spectrometry Society, v. 26, no.

3, p. 149-154 (in Chinese with English abstract).

Qinghai Institude of Geological Surevey (QIGS), 2004, Introduction of geological map of Kulangmiqiti area: Qinghai Insititute of Geological Survey, Xining, scale 1:250000, 1 sheet (in Chinese).

Qiu, N. S., 2002, Tectono-thermal evolution of the Qaidam Basin, China: evidence from Ro and apatite fission track data: Petroleum Geoscience, v. 8, no. 3, p. 279-285, doi: 10.1144/petgeo.8.3.279.

Quade, J., Breecker, D. O., Daëron, M., and Eiler, J., 2011, The paleoaltimetry of Tibet: An isotopic perspective: American Journal of Science, v. 311, no. 2, p. 77-115, doi:10.2475/02.2011.01.

Reid, A. J., Wilson, C. J., and Liu, S., 2005, Structural evidence for the Permo-Triassic tectonic evolution of the Yidun Arc, eastern Tibetan Plateau: Journal of Structural Geology, v. 27, no. 1, p. 119-137, doi: 10.1016/j.jsg.2004.06.011.

Rieser, A. B., Neubauer, F., Liu, Y., and Ge, X., 2005, Sandstone provenance of north-western sectors of the intracontinental Cenozoic Qaidam Basin, western China: tectonic vs. climatic control: Sedimentary Geology, v. 177, no. 1, p. 1-18, doi: 10.1016/j.sedgeo.2005.01.012.

Rieser, A. B., Liu, Y., Genser, J., Neubauer, F., Handler, R., Friedl, G., and Ge, X. H., 2006, $^{40}Ar/^{39}Ar$ ages of detrital white mica constrain the Cenozoic development of the intracontinental Qaidam Basin, China: GSA Bulletin, v. 118, no. 11/12, p. 1522-1534, doi: 10.1130/B25962.1.

Rieser, A. B., Neubauer, F., Liu, Y., Genser, J., Handler, R., Ge, X.-H., and Friedl, G., 2007, $^{40}Ar/^{39}Ar$ Dating of Detrital White Mica as a Complementary Tool for Provenance Analysis: a Case Study from the Cenozoic Qaidam Basin (China), in Nichols, G., Williams, E., and Paola, C. eds.: Sedimentary Processes, Environments and Basins - A Tribute to Peter Friend: Special Publication-International Association of Sedimentologists 38, p. 301-325, doi: 10.1002/9781444304411.ch14.

Rieser, A. B., Bojar, A.-V., Neubauer, F., Genser, J., Liu, Y., Ge, X.-H., and Friedl, G., 2009, Monitoring Cenozoic climate evolution of northeastern Tibet: stable isotope constraints from the western Qaidam Basin, China: International Journal of Earth Sciences, v. 98, no. 5, p. 1063-1075, doi: 10.1007/s00531-008-0304-5.

Robinson, D. M., Dupont-Nivet, G., Gehrels, G. E., and Zhang, Y., 2003, The Tula uplift, northwestern China: Evidence for regional tectonism of the northern Tibetan Plateau during late Mesozoic-early Cenozoic time: Geological Society of America Bulletin: v. 115 no. 1 p. 35-47, doi: 10.1130/0016-7606(2003)115<0035:TTUNCE>2.0.CO;2.

Roger, F., Arnaud, N., Gilder, S., Tapponnier, P., Jolivet, M., Brunel, M., Malavieille, J., Xu, Z., and Yang, J., 2003, Geochronological and geochemical constraints on Mesozoic suturing in east central Tibet: Tectonics, v. 22, no. 4, p. 1037, doi:10.1029/2002TC001466.

Roger, F., Jolivet, M., and Malavieille, J., 2008, Tectonic evolution of the Triassic fold belts of Tibet: Comptes Rendus Geoscience, v. 340, no. 2, p. 180-189, doi:10.1016/j.crte.2007.10.014.

Roger, F., Jolivet, M., and Malavieille, J., 2010, The tectonic evolution of the Songpan-Garzê (North Tibet) and adjacent areas from Proterozoic to Present: A synthesis: Journal of Asian Earth Sciences, v. 39, no. 4, p. 254-269, doi:10.1016/j.jseaes.2010.03.008.

Rohling, E., Fenton, M., Jorissen, F., Bertrand, P., Ganssen, G., and Caulet, J., 1998, Magnitudes of sea-level lowstands of the past 500,000 years: Nature, v. 394, no. 6689, p. 162-165, doi: 10.1038/28134.

Rowley, D. B., and Currie, B. S., 2006, Palaeo-altimetry of the late Eocene to Miocene Lunpola basin, central Tibet: Nature, v. 439, no. 7077, p. 677-681, doi: 10.1038/nature04506.

Shi, R. D., Yang, J. S., Wu, C. L., Tsuyoshi, I., and Takafumi, H., 2006, Island arc volcanic rocks in the north Qaidam UHP belt, northern Tibet plateau: Evidence for ocean-continent subduction preceding continent-continent Subduction: Journal of Asian Earth Sciences, v. 28, no. 2, p. 151-159, doi:10.1016/j.jseaes.2005.09.019.

Shi, D. N., Shen, Y., Zhao, W. J., and Li, A. B., 2009, Seismic evidence for a Moho offset and south-directed thrust at the easternmost Qaidam-Kunlun boundary in the Northeast Tibetan plateau: Earth and Planetary Science Letters, v. 288, p. 329-334, doi:10.1016/j.epsl.2009.09.036.

Shanxi Insititute of Geological Survey (SIGS), 2003, Introduction of geological map of Ayakumu area: Shanxi Insititute of Geological Survey, Xi'an, scale 1:250000, 1 sheet (in Chinese).

Spicer, R. A., Harris, N. B., Widdowson, M., Herman, A. B., Guo, S., Valdes, P. J., Wolfe, J. A., and Kelley, S. P., 2003, Constant elevation of southern Tibet over the past 15 million years: Nature, v. 421, no. 6923, p. 622-624, doi:10.1038/nature01356.

Sobel, E. R., and Arnaud, N., 1999, A possible middle Paleozoic suture in the Altyn Tagh, NW China: Tectonics, v. 18, no. 1, p. 64-74, doi: 10.1029/1998TC900023.

Sobel, E. R., Arnaud, N., Jolivet, M., Ritts, B. D., and Brunei, M., 2001, Jurassic to Cenozoic exhumation history of the Altyn Tagh range, northwest China, constrained by $^{40}Ar/^{39}Ar$ and apatite fission track thermochronologym, In Hendrix, M.S., and Davis, G.A., eds., Paleozoic and Mesozoic Tectonic Evolution ofCentral and Eastern Asia: From Continental Assembly to

Intracontinental Deformation: Geological Society of America Memoir 194, p. 247.

Song, S. G., 2001, Petrology, Mineralogy and Metamorphic Evolution of the Dulan UHP Terrane in North Qaidam, NW China, and Its Tectonic Implications [PH.D. thesis]: Chinese Academy of Geological Sciences, Beijing, 96 p (in Chinese with English abstract).

Song, S. G., Zhang, L. F., Niu, Y. L., Song, B., Zhang, G. B., and Wang, Q. J., 2004, Zircon U-Pb SHRIMP ages of eclogites from the North Qilian Mountains in NW China and their tectonic implication: Chinese Science Bulletin, v. 49, no. 8, p. 848-852, doi : 10.1007/BF02889759.

Song, S. G., Zhang, L. F., Niu, Y. L., Su, L., Song, B., and Liu, D. Y., 2006, Evolution from oceanic subduction to continental collision: a case study from the Northern Tibetan Plateau based on geochemical and geochronological data: Journal of Petrology, v. 47, no. 3, p. 435-455, doi: 10.1093/petrology/egi080.

Song, B., Zhang, K., Lu, J., Wang, C., and Xu, Y., 2013, The middle Eocene to early Miocene integrated sedimentary record in the Qaidam Basin and its implications for paleoclimate and early Tibetan Plateau uplift: Canadian Journal of Earth Sciences, v. 50, no. 2, p. 183-196, doi: 10.1139/cjes-2012-0048.

Staisch, L. M., Niemi, N. A., Hong, C., Clark, M. K., Rowley, D. B., and Currie, B., 2014, A Cretaceous-Eocene depositional age for the Fenghuoshan Group, Hoh Xil Basin: Implications for the tectonic evolution of the northern Tibet Plateau: Tectonics, v. 33, no. 3, p. 281-301, doi: 10.1002/2013TC003367.

Sun, Z. M., Yang, Z. Y., Pei, J. L., Ge, X. H., Wang, X. S., Yang, T. S., Li, W. M., and Yuan, S. H., 2005, Magnetostratigraphy of Paleogene sediments from northern Qaidam Basin, China: implications for tectonic uplift and block rotation in northern Tibetan plateau: Earth and Planetary Science Letters, v. 237, no. 3, p. 635-646, doi: 10.1016/j.epsl.2005.07.007.

Sun, Z. C., Jing M. C., Sun, N. D., Lu Y.L., Cao, L., 2007. Discussion on boundary between the upper and lower members of Xiaganchaigou Formation of Paleogene in Well Kun-2, Qaidam Basin. Journal of Palaeogeography, v. 9, no. 6, 611-618 (in Chinese with English abstract).

Tapponnier, P., Xu, Z. Q., Roger, F., Meyer, B., Arnaud, N., Wittlinger, G., and Yang, J. S., 2001, Oblique stepwise rise and growth of the Tibet Plateau: Science, v. 294, no. 5547, p. 1671-1677, doi: 10.1126/science.105978.

Taylor, M., and Yin, A., 2009, Active structures of the Himalayan-Tibetan orogen and their relationships to earthquake distribution, contemporary strain field, and Cenozoic volcanism: Geosphere, v. 5, no. 3, p. 199-214, doi: 10.1130/GES00217.1.

van Der Woerd, J., Tapponnier, P., Ryerson, F. J., Meriaux, A. S., Meyer, B., Gaudemer, Y., Finkel, R. C., Caffee, M. W., Guoguang, Z., and Zhiqin, X., 2002, Uniform postglacial slip-rate along the central 600 km of the Kunlun Fault (Tibet), from 26Al, 10Be, and 14C dating of riser offsets, and climatic origin of the regional morphology: Geophysical Journal International, v. 148, no. 3, p. 356-388, doi: 10.1046/j.1365-246x.2002.01556.x.

Wan, Y. S., Xu, Z. Q., Yang, J. S., and Zhang, J. X., 2001, Ages and Compositions of the Precambrian High-grade Basement of the Qilian Terrane and Its Adjacent Areas: Acta Geologica Sinica-English Edition, v. 75, no. 4, p. 375-384, doi: 10.1111/j.1755-6724.2001.tb00055.x.

Wang, Q., Zhang, P. Z., Freymueller, J. T., Bilham, R., Larson, K. M., Lai, X., You, X., Niu, Z., Wu, J., and Li, Y., 2001, Present-day crustal deformation in China constrained by global positioning system measurements: Science, v. 294, no. 5542, p. 574-577, doi: 10.1126/science.1063647.

Wang, F., Lo, C. H., Li, Q., Yeh, M. W., Wang, J., Zheng, D., and Wang, E., 2004a, Onset timing of significant unroofing around Qaidam basin, northern Tibet, China: constraints from $^{40}Ar/^{39}Ar$ and FT thermochronology on granitoids: Journal of Asian Earth Sciences, v. 24, p. 59-69, doi: 10.1130/B25778.

Wang, G. C., Wang, Q. H., Jian P. and Zhu Y. H., 2004b, Zircon SHRIMP ages of Precambrian metamorphic basement rocks and their tectonic significance in the eastern Kunlun Mountains, Qinghai Province, China: Earth Science Frontiers, v.11, no. 4, p. 481-490 (in Chinese with English abstract).

Wang, A., Wang, G., Xie, D., and Liu, D., 2006a, Fission track geochronology of Xiaonanchuan Pluton and the morphotectonic evolution of eastern Kunlun since Late Miocene: Journal of China University of Geosciences, v. 17, no. 4, p. 302-309, doi: 10.1016/S1002-0705(07)60003-X.

Wang, E., Xu, F. Y., Zhou, J. X., Wan, J., and Burchfiel, B. C., 2006b, Eastward migration of the Qaidam basin and its implications for Cenozoic evolution of the Altyn Tagh fault and associated river systems: Geological Society of America Bulletin, v. 118, no. 3-4, p. 349-365, doi: 10.1130/B25778.

Wang, C., Liu, L., Che, Z. C., Chen, D. L., Zhang, A. D., and Luo, J. H., 2006c, U-Pb geochronology and tectonic setting of the granitic gneiss in Jianggaleisayi Eclogite Belt: Geological Journal of China Universities, v. 12, no. 1, p. 74-82 (in Chinese with English abstract).

Wang, C., Zhao, X., Liu, Z., Lippert, P. C., Graham, S. A., Coe, R. S., Yi, H., Zhu, L., Liu, S.,

and Li, Y., 2008a, Constraints on the early uplift history of the Tibetan Plateau: Proceedings of the National Academy of Sciences, v. 105, no. 13, p. 4987-4992, doi: 10.1073pnas.0703595105.

Wang, C., Liu, L., Zhang, A. D., Yang, W. Q., and Cao, Y. T., 2008b, Geochemistry and petrography of early Paleozoic Yusupuleke Tagh Rapakivi-textured Granite Complex, South Altyn - an example for magma mixing: Acta Petrolei Sinica, v. 24, no. 12, p. 2809-2819 (in Chinese with English abstract).

Wang, Q., Wyman, D. A., Xu, J. F., Dong, Y. H., Vasconcelos, P. M., Pearson, N., Wan, Y. S., Dong, H., Li, C. F., and Yu, Y. S., 2008c, Eocene melting of subducting continental crust and early uplifting of central Tibet: evidence from central-western Qiangtang high-K calc-alkaline andesites, dacites and rhyolites: Earth and Planetary Science Letters, v. 272, no. 1, p. 158-171, doi:10.1016/j.epsl.2008.04.034.

Wang, Y. D., Nie, J. S., Zhang, T., Sun, G. Q., Yang, X., Liu, Y. H., and Liu, X. W., 2010a, Cenozoic tectonic evolution in the western Qaidam Basin inferred from subsurface data: Geosciences Journal, v. 14, no. 4, p. 335-344, doi: 10.1007/s12303-010-0033-1.

Wang, L., Xiao, A. C., Gong, Q. L., Liu, D., Wu, L., Zhou, S. P., Shen, Z. Y., Lou, Q. Q., and Sun, X. W., 2010b, The unconformity in Miocene sequence of western Qaidam Basin and its tectonic significance: SCIENCE CHINA Earth Sciences, v. 53, no. 8, p. 1126-1133, doi: 10.1007_s11430-010-4006-z.

Wang, C. S., Gao, R., Yin, A., Wang, H., Zhang, Y. X., Guo, T. L., Li, Q. S., and Li, Y. L., 2011, A mid-crustal strain-transfer model for continental deformation: A new perspective from high-resolution deep seismic-reflection profiling across NE Tibet: Earth and Planetary Science Letters, v. 306, no. 3, p. 279-288, doi: 10.1016/j.epsl.2011.04.010.

Wang, C., Liu, L., Yang, W. Q., Zhu, X. H., Cao, Y. T., Kang, L., Chen, S. F., Li, R. S., and He, S. P., 2013, Provenance and ages of the Altyn Complex in Altyn Tagh: implications for the early Neoproterozoic evolution of northwestern China: Precambrian Research. v. 230, p. 193-208, doi: 10.1016/j.precamres.2013.02.003.

Wang, C., Dai, J., Zhao, X., Li, Y., Graham, S. A., He, D., Ran, B., and Meng, J., 2014, Outward-growth of the Tibetan Plateau during the Cenozoic: A review: Tectonophysics, v. 621, p. 1-43, doi: 10.1016/j.tecto.2014.01.036.

Wiedenbeck, M., Alle, P., Corfu, F., Griffin, W., Meier, M., Oberli, F., Quadt, A. v., Roddick, J., and Spiegel, W., 1995, Three natural zircon standards for U-Th-Pb, Lu-Hf, trace element and REE analyses: Geostandards Newsletter, v. 19, no. 1, p. 1-23, doi: 10.1111/j.1751-908X.1995.tb00147.x.

Wu, H., Feng, Y., and Song, S., 1993, Metamorphism and deformation of blueschist belts and their tectonic implications, North Qilian Mountains, China: Journal of metamorphic Geology, v. 11, p. 523-523, doi: 10.1111/j.1525-1314.1993.tb00169.x.

Wu, C. L., Gao, Y. H., Wu, S. P., Chen, Q. L., Wooden, J. L., Mazadab, F. K., and Mattinson, C., 2008, Zircon SHRIMP dating and geochemical characteristics of granite from the Westem Qaidam: Science in China (D), v. 38, no. 8, p. 930-949 (in Chinese).

Wu, L., Xiao, A., Yang, S., Wang, L., Mao, L., Dong, Y., and Xu, B., 2012, Two-stage evolution of the Altyn Tagh Fault during the Cenozoic: new insight from provenance analysis of a geological section in NW Qaidam Basin, NW China: Terra Nova, v. 24, no.5, p.387-395, doi: 10.1111/j.1365-3121.2012.01077.x.

Wu, L., Xiao, A. C., Ma, D. D., Li, H. G., Xu, B., Shen, Y., and Mao, L. G., 2014, Cenozoic fault systems in southwest Qaidam Basin, northeastern Tibetan Plateau: Geometry, temporal development, and significance for hydrocarbon accumulation: AAPG Bulletin, v. 98, no. 6, p. 1213-1234, doi: 10.1306/11131313087.

Xia, W. C., Zhang, N., Yuan, X. P., Fan, L. S., and Zhang, B. S., 2001, Cenozoic Qaidam basin, China: A stronger tectonic inversed, extensional rifted basin: AAPG bulletin, v. 85, no. 4, p. 715-736, doi: 10.1306/8626C98D-173B-11D7-8645000102C1865D.

Xia, L. Q., Li, X. M., Ma, Z. P., Xu, X. Y., and Xia, Z. C., 2011, Cenozoic volcanism and tectonic evolution of the Tibetan plateau: Gondwana Research, v. 19, no. 4, p. 850-866, doi: doi:10.1016/j.gr.2010.09.005.

Xia, G. Q., 2012, The sedimentary records of the tectonic uplift of the East Kunlun in the Cenozoic [Ph.D. thesis]: Chengdu University of Technology, Chengdu, 150 p. (in Chinese with English abstract).

Xu, X. W., Chen, W. B., Ma, W. T., Yu, G. H., and Chen, G. H., 2002, Surface rupture of the Kunlunshan earthquake (Ms 8.1), northern Tibetan plateau, China: Seismological Research Letters, v. 73, no. 6, p. 884-892, doi: 10.1785/gssrl.73.6.884.

Xu, Q., Ding, L., Zhang, L., Cai, F., Lai, Q., Yang, D., and Liu-Zeng, J., 2013, Paleogene high elevations in the Qiangtang Terrane, central Tibetan Plateau: Earth and Planetary Science Letters, v. 362, p. 31-42, doi: 10.1016/j.epsl.2012.11.05.

Yang, F., Ma, Z. Q., Xu, T. C., and Ye, S. J., 1992, A Tertiary paleomagnetic stratigraphic profile in Qaidam basin: Acta Petrolei Sinica, v. 13, no. 2, p. 97-101 (in Chinese).

Yang, J. S., Robinson, P., Jiang, C. F., and Xu, Z. Q., 1996, Ophiolites of the Kunlun Mountains, China and their tectonic implications: Tectonophysics, v. 258, no. 1-4, p. 215-231, doi: 10.1016/0040-1951(95)00199-9.

Yang, J. S., Xu, Z. Q., Zhang, J. X., Chu, C. Y., Zhang, R. Y., and Liou, J. G., 2001, Tectonic significance of early Paleozoic high-pressure rocks in Altun-Qaidam-Qilian Mountains, northwest China in Hendrix, M.S., and Davis, G.A., eds., Paleozoic and Mesozoic Tectonic Evolution of Central and Eastern Asia: From Continental Assembly to Intracontinental Deformation:Geological Society of America Memoir 194, p. 151–170.

Yang, J. S., Xu, Z. Q., Zhang, J. X., Song, S. G., Wu, C. L., Shi, R. D., Li, H. B., and Maurice, B., 2002, Early Palaeozoic North Qaidam UHP metamorphic belt on the north‐eastern Tibetan plateau and a paired subduction model: Terra Nova, v. 14, no. 5, p. 397-404, doi: 10.1046/j.1365-3121.2002.00438.x.

Yang, J. S., Wu, C. L., Zhang, J. X., Shi, R. D., Meng, F. C., Wooden, J. L., and Yang, H. Y., 2006, Protolith of eclogites in the north Qaidam and Altun UHP terrane, NW China: Earlier oceanic crust?: Journal of Asian Earth Sciences, v. 28, no. 2, p. 185-204, doi: 10.1016/j.jseaes.2005.09.020.

Yang, W., Jolivet, M., Dupont-Nivet, G., Guo, Z., Zhang, Z., and Wu, C., 2013, Source to sink relations between the Tian Shan and Junggar Basin (northwest China) from Late Palaeozoic to Quaternary: evidence from detrital U-Pb zircon geochronology: Basin Research, v. 25, no. 2, p. 219-240, doi: 10.1111/j.1365-2117.2012.00558.x.

Yang, W., Jolivet, M., Dupont-Nivet, G., and Guo, Z., 2014, Mesozoic - Cenozoic tectonic evolution of southwestern Tian Shan: Evidence from detrital zircon U/Pb and apatite fission track ages of the Ulugqat area, Northwest China: Gondwana Research, v. 26, no. 3–4, p. 986-1008, doi: 10.1016/j.gr.2013.07.020.

Yi, H. S., Wang, C. S., Shi, Z. Q., Lin, J. H., and Zhu, L. D., 2008, Early uplift history of the Tibetan plateau: Records from paleocurrents and paleodrainage in the Hoh Xil basin: Acta Geologica Sinica‐English Edition, v. 82, no. 1, p. 206-213, doi: 10.1111/j.1755-6724.2008.tb00339.x.

Yin, A., Dang, Y. Q., Zhang, M., McRivette, M. W., Burgess, W. P., and Chen, X. H., 2007, Cenozoic tectonic evolution of Qaidam basin and its surrounding regions (part 2): Wedge tectonics in southern Qaidam basin and the Eastern Kunlun Range, in Sears, J.W., Harms, T.A., and Evenchick, C.A., eds., Whence the Mountains? Inquiries into the Evolution of Orogenic Systems: A Volume in Honor or Raymond A. Price: Geological Society of America Special Paper 433, p. 369–390, doi:10.1130/2007.2433(18)

Yin, A., Dang, Y. Q., Wang, L. C., Jiang, W. M., Zhou, S. P., Chen, X. H., Gehrels, G. E., and McRivette, M. W., 2008a, Cenozoic tectonic evolution of Qaidam basin and its surrounding regions (Part 1): The southern Qilian Shan-Nan Shan thrust belt and northern Qaidam basin:

Geological Society of America Bulletin, v. 120, no. 7-8, p. 813-846, doi:10.1130.B26180.1.

Yin, A., Dang, Y. Q., Zhang, M., Chen, X. H., and McRivette, M. W., 2008b, Cenozoic tectonic evolution of the Qaidam basin and its surrounding regions (Part 3): Structural geology, sedimentation, and regional tectonic reconstruction: Geological Society of America Bulletin, v. 120, no. 7-8, p. 847-876, doi: 10.1130/B26232.1.

Yu, X., Huang, B., Guan, S., Fu, S., Cheng, F., Cheng, X., Zhang, T., and Guo, Z., 2014, Anisotropy of magnetic susceptibility of Eocene and Miocene sediments in the Qaidam Basin, Northwest China: Implication for Cenozoic tectonic transition and depocenter migration: Geochemistry, Geophysics, Geosystems, v. 15, no. 6, p. 2095-2108, doi: 10.1002/2014GC005231.

Yuan, W. M., Zhang, X. T., Dong, J. Q., Tang, Y. H., Yu, F. S., and Wang, S. C., 2003, A new vision of the intracontinental evolution of the eastern Kunlun Mountains, Northern Qinghai-Tibet plateau, China: Radiation Measurements, v. 36, no. 1-6, p. 357-362, doi:10.1016/S1350-4487(03)00151-3.

Yuan, H. L., Gao, S., Liu, X. M., Li, H. M., Günther, D., and Wu, F. Y., 2004, Accurate U-Pb age and trace element determinations of zircon by laser ablation-inductively coupled plasma-mass spectrometry: Geostandards and Geoanalytical Research, v. 28, no. 3, p. 353-370, doi: 10.1111/j.1751-908X.2004.tb00755.x.

Yuan, W. M., Dong, J. Q., Wang, S. C., and Carter, A., 2006, Apatite fission track evidence for Neogene uplift in the eastern Kunlun Mountains, northern Qinghai-Tibet Plateau, China: Journal of Asian Earth Sciences, v. 27, no. 6, p. 847-856, doi: 10.1016/j.jseaes.2005.09.002.

Yue, Y., Ritts, B. D., Graham, S. A., Wooden, J. L., Gehrels, G. E., and Zhang, Z., 2004, Slowing extrusion tectonics: lowered estimate of post-Early Miocene slip rate for the Altyn Tagh fault: Earth and Planetary Science Letters, v. 217, no. 1, p. 111-122, doi: 10.1016/S0012-821X(03)00544-2.

Yue, Y. J., Graham, S. A., Ritts, B. D., and Wooden, J. L., 2005, Detrital zircon provenance evidence for large-scale extrusion along the Altyn Tagh fault: Tectonophysics, v. 406, no. 3, p. 165-178, doi: 10.1016/j.tecto.2005.05.023.

Zhang, J. X., Xu, Z. Q., Chen, W., and Xu, H. F., 1997, A tentative discussion on the ages of the subduction-accretionary complex/volcanic arcs in the middle sector of North Qilian Mountain: Acta Petrologica et Mineralogica, v. 16, no. 2, p. 112-119 (in Chinese with English abstract).

Zhang, J. X., Zhang, Z. M., Xu, Z. Q., Yang, J. S., and Cui, J. W., 2001, Petrology and geochronology of eclogites from the western segment of the Altyn Tagh, northwestern China:

Lithos, v. 56, no. 2, p. 187-206, doi: 10.1016/S0024-4937(00)00052-9.

Zhang, P. Z., Shen, Z., Wang, M., Gan, W., Bürgmann, R., Molnar, P., Wang, Q., Niu, Z., Sun, J., and Wu, J., 2004, Continuous deformation of the Tibetan Plateau from global positioning system data: Geology, v. 32, no. 9, p. 809-812, doi: 10.1130/G20554.1.

Zhang, J. X., Mattinson, C. G., Meng, F. C., and Wan, Y. S., 2005, An Early Palaeozoic HP/HT granulite–garnet peridotite association in the south Altyn Tagh, NW China: P–T history and U-Pb geochronology: Journal of Metamorphic Geology, v. 23, no. 7, p. 491-510, doi: 10.1111/j.1525-1314.2005.00585.x.

Zhang, W. L., 2006, High-resolution Magnetostratigraphy of the Cenozoic Qaidam Basin, implications for the uplift of Tibetan Plateau [Ph.D. thesis]: LanZhou University, Lanzhou, 158 p. (in Chinese with English abstract).

Zhang, J. X., Li, H. K., Meng, F. C., Xiang, Z. Q., Yu, S. Y., and Li, J. P., 2011, Polyphase tectonothermal events recorded in metamorphic basement from the Altyn Tagh, the southeastern margin of the Tarim basin, western China: constraint from U-Pb zircon geochronology -Pb zircon geochronology: Acta Petrologica Sinica, v. 27, no. 1, p. 23-46 (in Chinese with English abstract).

Zhang, W., Appel, E., Fang, X., Song, C., and Cirpka, O., 2012, Magnetostratigraphy of deep drilling core SG-1 in the western Qaidam Basin (NE Tibetan Plateau) and its tectonic implications: Quaternary Research, v. 78, no. 1, p. 139-148, doi: 10.1016/j.yqres.2012.03.011.

Zhang, C., Cheng, F., Huang, G., Huang, Y., Xing, C., Guan, B., Zhang, Q. and Xu, F., 2013a, Sediment and reservoir characteristics with reservior evaluation of the Lulehe Formation in Qie 16 block of Kunbei oildfield in Qaidam Basin. Acta Petrologica Sinica, v. 20, no. 8, p. 2883-2894 (in Chinese with English abstract).

Zhang, W., Fang, X., Song, C., Appel, E., Yan, M., and Wang, Y., 2013b, Late Neogene magnetostratigraphy in the western Qaidam Basin (NE Tibetan Plateau) and its constraints on active tectonic uplift and progressive evolution of growth strata: Tectonophysics, v. 599, p. 107-116, doi: 10.1016/j.tecto.2013.04.010.

Zhang, J., Mattinson, C., Yu, S., and Li, Y., 2014a, Combined rutile–zircon thermometry and U–Pb geochronology: New constraints on Early Paleozoic HP/UHT granulite in the south Altyn Tagh, north Tibet, China: Lithos, v. 200, p. 241-257, doi: 10.1016/j.lithos.2014.05.006.

Zhang, L. Y., Ding, L., Pullen, A., Xu, Q., Liu, D. L., Cai, F. L., Yue, Y. H., Lai, Q. Z., Shi, R. D., and Ducea, M. N., 2014b, Age and geochemistry of western Hoh-Xil–Songpan-Ganzi granitoids, northern Tibet: Implications for the Mesozoic closure of the Paleo-Tethys ocean: Lithos, v. 190, p. 328-348, doi: 10.1016/j.lithos.2013.12.019.

Zhao, J., Mooney, W. D., Zhang, X., Li, Z., Jin, Z., and Okaya, N., 2006, Crustal structure across the Altyn Tagh Range at the northern margin of the Tibetan plateau and tectonic implications: Earth and Planetary Science Letters, v. 241, no. 3, p. 804-814, doi: 10.1016/j.epsl.2005.11.003.

Zhou, J. X., Xu, F. Y., Wang, T. C., Cao, A. F., and Yin, C. M., 2006, Cenozoic deformation history of the Qaidam Basin, NW China: Results from cross-section restoration and implications for Qinghai-Tibet Plateau tectonics: Earth and Planetary Science Letters, v. 243, no. 1-2, p. 195-210, doi:10.1016/j.epsl.2005.11.033.

Zhu, Y. M., Weng, H. X., Su, A. G., Liang, D. G., and Peng, D. H., 2005, Geochemical characteristics of Tertiary saline lacustrine oils in the Western Qaidam Basin, northwest China: Applied Geochemistry, v. 20, no. 10, p. 1875-1889, doi: 10.1016/j.apgeochem.2005.06.003.

Zhuang, G., Hourigan, J. K., Ritts, B. D., and Kent-Corson, M. L., 2011, Cenozoic multiple-phase tectonic evolution of the northern Tibetan Plateau: Constraints from sedimentary records from Qaidam basin, Hexi Corridor, and Subei basin, northwest China: American Journal of Science, v. 311, no. 2, p. 116-152, doi: 10.2475/02.2011.02.

Zuffa, G. G., 1980, Hybrid arenites: their composition and classification: Journal of Sedimentary Research, v. 50, no. 1, p.21-29, doi: 10.1306/212F7950-2B24-11D7-8648000102C1865D.

Zuo, G. C., and Wu, H. Q., 1997, A bisubduction collision orogenic model of Early Paleozoic in the middle part of North Qilian area: Advance in Earth Science, v. 12, no. 4, p. 315-323 (in Chinese with English abstract).

Chapter 3 The interplay between the sediments within Qaidam basin and the active tectonic within Altyn Tagh Range

3.1 Initial rupture and displacement on the Altyn Tagh fault, northern Tibetan plateau: constraints based on residual Mesozoic to Cenozoic strata in the western Qaidam basin

Paper published in Geosphere, 2015, vol. 11, pp. 921–942

Initial rupture and displacement on the Altyn Tagh fault, northern Tibetan plateau: constraints based on residual Mesozoic to Cenozoic strata in the western Qaidam basin

Feng Cheng[1, 2], Zhaojie Guo[1, †], Hillary S. Jenkins[3], Suotang Fu[4], Xiang Cheng[1]

[1] Key Laboratory of Orogenic Belts and Crustal Evolution, Ministry of Education, School of Earth and Space Sciences, Peking University, Beijing, 100871, China

[2] Laboratoire Géosciences Rennes, CNRS-UMR6118, Université Rennes 1 - Observatoire des Sciences de l'Univers, Rennes, France

[3] Department of Environmental Studies, University of Redlands, Lewis Hall - 1200 E. Colton Avenue Redlands, CA 92373

[4] Qinghai Oilfield Company, PetroChina, Dunhuang, Gansu, 736202, China

[†] Corresponding author. E-mail address: cfcf.chengfeng@gmail.com

Note: The online version of this contribution can be found as: ***Cheng, F., Guo, Z., Jenkins, H.S., Fu, S., Cheng, X., 2015. Initial rupture and displacement on the Altyn Tagh fault, northern Tibetan Plateau: Constraints based on residual Mesozoic to Cenozoic strata in the western Qaidam Basin. Geosphere 11, 921-942, doi: 10.1130/GES01070.1.***

Abstract

The Altyn Tagh fault (ATF), located in the northern Tibetan plateau, is a large left-lateral strike-slip fault heavily responsible for the growth and formation of the plateau during Cenozoic time. Despite its significance, the initial timing and kinematic patterns of movement along the ATF remain highly debated. Here we present a detailed analysis of the stratigraphy and geochronology of three key lithologic sections (the Tula, Anxi, and Caishiling) along the

ATF to better understand this kinematic history. By correlating stratigraphic contacts and lithology with the U-Pb age spectra of Mesozoic samples within the western Qaidam basin, we find the ATF has experienced a total of ~360 km of displacement during the Cenozoic. By combining seismic profile data with geologic observations, we divide the activity along this fault into two distinct stages of motion: 1) an initial stage which occurred between early Eocene (~49 Ma) and mid-Miocene time (~15 Ma) and resulted in ~170 km of offset, and 2) an early stage which began in the late Miocene epoch and continues into the present, resulting in ~190 km of offset along the fault. We identify the Tula and Anxi sections as piercing points along the western segment of ATF and define these regions as residual parts of the original Qaidam basin. These estimates suggest that motion along the ATF has accelerated from an average left-lateral strike-slip rate of ~5.0 mm/yr during initial stage faulting to a rate of ~12.6 mm/yr between the late Miocene epoch and present day.

Keywords: northern Tibetan plateau; Altyn Tagh fault; Qaidam basin; strike-slip fault; displacement

3.1.1 Introduction

As a major strike-slip fault on the Tibetan plateau, the Altyn Tagh fault (ATF) plays a significant role in the Cenozoic deformation of northern Tibet (Fig. 1). Understanding the Cenozoic kinematic patterns of the ATF holds important implications for unraveling the evolution of northern Tibet, deciphering the growth history of the entire Tibetan plateau, and contributing to oil and gas exploration in the surrounding region (Yue and Liou, 1999; Yin and Harrison, 2000; Tapponnier et al., 2001; Yin et al., 2002; Wang et al., 2014). Recent studies have revealed much about the basic geology of the Altyn Tagh Range and the surrounding region (Wang, 1997; Cowgill et al., 2000; Yue et al., 2001; Yin et al., 2002; Chen et al., 2003; Cowgill et al., 2003; Dupont-Nivet et al.,2003, 2004; Ritts et al., 2004; Yue et al., 2004a; Wu et al., 2012a, 2012b; Cheng et al., 2014; Lu et al., 2014; Zhang et al., 2014); however, the immense size and extent of the Altyn Tagh Range make it difficult to locate ideal piercing points to estimate the initial timing of left-slip movement and total displacement along the ATF. As a result, both the timing and amount of slip along the fault are vigorously debated (e.g. Yin et al., 2002; Cowgill et al., 2003; Gehrels et al., 2003a, 2003b; Ritts et al., 2004; Wu et al., 2012a, 2012b).

Although some studies reference Mesozoic shearing in the Altyn Tagh Range, the growth of the Tibetan plateau is largely related to Cenozoic faulting along the ATF rather than any pre-Cenozoic shearing in the Altyn Tagh Range (Tapponnier et al., 1986, 2001; Arnaud et al.,

2003; Wang et al., 2005; Li et al., 2006; Liu et al., 2007b). A variety of approaches have been used to constrain the initial timing of left-slip movement along the ATF, and the estimates vary greatly. Initial movement along the ATF is estimated to have occured broadly between the Eocene and Miocene epochs (Chen et al., 2001; Meng et al., 2001; Wan et al., 2001; Yue et al., 2001; Yin et al., 2002; Robinson et al., 2003; Wu et al., 2012a, 2012b), and estimates of the total displacement along the ATF vary anywhere from ~1200 km to less than 90 km (Tapponnier et al., 1986; CSBS, 1992; Wang, 1997; Yin and Harrison, 2000; Yang et al., 2001; Yin et al., 2002; Cowgill et al., 2003; Gehrels et al., 2003a, 2003b; Ritts et al., 2004). The wide variety of estimates regarding the initial timing and offset of the ATF highlight the incomplete understanding of this remote region.

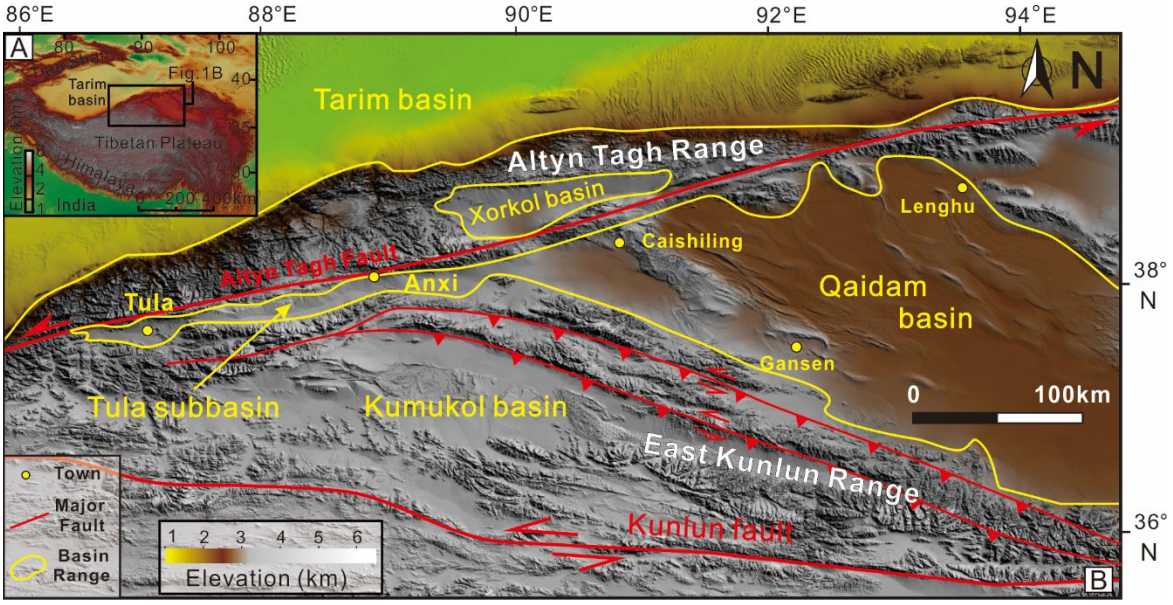

Figure 1. Digital topographic map of the center segment of the Altyn Tagh fault and surrounding area. Topography is from Shuttle Radar Topography Mission (SRTM) data.

In particular, Jurassic strata in both the southeast Tarim and northwest Qaidam basins across the ATF have been used as the geologic piercing point to constrain the total displacement along the ATF (e.g. Ritts and Biffi, 2000; Meng et al., 2001). However, Jurassic strata in western China are widespread and well developed in the foothills of several mountain belts (e.g. the Tian Shan, Altun Shan, Qilian Shan, and western Kunlun Mountains). These Jurassic strata are regionally similar, mainly characterized by a succession of terrestrial detrital rocks with coal-bearing deposits, locally intercalated with relatively few volcanic rocks (Hendrix et al., 1992, 2000; Li et al., 2004; Yue et al., 2004b; Yang et al., 2013; Liu et al., 2013a). While lithologically similar, these sedimentary features do not provide a distinct linear feature that can be matched across the ATF; thus Jurassic strata alone on either side of the ATF are inadequate and insufficient to document the total offset of the ATF.

In this paper, we present a detailed analysis of stratigraphy, sediment types, and detrital zircon U-Pb ages which enables us to establish stratigraphic correlations to source terranes and to constrain the amount of tectonic transport along the ATF (e.g. Gehrels, 2014). We present a synthesis of the stratigraphic and lithologic data along three sections (Tula, Anxi, and Caishiling sections) of the western segment of the ATF and the detrital zircon U-Pb geochronology for the Tula and Caishiling sections (Figs. 1 and 2). We use this information to constrain the timing of tectonic activity on the northern Tibetan plateau, to establish a more accurate estimate for the timing of initial movement along the ATF, and to provide a more accurate estimate of the total length of offset along the ATF during Cenozoic time.

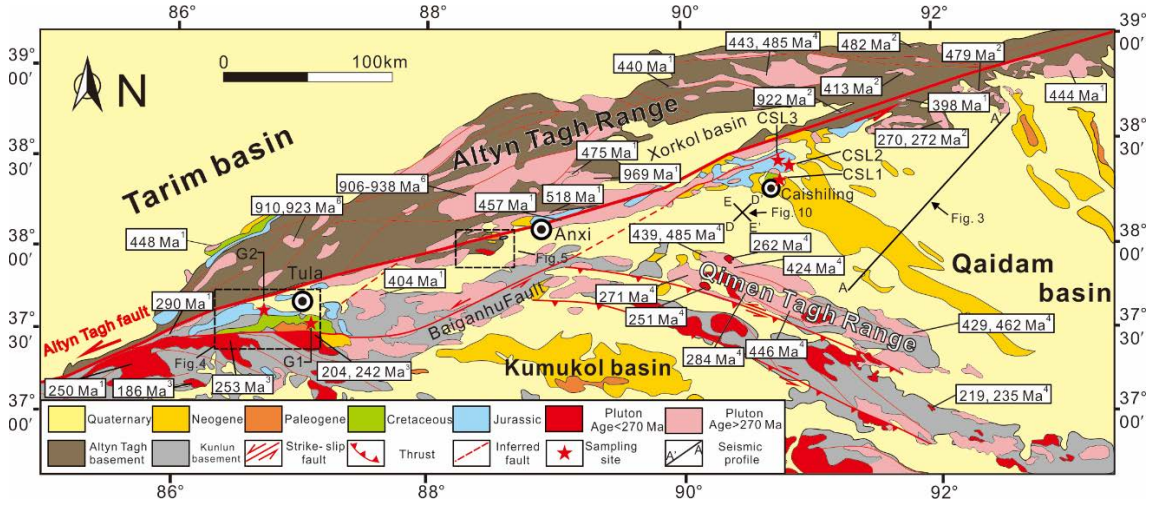

Figure 2. Geologic map of the center segment of the Altyn Tagh fault and the surrounding area, adapted from the Geologic Map of the Tibetan Plateau and Adjacent Areascompiled by Chengdu Institute of Geology and Mineral Resources and Chinese Geological Survey (map scale 1:1,500,000). Ages (zircon U-Pb) of plutons are mainly compiled from: 1—Cowgill et al. (2003); 2—Gehrels et al. (2003a); 3—HGSI (2003); 4—Chen et al. (2004); 5—Li et al. (2013); 6—Wang et al. (2013). See provenance analysis of Jurassic to Cretaceous strata sections for details.

3.1.2 Regional geology

3.1.2.1 Altyn Tagh Range

The Altyn Tagh Range is located at the northern edge of the Tibetan plateau, separating the Tarim basin to the northwest from the Qaidam basin to the southeast (Figs. 1 and 2). The bedrock of the Altyn Tagh Range is dominated by Precambrian igneous and metamorphic rocks and Paleozoic sedimentary rocks, whereas Mesozoic and Cenozoic strata are only sporadically represented (Wang, 1997; Sobel et al., 2001; Yin et al., 2002; Chen et al., 2003). Within the Altyn Tagh Range, the approximately 1600-km-long ENE-trending ATF starts in the western Kunlun Range in the southwest and terminates in the Qilian Shan Range in the

northeast, linking the Kunlun and Qilian Shan thrust belts (Burchfiel et al., 1989; Wang, 1997; Yue and Liou, 1999; Yin and Harrison, 2000; Yin et al., 2002). The origin of the ATF (Meyer et al., 1998; Chen et al., 2001; Meng et al., 2001; Wan et al., 2001; Yue et al., 2001; Yin et al., 2002; Ritts et al., 2004; Wu et al., 2012a, 2012b). The total displacement along the ATF fault remain heavily debated (CSBS, 1992; Ritts and Biffi, 2000; Yang et al., 2001; Cowgill et al., 2003; Gehrels et al., 2003a, 2003b). Quaternary slip rates of ~10 mm/yr on the ATF have been determined using field data, geodetic observations, and GPS measurements (Bendick et al., 2000; Shen et al., 2001; Yin et al., 2002; Zhang et al., 2004, 2007; Cowgill et al., 2009; Yin, 2010).

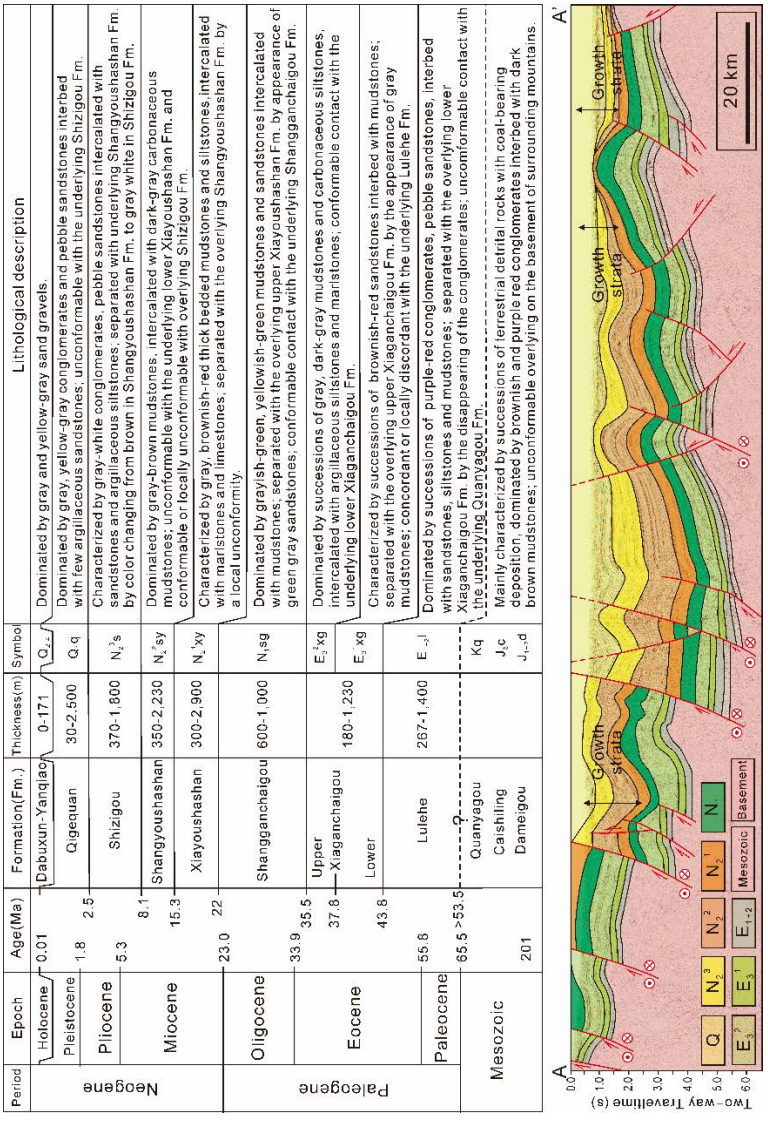

Figure 3. Stratigraphy and lithologic unit descriptions of the Qaidam Basin. The Cenozoic stratigraphy of the basin has been defined and dated in detail using magnetostratigraphy, palynology, and paleontology studies within the entire basin (Fang et al., 2007; Gao et al., 2009; Huang et al., 1996; Huo, 1990; Lu and Xiong, 2009; QBGMR, 1991; Qiu, 2002; Z.M. Sun et al., 2005; Xia et al., 2001; Yang et al., 1992; Zhao et al., 2006). See Figure 2 for seismic profile location. Note the growth strata above the Xiayoushashan Formation (N_2^1xy).

3.1.2.2 Qaidam basin

The triangular-shaped Qaidam basin, which lies on the southeastern side of the Altyn

Tagh Range, is the largest petroliferous basin within the northern Tibetan plateau (Figs. 1 and 2). The western Qaidam basin is bound by the Altyn Tagh Range to the northwest and the Qimen Tagh Range (western segment of the Eastern Kunlun Range) to the south. The westernmost part of the Qaidam basin is characterized by a unique NE-trending elongate landform known as the Tula trough (Wang et al., 2006a) or Tula subbasin (Guo et al., 1998) (Figs. 1 and 2). High-quality subsurface data have revealed that the southeastern Qaidam Basin is governed by a series of high-angle NW-trending reverse faults with considerable strike-slip component (Cheng et al., 2014, 2015) resulting in stratigraphic throw on either side of these faults in seismic profile (Fig. 3). The tectonic-sedimentary evolution of the Qaidam basin remains largely unknown though several hypotheses have been proposed (Métivier et al., 1996; Mock et al., 1999; Xia et al., 2001; Wang et al., 2006a; Yin et al., 2007; Meng and Fang, 2008; Yin et al., 2008a, 2008b; Wang et al., 2011). One hypothesis suggests that the western Qaidam basin experienced two Cenozoic structural phases: the first between the Paleocene and Eocene epochs and the second between the middle Miocene and Pleistocene epochs (Wang et al., 2010b). Growth strata and a regional angular unconformity between the early Miocene and late Miocene successions in the western Qaidam basin are identified as depositional responses to regional tectonic events in both the Altyn Tagh Range and the Eastern Kunlun Range during middle Miocene time (Song and Wang, 1993; Yin et al., 2007, 2008b; Wang et al., 2010a, 2010b; Wu et al., 2012a).

Geologic mapping and petroleum exploration have revealed that the Qaidam basin consists mainly of Cenozoic to Mesozoic nonmarine strata unconformably overlying an uncertain basement (Xia et al., 2001; Meng and Fang, 2008). The basement rock is too deep to be reached via drilling and its lithology therefore remains uncertain (Xia et al., 2001; Fang et al., 2007; Yin et al., 2008b). The Mesozoic strata are mainly located along the southern flank of the Altyn Tagh and the Qilian Shan ranges (Yin et al., 2008a; Wu et al., 2011). A succession of depo-centers of Cenozoic strata are present along the long axis of the basin and have gradually migrated eastward since the Eocene epoch (Song and Wang, 1993; Xia et al., 2001; Qiu, 2002; Sun et al., 2005a; Wang et al., 2006a; Yin et al., 2008b). Based on magnetostratigraphy, palynology and paleontology, the Mesozoic-Cenozoic strata of the Qaidam basin have been subdivided into 11 units and the chronostratigraphy of the Cenozoic units has been well constrained (Huo, 1990; QBGMR, 1991; Yang et al., 1992; Huang et al., 1996; Xia et al., 2001; Qiu, 2002; Sun et al., 2005a; Zhao et al., 2006; Fang et al., 2007; Yin et al., 2007; Gao et al., 2009; Lu and Xiong, 2009; Wu et al., 2011). These units are listed in order from oldest to youngest below, followed by the symbol for each unit, and the age range

capture of each unit, if available: (1) the Dameigou Fm., $J_{1+2}d$; (2) Caishiling Fm., J_3c; (3) Quanyagou Fm.., Kq; (4) the Lulehe Fm., $E_{1+2}l$, >53.5 - 43.8 Ma (Yang et al., 1992; Zhang, 2006; Ke et al., 2013); (5) the lower Xiaganchaigou Fm., E_31xg, 43.8 - 37.8 Ma (Zhang, 2006; Sun et al., 2007; Pei et al., 2009); (6) the upper Xiaganchaigou Fm., E_3^2xg, 37.8 - 35.5 Ma (Sun et al., 2005b, 2007; Pei et al., 2009); (7) the Shangganchaigou Fm., N_1sg, 35.5 - 22.0 Ma (Sun et al., 2005b; Lu and Xiong, 2009); (8) the lower Youshashan Fm., N_2^1xy, 22.0 - 15.3 Ma (Fang et al., 2007; Lu and Xiong, 2009); (9) the upper Youshashan Fm., N_2^2sy, 15.3 - 8.1 Ma (Fang et al., 2007); (10) the Shizigou Fm., N_2^3s, 8.1 - 2.5 Ma (Fang et al., 2007); (11) Quaternary deposits, including the Qigequan Fm. (Q_1q) and the Dabuxun-Yanqiao Fm. (Q_{2-4}), 2.5 - 0 Ma (Fang et al., 2007; Yin et al., 2008b). The lithologic features of each unit are summarized in detail Fig. 3.

3.1.3 Residual Mesozoic-Cenozoic stratigraphy along the Altyn Tagh Fault

3.1.3.1 Mesozoic to Eocene strata in the Tula section

The Tula section is bounded by the ATF to the north and the Kunlun Precambrian and Paleozoic basement to the south (Figs. 2 and 4). A narrow valley runs through this region at the westernmost part of the Qaidam basin. Precambrian, Ordovician, and Carboniferous rocks comprise the basement rock which is unconformably overlain by Mesozoic to Cenozoic strata (Guo et al., 1998; HGSI, 2003; Ritts et al., 2004). Mesozoic strata in the Tula section are dominantly terrestrial clastic rocks. Several faults are present on the south side of the Tula basin (Fig. 2). The left-lateral NE-SW trending strike-slip Baiganhu Fault can be identified by a series of distinctive fault scarps and structural lineaments within the mountains, although the fault later becomes obscured by Quaternary deposits in the Tula basin (Fig. 2; Cowgill et al., 2003; HGIS, 2003; Wang et al., 2014).

Jurassic clastic coal-bearing strata rest unconformably on the Altyn Tagh basement (Fig. 4). Based on lithologic associations, sequence stratigraphy, and paleontology, these strata have been divided into two units: the Dameigou Fm. ($J_{1+2}d$), located in the lower part of the section and the Caishiling Fm. (J_3c), located in the upper part of the section (XBGRM, 1993; HGIS, 2003; Robinson et al., 2003; Dupont-Nivet et al., 2004). The lower part of the Dameigou Fm. ($J_{1+2}d$) is composed of fining-upward gray-brown conglomerate beds interbedded with greenish-gray sandstone and siltstone beds. The upper part of the Dameigou Fm. ($J_{1+2}d$) is characterized by a set of sandstone beds interbedded with conglomerate, siltstone and lithic sandstone (Fig 5A). Grain size increases upsection, indicating gradual shallowing and

subsiding of the basin. In the Caishiling section, thick-bedded lithic sandstone and conglomerate (Fig. 5B) are developed at the base of the Dameigou Fm. (J_{1+2}d), indicating that denudation of the source area began in Early Jurassic time (Robinson et al., 2003).

The Caishiling Fm. (J_3c) is composed of yellowish massive sandy conglomerate (Fig. 5C) intercalated with quartzolithic sandstone at the base, and is characterized by purple red, gray purple siltstone in the lower part of the section. These rocks transition to variegated sandstone and siltstone intercalated with conglomerate in the middle and upper parts of the section (Ritts and Biffi, 2000; Robinson et al., 2003). In the upper part of the Caishiling Fm. (J_3c), cross-bedding is well developed in the sandstone and imbrication can be found in the conglomerate (Fig. 5D). The uppermost part of the Caishiling Fm. (J_3c) contains thick-bedded oil sands (Fig. 5E) and natural asphalt (Fig. 5F), indicating the Tula unit was once a subsidence area characterized by a topographic low different from the narrow valley that exists at present (Fig. 1). Geochemical fingerprints (e.g. carbon isotopic composition) in the Jurassic oil-bearing sandstone of the Tula basin is similar to that of the geochemical fingerprints in the Jurassic oil-bearing sandstone oil in the Qaidam Basin (Guo et al., 1998).

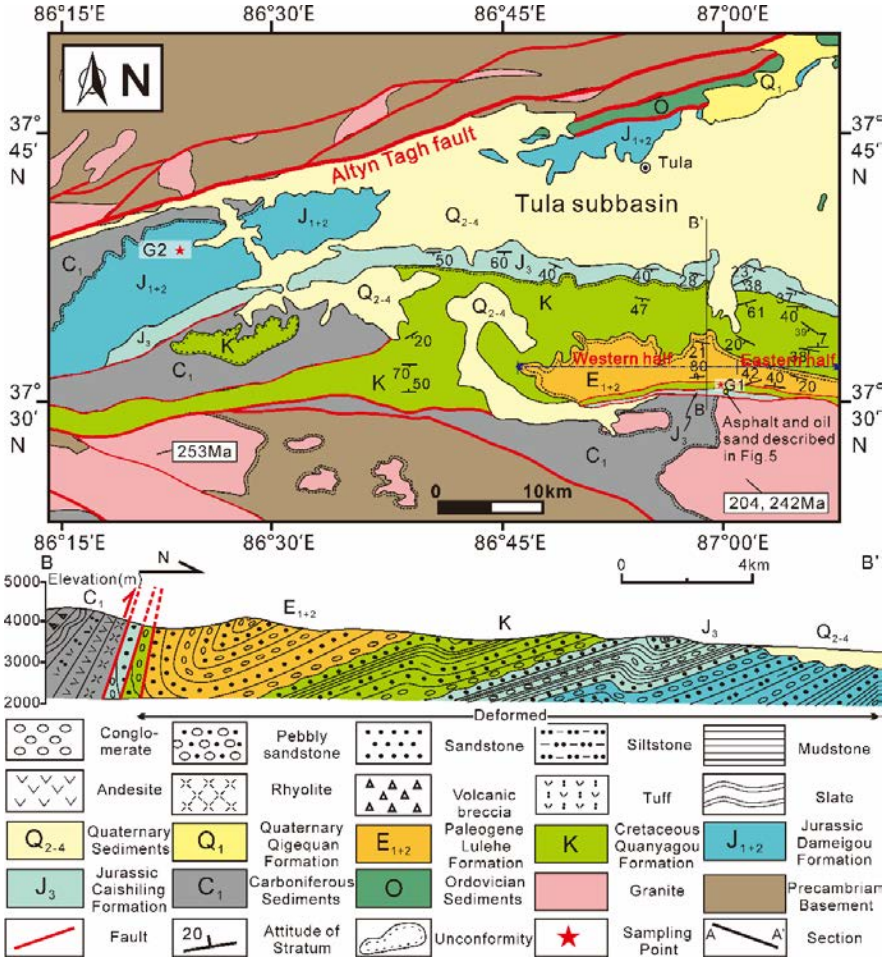

Figure 4. Geologic map (after Qiemo J45C003002 geologic map, scale 1:250,000) and geologic cross

section of the study area, compiled from HGSI (2003), Robinson et al. (2003), and XBGMR (1993). Red stars denote locations of U-Pb detrital zircon samples. Ages (zircon U-Pb) of plutons are mainly compiled from HGSI (2003). The western half and eastern half of the Eocene strata are based on the division of Dupont-Nivet et al. (2004).

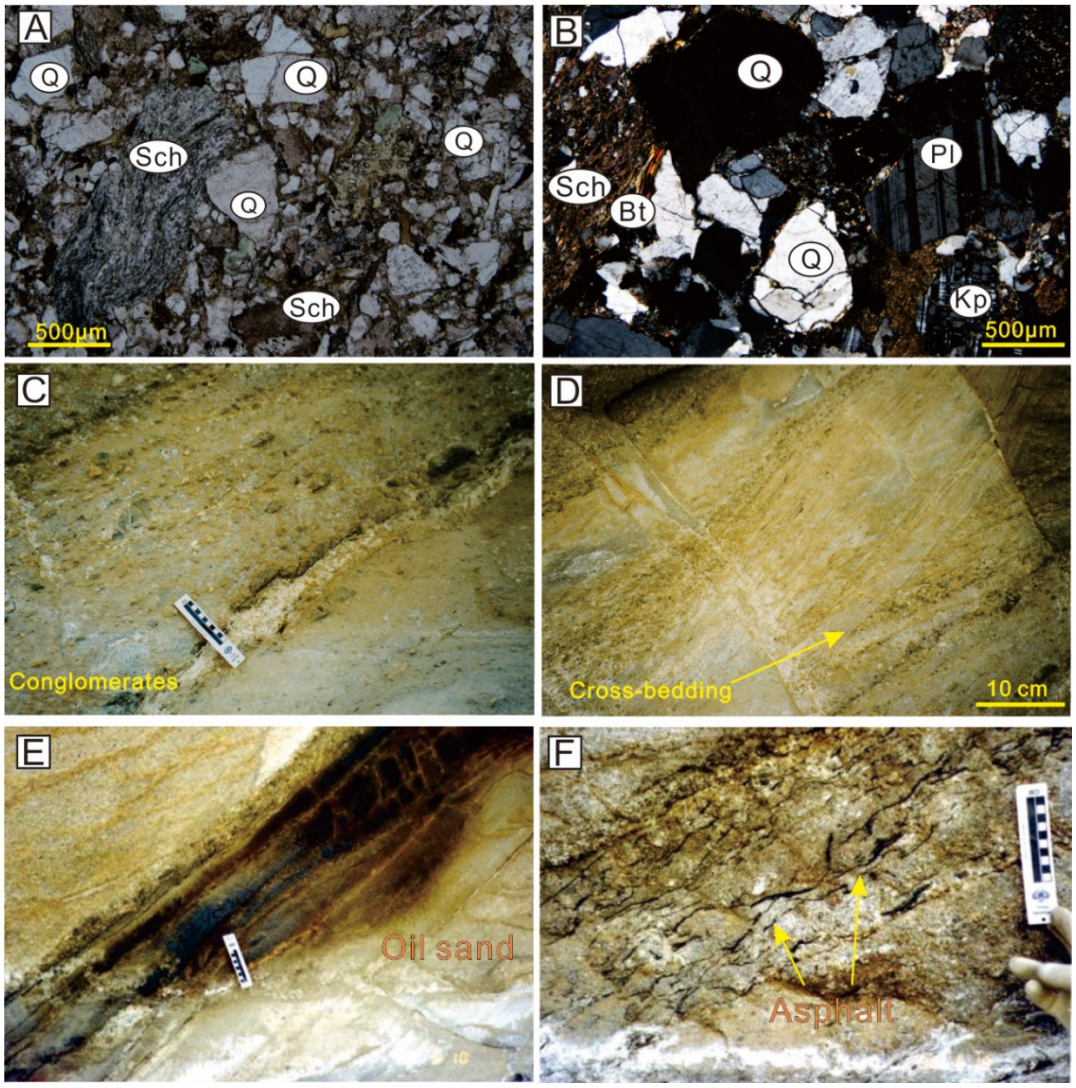

Figure 5. Typical photomicrographs and field photographs. (A) Lithic sandstone in early Jurassic strata ($J_{1+2}d$) of the Tula section, rich in lithic fragments, under plane polarized light. (B) Lithic sandstone in Early Jurassic strata ($J_{1+2}d$) of the Caishiling section, rich in various lithic fragments, under crossed polarized light. (C) Conglomerate and (D) cross-bedding in Late Jurassic (J_3c) strata of the Tula section. (E) Oil sand and (F) asphalt developed in Late Jurassic (J_3c) strata. Abbreviations: Sch—schist, Pl—plagioclase, Kp—potash feldspar, Q—quartz, Bt—biotite.

More than 2000 m of Cretaceous strata (Quanyagou Fm.) unconformably overlie the Late Jurassic strata Caishiling Fm. (XBGRM, 1993; Robinson et al., 2003). In the Tula section, Cretaceous plutons (~74 Ma) intrude Cretaceous strata, providing a minimum depositional age (XBGRM, 1993; Robinson et al., 2003). The lower part of the Cretaceous strata is dominated by purple-red conglomerate intercalated with sandstone, siltstone, and mudstone interpreted to represent lacustrine depositional environment. The upper part of Cretaceous strata consists

of purple red siltstone interbedded with silty mudstone interpreted to represent a lacustrine deltaic depositional environment (Ritts and Biffi, 2000; Robinson et al., 2003). The lacustrine to lacustrine delta deposits in the Tula unit reinforce the idea that the Tula unit was characterized by a topographic low during the Cretaceous, a setting very different from the narrow valley that exists at present (Fig. 1).

In the Tula unit, the well-exposed Paleocene to early Eocene Lulehe Fm. overlies the Mesozoic strata along a low-angle unconformity (XBGMR, 1993, HGSI, 2003; Robinson et al., 2003). The Lulehe Fm. consists mainly of purple red conglomerate interbedded with fine-grained sandstone at the base, which becomes coarser upsection with an increase in the abundance of conglomerate towards the top. The formation contains a high metamorphic lithic fraction and limestone clasts with coral fossils that suggest a proximal provenance and syntectonic deposits (Zuffa, 1980; Mack and Rasmussen, 1984; HGSI et al., 2003; Robinson et al., 2003). The distinctive purple red conglomerates found in the Lulehe Fm. are regionally similar to those found in the Qaidam basin. The Lulehe Fm. has been dated via magnetostratigraphy to between 65~53.5 and 43.8 Ma (Yang et al., 1992; Zhang et al., 2006; Ke et al., 2013). These dates further support a Paleocene to early Eocene age for the Lulehe Fm.

The Jurassic-early Eocene strata in the Tula section are heavily deformed, forming a major north-verging syncline with a steeply dipping south limb and a shallowly dipping north limb (Fig. 4). The Jurassic, Cretaceous, and Paleocene to early Eocene strata in the south limb of the syncline are inverted with a high dip angle (dipping mainly to the south from 180° to 200° at angles of 65°-80°). The contact between the Creteacous and Paleocene to early Eocene stata is characterized by a low-angle angular unconformity or a local fault boundary (XBGMR et al., 1993; HGSI et al., 2003; Robinson et al., 2003).

3.1.3.2 Cenozoic strata in the Anxi section

The Anxi section, ~150 km northeast of the Tula section, is located in the ATF zone and is bounded by the Altyn Tagh basement to the north and the Kunlun Precambrian and Paleozoic basement to the south (Figs. 2 and 6). Precambrian and early Paleozoic metamorphic rocks with igneous intrusions comprise this basement which is overlain by Mesozoic and Cenozoic strata (Guo et al., 1998; Ritts and Biffi, 2000; GGSI, 2003). The Cenozoic units in the Anxi section have been identified based on the detailed field mapping of previous studies, and depositional ages are estimated by correlating these units with the well-constrained Cenozoic strata of the Qaidam basin (Fig. 7; Huo, 1990; QBGMR, 1991; Yang et al., 1992;

Huang et al., 1996; Xia et al., 2001; Qiu, 2002; GGSI, 2003; Sun et al., 2005a; Zhao et al., 2006; Fang et al., 2007; Yin et al., 2007; Gao et al., 2009; Lu and Xiong, 2009; Wu et al., 2011).

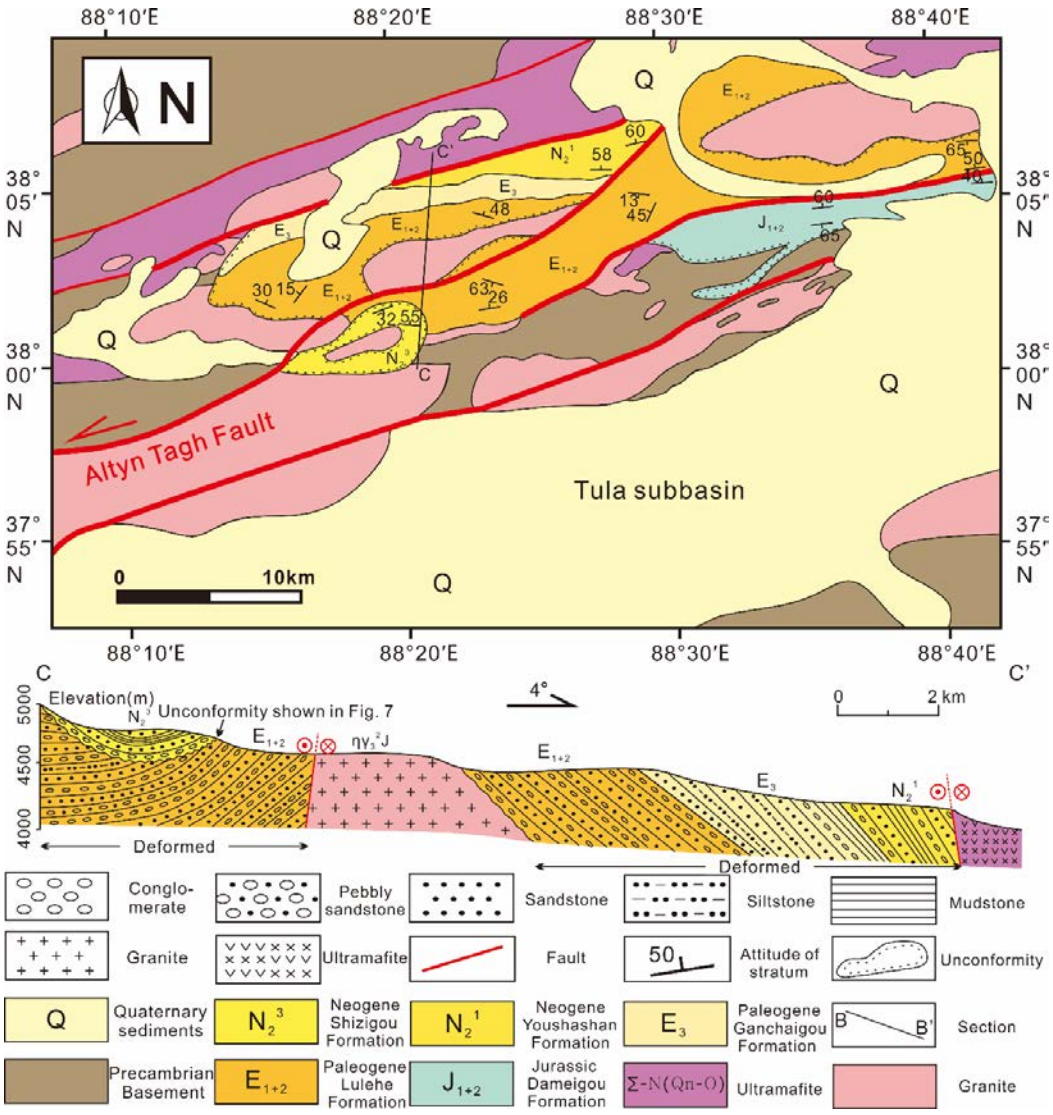

Figure 6. Geologic map (after the Washixia J45C002003 geologic map, scale 1:250,000) and geologic cross section of the study area, compiled from GGSI (2003) and XBGMR (1993).

Unlike the poorly preserved Cenozoic strata of the Tula section, the Anxi section contains a well-exposed Cenozoic stratigraphic succession that includes most of the Cenozoic units described above. The Anxi section includes the Paleocene to early Eocene Lulehe Fm., the Eocene to Oligocene Ganchaigou Fm., the Miocene Youshashan Fm. and the Pliocene Shizigou Fm. As visible in cross-sectional profile (Fig. 6), the Lulehe, Ganchaigou and Youshashan formations of the Anxi section are in conformable contact with one another and have been deformed synchronously after early Miocene time. However, in plan view, these

Paleocene to Miocene strata are cut by the left-lateral strike-slip ATF and separated from the overlying Pliocene strata of the Shizigou Fm. by an apparent angular unconformity (Fig. 6).

The Paleocene to early Eocene strata of the Lulehe Fm. crop out in the northern part of the valley and trend in a NE direction. These strata are characterized by brick-red conglomerates and pebble sandstones intercalated with sandstones and siltstones. This portion of the Lulehe Fm. is separated from the typically overlying Eocene strata of the Xiaganchaigou Fm. by the disappearance of the conglomerate layers (GGSI, 2003). The Eocene to Oligocene strata of the Ganchaigou Fm. only crop out in the northern part of the valley. The lack of paleomagnetic data in the Anxi section has thus far prevented a further division of these strata into two units as has been done in the western Qaidam basin (Fig. 3). The lower part of the Ganchaigou Fm. is dominated by grey to greyish-green sandstones intercalated with siltstones, biomicrites and mudstones. The upper part of the Ganchaigou Fm., however, is characterized by greyish-green calcareous shales and mudstones. The Gangchaigou Fm. is overlain by the Miocene Youshashan Fm., which contains brown granule conglomerate at its base (GGSI, 2003). Like the overlying Ganchaigou Fm., the Youshanshan Fm. crops out in the northern part of the valley. The Youghshanshan Fm. has not been subdivided into two units as has been done in the western Qaidam basin (Fig. 3; GGSI, 2003). The lower and middle sections of the Youshashan Fm. strata consist mainly of brown and maroon granule conglomerate interbedded with coarse sandstone while the upper part is characterized by purple and brown sandstone and pebble sandstone interbedded with conglomerate, siltstone and mudstone. These primarily brown strata distinguish the Youshashan Fm. from the overlying Pliocene strata of the Shizigou Fm., which is characterized by earthy yellow and grey pebble sandstone at its base (GGSI, 2003). The Pliocene strata are then overlain by Quaternary sand-gravel beds which lie atop an angular unconformity (Fig. 6). The lithology in the lower part of the Pliocene strata consists of sandstone interbedded with siltstone and mudstone while the middle and upper parts of the Pliocene strata are characterized by conglomerate and sandstone intercalated with siltstone (GGSI, 2003). These thickly-bedded conglomerates are interpreted to represent alluvial fan to fluvial facies (Ritts and Biffi, 2000).

3.1.4 Methods

3.1.4.1 Field investigation and seismic profile interpretation

We used three sections (Tula, Anxi, and Caishiling) along the western segment of the ATF to study stratigraphic features of the Mesozoic-Cenozoic deposits (Fig. 2). We integrate

three high-quality seismic profiles of the western Qaidam basin with our surficial field observation to explain the tectonic history of this region. Two of the seismic profiles (A-A' and D-D') trend along strike (northeast) of the ATF while one of the profiles (E-E') trends perpendicular (northwest) to the ATF (Fig. 2). Seismic data were interpreted using SMT Kingdom software.

Table 1. Summary of the major characteristics and corresponding statistical data for each of the samples.

Epoch	Formation (Fm.)	Sample number	Lithology	Detrital zircon age range (Ma)	Detrital zircon peaks (Ma)	Number of effective data points	Th/U ratios
Tula unit							
Cretaceous	Quanyagou Fm.	G1	Gray-yellow pebbly sandstone	218~2532	~238 ~414 ~904 ~1737	89	0.13~1.51
Early-Middle Jurassic	Dameigou Fm.	G2	Gray-white sandstones	254~2430	~250 ~447 ~1435 ~2465	99	0.09, 0.10~ 1.98
Caishiling unit							
Cretaceous	Quanyagou Fm.	CSL1	Gray-white sandstone	228~2915	~262 ~456 ~897	94	0.10~2.05
Late Jurassic	Caishiling Fm.	CSL2	Gray-white sandstones	246~2661	~254 ~445 ~926	100	0.03, 0.06, 0.12~1.55
Early-Middle Jurassic	Dameigou Fm.	CSL3	Gray-yellow sandstones	220~2480	~264 ~433	97	0.25~3.82

3.1.4.2 Sampling and analytical process

Detrital zircon geochronology is rapidly developing into an essential tool for sediment provenance analysis and geodynamic study (e.g. Fedo et al., 2003; Thomas, 2011; Gehrels et al., 2011; Gehrels, 2014). U-Pb dating of detrital zircons from sediments is widely used to reconstruct the provenance of ancient sedimentary systems. To identify appropriate piercing points along the ATF, five sandstone samples ranging in age from Lower Jurassic to Cretaceous were collected from the Tula and Caishiling sections. In the Tula section, we collected two samples: G1 and G2. Sample G1 is gray-yellow pebbly sandstone from the Cretaceous Quanyagou Fm. (Kq). Sample G2 is gray-white sandstone from the lower Jurassic Dameigou Fm. ($J_{1+2}d$). In the Caishiling section, we took three samples: CSL1, CSL2 and CSL3. Sample CSL1 is a gray-white fine-grained sandstone from the Cretaceous Quanyagou Fm. (Kq). Sample CSL2 is a gray-white medium-grained sandstone from the Upper Jurassic

Caishiling Fm. (J_3c). Sample CSL3 is a gray-yellow coarse-grained sandstone from the Lower Jurassic Dameigou Fm. (J_3c) (Fig. 2). Detailed descriptions of the zircon separation and LA-ICP-MS U–Pb dating of zircon are provided in the GSA Data Repository (see footnote 1[①]).

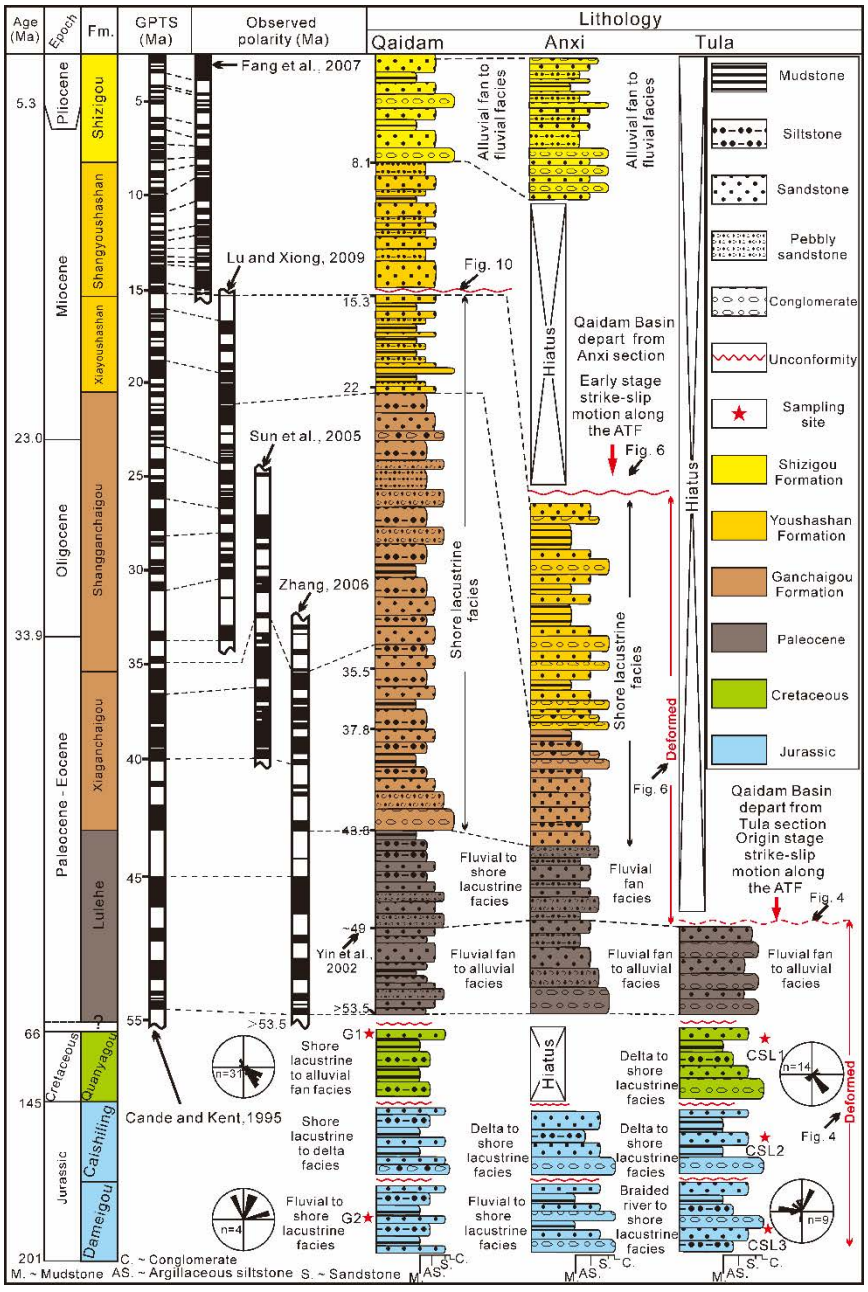

Figure 7. Chronostratigraphic correlation of the relic Mesozoic to Cenozoic strata along the Altyn Tagh fault. GPTS—geomagnetic polarity time scale of Cande and Kent (1995). Observed polarity was compiled from Yin et al. (2002), Z.M. Sun et al. (2005), Zhang (2006), Fang et al. (2007), and Lu and Xiong (2009). Paleocurrents are from Ritts and Biffi (2000). Chronostratigraphic correlation is based on field observation and previous studies (XBGMR, 1993; Guo et al., 1998; Ritts and Biffi, 2000; GGSI, 2003; HGSI, 2003; Robinson et al., 2003). ATF—Altyn Tagh fault.

[①] 1 Supplemental File. Description of zircon separation and LA-ICP-MS U-Pb dating of zircon, Figure DR1, and Tables DR1–DR2. Please visit http://dx .doi .org/10 .1130 /GES01070 .S1or the full-text article on www.gsapubs .org to view the Supplemental File

3.1.5 Results

3.1.5.1 U–Pb geochronology of detrital zircons

Isotopic ages with errors and related raw data are listed in full in Table DR1 (see footnote 1). The various zircon age groups and corresponding data for each sample are shown in Table 1. CL images of typical zircon grains are presented in Figure DR1 (see footnote 1).

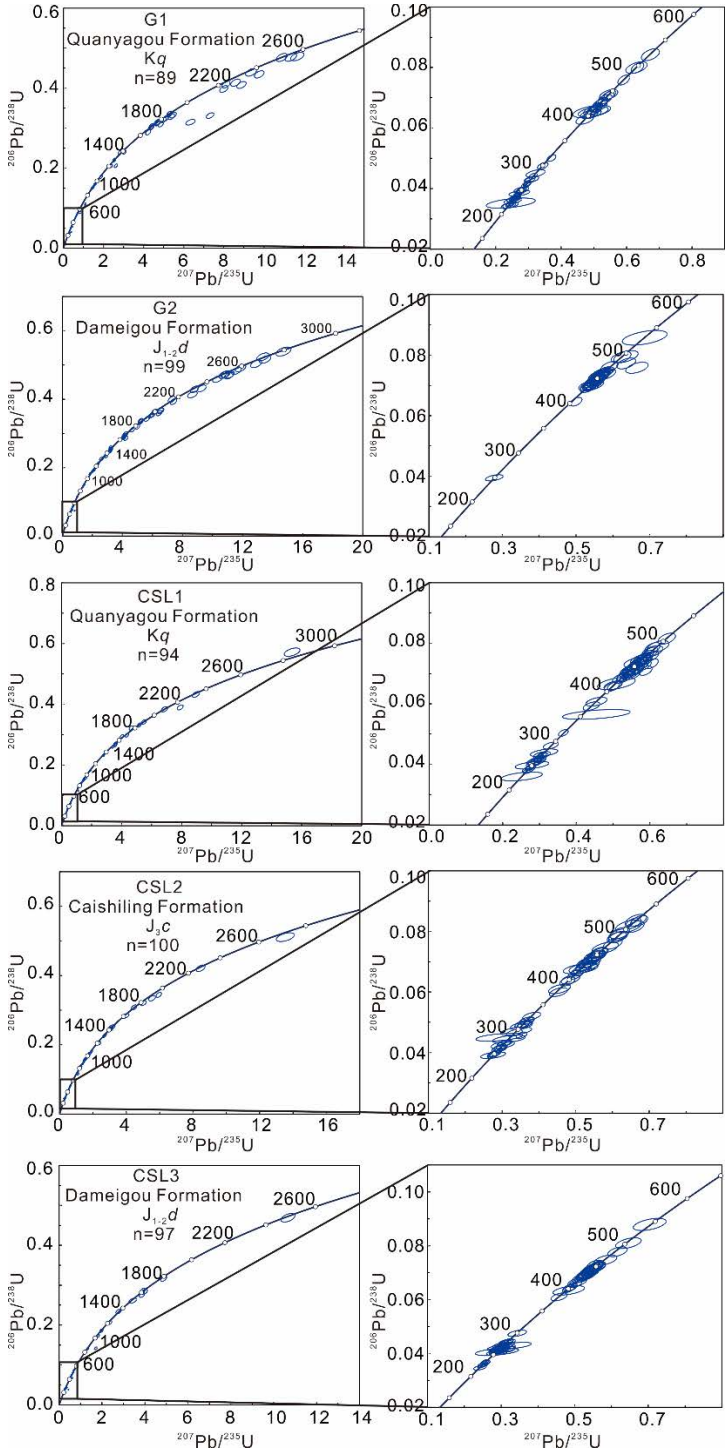

Figure 8. U-Pb concordia diagrams for zircon grains from the five sandstone samples

3.1.5.1.1 Jurassic samples

The zircons from sample G2 (Dameigou Fm.) are ~50-200 μm long and mainly subhedral to subrounded. The grains are generally colorless and exhibit prominent oscillatory zoning. Th/U ratios typically clustered between 0.09 and 1.98. Forty-eight out of 99 dated grains yielded a 206Pb/238U range of 530 to 404 Ma with a single peak in the age spectrum at 447 Ma (Fig. 9A). Only one zircon with a Triassic age (250 Ma) was obtained. The ages of all other zircons range from 2781 to 696 Ma.

In sample CSL3 (Dameigou Fm.), zircon grain morphology ranges from euhedral to abraded with an average size ranging between 50 μm and 250 μm. CL images show that most of these zircon crystals are characterized by relatively distinct oscillatory zoning. Th/U ratios vary between 0.25 and 3.82. The U-Pb ages range from 2480 to 220 Ma (Fig. 9B). The ages can be separated in three main groups with two peak ages at 264 Ma, 433 Ma, and eleven ages between 2480 to 852 Ma.

In sample CSL2 (Caishiling Fm.), zircon crystals display euhedral to abraded shapes for an average size ranging between 50 μm and 250 μm. The majority of the crystals display distinct oscillatory zoning in CL images indicating a magmatic origin confirmed by Th/U ratios varying between 0.12 and 1.55 (with two exception of 0.03 and 0.06). Among the 100 crystals analyzed, all zircon ages with a discordance degree of <10% were used. The U-Pb ages range from ~2661 to ~246 Ma (Fig. 9C). The age distributions are divided into four groups with two major peaks at ~254 Ma and ~445 Ma, a distribution spanning from 1073 Ma to 701 Ma with a peak at 926 Ma, and finally seven ages clustered around 1416 Ma.

3.1.5.1.2 Cretaceous samples

The zircons from sample G1 (Quanyagou Fm.) are predominantly colorless, euhedral to subhedral, and with a length of 50-150 μm. Most zircons show oscillatory zoning without inherited cores or overgrowths. All analyses have moderate U content, with variable Th/U from 0.13 to 1.51. In this study, 59 out of 89 dated grains yielded a 206Pb/238U range of 521 to 218 Ma with two age peaks at 414 Ma and 238 Ma (Fig. 9D). The age of the remaining zircons range from 2532 to 818 Ma with several subpeaks at 2502, 1737 and 904 Ma.

In sample CSL1 (Quanyagou Fm.), zircon grains show euhedral to abraded shapes with an average size between 50 μm and 200 μm. Most crystals show distinct oscillatory zoning. Th/U ratios vary from 0.10 to 2.05. 100 grains were analyzed and 94 effective data points were obtained. The U-Pb ages range from 2915 to 228 Ma. The ages can be separated in four main groups with three peaks at 897 Ma, 456 Ma and 262 Ma (Fig. 9E). In addition, fifteen

Proterozoic ages are given above 1000 Ma.

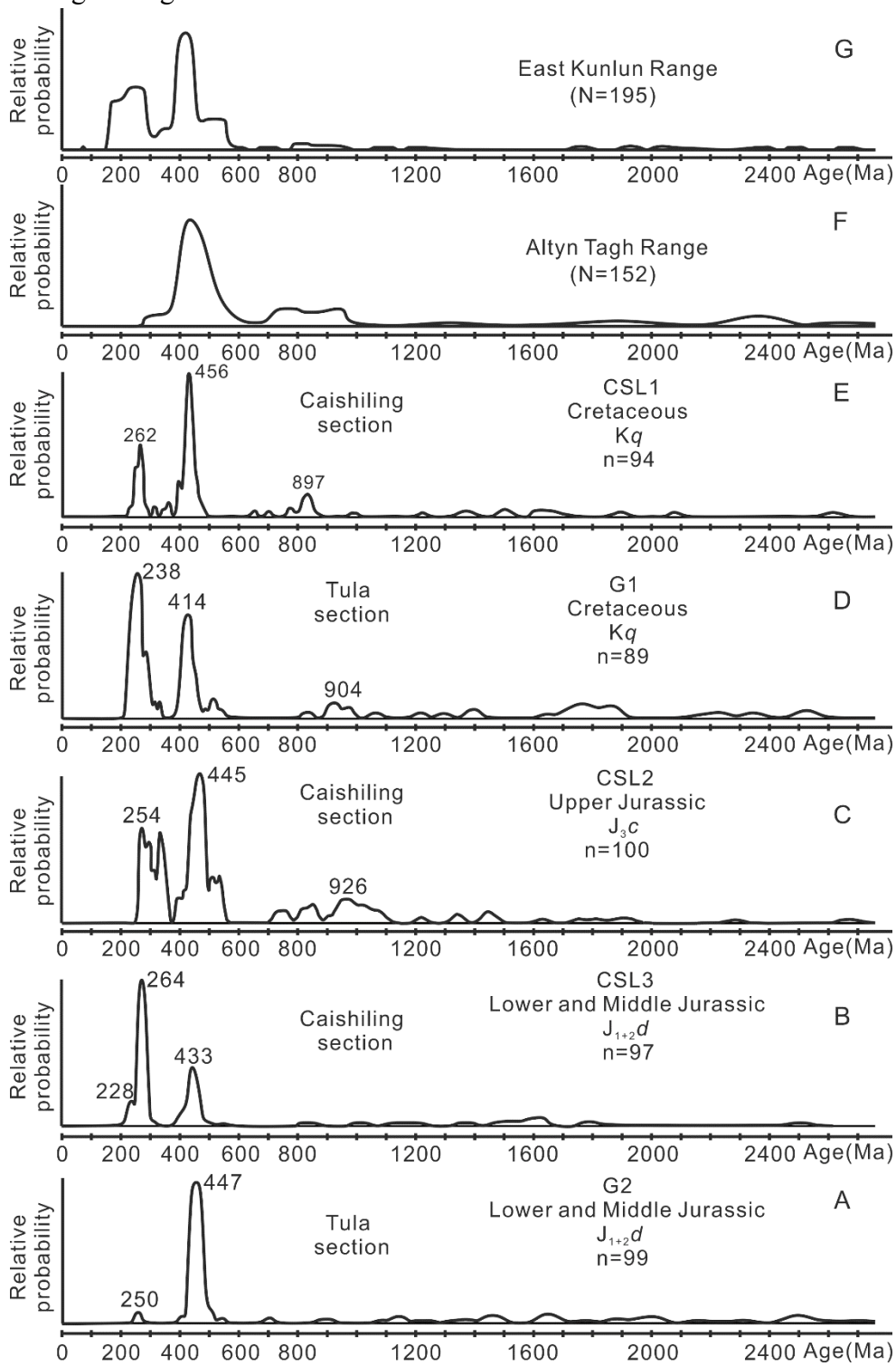

Figure 9. Relative probability histogram plots of U-Pb ages of detrital zircons from the five Jurassic and Cretaceous sandstone samples and relative probability histogram plots of pluton ages in the Altyn Tagh and Eastern Kunlun Ranges. Age data are from Yang et al. (2006), Zhang et al. (2001), Chen et al. (2003), Gehrels et al. (2003a, 2003b), Yue et al. (2005), Yang et al. (2006), L. Liu et al. (2007, 2013), Lu et al. (2008), Liu et al. (2009), Zhang et al. (2011), Li et al. (2013), and Wang et al. (2013). More information on dating and ages is provided in Table DR2 (see text footnote 1).

3.1.6 Discussion

3.1.6.1 New piercing points

Using lithologic and stratigraphic constraints, we conclude that both the Tula and Anxi sections were once regions of extensive subsidence characterized by topographic lows (Figs. 1 and 2). The dark mudstone, oil sands (Fig. 5E) and asphalt (Fig. 5F) found in the Upper Jurassic strata of the Tula section indicate Tula basin was once a depression during Late Jurassic time. In addition, matching geochemical fingerprints (e.g. carbon isotopic composition) between the Jurassic oil-bearing sandstone of the Tula basin and the Jurassic crude oil of Qaidam basin suggests that these two regions must have been parts of the same prototype basin (Guo et al., 1998). Recent studies confirm that the relatively rigid Qaidam basin was transported northeastward along the ATF during the Cenozoic, and has not undergone obvious basin-scale vertical axis rotation with respect to the Eurasian Plate since early Eocene time (Wang et al., 2006; Yu et al., 2014). Considering the large-scale left-lateral strike-slip displacement of the ATF during Cenozoic time, we suggest the Tula and Anxi sections were once part of the Qaidam basin but detached from the Qaidam during its northeasterward migration driven by faulting on the ATF. We propose the Qaidam basin may have actually been originally located much farther southwest along the ATF than its present position, likely located where the Tula and Anxi sections currently reside.

Stratigraphic successions are generally deposited during basin infilling processes, while periods of non-deposition or erosion are likely related to regional tectonic events (e.g. Wheeler, 1964; Allen and Allen, 1990; Boggs, 2006). In the Tula section, Paleocene strata correlate well with strata in the Caishiling section, however, post-Paleocene strata are missing (Figs. 4 and 7). In the Anxi section, Paleocene to early Miocene strata cross-correlate with comparable strata preserved in the Caishiling section, whereas the late Miocene are missing (Figs. 6 and 7). In the Qaidam basin, and particularly in the Caishiling section, the Paleocene to Quaternary strata are well developed (Figs. 2 and 7). If we consider a stepwise northeastward migration of the Qaidam basin along the ATF throughout the Cenozoic, the absence of post-Paleocene strata in the Tula section marks the detachment of the Qaidam basin from this section. Similarly, the absence of late Miocene strata in the Anxi section marks the detachment of the Qaidam basin from this section (Fig. 7). We therefore propose that the Paleocene strata in the Tula section and the Paleocene to early Miocene strata in the Anxi section represent the two piercing points to identify the initial position and early stages of Qaidam basin detachment and movement.

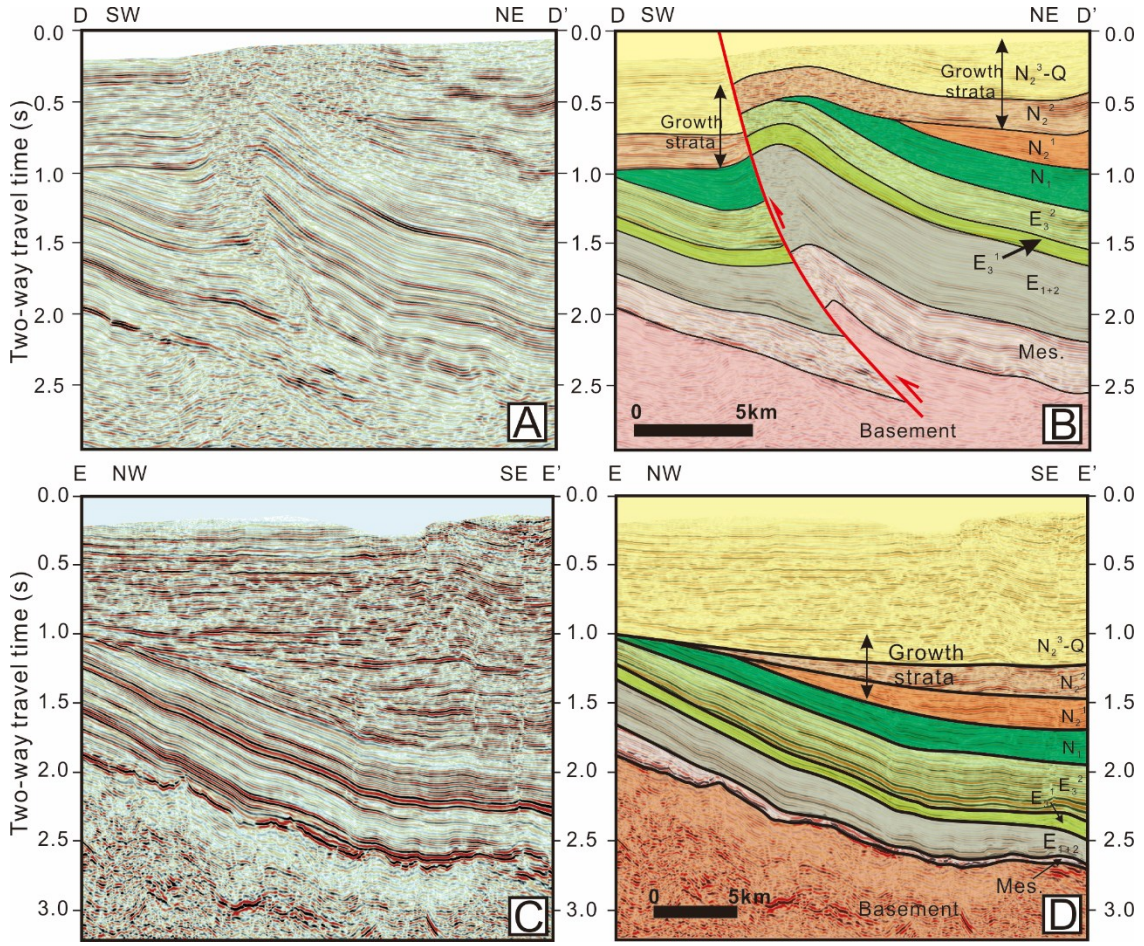

Figure 10. Seismic profiles in the southwestern Qaidam Basin; see Figure 2 for location. (A) Uninterpreted and (B) interpreted seismic profiles in the SW–NE direction; (C) uninterpreted and (D) interpreted seismic profiles in NW–SE direction. Note that the growth strata since the Xiayoushashan Formation (N_2^1xy) indicate the intense tectonic movement of the Altyn Tagh fault during middle Miocene time.

The Tula section contains consistently southward dipping strata on both sides of the low-angle (smaller than 10 degree) Jurassic-Cretaceous and Cretaceous-early Eocene unconformities (Fig. 4). These Jurassic-early Eocene sequences are heavily deformed, forming a major north-verging syncline with a steeply dipping south limb and a shallowly dipping north limb, indicating the deformation of these Jurassic-early Eocene sequences occurred during or after early Eocene time (Fig. 4). We therefore suggest that the topographic low in the Tula area became isolated during early Eocene time and the folding of the Tula syncline is related to motion on the fault to the south which was kinematically linked to the ATF during this time period. It is therefore likely that the Tula section was part of the Qaidam basin during early Eocene time and became isolated when the Qaidam basin migrated northward. This migration was induced by movement along the ATF, which is consistent with the initial timing of faulting along the ATF (ca. 49 Ma) as proposed by Yin et al. (2002). We therefore conclude that the

Tula section is an appropriate piercing point to constrain the initial stage (~49 Ma) of faulting along the ATF.

In Anxi section, the fine-grained deposits in the Oligocene to Miocene strata indicate that the Anxi unit was once a topographic low (HGSI, 2003). The lithofacies of the Pliocene Shizigou Fm. of the Anxi section are dominated by a succession of proximal fluvial deposits. In the western Qaidam basin, the Pliocene Shizigou Fm. is characterized by lacustrine facies (Yin et al., 2008b), suggesting that these two regions maintained different depositional systems during Pliocene time. The continuous sequences of Paleocene to early Miocene strata and the angular unconformity between the Youshanshan and Shizigou formations demonstrate that the Anxi section experienced a tectonic event between the early Miocene and Pliocene epochs, and this event in turn resulted in the deformation of the Paleocene to early Miocene strata (Figs. 6 and 7). Seismic profiles from the western Qaidam basin reveal that the Pliocene strata conformably overlie the Miocene strata and illustrate a distinctive unconformity between the Shangyoushashan and Xiayoushashan formations, both of which are Miocene in age. This unconformity becomes most prominent in the southern foothills of the Altyn Tagh Range, further indicating intense left-lateral strike-slip faulting along the ATF (Figs. 3 and 10; Meng and Fang, 2008; Wang et al., 2010a; Wu et al., 2012a). Within the western Qaidam basin, this unconformity is characterized by growth strata that started to develop after the initial deposition of Miocene strata. In profile DD' (Fig. 10), the deposits are cut by a branch fault of the ATF and the pre-Miocene strata are deformed by an anticline which was later cut and sealed by Miocene strata. Similarly, in profile EE' (Fig. 10), the growth strata are well developed and the thickness of the Eocene to Miocene pre-growth strata remains constant. The middle Miocene to Quaternary deposits thin northwestwards (toward the Altyn Tagh Range). Based on magnetostratigraphy, palynology and paleontology within the basin, the accurate timing of this regional unconformity has been constrained to ~15 Ma (Fang et al., 2007; Gao et al., 2009; Lu and Xiong, 2009; Wang et al., 2010a; Wu et al., 2012a). We thus suggest that the apparent unconformity between the Shangyoushashan and Xiayoushashan formations indicates middle Miocene (~15 Ma) motion of the Altyn Tagh fault system. Based on this, we propose that the deformed Paleocene to Miocene strata of the Anxi section represents another piercing point to constrain the historical position of the western Qaidam basin during mid-Miocene time. The initial stage of left-lateral strike-slip faulting along the ATF led to a gradual separation of the western Qaidam basin from the Anxi section. Tectonic movement precluded new deposition of strata, and the Anxi section became isolated from the Qaidam basin during late Miocene time. In addition to the ATF, we suggest the left-lateral strike-slip faulting of the

Baiganhu fault to the south of the basin also accommodated the northeastward motion of the Qaidam basin (Cowgill et al., 2003; HGIS, 2003; Wang et al., 2014). The Pliocene marginal conglomerate facies of the Anxi section formed via proximal accumulation sometime after initial stage left-lateral strike-slip faulting of the ATF.

3.1.6.2 Provenance analysis of Jurassic to Cretaceous strata

If the Cenozoic strata in the Tula and Anxi sections represent the initial timing and early stages of motion along the ATF and the postulated historical position of the Qaidam basin is reasonable, the pre-faulting deposits (Mesozoic strata) in the Tula section and the western Qaidam basin (Caishiling section) should be lithologically similar and their provenance comparable.

Paleocurrents in the Jurassic strata of the Tula, Anxi, and Caishiling sections all suggest northward current movement while Cretaceous strata show southward moving paleocurrents (Fig. 7; Ritts and Biffi, 2000). In general, there is relatively little paleocurrent data for Tula, Anxi, and Caishiling sections (e.g. n = 4 in the Tula section), however, the generally consistent orientation of paleocurrents across all three sections reflects a similar topography for these regions (Tula, Anxi and Caishiling) between Jurassic and Cretaceous time. Relative probability histogram plots of pluton ages in the Altyn Tagh and Eastern Kunlun ranges are shown in Fig. 9. Based on the morphological characteristics, internal textures and Th/U ratio of zircons, magmatic zircons (about 80 %) appear to dominate the section while metamorphic zircons (about 20 %) comprise the remainder (Corfu et al., 2003; Hanchar and Rudnick, 1995; Hoskin and Black, 2000).

In the Altyn Tagh Range, Archean and Proterozoic basement rocks are widely exposed with Archean zircon U-Pb ages ranging from ~3.6 Ga (Lu et al., 2008) to ~2.6 Ga (Lu and Yuan, 2003) and Proterozoic zircon U-Pb ages ranging from ~2.4 Ga to ~650 Ma (Gehrels et al., 2003a; Gehrels et al., 2003b; Wang et al., 2006b; Zhang et al., 2011; Wang et al., 2013). Paleozoic intrusions within this range show zircon U-Pb ages ranging from ~550 Ma to ~400 Ma (Sobel and Arnaud, 1999; Zhang et al., 2001; Cowgill et al., 2003; Gehrels et al., 2003a; Chen et al., 2004; Yue et al., 2004a, 2005; Yang et al., 2006; Wang et al., 2008; Liu et al., 2009) (Fig. 2). Only a few isolated Permian igneous rocks are distributed along the center of this range, with zircon U-Pb ages ranging between ~300 Ma and ~270 Ma (Cowgill et al., 2003; Gehrels et al., 2003a, 2003b).

With regard to the Eastern Kunlun Range, the Proterozoic basement rocks are isolated and show zircon U-Pb ages ranging from 1900 to 800 Ma (e.g. HGSI, 2003; Wang et al., 2013).

The Paleozoic to late Proterozoic intrusions show a zircon U-Pb age peak around 430 Ma which is based on early Paleozoic metamorphic rocks which represent the Ordovician - Silurian docking of the Kunlun and Tarim blocks (e.g. Matte et al., 1996; Cowgill et al., 2003; Li et al. 2013). The Kunlun basement age distribution is characterized by the occurrence of late Paleozoic - early Mesozoic ages (~300 to ~200 Ma) which correspond to the Permo-Triassic closure of the Paleotethys Ocean and the docking of the Qiangtang Block (Roger et al., 2003, 2008; Roger et al.,2010; Dai et al., 2013; Li et al., 2013). Finally, a few Mesozoic ages (e.g. ~74 Ma) have been obtained from the Tula section (Robinson et al., 2003).

In order to better constrain the provenance of the five sandstone samples, the plutons of the Altyn Tagh and Eastern Kunlun ranges are simply divided into two groups: those plutons with an age older than 270 Ma and those whose age is younger than 270 Ma. Older plutons are widespread in both the Altyn Tagh and Eastern Kunlun ranges, whereas younger plutons are confined to the Eastern Kunlun Range just south of our sample sites (Fig. 2). This distinctive pluton distribution can be used as a provenance signature to identify the source of detrital zircon for our Mesozoic samples. In general, detrital zircon age clusters in all five samples are basically similar and characterized by two main groups of Permian-Triassic and Paleozoic ages along with a small number of Precambrian ages (Figs. 8 and 9). The appearance of the Permian-Triassic zircon ages (<270 Ma) in all five samples strongly suggests an East Kunlun Range provenance. We consider that the slightly different peak ages of sample CSL1, CSL2, CSL3, G1 and G2 result from contributions of plutonic debris with a variety of ages (Fig. 9; Tab. 1).

In the Caishiling section, the sampling sites of the three Jurassic-Cretaceous samples (CSL1, CSL2 and CSL3) are located at the southern piedmont of the Altyn Tagh Range, where the basement is mainly dominated by Paleozoic and Precambrian plutons with ages older than 270 Ma (Fig. 9). If the Caishiling section has been situated in roughly the same region that it occupies today (Fig. 2), the Altyn Tagh Range must serve as the ultimate provenance for the zircons from the Jurassic-Cretaceous samples. If this is the case, the U-Pb age spectrum of these samples should display a Paleozoic and Precambrian age peak (>270 Ma). In samples CSL1, CSL2 and CSL3, the detrital zircon age spectra are similar and characterized by two main groups of Permian-Triassic and Paleozoic ages along with a small number of Precambrian ages. The widespread distribution of the Paleozoic and Precambrian plutons in both the Altyn Tagh and Eastern Kunlun Ranges prevents the use of zircon age spectra to estimate the estimate the source area of these Cretaceous and Jurassic samples. Nevertheless, all three samples contain a host of late Permian to Triassic zircon ages (<270 Ma) which are

found only in the plutons of the Eastern Kunlun Range, particularly those in the south Tula section (Figs. 2 and 9). In addition, the angular grains in the Jurassic samples shows poor sphericity and poor sorting, indicating deposition from a proximal source terrain (Figs. 5A and 5B). Based on the proximal source feature and the particular age spectrum (containing a host of late Permian to Triassic zircons) of these three samples, we suggest the Caishiling section was situated far closer to the Tula section in the past as compared with its current position. Meanwhile, plutons in the Eastern Kunlun Range had already been unroofed during early Jurassic time, representing a main source to the Dameigou (J1+2d), Caishiling (J3c) and Quanyagou (Kq) formations since that time.

In the Tula section, two Jurassic and Cretaceous samples (G1 and G2) were selected from the narrow Tula subbasin. The G1 sample was selected near the East Kunlun Mountains while the G2 sample was selected near the Altyn Tagh Range (Figs. 2 and 4). The age cluster of sample G1 features two main groups of Permian-Triassic and Paleozoic ages along with minor Precambrian ages, a pattern similar to that found in the Cretaceous sample from the Caishiling section (Figs. 9D and 9E). We thus suggest that the late Permian to Triassic strata of the Eastern Kunlun Range, and the Paleozoic and Precambrian plutons in both Eastern Kunlun and the Altyn Tagh ranges are the source rocks for the Cretaceous strata (Figs. 2 and 4). In particular, the age spectrum in the early Jurassic sample (G2) is characterized by an exceptionally unimodal distribution of detrital zircon (age ranging from 404 to 493 Ma, peak at 447 Ma) with only one Triassic age (250 Ma), whereas all of the other samples (G1, CSL1, CSL2 and CSL3) are characterized by bimodal distributions (Permian-Triassic and Paleozoic groups), suggesting that G2 is a distinct sample. The site location for G2 is extremely close to the Altyn Tagh Range and the older plutons within the Altyn Tagh Range serve as a major source of debris for sample G2 (Figs. 2 and 4). Older plutons from the Altyn Tagh Range represent the dominant source material, resulting in relatively little contribution from the East Kunlun Range as evidenced by very few Permian to Triassic zircons in the age distribution of sample G2 (Fig. 9A). However, the one zircon grain with a Triassic age found in sample G2 and the northward paleocurrents do suggest some small contribution may have come from the Permian-Triassic rocks of the East Kunlun Range (Figs. 7 and 9A; Ritts and Biffi, 2000). Therefore, we suggest the most plausible explanation for the anomalous detrital zircon ages found in the G2 sample is a mixture of source material from both the Altyn Tagh and the East Kunlun ranges. If the plutons from both locations (Paleozoic and Precambrian in the Altyn Tagh Range and Permian to Triassic on the East Kunlun Range) were exhumed during Jurassic time, they would represent a mixed source for samples G2 and CSL3 during that time.

By reconciling the detrital zircon ages of the sediments from the Altyn Tagh and Eastern Kunlun Ranges and combining this data with the large-scale left-lateral strike-slip displacements measured along the ATF, we deduce that the Caishiling section must have been located much closer to the Eastern Kunlun Range between Jurassic and Cretaceous time. The Tula unit, on the other hand, likely has not moved since Jurassic time. The lithologic and stratigraphic contact features of the residual Mesozoic to Cenozoic strata along the ATF combined with U-Pb dating of the Jurassic and Cretaceous samples of the Tula and Caishiling sections enable us to establish the timing of movement along the ATF. We resolve the motion along the ATF into two distinct stages: initial movement occurring at ~49 Ma and a subsequent early stage movement occurring at ~15 Ma. Both stages promote strike-slip motion along the fault. The Tula and Anxi sections can be used as piercing points along the western segment of ATF and we identify these regions as residual components of the original Qaidam basin.

3.1.6.3 Implications for the initial timing and total offset of the ATF

3.1.6.3.1 A general review of previous estimates

In the past few decades, a number of approaches have been used to estimate the overall displacement along the ATF. By comparing Paleozoic suture zones in the western Kunlun range with those in the Qilian Shan, CSBS (1992) argued for ~ 1200 km of offset along the fault. By matching similar geological features, particularly Late Paleozoic magmatic belts in the western and eastern Kunlun Shan, ranges of 300~500 km, 475 ± 70 km and ~550 km of displacement have all been estimated (Tapponnier et al., 1986; Peltzer and Tapponnier, 1988; Cowgill et al., 2003). Comprehensive correlations of the geologic features with the magmatic histories in the Altyn Tagh Range, Qilian Shan and Nasn Shan enabled Gehrels et al. (2003a) to suggest offsets of ~370 km, 375 km and ~400 km along the ATF. By reconstructing the shortening of the Nan Shan thrust belt, Yin and Harrison (2000) inferred 360 ± 50 km of displacement. A comprehensive analysis of the geologic features along the north margin of the Tibetan plateau has yielded estimates of ~400 km of offset (Molnar and Tapponnier, 1975). Using the measured Pliocene-Quaternary slip rate over the inferred duration of faulting along the ATF, Burchfiel and Royden (1991) estimated a ~200 km fault displacement. By matching the Tertiary rocks along the northern and the central segments of the ATF, Wang (1997) ascertained 69-90 km of displacement. Chen et al. (2002) suggested an offset of 500 ± 130 km between 24 Ma and present based on paleomagmatic data from the Qaidam basin. Notably, 400 ± 60 km has also been suggested based on the reconstruction of a Jurassic facies boundary

across the ATF (Ritts and Biffi, 2000).

On the other hand, magnetostratigraphy and sedimentological analysis has led some to suggest the ATF has been active since ca. 49 Ma rather than simply 24 Ma (Yin et al., 2002). Thermochronological data from the Altyn Tagh Range in conjunction with sedimentological evidence suggests that left-lateral strike-slip faulting occurred from late Eocene to early Oligocene time (Chen et al., 2001; Meng et al., 2001; Yue et al., 2001; Ritts et al., 2004). Yet still others point to geologic evidence within the northern Tibetan plateau that shows the onset of this left-lateral faulting occurred sometime during Miocene epoch (Wan et al., 2001; Wu et al., 2012a, 2012b).

As is apparent, the tremendous discrepancies both in total displacement and the timing of initial left-lateral movement along the fault may be attributed partially to an incomplete understanding of the lithology and tectonic history of the Altyn Tagh Range. This also makes is particularly challenging to find an ideal piercing point. Some estimates on the displacement of the ATF use plutonic belts or suture zones as the offset markers, but these large tectonic features have poor spatial definition because of high uncertainties in their shape and the extent of their geologic margins (Yin and Harrison, 2000; Yin et al., 2002). The intense deformation and shortening of the eastern and western Kunlun Ranges throughout geologic history as well as the deformation along the Qilian Shan has served to profoundly complicate any measurement of the actual displacement of the ATF.

3.1.6.3.2 Reassessing Cenozoic kinematic patterns on the ATF using new piercing points

The Qaidam and Tarim basins are both relatively rigid blocks when compared with the Altyn Tagh Range, which gives them relatively higher crustal strength (Wang et al., 2006a; Zhou et al., 2006). Paleomagnetic studies have revealed a 13.3°± 8.8° difference in paleomagnetic declination between the two halves of the arcuate structure outlined in the uplifted region of the Tula section (Fig. 4; see also Figure 3 in Dupont-Nivet et al., 2004) and suggest northwards transport along the ATF of this section, the western segment of the Eastern Kunlun Range (Qimen Tagh Range) and the Qaidam basin (Dupont-Nivet et al., 2004; Yu et al., 2014). The absence of a large vertical axis of rotation in the area adjacent to the ATF indicates that the left-lateral shear strain between the Tarim basin and the northern Tibetan plateau is concentrated on the relative weak ATF (Dupont-Nivet et al., 2002, 2003, 2004; Sun et al., 2005a). The relative movement of the Qaidam and Tarim basins is therefore representative of the actual displacement along the ATF. The distinctive sediment features that manifest along the ATF identify this displacement history can be used to locate appropriate

piercing points which can further be used to restrict the timing of this displacement (Yin and Harrison, 2000; Chen et al., 2003; Cowgill et al., 2003; Wang et al., 2006a; Yin et al., 2002, 2008b). In this paper, the residual Mesozoic to Cenozoic strata within the western Qaidam basin are documented as the piercing points that identify the Cenozoic kinematic pattern of the ATF. In order to account for the fact that the Qaidam basin and the relic Tula and Anxi units are situated south of the currently active ATF trace, two faults or major unconformities are required to act as boundaries between the detached Qaidam basin and relic Tula subbasin (Fig. 11).

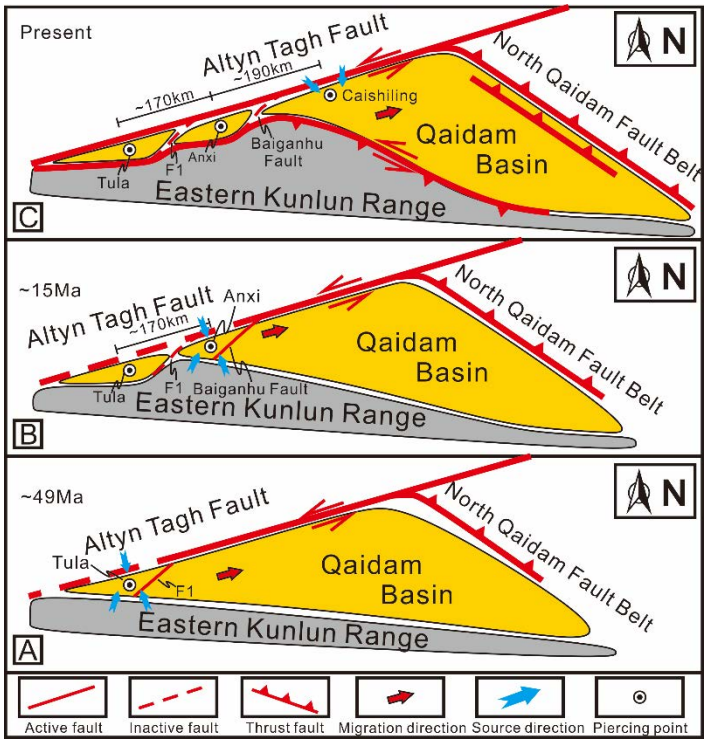

Figure 11. Proposed accelerated motion model for the Cenozoic Altyn Tagh fault (ATF). Note the piercing points along the Altyn Tagh fault. (A) Before early Eocene time, the Caishiling section was originally located where the Tula section is situated today. During early Eocene time (ca. 49 Ma), the left-lateral strike-slip faulting along the Altyn Tagh fault initiated, transporting the Qaidam Basin northeastward. Since then, the Tula unit remained stationary and was separated from the Qaidam Basin (B) during middle Miocene time (ca. 15 Ma), when the Caishiling section migrated northeastward to where the Anxi section is situated today. During this period, an intense left-lateral strike-slip faulting along the Altyn Tagh fault occurred and deformed the pre-Miocene strata in the Anxi section. Since then, the Anxi unit was left and separated from the Qaidam Basin (C) during continuous left-lateral strike-slip faulting along the Altyn Tagh fault that transported the Caishiling section to its present position. Consequently, ~360 km total Cenozoic offset is constrained along the Altyn Tagh fault, which is divided into ~170 km of offset between early Eocene and middle Miocene time and ~190 km of offset from the late Miocene until present.

Between the Jurassic and early Eocene, the westernmost part of the originally rigid Qaidam basin was located where the Tula section is situated today (Fig. 11A). Strike-slip movement along the ATF began shortly after the early Eocene. Faulting on the ATF induced the NE-SW trending branch fault (F1) in this region, now covered by Quaternary alluvium, deforming the Jurassic to early Eocene strata in the Tula section as it did so (Figs. 2 and 4). The initial strike-slip movement of the ATF also transported the original Qaidam basin northeastwards

and gradually separated the Qaidam basin from the Tula section. The depression in the Tula section then uplifted and was gradually isolated, leading to a pause in deposition during the Upper Paleogene to Neogene. This left-lateral faulting also lead to compression in the northern Qaidam basin, which began in the Paleocene to early Eocene as revealed by seismic profile data (Yin et al., 2008a; Fig. 11A). Systematic analysis of the Cenozoic stratigraphic sections along the ATF suggests that strike-slip movement along the western and central ATF was initiated at ca. 49 Ma (Yin et al., 2002), roughly consistent with the speculated sediment termination age of the Tula section. This onset age for large strike-slip faulting in the northern Tibetan plateau is also synchronous with the India-Asia collision as revealed by newly acquired palaeomagnetic evidence in southern Tibet (Dupont-Nivet et al., 2010; Huang et al., 2013; Lippert et al., 2014). This indicates that the deformation in northern Tibet may have begun as India and Eurasia began colliding. It is possible that the dominant cause of the large-scale strike-slip faults in the Asian interior (especially the ATF) is the India-Asia collision itself, the effects of which may still be felt on the northern Tibetan plateau today.

Between early Eocene and mid-Miocene time, movement of the ATF transported the westernmost part of the original Qaidam basin northeastwards to the position where the Anxi unit is at present. During the mid-Miocene, an intense left-lateral strike-slip motion occurred along the ATF and the originally rigid Qaidam separated from the Anxi unit and migrated northeastwards continuously (Fig. 11B). This fault motion tilted the Late Paleocene to early Miocene strata of the Anxi section and created a regional unconformity between the Shangyoushashan and Xiayoushashan formations. This unconformity matches the widespread unconformity within the western Qaidam basin (Figs. 3 and 7; Wang et al., 2010a, 2010b; Wu et al., 2012a, 2012b). The growth strata above this unconformity reveal a rapid tectonic event occurred just after the mid-Miocene epoch (~15 Ma). Based on the widespread potassic volcanism in northern Tibet, Yue and Liou (1999) also infer intense fault movement along the ATF ca. 13-16 Ma. This mid-Miocene faulting is recorded by the fission track present in both the Altyn Tagh Range and the north Qaidam basin (Jolivet et al., 2001; Wan et al., 2001). Overall, the tectonic events of the mid-Miocene are widespread and well developed in the Tibetan plateau (e.g. Yue and Liou, 1999; Kirby et al., 2002; Clark et al., 2004; Ding et al., 2004; Sun et al., 2005a; Wang et al., 2012), which may reflect a critical period in the process of Tibetan plateau growth. Following this, as seen in the Anxi section, the depression in the Anxi section becomes folded, uplifted and isolated gradually leading to a pause in deposition during the late Miocene (Figs. 6 and 7).

Since late Miocene epoch, the continuous left-lateral strike-slip faulting along the ATF

has gradually transported the Qaidam basin to its present position (Fig. 11C). Finally, recent left-lateral strike-slip faulting occurs along the entire ATF, reshaping the original faulting style. The Tula and Anxi units can be selected as piercing points to constrain the Cenozoic kinematic patterns of the ATF. Based on these offset markers, we estimate ~170 km of offset occurred between the mid-Eocene and mid-Miocene epochs, and ~190 km of offset occurred between the late Miocene epoch and the present, resulting in a total offset of ~360 km along the ATF during the Cenozoic (Fig. 11). This estimate suggests an average sinistral slip rate of ~5.0 mm/yr between the middle Eocene and the middle Miocene and an increase to ~12.6 mm/yr between the Miocene and the present. Our estimates for the overall displacement (~360 km) and average sinistral slip rate since the mid-Miocene are consistent with previous studies (Peltzer and Tapponnier, 1988; Ritts and Biffi, 2000; Yin and Harrison, 2000; Shen et al., 2001; Yin et al., 2002; Cowgill et al., 2003; Zhang et al., 2004, 2007; Cowgill et al., 2009). The accelerated strike-slip motion along the ATF between the mid-Miocene epoch and present day implies that the increased regional deformation of the northern Tibetan plateau may be related to the penetrative and far-reaching effects of the India-Asia collision.

3.1.7 Conclusions

As the major strike-slip fault on the northern Tibetan plateau, the ATF holds important implications for unraveling the Cenozoic growth history of the entire Tibetan plateau.

By correlating the lithology and sedimentary features of the Cenozoic strata along the ATF, and analyzing the detrital zircon U-Pb ages from Mesozoic strata in three sections along the fault, we find that these strata record the northward migration of the Qaidam basin and can be identified as the piercing points for defining the Cenozoic offset of the ATF. Specifically, the Tula section records the early Eocene position of the western Qaidam basin (e.g. Caishiling section), while the Anxi section documents its middle Miocene position. Based on this, we estimate ~170 km of offset occurred between the early Eocene (~49 Ma) to middle Miocene (~15 Ma) epochs and ~190 km of offset occurred between the late Miocene epoch and the present day, yielding ~360 km of total offset along the ATF during the Cenozoic period. This estimate implies that motion along the ATF has accelerated in recent time from an average sinistral slip rate of ~5.0 mm/yr between the early Eocene (~49 Ma) to middle Miocene (~15 Ma) epochs to an accelerated rate of ~12.6 mm/yr from the middle Miocene epoch to the present day.

Acknolegdements

This work was supported by the National Oil and Gas Scientific and Technologic Major Programs of China (Grant ZX05003) and China Scholarship Council (Egide Cai Yuanpei program 2014). We gratefully acknowledge the assistance of Dr. Suping Zhou, and Xiangjiang Yu for their contributions in the field. We are very grateful to Prof. Li Su of the Geological Lab Center, China University of Geosciences (Beijing), for her help with detrital zircon analysis and to Dr. Bo Zhang for his help with cathodoluminescence (CL) imaging. We are particularly grateful to Dr. Dupont-Nivet Guillaume for his helpful suggestions. Communications with Dr. Marc Jolivet, Jianxun Zhou, Dr. Dewen Zheng and Dr. Jinjiang Zhang had sharpened the discussion on the appropriate piercing points. We would like to thank Dr. An Yin and an anonymous reviewer for reviewing the earlier version of this manuscript. We also would like to thank science editor Dr. Shanaka de Silva, associate editor Dr. Todd LaMaskin, and two anonymous reviewers, who provided constructive feedback that helped improve this manuscript.

References Cited

Allen, P.A., and Allen, J.R., 1990, Basin analysis: Principles and applications: Cambridge, UK, Blackwell Scientific Publications, 451 p.

Arnaud, N., Tapponnier, P., Roger, F., Brunel, M., Scharer, U., Wen, C., and Zhiqin, X., 2003, Evidence for Mesozoic shear along the western Kunlun and Altyn‐Tagh fault, northern Tibet (China): Journal of Geophysical Research: Solid Earth (1978–2012), v. 108, no. B1, doi: 10.1029/2001JB000904.

Bendick, R., Bilham, R., Freymueller, J., Larson, K., and Yin, G., 2000, Geodetic evidence for a low slip rate in the Altyn Tagh fault system: Nature, v. 404, no. 6773, p. 69-72, doi: 10.1038/35003555.

Boggs, S., Jr., 2006, Principles of Sedimentology and Stratigraphy, 4th Edition: New Jersey, Pearson Prentice Hall, p. 326–333.

Burchfiel, B. C., Quidong, D., Molnar, P., Royden, L., Yipeng, W., Peizhen, Z., and Weiqi, Z., 1989, Intracrustal detachment within zones of continental deformation: Geology, v. 17, no. 8, p. 748-752., doi: 10.1130/0091-7613(1989)017<0448:IDWZOC>2.3.CO;2.

Burchfiel, B. C., and Royden, L. H., 1991, Tectonic of Asia 50 years after the death of Emile Argand: Eclogae Geologicae Helvetiae, v. 84, no. 3, p. 599-629.

Cande, S. C., and Kent, D. V., 1995, Revised calibration of the geomagnetic polarity timescale for the Late Cretaceous and Cenozoic: Journal of Geophysical Research: Solid Earth (1978–

2012), v. 100, no. B4, p. 6093-6095, doi: 10.1029/94JB03098.

Chen, Z. L., Zhang, Y. Q., Wang, X. F., and Chen, X. H., 2001, Fission Track Dating of Apatite Constrains on the Cenozoic Uplift of the Altyn Tagh Mountain: GEOSCIENTIA SINICA Acta Geoscientia Sinica, v. 22, no. 5, p. 413-418 (in Chinese with English).

Chen, Y., Gilder, S., Halim, N., Cogné, J. P., and Courtillot, V., 2002, New paleomagnetic constraints on central Asian kinematics: Displacement along the Altyn Tagh fault and rotation of the Qaidam Basin: Tectonics, v. 21, no. 5, p. 1042, doi: 10.1029/2001TC901030.

Chen, X. H., Yin, A., Gehrels, G. E., Cowgill, E. S., Grove, M., Harrison, T. M., and Wang, X. F., 2003, Two phases of Mesozoic north-south extension in the eastern Altyn Tagh range, northern Tibetan Plateau: Tectonics, v. 22, no. 5, p. 1053, doi: 10.1029/2001TC001336.

Chen, X. H., Wang, X. F., George, G. E., Yang, Y., Qin, H., Chen, Z. L., Yang, F., Chen, B. L., and Li, X. Z., 2004, Early Paleozoic Magmatism and Gold Mineralization in the Northern Altun, NW China: Acta Geologica Sinica-English Edition, v. 78, no. 2, p. 515-523, doi: 10.1111/j.1755-6724.2004.tb00161.x.

Cheng, F., Jolivet, M., Fu, S., Zhang, Q., Guan, S., Yu, X., and Guo, Z., 2014, Northward growth of the Qimen Tagh Range: A new model accounting for the Late Neogene strike-slip deformation of the SW Qaidam Basin: Tectonophysics, v. 632, p. 32-47, doi: 10.1016/j.tecto.2014.05.034.

Cheng, X., Fu, S., Wang, H., Yu, X., Cheng, F., Liu, R., Du, W., and Guo, Z., 2015, Geometry and kinematics of the Arlar strike-slip fault, SW Qaidam basin, China: New insights from 3-D seismic data: Journal of Asian Earth Sciences, v. 98, p. 198-208, doi: 10.1016/j.jseaes.2014.09.039.

Clark, M., Schoenbohm, L., Royden, L., Whipple, K., Burchfiel, B., Zhang, X., Tang, W., Wang, E., and Chen, L., 2004, Surface uplift, tectonics, and erosion of eastern Tibet from large-scale drainage patterns: Tectonics, v. 23, no. 1, p. TC1006, doi: 10.1029/2002TC001402.

Cowgill, E., Yin, A., Feng, W. X., and Qing, Z., 2000, Is the North Altyn fault part of a strike-slip duplex along the Altyn Tagh fault system?: Geology, v. 28, no. 3, p. 255-258, doi: 10.1130/0091-7613(2000)28<255:ITNAFP>2.0.CO;2.

Corfu, F., Hanchar, J. M., Hoskin, P. W., and Kinny, P., 2003, Atlas of zircon textures: Reviews in mineralogy and geochemistry, v. 53, no. 1, p. 469-500, doi: 10.2113/0530469.

Cowgill, E., Yin, A., Harrison, T. M., and Xiao-Feng, W., 2003, Reconstruction of the Altyn Tagh fault based on U-Pb geochronology: Role of back thrusts, mantle sutures, and heterogeneous crustal strength in forming the Tibetan Plateau: Journal of Geophysical Research, v. 108, no. B7, p. 2346, doi:10.1029/2002JB002080.

Cowgill, E., Gold, R. D., Xuanhua, C., Xiao-Feng, W., Arrowsmith, J. R., and Southon, J., 2009, Low Quaternary slip rate reconciles geodetic and geologic rates along the Altyn Tagh fault, northwestern Tibet: Geology, v. 37, no. 7, p. 647-650, doi: 10.1130/G25623A.1.

CSBS (Chinese Stata Bureau of Seismology), 1992. The Altyn Tagh Active Fault System. Seismology Publishing House, Beijing, pp. 319 (in Chinese).

Dai, J., Wang, C., Hourigan, J., and Santosh, M., 2013, Multi-stage tectono-magmatic events of the Eastern Kunlun Range, northern Tibet: Insights from U–Pb geochronology and (U–Th)/He thermochronology: Tectonophysics, v. 599, p. 97-106, doi: 10.1016/j.tecto.2013.04.005.

Ding, G., Chen, J., Tian, Q., Shen, X., Xing, C., and Wei, K., 2004, Active faults and magnitudes of left-lateral displacement along the northern margin of the Tibetan Plateau: Tectonophysics, v. 380, no. 3-4, p. 243-260, doi: 10.1016/j.tecto.2003.09.022.

Dupont-Nivet, G., Butler, R. F., Yin, A., and Chen, X., 2002, Paleomagnetism indicates no Neogene rotation of the Qaidam Basin in northern Tibet during Indo-Asian collision: Geology, v. 30, no. 3, p. 263, doi: 10.1130/0091-7613(2002)030<0263:PINNRO>2.0.CO;2.

Dupont-Nivet, G., Butler, R. F., Yin, A., and Chen, X., 2003, Paleomagnetism indicates no Neogene vertical axis rotations of the northeastern Tibetan Plateau: J. geophys. Res, v. 108, no. B8, p. 2386, doi: 10.1029/2003JB002399.

Dupont-Nivet, G., Robinson, D., Butler, R. F., Yin, A., and Melosh, H. J., 2004, Concentration of crustal displacement along a weak Altyn Tagh fault: Evidence from paleomagnetism of the northern Tibetan Plateau: Tectonics, v. 23, no. 1, p. TC1020, doi:10.1029/2002TC001397.

Dupont-Nivet, G., Lippert, P. C., Van Hinsbergen, D. J. J., Meijers, M. J. M., and Kapp, P., 2010, Palaeolatitude and age of the Indo–Asia collision: palaeomagnetic constraints: Geophysical Journal International, v. 182, no. 3, p. 1189-1198, doi: 10.1111/j.1365-246X.2010.04697.x.

Fang, X., Zhang, W., Meng, Q., Gao, J., Wang, X., King, J., Song, C., Dai, S., and Miao, Y., 2007, High-resolution magnetostratigraphy of the Neogene Huaitoutala section in the eastern Qaidam Basin on the NE Tibetan Plateau, Qinghai Province, China and its implication on tectonic uplift of the NE Tibetan Plateau: Earth and Planetary Science Letters, v. 258, no. 1-2, p. 293-306, doi:10.1016/j.epsl.2007.03.042.

Fedo, C. M., Sircombe, K. N., and Rainbird, R. H., 2003, Detrital zircon analysis of the sedimentary record: Reviews in mineralogy and geochemistry, v. 53, no. 1, p. 277-303, doi: 10.2113/0530277.

Gao, J., Li, S., Dai, S., Li, A., and Peng, Y., 2009. Constraints of tectonic evolution in

provenance from detrital zircon fission-track data of Cenozoic strata of Xichagou district in western Qaidam basin. Journal of Lanzhou University (Natural Sciences), v. 45, no. 3, p. 639-643 (in Chinese with English abstract).

Gehrels, G. E., Yin, A., and Wang, X. F., 2003a, Detrital-zircon geochronology of the northeastern Tibetan plateau: Geological Society of America Bulletin, v. 115, no. 7, p. 881-896, doi: 10.1130/0016-7606(2003)115<0881:DGOTNT>2.0.CO;2.

Gehrels, G. E., Yin, A., and Wang, X. F., 2003b, Magmatic history of the northeastern Tibetan Plateau: Journal of Geophysical Research, v. 108, no. B9, p. 2423, doi: 10.1029/2002JB001876.

Gehrels, G., 2014, Detrital Zircon U-Pb Geochronology Applied to Tectonics: Annual Review of Earth and Planetary Sciences, v. 42, no. 1, p. 127-149, doi: 10.1146/annurev-earth-050212-124012.

GGSI (Guangxi Geological Survey Institute), 2003. The Report of Regional Geological Survey of Washixia at Scale 1:250000. P.R.C.: Beijing, China Industry Press, 261 p. (in Chinese).

Guo, Z. J., Zhang, Z. C., and Zeng, F. G., 1998, Discovery of mega-thick oil sandstone and asphalt in the Jurassic System in the Tula Basin and its significance: Chinese Science Bulletin, v. 43, no. 22, p. 1898-1901, doi: 10.1007/BF02883468.

Hanchar, J., and Rudnick, R., 1995, Revealing hidden structures: the application of cathodoluminescence and back-scattered electron imaging to dating zircons from lower crustal xenoliths: Lithos, v. 36, no. 3, p. 289-303, doi: 10.1016/0024-4937(95)00022-4.

Hoskin, P., and Black, L., 2000, Metamorphic zircon formation by solid-state recrystallization of protolith igneous zircon: Journal of metamorphic Geology, v. 18, no. 4, p. 423-439, doi:10.1046/j.1525-1314.2000.00266.x.

Hendrix, M. S., Graham, S. A., Carroll, A. R., Sobel, E. R., McKNIGHT, C. L., Schulein, B. J., and Wang, Z., 1992, Sedimentary record and climatic implications of recurrent deformation in the Tian Shan: Evidence from Mesozoic strata of the north Tarim, south Junggar, and Turpan basins, northwest China: Geological Society of America Bulletin, v. 104, no. 1, p. 53-79, doi: 10.1130/0016-7606(1992)104<0053:SRACIO>2.3.CO;2.

Hendrix, M. S., 2000, Evolution of Mesozoic Sandstone Compositions, Southern Junggar, Northern Tarim, and Western Turpan Basins, Northwest China: A Detrital Record of the Ancestral Tian Shan: Journal of Sedimentary Research, v. 70, no. 3, p. 520-532, doi: 10.1306/2DC40924-0E47-11D7-8643000102C1865D.

HGSI (Hunan Geological Survey Institute), 2003, The Report of Regional Geological Survey

of Qiemo at Scale 1:250000. P.R.C.: Beijing, China Industry Press, 281 p. (in Chinese).

Huang, H., Huang, Q., and Ma, Y., 1996, Geology of Qaidam Basin and its petroleum prediction. Geological Publishing House, Beijing, 257 p. (in Chinese).

Huang, W., Dupont-Nivet, G., Lippert, P. C., van Hinsbergen, D. J., and Hallot, E., 2013, Inclination shallowing in Eocene Linzizong sedimentary rocks from Southern Tibet: correction, possible causes and implications for reconstructing the India-Asia collision: Geophysical Journal International, v. 1, p. 309, doi: 10.1093/gji/ggt188.

Huo, G. M., 1990, Petroleum geology of China: Oil fields in Qianghai and Xizang. Chinese Petroleum Industry Press, Beijing, 483 p. (in Chinese with English abstract).

Jolivet, M., Brunel, M., Seward, D., Xu, Z., Yang, J., Roger, F., Tapponnier, P., Malavieille, J., Arnaud, N., and Wu, C., 2001, Mesozoic and Cenozoic tectonics of the northern edge of the Tibetan plateau: fission-track constraints: Tectonophysics, v. 343, no. 1-2, p. 111-134, doi: 10.1016/S0040-1951(01)00196-2.

Ke, X., Ji, J., Zhang, K., Kou, X., Song, B., and Wang, C., 2013, Magnetostratigraphy and Anisotropy of Magnetic Susceptibility of the Lulehe Formation in the Northeastern Qaidam Basin: Acta Geologica Sinica-English Edition, v. 87, no. 2, p. 576-587, doi: 10.1111/1755-6724.12069.

Kirby, E., Reiners, P. W., Krol, M. A., Whipple, K. X., Hodges, K. V., Farley, K. A., Tang, W., and Chen, Z., 2002, Late Cenozoic evolution of the eastern margin of the Tibetan Plateau: Inferences from $^{40}Ar/^{39}Ar$ and (U-Th)/He thermochronology: Tectonics, v. 21, no. 1, p. 1-1-1-20, doi: 10.1029/2000TC001246.

Li, Z., Song, W. J., Peng, S. T., Wang, D. X., and Zhang, Z. P., 2004, Mesozoic-Cenozoic tectonic relationships between the Kuqa subbasin and Tian Shan, northwest China: constraints from depositional records: Sedimentary Geology, v. 172, no. 3, p. 223-249, doi: 10.1016/j.sedgeo.2004.09.002.

Li, H.B., Yang, J.S., Xu, Z.Q., Sun, Z.M., Tapponnier, P., van der Woerd, J., and Meriaux, A. S., 2006. The constraint of the Altyn Tagh fault system to the growth and rise of the northern Tibetan Plateau: Earth Science Frontiers, v. 13, no. 4, 59-79 (in Chinese with English abstract).

Li, W., Neubauer, F., Liu, Y. J., Genser, J., Ren, S. M., Han, G. Q., and Liang, C. Y., 2013, Paleozoic evolution of the Qimantagh magmatic arcs, Eastern Kunlun Mountains: constraints from zircon dating of granitoids and modern river sands: Journal of Asian Earth Sciences, v. 77, p. 183-202, doi: 10.1016/j.jseaes.2013.08.030.

Lippert, P., van Hinsbergen, D., and Dupont-Nivet, G., 2014, The Early Cretaceous to present 31 latitude of the central Lhasa-plano (Tibet): A paleomagnetic synthesis with implications for

Cenozoic 32 tectonics, paleogeography, and climate of Asia: Nie, JS, Hoke, GD, and Horton, BK, editors, v. 33, p. 2, doi: 10.1130/2014.2507(01).

Liu, L., Zhang, A., Chen, D., Yang, J., Luo, J., and Wang, C., 2007a, Implications Based on LA-ICP-MS Zircon U-Pb Ages of Eclogite and Its Country Rock from Jianggalesayi Area, Altyn Tagh, China: Earth Science Frontiers, v. 14, no. 1, p. 98-107, doi: 10.1016/S1872-5791(07)60004-9.

Liu, Y. J., Neubauer, F., Genser, J., Ge, X. H., Takasu, A., Yuan, S. H., Chang, L. H., and Li, W. M., 2007b, Geochronology of the initiation and displacement of the Altyn Strike-Slip Fault, western China: Journal of Asian Earth Sciences, v. 29, no. 2, p. 243-252, doi:10.1016/j.jseaes.2006.03.002.

Liu, L., Wang, C., Chen, D., Zhang, A., and Liou, J., 2009, Petrology and geochronology of HP–UHP rocks from the South Altyn Tagh, northwestern China: Journal of Asian Earth Sciences, v. 35, no. 3, p. 232-244, doi: 10.1016/j.jseaes.2008.10.007.

Liu, D. D., Jolivet, M., Yang, W., Zhang, Z. Y., Feng, C., Zhu, B., and Guo, Z. J., 2013a, Latest Palaeozoic-Early Mesozoic basin-range interactions in South Tian Shan (Northwest China) and their tectonic significance: Constraints from detrital zircon U-Pb ages: Tectonophysics v. 599, 197-213, 10.1016/j.tecto.2013.04.018.

Liu, L., Cao, Y. Y., Chen, D. L., Zhang, C. L., Yang, W. Q., Kang, L., and Liao, X. Y., 2013b, New progresses on the HP-UHP metamorphism in the South Altyn Tagh and the North Qinling: Chin Sci Bull, v. 58, p. 2113-2123 (in Chinese).

Lu, S. N., and Yuan, G. B., 2003, Geochronology of early Precambrian magmatic activities in Aketasdhtage, east Altyn Tagh: Journal of Acta Geologica Sinica, v. 77, no. 1, p. 61-68 (in Chinese with English abstract).

Lu, S. N., Li, H. K., Zhang, C. L., and Niu, G. H., 2008, Geological and geochronological evidence for the Precambrian evolution of the Tarim Craton and surrounding continental fragments: Precambrian Research, v. 160, no. 1, p. 94-107, doi: 10.1016/j.precamres.2007.04.025.

Lu, H., and Xiong, S., 2009, Magnetostratigraphy of the Dahonggou section, northern Qaidam Basin and its bearing on Cenozoic tectonic evolution of the Qilian Shan and Altyn Tagh Fault: Earth and Planetary Science Letters, v. 288, no. 3, p. 539-550, doi: 10.1016/j.epsl.2009.10.016.

Lu, H., Wang, E., and Meng, K., 2014, Paleomagnetism and anisotropy of magnetic susceptibility of the Tertiary Janggalsay section (southeast Tarim basin): Implications for Miocene tectonic evolution of the Altyn Tagh Range: Tectonophysics, v. 618, p. 67-78, doi: 10.1016/j.tecto.2014.01.031.

Mack, G. H., and Rasmussen, K. A., 1984, Alluvial-fan sedimentation of the Cutler Formation (Permo-Pennsylvanian) near Gateway, Colorado: Geological Society of America Bulletin, v. 95, no. 1, p. 109-116, doi: 10.1130/0016-7606(1984)95<109:ASOTCF>2.0.CO;2.

Matte, P., Tapponnier, P., Arnaud, N., Bourjot, L., Avouac, J., Vidal, P., Qing, L., Yusheng, P., and Yi, W., 1996, Tectonics of Western Tibet, between the Tarim and the Indus: Earth and Planetary Science Letters, v. 142, no. 3, p. 311-330, doi: 10.1016/0012-821X(96)00086-6.

Meng, Q. R., Hu, J. M., and Yang, F. Z., 2001, Timing and magnitude of displacement on the Altyn Tagh fault: constraints from stratigraphic correlation of adjoining Tarim and Qaidam basins, NW China: Terra Nova, v. 13, no. 2, p. 86-91, doi: 10.1046/j.1365-3121.2001.00320.x.

Meng, Q. R., and Fang, X., 2008, Cenozoic tectonic development of the Qaidam Basin in the northeastern Tibetan Plateau: Geological Society of America Special Papers, v. 444, p. 1-24, doi: 10.1130/2008.2444(01).

Métivier, F., Gaudemer, Y., Tapponnier, P., and Meyer, B., 1998, Northeastward growth of the Tibet plateau deduced from balanced reconstruction of two depositional areas: The Qaidam and Hexi Corridor basins, China: Tectonics, v. 17, no. 6, p. 823-842, doi: 10.1029/98TC02764.

Meyer, B., Tapponnier, P., Bourjot, L., Metivier, F., Gaudemer, Y., Peltzer, G., Shunmin, G., and Zhitai, C., 1998, Crustal thickening in Gansu‐Qinghai, lithospheric mantle subduction, and oblique, strike‐slip controlled growth of the Tibet plateau: Geophysical Journal International, v. 135, no. 1, p. 1-47, doi: 10.1046/j.1365-246X.1998.00567.x.

Mock, C., Arnaud, N. O., and Cantagrel, J. M., 1999, An early unroofing in northeastern Tibet? Constraints from $^{40}Ar/^{39}Ar$ thermochronology on granitoids from the eastern Kunlun range (Qianghai, NW China): Earth and Planetary Science Letters, v. 171, no. 1, p. 107-122, doi: 10.1016/S0012-821X(99)00133-8.

Molnar, P., and Tapponnier, P., 1975, Cenozoic tectonics of Asia: Effects of a continental collision: Science, v. 189, no. 4201, p. 419-426, doi: 10.1126/science.189.4201.419.

Pei, J., Sun, Z., Wang, X., Zhao, Y., Ge, X., Guo, X., Li, H., and Si, J., 2009, Evidence for Tibetan plateau uplift in Qaidam basin before Eocene-Oligocene boundary and its climatic implications: Journal of Earth Science, v. 20, p. 430-437, doi: 10.1007/s12583-009-0035-y.

Peltzer, G., and Tapponnier, P., 1988, Formation and evolution of strike-slip faults, rifts, and basins during the India-Asia collision: An experimental approach: Journal of Geophysical Research: Solid Earth (1978–2012), v. 93, no. B12, p. 15085-15117, doi: 10.1029/JB093iB12p15085.

QBGMR, 1991, Regional Geology of Qinghai Province. Geological Publishing House, Beijing, 662 p. (in Chinese).

Qiu, N. S., 2002, Tectono-thermal evolution of the Qaidam Basin, China: evidence from Ro and apatite fission track data: Petroleum Geoscience, v. 8, no. 3, p. 279-285, doi: 10.1144/petgeo.8.3.279.

Ritts, B. D., and Biffi, U., 2000, Magnitude of post-Middle Jurassic (Bajocian) displacement on the central Altyn Tagh fault system, northwest China: Geological Society of America Bulletin, v. 112, no. 1, p. 61-74, doi: 10.1130/0016-7606(2000)112<61:MOPJBD>2.0.CO;2.

Ritts, B. D., Yue, Y., and Graham, S. A., 2004, Oligocene–Miocene Tectonics and Sedimentation along the Altyn Tagh Fault, Northern Tibetan Plateau: Analysis of the Xorkol, Subei, and Aksay Basins: The Journal of geology, v. 112, no. 2, p. 207-229, doi: 10.1086/381658.

Robinson, D. M., Dupont-Nivet, G., Gehrels, G. E., and Zhang, Y., 2003, The Tula uplift, northwestern China: Evidence for regional tectonism of the northern Tibetan Plateau during late Mesozoic–early Cenozoic time: Geological Society of America Bulletin, v. 115, no. 1, p. 35-47, doi: 10.1130/0016-7606(2003)115<0035:TTUNCE>2.0.CO;2.

Roger, F., Arnaud, N., Gilder, S., Tapponnier, P., Jolivet, M., Brunel, M., Malavieille, J., Xu, Z., and Yang, J., 2003, Geochronological and geochemical constraints on Mesozoic suturing in east central Tibet: Tectonics, v. 22, no. 4, p. 1037, doi:10.1029/2002TC001466.

Roger, F., Jolivet, M., and Malavieille, J., 2008, Tectonic evolution of the Triassic fold belts of Tibet: Comptes Rendus Geoscience, v. 340, no. 2, p. 180-189, doi:10.1016/j.crte.2007.10.014.

Roger, 2010, The tectonic evolution of the Songpan-Garzê (North Tibet) and adjacent areas from Proterozoic to Present: A synthesis: Journal of Asian Earth Sciences, v. 39, no. 4, p. 254-269, doi:10.1016/j.jseaes.2010.03.008.

Shen, Z. K., Wang, M., Li, Y. X., Jackson, D. D., Yin, A., Dong, D. N., and Fang, P., 2001, Crustal deformation along the Altyn Tagh fault system, western China, from GPS: Journal of Geophysical Research: Solid Earth (1978–2012), v. 106, no. B12, p. 30607-30621, doi: 10.1029/2001JB000349.

Sobel, E. R., and Arnaud, N., 1999, A possible middle Paleozoic suture in the Altyn Tagh, NW China: Tectonics, v. 18, no. 1, p. 64-74, doi: 10.1029/1998TC900023.

Sobel, E. R., Arnaud, N., Jolivet, M., Ritts, B. D., and Brunei, M., 2001, Jurassic to Cenozoic exhumation history of the Altyn Tagh range, northwest China, constrained by $^{40}Ar/^{39}Ar$ and apatite fission track thermochronology: Paleozoic and Mesozoic tectonic evolution of central and eastern Asia, v. 194, p. 247-267, doi: doi: 10.1130/0-8137-1194-0.247.

Song, T., and Wang, X., 1993, Structural styles and stratigraphic patterns of syndepositional

faults in a contractional setting: Examples from Quaidam basin, northwestern China: AAPG bulletin, v. 77, no. 1, p. 102-117.

Sun, J. M., Zhu, R. X., and An, Z. S., 2005a, Tectonic uplift in the northern Tibetan Plateau since 13.7 Ma ago inferred from molasse deposits along the Altyn Tagh Fault: Earth and Planetary Science Letters, v. 235, no. 3, p. 641-653, doi: doi:10.1016/j.epsl.2005.04.034.

Sun, Z. M., Yang, Z. Y., Pei, J. L., Ge, X. H., Wang, X. S., Yang, T. S., Li, W. M., and Yuan, S. H., 2005b, Magnetostratigraphy of Paleogene sediments from northern Qaidam Basin, China: implications for tectonic uplift and block rotation in northern Tibetan plateau: Earth and Planetary Science Letters, v. 237, no. 3, p. 635-646, doi: 10.1016/j.epsl.2005.07.007.

Sun, Z. C., Jing M. C., Sun, N. D., Lu Y.L., Cao, L., 2007. Discussion on boundary between the upper and lower members of Xiaganchaigou Formation of Paleogene in Well Kun-2, Qaidam Basin. Journal of Palaeogeography, 9(6), 611-618 (in Chinese with English abstract).

Tapponnier, P., Peltzer, G., and Armijo, R., 1986, On the mechanics of the collision between India and Asia: Geological Society, London, Special Publications, v. 19, no. 1, p. 113-157, doi: 10.1144/GSL.SP.1986.019.01.07.

Tapponnier, P., Xu, Z. Q., Roger, F., Meyer, B., Arnaud, N., Wittlinger, G., and Yang, J. S., 2001, Oblique stepwise rise and growth of the Tibet Plateau: Science, v. 294, no. 5547, p. 1671-1677, doi: 10.1126/science.105978.

Thomas, W. A., 2011, Detrital-zircon geochronology and sedimentary provenance: Lithosphere, v. 3, no. 4, p. 304-308, doi: 10.1130/RF.L001.1.

Wan, J. L., Wang, Y., Li, Q., Wang, F., and Wang, E., 2001, FT Evidence of Northern Altyn Uplift in Late-Cenozoic: Bulletin of Mineralogy, Petrology and Geochemistry, v. 20, no. 4, p. 222-224 (in Chinese with English abstract).

Wang, E., 1997, Displacement and timing along the northern strand of the Altyn Tagh fault zone, northern Tibet: Earth and Planetary Science Letters, v. 150, no. 1, p. 55-64, doi: 10.1016/S0012-821X(97)00085-X.

Wang, X. F., Metcalfe, I., Jian, P., He, L. Q., and Wang, C. S., 2000, The Jinshajiang-Ailaoshan suture zone, China: tectonostratigraphy, age and evolution: Journal of Asian Earth Sciences, v. 18, no. 6, p. 675-690, doi: 10.1016/S1367-9120(00)00039-0.

Wang, Y., Zhang, X., Wang, E., Zhang, J., Li, Q., and Sun, G., 2005, $^{40}Ar/^{39}Ar$ thermochronological evidence for formation and Mesozoic evolution of the northern-central segment of the Altyn Tagh fault system in the northern Tibetan Plateau: Geological Society of America Bulletin, v. 117, no. 9-10, p. 1336-1346, doi: 10.1130/B25685.

Wang, E., Xu, F. Y., Zhou, J. X., Wan, J., and Burchfiel, B. C., 2006a, Eastward migration of

the Qaidam basin and its implications for Cenozoic evolution of the Altyn Tagh fault and associated river systems: Geological Society of America Bulletin, v. 118, no. 3-4, p. 349-365, doi: 10.1130/b25778.1.

Wang, C., Liu, L., Che, Z. C., Chen, D. L., Zhang, A. D., and Luo, J. H., 2006b, U-Pb geochronology and tectonic setting of the granitic gneiss in Jianggaleisayi Eclogite Belt: Geological Journal of China Universities, v. 12, no. 1, p. 74-82 (in Chinese with English abstract).

Wang, C., Liu, L., Zhang, A. D., Yang, W. Q., and Cao, Y. T., 2008, Geochemistry and petrography of early Paleozoic Yusupuleke Tagh Rapakivi-textured Granite Complex, South Altyn - an example for magma mixing: Acta Petrolei Sinica, v. 24, no. 12, p. 2809-2819 (in Chinese with English abstract).

Wang, L., Xiao, A. C., Gong, Q. L., Liu, D., Wu, L., Zhou, S. P., Shen, Z. Y., Lou, Q. Q., and Sun, X. W., 2010a, The unconformity in Miocene sequence of western Qaidam Basin and its tectonic significance: SCIENCE CHINA Earth Sciences, v. 53, no. 8, p. 1126-1133, doi: 10.1007/s11430-010-4006-z.

Wang, Y. D., Nie, J. S., Zhang, T., Sun, G. Q., Yang, X., Liu, Y. H., and Liu, X. W., 2010b, Cenozoic tectonic evolution in the western Qaidam Basin inferred from subsurface data: Geosciences Journal, v. 14, no. 4, p. 335-344, doi: 10.1007/s12303-010-0033-1.

Wang, C. S., Gao, R., Yin, A., Wang, H., Zhang, Y. X., Guo, T. L., Li, Q. S., and Li, Y. L., 2011, A mid-crustal strain-transfer model for continental deformation: A new perspective from high-resolution deep seismic-reflection profiling across NE Tibet: Earth and Planetary Science Letters, v. 306, no. 3, p. 279-288, doi: 10.1016/j.epsl.2011.04.010.

Wang, C., Dai, J., Zhao, X., Li, Y., Graham, S. A., He, D., Ran, B., and Meng, J., 2014, Outward-growth of the Tibetan Plateau during the Cenozoic: A review: Tectonophysics, v. 621, p. 1-43, doi: 10.1016/j.tecto.2014.01.036.

Wang, E., Kirby, E., Furlong, K. P., van Soest, M., Xu, G. Q., Shi, X., Kamp, P. J. J., and Hodges, K. V., 2012, Two-phase growth of high topography in eastern Tibet during the Cenozoic: Nature Geoscience, v. 5, no. 9, p. 640-645, doi: 10.1038/NGEO1538.

Wang, C., Liu, L., Yang, W. Q., Zhu, X. H., Cao, Y. T., Kang, L., Chen, S. F., Li, R. S., and He, S. P., 2013, Provenance and ages of the Altyn Complex in Altyn Tagh: implications for the early Neoproterozoic evolution of northwestern China: Precambrian Research, v. 230, p. 193-208, doi: 10.1016/j.precamres.2013.02.003.

Wang, Z. Z., Han B. F., Feng C. Y. and Li, G. C., 2009.Geochronology, geochemistry and tectonic significance of granites in Baiganhu area, Xinjiang. Acta Petrologica et Mineralogica,

v. 33, no. 4, p. 597-616 (in Chinese with English abstract).

Wheeler, H. E., 1964, Baselevel, lithosphere surface, and time-stratigraphy: Geological Society of America Bulletin, v. 75, no. 7, p. 599-610, doi: 10.1130/0016-7606(1964)75[599:BLSAT]2.0.CO;2.

Wu, L., Xiao, A., Wang, L., Shen, Z., Zhou, S., Chen, Y., Wang, L., Liu, D., and Guan, J., 2011, Late Jurassic–Early Cretaceous Northern Qaidam Basin, NW China: Implications for the earliest Cretaceous intracontinental tectonism: Cretaceous Research, v. 32, no. 4, p. 552-564, doi: 10.1016/j.cretres.2011.04.002.

Wu, L., Xiao, A., Wang, L., Mao, L., Wang, L., Dong, Y., and Xu, B., 2012a, EW-trending uplifts along the southern side of the central segment of the Altyn Tagh Fault, NW China: Insight into the rising mechanism of the Altyn Mountain during the Cenozoic: SCIENCE CHINA Earth Sciences, v. 55, no. 6, p. 926-939, doi: 10.1007/s11430-012-4402-7.

Wu, L., Xiao, A. C., Yang, S. F., Wang, L. Q., Mao, L. G., Wang, L., Dong, Y. P., and Xu, B., 2012b, Two-stage evolution of the Altyn Tagh Fault during the Cenozoic: new insight from provenance analysis of a geological section in NW Qaidam Basin, NW China: Terra Nova, v. 24, no. 5, p. 387-395, doi: 10.1111/j.1365-3121.2012.01077.x.

XBGMR (Xinjiang Bureau of Geology and Mineral Resources), 1993, Regional Geology of Xinjiang Uygur Autonomous Region: Beijing, Geological Publishing House, 841 p. (in Chinese with English summary).

Xia, W. C., Zhang, N., Yuan, X. P., Fan, L. S., and Zhang, B. S., 2001, Cenozoic Qaidam basin, China: A stronger tectonic inversed, extensional rifted basin: AAPG bulletin, v. 85, no. 4, p. 715-736, doi: 10.1306/8626C98D-173B-11D7-8645000102C1865D.

Yang, F., Ma, Z. Q., Xu, T. C., and Ye, S. J., 1992, A Tertiary paleomagnetic stratigraphic profile in Qaidam basin. Acta Petrolei Sinica, v. 13, no. 2, 97-101 (in Chinese).

Yang, J. S., Xu, Z. Q., Zhang, J. X., Chu, C. Y., Zhang, R. Y., and Liou, J. G., 2001, Tectonic significance of early Paleozoic high-pressure rocks in Altun-Qaidam-Qilian Mountains, northwest China: MEMOIRS-GEOLOGICAL SOCIETY OF AMERICA, p. 151-170.

Yang, J. S., Wu, C. L., Zhang, J. X., Shi, R. D., Meng, F. C., Wooden, J. L., and Yang, H. Y., 2006, Protolith of eclogites in the north Qaidam and Altun UHP terrane, NW China: Earlier oceanic crust?: Journal of Asian Earth Sciences, v. 28, no. 2, p. 185-204, doi: 10.1016/j.jseaes.2005.09.020.

Yang, W., Jolivet, M., Dupont‐Nivet, G., Guo, Z., Zhang, Z., and Wu, C., 2013, Source to sink relations between the Tian Shan and Junggar Basin (northwest China) from Late Palaeozoic to Quaternary: evidence from detrital U‐Pb zircon geochronology: Basin

Research, v. 25, no. 2, p. 219-240, doi: 10.1111/j.1365-2117.2012.00558.x.

Yin, A., and Harrison, T. M., 2000, Geologic evolution of the Himalayan-Tibetan orogen: Annual Review of Earth and Planetary Sciences, v. 28, no. 1, p. 211-280, doi: 10.1146/annurev.earth.28.1.211.

Yin, A., Rumelhart, P., Butler, R., Cowgill, E., Harrison, T., Foster, D., Ingersoll, R., Qing, Z., Xian-Qiang, Z., and Xiao-Feng, W., 2002, Tectonic history of the Altyn Tagh fault system in northern Tibet inferred from Cenozoic sedimentation: Geological Society of America Bulletin, v. 114, no. 10, p. 1257-1295, doi: 10.1130/0016-7606(2002)114<1257:THOTAT>2.0.CO;2.

Yin, A., Dang, Y. Q., Zhang, M., McRivette, M. W., Burgess, W. P., and Chen, X. H., 2007, Cenozoic tectonic evolution of Qaidam basin and its surrounding regions (part 2): Wedge tectonics in southern Qaidam basin and the Eastern Kunlun Range: Geological Society of America Special Papers, v. 433, p. 369-390, doi: 10.1130/2007.2433(18).

Yin, A., Dang, Y.Q., Wang, L.C., Jiang, W.M., Zhou, S.P., Chen, X.H., Gehrels, G.E., and McRivette, M.W., 2008a. Cenozoic tectonic evolution of Qaidam basin and its surrounding regions (Part 1): The southern Qilian Shan-Nan Shan thrust belt and northern Qaidam basin. Geological Society of America Bulletin 120, 813-846, doi:10.1130.B26180.1.

Yin, A., Dang, Y. Q., Zhang, M., Chen, X. H., and McRivette, M. W., 2008b, Cenozoic tectonic evolution of the Qaidam basin and its surrounding regions (Part 3): Structural geology, sedimentation, and regional tectonic reconstruction: Geological Society of America Bulletin, v. 120, no. 7-8, p. 847-876, doi: 10.1130/B26232.1.

Yin, A., 2010, Cenozoic tectonic evolution of Asia: A preliminary synthesis: Tectonophysics, v. 488, no. 1, p. 293-325, doi:10.1016/j.tecto.2009.06.002.

Yu, X. J., Fu, S. T., Guan, S. W., Huang, B., Cheng, F., Cheng, X., Zhang, T., and Guo, Z. J., 2014, Paleomagnetism of Eocene and Miocene sediments from the Qaidam basin: Implication for no integral rotation since the Eocene and a rigid Qaidam block: Geochemistry, Geophysics, Geosystems, v. 15, no. 6, p. 2109-2127, doi: 10.1002/2014GC005230.

Yue, Y. J., and Liou, J. G., 1999, Two-stage evolution model for the Altyn Tagh fault, China: Geology, v. 27, no. 3, p. 227-230, doi: 10.1130/0091-7613(1999)027<0227:TSEMFT>2.3.CO;2.

Yue, Y. J., Ritts, B. D., and Graham, S. A., 2001, Initiation and long-term slip history of the Altyn Tagh Fault, v. 43, no. 12, p. 1087-1093, doi: 10.1080/00206810109465062.

Yue, Y., Ritts, B. D., Graham, S. A., Wooden, J. L., Gehrels, G. E., and Zhang, Z., 2004a, Slowing extrusion tectonics: lowered estimate of post-Early Miocene slip rate for the Altyn Tagh fault: Earth and Planetary Science Letters, v. 217, no. 1, p. 111-122, doi:10.1016/S0012-

821X(03)00544-2.

Yue, Y. J., Ritts, B. D., Hanson, A. D., and Graham, S. A., 2004b, Sedimentary evidence against large strike-slip translation on the Northern Altyn Tagh fault, NW China: Earth and Planetary Science Letters, v. 228, no. 3, p. 311-323, doi: doi:10.1016/j.epsl.2004.10.008.

Yue, Y. J., Graham, S. A., Ritts, B. D., and Wooden, J. L., 2005, Detrital zircon provenance evidence for large-scale extrusion along the Altyn Tagh fault: Tectonophysics, v. 406, no. 3, p. 165-178, doi: 10.1016/j.tecto.2005.05.023.

Zhang, J. X., Zhang, Z. M., Xu, Z. Q., Yang, J. S., and Cui, J. W., 2001, Petrology and geochronology of eclogites from the western segment of the Altyn Tagh, northwestern China: Lithos, v. 56, no. 2, p. 187-206, doi: 10.1016/S0024-4937(00)00052-9.

Zhang, P. Z., Shen, Z., Wang, M., Gan, W., Bürgmann, R., Molnar, P., Wang, Q., Niu, Z., Sun, J., and Wu, J., 2004, Continuous deformation of the Tibetan Plateau from global positioning system data: Geology, v. 32, no. 9, p. 809-812, doi: 10.1130/G20554.1.

Zhang, W. L., 2006, High-resolution megnetostratigraphy of the Cenozoic Qaidam Basin, implications for the uplift of Tibetan Plateau [Ph.D. thesis]: LanZhou University, 158p. (in Chinese).

Zhang, P. Z., Molnar, P., and Xu, X. W., 2007, Late Quaternary and present-day rates of slip along the Altyn Tagh Fault, northern margin of the Tibetan Plateau: Tectonics, v. 26, no. 5, doi: 10.1029/2006TC002014.

Zhang, J. X., Li, H. K., Meng, F. C., Xiang, Z. Q., Yu, S. Y., and Li, J. P., 2011, Polyphase tectonothermal events recorded in “metamorphic basement” from the Altyn Tagh, the southeastern margin of the Tarim basin, western China: Constraint from U-Pb zircon geochronology: Acta Petrologica Sinica, v. 27, no. 1, p. 23-46 (in Chinese with English abstract).

Zhang, H. P., Zhang, P. Z., Zheng, D. W., Zheng, W. J., Chen, Z. W., and Wang, W. T., 2014, Transforming the Miocene Altyn Tagh fault slip into shortening of the north-western Qilian Shan: insights from the drainage basin geometry: Terra Nova, v. 26, no. 3, p. 216-221, doi: 10.1111/ter.12089.

Zhao, J. M., Mooney, W. D., Zhang, X. K., Li, Z. C., Jin, Z. J., and Okaya, N., 2006, Crustal structure across the Altyn Tagh Range at the northern margin of the Tibetan plateau and tectonic implications: Earth and Planetary Science Letters, v. 241, no. 3, p. 804-814, doi: 10.1016/j.epsl.2005.11.003.

Zhou, J. X., Xu, F. Y., Wang, T. C., Cao, A. F., and Yin, C. M., 2006, Cenozoic deformation history of the Qaidam Basin, NW China: Results from cross-section restoration and

implications for Qinghai–Tibet Plateau tectonics: Earth and Planetary Science Letters, v. 243, no. 1-2, p. 195-210, doi: 10.1016/j.epsl.2005.11.033.

Zuffa, G.G., 1980. Hybrid arenites: their composition and classification. Journal of Sedimentary Research 50, 21-29, doi: 10.1306/212F7950-2B24-11D7-8648000102C1865D.

3.2 Large-scale displacement along the Altyn Tagh Fault (North Tibet) since its Eocene initiation: insight from detrital zircon U-Pb geochronology and subsurface data

Paper published in Tectonophysics, 2016(Accepted with minor revision)

Large-scale displacement along the Altyn Tagh Fault (North Tibet) since its Eocene initiation: insight from detrital zircon U-Pb geochronology and subsurface data

Feng Cheng [1, 2], Marc Jolivet [2], Suotang Fu [3], Changhao Zhang [3], Qiquan Zhang [3], Zhaojie Guo [1, †]

[1] Key Laboratory of Orogenic Belts and Crustal Evolution, Ministry of Education, School of Earth and Space Sciences, Peking University, Beijing, 100871, China

[2] Laboratoire Géosciences Rennes, CNRS-UMR6118, Université Rennes 1 - Observatoire des Sciences de l'Univers, Rennes, 35042, France

[3] Qinghai Oilfield Company, PetroChina, Dunhuang, Gansu, 736202, China

[†] Corresponding author. Tel.: + 86-10-62753545; fax: + 86-10-62758610. E-mail address: zjguo@pku.edu.cn (Z.J. Guo)

Note: This work is submitted to the Tectonophysics and is undergoing peer-review process.

Abstract

Marking the northern boundary of the Tibetan plateau, the Altyn Tagh fault plays a crucial role in accommodating the Cenozoic crustal deformation affecting the plateau. However, its initiation time and amount of offset are still controversial despite being key information for the understanding of Tibet evolution. In this study, we present 1122 single LA-ICP-MS detrital zircon U-Pb ages obtained from 11 Mesozoic and Cenozoic sandstone samples, collected along two sections in the northwestern Qaidam basin (Eboliang and Huatugou). These data which are associated with new 3D seismic reflection profiles to demonstrate: (1) From the Paleocene to early Eocene, the Eboliang section was approximately located near the present

position of Anxi, ca. 360 ± 40 km southwest to its current location along the Altyn Tagh fault, and sediments were mainly derived from the Altyn Tagh Range. At the same period, the Huatugou section was approximately located near the present position of Tula, ca. 360 km southwest to its current location along the Altyn Tagh fault, and the Eastern Kunlun Range represented the significant sediment source. (2) Left-lateral strike-slip movement along the Altyn Tagh fault initiated during the early to middle Eocene, resulting in northeastward displacement of the two sections. (3) By the early Miocene, the intensive deformation within the Altyn Tagh Range and northwestern Qaidam basin strongly modified the drainage system, preventing the materials derived from the Altyn Tagh Range to reach the Eboliang and the Huatugou sections. The post-Oligocene clastic material in the western Qaidam basin is generally derived from local sources and recycling of the deformed Paleocene to Oligocene strata. From these data, we suggest enhanced tectonic activity within the Altyn Tagh Range and northwestern Qaidam basin since Miocene time, and propose an early to middle Eocene initiation of left-lateral strike-slip faulting and a 360 ± 40 km offset along the Altyn Tagh fault.
Keywords：Detrital zircon U-Pb geochronology, Cenozoic tectonics, North Tibet, Altyn Tagh fault, Qaidam basin.

3.2.1 Introduction

Two competing end-member mechanisms have been proposed to explain the accommodation of the ongoing convergence between India and Eurasia since the early Eocene collision: (1) a homogeneous crustal thickening of the Tibetan plateau (e.g. England and Houseman, 1989; Searle, 1996); and (2) an eastward extrusion of the Tibetan plateau and southeast Asia away from the indenting Indian plate (Molnar and Tapponnier, 1975; Peltzer and Tapponnier, 1988; Avouac and Tapponnier, 1993; Tapponnier, et al., 2001). The second model requires large-scale displacement along lithospheric strike-slip fault zones to allow extrusion of the Tibetan crust. (e.g. Searle, 1996; Tapponnier, et al., 2001). Marking the northern boundary of the Tibetan plateau (Fig. 1), the lithospheric-scale left-lateral strike-slip Altyn Tagh fault (ATF) plays a crucial role in accommodating the crustal deformation and appears to be an ideal field laboratory for ascertaining the dynamics of plateau formation (Molnar and Tapponnier, 1975; Wittlinger et al., 1998; Jolivet et al., 1999, 2001; Yin and Harrison, 2000; Yin et al., 2002; Searle et al., 2011). Understanding the kinematic pattern of the ATF, especially the exact Cenozoic initiation time and the amount of Cenozoic offset, is of major importance for unraveling the crustal accommodation processes within the plateau since the India-Eurasian collision and for deciphering the growth history of the entire Tibetan

plateau.

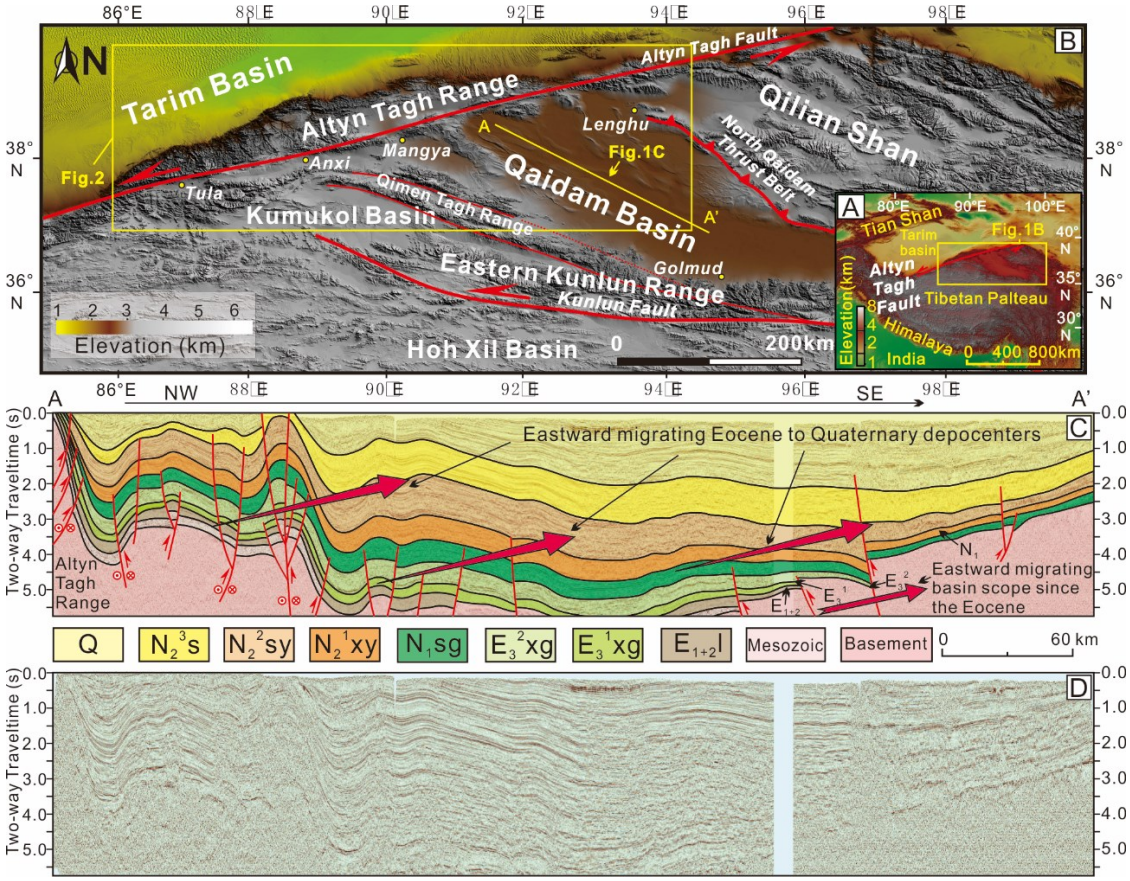

Fig. 1 (A) SRTM based digital topographic map of the Tibetan plateau. (B) Digital elevation model (DEM) and major tectonic elements of the Altyn Tagh Range, the Qaidam basin and the surrounding regions. The location of Fig. 2 is identified by the solid box. The DEM map was generated from the 90 m SRTM data. Note that the yellow solid line refers to the location of seismic profile AA'. (C) Interpreted and (D) non-interpreted seismic profile AA'. Note that the succession of Cenozoic depo-centers is marked along the long axis of the basin. These depo-centers gradually migrated eastward since the Eocene.

In spite of its widely recognized significance, the Cenozoic initial rupture and displacement on the ATF are still controversial and highly debated. Several authors proposed that a large scale Jurassic basement cooling event associated to tectonic exhumation affected a corridor along the ATF (e.g. Delville et al., 2001; Sobel et al., 2001; Wang et al., 2005). In addition, many researchers consider that deformation along the ATF initiated after the late Mesozoic, during the early Cenozoic, or even not before Neogene (e.g. Tapponnier et al., 1986; Jolivet et al., 1999; Chen et al., 2001; Jolivet et al., 2001; Yin et al., 2002; Wang et al., 2006a; Wu et al., 2012a, 2012b; Zhang et al., 2012, 2014a). Similarly, estimations of the total displacement along the ATF vary widely from ~1200 km to less than 90 km (e.g. Tapponnier et al., 1986; Wang, 1997; CSBS, 1992; Ritts and Biffi, 2000; Yin and Harrison, 2000; Yang et al., 2001; Yue et al., 2001; Chen et al., 2002; Yin et al., 2002; Cowgill et al., 2003; Gehrels et

al., 2003a, 2003b; Darby et al., 2005; Yue et al., 2005; Searle et al., 2011; Cheng et al., 2015a). These tremendous discrepancies may be partially attributed to the immense size and extent of the Altyn Tagh Range, making it difficult to locate ideal piercing points to estimate the total displacement along the ATF. Furthermore, due to strong Cenozoic deformation, continuous Mesozoic to Cenozoic stratigraphic sections useful to estimate the time of initiation of left-slip movement are seldom preserved (e.g. Yin and Harrison, 2000; Cheng et al., 2015a).

Detrital zircon analysis of a continuous, well dated stratigraphic succession has become a powerful tool for unraveling source to sink relationships and constraining the tectonic and topographic evolution of an area (e.g. Fedo et al., 2003; Thomas, 2011; Gehrels, 2014). To bring more constraints on the kinematic evolution of the ATF, we conducted an integrated analysis on two Jurassic to Pleistocene sedimentary sections in the western part of the Qaidam basin, adjacent to the ATF (Fig. 2). Detrital zircon U-Pb geochronology data obtained from these sections are associated to high-quality subsurface data, including newly acquired seismic profiles and drill core sandstone samples.

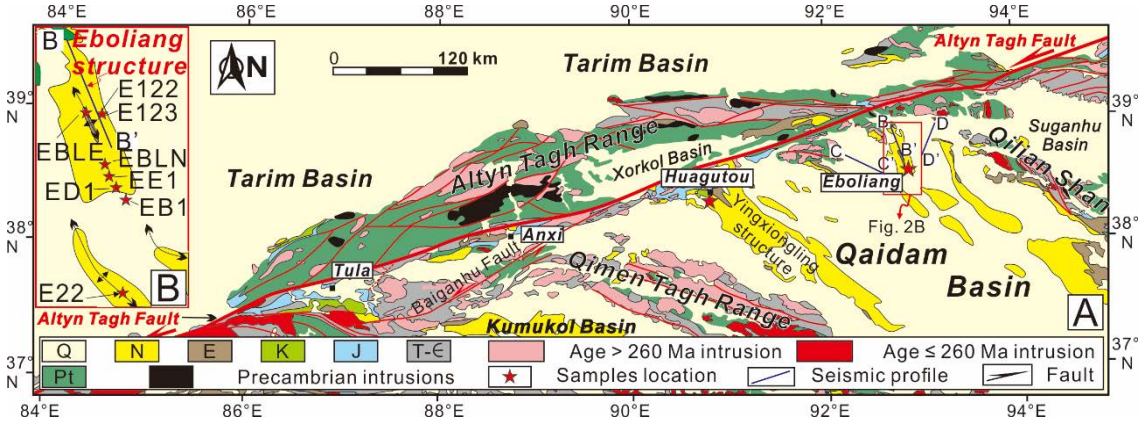

Fig. 2 Simplified geological map of the northwestern Qaidam basin and eastern segment of the Altyn Tagh Range, adapted from the Geologic Map of the Tibetan plateau and adjacent areas compiled by the Chengdu Institute of Geology and Mineral Resources and Chinese Geological Survey (map scale, 1:1,500,000).

3.2.2 Geological Background

3.2.2.1 Altyn Tagh Range

The Altyn Tagh Range is located along the northern edge of the Tibetan plateau, separating the Tarim basin to the northwest from the Tibetan plateau and the Qaidam basin to the south (Figs. 1 and 2). The bedrock of the Altyn Tagh Range mainly consists of Precambrian igneous and metamorphic rocks and Paleozoic igneous and sedimentary rocks (e.g. Sobel and Arnaud, 1999; Yin et al., 2002). It has been shown that the Altyn Tagh Range experienced

multiple-stage deformation and tectonic exhumation from the Jurassic to the Holocene (Tapponnier et al., 1986; Jolivet et al., 1999; Yue and Liou, 1999; Chen et al., 2001; Delville et al., 2001; Jolivet et al., 2001; Sobel et al., 2001; Yin et al., 2002; Wang et al., 2005, 2006a; Zhang et al., 2012). Within this range, the over 1600 km long ENE-trending ATF links the western Kunlun thrust belt in the southwest and the Qilian Shan thrust belt in the northeast (Fig. 1; Burchfiel et al., 1989; Wang, 1997; Yue and Liou, 1999; Yin and Harrison, 2000; Yin et al., 2002). Although Mesozoic shearing occurred in the Altyn Tagh Range, the northern Tibetan plateau growth is largely influenced by Cenozoic sinistral strike-slip faulting along the ATF (Tapponnier et al., 1986, 2001; Arnaud et al., 2003; Wang et al., 2005; Li et al., 2006; Liu et al., 2007). As previously mentioned, the estimation of the total displacement along the fault remains heavily debated, varying from about 1200 km to less than 90 km (e.g. CSBS, 1992; Ritts and Biffi, 2000; Yang et al., 2001; Chen et al., 2002; Cowgill et al., 2003; Gehrels et al., 2003a, 2003b; Yue et al., 2005; Cheng et al., 2015a).

3.2.2.2 Qaidam basin

The rhomb-shaped Qaidam basin, is the largest petroliferous basin within the entire Tibetan plateau (Figs. 1 and 2). Geomorphologically, the basin is surrounded by the Altyn Tagh Range to the northwest, the Qilian Shan to the northeast and the Eastern Kunlun Range to the south. Geological mapping and petroleum exploration revealed that the Qaidam basin is filled with Mesozoic to Cenozoic clastic sediment series unconformably overlying an uncertain basement (Xia et al., 2001; Meng and Fang, 2008; Yin et al., 2008a, 2008b). The Mesozoic strata, especially the Jurassic and lower Cretaceous sequences, are mainly distributed along the foreland of both the Altyn Tagh Range and the Qilian Shan (Ritts et al., 1999; Wu et al., 2011), while the Cenozoic series are generally deposited within the entire basin (Yin et al., 2008b). The Cenozoic sedimentation pattern is largely controlled by a succession of depocenters consistently located along the long axis of the basin and gradually migrating eastward since Eocene times, indicating the gradual uplift of the Altyn Tagh Range (Fig. 1; Song and Wang, 1993; Qiu, 2002; Sun et al., 2005; Wang et al., 2006a; Yin et al., 2008b). Using magnetostratigraphy, palynology and paleontology, the Mesozoic-Cenozoic strata have been precisely subdivided into 11 chronostratigraphically constrained units (Fig. 3; Huo, 1990; QBGMR, 1991; Yang et al., 1992; Huang et al., 1996; Xia et al., 2001; Qiu, 2002; Deng et al., 2004a, 2004b; Sun et al., 2005; Zhang, 2006; Zhao et al., 2006; Fang et al., 2007; Sun et al., 2007; Yin et al., 2008b; Gao et al., 2009; Pei et al., 2009; Lu and Xiong, 2009; Ke et al., 2013). These units are: (1) the Dameigou Formation, $_{J1+2}$d; (2) the Caishiling Formation,

J_3c; (3) the Quanyagou Formation, Kq; (4) the Lulehe Formation, $E_{1+2}l$, >53.5 - 43.8 Ma (Yang et al., 1992; Zhang, 2006; Ke et al., 2013); (5) the lower Xiaganchaigou Formation, E_3^1xg, 43.8 - 37.8 Ma (Zhang, 2006; Sun et al., 2007; Pei et al., 2009); (6) the upper Xiaganchaigou Formation, E_3^2xg, 37.8 - 35.5 Ma (Sun et al., 2005; Sun, 2007; Pei et al., 2009); (7) the Shangganchaigou Formation, N_1sg, 35.5 - 22.0 Ma (Sun et al., 2005; Lu and Xiong, 2009); (8) the Xiayoushashan Formation, N_2^1xy, 22.0 - 15.3 Ma (Fang et al., 2007; Lu and Xiong, 2009); (9) the Shangyoushashan Formation, N_2^2sy, 15.3 - 8.1 Ma (Fang et al., 2007); (10) the Shizigou Formation, N_2^3s, 8.1 - 2.5 Ma (Fang et al., 2007); (11) the Quaternary deposits, including the Qigequan Formation (Q_1q) and the Dabuxun-Yanqiao Formation (Q_2d), 2.5 - 0.01 Ma (Fang et al., 2007; Yin et al., 2008b). Effective elastic thickness calculation implies that the mechanical strength of the Qaidam crust is exceptionally strong compared to the rest of the Tibetan plateau (Braitenberg et al., 2003). Based on balanced cross section results, Zhou et al. (2006) proposed that the Qaidam basin experienced an average of 10% of NE-SW shortening during the Cenozoic, whereas Yin et al. (2008b) suggested that the shortening strain across the basin decreases systematically eastward from ca. 48% in the west, to ca. 11% in the center, and <1% in the east.

3.2.3 Stratigraphy and sedimentary characteristics of the studied sections

In this study, the Eboliang and Huatugou sections, situated along the eastern and central segments of the ATF, have been chosen for their exceptional preservation and exposure of the Jurassic to Pleistocene sedimentary series (Figs. 2 and 3). In order to give a continuous description of the Jurassic to Quaternary sediment evolution of the northwestern Qaidam basin, we constructed the Eboliang and Huatugou sections based on the lithologies, sediment facies and paleocurrent directions obtained from fieldwork, drill-core and literature data as summarized in the Figure 3 and in the text below. The strata in Huatugou and Eboliang sections have already been established by previous field geological studies which give age constraint based on fossil assemblages, distinctive lithology feature, magnetostratigraphy, palynology and paleontology (e.g. XBGRM, 1993; HGSI, 2003; IGSQP, 2004). Consequently, we follow the previous division of formations.

3.2.3.1 Eboliang section

The Eboliang section is located along the southern flank of the Altyn Tagh Range (Fig. 2). The upper Jurassic-Cretaceous strata are missing, and the Paleogene deposits rest unconformably on lower - middle Jurassic series. Except for the absence of the Paleocene

Lulehe Formation, the Cenozoic sequence is complete and exceptionally well exposed.

High-quality seismic profiles and drill core data reveal that the base of the Eboliang section is formed by the lower to middle Jurassic Dameigou Formation (J_{1+2}d), resting unconformably on the basement rocks (Yin et al., 2008). This Jurassic sequence generally contains a succession of three well-developed fining upward cycles. Each cycle characteristically begins with medium- to coarse-grained sandstone deposits (Fig. 4A), fining upwards to silty mudstone. The sequence, as in general for the Qaidam basin, is considered to represent shore shallow lacustrine facies at the base, evolving into flood plain sediments upward (Ritts et al., 1999; Ritts and Biffi, 2000; Wu et al., 2011; Jian et al., 2013). Trough and planar cross-stratification and clast imbrication from those fluvial strata indicates northward paleoflows during the Jurassic (Fig. 3; Ritts and Biffi, 2000).

The entire upper Jurassic and Cretaceous sequence is missing and the Paleocene Lulehe Formation (E_{1+2}l,) unconformably overlies the lower and middle Jurassic series (Wu et al., 2011). The strata are composed of dark brown mudstone (Fig. 4B) and sandy mudstone intercalated with gray siltstone at the base, evolving towards brown pebbly sandstone intercalated with conglomerates and gypsum-salt layers in the middle and upper parts of the section. The Lulehe Formation is generally interpreted as braided river and alluvial fan depositional environments (Zhuang et al., 2011; Jian et al., 2013; Song et al., 2013). Based on heavy mineral contents, calculated zircon-tourmaline-rutile (ZTR) indices, and the heavy mineral assemblages from drill-core samples from a large number of oil wells in the Eboliang section, Fu et al. (2013) suggested that during the deposition of the Paleocene-early Eocene Lulehe Formation, the material deposited in the Eboliang area was derived from the north, probably from the Altyn Tagh Range.

The Eocene to Oligocene strata of the Xiaganchaigou Formation unconformably rest on the Lulehe Formation. The strata are mainly composed of grey and brown sandstone (Fig. 4C) and conglomerate at the bottom corresponding to alluvial facies deposits (Zhuang et al., 2011; Jian et al., 2013; Wang et al., 2013) and contain a succession of fining upward cycles. The middle part of the Xiaganchaigou Formation is dominated by brownish red mudstone and sandy mudstone intercalated with gray calcareous mudstone and marlstone. The upper part of the Xiaganchaigou Formation, however, is dominated by variegated mudstone intercalated with thin-layers of sandy conglomerate, sandstone and limestone, generally associated to a lacustrine depositional environment (Zhuang et al., 2011; Jian et al., 2013; Wang et al., 2013). Conglomerate fabrics in the Eboliang area show north-directed or south-directed bilateral paleoflows, suggesting a low-energy lacustrine-offshore environment at the time (Fig. 3; Wu

et al., 2012b).

The Oligocene Shangganchaigou Formation (N1sg), conformably rests on the Xiaganchaigou Formation. It consists of brownish red, gray siltstone, grey mudstone, sandy mudstone and siltstone, intercalated with gray sandstone and marlstone (Fig. 4D) mostly corresponding to lacustrine sediment facies (Zhuang et al., 2011; Jian et al., 2013; Wang et al., 2013). Paleocurrents measured from the conglomerate fabrics become dominantly south-directed away from the Altyn Tagh Range (Fig. 3; Wu et al., 2012b).

The early Miocene Xiayoushashan Formation (N_2^1xy) conformably lies on the Shangganchaigou Formation. The lower part of the formation is composed of gray and brownish red mudstone and sandy mudstone intercalated with gray siltstone, grayish yellow sandstone and grayish brown marlstone. It evolves upwards to gray mudstone, argillaceous sandstone and argillaceous siltstone intercalated with grey siltstone, brownish red mudstone and gray marlstone (Fig. 4E). The early Miocene sequence in the north Qaidam basin is generally considered as deposited in a fluvial to marginal lacustrine environment (Zhuang et al., 2011; Jian et al., 2013; Wang et al., 2013). Conglomerate fabrics in the section suggest south-directed paleocurrents during the early Miocene (Fig. 3; Wu et al., 2012b).

The late Miocene Shangyoushashan Formation (N_2^2sy) conformably rests on the Xiayoushashan Formation. The deposits are mainly composed of grey mudstone and sandy mudstone intercalated with grey argillaceous sandstone, argillaceous siltstone, grayish yellow marlstone and some limited gray sandy limestone corresponding again to a fluvial to marginal lacustrine environment (Zhuang et al., 2011; Jian et al., 2013; Wang et al., 2013). Paleocurrent measurements from the sandstone layers around the Eboliang area indicate southwest-directed paleoflows (Fig. 3; Wu et al., 2012b).

The Pliocene Shizigou Formation (N_2^3s) generally conformably and locally unconformably rests on the Shangyoushashan Formation. The series are composed of gray mudstone and silty mudstone intercalated with brown siltstone, pebbly sandstone and gypsum-salt layers. It is generally interpreted as marginal lacustrine to alluvial fan environment (Fig. 4F; Zhuang et al., 2011; Heermance et al., 2013; Jian et al., 2013; Wang et al., 2013). Trough cross-bedding within the strata suggests generally southwestward paleoflows during the Pliocene (Fig. 3; Heermance et al., 2013).

Finally, the Pleistocene sequence, dominated by the Qigequan Formation (Q_1q), unconformably overlies the Shizigou Formation. The sediments are characterized by brown sandstone, pebbly sandstone and conglomerate intercalated with gypsum layers, corresponding to fluvial to evaporatic lacustrine facies (Heermance et al., 2013; Jian et al.,

2013). Well-developed cross-bedding within the strata shows primarily unidirectional paleocurrents toward the south (Fig. 3; Heermance et al., 2013).

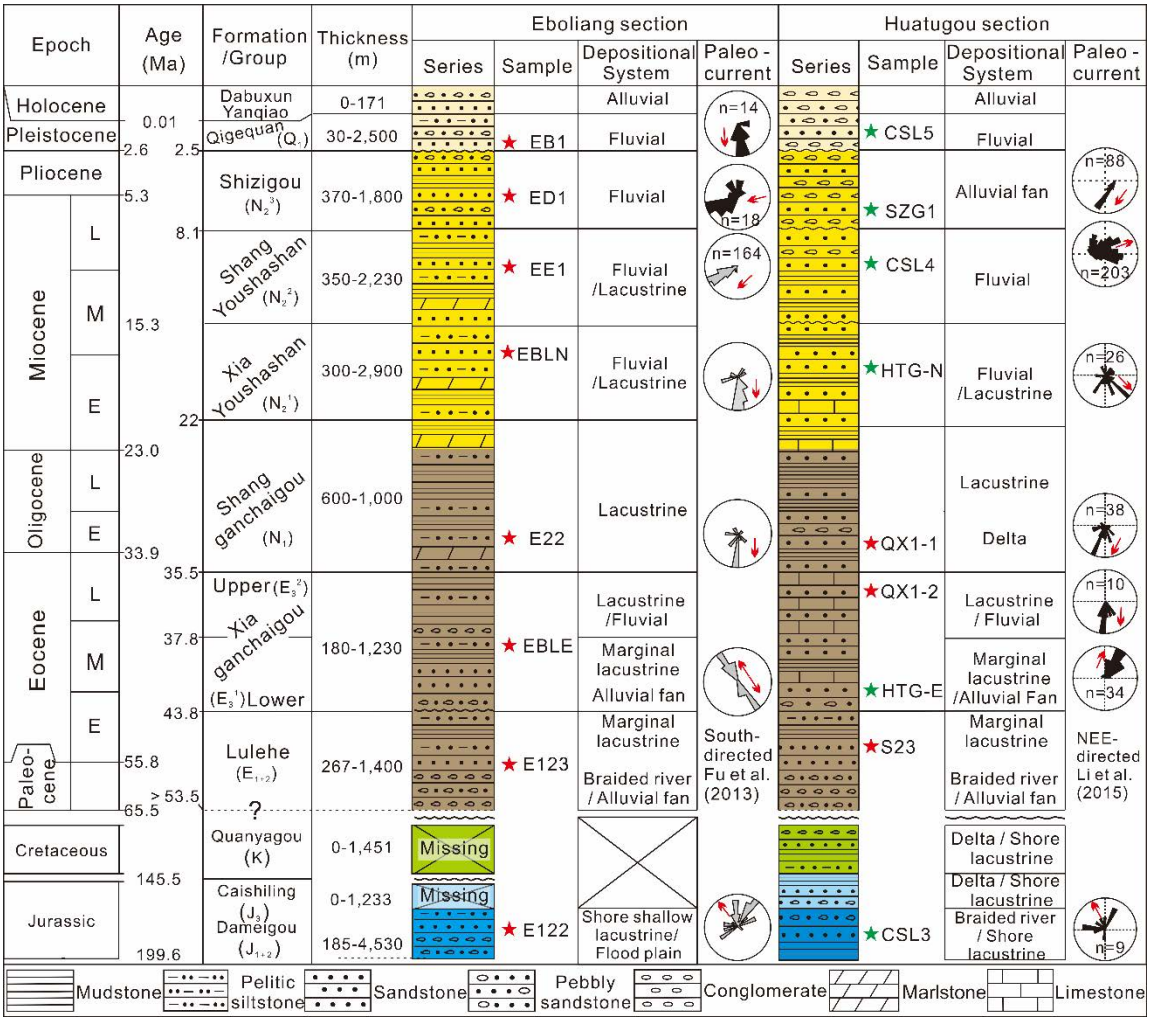

Fig. 3 Generalized stratigraphic column of the studied Mesozoic to Cenozoic series. Paleocurrent directions in the Huatugou section were obtained from Meng and Fang, (2008), Wu et al. (2012b) and Zhuang, et al. (2011). Paleocurrent directions in the Eboliang section were obtained from Zhuang, et al. (2011), Wu et al. (2012b) and Heermance et al. (2013). Note that sample CSL3 is cited from Cheng et al. (2015a), and samples HTG-E, HTG-N, CSL4, SZG1 and CSL5 are cited from Cheng et al. (2016). Red arrows refer to the general paleocurrent directions.

3.2.3.2 Huatugou section

The Huatugou section is located in the northernmost part of the prominent Yingxiongling uplift structure (Fig. 2). Except again for the Paleocene Lulehe Fm., the whole Mesozoic-Cenozoic sequence is well exposed (Figs. 2 and 3).

Subsurface data reveal that the Jurassic clastic coal-bearing strata rest unconformably on the Altyn Tagh Range basement (Xia et al., 2001; Yin et al., 2008). The Dameigou Formation ($J_{1+2}d$) is dominated by a set of sandstone beds interbedded with conglomerate, siltstone and

mudstone (Ritts et al., 1999; Ritts and Biffi, 2000). The sediment facies vary from fluvial to shallow lake deposits (Ritts and Biffi, 2000). Trough and planar cross-stratification as well as clast imbrication within the strata indicate northward paleoflows during the Jurassic (Fig. 3; Ritts and Biffi, 2000).

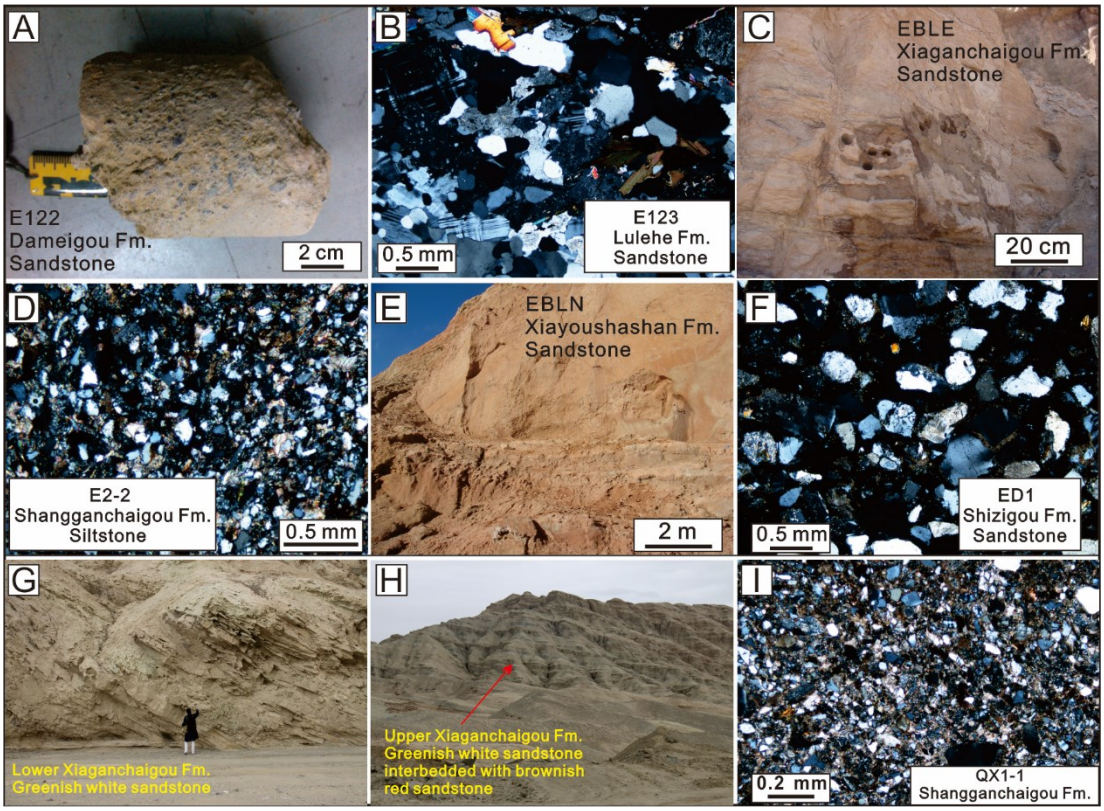

Fig. 4 Typical photomicrographs and field photographs of the various analyzed sediments. (A) Drill core sample of early to middle Jurassic (J_{1+2}) lithic sandstone obtained from drill well in the Eboliang section; (B) Thin section image of lithic sandstone from the Paleocene to early Eocene strata (E_{1+2}) in the Eboliang section, under crossed polarized light. (C) Horizontally stratified sandstone interbedded with mudstones of the Xiaganchaigou Formation (E_3^1) in the Eboliang section. (D) Thin section image of siltstone from the Oligocene strata (N_1), under crossed polarized light, obtained from drill well in the Eboliang section. (E) Thick-bedded sandstone in the early Miocene strata, Xiayoushashan Formation (N_2^1), Eboliang section. (F) Thin section image of siltstone from the Pliocene strata (N_2^3), in the Eboliang section, under crossed polarized light. (G) Greenish white sandstone intercalated with mudstone in the middle Eocene strata (E_3^1), Huatugou section. (H) Greenish white sandstone intercalated with brownish red mudstone in the late Eocene strata (E_3^1), Huatugou section. (I) Thin section image of sandstone in the Oligocene strata (N_1), Huatugou section, under crossed polarized light.

Based on the subsurface data (core and seismic profile data), the Paleocene to early Eocene Lulehe Formation (E_{1+2}l) is dominated by successions of purple-red conglomerate interbedded with sandstone at the base, evolving upward towards grey sandstone, siltstone and sandy mudstone. The sediment facies vary from fluvial to shallow lake deposits upward and

basinward (Fu et al., 2013; Li et al., 2015). Heavy mineral contents in surface samples, calculated zircon-tourmaline-rutile (ZTR) indices, and the heavy mineral assemblages from the drill-core samples from a large number of oil wells in the Huatugou area suggest that during the deposition of the Paleocene-early Eocene Lulehe Formation, the material deposited in the Huatugou area was mainly derived from the southwest, probably from the Eastern Kunlun Range (Fu et al., 2013; Li et al., 2015).

The middle Eocene lower Xiaganchaigou Formation (E_3^1xg) is mainly composed of grey-green, brownish-red sandstone and pebbly sandstone at the base, evolving upward towards brown red sandstone and siltstone (Fig. 4G). The sediment facies vary from fluvial to shallow lacustrine deposits upward (Zhuang et al., 2011; Wu et al., 2012a, 2012b). Paleocurrents from the pebble imbrication and cross-stratification in the fluvial sandstone layers are directed towards the NE (Fig. 3; Meng and Fang, 2008).

The late Eocene upper Xiaganchaigou Formation (E_3^2xg) rests conformably on the lower Xiaganchaigou Formation. This sequence is dominated by successions of grey-green, brownish-red mudstone and carbonaceous siltstone, intercalated with argillaceous siltstone and marlstone (Fig. 4H). The sediment facies vary upward from braided river to shallow lake deposits (Wu et al., 2012a, 2012b). Clast imbrications within the fluvial strata suggest that paleocurrents were directed towards the south during the deposition of the upper Xiaganchaigou Formation. (Fig. 3; Wu et al., 2012a).

The Oligocene Shangganchaigou Formation (N_1sg), conformably resting on the upper Xiaganchaigou Formation, is mainly composed of greyish-green carbonaceous mudstone and sandstone interbedded with grey-white mudstone. This series is dominated by deltaic to shallow lake facies deposits (Wu et al., 2012a, 2012b). Reported paleocurrents from clast imbrications are generally directed towards the south (Fig. 3; Wu et al., 2012a).

The Xiayoushashan Formation (N_2^1xy), conformable with the Shangganchaigou Formation, is mainly composed of yellowish-brown, pebbly sandstone, sandstone and argillaceous siltstone with intercalations of limestone. The facies vary from shallow lake to fluvial deposits (Wu et al., 2012a, 2012b). Clast imbrications within the sequences suggest generally southwestward paleoflows during the early Miocene.

The Shangyoushashan Formation (N_2^2sy), resting unconformably on the Xiayoushashan Formation (Wang et al., 2010), mainly consists of yellow pebbly sandstone, sandstone and silty mudstone. The sediment facies is dominated by shallow lake, alluvial plain and braided river deposits (Wu et al., 2012a, 2012b). Clast imbrication as well as trough (and lesser planar) cross-stratification within the layers in the section suggest generally northwestward

paleoflows (Zhuang et al., 2011).

The Shizigou Formation (N_2^3s), again lying unconformably on the Shangyoushashan Formation, is mainly composed of earth-yellow sandstone and silty mudstone corresponding to fluvial facies sediments (Wu et al., 2012a, 2012b). Paleocurrents from clast imbrications indicate generally south-directed paleoflows away from the Altyn Tagh Range during the deposition of the Shizigou Formation (Fig. 3; Zhuang et al., 2011).

The Qigequan (Q_1q) and Dabuxun-Yanqiao (Q_2) formations, unconformably overly the Shizigou Formation, and mainly consists of grey and brown sandstone and conglomerate corresponding to flood plain and alluvial facies deposits.

3.2.4 Methods and analytical procedures

3.2.4.1 Detrital zircon geochronology

Detrital zircon U-Pb geochronology has rapidly developed into a very powerful tool for determining sediment provenances (e.g. Fedo, et al., 2003; Thomas, 2011; Liu et al., 2013; Yang et al., 2013; Gehrels et al., 2014; Cheng et al., 2015a). By systematically comparing the detrital zircon U-Pb age spectrum obtained from sedimentary sequences in basins with the known ages of potential source terranes, it is possible to describe the source to sink relations through time within a given area and to reconstruct the landscape evolution of the region (e.g. Fedo, et al., 2003; Gehrels et al., 2011; Thomas, 2011; Liu et al., 2013; Yang et al., 2013; Gehrels et al., 2014; Yang et al., 2014; Cheng et al., 2015a). In the Eboliang section, eight samples were collected, ranging in age from Jurassic to Pleistocene (Fig. 2), and including three samples from drill cores. In the Huatugou section, three core samples were obtained from drill wells, ranging in age from Paleocene to Oligocene. In order to derive a continuous Jurassic to Pleistocene source to sink relation between the Altyn Tagh Range and the western Qaidam basin, we also integrated six published detrital zircon U-Pb dating results obtained on samples collected from the Huatugou section (Cheng et al., 2015a, 2016). The major petrological characteristics of all the samples are described in Table 1.

Zircon grains for U-Pb age dating were concentrated from each sample following the standard procedures outlined in Liu et al. (2013). This work was conducted at the Chengxin Geology Service Co. Ltd, Langfang, Hebei Province, China. Individual zircon crystals (generally more than 200 grains) were mounted in epoxy resin without handpicking to avoid sampling bias. Samples were then polished to obtain a smooth flat internal surface. Reflected and transmitted light as well as cathodoluminescence (CL) images were made to reveal

internal heterogeneities and allow choosing potential internal targets for isotopic dating. U-Pb analysis was performed on an Agilent 7500a ICP-MS connected to an American New Wave UP 193 SS 193 nm Excimer laser ablation system at the China University of Geosciences, Beijing. All samples were analyzed using a laser spot size of 36 μm and a frequency of 10 Hz. Two standards (Black et al., 2003; Qi et al., 2005) were analyzed every 10 to 20 grains, to correct for instrument fluctuations and determine fractionation factors. Zircons Qinghu and 91500 (Wiedenbeck et al., 1995) were the monitoring standards. For elemental concentration analysis, NIST610 was the external standard, and 29Si was the internal standard. Meanwhile, NIST612 and NIST614 were used as monitoring standards. The GLITTER 4.4 software was used to calculate the U-Pb isotope ratios and element contents (China University of Geosciences, Lab. of Prof. Y.S. Liu, Beijing, China). The U-Pb ages obtained were checked for discordance by plotting the analyses on concordia diagrams using the Isoplot 3.0 software (Ludwig, 2003). The common-Pb correction followed the method described by Andersen (2002). Ages younger than ca. 1000 Ma are based on common Pb-corrected 206Pb/238U ratios, whereas ages older than ca. 1000 Ma are based on common Pb-corrected 207Pb/206Pb ratios. For ICP-MS analyses, those ages with discordance degree >10% were excluded from analysis (e.g. Gehrels et al., 2003a; Yang et al., 2013; Liu et al., 2015). A more complete description of the sample separation methods and analytical procedures is given in Yuan et al. (2004).

3.2.4.2 Seismic profile

Extensive petroleum exploration of the Qaidam basin in recent years has provided abundant subsurface data, including high-quality seismic profiles and drill core data. In this study, we integrated two 3D and two 2D seismic profiles (A-A', B-B', CC' and DD', see locations in Figs. 1 and 2) from the western Qaidam basin with our surface field investigation to describe the tectonic history of the western Qaidam basin. Seismic data were interpreted using the SMT Kingdom software.

3.2.5 U–Pb geochronology results of detrital zircons

Representative CL images of typical zircon grains are presented in Figure 5. U-Pb isotopic ages with errors and related raw data are listed in full as Appendix S1. Concordia plots for the eleven samples are shown in Figure 6. The zircon age spectrum of the samples from the Eboliang and Huatugou sections are shown in Figs. 7 and 8, respectively. In the following, age peaks are considered major when corresponding to an age group including at least 50% of the total number of data, whereas a minor peak refers to those representing less

than 20% of the total number of data.

Table 1. Summary of the major characteristics and corresponding U-Pb age data for each sample

Epoch	Formation (Fm.)	Sample number	Lithology	Detrital zircon age range (Ma)	Detrital zircon peaks (Ma)	Number of effective data points	Th/U ratios
Eboliang section							
Pleistocence	Qigequan Fm. (Q_1q)	EB1	Greyish green sandstone	232~1053	~253 ~417	100	0.08, 0.09, 0.14~2.19
Pliocene	Shizigou Fm. (N_2^3s)	ED1	Gray-white sandstone	234~1252	~242 ~401	94	0.10~2.43
Late Miocene	Shangyoushashan Fm. (N_2^2sy)	EE1	Greyish green sandstone	232~2114	~253 ~424	87	0.03, 0.04, 0.05, 0.07, 0.11~1.52
Early Miocene	Xiayoushashan Fm. (N_2^1xy)	EBLN	Gray-white sandstone	231~1746	~258 ~444	100	0.01, 0.08, 0.14~1.46
Oligocene	Shangganchaigou Fm. (N_1sg)	E22	Gray-white sandstone	212~2608	~246 ~414	84	0.13~3.28
Eocene	Xiaganchaigou Fm. (E_3^1xg)	EBLE	Greyish green sandstone	57~2513	~255 ~461	95	0.02, 0.06, 0.08, 0.09, 0.15~4.04
Paleocene	Lulehe Fm. ($E_{1+2}l$)	E123	Gray-white sandstone	221~1429	~246 ~426 ~911	93	0.09, 0.10~1.66
Jurassic	Dameigou Fm. ($J_{1+2}d$)	E122	Gray-white sandstone	241~1871	~253 ~422	87	0.09, 0.12~2.51
Huatugou section							
Pleistocene	Qigequan Fm. (Q_1q)	CSL5*	Gray-white fine-grained sandstones, well- sorted.	211~2430	~260 ~420 ~860	98	0.04, 0.07, 0.09, 0.15~ 1.48
Pliocene	Shizigou Fm. (N_2^3s)	SZG1*	Gray-yellow fine-grained sandstones, well- sorted.	211~2430	~240 ~430 ~890	93	0.03, 0.09, 0.14~2.15
Middle Miocene	Shangyoushashan Fm. (N_2^2sy)	CSL4*	Brown fine-grained sandstones, well-sorted.	202~2378	~220 ~430 ~880	95	0.03, 0.06, 0.08, 0.09, 0.11~2.00
Early Miocene	Xiayoushashan Fm. (N_2^1xy)	HTG-N*	Gray-white fine-grained sandstones, well- sorted.	235~2378	~260 ~400	95	0.12~1.56
Oligocene	Shangganchaigou Fm. (N_1sg)	QX1-1	Gray-yellow pebbly sandstone	193~3188	~268 ~422 ~926	93	0.001, 0.08, 0.14~1.53
Late Eocene	Upper Xiaganchaigou Fm. (E_3^2xg)	QX1-2	Gray-white pebbly sandstone	215~2513	~285 ~461 ~920	98	0.08, 0.12~ 4.95
Middle Eocene	Lower Xiaganchaigou Fm. (E_3^1xg)	HTG-E*	Gray-white medium - grained sandstones, well- sorted.	181~2662	~260 ~430	98	0.22~1.59
Paleocene to Early Eocene	Lulehe Fm. ($E_{1+2}l$)	S23	Gray-white sandstone	188~1804	~247 ~412	59	0.14~1.84

Early-Middle Jurassic	Dameigou Fm. (J_{1+2}d)	CSL3#	Gray-yellow sandstones	220~2480	~264 ~433	97	0.25~3.82

Note: * Samples cited from Cheng et al. (in press); # Sample cited from Cheng et al. (2015a).

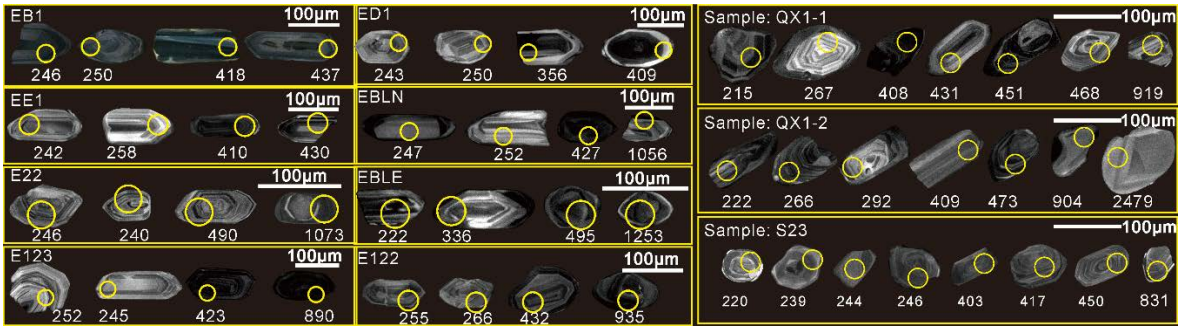

Fig. 5 Representative CL images of zircons from the 11 sandstone samples. The yellow circles show the location of the U-Pb analysis. Numbers are U-Pb ages in Ma.

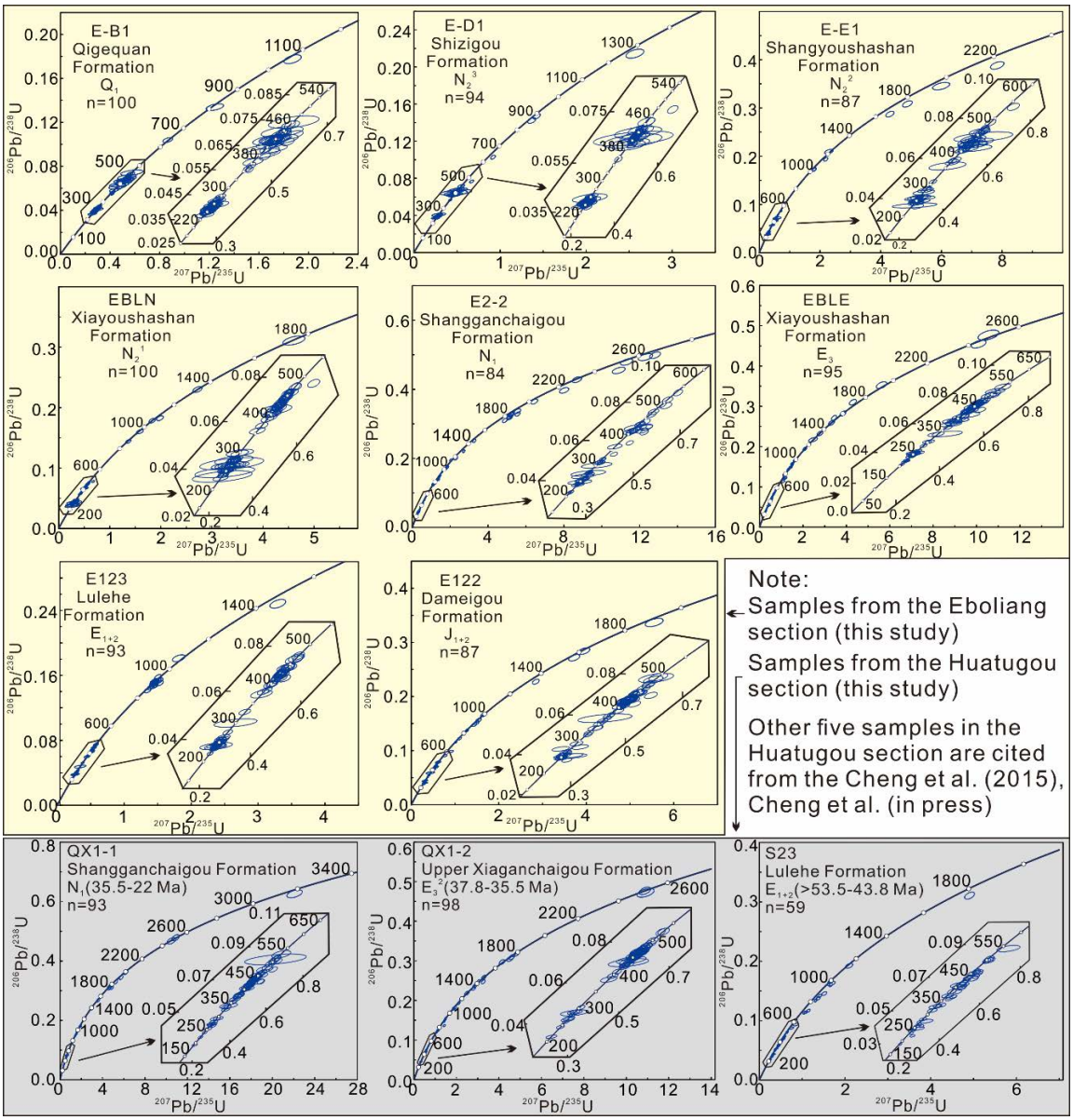

Fig. 6 U-Pb concordia diagrams for zircon grains of the 11 sandstone samples.

3.2.5.1 Eboliang section

Sample E122 (Dameigou Fm., early to middle Jurassic)

In sample E122, zircon grain morphologies range from subhedral to subrounded with an average size of 80 - 200 μm. The grains are generally colorless and exhibit obvious oscillatory zoning, with a few ones showing inherited cores and rims. Except for one grain with a Th/U ratio of 0.09, all the crystals show high Th/U ratios from 0.12 to 2.51, indicative of a magmatic origin (Corfu et al., 2003; Hanchar and Rudnick, 1995; Hoskin and Black, 2000). 87 out of 105 dated grains yielded a 206Pb/238U age ranging between 1871 to 241 Ma with two major peaks at ~422 Ma and ~253 Ma (Fig. 7A).

Sample E123 (Lulehe Fm., 53.5-43.8 Ma)

In sample E123, zircon crystals display subhedral to abraded shapes and an average size ranging between 50 μm and 350 μm. The majority of crystals (~90% of the total) display distinct oscillatory zoning in CL images indicating a magmatic origin, confirmed by Th/U ratios varying between 0.1 and 1.66 with only one grain having a slightly lower value of 0.09. Among 100 crystals analyzed, 93 concordant analyses yielded ages ranging from 1429 Ma to 221 Ma (Fig. 7B). The zircon age population is distributed in four groups with two major peaks at ~426 Ma and ~246 Ma, and one more restricted peak at ~911 Ma. Finally, two outlying ages of 1429 Ma and 1073 Ma were also obtained.

Sample EBLE (Lower Xiaganchaigou Fm., 43.8-37.8 Ma)

In sample EBLE, zircon grain morphologies range from subhedral to subrounded with an average size of 50 - 150 μm. CL images show that most zircon crystals (over 90% of the total) are characterized by relatively distinct oscillatory zoning suggesting a magmatic origin. Except for four grains with Th/U ratio of 0.02, 0.06, 0.08 and 0.09, all zircons show high Th/U ratios from 0.15 to 4.04, confirming the magmatic origin (Tab. 1). Among 100 crystals analyzed, 95 analyses are concordant and yielded ages mainly ranging from 2513 Ma to 207 Ma, with two peak ages at 461 Ma and 255 Ma (Fig. 7C). The age of the remaining zircons are evenly distributed from 2469 Ma to 690 Ma. One outlying grain yielded a much younger age of 57 Ma.

Sample E22 (Upper Xiaganchaigou Fm., 37.8-35.5 Ma)

Zircons from sample E22 are predominantly colorless, euhedral to abraded, with a length of 50 - 150 μm. Over 90% of the crystals show oscillatory zoning and some of them show inherited cores or overgrowths (Fig. 5). All analyses show high Th/U ratios ranging from 0.13 to 3.28 indicating a magmatic origin. 53 out of 105 dated grains yielded a 206Pb/238U age of

530 Ma to 212 Ma with two age peaks at 414 Ma and 246 Ma (Fig. 7D). The age of the remaining zircons are evenly distributed from 2608 Ma to 742 Ma.

Sample EBLN (Xiayoushashan Fm., 22.0-15.3 Ma)

In sample EBLN, zircon grains show euhedral to subhedral shapes with an average size ranging between 100 μm and 300 μm. Over 80% of crystals show distinct oscillatory zoning suggesting a magmatic origin, with a few showing inherited cores and rims. Except for two grains with Th/U ratio of 0.01 and 0.08, all the zircons show high Th/U ratios ranging from 0.14 to 1.46, indicative of their magmatic origin. The 100 crystals analyzed have a discordance degree of <10% and provided U-Pb ages ranging from 2114 Ma to 231 Ma (Fig. 7E). The ages can be separated in two main populations with two peak ages at 424 Ma and 253 Ma. In addition, 4 isolated grains have Proterozoic ages.

Sample EE1 (Shangyoushashan Fm., 15.3-8.1 Ma)

Zircons from sample EE1 are predominantly colorless, euhedral to abraded, with a length of 50 μm to 200 μm. CL images show that 90% of these grains are characterized by relatively distinct oscillatory zoning and some of them exhibit inherited cores or overgrowths. Except for four grains with Th/U ratio of 0.03, 0.04, 0.05 and 0.07, all zircons show high Th/U ratios ranging from 0.15 to 4.04, typical of a magmatic origin. All 105 U-Pb analyses are concordant and yielded ages mainly ranging from 2114 Ma to 232 Ma. The large majority of those ages can be divided in two groups with peak ages at 424 Ma (47 % of total) and 253 Ma (39 % of total), respectively (Fig. 7F). Eight zircons yielded single Proterozoic ages of 2114, 1912, 1732, 1627, 1226, 1140, 1026 and 1023 Ma.

Sample ED1 (Shizigou Fm., 8.1-2.5Ma)

In sample ED1, the majority of zircon grains (90 % of the total) are subhedral to subrounded, ranging from 100 to 250 μm in length. Most zircon crystals (~80 % of the total) exhibit oscillatory growth zoning, with some (~20 % of the total) showing inherited cores and rims. All zircons give high Th/U ratios from 0.10 to 2.43, indicating their magmatic origin. Among a total of 105 analyses, 94 concordant analyses yielded ages ranging from 1252 Ma to 234 Ma, falling into two main age population with peaks at 401 Ma (50 % of total) and 242 Ma (45 % of total) respectively (Fig. 7G). Five zircons yielded outlying ages of 1461, 1252, 883, 857 and 631 Ma.

Sample EB1 (Qigequan Fm., 2.5-0.01 Ma)

Zircons from sample EB1 are 80 - 250 μm long and mainly subhedral to subrounded. Over 90% of the zircons show oscillatory zoning and some of them show inherited cores or overgrowths. Except for two grains with Th/U ratio of 0.08 and 0.09, all the zircons have high

Th/U ratios ranging from 0.14 to 2.19, indicating their magmatic origin. All the 100 analyses have age discordance degree of <10%, and span from 1053 Ma to 232 Ma (Fig. 7H). The data group into two age populations with peaks at 417 Ma (48 % of total) and 253 Ma (46 % of total) respectively. Three zircons yielded ages of 1053, 809 and 637 Ma.

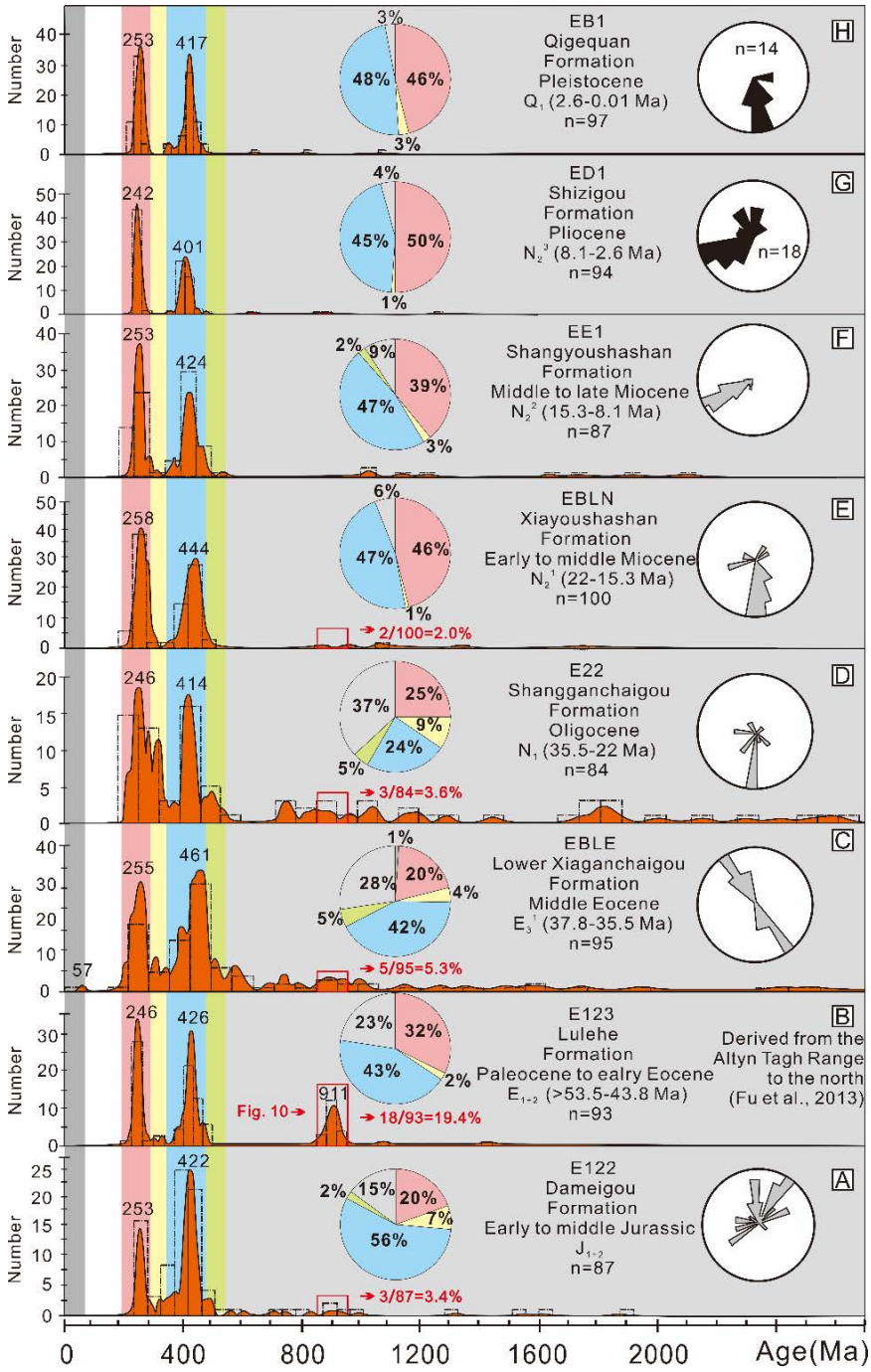

Fig. 7 Combined probability density functions (lines) and histogram plots (bars) depicting detrital zircon U-Pb ages of samples from the Eboliang section, arranged in stratigraphic order. Age distributions are colored according to age groups, and the pie diagrams show percentages of grains in those age categories. Paleocurrents rose diagrams in black are compiled from Heermance et al. (2013) and rose diagrams in gray are compiled from Wu et al. (2012b) and Ritts and Biffi (2000).

Overall, the U-Pb ages of detrital zircons from the 9 Jurassic to Pleistocene samples range from 2608 Ma to 57 Ma. Based on their morphological characteristics, internal textures and Th/U ratio, magmatic zircons appear to dominate (about 90 %) the section while the remaining ones are metamorphic zircons (about 10 %).

3.2.5.2 Huatugou section

Sample CSL3 (Dameigou Fm., early to middle Jurassic)

Zircons from sample CSL3 are predominantly euhedral to abraded, with a length of 50-250 μm. CL images show that most zircon crystals (90% of the total) are characterized by relatively distinct oscillatory zoning. Th/U ratios vary between 0.25 and 3.82. Among 100 zircons analyzed, 97 concordant analyses yielded ages ranging from 2480 to 220 Ma (Fig. 8A; Cheng et al., 2015a). The ages can be separated in three main groups with two peak ages at 433 Ma and 264 Ma, and some isolated ages between 2480 to 852 Ma (Fig. 8A).

Sample S23 (Lulehe Fm., 53.5-43.8 Ma)

In sample S23, zircon crystals display subhedral to abraded shapes for an average size ranging between 50 μm and 100 μm. The majority of crystals (90% of the total) display distinct oscillatory zoning in CL images indicating a magmatic origin, confirmed by Th/U ratios varying between 0.14 and 1.84. 59 usable data points were obtained among 102 analyzed zircon grains. U-Pb ages range from ~1804 Ma to ~188 Ma, with two peaks at ~412 Ma and ~247 Ma. Finally, a few isolated ages range from 1200 Ma to 600 Ma (Fig. 8B).

Sample HTG-E (Lower Xiaganchaigou Fm., 43.8-37.8 Ma)

In sample HTG-E, zircon grains show well-preserved euhedral shapes with an average size ranging between 50 μm and 150 μm. Over 90% of the crystals are characterized by relatively distinct oscillatory zoning indicating a magmatic origin confirmed by Th/U ratios varying from 0.22 to 1.59. Among 100 zircons analyzed, 98 concordant analyses yielded ages ranging from ~2662 Ma to ~181 Ma, with two peaks at ~430 Ma and ~260 Ma. A number of ages are spread between 2662 Ma and 500 Ma with 18% of the data clustering between 1500 Ma and 500 Ma (Fig. 8C; Cheng et al., 2016).

Sample QX1-2 (Upper Xiaganchaigou Fm., 37.8-35.5 Ma)

In sample QX1-2, zircon grain morphologies range from euhedral to subhedral with an average size of 100 ~ 200 μm. CL images show that most of these zircon crystals (~90% of the total) display relatively distinct oscillatory zoning suggesting a magmatic origin. Except for one grain with Th/U ratio of 0.08, all zircons show high Th/U ratios from 0.12 to 4.95, confirming the magmatic origin. Among a total of 105 analyses, 98 concordant analyses

yielded ages ranging from 2513 Ma to 215 Ma with two peak ages at 461 Ma and 285 Ma, and a potential sub-peak at 920 Ma (Fig. 8D).

Sample QX1-1(Shangganchaigou Fm., 35.5-22 Ma)

Zircons from sample QX1-1 are predominantly colorless, euhedral to abraded, with a length of 50-200 μm. Over 90 percent of the crystals show oscillatory zoning. Except for two grains with Th/U ratio of 0.001 and 0.08, all zircons show high Th/U ratios ranging from 0.14 to 1.53 indicating a magmatic origin. Among 100 crystals analyzed, 93 concordant analyses yielded ages ranging from 3188 Ma to 193 Ma, with a major age peak at ~422 Ma, a minor age peak at ~268 Ma, and a potential sub-peak at ~926 Ma (Fig. 8E).

Sample HTG-N (Xiayoushashan Fm., 22-15.3 Ma)

In sample HTG-N, zircon grain morphologies range from euhedral to abraded with an average size ranging between 80 μm and 200 μm. A large majority of zircon crystals (about 90%) display distinct oscillatory zoning on CL images indicating a magmatic source, which is also confirmed by Th/U ratios varying from 0.12 to 1.56. Among a total of 100 analyses, 95 concordant analyses yielded ages ranging from 2378 Ma to 235 Ma with two peak ages at 400 Ma and 260 Ma, and a number of ages clustering between 1200 Ma and 700 Ma (Fig. 8F; Cheng et al., 2016).

Sample CSL4 (Shangyoushashan Fm., 15.3-8.1 Ma)

Zircons from sample CSL4 are predominantly euhedral to abraded, with a length of 50 - 250 μm. More than 90% of the crystals display distinct oscillatory zoning on CL images implying a magmatic origin as attested by Th/U ratios varying from 0.11 to 2.00. Among 100 crystals analyzed, 95 concordant analyses yielded U-Pb ages ranging from ~2378 Ma to ~235 Ma, with three peaks at ~880 Ma, ~430 Ma and ~220 Ma. Finally, some ages are again spread from 1020 Ma to 800 Ma (Fig. 8G; Cheng et al., 2016).

Sample SZG1 (Shizigou Fm., 8.1-2.5Ma)

In sample SZG1, zircon grain morphologies range from euhedral to abraded with an average size of 80 - 200 μm. Most crystals (more than 90%) display a distinct oscillatory zoning on CL images indicating a magmatic origin. The Th/U ratios vary from 0.14 to 2.15, with two exceptions of 0.03 and 0.09, confirming a generally magmatic origin. 93 usable data points were obtained among 100 analyzed zircon grains. U-Pb ages range from ~2421 Ma to ~222 Ma, with three peaks at ~890 Ma, ~430 Ma and ~240 Ma (Fig. 8H; Cheng et al., 2016).

Sample CSL5 (Qigequan Fm., 2.5-0.01 Ma)

Zircons from sample CSL5 are predominantly well-preserved euhedral, with a length of 50-200 μm. Only a few grains (about 5%) show faint zoning in CL suggesting a metamorphic

origin. Most crystals display distinct oscillatory zoning characteristic of their magmatic origin. This is confirmed by Th/U ratios varying from 0.15 to 1.48, with three exceptions of 0.04, 0.07 and 0.09. Among 100 analyzed zircons, 98 U-Pb ages with discordance degree <10% obtained, ranging from ~2430 Ma to ~211 Ma, with two major peaks at ~420 Ma and ~260 Ma and a minor peak at ~860 Ma (Fig. 8I; Cheng et al., 2016).

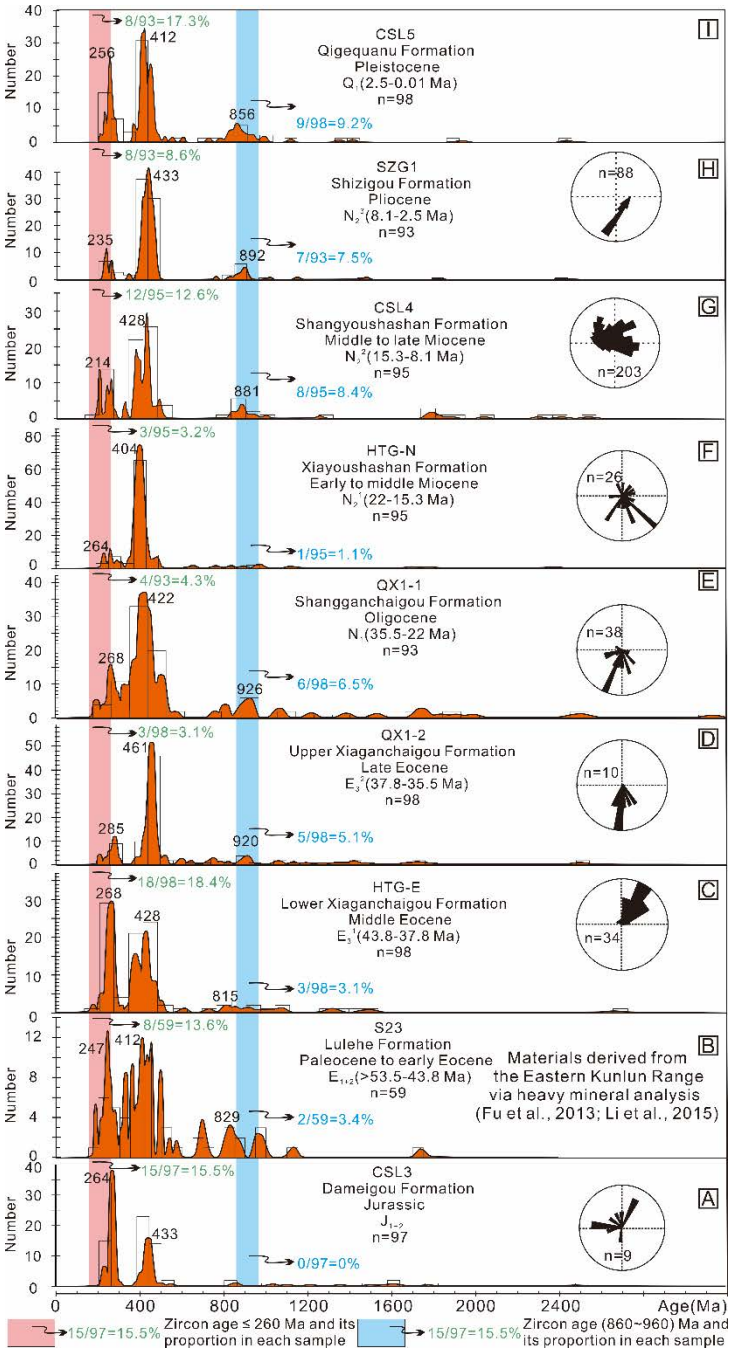

Fig. 8 Combined probability density functions (lines) and histogram plots (bars) depicting detrital zircon U-Pb ages of samples from the Huatugou section, arranged in stratigraphic order. Two distinctive age groups, indicative of separate sources, are colored. Paleocurrents rose diagrams are compiled from Meng and Fang, (2008), Wu et al. (2012b) and Zhuang, et al. (2011).

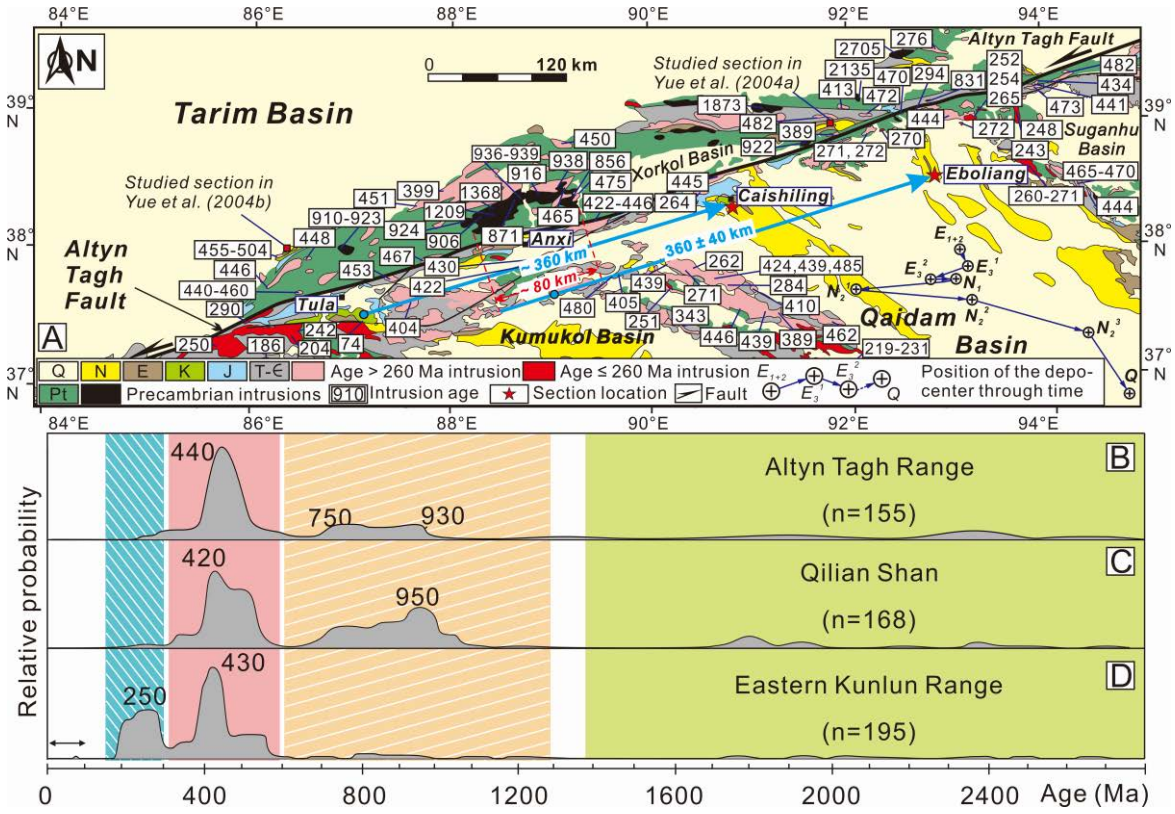

Fig. 9 (A) Sketched geological map of the Altyn Tagh Range and surrounding areas, showing the distribution of zircon U–Pb ages for granitoids. The numbers denote ages in Ma. Relative probability plots of zircon U-Pb ages from basement rocks and intrusives in: (B) the Altyn Tagh Range, (C) the Qilian Shan, and (D) the Eastern Kunlun Range. Age data are mainly cited from: Guo and Li, (1999), Sobel and Arnaud, (1999), Yang et al. (2001), Zhang et al. (2001), Yang and Song, (2002), Cowgill et al. (2003), Gehrels et al. (2003a, 2003b), Jolivet et al. (2003), Lu and Yuan, (2003), Robinson et al. 2003, Roger et al. (2003), Chen et al. (2004), IGSQP, (2004), Yue et al. (2004, 2005), Liu et al. (2006), Shi et al. (2006), Song et al. (2006), Wang et al. (2006b), Yang et al. (2006), Lu et al. (2008), Roger et al. (2008), Bovet et al. (2009), Liu et al. (2009), Wu et al. (2009), Xiao et al. (2009), Roger et al. (2010), Zhang et al. (2011), Dai et al. (2013), Li et al. (2013), Wang et al. (2013), Long et al. (2014), Song et al (2014), Wang et al.(2014b) , Zhang et al. (2014a), Dong et al. (2014, 2015), Chen et al. (2015) and references therein. The blue arrow refers to the northeastward migration of the Huatugou and Eboliang sections from their origins.

3.2.6 Discussion

3.2.6.1 Geochronological characteristics of potential sources for the sedimentary rocks in the western Qaidam basin

Highlands surrounding the basin is the priori potential source for the deposited clastic material (e.g. Bruguier et al., 1997; Allen and Allen, 2005). The Altyn Tagh Range, the Qilian Shan, as well as the Eastern Kunlun Range are all potential source regions likely to provide zircons to the Qaidam basin (e.g. Métivier et al., 1998; Xia et al., 2001; Meng and Fang, 2008;

Yin et al., 2007, 2008a, 2008b). In order to better constrain the provenance area of the samples collected in the western Qaidam basin (Fig. 9A), we compiled the zircon U-Pb ages available on basement rocks of the Altyn Tagh Range (Fig. 9B), the Qilian Shan (Fig. 9C) and the Eastern Kunlun Range (Fig. 8D).

In the Altyn Tagh Range, the basement mainly consists of Archean and Proterozoic rocks with Archean zircon U-Pb ages ranging from ~3.6 Ga to ~2.6 Ga (Lu and Yuan, 2003; Lu et al., 2008; Long et al., 2014; Zhang et al., 2014b and references therein), and Proterozoic zircon U-Pb ages ranging from ~2.4 Ga to ~650 Ma (Gehrels et al., 2003a, 2003b; Wang et al., 2006b; Lu et al., 2008 and references therein; Zhang et al., 2011; Wang et al., 2013). A few scattered Neoproterozoic intrusions are exposed, with a large, distinctive early Neoproterozoic intrusion (ca. 850 Ma to ca. 1000 Ma in age) exposed west of the Xorkol basin (Fig. 9A). Wang et al. (2013) recently reported a mean crystallization age of ~910 Ma for the basement rocks near the Anxi area, in the western part of the Altyn Tagh Range (Fig. 9A). Paleozoic intrusions with ages spanning from ~550 Ma to ~400 Ma are widely distributed (Jolivet et al., 1999; Sobel and Arnaud, 1999; Zhang et al., 2001; Cowgill et al., 2003; Gehrels et al., 2003a; Chen et al., 2004; Yue et al., 2004a, 2005; Yang et al., 2006; Wang et al., 2014b and references therein). Finally a few Permian igneous rocks are sporadically distributed along the central part of the Altyn Tagh Range, with zircon U-Pb ages ranging between ~300 Ma and ~260 Ma (Fig. 9A; Cowgill et al., 2003; Gehrels et al., 2003a; Gehrels et al., 2003b; Wu et al., 2014).

Zircon age from the North Qaidam and South Qilian Shan terranes mainly group between 2700 to 1100 Ma, 550 to 400 Ma, and 300 to 200 Ma (Fig. 9B; Yang and Song, 2002; Cowgill et al., 2003; Gehrels et al., 2003a, 2003b; Yue et al., 2005; Shi et al., 2006; Song et al., 2014 and references therein). The North Qilian Shan basement mainly consists of early Paleozoic marine strata associated with a series of Ordovician volcanics and Silurian granitic plutons (Bovet et al., 2009; Xiao et al., 2009; Song et al., 2014 and references therein). These granitoid intrusions yielded U-Pb zircon ages ranging from ca. 550 to ca. 440 Ma (Wu et al., 2001; Gehrels et al., 2003a, 2003b; Yue et al., 2005; Song et al., 2014 and references therein). Finally, the central Qilian Shan basement is composed of Mesoproterozoic to Neoproterozoic marine sequences intruded by early Paleozoic plutons, with detrital and plutonic zircon ages comprised between 2333 to 874 Ma and 442 to 424 Ma respectively (Guo and Li, 1999; Lu, 2002; Yue et al., 2005; Bovet et al., 2009; Song et al., 2014 and references therein). The Qilian Shan basement was affected by a Devonian phase of metamorphism (400-360 Ma), with a metamorphic peak at 440-423 Ma within the north Qaidam ultrahigh pressure belt (Yang et al., 2001, Yang and Song, 2002; Song et al., 2006; Yang et al., 2006; Song et al., 2014 and

references therein). Finally, sporadically distributed late Permian to early Triassic granitoids are exposed along the western edge of the South Qilian Shan terrane, yielding zircon U-Pb ages ranging from ca. 270 Ma to ca. 230 Ma (Fig. 9A and 9C; Yang and Song, 2002; Wu et al., 2009; Dong et al., 2014, 2015).

Within the Eastern Kunlun Range, Proterozoic ages are rare (Fig. 9A and 9D). Several early Paleozoic intrusions with U-Pb zircon ages ranging from ca. 500 Ma to 400 Ma have been reported by previous studies (Fig. 9C; Cowgill et al., 2003; IGSQP, 2004; Dai et al., 2013; Li et al. 2013). Late Paleozoic - early Mesozoic granitoids (ca. 300 Ma to ca. 200 Ma), corresponding to the magmatism associated to the Permo-Triassic closure of the Paleo-Tethys Ocean and to the post-collision magmatism that followed the docking of the Qiangtang Block, are extensively distributed (Fig. 9A; e.g. Roger et al., 2003, 2008, 2010; Liu et al., 2006; Li et al., 2013; Jolivet et al., 2015; Chen et al., 2015). Finally, a few Cretaceous ages have been obtained from the Tula Uplift in the western reach of the Eastern Kunlun Range (Figs. 2A and 9A; Robinson et al., 2003; Cheng et al., 2015a) and some Miocene to Quaternary volcanism was occurring in the southwestern part of the range (Jolivet et al., 2003).

3.2.6.2 Provenance analyses of the Mesozoic-Cenozoic strata in the western Qaidam basin

3.2.6.2.1 Eboliang section

On a first order analysis, the detrital zircon U-Pb age spectrum obtained from the eight samples collected on the Eboliang section are largely similar (Fig. 7), suggesting that the provenance area was largely homogeneous through time. However, second-order variations in age cluster proportions among those samples record source changes during basin filling. In general, the detrital zircons U-Pb ages can be statistically subdivided into three major groups of Precambrian (spanning from ca. 2.8 Ga to 550 Ma), early to middle Paleozoic (peaks at 460~400 Ma) and late Paleozoic to Mesozoic (peaks at ca. 260~240 Ma) (Fig. 7). Aside from these major groups, the restricted early Neoproterozoic age group spanning from ca. 850 to ca. 1100 Ma with a peak age around 911 Ma (for example in sample E123, Lulehe Formation) represents the contribution from a distinctive source in the Altyn Tagh Range that will be discussed in details below.

Based on isopachs distribution, the Jurassic depocenter was situated farther south of the Eboliang section, which rules out any contribution from the Eastern Kunlun Range in the Jurassic sediments from that section (Fig. 9A; also see Fig. 3b in Meng et al., 2001). We thus consider that the paleocurrents in the northwestern Qaidam basin (Ritts and Biffi, 2000)

probably provided sediments from mixed sources both in the Qilian Shan and Altyn Tagh Range. Based on $^{40}Ar/^{39}Ar$ thermochronology as well as zircon and apatite fission track analysis, previous researches have reported Jurassic exhumation in the Altyn Tagh Range (Delville et al., 2001; Jolivet et al., 2001; Sobel et al., 2001; Wang et al., 2005). The detrital zircon age distribution of the Jurassic sediments in the Eboliang section (sample E122, Fig. 7D), is very similar to those of the Cenozoic samples, including early to middle Paleozoic zircons (peaks at 422 Ma; 56 % of total), late Paleozoic to Mesozoic zircons (peaks at ca. 253 Ma; 20 % of total) and a few Precambrian zircon (15 % of total). This similarity suggests that the source of the material deposited in the Eboliang region has been largely stable since the early Jurassic including both Permian granitoids and Ordovician to Devonian basement from either or both the Altyn Tagh Range and the Qilian Shan (Figs. 7A and 9).

The Paleogene depocenters of the Qaidam basin were consistently located south of the Eboliang section (see Fig. 12A in Yin et al., 2008b), again excluding material contribution from the Eastern Kunlun Range (Fig. 9A; Meng and Fang, 2008; Yin et al., 2008b; Mao et al., 2014). Paleocurrent directions obtained from conglomerate fabrics (clast imbrications) as well as heavy mineral assemblages suggest that the Paleogene clastic materials deposited in the northwestern Qaidam basin mainly derived from the Qilian Shan to the northeast and the Altyn Tagh Range to the north (Fig. 7; Wu et al., 2011; Fu et al., 2013; Jian et al., 2013). The age spectrum obtained from the three Paleogene samples (E123, EBLE, and E22) are characterized by early to middle Paleozoic zircons (peaks at ca. 414 to ca. 461 Ma; 20 % ~ 43 % of total), late Paleozoic to early Mesozoic zircons (peaks at ca. 246 Ma to ca. 255 Ma; 20 % ~ 23 % of total), and a progressively increasing proportion of Precambrian zircons (from 23 % to 37 %).

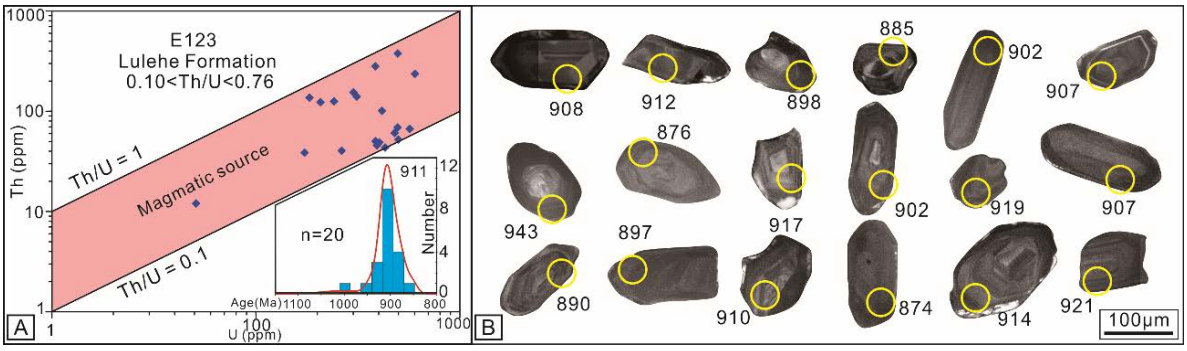

Fig. 10 (A) Frequency histograms for restricted early Neoproterzoic ages groups of detrital zircons from the Paleocene to early Eocene Lulehe Fm. (E_{1+2}) and the Th/U ratio for those zircon ages. (B) CL images of zircons for all early Neoproterzoic ages zircons from the Paleocene to early Eocene Lulehe Fm. The yellow circles show the location of the U-Pb analysis. Numbers are U-Pb ages in Ma. Note that the ~911 Ma peak age for the Neoproterozoic ages groups coincides with the mean crystallization age of ~910 Ma for the basement rocks in the western segment of the Altyn Tagh Range (Fig. 9A;

Wang et al., 2013). The distinctive Th/U ratio and oscillatory zones for those zircons indicate magmatic sources.

The age spectrum of sample E123 displays a distinctive early Neoproterozoic age group (Fig. 7B; 1100 Ma to 850 Ma; peak at 911 Ma). The oscillatory zoning in CL images and the relatively high Th/U ratios (over 0.1, average value 0.3) of those early Neoproterozoic zircons in sample E123 indicate a clear magmatic origin (Fig. 10; Hanchar and Rudnick, 1995; Hoskin and Black, 2000; Corfu et al., 2003). As shown in Figure 9A, the early Neoproterozoic sources are few and small in the Altyn Tagh Range and Qilian Shan, but for a large magmatic complex north of the Anxi area. Wang et al. (2013) recently reported a mean zircon U-Pb crystallization age of ~910 Ma for these intrusives, consistent with the 911 Ma peak age in the Paleocene to early Eocene sample E123 (Fig. 9A). The enriched early Neoproterozoic zircon age groups (ca. 1100 to ca. 850 Ma) in sample E123 that accounts for over 20% of the total analysis represents a major difference from the age spectrum of the Jurassic and post-Paleocene samples. We suggest that this group indicates that the extensive early Neoprotozoic intrusive north of Anxi area (Fig. 9A) formed a potential source area for the Paleocene to early Eocene strata in the Eboliang section. According to the isopach map of the Paleocene to early Eocene Lulehe Formation provided by Yin et al. (2008b), the main depocenter was located south of the Eboliang section and the strata in the Eboliang section generally thicken southwards and westwards (Fig. 8). In addition, a sub-depocenter developed in the western Qaidam basin close to the early Neoproterozoic basement rocks in the Altyn Tagh Range (see Fig. 12A in Yin et al., 2008b). If the Eboliang section had been continuously situated in roughly the same region as it occupies today (Fig. 2), the clastic materials derived from the early Neoproterozoic basement would thus not have been transported to the northwestern Qaidam basin. In addition, the few Neoproterozoic intrusions in the central and northern Qilian Shan region are not only far away from the Eboliang section, but also completely obstructed by the Paleocene uplift of the northern Qaidam thrust belt, clearly revealed by the seismic profiles in the southwestern flank of the Qilian Shan (Yin et al., 2008a). Based on these results combined with the generally southward paleoflows data reported from the northern Qaidam basin (e.g. Fu et al., 2013; Jian et al., 2013) and the largely accepted hundreds of kilometers of Cenozoic offset along the lithospheric ATF (e.g. Wittlinger et al., 1998; Wang et al., 2006a; Yu et al., 2014; Cheng et al., 2015a, 2015b), we conclude that the Eboliang section must have been located much closer to the present day position of Anxi (Figs. 1 and 2). The single Paleogene age observed in sample EBLE (Fig. 7C) is difficult to interpret since no Cenozoic magmatism has been reported in the Qaidam basin, Altyn Tagh Range or Qilian Shan. Our preferred interpretation is that the single

Paleocene zircon (57 Ma) was derived from the Cenozoic volcanic ash emitted from the volcanic centers along the northern edge of the Qiangtang Block (e.g. Jolivet et al., 2003; Ding et al., 2007; Staisch et al., 2015).

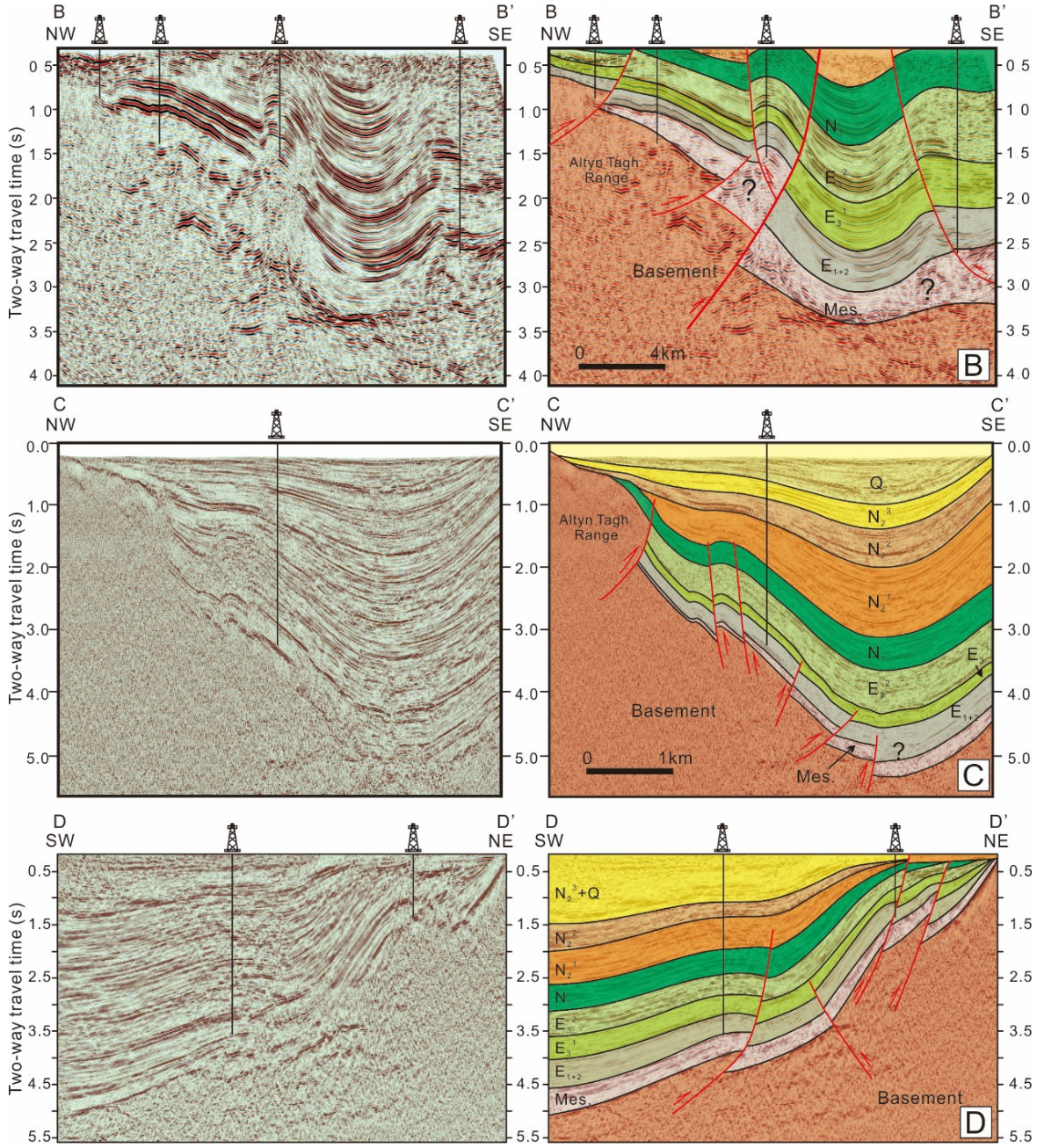

Fig. 11 Seismic profiles in the southwestern Qaidam basin. See Fig. 2A for location. Note the fold and thrusts in seismic profile BB', indicating the deformation in the northwestern Qaidam basin since the early Miocene. Offset of the Paleogene strata in seismic profiles CC' and DD' indicates the Eocene to Oligocene deformation in the northwestern Qaidam basin which would be associated with deformation along the ATF. Growth strata of the post-Oligocene strata in seismic profiles BB' and CC' indicate intense tectonic movements along the ATF since the Miocene.

The post-Oligocene depocenters are all located in the center of the Qaidam basin, south

of the Eboliang section (Fig. 8; Meng and Fang, 2008; Yin et al., 2008b; Mao et al., 2014). This again excludes the possibility that the Neogene Eboliang sediments issued from the Eastern Kunlun Range to the south. Consistently, the generally south-directed paleocurrents indicate that the sources of the post-Oligocene sediments in the Eboliang section were to the north, probably in the Altyn Tagh Range and the Qilian Shan (Wu et al., 2012b). However, the paleoflows changed from south-directed during the early Miocene, to generally southwest-directed during the Pliocene (Fig. 7). Unidirectional, south-directed paleocurrents are dominating during the Quaternary (Fig. 7). Although Miocene to Quaternary strata are still dominated by early to middle Paleozoic zircons (peaks at ca. 444 Ma to ca. 401 Ma; 45 % ~ 48 % of total) and late Paleozoic to Mesozoic zircons (peaks at ca. 258 Ma to ca. 242 Ma; 39 % ~ 50 % of total), Precambrian zircons become scarce (3% ~ 9 % of total), especially in Pliocene and Quaternary strata (Fig. 7F, 7G and 7H). As shown in the 3D seismic profile (Fig. 11), growth strata that developed during the deposition of the early Miocene series most probably indicate intense tectonic deformation along the adjacent ATF. Based on sediment facies studies and provenance analysis of the Oligocene to Miocene strata in the Xorkol basin, Ritts et al. (2004) concluded that the Oligocene to early Miocene sequence coarsens upwards from low-energy playa and alluvial mudflat deposits to proximal alluvial fan deposits, again supporting early Miocene deformation within the Altyn Tagh Range. A similar transition has been observed in the Oligocene to Miocene strata along the northern flank of the Altyn Tagh Range (Yue et al., 2004a). In addition, Miocene deformation within the Altyn Tagh Range has been clearly registered by thermochronology and paleomagnetism data (e.g. Jolivet et al., 1999; Chen et al., 2001; Jolivet et al., 2001; Wang et al., 2006; Liu et al., 2007; Lu et al., 2014). We thus propose that the disappearance of the Precambrian zircon in the post-Oligocene strata is linked to a major change in drainage pattern within the Altyn Tagh Range. The early Miocene deformation along the ATF led to the growth of a prominent topographic barrier, cutting off the link between the Precambrian source rocks in the Altyn Tagh Range and the Eboliang section area. Furthermore, the post-Oligocene samples (EBLN, EB1, ED1 and EE1) were collected in the south of the Eboliang fold structure that formed during or after the early Miocene (Figs. 2 and 11 A; e.g. Shang, 2001). Similarly to that produced in the Altyn Tagh Range, material sourced from the Qilian Shan was thus blocked east of the elevated growing structure and was not able to reach the deposition area to the south (Figs. 2, 9 and 11A). These results imply that the post-Oligocene clastic material deposited in the northwestern Qaidam basin was mainly derived from restricted local sources and/or recycling of the deformed pre-Oligocene strata.

3.2.6.2.2 Huatugou section

Along this section the detrital zircons U-Pb ages are again statistically subdivided into three major populations of Precambrian (spanning from ca. 3.2 Ga to 600 Ma), early to middle Paleozoic (peaks at 460~400 Ma) and late Paleozoic to Mesozoic (peaks at ca. 290~210 Ma) (Fig. 8). The Jurassic to Pleistocene basin depocenters were consistently situated farther southeast to Huatugou section, which rules out any material contribution from the Qilian Shan to the Huatugou section (Fig. 9A; Meng and Fang, 2008; Yin et al., 2008b; Mao et al., 2014).

Late Paleozoic - early Mesozoic granitic intrusions are widespread in the Altyn Tagh and Eastern Kunlun ranges, however, most of the early Mesozoic intrusions (younger than ca. 260 Ma) are confined to the Eastern Kunlun Range just south of our sample sites (Fig. 9A). This distinctive pluton distribution, together with the early Neoproterozoic zircons (1100~850 Ma) issued from the remarkably large intrusion in the Altyn Tagh Range (Fig. 9A; Wang et al., 2013; Cheng et al., 2015a) can be used as provenance signatures to identify the source of detrital zircons within our nine sandstone samples.

The poorly sorted, angular grains in the Jurassic samples suggest deposition from a proximal source terrain (see Figs. 5A and 5B in Cheng et al., 2015a). The zircon ages spectrum of the Jurassic sample (CSL3, Fig. 8A) is characterized by an exceptionally bimodal distribution (Permian-Triassic and Paleozoic groups). The zircons with ages younger than 260 Ma accounts for 15.5 % of the total number of analysis, suggesting that the Eastern Kunlun Range was a significant source of material for the Jurassic strata in the Huatugou section. This result is consistent with the general north- to west- directed paleoflows (Fig. 8A). The few Precambrian zircons (no early Neoproterozoic zircons) as well as the few south-directed paleocurrents might indicate limited contribution from the Altyn Tagh Range to the north, which suggests a limited topographic relief within that range, locally exposing basement rocks (Delville et al., 2001; Sobel et al., 2001; Ritts and Biffi, 2000).

In the Paleocene-early Eocene sample (S23) and the middle Eocene sample (HTG-E), the age spectrums from both samples are still largely bimodal, with about 15% of < 260 Ma zircons, suggesting that the Eastern Kunlun Range was still a significant material source for these samples. This assumption is consistent with the N-NE-directed paleoflows observed in the Paleocene to middle Eocene series (Fig. 8B and 8C; Meng and Fang, 2008; Fu et al., 2013; Li et al., 2015). On the other hand, the increasing proportion of Precambrian zircons (over 3% of early Neoproterozoic zircons in both samples) indicates that the Altyn Tagh Range was gradually becoming a significant source of clastic material for the Paleocene to middle Eocene

strata in the Huatugou section.

The late Eocene to Oligocene sample (QX1-2) displays a significant change in the detrital zircon age distribution pattern (Fig. 8C, 8D and 8E): the major Mesozoic age peak observed in the previous samples becomes nearly negligible with the proportion of < 260 Ma zircons decreasing dramatically (from 13.6% in sample S23 and 18.4% in sample HTG-E to 3.1% in sample QX1-2). In addition, the paleocurrent directions changed abruptly from generally north-directed in the Paleocene to middle Eocene strata to south-directed in the late Eocene strata (Fig. 8C and 8D). This implies major shift in the source region from the Eastern Kunlun Range to the Altyn Tagh Range during the middle to late Eocene time. The proportion of early Neoproterozoic zircons gradually increased (e.g. from 3.1% in sample HTG-E to 5.1% in sample QX1-2) further attesting that basement rocks in the Altyn Tagh Range served as a significant source for the sediments in the Huatugou section.

Recent sedimentology and paleomagnetic studies demonstrated that the relatively rigid Qaidam basin, together with the western segment of the Eastern Kunlun Range, have been transported northeastward along the ATF during the Cenozoic (Wang et al., 2006a; Yu et al., 2014; Cheng et al., 2015a, 2015b). This translation occurred without obvious basin-scale vertical axis rotation with respect to the Eurasia Plate since the early Eocene (Dupont-Nivet et al., 2002; Yu et al., 2014). We suggest that this sharp change in the detrital zircon age distribution pattern was directly related to the onset of large-scale left-lateral strike-slip displacement along the ATF. Except for the still slightly increasing proportion of Precambrian ages, the detrital zircon U-Pb age distributions registered in the Oligocene sample (QX1-1) is similar to those in the late Eocene sample (QX1-2), suggesting a relatively stable drainage pattern from the late Eocene to the Oligocene (Fig. 8D and 8E).

The age spectrum of the early Miocene sample (HTG-N) is again characterized by a major Paleozoic age peak and a minor Mesozoic age sub-peak (Fig. 8F). However, the amount of Precambrian zircons decreased significantly (early Neoproterozoic ages only represent 1.1% of the total analysis). A similar decrease in the proportion of Precambrian zircons was also registered in the early Miocene sample of the Eboliang section (sample EBLN in Fig. 7E), indicating of a regional change in source area and/or drainage pattern throughout the Altyn Tagh Range. As already mentioned in the provenance analysis of samples from the Eboliang section, we suggest that the regional early Miocene deformation within the Altyn Tagh Range cut off the link between the Precambrian source rocks in the Altyn Tagh and Qilian Shan ranges and the depositional area in the Huatugou and Eboliang sections. The early Miocene clastic material in these two sections was mainly derived from more restricted local source

regions and recycling of the deformed Paleocene to Oligocene strata.

Detrital zircon age distributions in the middle Miocene to Pleistocene samples (CSL4, SZG1 and CSL5) are similar, characterized by a major middle Paleozoic age peak, a minor but consistent Mesozoic age peak as well as few Precambrian zircons (Fig. 8G, 8H and 8I). Based on seismic profile interpretation, the fold structures developing perpendicular to the Altyn Tagh fault trend (e.g. the Yingxiongling structure, Fig. 2) initiated during or after the Oligocene (Yin et al., 2007; Yin et al., 2008a; Wu et al., 2014). After the Oligocene onset of deformation, the Huatugou section, located in the northernmost part of the prominent Yingxiongling uplift structure, was gradually isolated from the main Qaidam basin. A complex, local drainage pattern developed while recycling of the deformed Paleocene to Oligocene strata served as a major material source (Fig. 8).

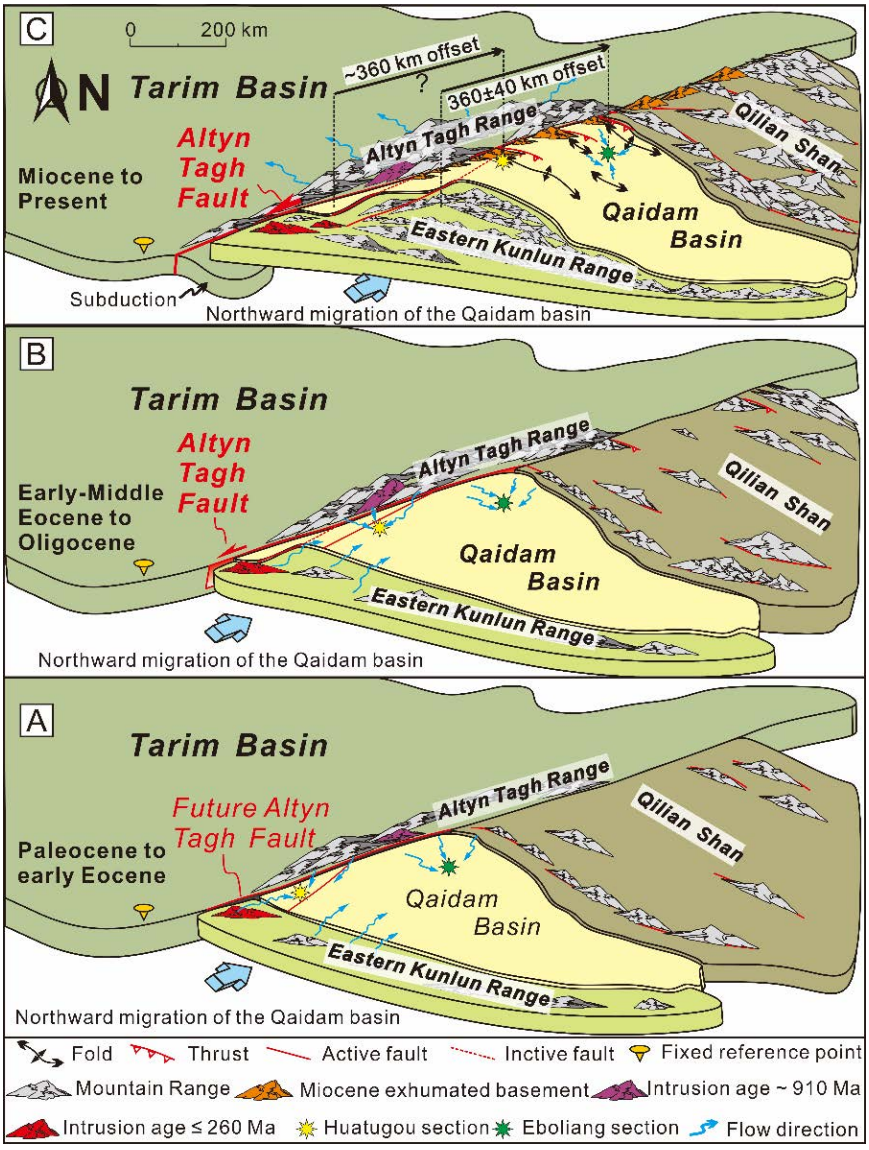

Fig. 12 Cenozoic kinematic model of the Altyn Tagh Fault and source to sink relation between the

western Qaidam basin and the surrounding regions. (A) during the Paleocene to early Eocene, the basement rocks in the Altyn Tagh Range served as the major source for the clastic material deposited in the Eboliang section, while sediments in the Huatugou section were derived from the Eastern Kunlun Range; (B) during the early Eocene to the Oligocene, the Qaidam basin migrated northeastward due to left-lateral strike-slip faulting along the ATF; (3) since the Miocene, intense left-lateral faulting along the ATF continuously offset the Qaidam basin towards the northeast and triggered post-Oligocene crustal deformation within the Altyn Tagh Range and western Qaidam basin. See text for detailed discussion.

3.2.6.3 Tectonics implications

3.2.6.3.1 Source to sink relation between the Qaidam basin and the Altyn Tagh Range

Provenance analysis results obtained from the two studied sections along the ATF reveal that the source to sink relation between the Qaidam basin and the Altyn Tagh Range underwent a three stages evolution:

During the Paleocene and early Eocene, the Eboliang and Huatugou sections were respectively located near the present day position of Anxi, and Tula (Figs. 2A and 12A). The basement rocks in the Altyn Tagh Range (including the early Neoproterozoic intrusive north of Anxi area) served as the major source area for the Eboliang section while a number of materials deposited in the Huatugou section derived from the Eastern Kunlun Range.

By early to middle Eocene, left-lateral strike-slip movement along the ATF initiated, resulting in gradually northeastward migration of the Qaidam basin (including the Eboliang and Huatugou sections). This migration ultimately disconnected the Eboliang section from the early Neoproterozoic source north of Anxi area (Fig. 12B), as attested by the decreasing proportion of early Neoprotozoic zircons (from 19.4% in Paleocene to early Eocene sample E123, to 5.3% in middle-late Eocene sample EBLE and 3.6% in the Oligocene sample E22). Similarly, the Huatugou section gradually moved away from the Tula area towards Anxi (Fig. 12B). This led to a decreasing proportion of < 260 Ma zircons (from ca. 15% in the Paleocene to middle Eocene samples S23 and HTG-E to ca. 3% in the late Eocene sample QX1-2; Fig. 8B, 8C and 8D) and an abrupt change in paleocurrent directions (Fig. 8C and 8D). In parallel, the gradual increase in early Neoproterozoic zircons (from ca. 3% in middle Eocene sample HTG-E to 6.5% in Oligocene sample QX1-1; Fig. 8C, 8D and 8E) suggests that the Huatugou section might be close to the early Neoproterozoic intrusives north of Anxi area during the middle Eocene to Oligocene.

On seimic profiles BB’ and CC’ (trending perpendicular to the Altyn Tagh Range; Figs. 2, 11A and 11B), several basement-involved thrust faults offset the Mesozoic strata and die

out in the Eocene and Oligocene strata. In addition, the Eocene to Oligocene strata slightly thicken towards the depocenter exhibiting a growth-strata structure (Fig. 11B). The oldest unit affected by growth strata is the middle Eocene lower Xiaganchaigou Fm., suggesting that the deformation along the ATF initiated around that time. Paleocurrents measurements and provenance analysis of conglomerates in the Xorkol basin (Fig. 2) and western Qaidam basin indicate that uplift along the central segment of ATF occurred prior to the Oligocene (Yue et al., 2001; Ritts et al., 2004; Wu et al., 2012a, 2012b), probably during the early to middle Eocene.

Since the early Miocene, the Eboliang and Huatugou sections continuously migrated northeastwards along the left-lateral strike-slip ATF. However, the scarcity of the Precambrain zircons, especially the early Neoproterozoic zircons, in the post-Oligocene sediments (e.g. sample EBLN in the Eboliang section and sample HTG-N in the Huatugou section) indicates a major change in the drainage pattern leading to disruption of the source to sink relation between the Altyn Tagh Range and the western Qaidam basin. On seimic profiles BB' and CC' (Fig. 11A and 11B), generally northward-tapering growth strata within the Miocene to Pliocene deposits are well-developed, likely associated with the left-lateral faulting along the ATF and deformation within the Altyn Tagh Range since the early Miocene. The post-Oligocene deformation and uplift within the Altyn Tagh Range and northwestern Qaidam basin largely modified the regional drainage pattern. Most of the material derived from the erosion of the Altyn Tagh Range was directed towards the Tarim basin to the north (Fig. 12C; Yue et al., 2004b). The post-Oligocene clastic materials deposited in the western Qaidam basin was derived from local sources including recycling of the deformed Paleocene to Oligocene strata.

3.2.6.3.2 Implications for the Miocene deformation within the Altyn Tagh Range

In this study, the disappearance of an early Neophrotozoic component in the detrital zircon age spectra of the Miocene strata both in the Eboliang and Huatugou sections as well as the Mioecene initiation of growth strata within the northwestern Qaidam basin are indicative of enhanced tectonic activity within the Altyn Tagh Range and Qaidam basin since the Miocene. This finding is consistent with the results of several previous multi-faceted studies including: thermochronology on the basement rocks within the Altyn Tagh Range (e.g. Chen et al., 2001; Jolivet et al., 1999, 2001; Sobel et al., 2001; Zhang et al., 2012); paleomagnetism studies on the Cenozoic strata within the northwestern Qaidam basin (e.g. Zhang et al., 2013; Lu et al., 2014; Chang et al., 2015); basin-scale seismic profile interpretation (Meng and Fang,

2008; Yin et al., 2008a, 2008b; Wang et al., 2010; Cheng et al., 2015a); provenance analyses along the Altyn Tagh Range (e.g. Yue et al., 2001; Yin et al., 2002; Wu et al., 2012a, 2012b) and synthetized tectonic analysis (e.g. Burchfiel et al.,1989; Meyer et al., 1998; Fu et al., 2015). In addition, the Miocene deformation has been widely recognized in the northern and eastern Tibetan plateau, including the Eastern Kunlun Range, the Altyn Tagh Range, the Longmen Shan and the Qilian Shan (e.g., Kirby et al., 2002; Clark et al., 2004; Ding et al., 2004; Ritts et al., 2004; Sun et al., 2005; Duvall et al., 2013; Yuan et al., 2013; Cheng et al., 2014, 2015a, 2016; Lease, 2014; Chang et al., 2015; Jolivet et al., 2015), which may reflect a critical period in the growth process of the Tibetan plateau.

3.2.6.3.3 Implications for the Cenozoic offset of the ATF

The Eboliang and Huatugou sections record the northward migration of the Qaidam basin and can be used as two piercing points for defining the Cenozoic offset of the ATF. A 360 ± 40 km offset can be estimated by corelating the Eboliang section to the early Neoprotozoic intrusive north of Anxi. Similarly, a ~360 km offset is obtained by corelating the Huatugou section to the Mesozoic plutons south of Tula area. We concede that, from analyzing detrital zircon spectra of Mesozoic to Cenozoic strata, the Eboliang-Anxi piercing point is much more convicing than the Tula-Huatugou piercing. However, by correlating the lithology and sedimentary features of the Cenozoic strata and analyzing the detrital zircon U-Pb ages from Mesozoic strata in both Tula and Huatugou sections, we previously found potential links between the Tula and Huatugou sections (Cheng et al., 2015a). We thus considered that the Tula section used to be a part of the Qaidam basin and was left behind due to the northeastward migration of the Qaidam basin. Two faults which have been indentified by previous research (Figs. 1, 2 and 12; e.g. Cowgill, et al., 2003) are acting as boundaries between the detached Qaidam basin and the relic Tula sub-basin (Cheng et al., 2015a). Since the early Eocene, faulting on the ATF induced these NE-SW–trending branch faults, now covered by Quaternary deposits. Northwards migration of the rigid Qaidam basin left the Tula section and parts of the Kunlun basement behind (Cheng et al., 2015a). Moreover, considering the strong mechanical behaviour of the rigid Qaidam basin, the Huatugou section should be approximately located near the present-day position of the Tula section if we restore the horizontal offset along the AFT based on the convincing Eboliang-Anxi piercing point. Consequently, we suggest a 360 ± 40 km offset along the ATF, which contradicts the extraordinary ~1200 km offset estimation (CSBS, 1992), but is in excellent agreement with independent, albeit indirect piercing points suggesting 300 to 400 km of displacement along the Altyn Tagh Range: (1) 400 ± 60 km offset

based on Jurassic lacustrine shorelines along the northern and southern sides of the Altyn Tagh fault (Ritts and Biffi, 2000), (2) ~375 km offset of the Cambrian magmatic arc in the Qilian Shan and the Altyn Tagh Range (Gehrels et al., 2003a), (3) ~375 ± 25 km offset of pre-Oligocene strata between the Qaidam and Xorkol basins (Yue et al., 2001), (4) ~360 ± 40 km offset estimation based on source to sink relation between the Xorkol basin and the North Qilian Shan (Yue et al., 2005), (5) 350~400 km offset based on eclogite, ophiolite and blueschist facies units in the Altyn Tagh Range and Qilian Shan (Yang et al., 2001; Zhang et al., 2001), (6) ~350 km offset based on similar early to middle Jurassic cooling zones on both side of the Altyn Tagh fault (Sobel et al., 2001). This large-scale lithospheric offset along the ATF would be totally accomodated by crustal deformation within the terrane to the east, especially by the NE-SW shortening and eastward extrusion along the faults within the Qilian Shan (e.g. Yin et al., 2002, 2008a; Cheng et al., 2015b). The confirmation of the hundreds of kilometers of displacement along the strike-slip ATF again supports the eastward extrusion of the Tibetan plateau driven by the India-Asia collision.

3.2.7 Conclusions

Detrital zircon U-Pb age patterns evolution from two Jurassic to Pleistocene stratigraphic sections in the northwestern Qaidam basin associated to high-quality seismic-reflection profiles revealed that: a) During the Paleocene to early Eocene, the Eboliang and Huatugou sections were respectively located near the present-day position of Anxi area and Tula area. The basement rocks in Altyn Tagh Range served as the significant source for the sediments to the Eboliang section, while the material deposited in the Huatugou section mostly derived from the Eastern Kunlun Range; b) Left-lateral strike-slip movement along the ATF initiated during the early-middle Eocene, resulting in gradually northeastward migration of the Qaidam basin; c) The post-Oligocene deformation within the Altyn Tagh Range and northwestern Qaidam basin strongly modified the regional drainage pattern. By Oligocene times, most of the material issued from the erosion of the Altyn Tagh Range was directed towards the Tarim basin to the north. The post-Oligocene clastic materials in the western Qaidam basin was mainly derived from local sources largely including recycling of the deformed Paleocene to Oligocene strata. Using the Eboliang and Huatugou sections as piercing points, we estimate a 360 ± 40 km offset along the ATF.

Acknolegdements

This work was supported by the Oil and Gas Scientific and Technologic Major Programs

of China (Grant ZX05003) and the China Scholarship Council – Campus France Egide Cai Yuanpei program N° 32393WL (2014). We gratefully acknowledge the assistance of Shuwei Guan, Qinyang Meng, Ruiying Chen, Chuanmin Zhou, Suping Zhou, Xiangjiang Yu, Xiang Cheng, Wei Du, Runchao Liu and Tuo Zhang during field work. We thank Li Su of the Geological Lab Center, China University of Geosciences (Beijing), for her help during detrital zircon analysis and to Prof. Chaodong Wu, Chuanwu Wang, Yan Chen for their helpful suggestions on the Cenozoic evolution of the Qaidam basin. Communications with Michel Ballevre, Sylvie Bourquin, Hervé Régnauld, Baofu Han and Zhicheng Zhang had sharpened the discussion on the appropriate piercing points. We particularly thank Science Editor Jean-Philippe Avouac and two anonymous reviewers for careful and insightful comments.

References

Allen, P.A., Allen, J.R., 2005. Basin Analysis: Principles and Applications. Blackwell Publishing Company, Oxford. 549 pp.

Andersen, T., 2002. Correction of common lead in U-Pb analyses that do not report 204Pb. Chemical Geology 192, 59-79.

Arnaud, N., Tapponnier, P., Roger, F., Brunel, M., Scharer, U., Chen, W., Xu, Z., 2003. Evidence for Mesozoic shear along the western Kunlun and Altyn-Tagh fault, northern Tibet (China). Journal of Geophysical Research: Solid Earth (1978-2012) 108.

Avouac, J.P., Tapponnier, P., 1993. Kinematic model of active deformation in central Asia. Geophysical Research Letters 20, 895-898.

Black, L.P., Kamo, S.L., Allen, C.M., Aleinikoff, J.N., Davis, D.W., Korsch, R.J., Foudoulis, C., 2003. TEMORA 1: a new zircon standard for Phanerozoic U–Pb geochronology. Chemical Geology 200, 155-170.

Bovet, P.M., Ritts, B.D., Gehrels, G., Abbink, A.O., Darby, B., Hourigan, J., 2009. Evidence of Miocene crustal shortening in the north Qilian Shan from Cenozoic stratigraphy of the western Hexi Corridor, Gansu Province, China. American Journal of Science 309, 290-329.

Braitenberg, C., Wang, Y., Fang, J., Hsu, H., 2003. Spatial variations of flexure parameters over the Tibet–Quinghai plateau. Earth and Planetary Science Letters 205, 211-224.

Bruguier, O., Lancelot, J., Malavieille, J., 1997. U–Pb dating on single detrital zircon grains from the Triassic Songpan–Ganze flysch (Central China): provenance and tectonic correlations. Earth and Planetary Science Letters 152, 217-231.

Burchfiel, B.C., Quidong, D., Molnar, P., Royden, L., Yipeng, W., Peizhen, Z., Weiqi, Z., 1989. Intracrustal detachment within zones of continental deformation. Geology 17, 748-752.

Chang, H., Li, L., Qiang, X., Garzione, C.N., Pullen, A., An, Z., 2015. Magnetostratigraphy of Cenozoic deposits in the western Qaidam Basin and its implication for the surface uplift of the northeastern margin of the Tibetan Plateau. Earth and Planetary Science Letters 430, 271-283.

Chen, Z.L., Zhang, Y.Q., Wang, X.F., Chen, X.H., 2001. Fission Track Dating of Apatite Constrains on the Cenozoic Uplift of the Altyn Tagh Mountain. Acta Geoscientia Sinica 22, 413-418 (in Chinese with English abstract).

Chen, X.H., Wang, X.F., E. George, G., Yang, Y., Qin, H., Chen, Z.L., Yang, F., Chen, B.L., Li, X.Z., 2004. Early Paleozoic Magmatism and Gold Mineralization in the Northern Altun, NW China. Acta Geologica Sinica-English Edition 78, 515-523.

Chen, Y., Gilder, S., Halim, N., Cogné, J.P., Courtillot, V., 2002. New paleomagnetic constraints on central Asian kinematics: Displacement along the Altyn Tagh fault and rotation of the Qaidam Basin. Tectonics 21, 1042.

Chen, X., Gehrels, G., Yin, A., Zhou, Q., Huang, P., 2015. Geochemical and Nd–Sr–Pb–O isotopic constrains on Permo–Triassic magmatism in eastern Qaidam Basin, northern Qinghai-Tibetan plateau: Implications for the evolution of the Paleo-Tethys. Journal of Asian Earth Sciences 114, Part 4, 674-692.

Cheng, F., Jolivet, M., Fu, S., Zhang, Q., Guan, S., Yu, X., Guo, Z., 2014. Northward growth of the Qimen Tagh Range: A new model accounting for the Late Neogene strike-slip deformation of the SW Qaidam Basin. Tectonophysics 632, 32-47.

Cheng, F., Guo, Z., Jenkins, H.S., Fu, S., Cheng, X., 2015a. Initial rupture and displacement on the Altyn Tagh fault, northern Tibetan Plateau: Constraints based on residual Mesozoic to Cenozoic strata in the western Qaidam Basin. Geosphere 11, 921-942.

Cheng, F., Jolivet, M., Dupont-Nivet, G., Wang, L., Yu, X., Guo, Z., 2015b. Lateral extrusion along the Altyn Tagh Fault, Qilian Shan (NE Tibet): insight from a 3D crustal budget. Terra Nova 27, 416-425.

Cheng, F., Fu, S., Jolivet, M., Zhang, C., Guo, Z., 2016. Source to sink relation between the Eastern Kunlun Range and the Qaidam Basin, northern Tibetan Plateau, during the Cenozoic. Geological Society of America Bulletin 128, 258-283, doi: 10.1130/B31260.1.

Clark, M., Schoenbohm, L., Royden, L., Whipple, K., Burchfiel, B., Zhang, X., Tang, W., Wang, E., Chen, L., 2004. Surface uplift, tectonics, and erosion of eastern Tibet from large-scale drainage patterns. Tectonics 23, TC1006.

Corfu, F., Hanchar, J.M., Hoskin, P.W., Kinny, P., 2003. Atlas of zircon textures. Reviews in mineralogy and geochemistry 53, 469-500.

Cowgill, E., Yin, A., Harrison, T.M., Xiao-Feng, W., 2003. Reconstruction of the Altyn Tagh fault based on U-Pb geochronology: Role of back thrusts, mantle sutures, and heterogeneous crustal strength in forming the Tibetan Plateau. Journal of Geophysical Research 108, 2346.

CSBS (Chinese Stata Bureau of Seismology), 1992. The Altyn Tagh Active Fault System. Seismology Publishing House, Beijing, pp. 1-319 (in Chinese).

Dai, J., Wang, C., Hourigan, J., Santosh, M., 2013. Multi-stage tectono-magmatic events of the Eastern Kunlun Range, northern Tibet: Insights from U–Pb geochronology and (U–Th)/He thermochronology. Tectonophysics 599, 97-106.

Darby, B.J., Ritts, B.D., Yue, Y., Meng, Q., 2005. Did the Altyn Tagh fault extend beyond the Tibetan Plateau? Earth and Planetary Science Letters 240, 425-435.

Delville, N., Arnaud, N., Montel, J.-M., Roger, F., Brunel, M., Tapponnier, P., Sobel, E., 2001. Paleozoic to Cenozoic deformation along the Altyn Tagh fault in the Altun Shan massif area, eastern Qilian Shan, northeastern Tibet, China. Geological Society of America Memoirs 194, 269-292.

Deng, T., Wang, X.M., 2004a. New material of the Neogene rhinocerotids from the Qaidam Basin in Qinghai, China. Vert. PalAsiat. 42 (3), 216–229.

Deng, T., Wang, X.M., 2004b. Late Miocene Hipparion (Equidae, Mammalia) of eastern Qaidam Basin in Qinghai, China. Vert. PalAsiat. 42 (4), 316–333.

Ding, G., Chen, J., Tian, Q., Shen, X., Xing, C., Wei, K., 2004. Active faults and magnitudes of left-lateral displacement along the northern margin of the Tibetan Plateau. Tectonophysics 380, 243-260.

Ding, L., Kapp, P., Yue, Y., Lai, Q., 2007. Postcollisional calc-alkaline lavas and xenoliths from the southern Qiangtang terrane, central Tibet. Earth and Planetary Science Letters 254, 28-38.

Dong, Z., Pei, X., Gu, P., Zhang, H., Chen, R., Zhang, X., 2014. Geochronology, Geochemistry, and Hf Isoplot of Yanchangbeishan Granodiorite of Lenghu Area in Qinghai. Nonwestern Geology 47 (4), 141-155 (in Chinese with English abstract).

Dong, Z., Gu, P., Chen, R., Zhang, X., Zhang, H., 2015. Geochronology, Geochemistry, and Hf Isoplot of Yanchangbeishan Adamellite of Lenghu Area in Qinghai. Earth Science-Journal of China University of Geosciences 40 (1), 130-144 (in Chinese with English abstract).

Duvall, A.R., Clark, M.K., Kirby, E., Farley, K.A., Craddock, W.H., Li, C., Yuan, D.-Y., 2013. Low-temperature thermochronometry along the Kunlun and Haiyuan Faults, NE Tibetan Plateau: Evidence for kinematic change during late-stage orogenesis. Tectonics 32, 1190-1211.

Dupont-Nivet, G., Butler, R.F., Yin, A., Chen, X., 2002. Paleomagnetism indicates no

Neogene rotation of the Qaidam Basin in northern Tibet during Indo-Asian collision. Geology 30, 263.

Dupont-Nivet, G., Lippert, P.C., Van Hinsbergen, D.J.J., Meijers, M.J.M., Kapp, P., 2010. Palaeolatitude and age of the Indo–Asia collision: palaeomagnetic constraints. Geophysical Journal International 182, 1189-1198.

England, P., Houseman, G., 1989. Extension during continental convergence, with application to the Tibetan Plateau. Journal of Geophysical Research: Solid Earth (1978–2012) 94, 17561-17579.

Fang, X., Zhang, W., Meng, Q., Gao, J., Wang, X., King, J., Song, C., Dai, S., Miao, Y., 2007. High-resolution magnetostratigraphy of the Neogene Huaitoutala section in the eastern Qaidam Basin on the NE Tibetan Plateau, Qinghai Province, China and its implication on tectonic uplift of the NE Tibetan Plateau. Earth and Planetary Science Letters 258, 293-306.

Fedo, C.M., Sircombe, K.N., Rainbird, R.H., 2003. Detrital zircon analysis of the sedimentary record. Reviews in mineralogy and geochemistry 53, 277-303.

Fu, L., Guan, P., Zhao, W. Y., Wang, M., Zhang, Y., Lu, J. W., 2013. Heavy mineral feature and provenance analysis of Paleogene Lulehe Formation in Qaidam Basin. Acta Petrologica Sinica, 29, 2867-2875 (in Chinese with English abstract).

Gao, J., Li, S., Dai, S., Li, A., Peng, Y., 2009. Constraints of tectonic evolution in provenance from detrital zircon fission-track data of Cenozoic strata of Xichagou district in western Qaidam basin. Journal of Lanzhou University (Natural Sciences) 45, 1-7 (in Chinese with English abstract).

Gehrels, G.E., Yin, A., Wang, X.F., 2003a. Magmatic history of the northeastern Tibetan Plateau. Journal of Geophysical Research 108, 2423.

Gehrels, G.E., Yin, A., Wang, X.F., 2003b. Detrital-zircon geochronology of the northeastern Tibetan plateau. Geological Society of America Bulletin 115, 881-896.

Gehrels, G., Kapp, P., DeCelles, P., Pullen, A., Blakey, R., Weislogel, A., Ding, L., Guynn, J., Martin, A., McQuarrie, N., 2011. Detrital zircon geochronology of pre-Tertiary strata in the Tibetan-Himalayan orogen. Tectonics 30, TC5016.

Gehrels, G., 2014. Detrital Zircon U-Pb Geochronology Applied to Tectonics. Annual Review of Earth and Planetary Sciences 42, 127-149.

Guo, J.J., Li, H.K., 1999. Angular Unconformity between the Huashishan Group and Huangzhong Group in the Eastern Mid-Qilian Massif: Identification and Implications. Progress In Precambrian Research 22, 47-52.

Hanchar, J., Rudnick, R., 1995. Revealing hidden structures: the application of

cathodoluminescence and back-scattered electron imaging to dating zircons from lower crustal xenoliths. Lithos 36, 289-303.

Hoskin, P., Black, L., 2000. Metamorphic zircon formation by solid-state recrystallization of protolith igneous zircon. Journal of metamorphic Geology 18, 423-439.

Heermance, R.V., Pullen, A., Kapp, P., Garzione, C.N., Bogue, S., Ding, L., Song, P., 2013. Climatic and tectonic controls on sedimentation and erosion during the Pliocene–Quaternary in the Qaidam Basin (China). Geological Society of America Bulletin 125, 833-856.

Huang, H., Huang, Q., Ma, Y., 1996. Geology of Qaidam Basin and its Petroleum Prediction. Geological Publishing House, Beijing, pp. 1–257 (in Chinese with English abstract).

Huo, G.M., 1990. Petroleum Geology of China: Oil Fields in Qianghai and Xizang, 14. Chinese Petroleum Industry Press, Beijing, pp. 1-483 (in Chinese with English abstract).

IGSQP (Institute of Geological Survey of Qinhai Province), 2004. The Report of Regional Geological Survey at Scale 1:250000. P.R.C. China Industry Press, pp. 1–386 (in Chinese).

Jian, X., Guan, P., Zhang, D.W., Zhang, W., Feng, F., Liu, R.J., Lin, S.D., 2013. Provenance of Tertiary sandstone in the northern Qaidam basin, northeastern Tibetan Plateau: Integration of framework petrography, heavy mineral analysis and mineral chemistry. Sedimentary Geology 290, 109-125.

Jolivet, M., Roger, F., Arnaud, N., Brunel, M., Tapponnier, P., Seward, D., 1999. Histoire de l'exhumation de l'Altun Shan: indications sur l'âge de la subduction du bloc du Tarim sous le système de l'Altyn Tagh (Nord Tibet). Comptes Rendus de l'Académie des Sciences-Series IIA-Earth and Planetary Science 329, 749-755.

Jolivet, M., Brunel, M., Seward, D., Xu, Z., Yang, J., Roger, F., Tapponnier, P., Malavieille, J., Arnaud, N., Wu, C., 2001. Mesozoic and Cenozoic tectonics of the northern edge of the Tibetan plateau: fission-track constraints. Tectonophysics 343, 111-134.

Jolivet, M., Brunel, M., Seward, D., Xu, Z., Yang, J., Malavieille, J., Roger, F., Leyreloup, A., Arnaud, N., Wu, C., 2003. Neogene extension and volcanism in the Kunlun Fault Zone, northern Tibet: New constraints on the age of the Kunlun Fault. Tectonics 22, 1052.

Jolivet, M., Roger, F., Xu, Z.Q., Paquette, J.L., Cao, H., 2015. Mesozoic–Cenozoic evolution of the Danba dome (Songpan Garzê, East Tibet) as inferred from LA-ICPMS U–Pb and fission-track data. Journal of Asian Earth Sciences 102, 180-204.

Ke, X., Ji, J., Zhang, K., Kou, X., Song, B., Wang, C., 2013. Magnetostratigraphy and Anisotropy of Magnetic Susceptibility of the Lulehe Formation in the Northeastern Qaidam Basin. Acta Geologica Sinica-English Edition 87, 576-587.

Kirby, E., Reiners, P.W., Krol, M.A., Whipple, K.X., Hodges, K.V., Farley, K.A., Tang, W.Q.,

Chen, Z.L., 2002. Late Cenozoic evolution of the eastern margin of the Tibetan Plateau: Inferences from $^{40}Ar/^{39}Ar$ and (U-Th)/He thermochronology. Tectonics 21, 1001.

Lease, R.O., 2014. Cenozoic mountain building on the northeastern Tibetan Plateau. Geological Society of America Special Papers 507, 115-127.

Li, H.B., Yang, J.S., Xu, Z.Q., Sun, Z.M., Tapponnier, P., van der Woerd, J., Meriaux, A.-S., 2006. The constraint of the Altyn Tagh fault system to the growth and rise of the northern Tibetan Plateau. Earth Science Frontiers 13, 59-79 (in Chinese with English abstract).

Li, W., Neubauer, F., Liu, Y.J., Genser, J., Ren, S.M., Han, G.Q., Liang, C.Y., 2013. Paleozoic evolution of the Qimantagh magmatic arcs, Eastern Kunlun Mountains: constraints from zircon dating of granitoids and modern river sands. Journal of Asian Earth Sciences 77, 183-202.

Li, L., Guo, Z., Guan, S., Zhou, S., Wang, M., Fang, Y., Zhang, C., 2015. Heavy mineral assemblage characteristics and the Cenozoic paleogeographic evolution in southwestern Qaidam Basin. Science China Earth Sciences, 1-17.

Liu, Y. H., Mo, X. X., Yu, X. H., Zhang, X. T. and Xu, G. W., 2006. Zircon SHRIMP U-Pb dating of the Jingren granite, Yemaquan region of the east Kunlun and its geological significance: Acta Petrologica Sinica 22, 2457-2463 (in Chinese with English abstract).

Liu, Y.J., Neubauer, F., Genser, J., Ge, X.H., Takasu, A., Yuan, S.H., Chang, L.H., Li, W.M., 2007. Geochronology of the initiation and displacement of the Altyn Strike-Slip Fault, western China. Journal of Asian Earth Sciences 29, 243-252.

Liu, D., Jolivet, M., Yang, W., Zhang, Z., Cheng, F., Zhu, B., Guo, Z., 2013. Latest Paleozoic–Early Mesozoic basin–range interactions in South Tian Shan (northwest China) and their tectonic significance: Constraints from detrital zircon U–Pb ages. Tectonophysics 599, 197-213.

Liu, D., Cheng, F., Guo, Z., Jolivet, M., Song, Y., 2015. Lahar facies of the Latest Paleozoic Arbasay Formation: Geomorphological characters and paleoenvironment reconstruction of Northern Tian Shan, NW China. Journal of Asian Earth Sciences 113, Part 1, 282-292.

Long, X., Yuan, C., Sun, M., Kröner, A., Zhao, G., 2014. New geochemical and combined zircon U–Pb and Lu–Hf isotopic data of orthogneisses in the northern Altyn Tagh, northern margin of the Tibetan plateau: Implication for Archean evolution of the Dunhuang Block and crust formation in NW China. Lithos 200–201, 418-431.

Lu, S.N., 2002. Preliminary Study of Precambrian Geology in the North Tibet–Qinghai Plateau. Geological Publishing House, Beijing, pp. 1-125 (in Chinese).

Lu, S.N., Yuan, G.B., 2003. Geochronology of early Precambrian magmatic activities in

Aketasdhtage, East Altyn Tagh. Acta Geological Sinica 77, 61–68 (in Chinese with English abstract).

Lu, S.N., Li, H.K., Zhang, C.L., Niu, G.H., 2008. Geological and geochronological evidence for the Precambrian evolution of the Tarim Craton and surrounding continental fragments. Precambrian Research 160, 94-107.

Lu, H., Xiong, S., 2009. Magnetostratigraphy of the Dahonggou section, northern Qaidam Basin and its bearing on Cenozoic tectonic evolution of the Qilian Shan and Altyn Tagh Fault. Earth and Planetary Science Letters 288, 539-550.

Lu, H., Wang, E., Meng, K., 2014. Paleomagnetism and anisotropy of magnetic susceptibility of the Tertiary Janggalsay section (southeast Tarim basin): Implications for Miocene tectonic evolution of the Altyn Tagh Range. Tectonophysics 618, 67-78.

Ludwig, K.R., 2003. User's manual for Isoplot 3.0: a geochronological toolkit for Microsoft Excel. Berkeley Geochronology Center. Spec. Pub., 4, pp. 1-71.

Mao, L.G., Xiao, A.C., Wu, L., Li, B.L., Wang, L.Q., Lou, Q.Q., Dong, Y.P., Qin, S.H., 2014. Cenozoic tectonic and sedimentary evolution of southern Qaidam Basin, NE Tibetan Plateau and its implication for the rejuvenation of Eastern Kunlun Mountains. Science China Earth Sciences, 1-14 (in Chinese).

Meng, Q.R., Hu, J.M., Yang, F.Z., 2001. Timing and magnitude of displacement on the Altyn Tagh fault: constraints from stratigraphic correlation of adjoining Tarim and Qaidam basins, NW China. Terra Nova 13, 86-91.

Meng, Q.R., Fang, X., 2008. Cenozoic tectonic development of the Qaidam Basin in the northeastern Tibetan Plateau. Geological Society of America Special Papers 444, 1-24.

Métivier, F., Gaudemer, Y., Tapponnier, P., Meyer, B., 1998. Northeastward growth of the Tibet plateau deduced from balanced reconstruction of two depositional areas: The Qaidam and Hexi Corridor basins, China. Tectonics 17, 823-842.

Meyer, B., Tapponnier, P., Bourjot, L., Metivier, F., Gaudemer, Y., Peltzer, G., Shunmin, G., Zhitai, C., 1998. Crustal thickening in Gansu‐Qinghai, lithospheric mantle subduction, and oblique, strike-slip controlled growth of the Tibet plateau. Geophysical Journal International 135, 1-47.

Molnar, P., Tapponnier, P., 1975. Cenozoic tectonics of Asia: Effects of a continental collision. Science 189, 419-426.

Pei, J., Sun, Z., Wang, X., Zhao, Y., Ge, X., Guo, X., Li, H., Si, J., 2009. Evidence for Tibetan plateau uplift in Qaidam basin before Eocene-Oligocene boundary and its climatic implications. Journal of Earth Science 20, 430-437.

Peltzer, G., Tapponnier, P., 1988. Formation and evolution of strike-slip faults, rifts, and basins during the India-Asia collision: An experimental approach. Journal of Geophysical Research: Solid Earth (1978–2012) 93, 15085-15117.

QBGMR (Qinhai Bureau of Geology Mineral Resources), 1991. Regional Geology of Qinghai Province. Geological Publishing House, Beijing, pp. 1–662 (in Chinese).

Qi, C., Li, X., Liang, X., Liu, Y., Tu, X., 2005. High-precision measurement of Hf isotopic reference values for the U-Pb geochronology standard zircons by multi-collector inductively coupled plasma-mass spectrometry. J. Chin. Mass Spectrom. Soc 26, 149-154.

Qiu, N.S., 2002. Tectono-thermal evolution of the Qaidam Basin, China: evidence from Ro and apatite fission track data. Petroleum Geoscience 8, 279-285.

Ritts, B.D., Hanson, A.D., Zinniker, D., Moldowan, J.M., 1999. Lower-Middle Jurassic nonmarine source rocks and petroleum systems of the northern Qaidam basin, northwest China. AAPG bulletin 83, 1980-2005.

Ritts, B.D., Biffi, U., 2000. Magnitude of post-Middle Jurassic (Bajocian) displacement on the central Altyn Tagh fault system, northwest China. Geological Society of America Bulletin 112, 61-74.

Ritts, B.D., Yue, Y., Graham, S.A., 2004. Oligocene-Miocene Tectonics and Sedimentation along the Altyn Tagh Fault, Northern Tibetan Plateau: Analysis of the Xorkol, Subei, and Aksay Basins. The Journal of geology 112, 207-229.

Roger, F., Arnaud, N., Gilder, S., Tapponnier, P., Jolivet, M., Brunel, M., Malavieille, J., Xu, Z., Yang, J., 2003. Geochronological and geochemical constraints on Mesozoic suturing in east central Tibet. Tectonics 22, 1037.

Roger, F., Jolivet, M., Malavieille, J., 2008. Tectonic evolution of the Triassic fold belts of Tibet. Comptes Rendus Geoscience 340, 180-189.

Roger, F., Jolivet, M., Malavieille, J., 2010. The tectonic evolution of the Songpan-Garzê (North Tibet) and adjacent areas from Proterozoic to Present: A synthesis. Journal of Asian Earth Sciences 39, 254-269.

Robinson, D.M., Dupont-Nivet, G., Gehrels, G.E., Zhang, Y., 2003. The Tula uplift, northwestern China: Evidence for regional tectonism of the northern Tibetan Plateau during late Mesozoic–early Cenozoic time. Geological Society of America Bulletin 115, 35-47.

Searle, M., 1996. Geological evidence against large-scale pre-Holocene offsets along the Karakoram Fault: Implications for the limited extrusion of the Tibetan plateau. Tectonics 15, 171-186.

Searle, M., Elliott, J., Phillips, R., Chung, S. L., 2011. Crustal–lithospheric structure and

continental extrusion of Tibet. Journal of the Geological Society 168, 633-672.

Shang Erjie, 2001. Basic structural style of tertiary in the western part of the northern area in the Qaidam basin and its petroleum significance. Geoscience 12, 422-424 (in Chinese with English abstract).

Shi, R.D., Yang, J.S., Wu, C.L., Tsuyoshi, I., Takafumi, H., 2006. Island arc volcanic rocks in the north Qaidam UHP belt, northern Tibet plateau: Evidence for ocean–continent subduction preceding continent–continent Subduction. Journal of Asian Earth Sciences 28, 151-159.

Sobel, E.R., Arnaud, N., 1999. A possible middle Paleozoic suture in the Altyn Tagh, NW China. Tectonics 18, 64-74.

Sobel, E.R., Arnaud, N., Jolivet, M., Ritts, B.D., Brunel, M., 2001. Jurassic to Cenozoic exhumation history of the Altyn Tagh range, northwest China, constrained by $^{40}Ar/^{39}Ar$ and apatite fission track thermochronology. Geological Society of America Memoirs 194, 247-267.

Song, T., Wang, X., 1993. Structural styles and stratigraphic patterns of syndepositional faults in a contractional setting: Examples from Quaidam basin, northwestern China. AAPG bulletin 77, 102-117.

Song, S.G., Zhang, L.F., Niu, Y.L., Su, L., Song, B., Liu, D.Y., 2006. Evolution from oceanic subduction to continental collision: a case study from the Northern Tibetan Plateau based on geochemical and geochronological data. Journal of Petrology 47, 435-455.

Song, S., Niu, Y., Su, L., Zhang, C., Zhang, L., 2014. Continental orogenesis from ocean subduction, continent collision/subduction, to orogen collapse, and orogen recycling: The example of the North Qaidam UHPM belt, NW China. Earth-Science Reviews 129, 59-84.

Staisch, L.M., Niemi, N.A., Hong, C., Clark, M.K., Rowley, D.B., Currie, B., 2014. A Cretaceous‐Eocene depositional age for the Fenghuoshan Group, Hoh Xil Basin: Implications for the tectonic evolution of the northern Tibet Plateau. Tectonics 33, 281-301.

Sun, Z.M., Yang, Z.Y., Pei, J.L., Ge, X.H., Wang, X.S., Yang, T.S., Li, W.M., Yuan, S.H., 2005. Magnetostratigraphy of Paleogene sediments from northern Qaidam Basin, China: implications for tectonic uplift and block rotation in northern Tibetan plateau. Earth and Planetary Science Letters 237, 635-646.

Sun, Z.C., Jing, M.C., Sun, N.D., Lu, Y.L., Cao, L., 2007. Discussion on boundary between the upper and lower members of Xiaganchaigou Formation of Paleogene in Well Kun-2, Qaidam Basin. J. Palaeogeogr. 9 (6), 611–618 (in Chinese with English abstract).

Sun, Y., Chen, Z., Chen, B., Han F., Zhou, Y., Hao, R. and Li, S., 2014. Cenozoic Uplift and Denudation of the EW-trending Range of Northern Altun Mountains: Evidence from Apatite Fission Track Data. Acta Geoscientica Sinica, 37 (1), 67-75 (in Chinese with English abstract).

Tapponnier, P., Peltzer, G., Armijo, R., 1986. On the mechanics of the collision between India and Asia. Geological Society, London, Special Publications 19, 113-157.

Tapponnier, P., Xu, Z.Q., Roger, F., Meyer, B., Arnaud, N., Wittlinger, G., Yang, J.S., 2001. Oblique stepwise rise and growth of the Tibet Plateau. Science 294, 1671-1677.

Thomas, W.A., 2011. Detrital-zircon geochronology and sedimentary provenance. Lithosphere 3, 304-308.

Wang, E., 1997. Displacement and timing along the northern strand of the Altyn Tagh fault zone, northern Tibet. Earth and Planetary Science Letters 150, 55-64.

Wang, Y., Zhang, X., Wang, E., Zhang, J., Li, Q., Sun, G., 2005. $^{40}Ar/^{39}Ar$ thermochronological evidence for formation and Mesozoic evolution of the northern-central segment of the Altyn Tagh fault system in the northern Tibetan Plateau. Geological Society of America Bulletin 117, 1336-1346.

Wang, E., Xu, F.Y., Zhou, J.X., Wan, J., Burchfiel, B.C., 2006a. Eastward migration of the Qaidam basin and its implications for Cenozoic evolution of the Altyn Tagh fault and associated river systems. Geological Society of America Bulletin 118, 349-365.

Wang, C., Liu, L., Che, Z.C., Chen, D.L., Zhang, A.D., Luo, J.H., 2006b. U–Pb geochronology and tectonic setting of the granitic gneiss in Jianggaleisayi Eclogite Belt. Geological Journal of China Universities 12, 74-82.

Wang, L., Xiao, A.C., Gong, Q.L., Liu, D., Wu, L., Zhou, S.P., Shen, Z.Y., Lou, Q.Q., Sun, X.W., 2010. The unconformity in Miocene sequence of western Qaidam Basin and its tectonic significance. Science China Earth Sciences 53, 1126-1133 (in Chinese).

Wang, C., Liu, L., Yang, W.Q., Zhu, X.H., Cao, Y.T., Kang, L., Chen, S.F., Li, R.S., He, S.P., 2013. Provenance and ages of the Altyn Complex in Altyn Tagh: implications for the early Neoproterozoic evolution of northwestern China. Precambrian Research 230, 193-208.

Wang, C., Dai, J., Zhao, X., Li, Y., Graham, S.A., He, D., Ran, B., Meng, J., 2014a. Outward-growth of the Tibetan Plateau during the Cenozoic: A review. Tectonophysics 621, 1-43.

Wang, C., Liu, L., Xiao, P.X., Cao, Y.T., Yu, H.Y., Meert, J.G., Liang, W.T., 2014b. Geochemical and geochronologic constraints for Paleozoic magmatism related to the orogenic collapse in the Qimantagh–South Altyn region, northwestern China. Lithos 202–203, 1-20.

Wiedenbeck, M., Alle, P., Corfu, F., Griffin, W., Meier, M., Oberli, F., Quadt, A.v., Roddick, J., Spiegel, W., 1995. Three natural zircon standards for U‐Th‐Pb, Lu‐Hf, trace element and REE analyses. Geostandards Newsletter 19, 1-23.

Wittlinger, G., Tapponnier, P., Poupinet, G., Mei, J., Danian, S., Herquel, G., Masson, F., 1998. Tomographic evidence for localized lithospheric shear along the Altyn Tagh fault. Science 282,

74-76.

Wu, C.L., Yang, J.S., Ireland, T., Wooden, J.L., Li, H.B., Wan, Y.S., Shi, R.D., 2001. Zircon SHRIMP ages of Aolaoshan granite from the south margin of Qilianshan and its geological significance. Acta Petrologica Sinica 17, 215–221 (in Chinese with English abstract).

Wu, C.L., Wooden, J.L., Robinson, P.T., Gao, Y.H., Wu, S.P., Chen, Q.L., Mazdab, F.K., Mattinson, C., 2009. Geochemistry and zircon SHRIMP U–Pb dating of granitoids from the west segment of the North Qaidam. Sci. China, Ser. D Earth Sci. 52 (11), 1771–1790 (in Chinese).

Wu C. L., Gao Y. H., Lei M., Qin H. P., Liu C. H., Li M. Z., Frost. B. R., Wooden J. L., 2014. Zircon SHRIMP U-Pb dating, Lu-Hf isotopic characteristics and petrogenesis of the Palaeozoic granites in Mangya area, south Altun, NW China. Acta Petrologica Sinica, 30(8), 2297-2323 (in Chinese with English abstract).

Wu, L., Xiao, A., Wang, L., Shen, Z., Zhou, S., Chen, Y., Wang, L., Liu, D., Guan, J., 2011. Late Jurassic–Early Cretaceous Northern Qaidam Basin, NW China: Implications for the earliest Cretaceous intracontinental tectonism. Cretaceous Research 32, 552-564.

Wu, L., Xiao, A.C., Yang, S.F., Wang, L.Q., Mao, L.G., Wang, L., Dong, Y.P., Xu, B., 2012a. Two-stage evolution of the Altyn Tagh Fault during the Cenozoic: new insight from provenance analysis of a geological section in NW Qaidam Basin, NW China. Terra Nova 24, 387-395.

Wu, L., Xiao, A., Wang, L., Mao, L., Wang, L., Dong, Y., Xu, B., 2012b. EW-trending uplifts along the southern side of the central segment of the Altyn Tagh Fault, NW China: Insight into the rising mechanism of the Altyn Mountain during the Cenozoic. Science China Earth Sciences 55, 926-939 (in Chinese).

Wu, L., Xiao, A., Ma, D., Li, H., Xu, B., Shen, Y., Mao, L., 2014. Cenozoic fault systems in southwest Qaidam Basin, northeastern Tibetan Plateau: Geometry, temporal development, and significance for hydrocarbon accumulation. AAPG bulletin 98, 1213-1234.

Xia, W.C., Zhang, N., Yuan, X.P., Fan, L.S., Zhang, B.S., 2001. Cenozoic Qaidam basin, China: A stronger tectonic inversed, extensional rifted basin. AAPG bulletin 85, 715-736.

Xiao, W., Windley, B.F., Yong, Y., Yan, Z., Yuan, C., Liu, C., Li, J., 2009. Early Paleozoic to Devonian multiple-accretionary model for the Qilian Shan, NW China. Journal of Asian Earth Sciences 35, 323-333.

Xiao, Q., Shao, G., Liu-Zeng, J., Oskin, M.E., Zhang, J., Zhao, G., Wang, J., 2015. Eastern termination of the Altyn Tagh Fault, western China: Constraints from a magnetotelluric survey. Journal of Geophysical Research: Solid Earth 120, 2838-2858.

Yang, F., Ma, Z.Q., Xu, T.C., Ye, S.J., 1992. A Tertiary paleomagnetic stratigraphic profile in Qaidam basin. Acta Petrolei Sinica 13, 97-101 (in Chinese with English abstract).

Yang, J., Xu, Z., Song, S., Wu, C., Shi, R., Zhang, J., Wan, Y., Li, H., Jin, X., Jolivet, M., 2000. Discovery of eclogite in Dulan, Qinghai Province and its significance for studying the HP-UHP metamorphic belt along the central orogenic belt of China. Acta Geologica Sinica 74, 156-168 (in Chinese with English abstract).

Yang, J., Xu, Z., Zhang, J., Chu, C. Y., Zhang, R., Liou, J. G., 2001. Tectonic significance of early Paleozoic high-pressure rocks in Altun-Qaidam-Qilian Mountains, northwest China. Geological Society of America Memoirs 194, 151-170.

Yang, M.H., Song, J.J., 2002. Petrology of the Lenghu granite mass, northwestern Qaidam basin, China. Northwestern Geol. 35, 94-98 (in Chinese with English abstract).

Yang, J.S., Wu, C.L., Zhang, J.X., Shi, R.D., Meng, F.C., Wooden, J.L., Yang, H.Y., 2006. Protolith of eclogites in the north Qaidam and Altun UHP terrane, NW China: Earlier oceanic crust? Journal of Asian Earth Sciences 28, 185-204.

Yang, W., Jolivet, M., Dupont-Nivet, G., Guo, Z., Zhang, Z., Wu, C., 2013. Source to sink relations between the Tian Shan and Junggar Basin (northwest China) from Late Palaeozoic to Quaternary: evidence from detrital U-Pb zircon geochronology. Basin Research 25, 219-240.

Yang, W., Jolivet, M., Dupont-Nivet, G., Guo, Z., 2014. Mesozoic - Cenozoic tectonic evolution of southwestern Tian Shan: Evidence from detrital zircon U/Pb and apatite fission track ages of the Ulugqat area, Northwest China. Gondwana Research 26, 986-1008.

Yin, A., Harrison, T.M., 2000. Geologic evolution of the Himalayan-Tibetan orogen. Annual Review of Earth and Planetary Sciences 28, 211-280.

Yin, A., Rumelhart, P., Butler, R., Cowgill, E., Harrison, T., Foster, D., Ingersoll, R., Qing, Z., Xian-Qiang, Z., Xiao-Feng, W., 2002. Tectonic history of the Altyn Tagh fault system in northern Tibet inferred from Cenozoic sedimentation. Geological Society of America Bulletin 114, 1257-1295.

Yin, A., Dang, Y.Q., Zhang, M., McRivette, M.W., Burgess, W.P., Chen, X.H., 2007. Cenozoic tectonic evolution of Qaidam basin and its surrounding regions (part 2): Wedge tectonics in southern Qaidam basin and the Eastern Kunlun Range. Geological Society of America Special Papers 433, 369-390.

Yin, A., Dang, Y.Q., Wang, L.C., Jiang, W.M., Zhou, S.P., Chen, X.H., Gehrels, G.E., McRivette, M.W., 2008a. Cenozoic tectonic evolution of Qaidam basin and its surrounding regions (Part 1): The southern Qilian Shan-Nan Shan thrust belt and northern Qaidam basin.

Geological Society of America Bulletin 120, 813-846.

Yin, A., Dang, Y.Q., Zhang, M., Chen, X.H., McRivette, M.W., 2008b. Cenozoic tectonic evolution of the Qaidam basin and its surrounding regions (Part 3): Structural geology, sedimentation, and regional tectonic reconstruction. Geological Society of America Bulletin 120, 847-876.

Yu, X.J., Fu, S.T., Guan, S.W., Huang, B., Cheng, F., Cheng, X., Zhang, T., Guo, Z.J., 2014. Paleomagnetism of Eocene and Miocene sediments from the Qaidam basin: Implication for no integral rotation since the Eocene and a rigid Qaidam block. Geochemistry, Geophysics, Geosystems 15, 2109-2127.

Yuan, H.L., Gao, S., Liu, X.M., Li, H.M., Günther, D., Wu, F.Y., 2004. Accurate U-Pb age and trace element determinations of zircon by laser ablation‐inductively coupled plasma-mass spectrometry. Geostandards and Geoanalytical Research 28, 353-370.

Yuan, D.Y., Ge, W.P., Chen, Z.W., Li, C.Y., Wang, Z.C., Zhang, H.P., Zhang, P.Z., Zheng, D.W., Zheng, W.J., Craddock, W.H., Dayem, K.E., Duvall, A.R., Hough, B.G., Lease, R.O., Champagnac, J.-D., Burbank, D.W., Clark, M.K., Farley, K.A., Garzione, C.N., Kirby, E., Molnar, P., Roe, G.H., 2013. The growth of northeastern Tibet and its relevance to large-scale continental geodynamics: A review of recent studies. Tectonics 32, 2013TC003348.

Yue, Y.J., Liou, J.G., 1999. Two-stage evolution model for the Altyn Tagh fault, China. Geology 27, 227-230.

Yue, Y.J., Ritts, B.D., Graham, S.A., 2001. Initiation and long-term slip history of the Altyn Tagh Fault. International Geology Review 43, 1087-1093.

Yue, Y., Ritts, B.D., Graham, S.A., Wooden, J.L., Gehrels, G.E., Zhang, Z., 2004a. Slowing extrusion tectonics: lowered estimate of post-Early Miocene slip rate for the Altyn Tagh fault. Earth and Planetary Science Letters 217, 111-122.

Yue, Y.J., Ritts, B.D., Hanson, A.D., Graham, S.A., 2004b. Sedimentary evidence against large strike-slip translation on the Northern Altyn Tagh fault, NW China. Earth and Planetary Science Letters 228, 311-323.

Yue, Y.J., Graham, S.A., Ritts, B.D., Wooden, J.L., 2005. Detrital zircon provenance evidence for large-scale extrusion along the Altyn Tagh fault. Tectonophysics 406, 165-178.

Zhang, J.X., Zhang, Z.M., Xu, Z.Q., Yang, J.S., Cui, J.W., 2001. Petrology and geochronology of eclogites from the western segment of the Altyn Tagh, northwestern China. Lithos 56, 187-206.

Zhang, W., 2006. The High precise Cenozoic magnetostratigraphy of the Qaidam basin and uplift of the northern Tibetan Plateau. (Doctoral dissertation) Lanzhou University, Lanzhou,

pp. 1–105 (in Chinese with English abstract).

Zhang, J.X., Li, H.K., Meng, F.C., Xiang, Z.Q., Yu, S.Y., Li, J.P., 2011. Polyphase tectonothermal events recorded in metamorphic basement from the Altyn Tagh, the southeastern margin of the Tarim basin, western China: constraint from U-Pb zircon geochronology –Pb zircon geochronology. Acta Petrol. Sin. 27, 23-46.

Zhang, Z.C., Guo, Z.J., Li, J.F., Tang, W.H., 2012. Mesozoic and Cenozoic uplift-denudation along the Altyn Tagh fault, northwestern china: constraints from apatite fission track data. Quaternary Sciences, 32(3): 499-509 (in Chinese with English abstract).

Zhang, W., Fang, X., Song, C., Appel, E., Yan, M., Wang, Y., 2013. Late Neogene magnetostratigraphy in the western Qaidam Basin (NE Tibetan Plateau) and its constraints on active tectonic uplift and progressive evolution of growth strata. Tectonophysics 599, 107-116.

Zhang, J., Mattinson, C., Yu, S., Li, Y., 2014a. Combined rutile–zircon thermometry and U-Pb geochronology: New constraints on Early Paleozoic HP/UHT granulite in the south Altyn Tagh, north Tibet, China. Lithos 200, 241-257.

Zhang, H.P., Zhang, P.Z., Zheng, D.W., Zheng, W.., Chen, Z.W., Wang, W.T., 2014b. Transforming the Miocene Altyn Tagh fault slip into shortening of the north-western Qilian Shan: insights from the drainage basin geometry. Terra Nova 26, 216-221.

Zhao, J.M., Mooney, W.D., Zhang, X.K., Li, Z.C., Jin, Z.J., Okaya, N., 2006. Crustal structure across the Altyn Tagh Range at the northern margin of the Tibetan plateau and tectonic implications. Earth and Planetary Science Letters 241, 804-814.

Zhou, J.X., Xu, F.Y., Wang, T.C., Cao, A.F., Yin, C.M., 2006. Cenozoic deformation history of the Qaidam Basin, NW China: Results from cross-section restoration and implications for Qinghai–Tibet Plateau tectonics. Earth and Planetary Science Letters 243, 195-210.

Zhuang, G., Hourigan, J.K., Ritts, B.D., Kent-Corson, M.L., 2011. Cenozoic multiple-phase tectonic evolution of the northern Tibetan Plateau: Constraints from sedimentary records from Qaidam basin, Hexi Corridor, and Subei basin, northwest China. American Journal of Science 311, 116-152.

Chapter 4 Quantitative estimate of the lateral extrusion along the Altyn Tagh Fault-Qilian Shan tectonic system

Paper published in Terra Nova, 2015, vol. 27, pp. 416-425

Lateral extrusion along the Altyn Tagh Fault – Qilian Shan (NE Tibet): insight from a 3D crustal budget

Feng Cheng[1, 2], Marc Jolivet[2], Guillaume Dupont-Nivet[1, 2, 3], Lin Wang[4], Xiangjiang Yu[1], Zhaojie Guo[1, †]

[1] Key Laboratory of Orogenic Belts and Crustal Evolution, Ministry of Education, School of Earth and Space Sciences, Peking University, Beijing, 100871, China

[2] Laboratoire Géosciences Rennes, CNRS-UMR6118, Université Rennes 1, Rennes, 35042, France

[3] Institute of Earth and Environmental Science, University of Potsdam, Potsdam, 14476, Germany

[4] Institute of Remote Sensing and Geographic Information System, Peking University, Beijing, 100871, China

[†] Corresponding author. Tel.: + 86-10-62753545; fax: + 86-10-62758610. E-mail address: zjguo@pku.edu.cn (Z.J. Guo)

Note: The online version of this contribution can be found as: ***Cheng, F., Jolivet, M., Dupont-Nivet, G., Wang, L., Yu, X., Guo, Z., 2015. Lateral extrusion along the Altyn Tagh Fault, Qilian Shan (NE Tibet): insight from a 3D crustal budget. Terra Nova 27, 416-425, doi: 10.1111/ter.12173.***

Abstract

The lithospheric strike-slip Altyn Tagh Fault accommodated hundreds of kilometers of displacement between the Qaidam and Tarim blocks since its Eocene reactivation. However, the way the deformation is accommodated in the Qilian Shan and further east remains to be clarified. Based on the 360 km northeastward migration of the relatively rigid Qaidam block along the Altyn Tagh Fault and 3D isovolumetric balance of the crustal deformation within the

Altyn Tagh Fault – Qilian Shan system, we demonstrate that 250 ± 28 km (43.8~49.4 %) of N20E directed crustal shortening and an additional ~250 to ~370 km of eastward motion of the Qilian Shan crust that must be accounted for by strike-slip faulting in the Qilian Shan and crustal thickening in the Qinling area, as well as extension in the adjoining North China block graben systems.

Keywords: Tibetan Plateau; Altyn Tagh Fault; Qilian Shan; Extrusion; Qaidam Basin

4.1 Introduction

As one of the major strike-slip fault system on the Tibetan Plateau, the Altyn Tagh Fault (ATF) accommodates a significant amount of post-collisional convergence between India and Eurasia through left-lateral strike-slip faulting (Molnar and Tapponnier, 1975). The kinematics of the ATF itself has been studied in details and around 360 km Cenozoic offset has been confirmed (Jolivet et al., 1999; Ritts and Biffi, 2000; Sobel et al., 2001; Gehrels et al., 2003; Yue et al., 2005; Searle et al., 2011; Cheng et al., 2015). Nonetheless, the accommodation of the strike-slip motion along the fault within the Qilian Shan wedge that forms its eastern termination remains highly debated (Fig. 1; Meyer et al., 1998; Yue and Liou, 1999; Yin and Harrison, 2000; Yin et al., 2002; Darby et al., 2005; Yin et al., 2008a; Xiao et al., 2015).

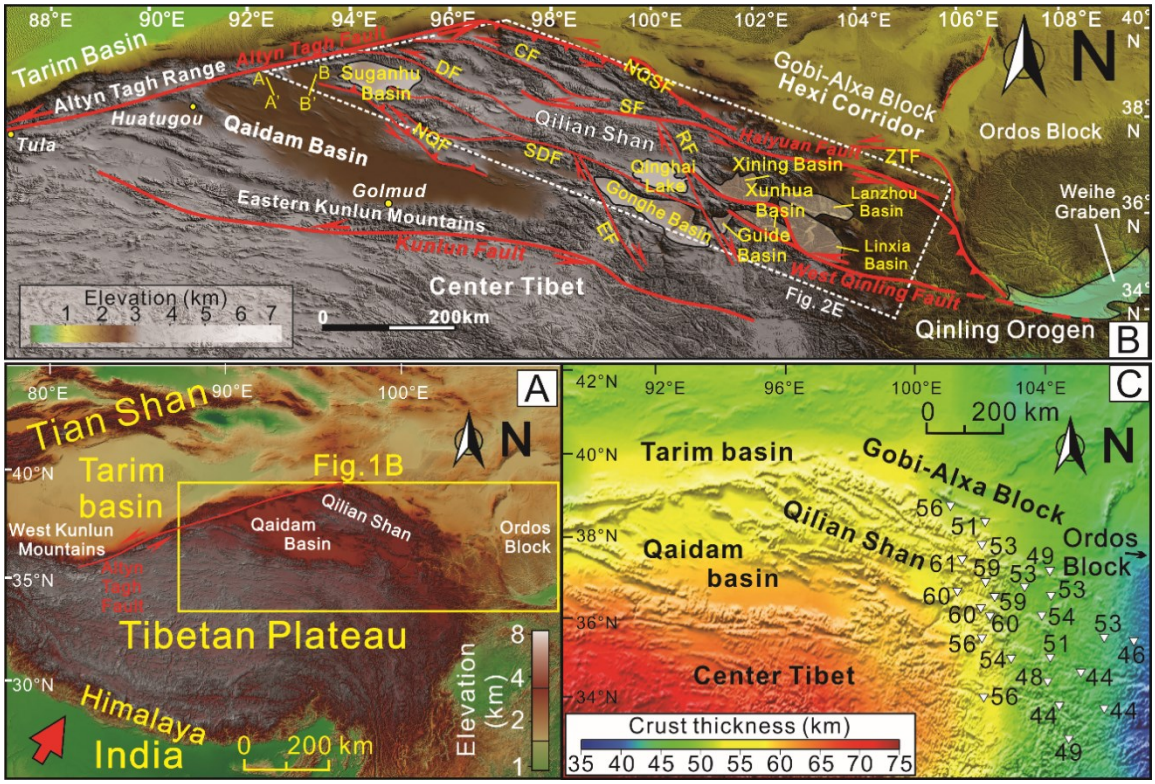

Fig.1 (A) SRTM-based digital topographic map of the Tibetan Plateau and the surrounding region. (B) SRTM-based digital topographic map of the northern Tibetan Plateau. NQSF, Northern Qilian Shan

Fault system; NQF, Northern Qaidam Fault; SDF, Saisitengshang-Dakendaban Fault; DF, Danghe-Nanshan Fault; DTF, Daxueshan Yuole-Nanshan Fault; SF, ShuleNanshan Fault; EF, Elashan Fault; RF, Riyueshan Fault; CF, Changma Fault; ZTF, Zhongwei-Tongxing Fault. Solid lines A–A' and B–B' represent the locations of the seismic profiles presented in Appendix S1. Dash-lined right trapezoid represents the studied Qilian Shan region. (C) SRTM-based present-day crustal-thickness map of the northern Tibetan Plateau and the surrounding region, modified from Li et al. (2014). The white solid triangles represent the locations of seismic stations, and numbers refer to the corresponding crustal thickness.

To understand lateral extrusion in the northern Tibetan Plateau, one major issue that remains to be explored within the kinematic pattern of the ATF – Qilian Shan system is whether the hundreds of kilometers of displacement along the ATF are totally absorbed by NE-SW crustal shortening within the Qilian Shan (Burchfiel et al., 1989; Yin and Harrision, 2000), or if they are transferred farther east in the Qinling region and possibly farther in North China (Fig. 1; Yue and Liou, 1999; Darby et al., 2005). Although large amounts of NE-SW directed shortening and eastward motion of the northern Tibetan crust has long been observed (e.g. Tapponnier and Molnar, 1977; Burchfiel et al., 1991; Dupont-Nivet et al., 2004; Zhang et al., 2004), proposed amounts of Cenozoic crustal shortening vary widely from ~20 % to ~60 % (Bally et al., 1986; Meyer, et al., 1998; Yin et al., 2008a; Zhang et al., 2014) and quantitative estimation of the amount of lateral extrusion in the northeastern Tibetan Plateau is deficient. More importantly, the large variation in crustal shortening estimation lead in turn to diverse understandings of the crustal deformation mechanism in the northern Tibetan Plateau, such as distributed or diffuse deformation (England and Seale, 1986; Burchfiel et al., 1991; Ratschbacher et al., 1994; Meyer et al., 1998), or lower crustal flow (Zhao and Morgan, 1987; Royden et al., 1997; Clark and Royden, 2000; Lease et al., 2012).

In this study, we propose a new quantitative evaluation of the Cenozoic crustal shortening and lateral extrusion budget in the northern Tibetan Plateau by considering both the northeastward migration of the relatively rigid Qaidam block along the ATF and restoring the 3D crustal deformation in the Qilian Shan.

4.2 Geological setting

The northern Tibetan Plateau is characterized by three key tectonic units: the left-lateral strike-slip lithospheric ATF, the Qilian Shan crustal wedge, and the near-rigid Qaidam block (Fig. 1; Wittlinger et al., 1998). The ATF bounds the northern part of the thickened Tibetan crust, and runs for over 1,600 km from the West Kunlun Mountains to the northwestern end of the Qilian Shan (Fig. 1; Cowgill et al., 2003). Proposed Cenozoic initiation of the ATF

generally varies from Eocene to Miocene and estimation on the offset between 300 and 400 km (Ritts and Biffi, 2000; Jolivet et al., 2001; Gehrels et al., 2003; Yue et al., 2005; Yin et al., 2008b; Wu et al., 2012; Cheng et al., 2015). The Qilian Shan separates the plateau from the Gobi-Alxa block to the northeast (Fig. 1B). This crustal-scale wedge consists of massive NW-SE striking mountain ranges growing on folds, thrusts or strike-slip faults accommodating the northward motion and eastward extrusion of the Tibetan Plateau (Meyer et al., 1998; Yin and Harrison, 2000; Tapponnier et al., 2001; Bovet et al., 2009). The proposed Paleocene to early Eocene initiation of the Cenozoic deformation and crustal shortening in the Qilian Shan (Métivier et al., 1998; Tapponnier et al., 2001; Jolivet et al. 2001; Yin et al., 2008a; Clark et al., 2010; Duvall et al., 2011; Zhuang et al., 2011; Yuan et al., 2013) challenges the model of post-Pliocene initial deformation in the northern Tibetan plateau inferred from northward progressive plateau growth hypothesis. The Qaidam block is bordered by the ATF to the northwest and the Qilian Shan to the northeast (Fig. 1B). Effective elastic thickness calculations indicate that the mechanical strength of the Qaidam crust is exceptionally high compared to that of the Qilian Shan (Braitenberg et al., 2003). Zhou et al. (2006) proposed that the Qaidam Basin experienced an average of 10 % of NE-SW shortening during the Cenozoic.

4.3 Methods

To estimate the amount of movement transferred from the ATF into the Qilian Shan, we followed the previously proposed 2D large-scale crustal deformation analyses of post-collision convergence between India and Eurasia (van Hinsbergen et al., 2011), to which we added the vertical component of crustal thickening. Recent studies demonstrated that the relatively rigid Qaidam block (Braitenberg et al., 2003; Zhou et al., 2006; Le Pape et al., 2012) has been transported northeastward along the ATF during the Cenozoic (Wang et al., 2006), without obvious post-Eocene basin-scale vertical axis rotation with respect to Eurasia (Dupont-Nivet et al., 2002; Yu et al., 2014). We thus consider that crustal shortening and vertical axis rotation of the Qaidam block have been minimal. The amount of northeastward migration of that block along the ATF must have been largely transferred into the Qilian Shan where it can be vertically partitioned into NE-SW directed crustal shortening and eastward extrusion (Fig. 2).

In the following analysis, we define the extent of the Qilian Shan to be the region comprised between the ATF, the Gobi-Alxa and the Qaidam blocks with an open boundary to the east. The general relations between the offset of the ATF, the amount of crustal shortening

and the shortening strain in the Qilian Shan are given by:

$$L_S = L_d \sin\alpha, \quad (1)$$

and

$$R_S = \frac{L_d \sin\alpha}{L_0 \sin\alpha} = \frac{L_d \sin\alpha}{(L_d + L_1)\sin\alpha} = \frac{L_d}{L_d + L_1}, \quad (2)$$

where α is the constant angle between the strike direction of the ATF and the average orientation of the Qilian Shan long-axis in plane view (Fig. 2E); L_d is the amount of offset along the ATF since its initiation; L_0 and L_1 are the average limb length of the Qilian Shan along the ATF before its initiation and at present day respectively; Ls is the average amount of crustal shortening since ATF initiation; finally Rs is the crustal shortening strain in the Qilian Shan since ATF initiation.

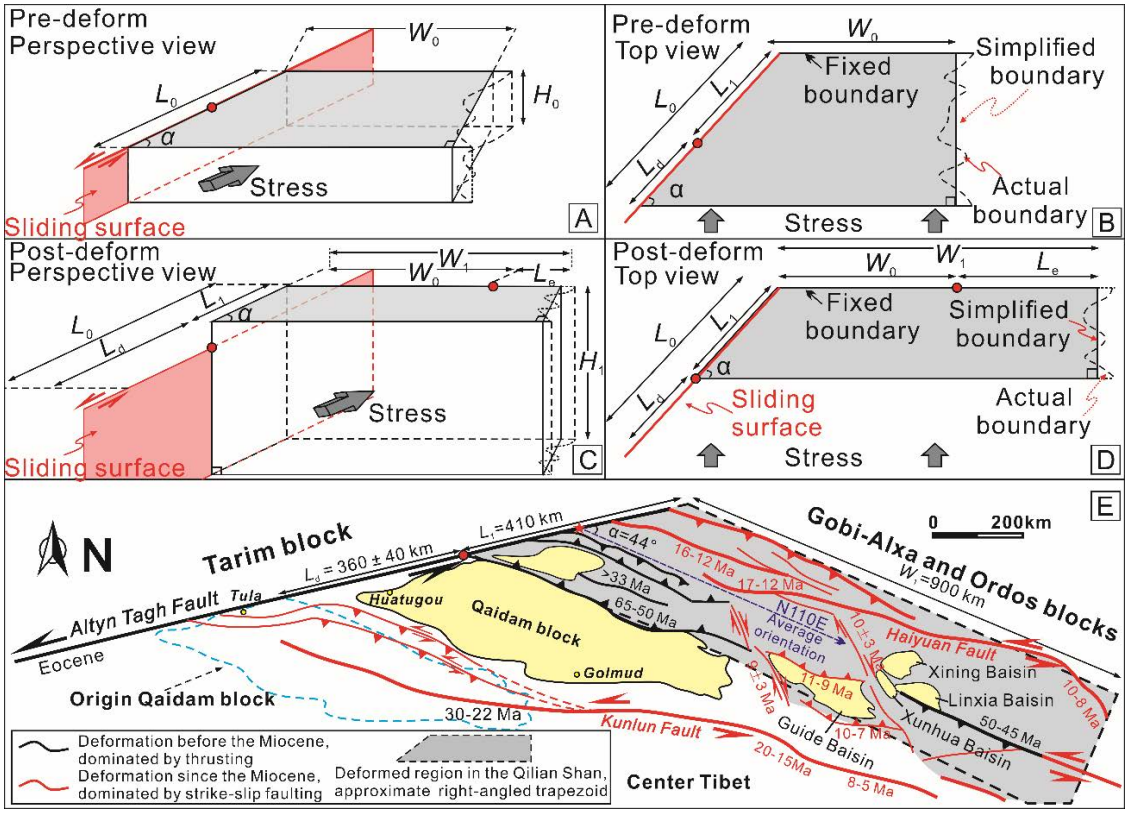

Fig.2 General model for balanced 3D crustal deformation in the Qilian Shan during the Cenozoic. (A) Perspective view of the Qilian Shan region before deformation. (B) Top view of the Qilian Shan region before deformation. (C) Perspective view of the Qilian Shan region after deformation. (D) Top view of the Qilian Shan region after deformation. (E) Sketch of the main active structures in the northern Tibetan plateau, modified from Duvallet al. (2013). To simplify the model, we consider the shape of the Qilian Shan to be an approximately right-angled trapezoid in plan view. The initiation ages are mainly compiled from previous work (e.g. Mocket al., 1999; Yin et al., 2002, 2007, 2008a,b; Jolivet et al., 2003; Lease et al., 2007; Bovet et al., 2009;Clarket al., 2010; Zheng et al., 2010; Craddock et al., 2011; Duvall et al., 2011, 2013; Hough et al., 2011; Yuan et al., 2011).

As shown by Yakovlev and Clark (2014), neglecting the density contrast between the upper and lower crust hardly changes the estimates of the modern orogenic mass. The occurrence of lower crustal flow in the northeastern Tibetan Plateau has recently been rejected (e.g. Lease et al., 2012; Li et al., 2014). From this conclusion and the lack of Cenozoic magmatism in the Qaidam Basin and Qilian Shan (Yin and Harrison, 2000), we consider the Cenozoic crust-mantle interaction and transition as sufficiently weak to be neglected in our model, and simplify the mass balance to volume balance.

Considering that both the Qaidam and Gobi-Alxa boundaries of the Qilian Shan are nearly parallel to the average orientation of the long-axis of the range during the deformation (Fig. 1B), we simplified the plane view geometry of the Qilian Shan into a right-angled trapezoid (Fig. 2). Based on isovolumetric balancing before and after crustal deformation in the Qilian Shan, the relations between the average amount of lateral crustal movement in the range, the initial crustal thickness, the present-day crustal thickness and the offset along the ATF, are described by:

$$V_0 = \frac{1}{2}\left[2\left(W_1 - L_e\right) + \left(L_d + L_1\right)\cos\alpha\right]\left(L_d + L_1\right)H_0\sin\alpha = V_1 = \frac{1}{2}\left(2W_1 + L_1\cos\alpha\right)L_1H_1\sin\alpha \quad (3)$$

where V_0 and V_1 are the constant crustal volumes of the Qilian Shan before the initiation of the ATF and at present, respectively; W_0 and W_1 are the widths of the northeastern front of the Qilian Shan before the initiation of the ATF and at present, respectively; H_0 and H_1 are the average crustal thicknesses of the Qilian Shan before the initiation of the ATF and at present, respectively; L_e is the average amount of lateral crustal movement in the Qilian Shan.

We define the Cenozoic offset along the ATF to be 360 ± 40 km based both on newly identified piercing points along the ATF (Cheng et al., 2015) and as synthesis of previous estimates (Fig. 3A). The limited crustal shortening (<20 km) within the near-rigid Qaidam block (Zhou et al., 2006) is obviously insufficient to accommodate the enormous sinistral displacement along the ATF. W_1, L_1 and α are respectively estimated to about 900 km, 410 km and 44° from Google Earth measurements (Fig. 2). The present-day crustal thickness (H_1) in the Qilian Shan was calculated adding the average crustal thickness below sea-level (~60 km) (Fig. 1C; Tian et al., 2013; Li et al., 2014), the average amount of Cenozoic exhumation (~6 km) estimated from fission-track analysis (Jolivet et al., 2001), and the average elevation of the range (~4 km) measured on Google Earth. The obtained value for H_1 is ~70 km. The estimated initial crustal thickness (H_0) of the Qilian Shan is generally ranging from 40 to 55 km (Tian et al., 2013), with a probable value around 45 km (Meyer et al., 1998; Lease et al., 2012). In order to account for this uncertainty we calculated solutions for multiple values of H0 (35, 40, 45, 50 and 55 km). Relevant parameter constraints in this study are listed in Table

1. Darby et al. (2005) favor the hypothesis that the ATF bypasses the northern margin of Qilian Shan. However, we feel that results from a recent magnetotelluric survey (Xiao et al., 2015) are opposed to the hypothesis of Darby et al. (2005), and favor the scenario that the ATF has its eastward termination within the Qilian Shan. Further details and discussion are given in Appendix S1.

Table 1. Relevant parameter estimates used in this study

Parameters	Estimation	Source
Cenozoic offset along the ATF (L_d)	300~400 km, mean offset of 360 ± 40 km	Yue and Liou, 1999; Ritts and Biffi, 2000; Yin and Harrison, 2000; Soble et al., 2001; Yue et al., 2001; Yue et al., 2005; Gehrels et al., 2003; Searle et al., 2011; Cheng et al., 2015
Average limb length of the Qilian Shan along the ATF at present day (L_1)	410 km	Measured on Google Earth
Width of the northeastern front of the Qilian Shan at present (W_1)	900 km	Measured on Google Earth
The average amount of Cenozoic exhumation since Eocene initiation (H_e)	~6 km	Jolivet et al., 2001; Yin et al., 2002; Zheng et al., 2010
Average elevation of the Qilian Shan range (H_a)	~4 km	Measured on Google Earth
Average crustal thickness of the Qilian Shan range below sea-level (H_b)	~60 km	Tian et al., 2011, 2013, 2014; Li et al., 2015
Average crustal thickness at present (H_1)	~70 km	$H_1 = H_e + H_a + H_b$
Initial crustal thickness of the Qilian Shan (H_0)	40~55 km Probable 45 km	Meyer et al., 1998; Tian et al., 2011; Lease et al., 2012; Tian et al., 2013, 2014
Constant angle between the strike direction of the ATF and the average orientation of the Qilian Shan long-axis in plane view (α)	44°	Measured on Google Earth
N110E directed crustal lateral (extrusion) movement (L_e)	$L_e = W_1 + 1/2(L_1 + L_d)\cos\alpha - 1/2(2W_1 + L_1\cos\alpha)[L_1/(L_1 + L_d)](H_1/H_0)$	
Crustal shortening within the Qilian Shan (N20E directed) (L_s)	$L_s = L_1\sin\alpha$	

Note: The Altyn Tagh Fault was defined as terminating at the northern margin of the Qilian Shan;

The Qaidam basin as a nearly-rigid block, which is based on the estimation by Braitenberg et al. (2003); Zhou et al. (2006), Pape et al. (2012). Detailed principles are given in Appendix S1.

4.4 Results

Considering a 360 ± 40 km offset along the ATF and a 45 km initial crustal thickness for the Qilian Shan, the calculated average N20E directed crustal shortening within the Qilian Shan is 250 ± 28 km, corresponding to a mean shortening strain of 43.8~49.4 %. From equation 3, using the previous values and the present-day crustal thickness of 70 km calculated above for the Qilian Shan, we obtain a value of ~250 to ~370 km of eastward crustal extrusion in the Qilian Shan during the Cenozoic. Detailed estimations of the crustal shortening and lateral extrusion are given in Figures 2-3, Tables 1-2 and Appendix S1.

Table. 2 N20E crustal shortening, shortening strain, and eastward extrusion estimates

Initial crust thickness H_0 (km)		ATF offsets $L_d > 0$ (km)		Eastward extrusion $L_e > 0$ (km)	Shortening $L_s > 0$ (km)	Shortening Rate Rs (%)
Total present crust thickness (including erosion) H_1 =70 km						
35		Max.	400	131	278	49.4
		Min.	320	-14	222	43.8
40		Max.	400	263	278	49.4
		Min.	320	133	222	43.8
45		Max.	400	367	278	49.4
		Min.	320	247	222	43.8
50		Max.	400	449	278	49.4
		Min.	320	339	222	43.8
55		Max.	400	517	278	49.4
		Min.	320	413	222	43.8
Probable	45	Probable	360	309	250	46.8

Note: In order to account for this uncertainty we calculated solutions for multiple values of H_0 (35, 40, 45, 50 and 55 km). Further considering a mean offset of 360 km along the ATF (L_d), the Qilian Shan would have accommodated as much as 309 km of lateral deformation since the Eocene activation of the ATF. Detailed parameter estimates are given in Table 1 and Appendix S1.

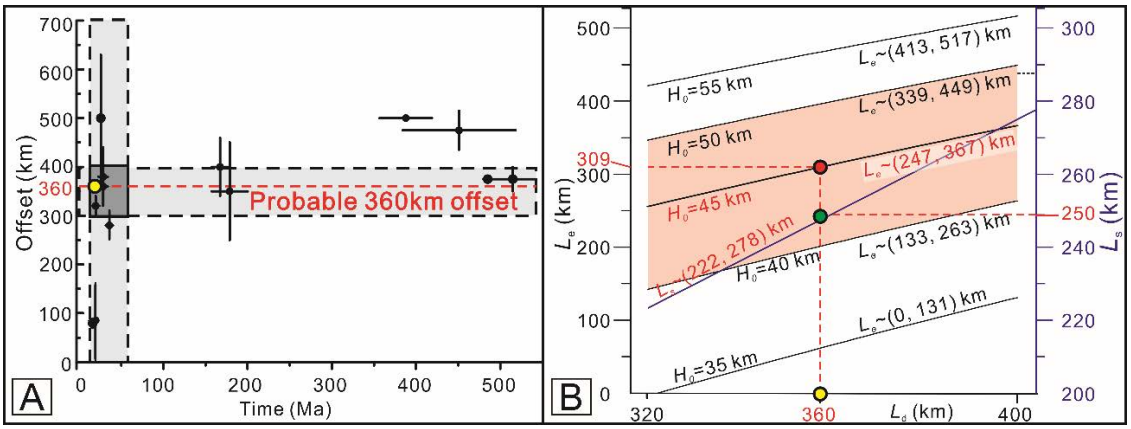

Fig.3 (A) Offset estimation along the Altyn Tagh Fault. Data were mainly compiled from Ritts and Biffi (2000), Yin et al. (2002), Gehrels et al. (2003), Yue et al. (2005); Searle et al. (2011) and Cheng et al. (2015). The grey rectangle represents the probable offset along the ATF and its probable time of initiation. In this study, we consider an offset of 360 ± 40 km along the ATF since its Eocene initiation based both on newly found piercing points in the western Qaidam Basin (Cheng et al., 2015) and on a summary of previous estimates, which is represented by the yellow circle. (B) Balanced calculation results. The black lines relate the amount of extrusion within the Qilian Shan (L_e) to the amount of offset along the ATF (L_d), while the blue line relates the amount of N20E directed crustal shortening within the Qilian Shan (L_s) to the amount of offset along the ATF (L_d). Considering the probable 360 km offset along the ATF (represented by the yellow circle in the figure) and an initial crustal thickness of 45 km in the Qilian Shan, there has been 309 km of eastward extrusion and 250 km of N20E directed crustal shortening in the Qilian Shan range, represented by the red circle and the green circle respectively. The pink region represents the possible range of L_e and L_s. In this study, we define the N110E-directed elongation of the Qilian Shan as the eastward extrusion.

4.5 Discussion and Conclusions

The dramatic decrease in GPS-measured velocities across the Qilian Shan implies large-scale N20E directed crustal shortening, accommodated along the major SE-NW thrust faults that structure the range (Fig. 4; Zhang et al., 2004; Duvall and Clark et al., 2010). The calculated 250 ± 28 km crustal shortening corresponding to a shortening strain of 47 ± 3 % are in good agreement with independent, albeit indirect evidence suggesting that the shortening strain in the Qilian Shan range between 30 % and 50 %: (1) geomorphological and geological features in the Qilian Shan as well as available subsurface data from the Qaidam Basin and the Hexi Corridor suggest a ~30-50 % of post-Neogene crustal shortening across the area (Bally et al.,1986; Meyer et al.,1998), (2) modeling of crustal deformation using the geometry of the drainage system within the Qilian Shan results in an estimate of ~39 % of shortening strain across the range (Zhang et al., 2014), (3) integration of receiver function analysis and wide-angle reflection/refraction profiles across the Qilian Shan indicate 250 to

350 km of N30E directed crustal shortening through the range (Tian et al., 2014).

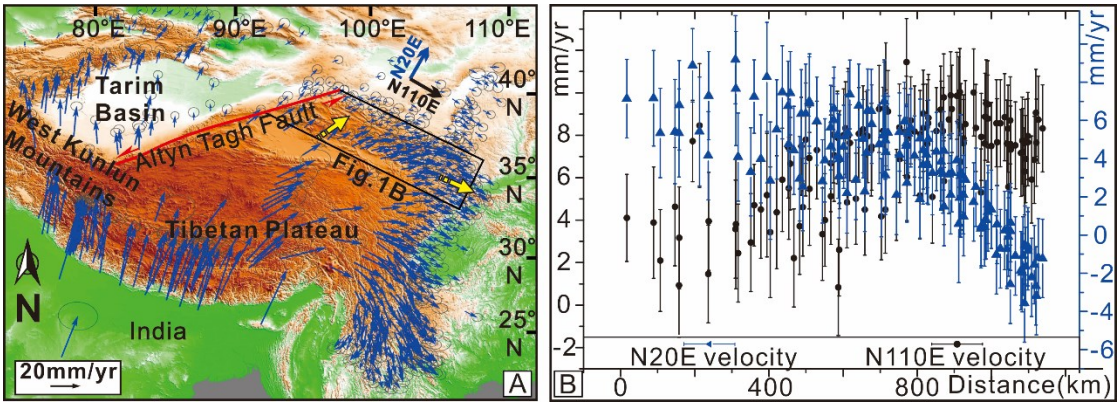

Fig.4 (A) Global Positioning System (GPS) velocities relative to stable Eurasia, modified from Zhang et al. (2004). The yellow arrows show the changes in orientation of the displacement vectors, clearly implying ongoing eastward crustal extrusion within the Qilian Shan region. (B) Strike-parallel and strike-perpendicular velocity (N110E) vs. distance. Solid-lined right trapezoid in the Fig. 4A represents the studied Qilian Shan region. GPS data from Gan et al. (2007). Details of the analytical method of geodetic velocities are given in Appendix S2. The sharp decrease in N20E directed GPS velocities from the northern Qaidam Basin to the Hexi Corridor and the large increase in N110E directed GPS velocities from the Altyn Tagh Range to the eastern Qilian Shan imply large amounts of crustal shortening and eastward extrusion within the Qilian Shan region at present.

Moreover, based on 3D isovolumetric deformation reconstruction, the Qilian Shan tectonic system accommodates between ~250 and ~370 km of eastward extrusion of the northeastern Tibetan Plateau crust (Fig. 3A). Although this eastward extrusion had already been evidenced by the N110E directed increase and N20E directed decrease of GPS velocities in the Qilian Shan (Fig. 4; Zhang et al., 2004), by strong earthquakes associated with sinistral faulting along strike-slip faults in the Qilian Shan (e.g. Haiyuan Fault; Lasserre et al., 1999), or by the occurrence of WNW–ESE and NW–SE oriented crustal and the upper mantle structures beneath the northeastern Tibetan Plateau (e.g. Li et al., 2011), few quantitative estimates of the total amount of Cenozoic displacement had been established up to now. Our estimate for crustal eastward extrusion in the Qilian Shan range provides one of the first quantitative budgets in the northeastern Tibetan Plateau.

We suggest that the >250 km eastward crustal extrusion is mainly accommodated by transcurrent motion on the main strike-slip faults that developed in the Qilian Shan (Fig. 1; Tab. 3). Since the eastward GPS velocities die out in the eastern margin of the plateau (Fig. 4; Zhang et al., 2004), this eastward crustal material flowing from the northeastern Tibetan Plateau should be partly absorbed by crustal thickening in the Qinling Orogen which initiated at 9~4 Ma slightly after the onset time of strike-slip faulting in the Qilian Shan (Fig. 5; Enkelmann et al., 2006). Finally, eastward crustal extrusion of the Qilian Shan would be a

possible driving mechanism for sinistral strike-slip faulting along the Haiyuan and West Qinling faults (Burchfiel et al., 1991; Duvall et al., 2011) and counter-clockwise rotation of the Ordos block (Zhang et al., 1998) leading to extension in the adjoining North China block graben systems, such as the Weihe Graben (Fig. 5B; Mercier et al., 2013).

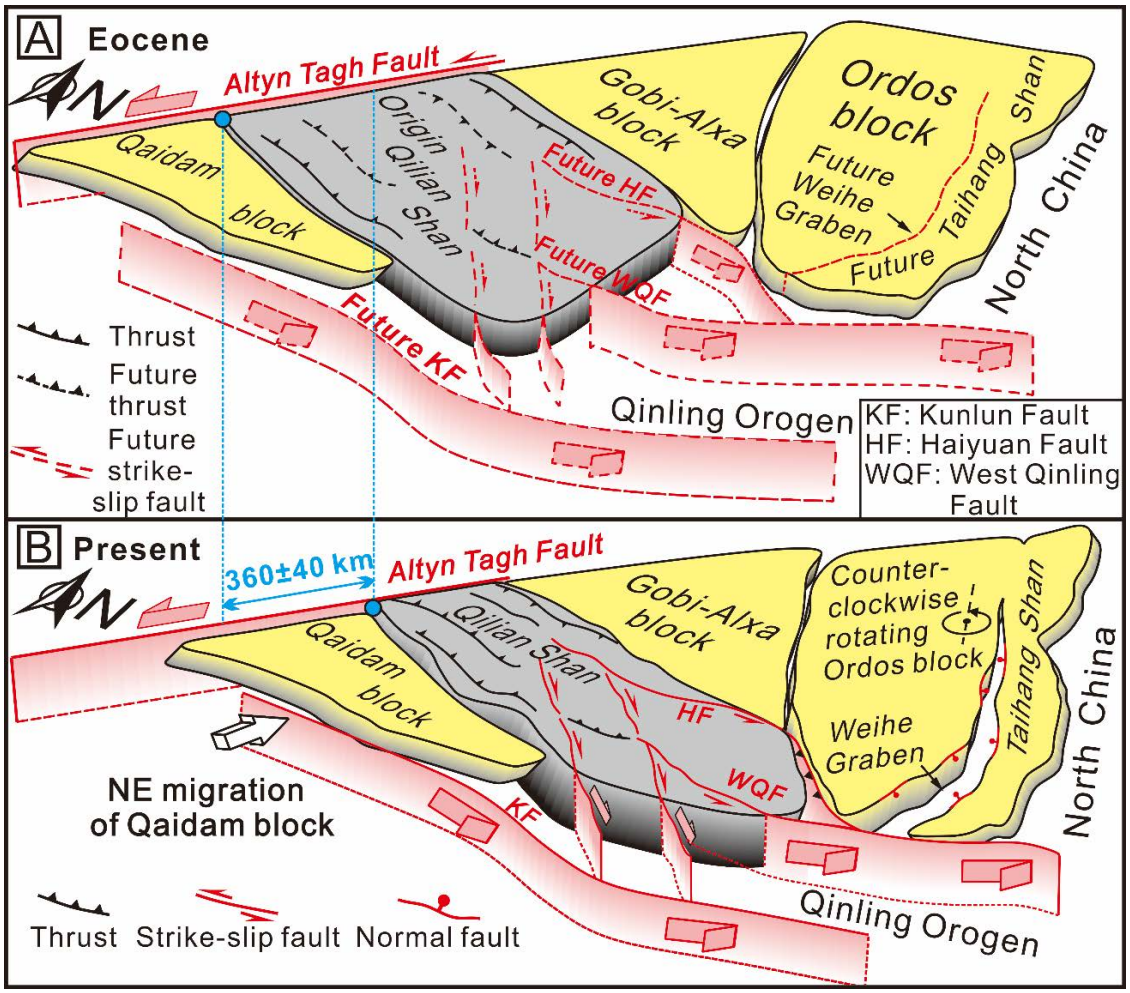

Fig.5 North-eastward migration model of the Qaidam block, corresponding to crustal shortening and eastward extrusion inthe Qilian Shan. (A) Pre-deformation phase. (B) Post-deformation phase. Note that hundreds of kilometres of offset along theATF have been absorbed within the Qilian Shan region and partly accommodated by N20E directed crustal shortening (250 ± 18 km). A large amount of this displacement was transferred further east through crustal transpression within the Qilian Shan. This eastward extrusion (~250–370 km) of crustal material from the north-eastern Tibetan Plateau is responsible for strike-slip faulting in the Qilian Shan region, crustal thickening in the Qinling region, anticlockwise rotation of the Ordos block, and extension in the Weihe Graben.

The lithospheric strike-slip Altyn Tagh Fault accommodated hundreds of kilometers of displacement between the Qaidam and Tarim blocks since its Eocene reactivation. However, the way the deformation is accommodated in the Qilian Shan and further east remains to be clarified. Based on the 360 km northeastward migration of the relatively rigid Qaidam block along the Altyn Tagh Fault and 3D isovolumetric balance of the crustal deformation within the

Altyn Tagh Fault – Qilian Shan system, we demonstrate that 250 ± 28 km (43.8~49.4 %) of N20E directed crustal shortening and an additional ~250 to ~370 km of eastward motion of the Qilian Shan crust that must be accounted for by strike-slip faulting in the Qilian Shan and crustal thickening in the Qinling area, as well as extension in the adjoining North China block graben systems.

Table.3 Potential structures that accommodate the eastward crustal extrusion in the Qilian Shan

Name of structure	Strike-slip faulting Initiation (Ma)	Slip rate (mm/yr)	Offset (km)
Haiyuan fault	17~12 (Duvall et al., 2013)	4~6 (Zhang et al., 1988; Gaudemer et al., 1995; Li et al., 2009; Zheng et al., 2012)	60~90 (Gaudemer et al., 1995;Ding et al., 2004)
Shulenanshan fault	23 (Ding et al., 2004)	6.5 (Ding et al., 2004)	~150 (Ding et al., 2004)
Zhongwei-Tongxing fault	5.3-3.4 (Ding et al., 2004)	4–7 (Ding et al., 2004)	20-25 (Ding et al., 2004)
West Qinling fault	16 (Wang et al., 2012)	2 (Li et al., 2005)	≥ 25 (Ratschbacher et al., 2003)
Northern Qilian fault	10 (Zheng et al., 2010)	~1 (Zheng et al., 2010)	~10 (Zheng et al., 2010)
Elashan fault	9 ± 3 (Yuan et al., 2011)	1.1 ± 0.3 mm/yr (Yuan et al., 2013)	9~12 (Yuan et al., 2011)
Riyueshan fault	10 ± 3 (Yuan et al., 2011)	1.2 ± 0.4 (Yuan et al., 2013)	6-12 (Yuan et al., 2011)
Changma fault	≤ 23 Oligocene (Kang et al., 1986)	1~5 (Peltzer et al., 1988; Zheng et al., 2012)	20~120

Acknowledgements

We thank Science Editor Jason Phipps Morgan for providing constructive feedback. This work was funded by the National S&T Major Project of China (No. 2011ZX05009-001) and the China Scholarship Council - Campus France Egide Cai Yuanpei program (201404490136; N° 32393WL(2014)).

Reference

Bally, A.W., Chou, I.M., Clayton, R., Heugster, H.P., Kidwell, S., Meckel, L.D., Ryder, R.T.,

Watts, A.B. and Wilson, A.A., 1986. Notes on Sedimentary Basins in China, Report of the American Sedimentary Basins Delegation to the People's Republic of China, August 17–September 8, open file report 86–327, USGS.

Bovet, P.M., Ritts, B.D., Gehrels, G., et al., 2009. Evidence of Miocene crustal shortening in the north Qilian Shan from Cenozoic stratigraphy of the western Hexi Corridor, Gansu Province, China. American Journal of Science, 309, 290-329.

Braitenberg, C., Wang, Y., Fang, J. and Hsu, H., 2003. Spatial variations of flexure parameters over the Tibet–Quinghai plateau. Earth and Planetary Science Letters, 205, 211-224.

Burchfiel, B.C., Quidong, D., Molnar, P., et al., 1989. Intracrustal detachment within zones of continental deformation. Geology, 17, 748-752.

Burchfiel, B., Zhang, P., Wang, Y., et al., 1991. Geology of the Haiyuan fault zone, Ningxia-Hui Autonomous Region, China, and its relation to the evolution of the northeastern margin of the Tibetan Plateau. Tectonics, 10, 1091-1110.

Cheng, F., Guo, Z., Jenkins, H.S., et al., 2015. Initial rupture and displacement on the Altyn Tagh fault, northern Tibetan Plateau: Constraints based on residual Mesozoic to Cenozoic strata in the western Qaidam Basin. Geosphere, 11, 921-942.

Clark, M.K. and Royden, L.H., 2000. Topographic ooze: Building the eastern margin of Tibet by lower crustal flow. Geology, 28, 703-706.

Clark, M.K., Farley, K.A., Zheng, D., et al., 2010. Early Cenozoic faulting of the northern Tibetan Plateau margin from apatite (U–Th)/He ages. Earth and Planetary Science Letters, 296, 78-88.

Cowgill, E., Yin, A., Harrison, T.M. and Xiao-Feng, W., 2003. Reconstruction of the Altyn Tagh fault based on U-Pb geochronology: Role of back thrusts, mantle sutures, and heterogeneous crustal strength in forming the Tibetan Plateau. Journal of Geophysical Research, 108, 2346.

Craddock, W., Kirby, E. and Zhang, H., 2011. Late Miocene-Pliocene range growth in the interior of the northeastern Tibetan Plateau. Lithosphere, 3, 420-438.

Darby, B.J., Ritts, B.D., Yue, Y. and Meng, Q., 2005. Did the Altyn Tagh fault extend beyond the Tibetan Plateau? Earth and Planetary Science Letters, 240, 425-435.

Ding, G., Chen, J., Tian, Q., et al., 2004. Active faults and magnitudes of left-lateral displacement along the northern margin of the Tibetan Plateau. Tectonophysics, 380, 243-260.

Dupont-Nivet, G., Butler, R.F., Yin, A. and Chen, X., 2002. Paleomagnetism indicates no Neogene rotation of the Qaidam Basin in northern Tibet during Indo-Asian collision. Geology, 30, 263-266.

Dupont-Nivet, G., Horton, B., Butler, R., et al., 2004. Paleogene clockwise tectonic rotation of the Xining-Lanzhou region, northeastern Tibetan Plateau. J. Geophys. Res, 109, B04401.

Duvall, A.R. and Clark, M.K., 2010. Dissipation of fast strike-slip faulting within and beyond northeastern Tibet. Geology, 38, 223-226.

Duvall, A.R., Clark, M.K., van der Pluijm, B.A. and Li, C., 2011. Direct dating of Eocene reverse faulting in northeastern Tibet using Ar-dating of fault clays and low-temperature thermochronometry. Earth and Planetary Science Letters, 304, 520-526.

Duvall, A.R., Clark, M.K., Kirby, E., et al., 2013. Low-temperature thermochronometry along the Kunlun and Haiyuan Faults, NE Tibetan Plateau: Evidence for kinematic change during late-stage orogenesis. Tectonics, 32, 1190-1211.

England, P. and Houseman, G., 1986. Finite strain calculations of continental deformation: 2. Comparison with the India-Asia collision zone. Journal of Geophysical Research: Solid Earth (1978–2012), 91, 3664-3676.

Enkelmann, E., Ratschbacher, L., Jonckheere, R., et al., 2006. Cenozoic exhumation and deformation of northeastern Tibet and the Qinling: Is Tibetan lower crustal flow diverging around the Sichuan Basin? Geological Society of America Bulletin, 118, 651-671.

Gaudemer, Y., Tapponnier, P., Meyer, B., et al., 1995. Partitioning of crustal slip between linked, active faults in the eastern Qilian Shan, and evidence for a major seismic gap, the 'Tianzhu gap', on the western Haiyuan Fault, Gansu (China). Geophysical Journal International, 120, 599-645.

Gehrels, G.E., Yin, A. and Wang, X.F., 2003. Magmatic history of the northeastern Tibetan Plateau. Journal of Geophysical Research, 108, 2423.

Hough, B.G., Garzione, C.N., Wang, Z., et al., 2011. Stable isotope evidence for topographic growth and basin segmentation: Implications for the evolution of the NE Tibetan Plateau. Geological Society of America Bulletin, 123, 168-185.

Jolivet, M., Roger, F., Arnaud, N., et al., 1999. Histoire de l'exhumation de l'Altun Shan: indications sur l'âge de la subduction du bloc du Tarim sous le système de l'Altyn Tagh (Nord Tibet). Comptes Rendus de l'Académie des Sciences-Series IIA-Earth and Planetary Science, 329, 749-755.

Jolivet, M., Brunel, M., Seward, D., et al., 2001. Mesozoic and Cenozoic tectonics of the northern edge of the Tibetan plateau: fission-track constraints. Tectonophysics, 343, 111-134.

Jolivet, M., Brunel, M., Seward, D., et al., 2003. Neogene extension and volcanism in the Kunlun Fault Zone, northern Tibet: New constraints on the age of the Kunlun Fault. Tectonics, 22, 1052.

Kang, L., 1986. Study of paleo-earthquakes in Changma Fault zone. Journal of seismology, 12, 16-22 (in Chinese with English abstract).

Lasserre, C., Morel, P.H., Gaudemer, Y., et al., 1999. Postglacial left slip rate and past occurrence of M≥ 8 earthquakes on the western Haiyuan fault, Gansu, China. Journal of Geophysical Research: Solid Earth (1978–2012), 104, 17633-17651.

Lease, R.O., Burbank, D.W., Gehrels, G.E., et al., 2007. Signatures of mountain building: Detrital zircon U/Pb ages from northeastern Tibet. Geology, 35, 239-242.

Lease, R.O., Burbank, D.W., Clark, M.K., et al., 2011. Middle Miocene reorganization of deformation along the northeastern Tibetan Plateau. Geology, 39, 359-362.

Lease, R.O., Burbank, D.W., Zhang, H., et al., 2012. Cenozoic shortening budget for the northeastern edge of the Tibetan Plateau: Is lower crustal flow necessary? Tectonics, 31, TC3011.

Le Pape, F., Jones, A.G., Vozar, J. and Wenbo, W., 2012. Penetration of crustal melt beyond the Kunlun Fault into northern Tibet. Nature Geoscience, 5, 330-335.

Li, C., 2005. Quantitative researches on several prominent faults in the NE Margin of the Tibetan plateau. Doctoral dissertation, China Earthquake Administration, Beijing, 230 pp (in Chinese with English abstract).

Li, C., Zhang, P.Z., Yin, J. and Min, W., 2009. Late Quaternary left-lateral slip rate of the Haiyuan fault, northeastern margin of the Tibetan Plateau. Tectonics, 28.

Li, J., Wang, X. and Niu, F., 2011. Seismic anisotropy and implications for mantle deformation beneath the NE margin of the Tibet plateau and Ordos plateau. Physics of the Earth and Planetary Interiors, 189, 157-170.

Li, X., Li, H., Shen, Y., et al., 2014. Crustal Velocity Structure of the Northeastern Tibetan Plateau from Ambient Noise Surface-Wave Tomography and Its Tectonic Implications. Bulletin of the Seismological Society of America, 104, 1045-1055.

Mercier, J.L., Vergely, P., Zhang, Y.Q., et al., 2013. Structural records of the Late Cretaceous–Cenozoic extension in Eastern China and the kinematics of the Southern Tan-Lu and Qinling Fault Zone (Anhui and Shaanxi provinces, PR China). Tectonophysics, 582, 50-75.

Métivier, F., Gaudemer, Y., Tapponnier, P. and Meyer, B., 1998. Northeastward growth of the Tibet plateau deduced from balanced reconstruction of two depositional areas: The Qaidam and Hexi Corridor basins, China. Tectonics, 17, 823-842.

Meyer, B., Tapponnier, P., Bourjot, L., et al., 1998. Crustal thickening in Gansu-Qinghai, lithospheric mantle subduction, and oblique, strike-slip controlled growth of the Tibet plateau. Geophysical Journal International, 135, 1-47.

Mock, C., Arnaud, N.O. and Cantagrel, J.M., 1999. An early unroofing in northeastern Tibet? Constraints from $^{40}Ar/^{39}Ar$ thermochronology on granitoids from the eastern Kunlun range (Qianghai, NW China). Earth and Planetary Science Letters, 171, 107-122.

Molnar, P. and Tapponnier, P., 1975. Cenozoic tectonics of Asia: Effects of a continental collision. Science, 189, 419-426.

Peltzer, G., Tapponnier, P., Gaudemer, Y., et al., 1988. Offsets of late Quaternary morphology, rate of slip, and recurrence of large earthquakes on the Chang Ma fault (Gansu, China). Journal of Geophysical Research: Solid Earth (1978–2012), 93, 7793-7812.

Ratschbacher, L., Frisch, W., Liu, G. and Chen, C., 1994. Distributed deformation in southern and western Tibet during and after the India-Asia collision. Journal of Geophysical Research: Solid Earth (1978–2012), 99, 19917-19945.

Ratschbacher, L., Hacker, B.R., Calvert, A., et al., 2003. Tectonics of the Qinling (Central China): tectonostratigraphy, geochronology, and deformation history. Tectonophysics, 366, 1-53.

Ritts, B.D. and Biffi, U., 2000. Magnitude of post-Middle Jurassic (Bajocian) displacement on the central Altyn Tagh fault system, northwest China. Geological Society of America Bulletin, 112, 61-74.

Royden, L.H., Burchfiel, B.C., King, R.W., et al., 1997. Surface deformation and lower crustal flow in eastern Tibet. Science, 276, 788-790.

Searle, M., Elliott, J., Phillips, R. and Chung, S.-L., 2011. Crustal–lithospheric structure and continental extrusion of Tibet. Journal of the Geological Society, 168, 633-672.

Sobel, E.R., Arnaud, N., Jolivet, M., et al., 2001. Jurassic to Cenozoic exhumation history of the Altyn Tagh range, northwest China, constrained by $^{40}Ar/^{39}Ar$ and apatite fission track thermochronology. Geological Society of America Memoirs, 194, 247-267.

Tapponnier, P. and Molnar, P., 1977. Active faulting and tectonics in China. Journal of Geophysical Research, 82, 2905-2930.

Tapponnier, P., Xu, Z.Q., Roger, F., et al., 2001. Oblique stepwise rise and growth of the Tibet Plateau. Science, 294, 1671-1677.

Tian, X., Teng, J., Zhang, H., et al., 2011. Structure of crust and upper mantle beneath the Ordos Block and the Yinshan Mountains revealed by receiver function analysis. Physics of the Earth and Planetary Interiors, 184, 186-193.

Tian, X. and Zhang, Z., 2013. Bulk crustal properties in NE Tibet and their implications for deformation model. Gondwana Research, 24, 548-559.

Tian, X., Liu, Z., Si, S. and Zhang, Z., 2014. The crustal thickness of NE Tibet and its

implication for crustal shortening. Tectonophysics, 634, 198-207.

van Hinsbergen, D.J., Kapp, P., Dupont-Nivet, G., et al., 2011. Restoration of Cenozoic deformation in Asia and the size of Greater India. Tectonics, 30, TC5003.

Wang, E., 1996. Early Tertiary Strike Slip Displacement AlongQilian Mountain Range And Associated Sedimentation And Deformation in the Lanzhou Basin, 30th International Geological Congress, Beijing, Abstracts, 1, 268.

Wang, E., Xu, F.Y., Zhou, J.X., et al., 2006. Eastward migration of the Qaidam basin and its implications for Cenozoic evolution of the Altyn Tagh fault and associated river systems. Geological Society of America Bulletin, 118, 349-365.

Wang, Z., Zhang, P., Garzione, C.N., et al., 2012. Magnetostratigraphy and depositional history of the Miocene Wushan basin on the NE Tibetan plateau, China: implications for middle Miocene tectonics of the West Qinling fault zone. Journal of Asian Earth Sciences, 44, 189-202.

Wittlinger, G., Tapponnier, P., Poupinet, G., et al., 1998. Tomographic evidence for localized lithospheric shear along the Altyn Tagh fault. Science, 282, 74-76.

Wu, L., Xiao, A.C., Yang, S.F., et al., 2012. Two-stage evolution of the Altyn Tagh Fault during the Cenozoic: new insight from provenance analysis of a geological section in NW Qaidam Basin, NW China. Terra Nova, 24, 387-395.

Xiao, Q., Shao G., Liu-Zeng J., et al., 2015. Eastern termination of the Altyn Tagh Fault, western China: Constraints from a magnetotelluric survey, J. Geophys. Res. Solid Earth, 120, doi: 10.1002/2014JB011363.

Yakovlev, P.V. and Clark, M.K., 2014. Conservation and redistribution of crust during the Indo-Asian collision .Tectonics, 33, 1016-1027.

Yin, A. and Harrison, T.M., 2000. Geologic evolution of the Himalayan-Tibetan orogen. Annual Review of Earth and Planetary Sciences, 28, 211-280.

Yin, A., Rumelhart, P., Butler, R., et al., 2002. Tectonic history of the Altyn Tagh fault system in northern Tibet inferred from Cenozoic sedimentation. Geological Society of America Bulletin, 114, 1257-1295.

Yin, A., Dang, Y.Q., Zhang, M., et al., 2007. Cenozoic tectonic evolution of Qaidam basin and its surrounding regions (part 2): Wedge tectonics in southern Qaidam basin and the Eastern Kunlun Range. Geological Society of America Special Papers, 433, 369-390.

Yin, A., Dang, Y.Q., Wang, L.C., et al., 2008a. Cenozoic tectonic evolution of Qaidam basin and its surrounding regions (Part 1): The southern Qilian Shan-Nan Shan thrust belt and northern Qaidam basin. Geological Society of America Bulletin, 120, 813-846.

Yin, A., Dang, Y.Q., Zhang, M., et al., 2008b. Cenozoic tectonic evolution of the Qaidam basin and its surrounding regions (Part 3): Structural geology, sedimentation, and regional tectonic reconstruction. Geological Society of America Bulletin, 120, 847-876.

Yu, X.J., Fu, S.T., Guan, S.W., et al., 2014. Paleomagnetism of Eocene and Miocene sediments from the Qaidam basin: Implication for no integral rotation since the Eocene and a rigid Qaidam block. Geochemistry, Geophysics, Geosystems, 15, 2109-2127.

Yuan, D.Y., Champagnac, J.D., Ge, W.P., et al., 2011. Late Quaternary right-lateral slip rates of faults adjacent to the lake Qinghai, northeastern margin of the Tibetan Plateau. Geological Society of America Bulletin, 123, 2016-2030.

Yuan, D.Y., Ge, W.P., Chen, Z.W., et al., 2013. The growth of northeastern Tibet and its relevance to large-scale continental geodynamics: A review of recent studies. Tectonics, 32, 2013TC003348.

Yue, Y.J. and Liou, J.G., 1999. Two-stage evolution model for the Altyn Tagh fault, China. Geology, 27, 227-230.

Yue, Y.J., Ritts, B.D. and Graham, S.A., 2001. Initiation and long-term slip history of the Altyn Tagh Fault. International Geology Review, 43, 1087-1093.

Yue, Y.J., Graham, S.A., Ritts, B.D. and Wooden, J.L., 2005. Detrital zircon provenance evidence for large-scale extrusion along the Altyn Tagh fault. Tectonophysics, 406, 165-178.

Zhang, P., Molnar, P., Burchfiel, B., et al., 1988. Bounds on the Holocene slip rate of the Haiyuan fault, north-central China. Quaternary Research, 30, 151-164.

Zhang, Y.Q., Mercier, J.L. and Vergély, P., 1998. Extension in the graben systems around the Ordos (China), and its contribution to the extrusion tectonics of south China with respect to Gobi-Mongolia. Tectonophysics, 285, 41-75.

Zhang, P.Z., Shen, Z., Wang, M., et al., 2004. Continuous deformation of the Tibetan Plateau from global positioning system data. Geology, 32, 809-812.

Zhang, H.P., Zhang, P.Z., Zheng, D.W., et al., 2014. Transforming the Miocene Altyn Tagh fault slip into shortening of the north-western Qilian Shan: insights from the drainage basin geometry. Terra Nova, 26, 216-221.

Zhao, W.L. and Morgan, W.J., 1987. Injection of Indian crust into Tibetan lower crust: A two-dimensional finite element model study. Tectonics, 6, 489-504.

Zheng, D., Clark, M.K., Zhang, P., et al., 2010. Erosion, fault initiation and topographic growth of the North Qilian Shan (northern Tibetan Plateau). Geosphere, 6, 937-941.

Zheng, W., Zhang, P., He, W., et al., 2013. Transformation of displacement between strike-slip and crustal shortening in the northern margin of the Tibetan Plateau: Evidence from decadal

GPS measurements and late Quaternary slip rates on faults. Tectonophysics, 584, 267-280.
Zhou, J.X., Xu, F.Y., Wang, T.C., et al., 2006. Cenozoic deformation history of the Qaidam Basin, NW China: Results from cross-section restoration and implications for Qinghai–Tibet Plateau tectonics. Earth and Planetary Science Letters, 243, 195-210.
Zhuang, G., Hourigan, J.K., Ritts, B.D. and Kent-Corson, M.L., 2011. Cenozoic multiple-phase tectonic evolution of the northern Tibetan Plateau: Constraints from sedimentary records from Qaidam basin, Hexi Corridor, and Subei basin, northwest China. American Journal of Science, 311, 116-152.

4.6 Chapter summary

The lithospheric strike-slip Altyn Tagh Fault accommodated hundreds of kilometers of displacement between the Qaidam and Tarim blocks since its Eocene reactivation. However, the way the deformation is accommodated in the Qilian Shan and further east remains to be clarified. Based on the 360 km northeastward migration of the relatively rigid Qaidam block along the Altyn Tagh Fault and 3D isovolumetric balance of the crustal deformation within the Altyn Tagh Fault – Qilian Shan system, we demonstrate that 250 ± 28 km (43.8~49.4 %) of N20E directed crustal shortening and an additional ~250 to ~370 km of eastward motion of the Qilian Shan crust that must be accounted for by strike-slip faulting in the Qilian Shan and crustal thickening in the Qinling area, as well as extension in the adjoining North China block graben systems.

Chapter 5 Strike-slip superimposed Qaidam Basin and its control on oil and gas accumulation

Paper published in Petroleum Exploration and Development, 2015, vol. 42, pp. 778-789

Strike-slip superimposed Qaidam Basin and its control on oil and gas accumulation, NW China

FU Suotang[1], MA Dade[1], GUO Zhaojie[2,†], **CHENG Feng**[2]

[1] Qinghai Oilfield Company, PetroChina, Dunhuang, Gansu 736202, China;
[2] Key Laboratory of Orogenic Belts and Crustal Evolution, Ministry of Education, School of Earth and Space Sciences, Peking University, Beijing 100871, China
[†] Corresponding author. Tel.: + 86-10-62753545; fax: + 86-10-62758610. E-mail address: zjguo@pku.edu.cn (Z.J. Guo)

Note: *This English version is translated from a Chinese version by the editorial office of the journal* ***Petroleum Exploration and Development***. The online version of this contribution can be found as: ***Fu, S., Ma, D., Guo, Z., Cheng, F., 2015. Strike-slip superimposed Qaidam Basin and its control on oil and gas accumulation, NW China. Petroleum Exploration and Development 42, 778-789, doi: 10.1016/S1876-3804(15)30074-4.***

Abstract

Based on detailed field survey in the western Qaidam Basin, combined with petroleum exploration practices in recent years, this study suggests that the Qaidam Basin is a strike-slip superimposed basin jointly controlled by the left-lateral strike-slip Altyn Tagh and East Kunlun faults. The Altyn Tagh fault acts as the major controlling boundary, while the East Kunlun fault only controls the local evolution of the southern edge of the basin. To the east, the northern Qaidam-Qilian Shan thrust-fold belt passively accommodates the northeastward displacement along the Altyn Tagh fault through NE-SW directed shortening. In the India-Asia collision background, the left-lateral strike-slip faulting along the Altyn Tagh fault initiated from the early Eocene, forcing the Qaidam Basin to move northeastward, causing the

thrust and slip deformation of the NW-SE faults in northern Qaidam margin-Qilian Mountain area, and the deposition of the Cenozoic since the Paleogene Lulehe Formation. During the Paleogene, the northern Qaidam Basin developed coarse-grained sediments like that in a foreland basin, forming poor quality source rocks; while the southwestern Qaidam Basin was an extensional sag basin where good quality source rocks deposited. By the early Miocene, left-lateral faulting along the Kunlun fault became active, leading to the formation of a series of en-echelon faults (e.g. the Kunbei fault, the Arlar fault and the Hongliuquan fault). These faults gradually migrated northward, their kinematics changing from left-lateral strike-slip motion to NE-SW transpression. Strike-slip-related structures controlled by those faults (e.g. the Yingxiongling structure) are ideal places for oil and gas accumulation from Paleogene source rocks. To sum up, the Qaidam Basin is a strike-slip superimposedbasin jointly controlled by the left-lateral strike-slip AltynTagh and East Kunlun faults. The temporal and spatial superimposition of these two strike-slip faults during the Cenozoic controlled theevolution of the basin as well as the oil and gas accumulation.

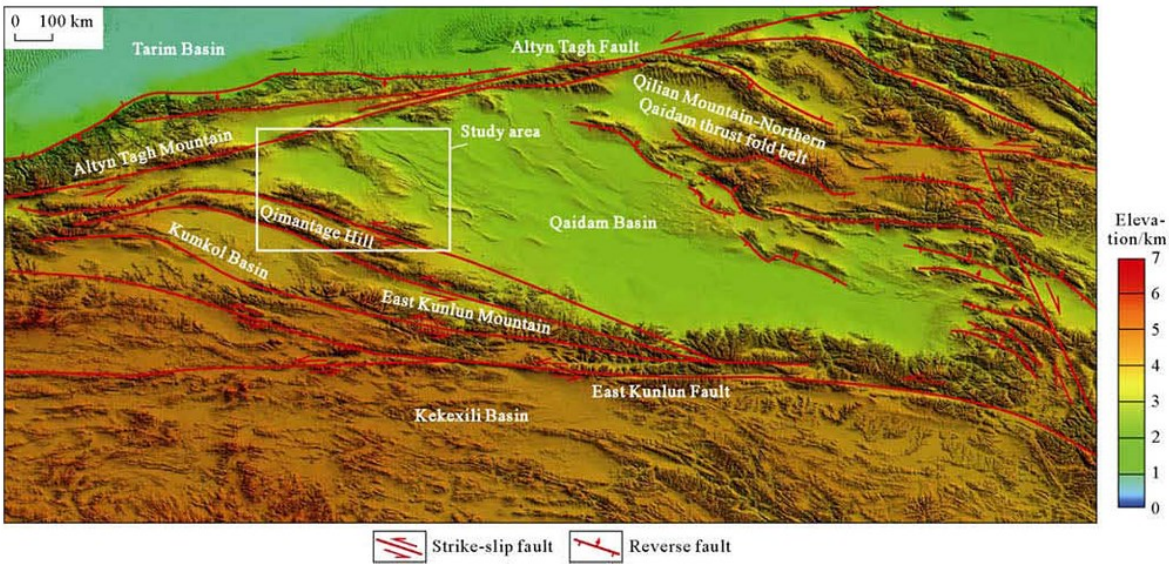

Fig. 1. Topography and distribution of the main faults of the Qaidam Basin and its periphery (Topographic data adopts the SRTMdata in 90 m resolution[17]).

5.1 Introduction

The Qaidam Basin in triangular shape is located in the northern margin of the Tibetan Plateau and held in between Altyn Tagh, East Kunlun and Qilian Mountain. It is the largest oil and gas basin in the Tibetan Plateau. Since Well Qie 6 drilled in the southwestern Qaidam Basin obtained high-yield industrial oil flow in 2007, a series of large oil and gas fields have been successively discovered in the Qiekelike, Yingdong, Dongping and Yingxi regions,

opening a new page of oil and gas exploration in plateau basins. The Qaidam Basin has not only unique tectonic setting and attributes, but also unique hydrocarbon accumulation process and pattern, since (1) it is the only basin held by two large strike-slip faults (Altyn Tagh and East Kunlun strike-slip faults) in the world; (2) it is the only large oil and gas-bearing basin in the interior Tibetan Plateau; (3) it is the only large oil and gas-bearing basin that develops Cenozoic continental reservoirs in western China. Therefore, the Qaidam Basin must have unique tectonic and hydrocarbon accumulation theory as it has different characteristics and petroleum exploration practice from other basins.

5.2 Similarities, differences and key points of the cognition

The genesis and attributes of the Qaidam Basin is a subject of intense debate for a long time. Previous petroleum geologists believed that the Qaidam Basin had experienced three tectonic evolution stages during the Mesozoic and Cenozoic, Jurassic to Cretaceous rifting stage, Paleogene depression stage and Neogene inversion stage[1]. With the deepening of exploration, some researchers advanced the Qaidam Basin experienced two tectonic evolution stages, Cretaceous to Paleogene extensional stage and Neogene compressional stage[2]. In recent years, some researchers put forward a new finding that the Qaidam Basin was a superimposed basin, which means it was an analogous foreland basin superimposed on the Jurassic to Paleogene fold basement pull-apart basin since the Neogene[3-4]. In addition, some researchers considered the Qaidam Basin had experienced four evolution stages based on the latest oil and gas exploration results, Jurassic rifting stage, Cretaceous compressional stage, Paleogene stable and wide basin/transpression stage and Neogene compressional and intracontinential depression stage[5]. The different recognitions on the tectonic evolution and attributes of the Qaidam Basin are ascribed to the different recognitions on the relationship between the Qaidam Basin and its peripheral orogenic belts (Fig. 1). Most studies in early stage reached the conclusion that the formation of the Qaidam Basin was related to the northward overthrust of the East Kunlun Mountain[6-9], which means the Qaidam Basin is the foreland basin of the East Kunlun Mountain which continues obducting northwards along a series south-dipping faults or converted transpression system in the southern Qaidam Basin[10-11]. However, based on the seismic profile collected from the interior basin, Yin et al.[12]put forward an opposite view point that a large set of wedge structure developed beneath the Qaidam Basin obducted the Qaidam Basin to the East Kunlun Mountain southwards from Qilian piedmont, indicating the Qaidam Basin was not only a foreland basin of the Qilian

Mountain, but also a piggyback basin of the East Kunlun Mountain[12-14]. In addition, some researchers believed the Qaidam Basin was part of the Tarim Basin before the Oligocene based on the stratigraphic correlation results between the southwestern margin of the Tarim Basin and the western Qaidam Basin, the left-lateral strike-slip of Altyn Tagh fault initiated from the Oligocene resulted in the separation of Qaidam Basin from the Tarim Basin, after that, the Qaidam Basin gradually evolved into a large inter-mountain compressional basin.

Moreover, they further pointed out that the flexural folding occurred in the upper crust of the northern Tibetan Plateau was the major cause of the formation of the Qaidam Basin[15-16]. Although there is controversy over the genesis and attributes of the Qaidam Basin, with the promotion of seismic exploration in recent years, the basic geological features of the Qaidam Basin have been gradually revealed. Based on the major breakthroughs in magnetic stratigraphy, paleobotany and seismic exploration, the Cenozoic stratigraphic sequence and age of the entire basin have been established and accurately constrained, in which eight sets of rock stratigraphic units are identified from bottom to top[18-24], including Lulehe Formation, Lower Member of Lower Ganchaigou Formation, Upper Member of Lower Ganchaigou Formation, Upper Ganchaigou Formation, Lower Youshashan Formation, Upper Youshashan Formation, Shizigou Formation and Qigequan Formation (Fig. 2). Moreover, the Cenozoic stratigraphic distribution across the entire basin reflects the depocenter of the Qaidam Basin has been located in the axis center of the basin since Lulehe Period, and gradually migrated eastwards[20-22].At the same time, controlled by the left-lateral strike-slip of Altyn Tagh faults, the entire Qaidam Basin migrated

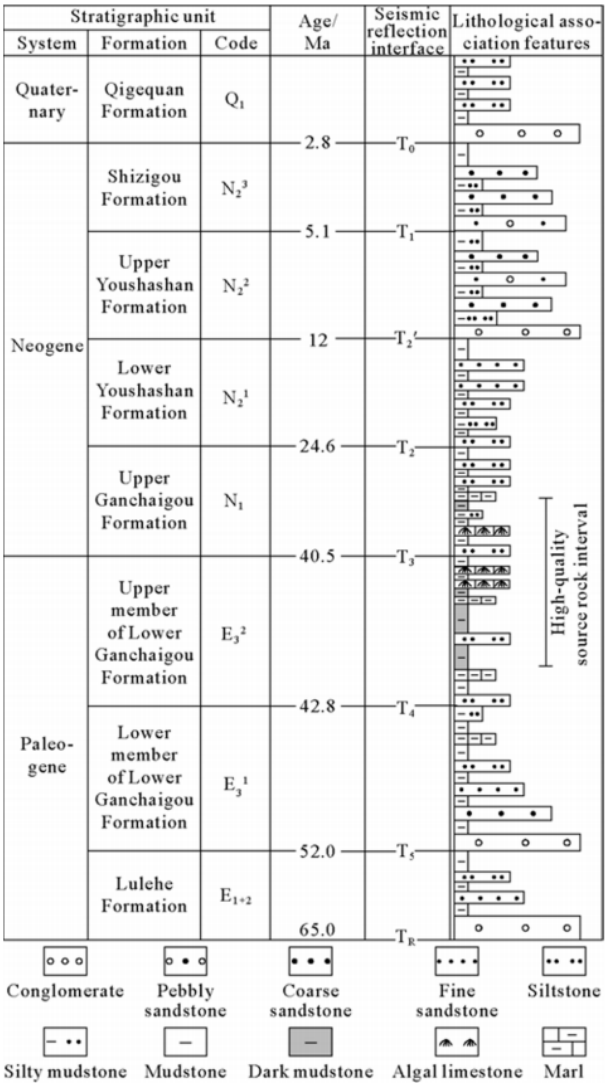

Fig. 2. Composite stratigraphic column of the Cenozoic strata in the western Qaidam Basin.

northeastwards as a rigid block[25-26]. Numerous high-resolution 2D and 3D seismic profiles reveal the crust deformation in northern margin of the Qaidam Basin started in the Eocene[12-13], but the Miocene growth strata developing in Altyn Tagh and East Kunlun piedmont in the western part of the Qaidam Basin indicate the crustal deformation of the East Kunlun Mountain occurred in the Miocene[12-13]. In addition, a set of fine-grained salty lacustrine deposits have been discovered in the Paleogene-Neogene strata in the western Qaidam Basin during oil and gas exploration, which are the major high-quality source rocks in the upper member of Lower Ganchaigou Formation and Upper Ganchaigou Formation (Fig. 2), while the Paleogene in the northern margin of the Qaidam Basin is a set of coarse clastic deposits of foreland basin without source rocks[27]. The geological features and exploration results have provided good foundation for further study of the Qaidam Basin. It can be seen that finding out the tectonic relationship between the Qaidam Basin and its peripheral orogenic belts is the key to revealing the Cenozoic evolution, clarifying the genesis and attributes and the hydrocarbon accumulation theory of the Qaidam Basin.

5.3 Structural features of peripheral Qaidam Basin

5.3.1 Altyn Tagh left-lateral strike-slip fault – North Qaidam thrust system

Altyn Tagh fault, a large left-lateral strike-slip fault at the margin of the Tibetan Plateau, defines the western boundary of the Qaidam Basin (Fig. 1), and its movement controlled the evolution of the Qaidam Basin during the Cenozoic, thereby, exploring the active regularity and tectonic evolution history of the Altyn Tagh fault during the Cenozoic is of great significance for recognizing the Cenozoic evolution of the Qaidam Basin[28-31]. Two key issues need to be clarified in studying the Cenozoic tectonic activity of Altyn Tagh strike-slip fault, the initial duration and displacement of the left-lateral strike-slip movement of Altyn Tagh fault during the Cenozoic. There is controversy over the time when Altyn Tagh fault began to move since India-Eurasia collision, but most researchers consider it is from the Eocene to Miocene[29,32-38](Table 1). For the left-lateral strike-slip displacement of Altyn Tagh fault during the Cenozoic, although different reference points were taken by previous researchers (suture zone, magmatic rock or Jurassic coal line), it is generally estimated at 300~400 km[15,38-48]. The latest paleomagnetic study shows the Qaidam Basin has migrated along Altyn Tagh fault northeastwards since the Eocene, during the course, large-scale vertical rotation doesn't occur[26]. Based on the above understandings, Cheng et al.[38]identified the syntectonic sedimentation related to the left-lateral strike-slip of Altyn Tagh fault during the Cenozoic

through correlating the stratigraphic depositional features between the Qaidam Basin and Tula Basin, and further pointed out that the left-lateral strike-slip movement of Altyn Tagh fault began in Lulehe Period, then sped up after the Miocene, that indicates the Eocene is the initial active time limit for the Altyn Tagh fault and its left-lateral strike-slip displacement is about 360 km.

Table 1. Summary of the initial strike-slip time limit of Altyn Tagh fault.

Number	Initial strike-slip time limit	Study method	Reference
1	About 49 Ma ago	Comprehensive analysis of the Cenozoic profile along Altyn Tagh Mountain	[29]
2	Eocene	Comparative analysis of the Cenozoic strata along Altyn Tagh fault	[38]
3	35.5 Ma ago	Studying the low temperature geochronology of Altyn Tagh basement (fission track)	[36]
4	Oligocene	Comparative analysis of the Oligocene strata between Tarim Basin and Qaidam Basin	[15]
5	Miocene	Analysis of the Cenozoic provenance along Altyn Tagh fault	[33-34]
6	Oligocene to early Miocene	Analysis of the Cenozoic strata along Altyn Tagh fault	[37]
7	Middle Miocene	Studying the low temperature geochronology of Altyn Tagh basement (fission track)	[32]

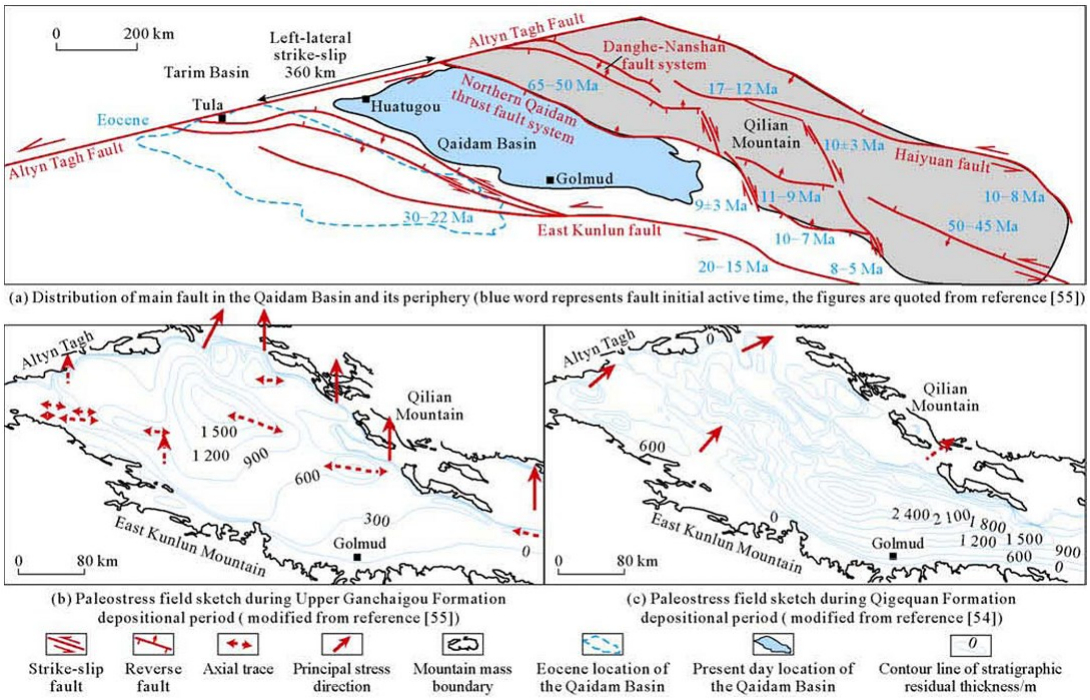

Fig. 3. Main fault distribution and the Paleogene and Neogene principal stress orientation in the Qaidam

Basin and its periphery.

There develop a series of NWW-trending thrust systems in North Qaidam – Qilian South Mountain, the northeastern boundary of the Qaidam Basin, such as the North Qaidam thrust system and Danghe-Nanshan fault system (Figs.1 and 3), among which, North Qaidam thrust system is NWW-SEE trending in plane and northward-dipping in vertical. The faults in this system generally obduct from Qilian Mountain to the basin, some faults have strike-slip component[14,49-50]. The seismic profiles of North Qaidam region reveal that these overthrust faults began to move in the Eocene and has lasted to present day[13-14]. According to field sedimentary record, it is generally believed the North Qaidam-Qilian Mountain began to deform in Eocene Lulehe Period since the collision between India and Eurasia plate[14,51], along with 20%~50% crustal shortening in NE-SW direction[13-14,52-53]. Based on the study on the magnetic fabric of the Cenozoic strata basinwide, Yu et al.[54]found that since the Paleogene, the North Qaidam began to experience compressional stress from north to south, while the southwestern Qaidam Basin was in extensional state, however, since the Neogene, the northern Qaidam Basin began to experience NE-SW compressional stress, the western Qaidam Basin also was affected by NE-SW compressional stress (Fig. 3). The overthrust and strike-slip events of the North Qaidam fault system have reformed the Mesozoic stratigraphic distribution pattern of the northern margin of the Qaidam Basin since Lulehe Period, and the transpression faults and related fold traps formed at the same time provide effective sealing conditions for Jurassic reservoirs[50].

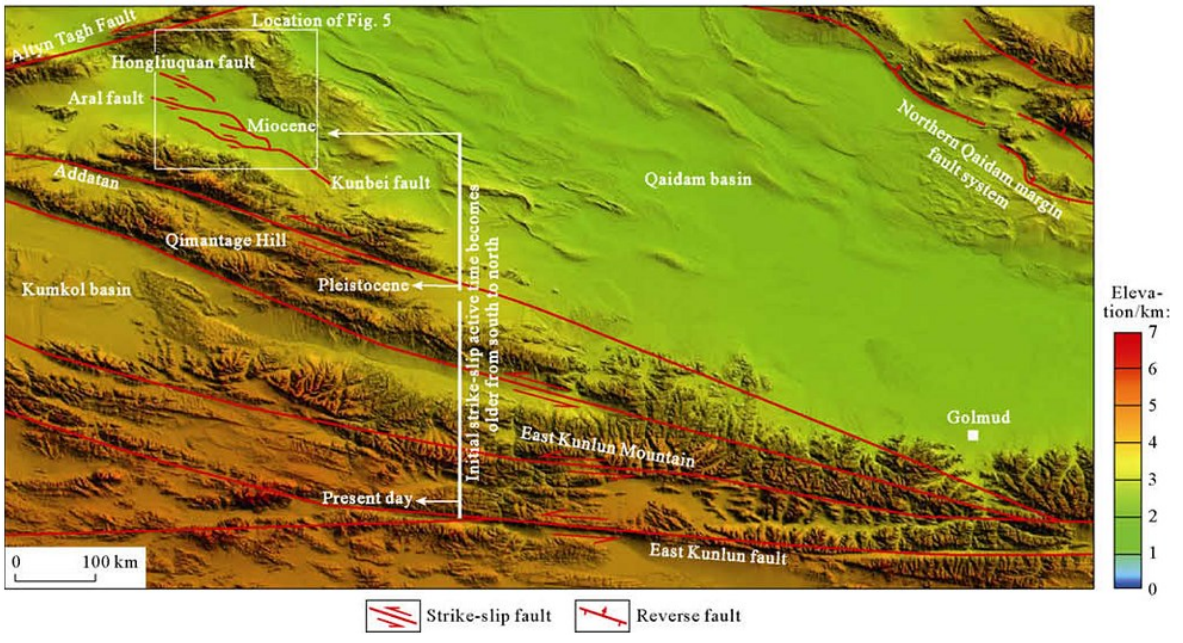

Fig. 4. Northward migration model of the strike-slip fault in the west segment of East Kunlun Mountain, Southwest Qaidam (topographic data adopts the SRTM data with 90 m resolution[17]).

The authors think that the left-lateral strike-slip faulting of the Altyn Tagh fault and the overthrust faulting of the North Qaidam might initiate from the Eocene. In other words, the Altyn Tagh left-lateral strike-slip faults and North Qadam fault system are in the same tectonic system: the Altyn Tagh left-lateral strike-slip initiating in the Paleocene-Eocene resulted in the NW-trending thrust activities of North Qaidam, at the same time the Qaidam began to subside in large scale as a whole. According to the evaluation that the left-lateral strike-slip displacement of Altyn Tagh fault is about 360 km, the Qaidam Basin with a relatively rigid basement has migrated 360 km northeastwards along Altyn Tagh fault as a whole since the Eocene, however, the displacement is adjusted by the NE-SW trending shortening and SE trending extrusion of the crust of North Qaidam-Qilian region. Thus, the Altyn Tagh strike-slip fault has been an important boundary for the Qaidam Basin since the Eocene and the North Qaidam-Qilian overthrust fold fault belt has been a passive adjustment boundary for the Qaidam Basin.

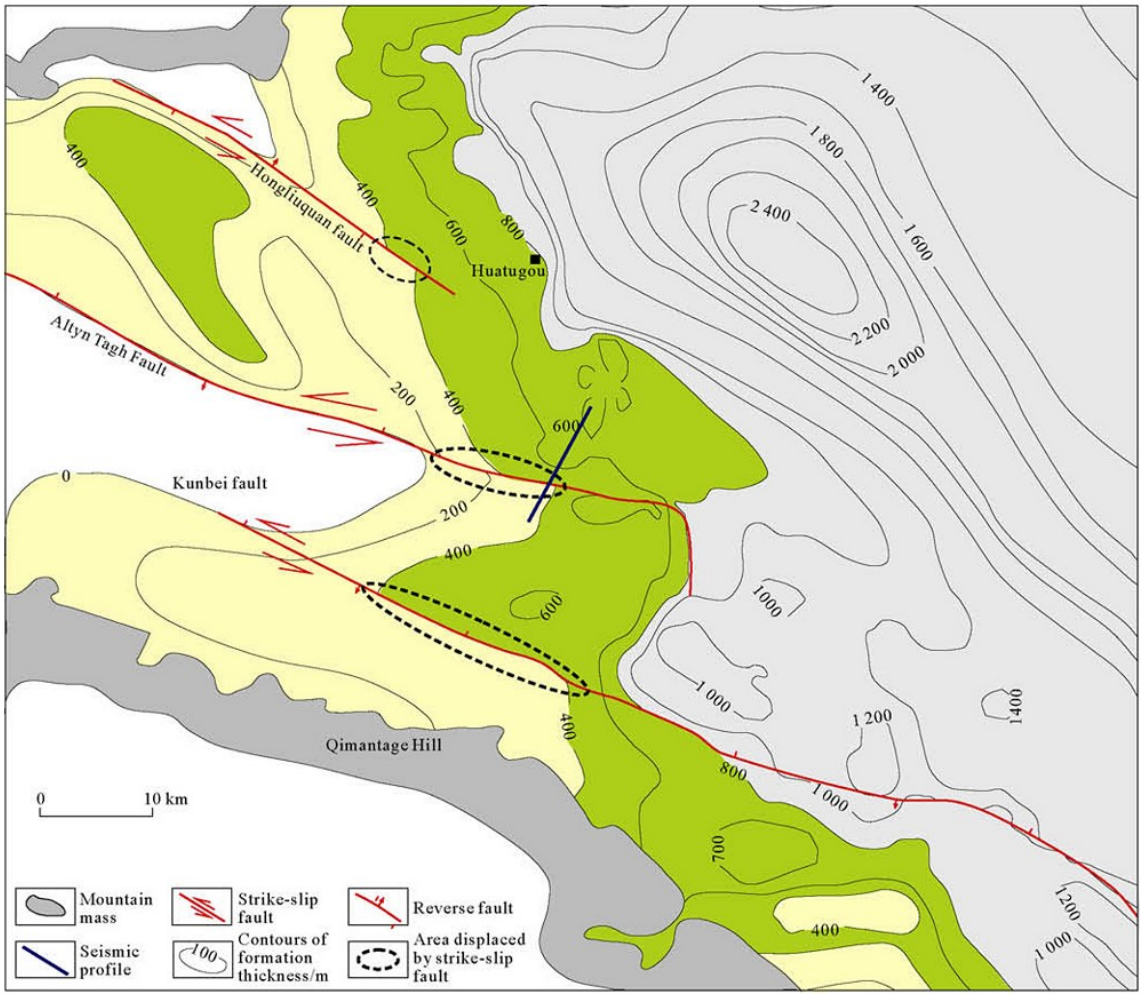

Fig. 5. Formation thickness and fault distribution of the upper member of Lower Ganchaigou Formation in Southwestern Qaidam Basin (Modified from reference [58]).

5.3.2 Left-lateral strike-slip of East Kunlun fault and its superimposed regulation on the basin since the Miocene

Located in the southern margin of the Qaidam Basin, and in W-E trend, the East Kunlun left-lateral strike-slip fault extends westwards through Kunlun Pass, giving rise to a series of arcuate structures composed of linear faults in Qimantage region in the west part[56-59](Figs. 1 and 4). The study on the fission track and $^{40}Ar/^{39}Ar$ low temperature thermochronology of the East Kunlun basement show several rapid cooling events happened to in the East Kunlun Mountain from the Oligocene to Early Miocene, which may be related to the large-scale tectonic movement of the East Kunlun Mountain occurred in the same period[10-11]. Based on the study on the fission track and (U-Th)/He low temperature thermochronology of the East Kunlun basement, Cheng et al.[58]and Duvall et al.[55]concluded the East Kunlun left-lateral strike-slip faulting might initiate from the Oligocene to Miocene, but Yin et al.[12]thought the East Kunlun left-lateral strike-slip faulting initiated in the Oligocene based on the Cenozoic growth strata identified in East Kunlun piedmont and the southern margin of the Qaidam Basin.

There are different opinions about the structural relationship between the East Kunlun Mountain and the Qaidam Basin[6-13]. Previous study reached the finding that there developed a large-scale transpressive system in East Kunlun region, with East Kunlun left-lateral strike-slip fault as southern boundary, and a series of south-dipping faults in the north which control the Cenozoic evolution of the southwestern margin of the Qaidam Basin[6-8,10-11]. But since this model can't reasonably explain the feature that the depocenter of the Qaidam Basin is not closed to East Kunlun Piedmont, Yin et al.[13] proposed an opposite point of view that a large wedge-shaped structure developed in the southern margin of the Qaidam Basin, which obducted the Qaidam Basin onto East Kunlun orogenic belt southwards, leading to the obduction of Qaidam Basin with low altitude onto the Qimantage Hill with relatively high altitude along a series of north-dipp ing Cenozoic faults southwards. This point of view is supported by some geophysical data collected from deep crust[60-61]. Although the southward thrust model can reasonably explain the dish distribution of the Cenozoic strata of the Qaidam Basin, but can't reasonably interpret the genesis of the arcuate structure of the Qimantage Hill in the west segment of the East Kunlun Mountain in plane[57].

Latest study on the distribution and mechanism of natural earthquake sources show the structures of the Southwest Qaidam and Qimantage Hill represent thrust and left-lateral strike-slip features[58] (Fig. 4). Remote sensing image and field geological survey show Qimantage mountain area has the Pleistocene sedimentary record of strike-slip tectonic deformation[58].

In addition, the tectonic and depositional framework of the Southwest Qaidam Basin represents a structural pattern of uplifts and depressions separated by a series of high-angle strike-slip faults, where the major faults include Kunbei Fault, Alar Fault and Hongliuquan Fault, their echelon shape and Eocene displaced by faults are signs of left-lateral strike-slip (Fig. 5). The growth strata identified in the seismic profiles of the southwestern Qaidam Basin indicate left-lateral strike-slip movement began in early Miocene (Fig. 6). In plane, the initial active time of the western branch fault of East Kunlun left-lateral strike-slip fault gradually becomes older from south (present East Kunlun left-lateral active fault) to north (Kunbei fault zone in the Southwest Qaidam Basin) (Fig. 4).

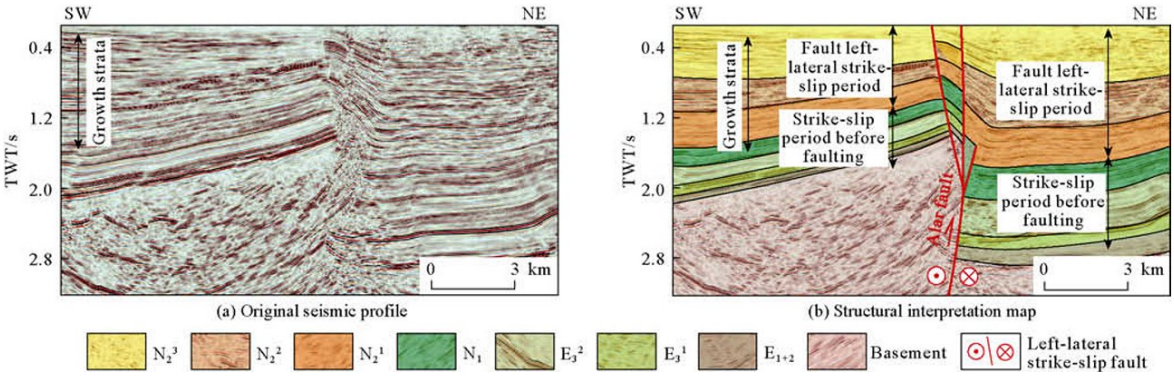

Fig. 6. Alar fault structural profile in Southwestern Qaidam Basin (Profile location is shown in Fig. 5).

Based on the analysis above, the author conclude that the boundary between the East Kunlun Mountain and the Qaidam Basin is neither southward thrust nor simple overthrust, but a strike-slip fault boundary, which is represented by Kunlun left-lateral strike-slip fault. Based on the fact that the initial time of the East Kunlun left-lateral strike-slip faulting in Qimantage region becomes younger from north to south, we think East Kunlun left-lateral strike-slip fault gradually has migrated northwards under the control of Altun Tagh left- lateral strike-slip faulting since early Miocene, during this process, left-lateral strike-slip attribute has gradually transited into northward thrust and left-lateral strike-slip attribute (Fig. 7), that means the East Kunlun left-lateral strike-slip fault has been an important strike-slip adjustment boundary since Neogene.

5.4 Structural control of the strike-slip superimposed Qaidam Basin on oil and gas accumulation

5.4.1 Distribution of sourcerocks in the Qaidam Basin

Exploration results reveal that there are three sets of important petroleum systems in the Qaidam Basin, including Jurassic, Paleogene-Neogene and Quaternary petroleum systems [62-

[63], among which, Jurassic petroleum system mainly occurs in the northern margin of the Qaidam basin, and its source rocks are predominantly composed of Lower Jurassic (J_{1+2}) dark coal measure mudstone (Fig. 8).

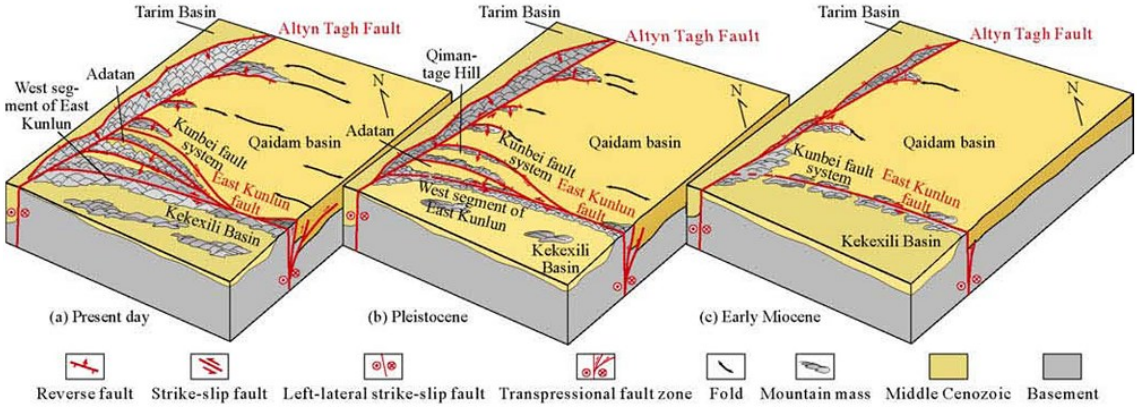

Fig. 7. Northward migration model of strike-slip fault in Southwestern Qaidam Basin (Modified from reference [58]).

Not developed in the northern margin of the Qaidam Basin, but developed in the Western Qaidam Basin, Paleogene-Neogene effective source rocks have features of typical salt lake source rocks [27,63]. The source rocks in the Western Qaidam Basin are characterized by low abundance of organic matter, high conversion rate and large hydrocarbon generation potential, leading to the occurrence of oil and gas rich sags in the Western Qaidam Basin (Fig. 8). Occurring in multiple series, wide in distribution and large in thickness, the Paleogene-Neogene source rocks in the Western Qaidam Basin predominantly are distributed in Upper Lulehe Formation (E_{1+2}), Lower Ganchaigou Formation (E_3), Upper Ganchaigou Formation (N_1), Lower Youshashan Formation (N_2^1) and Upper Youshashan Formation (N_2^2) in Mangya Sag, among which, the major source rocks in the upper member of Eocene Lower Ganchaigou Formation (E_3^2) and Oligocene Upper Ganchaigou Formation (N_1), are characterized by high carbonate content, low organic matter abundance and high hydrocarbon conversion rate, and give rise to various types of reservoirs, such as structural and stratigraphic-lithological reservoirs[27]. Previous researchers concluded the oil and gas reservoirs in the Western Qaidam Basin were mainly formed in middle-late Himalayan Period, especially in late N_2^1 and N_2^3-Q Period through dissecting the typical oilfield structures, such as Gasi, Wunan, Hongliuyan, Qie6, Nanyishan and Youquanzi in the Western Qaidam Basin and comprehensive regional geologic analysis[27]. The hydrocarbon accumulation features and time indicate the oil and gas reservoirs in the Western Qaidam Basin are closely related to the tectonic movement of late stage, the hydrocarbon accumulation phase and time correspond to the activity of East Kunlun strike-slip fault and its control on basin very well, especially for the reservoirs formed in 15-8

Ma ago (about late N_2^1) and the reservoirs formed in 4 Ma ago[27].

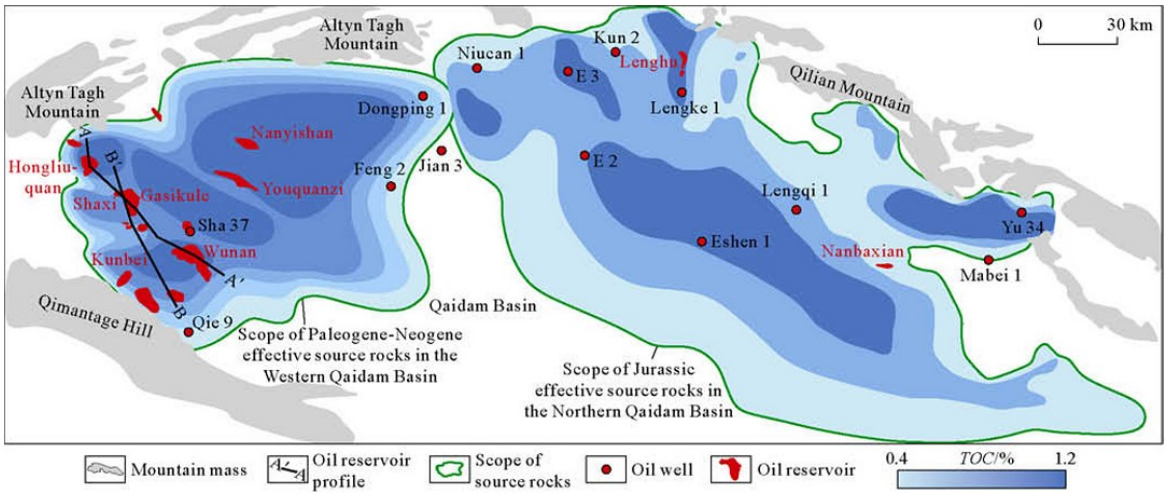

Fig. 8. Distribution of source rocks and oil and gasin Qaidam Basin (Modified from reference [27]).

Under the jointly effect of Qimantage Mountain thrust fault system and Altyn Tagh left-lateral strike-slip faults, a large number of NW-NWW trending, NE trending and nearly N-S trending faults develop in the Western Qaidam Basin[57,64].

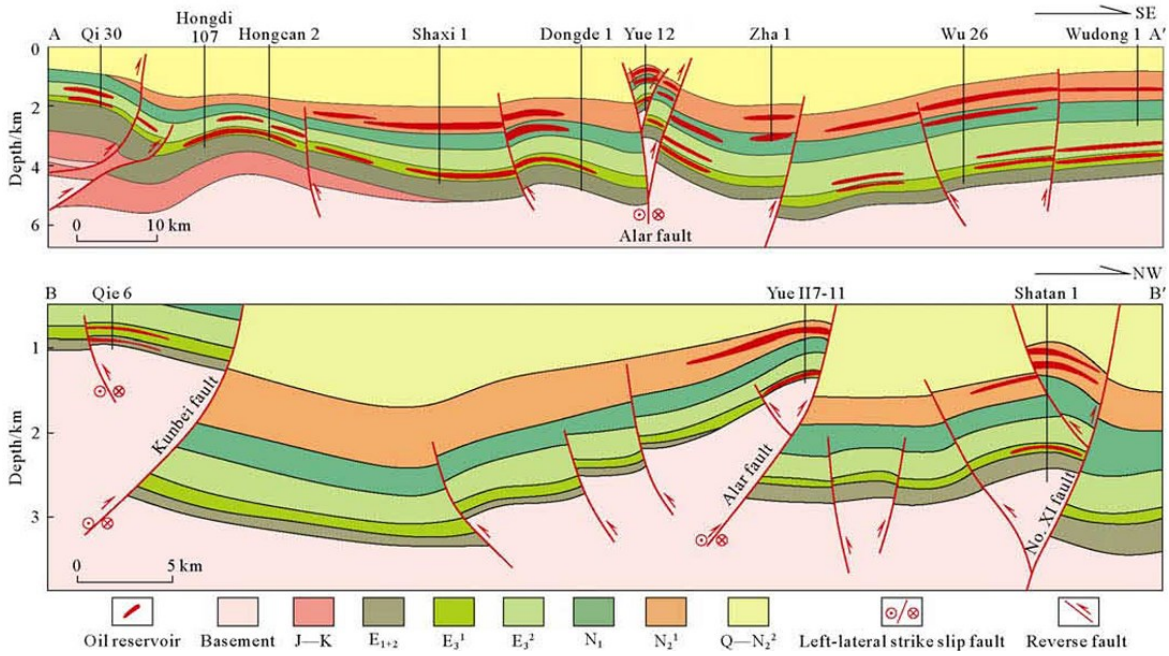

Fig. 9. Typical oil reservoir profile in Southwestern Qaidam Basin (Profile locatin is shown in Fig. 8).

The reservoirs in the Western Qaidam Basin are generally associated with fault structures[65]. Shaxi-Gasikule oil and gas accumulation zones distributing along Alar, No.XI fault (Figs. 8 and 9), the large oil and gas reservoirs discovered in Yingxi, Youshashan and Yingdong structure along the southern margin of Yingxiong Ridge are all closely related to the late Cenozoic fault belt; structural-stratigraphic-lithologic composite reservoirs distributing along Hongliuquan fault in Altyn Tagh piedmont zone, are controlled by fault nose

structure. In addition, structural-fractured reservoirs are distributed along Nanyishan fault and Jiandingshan fault (Figs. 8 and 9). Therefore, the strike-slip related faults developed since Neogene are of great significance for the trap formation and hydrocarbon accumulation in the western Qaidam Basin[64-65].

5.4.2 Control of strike-slip superimposed basin on oil and gas accumulation

A new theoretical model that the Qaidam Basin is a strike-slip superimposed basin jointly controlled by the left-lateral strike-slip Altyn Tagh and East Kunlun faults is proposed through systematically analyzing the structural relationship between the Qaidam Basin and its periphery orogenic belts.

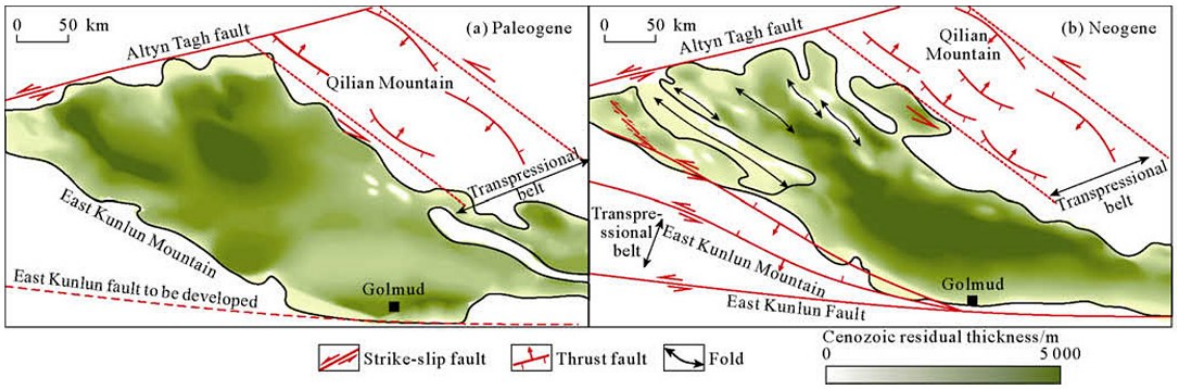

Fig. 10. Cenozoic tectonic - sedimentary evolution schematic of the Qaidam Basin and its periphery.

Since the Eocene (Fig. 10a), Altyn Tagh began left-lateral strike-slip movement, affected by which, the Qaidam Basin with a relatively rigid basement gradually has migrated northeastwards along Altyn Tagh left-lateral strike-slip fault, resulting in the shortening of crust in the northern Qaidam Basin-Qilian region in NE-SW direction since the Eocene, thereby, the northern Qaidam Basin seems a foreland basin of Qilian Mountain. There deposited a set of coarse-grained clastic strata but no high-quality source rocks in the northern Qaidam Basin during the Paleogene. At the same time, the southwestern Qaidam Basin was in extensional stress field, representing as a depression in tenso-shear context, thereby, a set of fine-grained strata deposited, acting as high-quality source rocks.

Since the Miocene (Fig. 10b), the East Kunlun fault system started left-lateral strike-slip movement, along with the northeastward migration of the Qaidam Basin, the west segment of the East Kunlun left-lateral strike-slip fault gradually migrated southwards, forming a series of en echelon faults (such as Kunbei fault, Alar fault, Qimantage Hill fault). The formation of these strike-slip fault systems and their continuous northward migration as well as the rapid uplifting of East Kunlun Mountain and Qimantage Mountain resulted in the transition from

extensional background into compressional background under the compressional stress of NE-NW trending in western Qaidam Basin since Miocene, thus, the Neogene strata in the western Qaidam Basin are composed of the clastic sediments with grain size gradually increasing from bottom to top. The strike-slip related structures formed during Miocene (Kunbei fault, No. XI fault, Alar fault, Hongliuquan fault and Yingxiong Ridge) are ideal places for oil and gas accumulation and the fracture systems developed along fault zone are one of the important factor to improve reservoir petrophysical properties.

Altyn Tagh strike-slip fault is an important controlling boundary of the Qaidam Basin, which controlled the development and migration of different Cenozoic depocenters since Eocene; North Qaidam-Qilian thrust fold fault zone is the passive adjustment boundary of Qaidam Basin, which has suffered compression and deformation in NE-SW direction since the Eocene; East Kunlun left-lateral strike-slip fault is the positive superimposed adjustment boundary of the basin, its left-lateral strike-slip movement and migration lay foundation for the tectonic style of the Western Qaidam Basin and has become an important oil and gas accumulation controlling factor. The temporal and spatial superimposition of Altyn Tagh and East Kunlun strike-slip faults as well as North Qaidam-Qilian fold thrust fault zone give rise to the unique tectonic features of strike-slip superimposed basin and has controlled the oil and gas accumulation of the Qaidam Basin since Cenozoic.

In recent years, along with thinking innovation and technical progress, major exploration breakthroughs have been successively achieved in Qiekelike, Yingdong, Dongping, Niudong and Yingxi regions, indicating the Qaidam Basin is a plateau basin with great exploration potential. The gradual maturation of the new concept of Qaidam “strike-slip superimposed basin” and the continuous improvement in the hydrocarbon accumulation theory with strike-slip superimposed basin characteristics will create a new phase for the oil and gas exploration of the Qaidam Basin and provide solid theoretical support for accelerating construction of a plateau oil and gas field of ten million tons order.

Reference

[1] Compiling Group of Petroleum Geology in Tibet Oil and Gas Area. Petroleum geology of China: Vol. 14. Beijing: Petroleum Industry Press, 1990: 331–482.

[2] Xia Wenchen, Zhang Ning, Yuan Xiaoping, et al. Cenozoic Qaidam Basin, China: A stronger tectonic inversed, extensional rifted basin. AAPG Bulletin, 2001, 85(4): 715–736.

[3] Zhao Wenzhi, Zhang Guangya, Wang Hongjun, et al. Basic features of petroleum geology in the superimposed petroliferous basins of China and their research methodologies.

Petroleum Exploration and Development, 2003, 30(2): 1–8.

[4] He Dengfa, Jia Chengzao, Tong Xiaoguang, et al. Discussion and analysis of superimposed sedimentary basins. Petroleum Exploration and Development, 2004, 31(1): 1–7.

[5] Jin Zhijun, Zhang Mingli, TangLiangjie, et al. Evolution of Meso-Cenozoic Qaidam Basin and its control on oil and gas. Oil & Gas Geology, 2004, 25(6): 603–608.

[6] Burchfiel B C, Deng Q D, Molnar P, et al. Intracrustal detachment within zones of continental deformation. Geology, 1989, 17(8): 748–752.

[7] Meyer B, Tapponnier P, Bourjot L, et al. Crustal thickening in Gansu-Qinghai, lithospheric mantle subduction, and oblique, strike-slip controlled growth ofthe Tibet Plateau. Geophysical Journal International, 1998, 135(1): 1–47.

[8] Tapponnier P, Xu Z Q, Roger F,et al. Oblique stepwise rise and growth of the Tibet Plateau. Science, 2001, 294: 1671–1677.

[9] Chen W P, Chen C Y, Nábelek J L. Present-day deformation of the Qaidam Basin with implications for intra-continental tectonics. Tectonophysics, 1999, 305(1/2/3): 165–181.

[10] Mock C, Arnaud N O, Cantagrel J M. An early unroofing in northeastern Tibet constraints from $^{40}Ar/^{39}Ar$ thermochronology on granitoids from the eastern Kunlun range (Qianghai, NW China). Earth and Planetary Science Letters, 1999, 171(1): 107–122.

[11] Jolivet M, Brunel M, Seward D, et al. Mesozoic and Cenozoic tectonics of the northern edge of the Tibetan Plateau: Fission-track constraints. Tectonophysics, 2001, 343(1/2): 111–134.

[12] Yin A, Dang Y Q, Zhang M,et al. Cenozoic tectonic evolution of Qaidam Basin and its surrounding regions (part 2): Wedge tectonics in southern Qaidam Basin and the Eastern Kunlun range. Geological Society of America, Special Papers, 2007, 433: 369–390.

[13] Yin A, Dang Y Q, Zhang M,et al. Cenozoic tectonic evolution of the Qaidam Basin and its surrounding regions (Part 3): Structural geology, sedimentation, and regional tectonic reconstruction. Geological Society of America Bulletin, 2008, 120(7/8): 847–876.

[14] Yin A, Dang Y Q, Wang L C, et al. Cenozoic tectonic evolution of Qaidam Basin and its surrounding regions (Part 1): The southern Qilian Shan-Nan Shan thrust belt and northern Qaidam Basin. Geological Society of America Bulletin, 2008, 120(7/8): 813–846.

[15] Meng Q R, Hu J M, Yang F Z. Timing and magnitude of displacement on the Altyn Tagh fault: Constraints from stratigraphic correlation of adjoining Tarim and Qaidam Basins, NW China. Terra Nova, 2001, 13(2): 86–91.

[16] Meng Q R, Fang X. Cenozoic tectonic development of the Qaidam Basin in the

northeastern Tibetan Plateau. Geological Society of America, Special Papers, 2008, 444: 1–24.

[17] CGIAR. SRTM 90m digital elevation data. (2008-08-19) [2015-05-20]. http://srtm.csi.cgiar.org.

[18] Fang Xiaoming, Zhang Weilin, Meng Qingquan, et al. High-resolution magnetostratigraphy of the Neogene Huaitoutala section in the eastern Qaidam Basin on the NE Tibetan Plateau, Qinghai Province, China and its implication on tectonic uplift of the NE Tibetan Plateau. Earth and Planetary Science Letters, 2007, 258(1/2): 293–306.

[19] Lu Haijian, Xiong Shangfa. Magnetostratigraphy of the Dahonggou Section, northern Qaidam Basin and its bearing on Cenozoic tectonic evolution ofthe Qilian Shan and Altyn Tagh fault. Earth and Planetary Science Letters, 2009, 288(3): 539–550.

[20] Huang Hanchun, Huang Qinghua, Ma Yongsheng. Geology of Qaidam Basin and its petroleum prediction. Beijing: Geological Publishing House, 1996.

[21] Yang Fan, Ma Zhiqiang, Xu Tongchun, et al. A Tertiary paleomagnetic stratigraphic profile in Qaidam Basin. Acta Petrolei Sinica, 1992, 13(2): 97–101.

[22] Sun Jimin, Zhu Rixiang, An Zhishen. Tectonic uplift in the northern Tibetan Plateau since 13.7 Ma ago inferred from molasse deposits along the Altyn Tagh fault. Earth and Planetary Science Letters, 2005, 235(3): 641–653.

[23] Ke Xue, Ji Junliang, Zhang Kexin, et al. Magnetostratigraphy and anisotropy of magnetic susceptibility of the Lulehe Formation in the Northeastern Qaidam Basin. Acta Geologica Sinica: English Edition, 2013, 87(2): 576–587.

[24] Rieser A B, Liu Yongjiang, Genser J, et al. $^{40}Ar/^{39}Ar$ ages of detrital white mica constrain the Cenozoic development of the intracontinental Qaidam Basin, China. GSA Bulletin, 2006, 118(11/12): 1522–1534.

[25] Yu Xiangjiang, Fu Suotang, Guan Shuwei, et al. Paleomagnetism of Eocene and Miocene sediments from the Qaidam Basin: Implication for no integral rotation since the Eocene and a rigid Qaidam Block. Geochemistry, Geophysics, Geosystems, 2014, 15(6): 2109–2127.

[26] Wang Erchie, Xu Fengyin, Zhou Jianxun, et al. Eastward migration of the Qaidam Basin and its implications for Cenozoic evolution of the Altyn Tagh fault and associated river systems. Geological Society of America Bulletin, 2006, 118(3/4): 349–365.

[27] Fu Suotang. Key controlling factors of oil and gas accumulation in the western Qaidam Basin and its implications for favorable exploration direction.Acta Sedimentologica Sinica, 2010, 28(2): 373–379.

[28] Molnar P, Tapponnier P. Cenozoic tectonics of Asia: Effects of a continental collision. Science, 1975, 189: 419–426.

[29] Yin An, Rumelhart P, Butler R, et al. Tectonic history of the Altyn Tagh fault system in northern Tibet inferred from Cenozoic sedimentation. GeologicalSociety of America Bulletin, 2002, 114(10): 1257–1295.

[30] Robinson D M, Dupont-Nivet G,Gehrels G E, et al. The Tula uplift, northwestern China: Evidence for regional tectonism of the northern Tibetan Plateau during late Mesozoic–early Cenozoic time. Geological Society of America Bulletin, 2003, 115(1): 35–47.

[31] Peltzer G, Tapponnier P. Formation and evolution of strike-slip faults, rifts, and basins during the India-Asia collision: An experimental approach. Journal of Geophysical Research: Solid Earth(1978-2012), 1988, 93(B12): 15085–15117.

[32] Wan Jinglin, Wang Yu, Li Qi, et al. FT evidence of northern Altyn uplift in Late-Cenozoic. Bulletin of Mineralogy, Petrology and Geochemistry, 2001, 20(4): 222–224.

[33] Wu Lei, Xiao Ancheng, Yang Shufeng, et al. Two-stage evolution of the Altyn Tagh fault during the Cenozoic: New insight from provenance analysis of a geological section in NW Qaidam Basin, NW China. Terra Nova, 2012, 24(5): 387–395.

[34] Wu Lei, Xiao Ancheng, Wang Liang, et al. EW-trending uplifts along the southern side of the central segment of the Altyn Tagh fault, NW China: Insight into the rising mechanism of the Altyn Mountain during the Cenozoic. SCIENCE CHINA Earth Sciences, 2012, 55(6): 926–939.

[35] Wang Liang, Xiao Ancheng,Gong Qinglin, et al. The unconformity in Miocene sequence of western Qaidam Basin and its tectonic significance. SCIENCE CHINA Earth Sciences, 2010, 53(8): 1126–1133.

[36] Chen Zhengle, Zhang Yueqiao, Wang Xiaofeng, et al. Fission track dating of apatite constrainson the Cenozoic uplift of the Altyn Tagh Mountain. Acta Geoscientia Sinica, 2001, 22(5): 413–418.

[37] Yue Yongjun, Ritts B D, Graham S A. Initiation and long-term slip history of the Altyn Tagh fault. International Geology Review, 2001, 43(12): 1087–1093.

[38] Cheng Feng, Guo Zhaojie, Jenkins H S, et al. Initial rupture and displacement on the Altyn Tagh fault, northern Tibetan Plateau: Constraints based on residual Mesozoic to Cenozoic strata in the western Qaidam Basin. Geosphere, 2015, 11(3): 921–942.

[39] Cowgill E, Yin An, Harrison T M, et al. Reconstruction of the Altyn Tagh fault based on U-Pb geochronology: Role of back thrusts, mantle sutures, and heterogeneous crustal

strength in forming the Tibetan Plateau. Journal of Geophysical Research, 2003, 108(B7): 2346.

[40] Che Zicheng, Liu Liang, Liu Hongfu, et al. The constituents of the Altun fault system and genetic characteristics of related Meso-Cenozoic petroleum-bearing basin. Regional Geology of China, 1998, 17(4): 377–384.

[41] Ge Xiaohong, Liu Junlai. Formation and tectonic background of the northern Qilian orogenic belt. Earth Science Frontiers, 1999, 6(4): 223–230.

[42] Yue Yongjun, Liou J G. Two-stage evolution model for the Altyn Tagh fault, China. Geology, 1999, 27(3): 227–230.

[43] Gehrels G E, Yin An, Wang Xiaofeng. Magmatic history of the northeastern Tibetan Plateau. Journal of Geophysical Research, 2003, 108(B9): 2423.

[44] Yang Jinsui, Xu Zhiqin, Zhang Jianxin, et al. Tectonic significance of early Paleozoic high-pressure rocks in Altun-Qaidam-Qilian Mountains, northwest China. Geological Society of America Memoirs, 2001, 194: 151–170.

[45] Zhang Jianxin, Zhang Zeming, Xu Zhiqin, et al. Petrology and geochronology of eclogites from the western segment of the Altyn Tagh, northwestern China. Lithos, 2001, 56(2): 187–206.

[46] Gehrels G, Yin A, Chen X, etal. Constraints on the offset of the eastern Altyn Tagh fault, western China. EOS: Transactions of the American Geophysical Union, 2000, 81: F1093.

[47] Sobel E R, Arnaud N, JolivetM, et al. Jurassic to Cenozoic exhumation history of the Altyn Tagh range, northwest China, constrained by $^{40}Ar/^{39}Ar$ and apatite fission track thermochronology. In: Paleozoic and Mesozoic tectonic evolution of central Asia: From continental assembly to intracontinental deformation. Boulder, CO: Geological Society of America, 2001, 194: 247–267.

[48] Ritts B D, Biffi U. Magnitude of post-Middle Jurassic (Bajocian) displacement on the central Altyn Tagh fault system, northwest China. Geological Society of America Bulletin, 2000, 112(1): 61–74.

[49] Wang Guihong, Ma Dade, Zhou Chuanmin, et al. The seismic profile interpretation and development mechanism of strike-slip faults in northern Qaidam Basin. Acta Geoscientica Sinica, 2011, 32(2): 204–210.

[50] Wei Guoqi, Li Benliang, XiaoAncheng, et al. Strike-thrust structures and petroleum exploration in northern Qaidam Basin. Earth Science Frontiers, 2005, 12(4): 397–402.

[51] Zhuang Guangsheng, Hourigan J K, Ritts B D, et al. Cenozoic multiple-phase tectonic

evolution of the northern Tibetan Plateau: Constraints from sedimentary records from Qaidam Basin, Hexi Corridor, and Subei Basin, northwest China. American Journal of Science, 2011, 311(2): 116–152.

[52] Bally A W, Chou I M, Clayton R, et al. Notes on sedimentary basins in China, report of the American sedimentary basins delegation to the People's Republic of China. Washington: US Geological Survey, 1986.

[53] Zhang Huiping, Zhang Peizheng, Zheng Dewen, et al. Transforming the Miocene Altyn Tagh fault slip into shortening of the north-western Qilian Shan: Insights from the drainage basin geometry. Terra Nova, 2014, 26(3): 216–221.

[54] Yu Xiangjiang, Huang Baochun, Guan Shuwei, et al. Anisotropy of magnetic susceptibility of Eocene and Miocene sediments in the Qaidam Basin, northwest China: Implication for Cenozoic tectonic transition and depocenter migration. Geochemistry, Geophysics, Geosystems, 2014, 15(6): 2095–2108.

[55] Duvall A R, Clark M K, Kirby E, et al. Low-temperature thermochronometry along the Kunlun and Haiyuan faults, NE Tibetan Plateau: Evidence for kinematic change during late-stage orogenesis. Tectonics, 2013, 32(5): 1190–1211.

[56] Kirby E, Reiners P W, Krol M A, et al. Late Cenozoic evolution of the eastern margin of the Tibetan Plateau: Inferences from $^{40}Ar/^{39}Ar$ and (U-Th)/He thermochronology. Tectonics, 2002, 21(1): 1–20.

[57] Fu Bihong, Awata Y. Displacement and timing of left-lateral faulting in the Kunlun fault zone, northern Tibet, inferred from geologic and geomorphic features. Journal of Asian Earth Sciences, 2007, 29(2): 253–265.

[58] Cheng Feng, Jolivet M, Fu Suotang, et al. Northward growth of the Qimen Tagh range: A new model accounting for the Late Neogene strike-slip deformation of the SW Qaidam Basin. Tectonophysics, 2014, 632: 32–47.

[59] Jolivet M, Brunel M, Seward D, et al. Neogene extension and volcanism in the Kunlun fault zone, northern Tibet: New constraints on the age of the Kunlun fault. Tectonics, 2003, 22(5): 1052.

[60] Shi Danian, Shen Yang, Zhao Wenjin, et al. Seismic evidence for a Moho offset and south-directed thrust at the easternmost Qaidam–Kunlun boundary in the Northeast Tibetan Plateau. Earth and Planetary Science Letters, 2009, 288(1/2): 329–334.

[61] Wang Chengshan, Gao Rui, Yin An, et al. A mid-crustal strain-transfer model for continental deformation: A new perspective from high-resolution deep seismic-reflection profiling across NE Tibet. Earth and Planetary Science Letters, 2011, 306(3): 279–288.

[62] Zhao Fan, Sun Deqiang, Yan Cunfeng, et al. Meso-Cenozoic evolution of the Qaidam Basin and its relationship with oil and gas accumulation. Natural Gas and Geoscience, 2013, 24(5): 940–947.

[63] Xu Fengyin, Peng Dehua, Hou Enke. Hydrocarbon accumulation and exploration potential in Qaidam Basin. Acta Petrolei Sinica, 2003, 24(4): 1–6.

[64] Fang Xiang, Jiang Bo, Zhang Yongshu. Faulted structure and hydrocarbon accumulation in western Qaidam Basin. Oil & Gas Geology, 2006, 27(1): 56–61.

[65] Chen Shaojun, Luo Qun, Wang Tiecheng, et al. Faulting characteristics and effects on the hydrocarbon distribution in Qaidam Basin. Xinjiang Petroleum Geology, 2004, 25(1): 22–25.

Chapter 6 Conclusions and Follow-up research

6.1 General Conclusions

The main objective of my PhD dissertation is to understand the Cenozoic evolution of the Qaidam basin and its surrounding regions, North Tibet (including Eastern Kunlun Range, Altyn Tagh Range, and Qilian Shan). The major contributions from this thesis are that:

A. The SW Qaidam Basin has been bordered by a series of strike-slip faults to the south since the Early Miocene, rather than by a continuous northward or southward thrusting system. The SW Qaidam Basin did not suffer a major N–S compression and shortening before the Early Miocene.

B. The Eastern Kunlun Range was already exhumed prior to the Paleocene. From the Late Eocene to Oligocene, the southward expanding Qaidam basin may locally inundate the eastern Kunlun Range and connect with the Kumukol basin or even the Hoh Xil basin to the south. Since the Miocene, the intense uplifting of the Eastern Kunlun Range separated the Qaidam basin and Hoh Xil basin.

C. An early-middle Eocene initiation of left-lateral strike-slip faulting is determined and a 360 ± 40 km offset along the Altyn Tagh fault since its Cenozoic reactivation is estimated. The enhanced tectonic activity within the Altyn Tagh Range and northwestern Qaidam basin from Miocene time is also suggested.

D. Based on the 360 km northeastward migration of the relatively rigid Qaidam block along the Altyn Tagh Fault and 3D isovolumetric balance of the crustal deformation within the Altyn Tagh Fault – Qilian Shan system, I demonstrate that 250 ± 28 km (43.8~49.4 %) of N20E directed crustal shortening and an additional ~250 to ~370 km of eastward motion of the Qilian Shan crust must be accounted for by strike-slip faulting in the Qilian Shan and crustal thickening in the Qinling area, as well as extension in the adjoining North China block graben systems.

E. Collectively, the Qaidam Basin is not a foreland basin nor an extensional basin, but a strike-slip superimposed basin jointly controlled by the left-lateral strike-slip Altyn Tagh and East Kunlun faults. The Altyn Tagh fault acts as the major controlling boundary, while the East Kunlun fault only controls the local evolution of the southern edge of the basin. The temporal and spatial superimposition of these two strike-slip faults during the Cenozoic controlled the evolution of the basin as well as the oil and gas accumulation.

6.2 Follow-up research

Based on my recent research on the Cenozoic tectonic evolution of the northern Tibetan plateau, I would like to address three issues:

A. The early stage (Paleocene-Eocene, Lulehe Fm.) of the northern Tibetan plateau since the India-Asian collision is still poorly constrained. In my thesis (Chapter 2.2), I suggest that the Eastern Kunlun Range was already exhumed prior to the Paleocene. In order to obtain better constraints on the early stage of the plateau, I would like to employ O isotopes and clumped isotopes to study the paleoelevation and paleoclimate. In addition, magnetostratigraphy study on well-exposed, continuous outcrops of Paleocene-Eocene strata (Lulehe Fm.) within the Qaidam basin would also provide a useful, detailed calendar for the deposition of that formation and the corresponding paleoenvironment evolution.

B. In recent years, the Miocene deformation phase (~15 Ma) has been widely studied in the northern Tibetan plateau. In particular, a middle Miocene reorganization of the deformation has been recognized. This reorganization can be summarized as: prior to the Miocene, the north-northeastern margin of the Tibetan Plateau was characterized primarily by compressive structures accommodating N or NE convergence beginning roughly at the onset of the India-Eurasia collision (Eocene); These compressive structures were gradually overprinted by the Miocene-Pliocene initiation of near E-W or NWW-SEE strike-slip faults, such as the Kunlun and Haiyuan faults. Identifying how the regional climate responded to this intense Miocene deformation in the northern Tibetan plateau would be a significant attempt for exploiting the interplay between tectonics and climate.

Reference

Arnaud, N., Tapponnier, P., Roger, F., Brunel, M., Scharer, U., Chen, W., Xu, Z., 2003. Evidence for Mesozoic shear along the western Kunlun and Altyn‐Tagh fault, northern Tibet (China). Journal of Geophysical Research: Solid Earth (1978–2012) 108.

Bally, A.W., Chou, I.-M., Clayton, R., Eugster, H.P., Kidwell, S., Meckel, L.D., Ryder, R.T., Watts, A.B., Wilson, A.A., 1986.Notes on sedimentary basins in China—report of the American Sedimentary Basins delegation to the People's Republic of China. U.S. Geological Survey Open-File Report, 108, pp. 86–327.

Basilevsky, A.T., Head, J.W., 2007. Beta Regio, Venus: Evidence for uplift, rifting, and volcanism due to a mantle plume. Icarus 192, 167-186.

Bovet, P.M., Ritts, B.D., Gehrels, G., Abbink, A.O., Darby, B., Hourigan, J., 2009. Evidence of Miocene crustal shortening in the north Qilian Shan from Cenozoic stratigraphy of the western Hexi Corridor, Gansu Province, China. American Journal of Science 309, 290-329.

Burchfiel, B.C., Quidong, D., Molnar, P., Royden, L., Yipeng, W., Peizhen, Z., Weiqi, Z., 1989. Intracrustal detachment within zones of continental deformation. Geology 17, 748-752.

Burchfiel, B., Zhang, P., Wang, Y., Zhang, W., Song, F., Deng, Q., Molnar, P., Royden, L., 1991. Geology of the Haiyuan fault zone, Ningxia‐Hui Autonomous Region, China, and its relation to the evolution of the northeastern margin of the Tibetan Plateau. Tectonics 10, 1091-1110.

Chen, W.P., Chen, C.Y., L Nábelek, J., 1999. Present-day deformation of the Qaidam basin with implications for intra-continental tectonics. Tectonophysics 305, 165-181.

Chen, Z.L., Zhang, Y.Q., Wang , X.F., Chen, X.H., 2001. Fission Track Dating of Apatite Constrains on the Cenozoic Uplift of the Altyn Tagh Mountain. GEOSCIENTIA SINICA Acta Geoscientia Sinica 22, 413-418 (in Chinese with English abstract).

Chen, X.H., Yin, A., Gehrels, G.E., Cowgill, E.S., Grove, M., Harrison, T.M., Wang, X.F., 2003. Two phases of Mesozoic north-south extension in the eastern Altyn Tagh range, northern Tibetan Plateau. Tectonics 22, 1053.

Chen, X., Gehrels, G., Yin, A., Zhou, Q., Huang, P., 2015. Geochemical and Nd–Sr–Pb–O isotopic constrains on Permo–Triassic magmatism in eastern Qaidam Basin, northern Qinghai-Tibetan plateau: Implications for the evolution of the Paleo-Tethys. Journal of Asian Earth Sciences 114, Part 4, 674-692.

Clark, M.K., Farley, K.A., Zheng, D., Wang, Z., Duvall, A.R., 2010. Early Cenozoic faulting of the northern Tibetan Plateau margin from apatite (U–Th)/He ages. Earth and Planetary Science Letters 296, 78-88.

Cheng, F., Jolivet, M., Fu, S., Zhang, Q., Guan, S., Yu, X., Guo, Z., 2014. Northward growth of the Qimen Tagh Range: A new model accounting for the Late Neogene strike-slip deformation of the SW Qaidam Basin. Tectonophysics 632, 32-47.

Cheng, F., Fu, S., Jolivet, M., Zhang, C., Guo, Z., 2016. Source to sink relation between the Eastern Kunlun Range and the Qaidam Basin, northern Tibetan Plateau, during the Cenozoic. Geological Society of America Bulletin 128, 258-283.

Cobbold, P., Davy, P., 1988. Indentation tectonics in nature and experiment. 2. Central Asia, Bull. Geol. Inst. Univ. Uppsala 14, 143-162.

Cowgill, E., Yin, A., Harrison, T.M., Xiao-Feng, W., 2003. Reconstruction of the Altyn Tagh fault based on U-Pb geochronology: Role of back thrusts, mantle sutures, and heterogeneous crustal strength in forming the Tibetan Plateau. Journal of Geophysical Research 108, 2346.

Davy, P., Cobbold, P., 1988. Indentation tectonics in nature and experiment. 1. Experiments scaled for gravity. Bull. Geol. Inst. Univ. Uppsala 14, 129-141.

Dai, J., Wang, C., Hourigan, J., Santosh, M., 2013. Multi-stage tectono-magmatic events of the Eastern Kunlun Range, northern Tibet: Insights from U–Pb geochronology and (U–Th)/He thermochronology. Tectonophysics 599, 97-106.

Dupont-Nivet, G., Butler, R.F., Yin, A., Chen, X., 2003. Paleomagnetism indicates no Neogene vertical axis rotations of the northeastern Tibetan Plateau. J. geophys. Res 108, 2386.

Dupont-Nivet, G., Robinson, D., Butler, R.F., Yin, A., Melosh, H.J., 2004. Concentration of crustal displacement along a weak Altyn Tagh fault: Evidence from paleomagnetism of

the northern Tibetan Plateau. Tectonics 23, TC1020.

Dupont-Nivet, G., Krijgsman, W., Langereis, C.G., Abels, H.A., Dai, S., Fang, X., 2007. Tibetan plateau aridification linked to global cooling at the Eocene–Oligocene transition. Nature 445, 635-638.

Duvall, A.R., Clark, M.K., 2010. Dissipation of fast strike-slip faulting within and beyond northeastern Tibet. Geology 38, 223-226.

Duvall, A.R., Clark, M.K., Kirby, E., Farley, K.A., Craddock, W.H., Li, C., Yuan, D.-Y., 2013. Low-temperature thermochronometry along the Kunlun and Haiyuan Faults, NE Tibetan Plateau: Evidence for kinematic change during late-stage orogenesis. Tectonics 32, 1190-1211.

England, P., Houseman, G., 1986. Finite strain calculations of continental deformation: 2. Comparison with the India‐Asia collision zone. Journal of Geophysical Research: Solid Earth (1978–2012) 91, 3664-3676.

Garzione, C.N., Ikari, M.J., Basu, A.R., 2005. Source of Oligocene to Pliocene sedimentary rocks in the Linxia basin in northeastern Tibet from Nd isotopes: Implications for tectonic forcing of climate. Geological Society of America Bulletin 117, 1156-1166.

Gehrels, G.E., Yin, A., Wang, X.F., 2003a. Magmatic history of the northeastern Tibetan Plateau. Journal of Geophysical Research 108, 2423.

Gehrels, G.E., Yin, A., Wang, X.F., 2003b. Detrital-zircon geochronology of the northeastern Tibetan plateau. Geological Society of America Bulletin 115, 881-896.

Kapp, P., DeCelles, P.G., Gehrels, G.E., Heizler, M., Ding, L., 2007. Geological records of the Lhasa-Qiangtang and Indo-Asian collisions in the Nima area of central Tibet. Geological Society of America Bulletin 119, 917-933.

Jolivet, M., Brunel, M., Seward, D., Xu, Z., Yang, J., Roger, F., Tapponnier, P., Malavieille, J., Arnaud, N., Wu, C., 2001. Mesozoic and Cenozoic tectonics of the northern edge of the Tibetan plateau: fission-track constraints. Tectonophysics 343, 111-134.

Jolivet, M., Brunel, M., Seward, D., Xu, Z., Yang, J., Malavieille, J., Roger, F., Leyreloup, A., Arnaud, N., Wu, C., 2003. Neogene extension and volcanism in the Kunlun Fault Zone, northern Tibet: New constraints on the age of the Kunlun Fault. Tectonics 22, 1052.

Jolivet, M., Roger, F., Xu, Z.Q., Paquette, J.L., Cao, H., 2015. Mesozoic–Cenozoic evolution of the Danba dome (Songpan Garzê, East Tibet) as inferred from LA-ICPMS U–Pb and fission-track data. Journal of Asian Earth Sciences 102, 180-204.

Li, H.B., Yang, J.S., Xu, Z.Q., Sun, Z.M., Tapponnier, P., van der Woerd, J., Meriaux, A.-S., 2006. The constraint of the Altyn Tagh fault system to the growth and rise of the northern Tibetan Plateau. Earth Science Frontiers 13, 59-79 (in Chinese with English abstract).

Liu, Y.J., Neubauer, F., Genser, J., Ge, X.H., Takasu, A., Yuan, S.H., Chang, L.H., Li, W.M., 2007. Geochronology of the initiation and displacement of the Altyn Strike-Slip Fault, western China. Journal of Asian Earth Sciences 29, 243-252.

Lu, H., Wang, E., Meng, K., 2014. Paleomagnetism and anisotropy of magnetic susceptibility of the Tertiary Janggalsay section (southeast Tarim basin): Implications for Miocene tectonic evolution of the Altyn Tagh Range. Tectonophysics 618, 67-78.

Mao, L., Xiao, A., Wu, L., Li, B., Wang, L., Lou, Q., Dong, Y., Qin, S., 2014. Cenozoic tectonic and sedimentary evolution of southern Qaidam Basin, NE Tibetan Plateau and its implication for the rejuvenation of Eastern Kunlun Mountains. Science China Earth Sciences 57, 2726-2739.

Meng, Q.R., Hu, J.M., Yang, F.Z., 2001. Timing and magnitude of displacement on the Altyn Tagh fault: constraints from stratigraphic correlation of adjoining Tarim and Qaidam basins, NW China. Terra Nova 13, 86-91.

Meng, Q.R., Fang, X., 2008. Cenozoic tectonic development of the Qaidam Basin in the northeastern Tibetan Plateau. Geological Society of America Special Papers 444, 1-24.

Métivier, F., Gaudemer, Y., Tapponnier, P., Meyer, B., 1998. Northeastward growth of the Tibet plateau deduced from balanced reconstruction of two depositional areas: The Qaidam and Hexi Corridor basins, China. Tectonics 17, 823-842.

Meyer, B., Tapponnier, P., Bourjot, L., Metivier, F., Gaudemer, Y., Peltzer, G., Shunmin, G., Zhitai, C., 1998. Crustal thickening in Gansu-Qinghai, lithospheric mantle subduction, and oblique, strike-slip controlled growth of the Tibet plateau. Geophysical Journal International 135, 1-47.

Mock, C., Arnaud, N.O., Cantagrel, J.M., 1999. An early unroofing in northeastern Tibet?

Constraints from $^{40}Ar/^{39}Ar$ thermochronology on granitoids from the eastern Kunlun range (Qianghai, NW China). Earth and Planetary Science Letters 171, 107-122.

Molnar, P., Tapponnier, P., 1975. Cenozoic tectonics of Asia: Effects of a continental collision. Science 189, 419-426.

Molnar, P., England, P., Martinod, J., 1993. Mantle dynamics, uplift of the Tibetan Plateau, and the Indian monsoon. Reviews of Geophysics 31, 357-396.

Ritts, B.D., Yue, Y., Graham, S.A., 2004. Oligocene–Miocene Tectonics and Sedimentation along the Altyn Tagh Fault, Northern Tibetan Plateau: Analysis of the Xorkol, Subei, and Aksay Basins. The Journal of geology 112, 207-229.

Robinson, D.M., Dupont-Nivet, G., Gehrels, G.E., Zhang, Y., 2003. The Tula uplift, northwestern China: Evidence for regional tectonism of the northern Tibetan Plateau during late Mesozoic–early Cenozoic time. Geological Society of America Bulletin 115, 35-47.

Shi, D.N., Shen, Y., Zhao, W.J., Li, A.B., 2009. Seismic evidence for a Moho offset and south-directed thrust at the easternmost Qaidam–Kunlun boundary in the Northeast Tibetan plateau. Earth and Planetary Science Letters 288, 329-334.

Tapponnier, P., Molnar, P., 1977. Active faulting and tectonics in China. Journal of Geophysical Research 82, 2905-2930.

Tapponnier, P., Peltzer, G., Armijo, R., Cobbold, P., 1982. Propagating extrusion tectonics in Asia; new insights from simple experiments with plasticine. Geology 10, 611-616.

Tapponnier, P., Peltzer, G., Armijo, R., 1986. On the mechanics of the collision between India and Asia. Geological Society, London, Special Publications 19, 113-157.

Tapponnier, P., Xu, Z.Q., Roger, F., Meyer, B., Arnaud, N., Wittlinger, G., Yang, J.S., 2001. Oblique stepwise rise and growth of the Tibet Plateau. Science 294, 1671-1677.

Taylor, M., Yin, A., 2009. Active structures of the Himalayan-Tibetan orogen and their relationships to earthquake distribution, contemporary strain field, and Cenozoic volcanism. Geosphere 5, 199-214.

Wan, J.L., Wang, Y., Li, Q., Wang, F., Wang, E., 2001. FT Evidence of Northern Altyn Uplift in Late-Cenozoic. Bulletin of Mineralogy, Petrology and Geochemistry 20, 222-224 (in

Chinese with English abstract).

Wang, E., 1997. Displacement and timing along the northern strand of the Altyn Tagh fault zone, northern Tibet. Earth and Planetary Science Letters 150, 55-64.

Wang, Y., Zhang, X., Wang, E., Zhang, J., Li, Q., Sun, G., 2005. $^{40}Ar/^{39}Ar$ thermochronological evidence for formation and Mesozoic evolution of the northern-central segment of the Altyn Tagh fault system in the northern Tibetan Plateau. Geological Society of America Bulletin 117, 1336-1346.

Wang, E., Xu, F.-Y., Zhou, J.-X., Wan, J., Burchfiel, B.C., 2006. Eastward migration of the Qaidam basin and its implications for Cenozoic evolution of the Altyn Tagh fault and associated river systems. Geological Society of America Bulletin 118, 349-365.

Wang, C., Zhao, X., Liu, Z., Lippert, P.C., Graham, S.A., Coe, R.S., Yi, H., Zhu, L., Liu, S., Li, Y., 2008. Constraints on the early uplift history of the Tibetan Plateau. Proceedings of the National Academy of Sciences 105, 4987-4992.

Wang, C.S., Gao, R., Yin, A., Wang, H., Zhang, Y.X., Guo, T.L., Li, Q.S., Li, Y.L., 2011. A mid-crustal strain-transfer model for continental deformation: A new perspective from high-resolution deep seismic-reflection profiling across NE Tibet. Earth and Planetary Science Letters 306, 279-288.

Wang, C., Dai, J., Zhao, X., Li, Y., Graham, S.A., He, D., Ran, B., Meng, J., 2014. Outward-growth of the Tibetan Plateau during the Cenozoic: A review. Tectonophysics.

Wu, L., Xiao, A., Wang, L., Mao, L., Wang, L., Dong, Y., Xu, B., 2012a. EW-trending uplifts along the southern side of the central segment of the Altyn Tagh Fault, NW China: Insight into the rising mechanism of the Altyn Mountain during the Cenozoic. SCIENCE CHINA Earth Sciences 55, 926-939.

Wu, L., Xiao, A.C., Yang, S.F., Wang, L.Q., Mao, L.G., Wang, L., Dong, Y.P., Xu, B., 2012b. Two-stage evolution of the Altyn Tagh Fault during the Cenozoic: new insight from provenance analysis of a geological section in NW Qaidam Basin, NW China. Terra Nova 24, 387-395.

Wu, L., Xiao, A.C., Ma, D.D., Li, H.G., Xu, B., Shen, Y., Mao, L.G., 2014. Cenozoic fault systems in southwest Qaidam Basin, northeastern Tibetan Plateau: Geometry, temporal

development, and significance for hydrocarbon accumulation. AAPG Bulletin 98, 1213-1234.

Xia, W.C., Zhang, N., Yuan, X.P., Fan, L.S., Zhang, B.S., 2001. Cenozoic Qaidam basin, China: A stronger tectonic inversed, extensional rifted basin. AAPG bulletin 85, 715-736.

Yang, J., Xu, Z., Zhang, J., Chu, C.-Y., Zhang, R., Liou, J.-G., 2001. Tectonic significance of early Paleozoic high-pressure rocks in Altun-Qaidam-Qilian Mountains, northwest China. Geological Society of America Memoirs 194, 151-170.

Yin, A., Harrison, T.M., 2000. Geologic evolution of the Himalayan-Tibetan orogen. Annual Review of Earth and Planetary Sciences 28, 211-280.

Yin, A., Rumelhart, P., Butler, R., Cowgill, E., Harrison, T., Foster, D., Ingersoll, R., Qing, Z., Xian-Qiang, Z., Xiao-Feng, W., 2002. Tectonic history of the Altyn Tagh fault system in northern Tibet inferred from Cenozoic sedimentation. Geological Society of America Bulletin 114, 1257-1295.

Yin, A., Dang, Y.Q., Zhang, M., McRivette, M.W., Burgess, W.P., Chen, X.H., 2007. Cenozoic tectonic evolution of Qaidam basin and its surrounding regions (part 2): Wedge tectonics in southern Qaidam basin and the Eastern Kunlun Range. Geological Society of America Special Papers 433, 369-390.

Yin, A., Dang, Y.Q., Zhang, M., Chen, X.H., McRivette, M.W., 2008a. Cenozoic tectonic evolution of the Qaidam basin and its surrounding regions (Part 3): Structural geology, sedimentation, and regional tectonic reconstruction. Geological Society of America Bulletin 120, 847-876.

Yin, A., Dang, Y.Q., Wang, L.C., Jiang, W.M., Zhou, S.P., Chen, X.H., Gehrels, G.E., McRivette, M.W., 2008b. Cenozoic tectonic evolution of Qaidam basin and its surrounding regions (Part 1): The southern Qilian Shan-Nan Shan thrust belt and northern Qaidam basin. Geological Society of America Bulletin 120, 813-846.

Yin, A., 2010. Cenozoic tectonic evolution of Asia: A preliminary synthesis. Tectonophysics 488, 293-325.

Yu, X., Huang, B., Guan, S., Fu, S., Cheng, F., Cheng, X., Zhang, T., Guo, Z., 2014. Anisotropy of magnetic susceptibility of Eocene and Miocene sediments in the Qaidam Basin,

Northwest China: Implication for Cenozoic tectonic transition and depocenter migration. Geochemistry, Geophysics, Geosystems 15, 2095-2108.

Yuan, W.M., Dong, J.Q., Wang, S.C., Carter, A., 2006. Apatite fission track evidence for Neogene uplift in the eastern Kunlun Mountains, northern Qinghai–Tibet Plateau, China. Journal of Asian Earth Sciences 27, 847-856.

Yuan, D.Y., Ge, W.P., Chen, Z.W., Li, C.Y., Wang, Z.C., Zhang, H.P., Zhang, P.Z., Zheng, D.W., Zheng, W.J., Craddock, W.H., Dayem, K.E., Duvall, A.R., Hough, B.G., Lease, R.O., Champagnac, J.-D., Burbank, D.W., Clark, M.K., Farley, K.A., Garzione, C.N., Kirby, E., Molnar, P., Roe, G.H., 2013. The growth of northeastern Tibet and its relevance to large-scale continental geodynamics: A review of recent studies. Tectonics 32, 2013TC003348.

Yue, Y.J., Liou, J.G., 1999. Two-stage evolution model for the Altyn Tagh fault, China. Geology 27, 227-230.

Yue, Y.J., Ritts, B.D., Graham, S.A., 2001. Initiation and long-term slip history of the Altyn Tagh Fault. International Geology Review 43, 1087-1093.

Zhang, P.Z., Shen, Z., Wang, M., Gan, W., Bürgmann, R., Molnar, P., Wang, Q., Niu, Z., Sun, J., Wu, J., 2004. Continuous deformation of the Tibetan Plateau from global positioning system data. Geology 32, 809-812.

Zhang, H.-p., Zhang, P.-z., Zheng, D.-W., Zheng, W.-J., Chen, Z.-W., Wang, W.-T., 2014. Transforming the Miocene Altyn Tagh fault slip into shortening of the north-western Qilian Shan: insights from the drainage basin geometry. Terra Nova 26, 216-221.

Zhuang, G., Hourigan, J.K., Ritts, B.D., Kent-Corson, M.L., 2011. Cenozoic multiple-phase tectonic evolution of the northern Tibetan Plateau: Constraints from sedimentary records from Qaidam basin, Hexi Corridor, and Subei basin, northwest China. American Journal of Science 311, 116-152.

Appendix

Appendix to Chapter 2.2

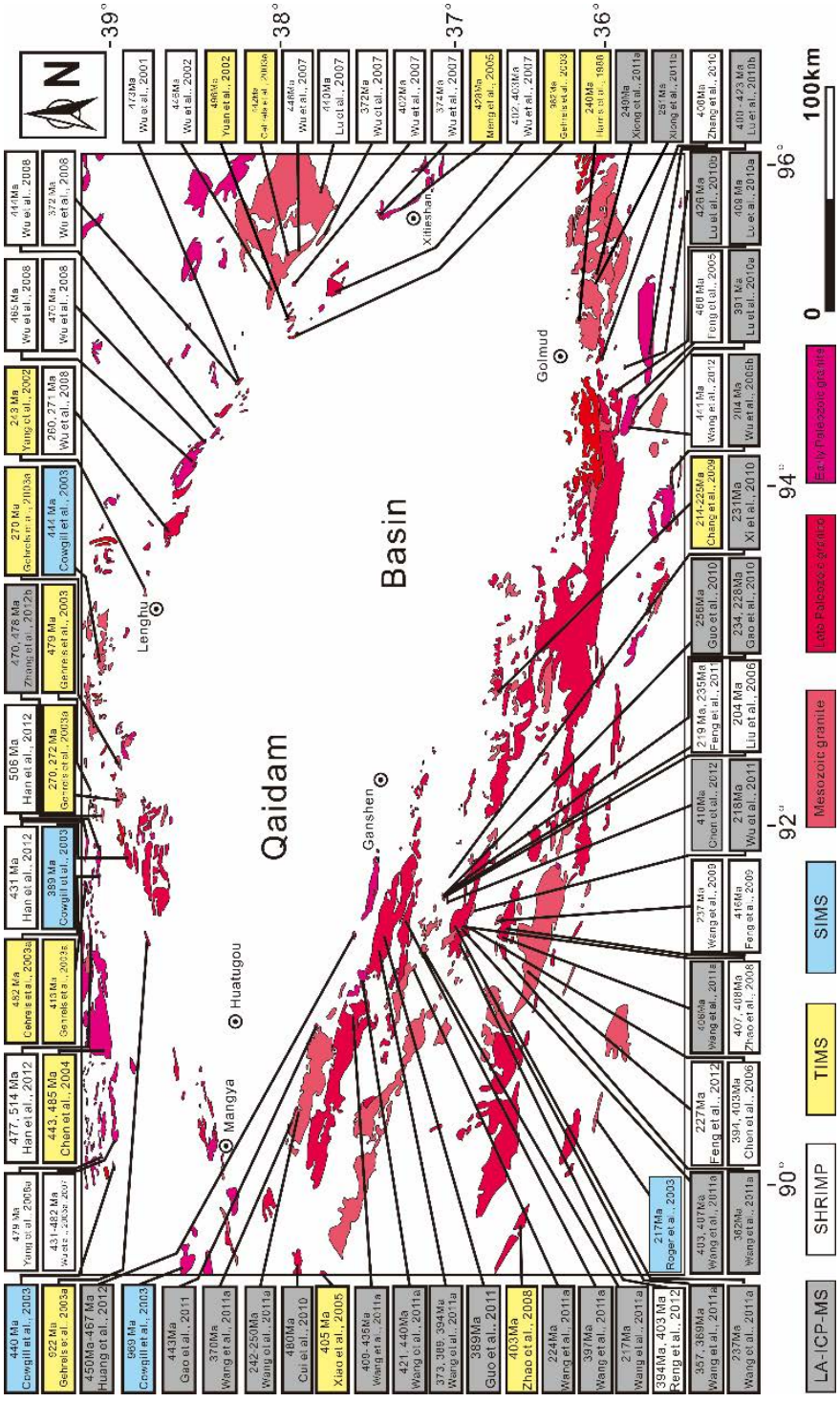

gure DR1 Distribution of magmatic rocks in the surrounding area of Qaidam basin and statistics of the zircon U-Pb ages. The statistics of the zircon U-Pb ages are mainly collected from references in Table DR1

Table DR1. Zircon U-Pb ages from plutons of the Eastern Kunlun Range, Altyn Tagh Range and Qilian Shan.

Altyn Tagh Range			Qilian Shan			East Kunlun Range		
Source	Year	Age(Ma)	Source	Year	Age(Ma)	Source	Year	Age(Ma)
Yue Yongjun et al.,	2005	413	Yue Yongjun et al.,	2005	1728	She Hongquan et al.,	2007	215
Yue Yongjun et al.,	2005	482	Yue Yongjun et al.,	2005	482	Li Shijin et al.,	2008	224
Yue Yongjun et al.,	2005	1870	Yue Yongjun et al.,	2005	424	Wang Song et al.,	2009	237
Yue Yongjun et al.,	2005	1877	Yue Yongjun et al.,	2005	472	Li Dongsheng et al.,	2009	206
Yue Yongjun et al.,	2005	479	Yue Yongjun et al.,	2005	480	Li Dongsheng et al.,	2009	223
Gehrels et al.,	2003	270	Yue Yongjun et al.,	2005	423	Feng Chengyou et al.,	2009	237
Gehrels et al.,	2003	272	Yue Yongjun et al.,	2005	406	Huang Limei et al.,	2012	459
Gehrels et al.,	2003	270	Yue Yongjun et al.,	2005	425	Guo Lei et al.,	2010	256
Gehrels et al.,	2003	440	Yue Yongjun et al.,	2005	366	Gao Yongbao et al.,	2012	228
Cowgill et al.,	2003	922	Yue Yongjun et al.,	2005	248	Gao Yongbao et al.,	2012	234
Cowgill et al.,	2003	389	Yue Yongjun et al.,	2005	434	Liu Chengdong et al.,	2003	242
Cowgill et al.,	2003	2720	Yue Yongjun et al.,	2005	441	Liu Yunhua et al.,	2006	204
Cowgill et al.,	2003	442	Yue Yongjun et al.,	2005	473	Wu Xiangke et al.,	2011	218
Cowgill et al.,	2003	290	Yue Yongjun et al.,	2005	430	Feng Chengyou et al.,	2011	219
Cowgill et al.,	2003	404	Gehrels et al.,	2003	461	Feng Chengyou et al.,	2011	235
Cowgill et al.,	2003	457	Cowgill et al.,	2003	459	Chen Danling et al.,	2011	212
Cowgill et al.,	2003	518	Cowgill et al.,	2003	922	Ren Erfeng et al.,	2012	403
Cowgill et al.,	2003	475	Cowgill et al.,	2003	928	Ren Erfeng et al.,	2012	394
Cowgill et al.,	2003	969	Cowgill et al.,	2003	442	Feng Chengyou et al.,	2010	227
Cowgill et al.,	2003	444	Cowgill et al.,	2003	422	Feng Chengyou et al.,	2010	220
Cowgill et al.,	2003	2396	Lu Songnian et al.,	2008	2366	Gao Yongbao et al.,	2011	430
Lu Songnian et al.,	2008	2582	Lu Songnian et al.,	2008	2412	Gao Yongbao et al.,	2011	431
Lu Songnian et al.,	2008	2604	Lu Songnian et al.,	2008	1939	Feng Chengyou et al.,	2009	417
Lu Songnian et al.,	2008	2830	Lu Songnian et al.,	2008	2348	Feng Chengyou et al.,	2009	468
Lu Songnian et al.,	2008	3574	Lu Songnian et al.,	2008	1852	Chen Junlu et al.,	2004	405

Lu Songnian et al.,	2008	3665	Lu Songnian et al.,	2008	1763	Chen Junlu et al.,	2004	2380
Lu Songnian et al.,	2008	2396	Lu Songnian et al.,	2008	844	Chen Junlu et al.,	2004	816
Lu Songnian et al.,	2008	1978	Lu Songnian et al.,	2008	740	Chen Junlu et al.,	2004	401
Lu Songnian et al.,	2008	2670	Lu Songnian et al.,	2008	1050	Cui Meihui et al.,	2011	480
Lu Songnian et al.,	2008	2830	Lu Songnian et al.,	2008	1020	Wang Bingzhang et al.,	2009	271
Lu Songnian et al.,	2008	1986	Lu Songnian et al.,	2008	1020	Wang Bingzhang et al.,	2009	284
Lu Songnian et al.,	2008	2374	Lu Songnian et al.,	2008	1020	Wang Bingzhang et al.,	2009	251
Lu Songnian et al.,	2008	2351	Lu Songnian et al.,	2008	987	Mo xuanxue et al.,	2005	212
Lu Songnian et al.,	2008	2358	Lu Songnian et al.,	2008	928	Qinghai Geology investigation institute	2008	214
Lu Songnian et al.,	2008	2366	Lu Songnian et al.,	2008	917	Qinghai Geology investigation institute	2008	225
Lu Songnian et al.,	2008	2412	Lu Songnian et al.,	2008	917	Xiao Aifang et al.,	2005	405
Lu Songnian et al.,	2008	2426	Lu Songnian et al.,	2008	878	Wang Xiangli et al.,	2010	1090
Lu Songnian et al.,	2008	1900	Lu Songnian et al.,	2008	953	Wang Xiangli et al.,	2010	312
Lu Songnian et al.,	2008	930	Lu Songnian et al.,	2008	875	Gao Yongbao et al.,	2010	430
Wu Cailai et al.,	2005	474	Lu Songnian et al.,	2008	878	Gao Yongbao et al.,	2010	430
Wu Cailai et al.,	2005	446	Lu Songnian et al.,	2008	864	Gao Yongbao et al.,	2010	430
Wu Cailai et al.,	2005	435	Lu Songnian et al.,	2008	855	Qinghai Geology investigation institute	2003	410
Wu Cailai et al.,	2005	431	Lu Songnian et al.,	2008	844	Qinghai Geology investigation institute	2003	419
Yang Jingsui et al.,	2008	479	Lu Songnian et al.,	2008	821	Ma Yongshou et al.,	2010	550
Yang Wenqiang et al.,	2012	453	Lu Songnian et al.,	2008	1776	Ma Yongshou et al.,	2010	2046
Hao Jie et al.,	2006	467	Lu Songnian et al.,	2008	740	Wu Shaofeng et al.,	2012	429
Sun Jiming et al.,	2012	497	Lu Songnian et al.,	2008	1793	Tan Shengxiang et al.,	2004	831
Wang Chao et al.,	2013	923	Lu Songnian et al.,	2008	1800	Cao Shitai et al.,	2011	429
Wang Chao et al.,	2013	910	Wang Chao et al.,	2013	976	Cao Shitai et al.,	2011	430

Wang Chao et al.,	2013	927	Wang Chao et al.,	2013	952	Wang Binzhang	2012	440
Wang Chao et al.,	2013	924	Wang Chao et al.,	2013	941	Wang Binzhang	2012	450
Wang Chao et al.,	2013	906	Wang Chao et al.,	2013	935	Feng Chengyou et al.,	2010	219
Wang Chao et al.,	2013	916	Wang Chao et al.,	2013	953	Xi Rengang et al.,	2011	231
Wang Chao et al.,	2013	938	Wang Chao et al.,	2013	915	Guo Tongzhen et al.,	2011	389
Wang Chao et al.,	2013	907	Wang Chao et al.,	2013	907	Qinghai Geology investigation institute	2010	224
Xiu Qunye et al.,	2007	449	Wang Chao et al.,	2013	932	Feng Chengyou et al.,	2012	227
Han Dengbin et al.,	2012	446	Wang Chao et al.,	2013	918	Feng Chengyou et al.,	2012	220
Han Dengbin et al.,	2012	477	Wang Chao et al.,	2013	930	Chang Youying et al.,	2009	223
Han Dengbin et al.,	2012	477	Liu Liang et al.,	2013	783	Chang Youying et al.,	2009	214
Han Dengbin et al.,	2012	514	Liu Liang et al.,	2013	748	Chang Youying et al.,	2009	225
Han Dengbin et al.,	2012	417	Liu Liang et al.,	2013	847	Liu Xiaokang et al.,	2011	419
Han Dengbin et al.,	2012	488	Liu Liang et al.,	2013	847	Chen Bo et al.,	2012	410
Han Dengbin et al.,	2012	479	Liu Liang et al.,	2013	457	Gao Xiaofeng et al.,	2011	443
Han Dengbin et al.,	2012	506	Liu Liang et al.,	2013	446	Luo Zhaohua et al.,	2002	212
Han Dengbin et al.,	2012	431	Liu Liang et al.,	2013	909	Mo xuanxue et al.,	2007	471
Han Dengbin et al.,	2012	443	Liu Liang et al.,	2013	1005	Mo xuanxue et al.,	2007	485
Han Dengbin et al.,	2012	417	Liu Liang et al.,	2013	891	Mo xuanxue et al.,	2005	387
Han Dengbin et al.,	2012	431	Liu Liang et al.,	2013	890	Mo xuanxue et al.,	2005	386
Han Dengbin et al.,	2012	440	Liu Liang et al.,	2013	516	Mo xuanxue et al.,	2005	408
Wu Cailai et al.,	2007	435	Shi Rendeng et al.,	2004	550	Mo xuanxue et al.,	2005	408
Wu Cailai et al.,	2007	433	Meng Fancong et al.,	2010	505	Mo xuanxue et al.,	2005	401
Wu Cailai et al.,	2007	435	Zeng Jianyuan et al.,	2007	497	Chen Hongwei et al.,	2006	403
Wu Cailai et al.,	2007	431	Wu Cailai et al.,	2010	501	Chen Hongwei et al.,	2006	394
Liu Han et al.,	2012	750	Wu Cailai et al.,	2010	512	Lu Songnian et al.,	2002	522
Liu Han et al.,	2012	763	Wu Cailai et al.,	2010	508	Lu Songnian et al.,	2002	2468
Liu Han et al.,	2012	754	Wu Cailai et al.,	2010	477	Lu Songnian et al.,	2002	1955

Liu Liang et al.,	1999	524	Wu Cailai et al.,	2010	463	Yang Jinsui et al.,	1996	518
Zeng Jianyuan et al.,	2006	776	Wu Cailai et al.,	2010	424	Feng Jianyun et al.,	2010	509
Zeng Jianyuan et al.,	2006	774	Wu Cailai et al.,	2010	435	Wang Binzhang	2012	509
Lu Songnian et al.,	2009	757	Wu Cailai et al.,	2010	429	Wang Binzhang	2012	434
Lu Songnian et al.,	2009	438	Song Zhongbao et al.,	2004	482	Wang Binzhang	2012	435
Lu Songnian et al.,	2009	425	Song Zhongbao et al.,	2007	458	Wang Binzhang	2012	419
	2009	2679	Huang Chuanjian et	1995	486	Wang Binzhang	2012	421
Wu Yuezhong et al.,			al.,					
Wu Yuezhong et al.,	2009	856	Wu Cailai et al.,	2007	477	Wang Binzhang	2012	413
Wu Yuezhong et al.,	2009	1312	Wu Cailai et al.,	2007	463	Wang Binzhang	2012	409
Wu Yuezhong et al.,	2009	1209	Wang Yusheng et al.,	2001	940	Wang Binzhang	2012	1782
Wu Yuezhong et al.,	2009	871	Wang Yusheng et al.,	2001	1030	Wang Binzhang	2012	2642
Wu Yuezhong et al.,	2009	1311	Wang Yusheng et al.,	2001	1020	Wang Binzhang	2012	881
Wu Yuezhong et al.,	2009	450	Wang Yusheng et al.,	2000	930	Wang Binzhang	2012	923
Wu Yuezhong et al.,	2009	465	Wang Yusheng et al.,	2000	930	Wang Binzhang	2012	427
Wu Yuezhong et al.,	2009	445	Wang Yusheng et al.,	2000	750	Wang Binzhang	2012	451
Wu Yuezhong et al.,	2009	452	Guo Jinjing et al.,	1999	920	Wang Binzhang	2012	189
Wu Yuezhong et al.,	2009	448	Guo Jinjing et al.,	1999	910	Wang Binzhang	2012	290
Wu Yuezhong et al.,	2009	327	Mei Hualin et al.,	1998	2670	Wang Binzhang	2012	397
Wu Yuezhong et al.,	2009	313	Mei Hualin et al.,	1999	880	Wang Binzhang	2012	683
Wu Yuezhong et al.,	2009	397	Xu Wanchun et al.,	2007	891	Wang Binzhang	2012	373
	2003	495	Wang Christina Yan	2005	445	Wang Binzhang	2012	394
Xiao Peixi et al.,			et al.,					
Song Zhongbao et al.,	2004	482	Xu Wangchun et al.,	2007	776	Wang Binzhang	2012	373
Liu Han et al.,	2011	462	Xu Wangchun et al.,	2007	774	Wang Binzhang	2012	369
Liu Han et al.,	2011	437	Li Xianhua et al.,	2004	827	Wang Binzhang	2012	370
Zhang Zhicheng et al.,	2008	521	Ayers et al.,	2002	1921	Wang Binzhang	2012	397
Kang Lei et al.,	2011	500	Mattinson et al.,	2006	433	Wang Binzhang	2012	395

Gherels et al.,	1999	480	Xia Xiaohong et al.,	2009	490	Wang Binzhang	2012	370
Chen Xuanhua et al.,	2003	443	He Shiping et al.,	2007	443	Wang Binzhang	2012	357
Dong Shunli et al.,	2013	450	He Shiping et al.,	2007	1782	Wang Binzhang	2012	284
Dong Shunli et al.,	2013	465	He Shiping et al.,	2007	385	Wang Binzhang	2012	241
Zhang Zhanwu et al.,	2012	478	He Shiping et al.,	2007	471	Wang Binzhang	2012	250
Zhang Zhanwu et al.,	2012	470	Li Shuguang et al.,	2004	447	Wang Binzhang	2012	217
Dong Zengchan et al.,	2011	445	Zhang Zhaowei et al.,	2012	441	Wang Binzhang	2012	224
Liu Han et al.,	2012	2007	Wei Fanghui et al.,	2012	441	Ma Shengchao et al.,	2012	219
Ma Zhongping et al.,	2012	467	Zhang Zhaowei et al.,	2012	443	Ma Shengchao et al.,	2012	235
Ma Zhongping et al.,	2012	462	Mao Jingwen et al.,	2000	460	Cui Meihui et al.,	2012	480
Ma Zhongping et al.,	2012	470	Xiong Ziliang et al.,	2012	424	Zhang Dequan et al.,	2001	438
Ma Zhongping et al.,	2012	464	Xiong Ziliang et al.,	2012	402	Cheng Nengsong et al.,	2008	517
Yang Qi et al.,	2004	443	Su Jianping et al.,	2004	444	Cheng Nengsong et al.,	2008	516
Yang Qi et al.,	2004	485	Yu Jiyuan et al.,	2012	455	Cheng Nengsong et al.,	2008	559
Liu Liang et al.,	2007	750	Wu Cailai et al.,	2006	476	Cheng Nengsong et al.,	2008	482
	2005	846	Wu Cailai et al.,	2006	463	Cheng Nengsong et al.,	2008	516
Zhang Jianxin	abc							
	2005	844	Wang Yinchuan et al.,	2012	1765	Cheng Nengsong et al.,	2008	549
Zhang Jianxin	abc							
Zhang Jianxin	2004	842	Wu Cailai et al.,	2004	383	Yang Jingsui et al.,	1995	518
Liu Liang	2009	1800	Chen Junlu et al.,	2006	440	Lu Songnian et al.,	2002	522
	2009	821	Wang Hongliang et	2007	1192	Yang Jingsui et al.,	1996	579
Liu Liang			al.,					
Qi Xuexiang	2005	482	Qi Ruirong et al.,	2012	463	Li Huaikun et al.,	2006	506
	2005	404	Huang Zengbao et al.,	2010	414	Guangxi Geology	2003	1209
Qi Xuexiang						investigation institute		
	2013	754	Xiang Zengqun et al.,	2007	504	Guangxi Geology	2003	871
Liu Liang						investigation institute		

	2013	752	Yang Jinsui et al.,	2008	479	Guangxi Geology investigation institute	2003	550
Liu Liang								
	2013	647	Xiao Lin et al.,	1997	2152	Guangxi Geology investigation institute	2003	408
Liu Liang								
	2013	730	Yong Yong et al.,	2008	454	Guangxi Geology investigation institute	2003	397
Liu Liang								
	2013	857	Yong Yong et al.,	2008	846	Guangxi Geology investigation institute	2003	320
Liu Liang								
	2013	719	Yong Yong et al.,	2008	756	Guangxi Geology investigation institute	2003	381
Liu Liang								
	2013	867	Yong Yong et al.,	2008	853	Guangxi Geology investigation institute	2003	271
Liu Liang								
	2013	563	Xu Xueyi et al.,	2008	723	Qinghai Geology investigation institute	2003	831
Liu Liang								
Wu Cailai et al.,	2001	446	Zeng Jianyuan et al.,	2006	776	Yang Jinsui et al.,	2005	417
Chen Xuanhua et al.,	2003	2926	Zeng Jianyuan et al.,	2006	774	Yang Jinsui et al.,	2005	421
Chen Xuanhua et al.,	2003	1728	Chen Junlu et al.,	2008	445	Yang Jinsui et al.,	2005	250
Chen Xuanhua et al.,	2003	405	Xia Xiaohong et al.,	2010	490	Yang Jinsui et al.,	2005	308
Wu Suoping et al.,	2007	385	He Yanhong et al.,	2005	447	Bian Qiantao et al.,	1999	402
Li Weidong et al.,	2012	462	Guo Jinjing et al.,	1999	917	Cheng Nengsong et al.,	2000	447
Cao Yuting et al.,	2013	579	Pei Xianzhi et al.,	2007	440	Gao Xiaofeng et al.,	2010	458
	2010	410	Pei Xianzhi et al.,	2007	450	Shanxi Geology investigation institute	2003	432
Liu Feng et al.,								
Liu Han et al.,	2013	457	He Yanhong et al.,	2005	1900	Feng Jianyun et al.,	2010	509
Liu Han et al.,	2013	419	He Yanhong et al.,	2005	2350	Zhang Yafeng et al.,	2010	515
Liu Han et al.,	2013	411	He Yanhong et al.,	2005	2500	Sun Yu et al.,	2009	255
Liu Han et al.,	2013	503	Wu Cailai et al.,	2008	465	Liu Chengdong et al.,	2004	239
Liu Han et al.,	2013	420	Wu Cailai et al.,	2008	470	Liu Chengdong et al.,	2004	242

Liu Han et al.,	2013	419	Wu Cailai et al.,	2008	444	Liu Chengdong et al.,	2000	236
Liu Han et al.,	2013	411	Wu Cailai et al.,	2008	372	Liu Chengdong et al.,	2000	235
Liu Han et al.,	2013	420	Wu Cailai et al.,	2008	271	Long Xiaoping et al.,	2006	411
Liu Han et al.,	2013	405	Wu Cailai et al.,	2008	260	Long Xiaoping et al.,	2006	396
Chen Xuanhua et al.,	2003	418	Li Jianfeng et al.,	2010	415	Zhang Jianxin et al.,	2003	402
Chen Xuanhua et al.,	2003	413	Li Jianfeng et al.,	2010	435	Liu Zhanqing et al.,	2011	516
Chen Xuanhua et al.,	2003	413	Dong Guoan et al.,	2007	930	Liu Zhanqing et al.,	2011	332
			Dong Guoan et al.,	2007	918	Liu Zhanqing et al.,	2011	441
			Dong Guoan et al.,	2007	790	Li Wangye et al.,	2007	493
			Wu Cailai et al.,	2007	446	Lu Lu et al.,	2010	423
			Wu Cailai et al.,	2007	409	Zhang Yaoling et al.,	2010	406
			Wu Cailai et al.,	2007	403	Sun Yu et al.,	2009	254
			Wu Cailai et al.,	2007	375	China University of Geosciences (Wuhan)	2003	205
			Wu Cailai et al.,	2007	372	Ren Junhu et al.,	2009	436
			Wu Peng et al.,	2012	499	Ren Junhu et al.,	2009	413
			Yu Jiyuan et al.,	2012	910	Ren Junhu et al.,	2009	403
			Xue Ning et al.,	2009	829	Xiong Fuhao et al.,	2011	249
			Xue Ning et al.,	2009	842	Liu Bin et al.,	2012	407
			Su Jianping et al.,	2004	751	Liu Bin et al.,	2012	406
			Lu Xinxiang et al.,	2007	440	Liu et al.,	2004	242
			Xia Xiaohong et al.,	2012	501	Liu et al.,	2004	239
			Xia Xiaohong et al.,	2012	495	Cheng Nengsong et al.,	2002	448
			Dang Jinhua et al.,	2011	345	Cheng Nengsong et al.,	2002	427
						Cheng Nengsong et al.,	2002	920
						Zhang Jianxin et al.,	2003	460
						Cheng Nengsong et al.,	1999	500
						Li Huaikun et al.,	2006	500

China University of Geosciences (Wuhan)	2003	438
Zhu Yunhai et al.,	2005	419
Zhu Yunhai et al.,	2005	401
Li Fudong et al.,	1993	222
Li Fudong et al.,	1993	206
Li Fudong et al.,	1993	223
Zhan fayu et al.,	2007	230
Zhan fayu et al.,	2007	222
Zhan fayu et al.,	2007	215
Zhan fayu et al.,	2007	228
Zhan fayu et al.,	2007	219
Zhang Hongfei et al.,	2006	218
Bian Qiantao et al.,	2007	402
Lu Lu et al.,	2010	409
Lu Lu et al.,	2010	391
Robbinson et al.,	2003	74
Li Wei et al.,	2013	485
Li Wei et al.,	2013	439
Li Wei et al.,	2013	424
Li Wei et al.,	2013	262
Li Wei et al.,	2013	462
Li Wei et al.,	2013	428
Li Wei et al.,	2013	446

Table DR2. LA-ICP-MS U-Pb data of detrital zircons from the 22 sandstone samples.

Analysis number	Th/U	Isotopic ratios and errors						Ages and errors (Ma)						Disc.%
		$^{207}Pb/^{206}Pb$	1σ	$^{207}Pb/^{235}U$	1σ	$^{206}Pb/^{238}U$	1σ	$^{207}Pb/^{206}Pb$	1σ	$^{207}Pb/^{235}U$	1σ	$^{206}Pb/^{238}U$	1σ	
HTG-E														
HTG-01	1.14	0.05583	0.00138	0.53192	0.0133	0.06909	0.00099	446	31	433	9	431	6	0.5
HTG-02	0.72	0.05142	0.0026	0.2838	0.01417	0.04002	0.00069	260	83	254	11	253	4	0.4
HTG-03	0.45	0.05474	0.00138	0.48562	0.01239	0.06433	0.00093	402	32	402	8	402	6	0
HTG-04	0.57	0.06984	0.00157	1.48928	0.03402	0.15464	0.00222	924	25	926	14	927	12	-0.1
HTG-05	0.61	0.05156	0.00179	0.30118	0.01037	0.04236	0.00067	266	50	267	8	267	4	0
HTG-06	0.98	0.05133	0.00371	0.29057	0.02058	0.04105	0.00087	256	123	259	16	259	5	0
HTG-07	0.54	0.05248	0.00142	0.28769	0.00786	0.03975	0.00058	306	36	257	6	251	4	2.4
HTG-08	0.49	0.05171	0.0016	0.30426	0.00936	0.04266	0.00065	273	43	270	7	269	4	0.4
HTG-09	1.08	0.05122	0.0019	0.28264	0.01042	0.04002	0.00063	251	56	253	8	253	4	0
HTG-10	1.55	0.09464	0.00214	3.45538	0.07954	0.26474	0.00386	1521	23	1517	18	1514	20	0.5
HTG-11	0.38	0.08592	0.00275	2.72175	0.08636	0.2297	0.0037	1336	37	1334	24	1333	19	0.2
HTG-12	1.59	0.06724	0.00205	1.30861	0.03942	0.14113	0.00224	845	37	850	17	851	13	-0.1
HTG-13	0.53	0.05514	0.00322	0.44021	0.02469	0.0579	0.00093	418	134	370	17	363	6	1.9
~~HTG-14~~	~~0.05~~	~~0.16236~~	~~0.00339~~	~~9.02601~~	~~0.19329~~	~~0.4031~~	~~0.00578~~	~~2480~~	~~18~~	~~2341~~	~~20~~	~~2183~~	~~27~~	~~13.6~~
HTG-15	0.53	0.05168	0.0021	0.30648	0.01237	0.043	0.00067	271	64	271	10	271	4	0
HTG-16	0.22	0.05626	0.00133	0.57136	0.01369	0.07365	0.00106	463	29	459	9	458	6	0.2
HTG-17	1.00	0.05085	0.00241	0.26975	0.01267	0.03847	0.00064	234	78	242	10	243	4	-0.4
HTG-18	1.06	0.05176	0.00203	0.30631	0.01185	0.04291	0.0007	275	59	271	9	271	4	0
HTG-19	0.69	0.05463	0.00393	0.47712	0.0338	0.06333	0.00126	397	124	396	23	396	8	0
HTG-20	1.06	0.05119	0.00492	0.28202	0.02671	0.03995	0.00092	249	171	252	21	253	6	-0.4
HTG-21	0.52	0.07792	0.00331	1.9669	0.07795	0.18309	0.0028	1145	87	1104	27	1084	15	5.6
HTG-22	0.91	0.07544	0.00267	1.86739	0.06482	0.17949	0.00311	1080	42	1070	23	1064	17	1.5

HTG-23	0.93	0.05701	0.0016	0.63664	0.01791	0.08098	0.00122	492	36	500	11	502	7	-0.4
HTG-24	0.42	0.05563	0.00194	0.52888	0.01823	0.06894	0.00111	438	48	431	12	430	7	0.2
HTG-25	0.73	0.07017	0.00475	1.38465	0.09204	0.14309	0.00296	933	102	882	39	862	17	2.3
HTG-26	0.54	0.04962	0.00947	0.19482	0.03663	0.02847	0.00103	177	315	181	31	181	6	0
HTG-27	0.65	0.05141	0.00806	0.28292	0.04384	0.03991	0.00114	259	287	253	35	252	7	0.4
HTG-28	0.78	0.05468	0.00183	0.47955	0.0159	0.0636	0.00101	399	46	398	11	397	6	0.3
HTG-29	0.40	0.05352	0.00287	0.28534	0.01512	0.03866	0.00067	351	88	255	12	245	4	4.1
HTG-30	0.62	0.05195	0.00188	0.32112	0.01154	0.04482	0.0007	283	54	283	9	283	4	0
HTG-31	0.63	0.05571	0.00279	0.52718	0.02613	0.06862	0.00116	441	80	430	17	428	7	0.5
HTG-32	0.56	0.05478	0.00211	0.48393	0.0183	0.06406	0.00109	403	54	401	13	400	7	0.2
HTG-33	0.33	0.06604	0.00205	1.22579	0.03787	0.1346	0.0021	808	39	812	17	814	12	-0.2
HTG-34	0.56	0.05158	0.00242	0.29437	0.01362	0.04138	0.00072	267	74	262	11	261	4	0.4
HTG-35	1.06	0.05136	0.00388	0.28391	0.02108	0.04008	0.00083	257	131	254	17	253	5	0.4
HTG-36	0.59	0.05392	0.00179	0.25385	0.0084	0.03413	0.00053	368	47	230	7	216	3	6.5
HTG-37	1.15	0.07332	0.002	1.73243	0.04735	0.17133	0.00261	1023	31	1021	18	1019	14	0.4
HTG-38	0.71	0.05173	0.00203	0.30579	0.01181	0.04286	0.00071	273	58	271	9	271	4	0
HTG-39	0.78	0.05354	0.004	0.40882	0.0301	0.05537	0.00111	352	131	348	22	347	7	0.3
HTG-40	0.99	0.05535	0.00333	0.55771	0.03316	0.07306	0.00133	426	100	450	22	455	8	-1.1
HTG-41	0.30	0.06283	0.00282	0.66466	0.02941	0.07671	0.0013	702	65	517	18	476	8	8.6
HTG-42	0.89	0.05179	0.00553	0.29852	0.03158	0.04179	0.00088	276	200	265	25	264	5	0.4
HTG-43	1.21	0.05586	0.00164	0.55139	0.01613	0.07158	0.00109	447	38	446	11	446	7	0
HTG-44	0.85	0.05555	0.00303	0.52298	0.02794	0.06826	0.00131	434	85	427	19	426	8	0.2
HTG-45	0.53	0.05412	0.00194	0.44413	0.01567	0.05951	0.00098	376	50	373	11	373	6	0
HTG-46	0.94	0.05621	0.00192	0.56264	0.01898	0.07258	0.00118	461	46	453	12	452	7	0.2
HTG-47	0.46	0.05137	0.0016	0.30107	0.00931	0.0425	0.00066	257	43	267	7	268	4	-0.4
HTG-48	0.58	0.05618	0.00161	0.58709	0.01675	0.07578	0.00116	459	37	469	11	471	7	-0.4
HTG-49	0.74	0.05167	0.00277	0.29782	0.0158	0.0418	0.00072	271	90	265	12	264	4	0.4
HTG-50	0.54	0.05082	0.00225	0.25119	0.01094	0.03584	0.00061	233	69	228	9	227	4	0.4

HTG-51	0.52	0.0553	0.00231	0.52488	0.02155	0.06882	0.00118	424	61	428	14	429	7	-0.2
HTG-52	0.42	0.09013	0.00358	2.79364	0.10182	0.2248	0.00353	1428	78	1354	27	1307	19	9.3
HTG-53	1.12	0.05286	0.00318	0.36331	0.02142	0.04984	0.00098	323	98	315	16	314	6	0.3
HTG-54	0.48	0.05524	0.00325	0.51835	0.03001	0.06804	0.00126	422	96	424	20	424	8	0
HTG-55	0.75	0.05183	0.00295	0.31339	0.0174	0.04385	0.00086	278	91	277	13	277	5	0
HTG-56	1.09	0.05133	0.00361	0.29415	0.02029	0.04155	0.00087	256	120	262	16	262	5	0
HTG-57	0.58	0.05376	0.00229	0.43579	0.01823	0.05878	0.00102	361	63	367	13	368	6	-0.3
HTG-58	0.52	0.05563	0.00228	0.53272	0.02144	0.06944	0.00119	438	59	434	14	433	7	0.2
HTG-59	0.58	0.05487	0.00179	0.49359	0.01597	0.06523	0.00103	407	44	407	11	407	6	0
HTG-60	0.62	0.06888	0.00191	1.42808	0.03958	0.15034	0.00233	895	32	901	17	903	13	-0.2
HTG-61	0.82	0.05432	0.00218	0.45526	0.01797	0.06077	0.00104	384	58	381	13	380	6	0.3
HTG-62	0.73	0.05492	0.00204	0.49022	0.01794	0.06472	0.00108	409	52	405	12	404	7	0.2
HTG-63	0.90	0.05445	0.00283	0.45999	0.0234	0.06125	0.00117	390	80	384	16	383	7	0.3
HTG-64	0.58	0.05656	0.00171	0.59192	0.01775	0.07588	0.00119	474	39	472	11	471	7	0.2
HTG-65	0.46	0.05727	0.00185	0.63645	0.0203	0.08059	0.0013	502	42	500	13	500	8	0
HTG-66	0.42	0.0549	0.00196	0.45753	0.01621	0.06043	0.00098	408	50	383	11	378	6	1.3
HTG-67	0.61	0.05161	0.00245	0.30802	0.01437	0.04328	0.00077	268	74	273	11	273	5	0
HTG-68	0.47	0.05632	0.00364	0.57228	0.03629	0.07368	0.00151	465	104	459	23	458	9	0.2
HTG-69	0.58	0.05438	0.00259	0.46854	0.02178	0.06248	0.00117	387	71	390	15	391	7	-0.3
HTG-70	0.38	0.09241	0.00301	3.25629	0.10488	0.25551	0.00425	1476	36	1471	25	1467	22	0.6
HTG-71	0.47	0.05474	0.00193	0.47067	0.01639	0.06235	0.00102	402	49	392	11	390	6	0.5
HTG-72	0.43	0.05077	0.00239	0.24517	0.01134	0.03502	0.00062	230	74	223	9	222	4	0.5
HTG-73	0.66	0.0544	0.0031	0.46269	0.02586	0.06168	0.00119	388	91	386	18	386	7	0
HTG-74	1.43	0.05412	0.00263	0.45702	0.0217	0.06123	0.00114	376	73	382	15	383	7	-0.3
HTG-75	0.77	0.05529	0.00186	0.52349	0.01742	0.06866	0.00112	424	45	427	12	428	7	-0.2
HTG-76	0.54	0.0554	0.00939	0.52627	0.08804	0.06888	0.00225	428	313	429	59	429	14	0
HTG-77	0.82	0.06618	0.00283	1.22955	0.05134	0.13472	0.00247	812	57	814	23	815	14	-0.1
HTG-78	0.69	0.05127	0.00273	0.29021	0.01512	0.04104	0.00079	253	84	259	12	259	5	0

HTG-79	0.59	0.05406	0.00407	0.45214	0.03325	0.06065	0.00141	374	124	379	23	380	9	-0.3
HTG-80	0.51	0.05518	0.00158	0.51989	0.01489	0.06832	0.00106	420	37	425	10	426	6	-0.2
HTG-81	0.56	0.05434	0.00272	0.44887	0.02218	0.0599	0.00107	385	79	376	16	375	7	0.3
HTG-82	0.59	0.05538	0.00221	0.52724	0.0207	0.06903	0.00118	428	57	430	14	430	7	0
HTG-83	0.60	0.05128	0.0021	0.28825	0.01155	0.04076	0.00071	253	60	257	9	258	4	-0.4
HTG-84	0.46	0.05165	0.00193	0.30158	0.01109	0.04234	0.00072	270	53	268	9	267	4	0.4
HTG-85	0.69	0.0563	0.00178	0.59529	0.01864	0.07667	0.00123	464	41	474	12	476	7	-0.4
HTG-86	0.29	0.05526	0.00203	0.53191	0.01923	0.0698	0.00118	423	51	433	13	435	7	-0.5
HTG-87	0.78	0.06486	0.00283	1.07174	0.04564	0.11982	0.00222	770	58	740	22	730	13	1.4
HTG-88	0.74	0.05406	0.00216	0.44507	0.01748	0.0597	0.00103	374	57	374	12	374	6	0
HTG-89	0.03	0.05631	0.00245	0.58798	0.02521	0.07572	0.00132	465	64	470	16	471	8	-0.2
HTG-90	1.07	0.05356	0.00255	0.43177	0.02026	0.05846	0.00104	353	74	364	14	366	6	-0.5
HTG-91	0.58	0.07473	0.0032	1.67484	0.06999	0.16251	0.00306	1061	54	999	27	971	17	2.9
HTG-92	0.34	0.06174	0.00324	0.84897	0.04384	0.09971	0.00182	665	79	624	24	613	11	1.8
HTG-93	0.63	0.05174	0.00232	0.29968	0.01321	0.042	0.00075	274	68	266	10	265	5	0.4
HTG-94	0.44	0.05574	0.00184	0.5427	0.01771	0.0706	0.00115	442	44	440	12	440	7	0
HTG-95	0.31	0.19336	0.00549	13.63387	0.38682	0.51131	0.00807	2771	26	2725	27	2662	34	4.1
HTG-96	0.57	0.0516	0.00204	0.29104	0.01131	0.0409	0.00071	268	57	259	9	258	4	0.4
HTG-97	0.30	0.05508	0.00231	0.5048	0.02076	0.06645	0.00119	415	60	415	14	415	7	0
~~HTG-98~~	~~0.70~~	~~0.08382~~	~~0.00303~~	~~1.99761~~	~~0.0706~~	~~0.17282~~	~~0.00307~~	~~1288~~	~~42~~	~~1115~~	~~24~~	~~1028~~	~~17~~	~~25.3~~
HTG-99	0.73	0.05563	0.00206	0.53124	0.01935	0.06925	0.00119	438	51	433	13	432	7	0.2
HTG-100	0.29	0.05194	0.00239	0.3252	0.0148	0.0454	0.00079	283	72	286	11	286	5	0
HTG-N														
HTG-01	0.42	0.05483	0.00228	0.45594	0.01891	0.0603	0.00097	405	64	381	13	377	6	1.1
HTG-02	1.07	0.05535	0.00145	0.51807	0.01383	0.06787	0.00103	426	33	424	9	423	6	0.2
HTG-03	0.64	0.05492	0.0021	0.49752	0.01909	0.06569	0.00102	409	58	410	13	410	6	0

HTG-04	0.44	0.05526	0.00141	0.50457	0.0131	0.06621	0.001	423	32	415	9	413	6	0.5
HTG-05	0.97	0.16334	0.00267	10.04928	0.181	0.44612	0.00625	2491	14	2439	17	2378	28	4.8
HTG-06	0.87	0.05181	0.00196	0.3077	0.0117	0.04307	0.00067	277	59	272	9	272	4	0
HTG-07	0.55	0.05517	0.00186	0.51483	0.01752	0.06767	0.00104	419	49	422	12	422	6	0
HTG-08	0.85	0.05483	0.00193	0.48262	0.01701	0.06382	0.00101	405	51	400	12	399	6	0.3
HTG-09	0.18	0.05689	0.00188	0.51447	0.01535	0.06558	0.00094	487	75	421	10	409	6	2.9
HTG-10	0.45	0.05713	0.00121	0.62606	0.01385	0.07947	0.00115	497	25	494	9	493	7	0.2
HTG-11	1.15	0.05669	0.00123	0.59684	0.01354	0.07635	0.0011	479	26	475	9	474	7	0.2
HTG-12	0.67	0.05548	0.00198	0.49205	0.01758	0.06431	0.00102	432	51	406	12	402	6	1
HTG-13	0.98	0.05143	0.00132	0.29634	0.00777	0.04178	0.00062	260	34	264	6	264	4	0
HTG-14	0.58	0.05462	0.00153	0.47635	0.0136	0.06324	0.00095	397	38	396	9	395	6	0.3
HTG-15	0.75	0.06008	0.00214	0.53638	0.01894	0.06474	0.00107	606	48	436	13	404	6	7.9
HTG-16	0.43	0.05468	0.00147	0.48626	0.01335	0.06448	0.00096	399	35	402	9	403	6	-0.2
HTG-17	0.64	0.05434	0.00127	0.46186	0.01116	0.06164	0.0009	385	29	386	8	386	5	0
~~HTG-18~~	~~0.69~~	~~0.06824~~	~~0.00175~~	~~0.5988~~	~~0.01567~~	~~0.06363~~	~~0.00095~~	~~876~~	~~30~~	~~476~~	~~10~~	~~398~~	~~6~~	~~19.6~~
~~HTG-19~~	~~0.74~~	~~0.08731~~	~~0.00303~~	~~0.59889~~	~~0.0206~~	~~0.04974~~	~~0.00082~~	~~1367~~	~~41~~	~~477~~	~~13~~	~~313~~	~~5~~	~~52.4~~
HTG-20	0.51	0.054	0.00181	0.45848	0.01542	0.06157	0.00097	371	48	383	11	385	6	-0.5
HTG-21	0.51	0.0769	0.00135	2.02718	0.0385	0.19116	0.00269	1119	18	1125	13	1128	15	-0.8
HTG-22	0.57	0.05487	0.00308	0.48245	0.02679	0.06376	0.00114	407	92	400	18	398	7	0.5
HTG-23	0.90	0.05471	0.00266	0.48406	0.02342	0.06416	0.00106	400	79	401	16	401	6	0
HTG-24	0.74	0.05571	0.00643	0.52488	0.05985	0.06832	0.00167	441	212	428	40	426	10	0.5
~~HTG-25~~	~~0.44~~	~~0.07525~~	~~0.00334~~	~~0.51288~~	~~0.02253~~	~~0.04942~~	~~0.00085~~	~~1075~~	~~60~~	~~420~~	~~15~~	~~311~~	~~5~~	~~35~~
HTG-26	0.82	0.05646	0.00147	0.58541	0.01539	0.07519	0.00114	471	32	468	10	467	7	0.2
HTG-27	0.43	0.05103	0.00178	0.27306	0.00948	0.0388	0.00061	242	51	245	8	245	4	0
HTG-28	0.55	0.05513	0.00317	0.50519	0.02859	0.06645	0.00128	417	92	415	19	415	8	0
HTG-29	0.52	0.05533	0.00373	0.43892	0.02861	0.05753	0.00099	426	155	369	20	361	6	2.2
HTG-30	0.50	0.05488	0.00748	0.50918	0.06852	0.06727	0.00186	407	252	418	46	420	11	-0.5
HTG-31	0.67	0.05452	0.00166	0.48416	0.0149	0.06439	0.00097	393	42	401	10	402	6	-0.2

HTG-32	0.32	0.05499	0.00222	0.5103	0.02056	0.06729	0.00108	412	61	419	14	420	7	-0.2
HTG-33	0.58	0.05488	0.00132	0.50346	0.01248	0.06652	0.00098	407	30	414	8	415	6	-0.2
HTG-34	1.05	0.05468	0.00345	0.47932	0.02981	0.06356	0.00125	399	104	398	20	397	8	0.3
HTG-35	0.88	0.05838	0.0014	0.5194	0.0128	0.06451	0.00095	544	29	425	9	403	6	5.5
HTG-36	1.07	0.05531	0.00151	0.48646	0.01355	0.06377	0.00095	425	36	402	9	399	6	0.8
HTG-37	0.55	0.05432	0.00854	0.46228	0.07146	0.06171	0.00207	384	287	386	50	386	13	0
HTG-38	0.12	0.05687	0.00225	0.61621	0.02418	0.07857	0.00133	486	57	487	15	488	8	-0.2
HTG-39	0.36	0.05618	0.00236	0.49847	0.01951	0.06435	0.00097	459	95	411	13	402	6	2.2
HTG-40	0.67	0.06582	0.00187	1.1536	0.0332	0.12709	0.00195	801	35	779	16	771	11	1
HTG-41	0.70	0.05261	0.0052	0.3578	0.03505	0.04931	0.00103	312	183	311	26	310	6	0.3
HTG-42	0.49	0.05481	0.00617	0.52101	0.05774	0.06892	0.0018	404	202	426	39	430	11	-0.9
HTG-43	0.47	0.05449	0.00358	0.46222	0.0301	0.06151	0.00111	391	114	386	21	385	7	0.3
HTG-44	0.53	0.05277	0.00179	0.36874	0.01249	0.05067	0.00081	319	48	319	9	319	5	0
HTG-45	0.77	0.05471	0.00179	0.48887	0.01605	0.0648	0.00101	400	46	404	11	405	6	-0.2
HTG-46	0.78	0.05472	0.00634	0.48458	0.05571	0.06421	0.0014	401	219	401	38	401	8	0
HTG-47	0.35	0.05636	0.00182	0.53117	0.01725	0.06834	0.00105	467	45	433	11	426	6	1.6
HTG-48	0.91	0.0549	0.0042	0.49953	0.03781	0.06598	0.00128	408	135	411	26	412	8	-0.2
HTG-49	0.49	0.05466	0.00265	0.49752	0.02384	0.066	0.00116	398	76	410	16	412	7	-0.5
HTG-50	0.57	0.05559	0.00106	0.47923	0.00969	0.06251	0.00088	436	22	398	7	391	5	1.8
HTG-51	1.09	0.05436	0.00564	0.46863	0.04817	0.06251	0.00133	386	193	390	33	391	8	-0.3
HTG-52	0.44	0.05502	0.002	0.49708	0.01793	0.06551	0.00107	413	52	410	12	409	6	0.2
HTG-53	0.15	0.07015	0.00129	1.58152	0.03115	0.16348	0.0023	933	20	963	12	976	13	-1.3
HTG-54	0.57	0.05536	0.00261	0.50629	0.02353	0.06631	0.00118	427	72	416	16	414	7	0.5
HTG-55	1.56	0.05495	0.00157	0.4969	0.01438	0.06557	0.001	410	38	410	10	409	6	0.2
HTG-56	0.87	0.05552	0.00379	0.51616	0.03492	0.06741	0.00126	433	118	423	23	421	8	0.5
HTG-57	0.27	0.05491	0.00172	0.49223	0.01545	0.06501	0.00102	409	43	406	11	406	6	0
HTG-58	0.29	0.05531	0.00147	0.5111	0.01383	0.067	0.001	425	34	419	9	418	6	0.2
HTG-59	0.87	0.05492	0.0013	0.48769	0.0119	0.06439	0.00093	409	30	403	8	402	6	0.2

HTG-60	1.15	0.05535	0.00235	0.53347	0.02245	0.06988	0.00117	426	64	434	15	435	7	-0.2
HTG-61	0.23	0.07007	0.00162	1.45321	0.03459	0.15039	0.00221	930	26	911	14	903	12	0.9
HTG-62	0.14	0.05622	0.00138	0.57296	0.01444	0.0739	0.00107	461	31	460	9	460	6	0
HTG-63	0.70	0.05599	0.00259	0.55147	0.02525	0.07142	0.00125	452	70	446	17	445	8	0.2
HTG-64	0.62	0.05562	0.00268	0.50381	0.02404	0.06569	0.00114	437	75	414	16	410	7	1
HTG-65	0.84	0.0549	0.00224	0.50223	0.02034	0.06633	0.0011	408	61	413	14	414	7	-0.2
HTG-66	0.68	0.05442	0.00188	0.47132	0.01624	0.0628	0.001	388	49	392	11	393	6	-0.3
HTG-67	1.33	0.05486	0.00376	0.49758	0.0337	0.06576	0.00126	407	118	410	23	411	8	-0.2
HTG-68	0.82	0.05514	0.00591	0.48278	0.0511	0.06349	0.00152	418	194	400	35	397	9	0.8
HTG-69	0.34	0.05562	0.00156	0.53587	0.01511	0.06987	0.00107	437	36	436	10	435	6	0.2
HTG-70	0.37	0.05549	0.0016	0.50319	0.01466	0.06575	0.001	432	38	414	10	410	6	1
HTG-71	1.30	0.05503	0.00188	0.5013	0.01701	0.06606	0.00109	413	47	413	12	412	7	0.2
HTG-72	0.95	0.0554	0.00254	0.51848	0.02355	0.06787	0.00114	428	71	424	16	423	7	0.2
HTG-73	0.56	0.05515	0.00134	0.50784	0.01269	0.06677	0.00098	418	31	417	9	417	6	0
HTG-74	0.34	0.07267	0.00262	1.64201	0.0591	0.16385	0.00266	1005	47	986	23	978	15	0.8
HTG-75	0.83	0.0516	0.00183	0.29721	0.01054	0.04177	0.00065	268	53	264	8	264	4	0
HTG-76	0.65	0.05571	0.00159	0.54565	0.01564	0.07102	0.00109	441	37	442	10	442	7	0
HTG-77	0.92	0.05481	0.00133	0.48169	0.01189	0.06373	0.00095	404	30	399	8	398	6	0.3
HTG-78	1.27	0.05106	0.00237	0.26332	0.01211	0.03739	0.00064	244	74	237	10	237	4	0
HTG-79	0.91	0.05457	0.00205	0.47846	0.01794	0.06358	0.00102	395	55	397	12	397	6	0
HTG-80	0.51	0.05521	0.00227	0.51026	0.02088	0.06702	0.00107	421	63	419	14	418	6	0.2
HTG-81	0.41	0.05228	0.00148	0.34119	0.00977	0.04733	0.00072	298	38	298	7	298	4	0
~~HTG-82~~	~~0.47~~	~~0.04619~~	~~0.00738~~	~~0.39454~~	~~0.06265~~	~~0.06194~~	~~0.0011~~	~~8~~	~~285~~	~~338~~	~~46~~	~~387~~	~~7~~	~~-12.7~~
~~HTG-83~~	~~13.32~~	~~0.05628~~	~~0.00107~~	~~0.44693~~	~~0.00899~~	~~0.05759~~	~~0.00081~~	~~463~~	~~22~~	~~375~~	~~6~~	~~361~~	~~5~~	~~3.9~~
HTG-84	0.88	0.05126	0.00127	0.26253	0.00664	0.03714	0.00054	253	32	237	5	235	3	0.9
HTG-85	1.05	0.0565	0.0018	0.60989	0.01944	0.07828	0.00123	472	43	483	12	486	7	-0.6
HTG-86	0.88	0.1092	0.00217	4.80437	0.09995	0.31903	0.00458	1786	19	1786	17	1785	22	0.1
HTG-87	0.15	0.06813	0.00144	1.31211	0.02877	0.13965	0.00201	873	23	851	13	843	11	0.9

HTG-88	0.66	0.0553	0.00158	0.52529	0.01515	0.06888	0.00105	424	38	429	10	429	6	0
HTG-89	0.60	0.05465	0.00352	0.4649	0.02931	0.06169	0.00128	398	104	388	20	386	8	0.5
HTG-90	0.74	0.0549	0.00113	0.49643	0.01068	0.06557	0.00094	408	24	409	7	409	6	0
HTG-91	1.12	0.05452	0.00387	0.46714	0.03279	0.06213	0.00118	393	124	389	23	389	7	0
HTG-92	1.36	0.05756	0.00131	0.49573	0.0116	0.06245	0.00091	513	27	409	8	391	6	4.6
HTG-93	0.54	0.0549	0.00475	0.49215	0.04229	0.06501	0.00126	408	159	406	29	406	8	0
HTG-94	0.40	0.05552	0.00161	0.51548	0.01501	0.06732	0.00103	433	38	422	10	420	6	0.5
HTG-95	1.11	0.05577	0.00164	0.54206	0.01593	0.07048	0.00109	443	38	440	10	439	7	0.2
HTG-96	0.57	0.05413	0.00172	0.45384	0.01451	0.0608	0.00093	376	45	380	10	380	6	0
HTG-97	0.37	0.06249	0.00188	0.92879	0.02798	0.10778	0.00167	691	38	667	15	660	10	1.1
HTG-98	0.77	0.05493	0.00144	0.49966	0.01324	0.06596	0.00099	409	33	411	9	412	6	-0.2
HTG-99	0.77	0.05119	0.00129	0.2972	0.0076	0.0421	0.00063	249	32	264	6	266	4	-0.8
HTG-100	0.40	0.10343	0.00223	4.31811	0.09611	0.30274	0.00445	1687	21	1697	18	1705	22	-1.1
SZG2														
SZG2-01	1.04	0.05166	0.0012	0.27265	0.00652	0.03827	0.00053	270	30	245	5	242	3	1.2
SZG2-02	0.24	0.09542	0.00206	3.2949	0.05673	0.25045	0.00327	1536	42	1480	13	1441	17	6.6
SZG2-03	0.12	0.11663	0.00123	5.44527	0.07158	0.33856	0.00437	1905	11	1892	11	1880	21	1.3
SZG2-04	0.37	0.05858	0.00078	0.59574	0.00908	0.07374	0.00097	552	15	475	6	459	6	3.5
SZG2-05	1	0.0566	0.00069	0.47699	0.00683	0.06111	0.0008	476	14	396	5	382	5	3.7
SZG2-06	0.43	0.056	0.00064	0.53683	0.0074	0.06951	0.0009	452	14	436	5	433	5	0.7
SZG2-07	0.26	0.05874	0.00142	0.55076	0.01121	0.068	0.00089	558	54	445	7	424	5	5
SZG2-08	0.32	0.05802	0.00063	0.66478	0.00892	0.08309	0.00108	531	13	518	5	515	6	0.6
SZG2-09	0.04	0.0657	0.00141	0.8723	0.01495	0.09629	0.00124	797	46	637	8	593	7	7.4
~~SZG2-10~~	~~0.83~~	~~0.06851~~	~~0.00655~~	~~0.45635~~	~~0.04277~~	~~0.04831~~	~~0.00092~~	~~884~~	~~205~~	~~382~~	~~30~~	~~304~~	~~6~~	~~25.7~~
SZG2-11	0.48	0.0555	0.00078	0.54847	0.00867	0.07165	0.00095	432	16	444	6	446	6	-0.4
~~SZG2-12~~	~~0.31~~	~~0.07484~~	~~0.00178~~	~~1.09644~~	~~0.02164~~	~~0.10625~~	~~0.0014~~	~~1064~~	~~49~~	~~752~~	~~10~~	~~651~~	~~8~~	~~15.5~~

SZG2-13	0.69	0.05602	0.0008	0.53375	0.00853	0.06908	0.00092	453	16	434	6	431	6	0.7
SZG2-14	0.39	0.07054	0.00082	1.45263	0.02023	0.14933	0.00195	944	13	911	8	897	11	1.6
SZG2-15	0.23	0.06068	0.00186	0.71153	0.0196	0.08505	0.00116	628	68	546	12	526	7	3.8
SZG2-16	0.41	0.05651	0.00065	0.57094	0.00789	0.07326	0.00095	472	14	459	5	456	6	0.7
SZG2-17	0.59	0.05601	0.00267	0.48669	0.02206	0.06303	0.00093	453	109	403	15	394	6	2.3
SZG2-18	0.03	0.09545	0.00101	3.26743	0.0432	0.24823	0.00321	1537	11	1473	10	1429	17	7.6
SZG2-19	1.15	0.05297	0.00083	0.2961	0.00511	0.04053	0.00054	328	18	263	4	256	3	2.7
SZG2-20	0.38	0.08432	0.00109	2.54203	0.03797	0.21861	0.00292	1300	13	1284	11	1275	15	2
SZG2-21	0.4	0.05931	0.0017	0.57604	0.01458	0.07045	0.00095	578	64	462	9	439	6	5.2
SZG2-22	0.46	0.05257	0.00073	0.28943	0.00458	0.03993	0.00053	310	16	258	4	252	3	2.4
SZG2-23	0.34	0.05675	0.00068	0.54767	0.00778	0.06998	0.00092	482	14	443	5	436	6	1.6
SZG2-24	0.48	0.05667	0.00067	0.5009	0.00706	0.06409	0.00084	479	14	412	5	400	5	3
SZG2-25	0.31	0.06002	0.00163	0.59686	0.0141	0.07213	0.00097	604	60	475	9	449	6	5.8
SZG2-26	0.22	0.06887	0.00079	1.38199	0.01918	0.14551	0.0019	895	13	881	8	876	11	0.6
SZG2-27	0.53	0.061	0.00068	0.67197	0.00912	0.07987	0.00104	639	13	522	6	495	6	5.5
~~SZG2-28~~	~~0.35~~	~~0.09522~~	~~0.00214~~	~~3.14908~~	~~0.05722~~	~~0.23986~~	~~0.00318~~	~~1532~~	~~43~~	~~1445~~	~~14~~	~~1386~~	~~17~~	~~10.5~~
SZG2-29	0.15	0.07031	0.00082	1.48543	0.02077	0.1532	0.00201	937	13	924	8	919	11	0.5
SZG2-30	0.37	0.05421	0.00205	0.29153	0.01026	0.03901	0.00055	380	87	260	8	247	3	5.3
SZG2-31	0.11	0.0698	0.00078	1.44376	0.01968	0.14998	0.00196	922	13	907	8	901	11	0.7
SZG2-32	0.31	0.05694	0.0016	0.56408	0.01391	0.07185	0.00097	489	63	454	9	447	6	1.6
SZG2-33	0.41	0.116	0.00128	5.11693	0.06929	0.31986	0.00418	1895	11	1839	12	1789	20	5.9
SZG2-34	0.33	0.06822	0.00195	1.26953	0.03203	0.13498	0.00183	875	61	832	14	816	10	2
SZG2-35	0.56	0.10643	0.00119	4.08699	0.05568	0.27845	0.00365	1739	11	1652	11	1584	18	9.8
SZG2-36	0.15	0.06563	0.00144	0.95848	0.01699	0.10592	0.00138	795	47	683	9	649	8	5.2
SZG2-37	1.13	0.05982	0.00072	0.60553	0.00865	0.0734	0.00097	597	14	481	5	457	6	5.3
SZG2-38	0.46	0.05719	0.00075	0.61505	0.0093	0.07798	0.00103	499	15	487	6	484	6	0.6
SZG2-39	0.48	0.05913	0.00186	0.56549	0.01598	0.06936	0.00095	572	70	455	10	432	6	5.3
SZG2-40	0.76	0.07137	0.00101	1.20034	0.01917	0.12196	0.00164	968	15	801	9	742	9	8

SZG2-41	0.62	0.05657	0.00088	0.5301	0.0091	0.06794	0.00091	475	18	432	6	424	5	1.9
SZG2-42	0.36	0.07492	0.00084	1.79853	0.02456	0.17408	0.00228	1066	12	1045	9	1035	13	3
SZG2-43	0.53	0.05675	0.00071	0.56798	0.00831	0.07257	0.00096	482	14	457	5	452	6	1.1
~~SZG2-44~~	~~0.94~~	~~0.06312~~	~~0.00077~~	~~0.54552~~	~~0.00785~~	~~0.06266~~	~~0.00083~~	~~712~~	~~14~~	~~442~~	~~5~~	~~392~~	~~5~~	~~12.8~~
SZG2-45	0.98	0.06185	0.00083	0.60239	0.00921	0.07062	0.00094	669	15	479	6	440	6	8.9
SZG2-46	1.2	0.05306	0.00111	0.28271	0.0062	0.03864	0.00054	331	26	253	5	244	3	3.7
SZG2-47	0.88	0.13459	0.00148	6.82656	0.09253	0.36779	0.00482	2159	11	2089	12	2019	23	6.9
SZG2-48	0.21	0.06698	0.0008	1.04012	0.01483	0.1126	0.00149	837	13	724	7	688	9	5.2
SZG2-49	0.81	0.06072	0.00078	0.58752	0.00874	0.07017	0.00093	629	14	469	6	437	6	7.3
SZG2-50	0.52	0.05404	0.00082	0.44511	0.00749	0.05972	0.00081	373	17	374	5	374	5	0
SZG2-51	0.19	0.06957	0.0015	1.39332	0.02394	0.14525	0.0019	916	45	886	10	874	11	1.4
SZG2-52	0.81	0.05617	0.00082	0.54119	0.00883	0.06987	0.00094	459	16	439	6	435	6	0.9
SZG2-53	0.43	0.05416	0.00069	0.45266	0.00673	0.06061	0.0008	378	15	379	5	379	5	0
SZG2-54	0.5	0.05703	0.00068	0.54709	0.00782	0.06956	0.00092	493	14	443	5	434	6	2.1
SZG2-55	0.59	0.05593	0.00199	0.53054	0.01736	0.06879	0.00095	450	81	432	12	429	6	0.7
~~SZG2-56~~	~~0.96~~	~~0.06041~~	~~0.00088~~	~~0.49136~~	~~0.00804~~	~~0.05898~~	~~0.00079~~	~~618~~	~~16~~	~~406~~	~~5~~	~~369~~	~~5~~	~~10~~
SZG2-57	0.33	0.0554	0.0023	0.4927	0.01916	0.0645	0.00095	428	95	407	13	403	6	1
SZG2-58	0.72	0.05346	0.00082	0.27293	0.00462	0.03702	0.0005	348	18	245	4	234	3	4.7
SZG2-59	0.44	0.0518	0.00137	0.30043	0.00809	0.04206	0.00061	277	36	267	6	266	4	0.4
SZG2-60	0.1	0.11535	0.00128	5.32413	0.07252	0.3347	0.00439	1885	11	1873	12	1861	21	1.3
SZG2-61	0.2	0.05176	0.00075	0.2758	0.0045	0.03864	0.00052	275	17	247	4	244	3	1.2
SZG2-62	0.91	0.12554	0.00152	6.18972	0.08865	0.35753	0.00479	2036	11	2003	13	1970	23	3.4
SZG2-63	0.92	0.0626	0.00274	1.02874	0.04246	0.11918	0.00175	695	96	718	21	726	10	-1.1
SZG2-64	0.98	0.05849	0.00073	0.55858	0.00822	0.06926	0.00092	548	14	451	5	432	6	4.4
SZG2-65	0.45	0.05682	0.00069	0.53543	0.0077	0.06833	0.0009	485	14	435	5	426	5	2.1
SZG2-66	0.44	0.05086	0.00084	0.27193	0.00489	0.03877	0.00053	234	19	244	4	245	3	-0.4
SZG2-67	0.64	0.05517	0.00069	0.4797	0.00706	0.06304	0.00084	419	15	398	5	394	5	1
SZG2-68	0.55	0.05175	0.00113	0.28566	0.00651	0.04002	0.00056	274	28	255	5	253	3	0.8

SZG2-69	0.1	0.05505	0.00115	0.47995	0.00785	0.06324	0.00083	414	48	398	5	395	5	0.8
SZG2-70	0.88	0.05629	0.00076	0.56422	0.00877	0.07268	0.00097	464	15	454	6	452	6	0.4
~~SZG2-71~~	~~0.17~~	~~0.11596~~	~~0.00233~~	~~4.57494~~	~~0.06956~~	~~0.28615~~	~~0.00375~~	~~1895~~	~~37~~	~~1745~~	~~13~~	~~1622~~	~~19~~	~~16.8~~
SZG2-72	0.33	0.0555	0.00075	0.51512	0.00801	0.06731	0.0009	432	16	422	5	420	5	0.5
SZG2-73	0.54	0.0558	0.00073	0.51289	0.0078	0.06665	0.00089	444	15	420	5	416	5	1
SZG2-74	0.73	0.05116	0.00149	0.31248	0.00921	0.04429	0.00065	248	41	276	7	279	4	-1.1
SZG2-75	0.97	0.08404	0.00101	2.45192	0.03519	0.21155	0.00282	1293	12	1258	10	1237	15	4.5
SZG2-76	0.56	0.05623	0.00067	0.59128	0.00841	0.07625	0.00101	461	14	472	5	474	6	-0.4
SZG2-77	0.95	0.05621	0.00076	0.50207	0.0078	0.06477	0.00087	461	15	413	5	405	5	2
SZG2-78	0.27	0.06992	0.00083	1.43413	0.02036	0.14874	0.00197	926	13	903	8	894	11	1
SZG2-79	0.53	0.1072	0.00145	4.6272	0.07142	0.313	0.00429	1752	13	1754	13	1755	21	-0.2
SZG2-80	0.36	0.0569	0.00068	0.56003	0.00804	0.07136	0.00095	488	14	452	5	444	6	1.8
SZG2-81	0.58	0.05166	0.00103	0.29257	0.00614	0.04107	0.00057	270	24	261	5	259	4	0.8
SZG2-82	0.28	0.05703	0.00069	0.55784	0.00807	0.07093	0.00094	493	14	450	5	442	6	1.8
~~SZG2-83~~	~~0.83~~	~~0.12455~~	~~0.00371~~	~~5.35921~~	~~0.13901~~	~~0.31208~~	~~0.00457~~	~~2022~~	~~54~~	~~1878~~	~~22~~	~~1751~~	~~22~~	~~15.5~~
SZG2-84	0.13	0.06722	0.00142	1.26539	0.02105	0.13654	0.00179	844	45	830	9	825	10	0.6
SZG2-85	0.24	0.06932	0.00187	1.2658	0.02953	0.13243	0.0018	908	57	831	13	802	10	3.6
SZG2-86	0.69	0.05543	0.00073	0.53214	0.00815	0.06961	0.00093	430	15	433	5	434	6	-0.2
SZG2-87	0.38	0.0801	0.00106	1.76899	0.02709	0.16015	0.00215	1199	13	1034	10	958	12	7.9
~~SZG2-88~~	~~0.16~~	~~0.24466~~	~~0.00469~~	~~18.20403~~	~~0.25457~~	~~0.53965~~	~~0.00707~~	~~3151~~	~~31~~	~~3001~~	~~13~~	~~2782~~	~~30~~	~~13.3~~
~~SZG2-89~~	~~0.6~~	~~0.12638~~	~~0.00364~~	~~5.16357~~	~~0.12723~~	~~0.29633~~	~~0.0044~~	~~2048~~	~~52~~	~~1847~~	~~21~~	~~1673~~	~~22~~	~~22.4~~
SZG2-90	0.38	0.06005	0.00169	0.6508	0.01609	0.0786	0.00107	605	62	509	10	488	6	4.3
SZG2-91	0.2	0.05599	0.00069	0.54817	0.00798	0.07099	0.00095	452	14	444	5	442	6	0.5
SZG2-92	0.43	0.05747	0.00078	0.5696	0.0089	0.07187	0.00097	510	15	458	6	447	6	2.5
SZG2-93	0.93	0.05172	0.00204	0.28214	0.01111	0.03956	0.00063	273	61	252	9	250	4	0.8
SZG2-94	0.8	0.0553	0.00073	0.50487	0.00769	0.06621	0.00089	424	15	415	5	413	5	0.5
SZG2-95	0.27	0.06089	0.00102	0.80018	0.01451	0.09529	0.00132	635	18	597	8	587	8	1.7
SZG2-96	0.08	0.05744	0.00079	0.62551	0.00987	0.07897	0.00107	508	16	493	6	490	6	0.6

SZG2-97	0.44	0.05707	0.00083	0.53608	0.00875	0.06812	0.00092	494	16	436	6	425	6	2.6
~~SZG2-98~~	~~0.85~~	~~0.0717~~	~~0.00122~~	~~0.60443~~	~~0.01111~~	~~0.06113~~	~~0.00085~~	~~977~~	~~18~~	~~480~~	~~7~~	~~382~~	~~5~~	~~25.7~~
SZG2-99	0.46	0.06944	0.00082	1.37194	0.01957	0.14326	0.0019	912	13	877	8	863	11	1.6
SZG2-100	0.32	0.05537	0.00081	0.5333	0.00877	0.06984	0.00095	427	17	434	6	435	6	-0.2
CSL4														
~~CSL4-01~~	~~0.75~~	~~0.06661~~	~~0.00149~~	~~0.67635~~	~~0.01605~~	~~0.07363~~	~~0.00111~~	~~826~~	~~26~~	~~525~~	~~10~~	~~458~~	~~7~~	~~14.6~~
CSL4-02	0.06	0.0701	0.00188	1.44133	0.03253	0.14912	0.00217	931	56	906	14	896	12	1.1
CSL4-03	0.7	0.05104	0.00159	0.28476	0.00907	0.04046	0.00064	243	45	254	7	256	4	-0.8
CSL4-04	0.08	0.07149	0.00196	1.57285	0.03653	0.15957	0.00233	971	57	960	14	954	13	0.6
CSL4-05	0.35	0.05498	0.00135	0.53496	0.01376	0.07055	0.00108	411	31	435	9	439	7	-0.9
CSL4-06	0.62	0.05567	0.00145	0.49032	0.0133	0.06387	0.00099	439	34	405	9	399	6	1.5
CSL4-07	0.7	0.05072	0.00148	0.24417	0.00727	0.03491	0.00056	228	40	222	6	221	3	0.5
CSL4-08	0.63	0.15355	0.0025	9.12499	0.16046	0.43093	0.006	2386	14	2351	16	2310	27	3.3
CSL4-09	0.84	0.06049	0.00106	0.56835	0.01065	0.06813	0.00093	621	19	457	7	425	6	7.5
CSL4-10	1.04	0.06007	0.00094	0.49181	0.00845	0.05937	0.0008	606	17	406	6	372	5	9.1
CSL4-11	0.28	0.07364	0.00126	1.71318	0.03153	0.16869	0.00232	1032	18	1013	12	1005	13	2.7
CSL4-12	0.11	0.06982	0.00107	1.4347	0.02429	0.14899	0.00201	923	16	904	10	895	11	1
CSL4-13	0.78	0.05769	0.00099	0.4829	0.00889	0.0607	0.00083	518	19	400	6	380	5	5.3
CSL4-14	0.72	0.05424	0.00104	0.448	0.00908	0.05989	0.00083	381	23	376	6	375	5	0.3
CSL4-15	0.4	0.05538	0.00132	0.5355	0.01313	0.07012	0.00099	428	30	435	9	437	6	-0.5
CSL4-16	0.4	0.05699	0.00112	0.62277	0.01282	0.07925	0.00111	491	23	492	8	492	7	0
CSL4-17	1.75	0.0556	0.00105	0.53325	0.01068	0.06955	0.00096	436	22	434	7	433	6	0.2
CSL4-18	0.44	0.05034	0.0009	0.22084	0.00422	0.03181	0.00044	211	21	203	4	202	3	0.5
CSL4-19	0.63	0.05476	0.00137	0.46215	0.01189	0.0612	0.00087	402	33	386	8	383	5	0.8
CSL4-20	0.22	0.05592	0.00097	0.53339	0.00995	0.06917	0.00095	449	20	434	7	431	6	0.7
CSL4-21	0.67	0.05571	0.00094	0.52308	0.00953	0.06808	0.00093	441	19	427	6	425	6	0.5

CSL4-22	0.9	0.05685	0.00104	0.54372	0.01058	0.06935	0.00096	486	21	441	7	432	6	2.1
CSL4-23	0.5	0.05148	0.00121	0.29352	0.00713	0.04134	0.00059	262	31	261	6	261	4	0
CSL4-24	0.86	0.05268	0.003	0.27652	0.01516	0.03807	0.00058	315	133	248	12	241	4	2.9
CSL4-25	1.23	0.05625	0.00091	0.50521	0.00895	0.06513	0.00089	462	18	415	6	407	5	2
CSL4-26	0.59	0.05473	0.00237	0.46138	0.01985	0.06113	0.00101	401	67	385	14	382	6	0.8
CSL4-27	0.39	0.05539	0.00104	0.53299	0.01065	0.06978	0.00097	428	22	434	7	435	6	-0.2
CSL4-28	0.75	0.05692	0.00153	0.3255	0.00893	0.04146	0.0006	488	36	286	7	262	4	9.2
CSL4-29	0.49	0.11291	0.00167	5.02692	0.08315	0.32285	0.00437	1847	14	1824	14	1804	21	2.4
CSL4-30	0.64	0.0571	0.00106	0.54286	0.0107	0.06894	0.00095	495	21	440	7	430	6	2.3
CSL4-31	0.88	0.05124	0.00116	0.25021	0.00585	0.03541	0.0005	252	29	227	5	224	3	1.3
CSL4-32	0.61	0.05453	0.00336	0.46407	0.02848	0.06171	0.00104	393	108	387	20	386	6	0.3
CSL4-33	0.93	0.0551	0.00184	0.49158	0.01634	0.06469	0.00104	416	46	406	11	404	6	0.5
CSL4-34	0.44	0.05559	0.00108	0.52376	0.01077	0.06833	0.00095	436	23	428	7	426	6	0.5
CSL4-35	1.42	0.06015	0.00102	0.58382	0.01076	0.07038	0.00097	609	19	467	7	438	6	6.6
CSL4-36	0.03	0.05504	0.00104	0.50182	0.01006	0.06611	0.00092	414	22	413	7	413	6	0
CSL4-37	0.2	0.0551	0.00088	0.48671	0.00855	0.06405	0.00087	416	18	403	6	400	5	0.8
CSL4-38	0.89	0.05671	0.00112	0.53487	0.01121	0.06839	0.00095	480	24	435	7	426	6	2.1
CSL4-39	0.09	0.07199	0.00159	1.5408	0.02714	0.15523	0.00207	986	46	947	11	930	12	1.8
CSL4-40	0.81	0.05556	0.00236	0.53383	0.0225	0.06968	0.00114	435	65	434	15	434	7	0
CSL4-41	0.58	0.05502	0.00148	0.49155	0.01347	0.06479	0.00095	413	36	406	9	405	6	0.2
CSL4-42	0.5	0.05407	0.00153	0.45069	0.01303	0.06044	0.00088	374	39	378	9	378	5	0
CSL4-43	0.59	0.05403	0.0015	0.43669	0.0124	0.05861	0.00084	372	38	368	9	367	5	0.3
CSL4-44	0.57	0.05525	0.00106	0.46991	0.0096	0.06168	0.00086	422	23	391	7	386	5	1.3
CSL4-45	0.08	0.05895	0.00101	0.65507	0.01221	0.08057	0.00111	565	19	512	7	500	7	2.4
CSL4-46	0.39	0.06619	0.00216	1.26537	0.03714	0.13865	0.00197	812	70	830	17	837	11	-0.8
CSL4-47	0.37	0.05595	0.00093	0.48462	0.00879	0.06281	0.00087	450	19	401	6	393	5	2
CSL4-48	1	0.05782	0.00122	0.4925	0.01092	0.06176	0.00088	523	25	407	7	386	5	5.4
CSL4-49	0.38	0.08264	0.00263	2.46524	0.06965	0.21635	0.00314	1261	64	1262	20	1263	17	-0.2

CSL4-50	0.42	0.1141	0.00187	5.17229	0.09296	0.32871	0.00459	1866	15	1848	15	1832	22	1.9
CSL4-51	1.3	0.05637	0.00132	0.58571	0.0142	0.07535	0.00108	467	29	468	9	468	6	0
CSL4-52	1.28	0.05114	0.00105	0.27415	0.00593	0.03887	0.00055	247	26	246	5	246	3	0
CSL4-53	0.72	0.13755	0.00218	7.09205	0.12433	0.37388	0.00518	2197	14	2123	16	2048	24	7.3
CSL4-54	0.46	0.05204	0.00286	0.3215	0.01758	0.04479	0.00074	287	95	283	14	282	5	0.4
CSL4-55	0.3	0.05676	0.00106	0.56289	0.01121	0.07192	0.00101	482	21	453	7	448	6	1.1
CSL4-56	0.3	0.05767	0.00177	0.5607	0.01527	0.07051	0.00099	517	69	452	10	439	6	3
CSL4-57	~~0.37~~	0.05451	0.00101	0.46422	0.0092	0.06175	0.00087	392	22	387	6	386	5	0.3
~~CSL4-58~~	0.56	~~0.08232~~	~~0.00294~~	~~2.11361~~	~~0.06872~~	~~0.18621~~	~~0.00273~~	~~1253~~	~~71~~	~~1153~~	~~22~~	~~1101~~	~~15~~	~~13.8~~
CSL4-59	0.28	0.05705	0.00209	0.55942	0.01885	0.07112	0.00103	493	83	451	12	443	6	1.8
CSL4-60	0.29	0.05155	0.00107	0.23511	0.00513	0.03307	0.00047	266	26	214	4	210	3	1.9
CSL4-61	0.96	0.05177	0.00123	0.27988	0.0069	0.0392	0.00057	275	31	251	5	248	4	1.2
CSL4-62	2	0.11371	0.00225	5.04151	0.10521	0.32149	0.00472	1860	18	1826	18	1797	23	3.5
CSL4-63	0.84	0.05486	0.0065	0.47453	0.05577	0.06272	0.00143	407	223	394	38	392	9	0.5
CSL4-64	0.78	0.05515	0.00118	0.51491	0.01159	0.06771	0.00097	418	26	422	8	422	6	0
CSL4-65	0.47	0.05706	0.00098	0.60295	0.01131	0.07662	0.00107	494	20	479	7	476	6	0.6
CSL4-66	0.54	0.05183	0.00143	0.23891	0.00673	0.03343	0.0005	278	38	218	6	212	3	2.8
CSL4-67	0.7	0.0564	0.00109	0.52662	0.01088	0.0677	0.00096	468	23	430	7	422	6	1.9
CSL4-68	1.42	0.05162	0.00124	0.27326	0.00682	0.03839	0.00056	269	32	245	5	243	3	0.8
CSL4-69	0.46	0.05612	0.00103	0.52516	0.01038	0.06785	0.00096	457	21	429	7	423	6	1.4
CSL4-70	0.28	0.05347	0.00108	0.38775	0.00833	0.05259	0.00075	349	25	333	6	330	5	0.9
CSL4-71	0.26	0.11397	0.00283	5.01459	0.10304	0.31911	0.00446	1864	46	1822	17	1785	22	4.4
CSL4-72	~~0.55~~	0.05703	0.00131	0.5796	0.01376	0.0737	0.00109	493	28	464	9	458	7	1.3
CSL4-73	0.57	0.05483	0.00132	0.45158	0.01125	0.05972	0.00087	405	31	378	8	374	5	1.1
CSL4-74	0.31	0.05655	0.001	0.54547	0.01049	0.06995	0.00098	474	20	442	7	436	6	1.4
CSL4-75	0.63	0.05162	0.00156	0.30013	0.00925	0.04216	0.00063	269	44	267	7	266	4	0.4
CSL4-76	~~0.54~~	0.05488	0.00116	0.51526	0.01152	0.06808	0.00098	407	26	422	8	425	6	-0.7
CSL4-77	1.16	0.18018	0.00302	12.05815	0.22267	0.48527	0.00684	2655	14	2609	17	2550	30	4.1

CSL4-78	0.14	0.0548	0.00103	0.48859	0.00987	0.06466	0.00092	404	22	404	7	404	6	0
CSL4-79	0.67	0.05429	0.00153	0.45714	0.0132	0.06106	0.00091	383	39	382	9	382	6	0
CSL4-80	0.37	0.05025	0.00207	0.23283	0.00963	0.03359	0.00053	207	67	213	8	213	3	0
CSL4-81	0.47	0.05655	0.00132	0.54124	0.01319	0.06941	0.00101	474	29	439	9	433	6	1.4
CSL4-82	0.17	0.06929	0.00124	1.34381	0.02619	0.14063	0.002	907	19	865	11	848	11	2
CSL4-83	0.56	0.05691	0.00164	0.62053	0.01817	0.07906	0.0012	488	38	490	11	491	7	-0.2
CSL4-84	0.56	0.05603	0.00187	0.49409	0.01657	0.06394	0.00103	454	46	408	11	400	6	2
CSL4-85	0.67	0.05741	0.00115	0.56127	0.01198	0.0709	0.00102	507	24	452	8	442	6	2.3
CSL4-86	0.37	0.05752	0.00509	0.64173	0.05631	0.0809	0.00165	512	159	503	35	501	10	0.4
CSL4-87	0.7	0.12415	0.00215	5.8487	0.11113	0.3416	0.00484	2017	16	1954	16	1894	23	6.5
CSL4-88	0.29	0.07054	0.00129	1.43026	0.02843	0.14702	0.0021	944	20	902	12	884	12	2
~~CSL4-89~~	0.59	~~0.06245~~	~~0.00254~~	~~0.52486~~	~~0.02141~~	~~0.06094~~	~~0.00098~~	~~690~~	~~59~~	~~428~~	~~14~~	~~381~~	~~6~~	~~12.3~~
CSL4-90	0.82	0.16199	0.00279	10.194	0.19322	0.45633	0.00645	2477	15	2453	18	2423	29	2.2
CSL4-91	0.58	0.05082	0.00273	0.23788	0.01219	0.03395	0.00054	232	125	217	10	215	3	0.9
~~CSL4-92~~	0.71	~~0.06308~~	~~0.00219~~	~~0.54332~~	~~0.01894~~	~~0.06246~~	~~0.001~~	~~711~~	~~47~~	~~441~~	~~12~~	~~391~~	~~6~~	~~12.8~~
CSL4-93	0.82	0.05602	0.00127	0.49195	0.01168	0.06367	0.00094	453	28	406	8	398	6	2
CSL4-94	1.11	0.05547	0.0013	0.53882	0.01315	0.07044	0.00104	431	29	438	9	439	6	-0.2
~~CSL4-95~~	0.75	~~0.06274~~	~~0.00136~~	~~0.34994~~	~~0.008~~	~~0.04045~~	~~0.00059~~	~~699~~	~~25~~	~~305~~	~~6~~	~~256~~	~~4~~	~~19.1~~
CSL4-96	0.21	0.06964	0.0013	1.41985	0.02864	0.14785	0.00212	918	20	897	12	889	12	0.9
CSL4-97	0.16	0.06966	0.00187	1.38716	0.03152	0.14442	0.00205	918	56	883	13	870	12	1.5
CSL4-98	0.53	0.05512	0.00117	0.52034	0.01167	0.06845	0.001	417	26	425	8	427	6	-0.5
CSL4-99	0.46	0.05672	0.00111	0.41268	0.00866	0.05276	0.00076	481	23	351	6	331	5	6
CSL4-100	0.67	0.05523	0.00202	0.32164	0.01181	0.04223	0.00067	422	54	283	9	267	4	6
SZG1														
SZG1-01	0.65	0.05588	0.0009	0.53076	0.0094	0.06888	0.00095	448	18	432	6	429	6	0.7
SZG1-02	2.15	0.05625	0.0008	0.5744	0.00924	0.07405	0.001	462	16	461	6	461	6	0

~~SZG1-03~~	~~0.66~~	~~0.05823~~	~~0.00079~~	~~0.34527~~	~~0.00539~~	~~0.043~~	~~0.00058~~	~~538~~	~~15~~	~~301~~	~~4~~	~~271~~	~~4~~	~~11.1~~
SZG1-04	0.54	0.05559	0.00082	0.54161	0.00899	0.07065	0.00096	436	17	439	6	440	6	-0.2
SZG1-05	0.4	0.06859	0.00086	1.19076	0.01764	0.12587	0.00168	886	14	796	8	764	10	4.2
SZG1-06	0.61	0.05934	0.00077	0.52475	0.00796	0.06412	0.00086	580	15	428	5	401	5	6.7
SZG1-07	0.21	0.05625	0.00074	0.57964	0.00886	0.07473	0.00101	462	15	464	6	465	6	-0.2
SZG1-08	0.41	0.06597	0.00106	1.36305	0.02391	0.14981	0.00208	805	17	873	10	900	12	-3
SZG1-09	0.47	0.0549	0.00073	0.49679	0.00766	0.06561	0.00088	408	15	410	5	410	5	0
SZG1-10	0.93	0.05793	0.00078	0.58728	0.00911	0.07351	0.00099	527	15	469	6	457	6	2.6
SZG1-11	0.37	0.05586	0.00086	0.5513	0.00946	0.07157	0.00098	447	17	446	6	446	6	0
SZG1-12	0.35	0.0599	0.00078	0.54695	0.00832	0.06621	0.00089	600	15	443	5	413	5	7.3
SZG1-13	0.47	0.06152	0.00086	0.55101	0.00876	0.06494	0.00088	657	15	446	6	406	5	9.9
~~SZG1-14~~	~~1.24~~	~~0.06143~~	~~0.00092~~	~~0.35486~~	~~0.00592~~	~~0.04188~~	~~0.00057~~	~~654~~	~~16~~	~~308~~	~~4~~	~~264~~	~~4~~	~~16.7~~
SZG1-15	1	0.05919	0.00083	0.6048	0.00969	0.07409	0.00101	574	16	480	6	461	6	4.1
~~SZG1-16~~	~~0.85~~	~~0.07747~~	~~0.00158~~	~~0.66341~~	~~0.01408~~	~~0.06209~~	~~0.0009~~	~~1133~~	~~21~~	~~517~~	~~9~~	~~388~~	~~5~~	~~33.2~~
~~SZG1-17~~	~~1.34~~	~~0.06433~~	~~0.00114~~	~~0.57329~~	~~0.01092~~	~~0.06462~~	~~0.00091~~	~~752~~	~~19~~	~~460~~	~~7~~	~~404~~	~~6~~	~~13.9~~
SZG1-18	0.72	0.05242	0.00088	0.30433	0.00558	0.0421	0.00058	304	20	270	4	266	4	1.5
SZG1-19	0.77	0.05117	0.00124	0.29065	0.00727	0.04118	0.00059	248	32	259	6	260	4	-0.4
SZG1-20	0.24	0.05632	0.00074	0.53707	0.00823	0.06915	0.00093	465	15	436	5	431	6	1.2
SZG1-21	0.3	0.0797	0.00104	2.15135	0.03283	0.19573	0.00265	1190	13	1165	11	1152	14	3.3
SZG1-22	0.57	0.0555	0.00078	0.56501	0.00908	0.07381	0.00101	432	16	455	6	459	6	-0.9
SZG1-23	0.45	0.0562	0.00085	0.51628	0.0087	0.06661	0.00091	460	17	423	6	416	5	1.7
SZG1-24	0.51	0.05587	0.00106	0.53713	0.01084	0.0697	0.00098	447	22	437	7	434	6	0.7
SZG1-25	0.77	0.05548	0.00126	0.52681	0.01248	0.06885	0.00099	432	28	430	8	429	6	0.2
SZG1-26	1.44	0.05719	0.00084	0.56945	0.00941	0.0722	0.00099	499	16	458	6	449	6	2
SZG1-27	0.17	0.06986	0.00085	1.4282	0.02082	0.14825	0.00198	924	13	901	9	891	11	1.1
SZG1-28	0.49	0.05637	0.00071	0.57296	0.00854	0.0737	0.00099	467	15	460	6	458	6	0.4
SZG1-29	0.39	0.05599	0.00076	0.5899	0.00922	0.0764	0.00103	452	16	471	6	475	6	-0.8
SZG1-30	1.81	0.05535	0.00077	0.54808	0.00869	0.0718	0.00097	426	16	444	6	447	6	-0.7

SZG1-31	0.2	0.05528	0.00072	0.57489	0.00871	0.07541	0.00101	424	15	461	6	469	6	-1.7
SZG1-32	1.3	0.05606	0.00082	0.50832	0.00834	0.06575	0.0009	455	16	417	6	410	5	1.7
SZG1-33	0.46	0.09484	0.00115	3.39229	0.04921	0.25938	0.00347	1525	12	1503	11	1487	18	2.6
SZG1-34	0.48	0.0565	0.00076	0.58355	0.00904	0.07489	0.00101	472	15	467	6	466	6	0.2
SZG1-35	0.54	0.05678	0.00072	0.57755	0.00865	0.07375	0.00099	483	15	463	6	459	6	0.9
~~SZG1-36~~	~~1.03~~	~~0.0615~~	~~0.00105~~	~~0.32217~~	~~0.00594~~	~~0.03799~~	~~0.00053~~	~~657~~	~~19~~	~~284~~	~~5~~	~~240~~	~~3~~	~~18.3~~
SZG1-37	0.71	0.05329	0.00094	0.30556	0.0058	0.04157	0.00058	341	20	271	5	263	4	3
SZG1-38	0.09	0.06929	0.00085	1.45179	0.02129	0.15193	0.00204	907	13	911	9	912	11	-0.1
SZG1-39	0.18	0.05496	0.00135	0.53531	0.01103	0.07064	0.00095	411	56	435	7	440	6	-1.1
SZG1-40	1.17	0.05887	0.00125	0.5706	0.01266	0.07029	0.00101	562	25	458	8	438	6	4.6
SZG1-41	0.16	0.06835	0.00153	1.3596	0.0244	0.14427	0.00192	879	47	872	11	869	11	0.3
~~SZG1-42~~	~~0.18~~	~~0.10095~~	~~0.00289~~	~~1.9977~~	~~0.04911~~	~~0.14352~~	~~0.00212~~	~~1642~~	~~54~~	~~1115~~	~~17~~	~~865~~	~~12~~	~~28.9~~
SZG1-43	0.92	0.05607	0.00077	0.52981	0.00837	0.06851	0.00093	455	16	432	6	427	6	1.2
SZG1-44	1.18	0.05767	0.0008	0.54584	0.00865	0.06863	0.00093	517	16	442	6	428	6	3.3
SZG1-45	0.48	0.06105	0.00096	0.57864	0.01002	0.06873	0.00095	641	17	464	6	428	6	8.4
SZG1-46	0.95	0.05666	0.0012	0.49478	0.011	0.06333	0.0009	478	26	408	7	396	5	3
SZG1-47	0.4	0.05594	0.00119	0.50853	0.0113	0.06591	0.00094	450	26	417	8	411	6	1.5
SZG1-48	0.69	0.05384	0.00074	0.46317	0.00731	0.06238	0.00085	364	16	386	5	390	5	-1
SZG1-49	0.19	0.05524	0.0008	0.49859	0.00817	0.06545	0.00089	422	17	411	6	409	5	0.5
SZG1-50	0.45	0.05557	0.00104	0.50585	0.01014	0.06601	0.00093	435	22	416	7	412	6	1
SZG1-51	0.32	0.05608	0.00114	0.52362	0.01126	0.06772	0.00099	456	24	428	8	422	6	1.4
SZG1-52	0.21	0.05429	0.0015	0.47056	0.0112	0.06287	0.00088	383	63	392	8	393	5	-0.3
SZG1-53	0.73	0.05507	0.00318	0.52263	0.02966	0.06882	0.00138	415	91	427	20	429	8	-0.5
SZG1-54	0.63	0.05541	0.00121	0.53331	0.01218	0.0698	0.00103	429	26	434	8	435	6	-0.2
SZG1-55	0.22	0.06947	0.00182	1.36166	0.03007	0.14216	0.00199	913	55	873	13	857	11	1.9
SZG1-56	0.45	0.05478	0.00206	0.5191	0.01795	0.06873	0.00102	403	86	425	12	428	6	-0.7
SZG1-57	0.46	0.05679	0.00102	0.55204	0.01076	0.07049	0.00101	483	21	446	7	439	6	1.6
SZG1-58	0.84	0.05812	0.00202	0.57752	0.01996	0.07206	0.00121	534	47	463	13	449	7	3.1

SZG1-59	0.58	0.06138	0.00247	0.59599	0.0236	0.07042	0.00127	653	54	475	15	439	8	8.2
SZG1-60	0.66	0.05181	0.00102	0.25061	0.00527	0.03508	0.00051	277	24	227	4	222	3	2.3
SZG1-61	1.24	0.05051	0.00531	0.25674	0.02641	0.03686	0.00079	219	240	232	21	233	5	-0.4
SZG1-62	0.72	0.05977	0.00153	0.59523	0.01556	0.07221	0.00111	595	31	474	10	449	7	5.6
SZG1-63	0.51	0.0568	0.00105	0.50817	0.01012	0.06488	0.00093	484	21	417	7	405	6	3
SZG1-64	0.51	0.05632	0.00088	0.5228	0.00924	0.06732	0.00094	465	18	427	6	420	6	1.7
SZG1-65	0.67	0.05084	0.00236	0.27026	0.01237	0.03855	0.0007	234	72	243	10	244	4	-0.4
SZG1-66	0.65	0.05744	0.00117	0.54794	0.01182	0.06918	0.00101	508	24	444	8	431	6	3
SZG1-67	1.4	0.05753	0.00119	0.54781	0.012	0.06906	0.00101	512	24	444	8	430	6	3.3
SZG1-68	0.41	0.05771	0.00105	0.6149	0.01214	0.07727	0.00111	519	21	487	8	480	7	1.5
SZG1-69	1.05	0.05766	0.00125	0.56148	0.01273	0.07061	0.00105	517	25	452	8	440	6	2.7
SZG1-70	0.33	0.05801	0.00131	0.57613	0.01349	0.07202	0.00108	530	27	462	9	448	6	3.1
SZG1-71	0.38	0.05596	0.00128	0.51598	0.01228	0.06687	0.001	451	28	422	8	417	6	1.2
SZG1-72	1.13	0.05632	0.00097	0.55038	0.01039	0.07087	0.00101	465	20	445	7	441	6	0.9
SZG1-73	0.53	0.07498	0.00122	1.77203	0.03202	0.17138	0.00243	1068	17	1035	12	1020	13	4.7
SZG1-74	1.41	0.05076	0.00107	0.25576	0.00569	0.03654	0.00053	230	26	231	5	231	3	0
SZG1-75	0.23	0.05578	0.00126	0.51792	0.01221	0.06734	0.00101	444	27	424	8	420	6	1
SZG1-76	0.71	0.05578	0.00109	0.51357	0.01072	0.06677	0.00097	444	23	421	7	417	6	1
~~SZG1-77~~	~~0.21~~	~~0.10062~~	~~0.00328~~	~~1.90619~~	~~0.05542~~	~~0.1374~~	~~0.00203~~	~~1636~~	~~62~~	~~1083~~	~~19~~	~~830~~	~~11~~	~~30.5~~
SZG1-78	1.35	0.05627	0.00118	0.54406	0.01203	0.07012	0.00103	463	25	441	8	437	6	0.9
SZG1-79	0.63	0.05447	0.00121	0.45007	0.01047	0.05992	0.00089	391	27	377	7	375	5	0.5
SZG1-80	0.35	0.05664	0.00123	0.57195	0.01305	0.07322	0.00109	478	26	459	8	456	7	0.7
SZG1-81	0.74	0.16803	0.00257	10.56279	0.18308	0.45586	0.00647	2538	13	2485	16	2421	29	0
SZG1-82	0.64	0.05479	0.00126	0.5434	0.01304	0.07192	0.00108	404	28	441	9	448	6	-1.6
SZG1-83	2.07	0.05764	0.00099	0.54685	0.01035	0.0688	0.00098	516	20	443	7	429	6	3.3
SZG1-84	0.47	0.0549	0.00102	0.54351	0.01091	0.0718	0.00103	408	22	441	7	447	6	-1.3
SZG1-85	0.91	0.05045	0.00148	0.25552	0.00758	0.03673	0.00058	216	40	231	6	233	4	-0.9
SZG1-86	1.14	0.05844	0.00392	0.61089	0.03962	0.07581	0.00129	546	151	484	25	471	8	2.8

SZG1-87	0.58	0.05802	0.00149	0.44026	0.01156	0.05503	0.00085	531	32	370	8	345	5	7.2
SZG1-88	0.83	0.05576	0.00146	0.49949	0.01336	0.06496	0.00101	443	33	411	9	406	6	1.2
SZG1-89	1.59	0.05627	0.00136	0.55844	0.01393	0.07197	0.0011	463	30	451	9	448	7	0.7
SZG1-90	0.27	0.05601	0.00412	0.55412	0.03962	0.07175	0.00121	453	168	448	26	447	7	0.2
SZG1-91	0.97	0.05021	0.00196	0.26187	0.01014	0.03782	0.00065	205	58	236	8	239	4	-1.3
SZG1-92	0.44	0.07082	0.00124	1.45347	0.02781	0.14884	0.00214	952	18	911	12	894	12	1.9
SZG1-93	0.38	0.05716	0.00135	0.59523	0.01458	0.07551	0.00115	498	29	474	9	469	7	1.1
SZG1-94	0.4	0.05746	0.0027	0.58618	0.0259	0.07398	0.00117	509	106	468	17	460	7	1.7
SZG1-95	1.59	0.0575	0.00121	0.56055	0.01243	0.0707	0.00105	511	25	452	8	440	6	2.7
SZG1-96	0.14	0.07083	0.00119	1.48002	0.0275	0.15154	0.00216	953	18	922	11	910	12	1.3
SZG1-97	0.97	0.11551	0.00183	5.23981	0.09359	0.32896	0.00468	1888	15	1859	15	1833	23	3
SZG1-98	0.03	0.0587	0.00143	0.54239	0.01081	0.06701	0.00094	556	54	440	7	418	6	5.3
SZG1-99	0.17	0.0682	0.00183	1.28441	0.0291	0.1366	0.00195	875	57	839	13	825	11	1.7
SZG1-100	0.75	0.04971	0.00283	0.26029	0.01457	0.03797	0.00074	181	93	235	12	240	5	-2.1
CSL5														
CSL5-01	0.53	0.05616	0.00115	0.56648	0.01232	0.07314	0.00103	459	25	456	8	455	6	0.2
CSL5-02	0.43	0.05187	0.00077	0.27698	0.00465	0.03872	0.00053	280	17	248	4	245	3	1.2
CSL5-03	0.38	0.06803	0.00095	1.32025	0.02122	0.14073	0.00192	869	15	855	9	849	11	0.7
CSL5-04	0.55	0.05155	0.001	0.29626	0.00612	0.04167	0.00058	266	24	263	5	263	4	0
CSL5-05	0.39	0.05737	0.00114	0.58271	0.01235	0.07365	0.00103	506	24	466	8	458	6	1.7
CSL5-06	0.8	0.05569	0.00082	0.49368	0.00823	0.06428	0.00087	440	17	407	6	402	5	1.2
CSL5-07	0.69	0.0547	0.00101	0.5078	0.01005	0.06732	0.00094	400	22	417	7	420	6	-0.7
CSL5-08	0.85	0.05593	0.00096	0.54454	0.01021	0.0706	0.00099	450	20	441	7	440	6	0.2
CSL5-09	0.36	0.07085	0.00095	1.40496	0.02205	0.14378	0.00195	953	14	891	9	866	11	2.9
CSL5-10	0.65	0.0509	0.00159	0.27486	0.0087	0.03916	0.00058	236	46	247	7	248	4	-0.4
CSL5-11	0.68	0.05375	0.00177	0.43662	0.01445	0.0589	0.00092	361	47	368	10	369	6	-0.3

CSL5-12	0.36	0.05638	0.00088	0.51831	0.00906	0.06667	0.00092	467	18	424	6	416	6	1.9
CSL5-13	0.46	0.05588	0.00118	0.55057	0.01228	0.07145	0.00101	448	26	445	8	445	6	0
CSL5-14	1.35	0.05853	0.00135	0.71908	0.01724	0.08908	0.00128	550	28	550	10	550	8	0
CSL5-15	1.48	0.04609	0.00412	0.23903	0.02099	0.03761	0.00062	2	195	218	17	238	4	-8.4
CSL5-16	0.31	0.16406	0.00346	10.35702	0.16753	0.45786	0.00621	2498	36	2467	15	2430	27	2.8
CSL5-17	0.36	0.05647	0.00112	0.60673	0.01286	0.0779	0.0011	471	24	481	8	484	7	-0.6
CSL5-18	0.65	0.05153	0.00126	0.30319	0.00768	0.04267	0.00062	265	32	269	6	269	4	0
CSL5-19	0.7	0.05453	0.00078	0.47941	0.00786	0.06375	0.00087	393	17	398	5	398	5	0
CSL5-20	0.15	0.06955	0.00153	1.38151	0.02401	0.14407	0.00193	915	46	881	10	868	11	1.5
CSL5-21	0.3	0.07085	0.00102	1.45701	0.02405	0.14912	0.00205	953	15	913	10	896	12	1.9
CSL5-22	0.39	0.05609	0.00123	0.54832	0.01264	0.07089	0.00101	456	27	444	8	442	6	0.5
CSL5-23	0.59	0.05097	0.00335	0.27532	0.01801	0.03917	0.00067	239	119	247	14	248	4	-0.4
CSL5-24	0.92	0.05635	0.00126	0.54878	0.01279	0.07062	0.00101	466	28	444	8	440	6	0.9
CSL5-25	0.47	0.05578	0.00101	0.55808	0.01095	0.07255	0.00101	444	21	450	7	452	6	-0.4
CSL5-26	0.44	0.07836	0.00111	2.0417	0.03319	0.18894	0.0026	1156	14	1130	11	1116	14	3.6
CSL5-27	0.81	0.0566	0.00094	0.56015	0.01023	0.07176	0.00099	476	19	452	7	447	6	1.1
CSL5-28	0.22	0.05106	0.00094	0.27732	0.00549	0.03938	0.00055	244	22	249	4	249	3	0
CSL5-29	0.45	0.05151	0.00124	0.28808	0.00726	0.04056	0.00057	264	33	257	6	256	4	0.4
CSL5-30	0.47	0.05051	0.0013	0.23159	0.00612	0.03325	0.00048	219	35	212	5	211	3	0.5
CSL5-31	0.5	0.07197	0.00097	1.56049	0.02454	0.15723	0.00214	985	14	955	10	941	12	1.5
CSL5-32	0.67	0.05648	0.0015	0.58891	0.01597	0.0756	0.00113	471	34	470	10	470	7	0
CSL5-33	1.01	0.07166	0.00108	1.53535	0.02608	0.15536	0.00215	976	16	945	10	931	12	1.5
CSL5-34	0.6	0.09182	0.00134	3.09862	0.05129	0.2447	0.0034	1464	14	1432	13	1411	18	3.8
CSL5-35	1.33	0.05461	0.00075	0.4676	0.00745	0.06208	0.00084	396	16	390	5	388	5	0.5
CSL5-36	0.71	0.05577	0.00106	0.5515	0.01125	0.0717	0.00101	443	22	446	7	446	6	0
CSL5-37	0.22	0.05459	0.00152	0.48417	0.01173	0.06433	0.00089	395	64	401	8	402	5	-0.2
CSL5-38	0.23	0.0657	0.0016	1.217	0.02464	0.13434	0.00183	797	52	808	11	813	10	-0.6
CSL5-39	0.56	0.0564	0.00117	0.54295	0.01192	0.06981	0.00099	468	25	440	8	435	6	1.1

CSL5-40	0.88	0.05554	0.00172	0.52436	0.0164	0.06847	0.00105	434	43	428	11	427	6	0.2
CSL5-41	1.2	0.11908	0.00457	5.73027	0.19984	0.349	0.0056	1942	70	1936	30	1930	27	0.6
CSL5-42	0.83	0.05152	0.00136	0.25797	0.007	0.03631	0.00053	264	36	233	6	230	3	1.3
CSL5-43	0.85	0.05645	0.00081	0.52431	0.00863	0.06735	0.00092	470	16	428	6	420	6	1.9
CSL5-44	0.49	0.05764	0.00128	0.66151	0.01543	0.08322	0.00119	516	27	516	9	515	7	0.2
CSL5-45	0.45	0.05564	0.00084	0.51702	0.00881	0.06738	0.00092	438	17	423	6	420	6	0.7
CSL5-46	0.58	0.0565	0.00114	0.5639	0.01211	0.07237	0.00102	472	24	454	8	450	6	0.9
CSL5-47	0.58	0.05467	0.00166	0.47872	0.01485	0.0635	0.00095	399	43	397	10	397	6	0
CSL5-48	0.61	0.05135	0.00185	0.28583	0.01036	0.04037	0.00062	257	55	255	8	255	4	0
CSL5-49	0.66	0.05588	0.00082	0.51544	0.00865	0.06689	0.00092	448	17	422	6	417	6	1.2
CSL5-50	0.63	0.05623	0.001	0.57696	0.01115	0.0744	0.00104	461	21	463	7	463	6	0
CSL5-51	0.04	0.05738	0.00085	0.55515	0.00934	0.07016	0.00096	506	17	448	6	437	6	2.5
CSL5-52	0.5	0.05572	0.00083	0.50319	0.00856	0.06548	0.0009	441	17	414	6	409	5	1.2
CSL5-53	1.08	0.05564	0.00075	0.49459	0.00782	0.06446	0.00088	438	16	408	5	403	5	1.2
CSL5-54	0.47	0.07125	0.00101	1.4438	0.02359	0.14695	0.00202	965	15	907	10	884	11	2.6
CSL5-55	0.37	0.0552	0.00087	0.5137	0.00903	0.06748	0.00093	420	18	421	6	421	6	0
CSL5-56	0.25	0.05471	0.00094	0.4926	0.00928	0.06529	0.00091	400	20	407	6	408	6	-0.2
CSL5-57	0.47	0.05582	0.00136	0.52153	0.01317	0.06775	0.00098	445	31	426	9	423	6	0.7
CSL5-58	0.62	0.05073	0.00075	0.25318	0.00425	0.03619	0.0005	229	18	229	3	229	3	0
CSL5-59	0.07	0.06874	0.0009	1.34217	0.02079	0.1416	0.00193	891	14	864	9	854	11	1.2
CSL5-60	0.47	0.05553	0.00106	0.51573	0.0106	0.06735	0.00095	434	23	422	7	420	6	0.5
CSL5-61	0.62	0.05128	0.00107	0.29122	0.00642	0.04118	0.00059	253	26	260	5	260	4	0
CSL5-62	0.69	0.05119	0.00156	0.28494	0.0088	0.04037	0.00061	249	44	255	7	255	4	0
~~CSL5-63~~	~~0.49~~	~~0.0945~~	~~0.00289~~	~~2.49045~~	~~0.06714~~	~~0.19113~~	~~0.00278~~	~~1518~~	~~59~~	~~1269~~	~~20~~	~~1128~~	~~15~~	~~34.6~~
CSL5-64	0.71	0.05671	0.00092	0.50792	0.00914	0.06495	0.0009	480	19	417	6	406	5	2.7
CSL5-65	0.65	0.05174	0.00275	0.31247	0.01654	0.04379	0.00073	274	91	276	13	276	5	0
CSL5-66	0.44	0.05506	0.00254	0.49912	0.02298	0.06573	0.0011	415	73	411	16	410	7	0.2
CSL5-67	0.51	0.0551	0.00089	0.51769	0.00928	0.06813	0.00095	416	19	424	6	425	6	-0.2

CSL5-68	1.04	0.05586	0.00091	0.50255	0.00912	0.06524	0.0009	447	19	413	6	407	5	1.5
CSL5-69	0.74	0.05143	0.00293	0.2918	0.0165	0.04114	0.00071	260	98	260	13	260	4	0
CSL5-70	0.79	0.07028	0.00094	1.37501	0.02162	0.14188	0.00194	937	14	878	9	855	11	2.7
CSL5-71	0.31	0.0553	0.00086	0.52189	0.00916	0.06844	0.00095	424	18	426	6	427	6	-0.2
CSL5-72	0.54	0.08539	0.00143	2.72967	0.05026	0.23182	0.00331	1324	17	1337	14	1344	17	-1.5
CSL5-73	0.28	0.07351	0.00109	1.6933	0.02853	0.16705	0.00232	1028	15	1006	11	996	13	1
CSL5-74	1.44	0.05432	0.00123	0.29978	0.00711	0.04002	0.00057	384	29	266	6	253	4	5.1
CSL5-75	0.53	0.06817	0.00119	1.28128	0.02442	0.1363	0.00193	874	19	837	11	824	11	1.6
CSL5-76	0.75	0.05457	0.00108	0.48333	0.0102	0.06422	0.00091	395	24	400	7	401	6	-0.2
CSL5-77	0.75	0.05145	0.0012	0.2699	0.00658	0.03804	0.00054	261	31	243	5	241	3	0.8
CSL5-78	0.87	0.05476	0.00123	0.49538	0.01167	0.06561	0.00095	402	28	409	8	410	6	-0.2
CSL5-79	0.18	0.0707	0.00097	1.34168	0.02156	0.13762	0.00189	949	15	864	9	831	11	4
CSL5-80	0.27	0.05523	0.00086	0.515	0.00906	0.06762	0.00094	422	18	422	6	422	6	0
CSL5-81	0.19	0.05141	0.00103	0.29391	0.00626	0.04146	0.00059	259	25	262	5	262	4	0
CSL5-82	0.68	0.05118	0.00176	0.27367	0.00952	0.03878	0.0006	249	52	246	8	245	4	0.4
CSL5-83	0.09	0.05694	0.00089	0.57554	0.01008	0.0733	0.00102	489	18	462	6	456	6	1.3
CSL5-84	0.53	0.06495	0.00107	1.06917	0.01955	0.11937	0.00168	773	18	738	10	727	10	1.5
CSL5-85	0.35	0.05501	0.00093	0.49455	0.0092	0.06519	0.00091	413	20	408	6	407	6	0.2
CSL5-86	0.19	0.05611	0.00085	0.56453	0.0097	0.07296	0.00101	457	17	454	6	454	6	0
CSL5-87	0.2	0.06972	0.00175	1.45679	0.03042	0.15155	0.0021	920	53	913	13	910	12	0.3
CSL5-88	0.91	0.05502	0.00413	0.50933	0.03793	0.06713	0.00129	413	133	418	26	419	8	-0.2
CSL5-89	0.6	0.05558	0.00218	0.48639	0.0177	0.06347	0.00092	436	89	402	12	397	6	1.3
CSL5-90	0.68	0.05124	0.00114	0.28524	0.00666	0.04037	0.00059	252	28	255	5	255	4	0
CSL5-91	0.9	0.05418	0.00108	0.44756	0.0095	0.0599	0.00086	379	24	376	7	375	5	0.3
CSL5-92	1.15	0.05517	0.00107	0.56565	0.01171	0.07435	0.00107	419	23	455	8	462	6	-1.5
CSL5-93	0.63	0.0538	0.00112	0.43081	0.00946	0.05807	0.00085	363	25	364	7	364	5	0
CSL5-94	0.48	0.06389	0.00149	1.12979	0.02716	0.12824	0.00194	738	27	768	13	778	11	-1.3
CSL5-95	0.41	0.05679	0.00095	0.55781	0.01029	0.07123	0.001	483	19	450	7	444	6	1.4

~~CSL5-96~~	~~0.42~~	~~0.09896~~	~~0.00135~~	~~3.07143~~	~~0.04911~~	~~0.22508~~	~~0.0031~~	~~1605~~	~~13~~	~~1426~~	~~12~~	~~1309~~	~~16~~	~~22.6~~
CSL5-97	0.58	0.07101	0.00103	1.6102	0.02689	0.16443	0.00228	958	15	974	10	981	13	-0.7
CSL5-98	0.7	0.05945	0.00109	0.54633	0.01083	0.06664	0.00096	584	21	443	7	416	6	6.5
CSL5-99	0.47	0.05978	0.00211	0.80654	0.02588	0.09785	0.00142	596	78	601	15	602	8	-0.2
CSL5-100	0.67	0.05265	0.00109	0.32001	0.00699	0.04408	0.00064	314	25	282	5	278	4	1.4
GS-E														
GSE-01	0.46	0.0554	0.00182	0.51894	0.01656	0.06792	0.00112	428	42	424	11	424	7	0
GSE-02	0.57	0.13755	0.00312	7.12679	0.1611	0.37568	0.00548	2197	20	2127	20	2056	26	6.9
GSE-03	0.34	0.0776	0.00305	2.09061	0.07583	0.1954	0.00299	1137	80	1146	25	1151	16	-1.2
GSE-04	0.52	0.05179	0.00212	0.30864	0.01239	0.04321	0.00071	276	62	273	10	273	4	0
GSE-05	0.96	0.05605	0.00192	0.56976	0.01901	0.07371	0.00121	454	45	458	12	458	7	0
GSE-06	0.47	0.05652	0.00188	0.57846	0.01879	0.07421	0.00121	473	43	463	12	461	7	0.4
GSE-07	0.57	0.05111	0.00311	0.27488	0.01644	0.039	0.00072	246	103	247	13	247	4	0
GSE-08	2.19	0.05143	0.00337	0.29312	0.01879	0.04133	0.00082	260	111	261	15	261	5	0
GSE-09	0.69	0.18101	0.00417	12.23168	0.28122	0.48998	0.00721	2662	20	2622	22	2571	31	3.5
~~GSE-10~~	~~1.12~~	~~0.06867~~	~~0.00594~~	~~0.65556~~	~~0.05539~~	~~0.06923~~	~~0.00167~~	~~889~~	~~135~~	~~512~~	~~34~~	~~432~~	~~10~~	~~18.5~~
GSE-11	0.43	0.05505	0.00278	0.50966	0.02516	0.06713	0.00123	414	77	418	17	419	7	-0.2
GSE-12	0.3	0.05547	0.00226	0.53388	0.02114	0.06979	0.00123	431	57	434	14	435	7	-0.2
GSE-13	0.5	0.05583	0.00318	0.55756	0.03102	0.07242	0.00139	446	89	450	20	451	8	-0.2
GSE-14	1.11	0.05328	0.00186	0.45561	0.0155	0.06201	0.00102	341	48	381	11	388	6	-1.8
GSE-15	1.49	0.06058	0.0033	0.81885	0.04374	0.09801	0.00184	624	83	607	24	603	11	0.7
GSE-16	0.21	0.11511	0.00304	5.39927	0.14019	0.34012	0.00536	1882	25	1885	22	1887	26	-0.3
GSE-17	0.3	0.15323	0.0039	9.32284	0.23446	0.4412	0.00684	2382	23	2370	23	2356	31	1.1
GSE-18	0.39	0.06964	0.0019	1.46593	0.0393	0.15265	0.00237	918	31	916	16	916	13	0
GSE-19	0.77	0.05087	0.00306	0.27405	0.01614	0.03906	0.00075	235	100	246	13	247	5	-0.4
GSE-20	0.74	0.05559	0.00564	0.54104	0.05412	0.07057	0.00165	436	183	439	36	440	10	-0.2
GSE-21	1.56	0.20685	0.00548	15.79196	0.41246	0.55361	0.00886	2881	23	2864	25	2840	37	1.4

GSE-22	0.2	0.06894	0.00192	1.39497	0.0382	0.14673	0.00229	897	32	887	16	883	13	0.5
GSE-23	1	0.05601	0.00208	0.55042	0.0199	0.07126	0.00124	453	50	445	13	444	7	0.2
GSE-24	0.61	0.05569	0.00326	0.53598	0.03052	0.06979	0.00144	440	90	436	20	435	9	0.2
GSE-25	0.36	0.23417	0.0076	18.7828	0.52856	0.58173	0.00941	3081	53	3031	27	2956	38	4.2
GSE-26	0.05	0.07028	0.00206	1.63752	0.04709	0.16895	0.00273	937	33	985	18	1006	15	-6.9
GSE-27	0.44	0.06944	0.00259	1.40525	0.05071	0.14674	0.00264	912	45	891	21	883	15	0.9
GSE-28	0.14	0.10615	0.00308	4.43759	0.12639	0.30315	0.00494	1734	29	1719	24	1707	24	1.6
GSE-29	0.02	0.0556	0.00229	0.53839	0.02162	0.07021	0.00125	436	58	437	14	437	8	0
~~GSE-30~~	~~1.47~~	~~0.07381~~	~~0.00313~~	~~0.5377~~	~~0.02208~~	~~0.05283~~	~~0.00098~~	~~1036~~	~~53~~	~~437~~	~~15~~	~~332~~	~~6~~	~~31.6~~
GSE-31	0.44	0.12816	0.00384	7.0095	0.20608	0.39662	0.0066	2073	29	2113	26	2153	30	-3.7
GSE-32	0.69	0.05582	0.00214	0.55226	0.02051	0.07174	0.00129	445	51	446	13	447	8	-0.2
GSE-33	0.58	0.0564	0.00196	0.59787	0.02027	0.07687	0.00132	468	45	476	13	477	8	-0.2
GSE-34	0.59	0.10047	0.00325	4.06593	0.12814	0.29346	0.00511	1633	33	1647	26	1659	25	-1.6
GSE-35	0.85	0.05179	0.00193	0.31882	0.01158	0.04464	0.00079	276	51	281	9	282	5	-0.4
GSE-36	0.23	0.05822	0.00198	0.62031	0.02056	0.07726	0.00132	538	43	490	13	480	8	2.1
GSE-37	0.63	0.05619	0.00263	0.31815	0.01447	0.04105	0.00078	460	67	280	11	259	5	8.1
GSE-38	0.9	0.05142	0.00317	0.27843	0.01672	0.03927	0.00083	260	99	249	13	248	5	0.4
GSE-39	0.12	0.11218	0.00356	4.86847	0.15153	0.3147	0.0053	1835	33	1797	26	1764	26	4
GSE-40	0.3	0.07331	0.00274	1.76356	0.06414	0.17444	0.00317	1023	45	1032	24	1037	17	-1.4
GSE-41	0.59	0.05609	0.00235	0.55924	0.0228	0.07229	0.00133	456	58	451	15	450	8	0.2
GSE-42	0.32	0.07014	0.00254	1.44329	0.0508	0.14922	0.00269	932	43	907	21	897	15	1.1
GSE-43	0.95	0.16586	0.00558	10.56064	0.34751	0.46169	0.00808	2516	32	2485	31	2447	36	2.8
GSE-44	0.68	0.05682	0.00235	0.59547	0.02401	0.07599	0.00141	485	56	474	15	472	8	0.4
GSE-45	1.78	0.05699	0.00213	0.59498	0.02164	0.0757	0.00137	491	49	474	14	470	8	0.9
GSE-46	0.02	0.07132	0.00274	1.58745	0.0593	0.16139	0.003	967	46	965	23	964	17	0.1
GSE-47	0.24	0.05582	0.00219	0.53115	0.02024	0.069	0.00128	445	52	433	13	430	8	0.7
~~GSE-48~~	~~0.39~~	~~0.06999~~	~~0.00323~~	~~0.89749~~	~~0.04022~~	~~0.09298~~	~~0.00185~~	~~928~~	~~59~~	~~650~~	~~22~~	~~573~~	~~11~~	~~13.4~~
GSE-49	0.29	0.11537	0.00426	5.48605	0.19701	0.34481	0.00642	1886	38	1898	31	1910	31	-1.3

GSE-50	0.87	0.05646	0.00295	0.58369	0.02971	0.07496	0.00153	471	76	467	19	466	9	0.2
GSE-51	0.34	0.05524	0.00235	0.49804	0.0206	0.06537	0.00125	422	58	410	14	408	8	0.5
GSE-52	0.71	0.05631	0.00463	0.57437	0.04637	0.07395	0.00172	465	138	461	30	460	10	0.2
GSE-53	0.58	0.05099	0.00288	0.27157	0.01494	0.03862	0.00081	240	88	244	12	244	5	0
GSE-54	0.2	0.11851	0.00445	5.65569	0.20719	0.34604	0.0064	1934	39	1925	32	1916	31	0.9
GSE-55	1.38	0.05173	0.00348	0.29077	0.01908	0.04076	0.00091	273	109	259	15	258	6	0.4
~~GSE-56~~	~~0.74~~	~~0.13276~~	~~0.00509~~	~~6.40543~~	~~0.23956~~	~~0.34985~~	~~0.00658~~	~~2135~~	~~39~~	~~2033~~	~~33~~	~~1934~~	~~31~~	~~10.4~~
STB2														
STB2-01	0.74	0.05108	0.00203	0.26568	0.01065	0.03772	0.00057	244	64	239	9	239	4	0
STB2-02	0.39	0.05186	0.00116	0.22909	0.00536	0.03203	0.00045	279	29	209	4	203	3	3
STB2-03	0.57	0.05555	0.00109	0.48745	0.01016	0.06363	0.00089	434	23	403	7	398	5	1.3
STB2-04	0.26	0.06829	0.00116	1.30465	0.02417	0.13853	0.00192	877	18	848	11	836	11	1.4
STB2-05	0.27	0.07074	0.00125	1.42152	0.02721	0.14571	0.00204	950	19	898	11	877	11	2.4
STB2-06	0.4	0.05383	0.0011	0.45872	0.00989	0.06179	0.00087	364	25	383	7	387	5	-1
STB2-07	0.79	0.05499	0.00126	0.48093	0.01146	0.06342	0.00091	412	29	399	8	396	6	0.8
STB2-08	0.6	0.05513	0.00151	0.47581	0.01337	0.06259	0.00092	417	37	395	9	391	6	1
STB2-09	0.41	0.06769	0.00138	1.27863	0.02759	0.13696	0.00196	859	23	836	12	827	11	1.1
STB2-10	0.42	0.0539	0.00104	0.46264	0.00954	0.06224	0.00087	367	23	386	7	389	5	-0.8
STB2-11	0.23	0.07038	0.00122	1.43096	0.02702	0.14744	0.00206	939	18	902	11	887	12	1.7
STB2-12	0.38	0.05661	0.00099	0.526	0.00997	0.06738	0.00093	476	20	429	7	420	6	2.1
STB2-13	0.65	0.0553	0.00183	0.47447	0.01588	0.06221	0.00093	424	48	394	11	389	6	1.3
STB2-14	0.62	0.05409	0.00107	0.46618	0.00983	0.0625	0.00088	375	24	389	7	391	5	-0.5
STB2-15	0.67	0.06864	0.00136	1.09883	0.02317	0.11608	0.00164	888	22	753	11	708	9	6.4
STB2-16	0.26	0.06801	0.0013	1.37557	0.02816	0.14666	0.00207	869	21	879	12	882	12	-0.3
~~STB2-17~~	~~0.51~~	~~0.0926~~	~~0.0027~~	~~2.71415~~	~~0.06922~~	~~0.21259~~	~~0.00302~~	~~1480~~	~~57~~	~~1332~~	~~19~~	~~1243~~	~~16~~	~~19.1~~
STB2-18	0.17	0.06949	0.00107	1.38493	0.02389	0.14452	0.00199	913	16	883	10	870	11	1.5

STB2-19	0.34	0.05507	0.00122	0.46813	0.01082	0.06164	0.00088	415	27	390	7	386	5	1
STB2-20	0.96	0.05625	0.00114	0.52233	0.01125	0.06733	0.00095	462	24	427	8	420	6	1.7
STB2-21	0.73	0.0545	0.00189	0.46393	0.01627	0.06173	0.00093	392	52	387	11	386	6	0.3
STB2-22	0.76	0.05051	0.0025	0.26465	0.01308	0.03799	0.00061	219	85	238	11	240	4	-0.8
STB2-23	0.34	0.06996	0.00155	1.45226	0.03366	0.15052	0.00217	927	25	911	14	904	12	0.8
STB2-24	0.29	0.05432	0.00118	0.46105	0.01055	0.06154	0.00087	384	27	385	7	385	5	0
~~STB2-25~~	~~0.36~~	~~0.12371~~	~~0.00207~~	~~5.41064~~	~~0.09887~~	~~0.31713~~	~~0.00451~~	~~2010~~	~~15~~	~~1887~~	~~16~~	~~1776~~	~~22~~	~~13.2~~
STB2-26	0.74	0.05111	0.00224	0.25851	0.01135	0.03668	0.00058	246	72	233	9	232	4	0.4
STB2-27	0.46	0.05405	0.00233	0.24654	0.01065	0.03307	0.00053	373	68	224	9	210	3	6.7
~~STB2-28~~	~~0.46~~	~~0.06242~~	~~0.00236~~	~~0.51364~~	~~0.01792~~	~~0.05968~~	~~0.00087~~	~~689~~	~~83~~	~~421~~	~~12~~	~~374~~	~~5~~	~~12.6~~
STB2-29	0.42	0.05588	0.00105	0.48131	0.0097	0.06246	0.00088	448	22	399	7	391	5	2
STB2-30	0.7	0.05175	0.00337	0.27661	0.01794	0.03876	0.00065	274	118	248	14	245	4	1.2
STB2-31	0.54	0.05489	0.0012	0.49135	0.01128	0.06491	0.00093	408	27	406	8	405	6	0.2
STB2-32	0.44	0.05011	0.00254	0.23658	0.012	0.03423	0.00054	200	88	216	10	217	3	-0.5
STB2-33	0.31	0.07017	0.0013	1.43515	0.02854	0.14831	0.00209	933	20	904	12	891	12	1.5
STB2-34	0.38	0.06305	0.0019	0.96753	0.02949	0.11128	0.00172	710	39	687	15	680	10	1
STB2-35	0.26	0.07097	0.00122	1.39414	0.02619	0.14245	0.00199	957	18	886	11	859	11	3.1
STB2-36	0.4	0.06545	0.00146	1.05187	0.02449	0.11654	0.00169	789	26	730	12	711	10	2.7
STB2-37	0.8	0.05474	0.00143	0.49225	0.01315	0.06521	0.00096	402	34	406	9	407	6	-0.2
STB2-38	0.78	0.05518	0.00144	0.48514	0.01305	0.06375	0.00092	420	35	402	9	398	6	1
STB2-39	0.52	0.05528	0.00123	0.53005	0.01232	0.06952	0.00099	424	28	432	8	433	6	-0.2
STB2-40	0.38	0.07056	0.00116	1.45888	0.02639	0.14994	0.00208	945	17	914	11	901	12	1.4
STB2-41	0.43	0.07034	0.00235	1.58597	0.04781	0.16352	0.00236	938	70	965	19	976	13	-1.1
STB2-42	0.92	0.05533	0.00109	0.51841	0.01087	0.06794	0.00096	426	23	424	7	424	6	0
STB2-43	0.42	0.05078	0.00267	0.24083	0.01264	0.03439	0.00056	231	91	219	10	218	3	0.5
STB2-44	0.12	0.05594	0.00161	0.48186	0.01214	0.06247	0.00086	450	65	399	8	391	5	2
STB2-45	0.2	0.06919	0.00119	1.41662	0.02664	0.14848	0.00207	904	18	896	11	892	12	0.4
STB2-46	0.87	0.05089	0.00196	0.23634	0.00918	0.03368	0.00051	236	62	215	8	214	3	0.5

STB2-47	0.61	0.06822	0.00186	1.29267	0.03605	0.1374	0.00204	875	34	842	16	830	12	1.4
STB2-48	0.42	0.0564	0.00182	0.50507	0.01656	0.06494	0.00097	468	46	415	11	406	6	2.2
STB2-49	0.59	0.05614	0.00129	0.55358	0.01321	0.0715	0.00103	458	29	447	9	445	6	0.4
STB2-50	0.66	0.05462	0.00138	0.49391	0.01282	0.06558	0.00096	397	33	408	9	409	6	-0.2
STB2-51	0.68	0.0537	0.00171	0.26627	0.00862	0.03596	0.00054	358	46	240	7	228	3	5.3
STB2-52	0.62	0.05492	0.00288	0.25629	0.01341	0.03384	0.00055	409	88	232	11	215	3	7.9
STB2-53	0.45	0.05485	0.0014	0.49394	0.01298	0.06531	0.00095	406	34	408	9	408	6	0
STB2-54	0.22	0.07053	0.0012	1.39886	0.02596	0.14383	0.00201	944	18	888	11	866	11	2.5
STB2-55	0.5	0.05519	0.00113	0.50883	0.01104	0.06685	0.00095	420	25	418	7	417	6	0.2
STB2-56	0.36	0.07002	0.00129	1.42923	0.0283	0.14801	0.00209	929	20	901	12	890	12	1.2
STB2-57	0.46	0.05426	0.00204	0.48288	0.01829	0.06453	0.00099	382	57	400	13	403	6	-0.7
STB2-58	0.49	0.05036	0.00264	0.23994	0.01259	0.03455	0.00055	212	92	218	10	219	3	-0.5
STB2-59	0.93	0.05562	0.00116	0.475	0.01042	0.06193	0.00088	437	25	395	7	387	5	2.1
STB2-60	0.56	0.05574	0.00125	0.51992	0.01221	0.06763	0.00097	442	28	425	8	422	6	0.7
STB2-61	0.48	0.0506	0.00204	0.25002	0.01011	0.03583	0.00056	223	64	227	8	227	3	0
STB2-62	0.16	0.06526	0.00171	1.16384	0.02583	0.12934	0.0018	783	56	784	12	784	10	0
STB2-63	0.88	0.05093	0.00165	0.24897	0.00814	0.03545	0.00053	238	48	226	7	225	3	0.4
STB2-64	0.7	0.05153	0.00148	0.30867	0.00907	0.04344	0.00064	265	41	273	7	274	4	-0.4
STB2-65	1.03	0.06831	0.00153	1.40148	0.03277	0.14878	0.00216	878	26	890	14	894	12	-0.4
STB2-66	0.54	0.05522	0.00116	0.49909	0.01102	0.06553	0.00094	421	25	411	7	409	6	0.5
STB2-67	0.44	0.05223	0.00232	0.24632	0.0103	0.0342	0.00051	295	104	224	8	217	3	3.2
STB2-68	0.42	0.05013	0.0014	0.23331	0.00664	0.03375	0.0005	201	39	213	5	214	3	-0.5
STB2-69	0.69	0.05097	0.00238	0.26343	0.01232	0.03748	0.0006	239	78	237	10	237	4	0
STB2-70	0.5	0.05055	0.00229	0.23588	0.01071	0.03384	0.00053	220	76	215	9	215	3	0
~~STB2-71~~	~~0.7~~	~~0.07549~~	~~0.00516~~	~~0.33641~~	~~0.02225~~	~~0.03232~~	~~0.00056~~	~~1082~~	~~141~~	~~294~~	~~17~~	~~205~~	~~3~~	~~43.4~~
STB2-72	0.35	0.07011	0.00153	1.45202	0.03327	0.15017	0.00217	932	25	911	14	902	12	1
STB2-73	0.79	0.055	0.00134	0.47823	0.01209	0.06306	0.00091	412	32	397	8	394	6	0.8
STB2-74	0.3	0.07061	0.0013	1.39053	0.02747	0.14281	0.00202	946	20	885	12	861	11	2.8

STB2-75	0.45	0.05556	0.00143	0.2566	0.00681	0.03349	0.00049	435	34	232	6	212	3	9.4
STB2-76	0.51	0.0544	0.0013	0.46397	0.0115	0.06185	0.0009	388	31	387	8	387	5	0
STB2-77	0.48	0.05557	0.0019	0.49954	0.01722	0.06518	0.001	435	49	411	12	407	6	1
STB2-78	0.93	0.12231	0.0022	5.73487	0.11133	0.34002	0.00486	1990	16	1937	17	1887	23	5.5
STB2-79	0.63	0.10153	0.00183	3.78764	0.07348	0.27052	0.00385	1652	17	1590	16	1543	20	7.1
STB2-80	0.51	0.05548	0.00118	0.52408	0.01175	0.0685	0.00098	432	26	428	8	427	6	0.2
STB2-81	0.53	0.05038	0.00309	0.22811	0.01394	0.03283	0.00056	213	109	209	12	208	3	0.5
STB2-82	0.7	0.05098	0.00228	0.26181	0.01171	0.03724	0.0006	240	73	236	9	236	4	0
STB2-83	0.63	0.05424	0.00207	0.45925	0.01765	0.0614	0.00095	381	58	384	12	384	6	0
STB2-84	0.45	0.05463	0.00113	0.48562	0.01064	0.06446	0.00092	397	25	402	7	403	6	-0.2
STB2-85	0.37	0.06696	0.00242	1.07991	0.0356	0.11696	0.00173	837	77	744	17	713	10	4.3
STB2-86	0.19	0.06944	0.00141	1.41837	0.03052	0.14811	0.00213	912	22	897	13	890	12	0.8
STB2-87	0.25	0.06966	0.00127	1.30208	0.02567	0.13554	0.00192	918	20	847	11	819	11	3.4
STB2-88	0.41	0.05079	0.00257	0.2421	0.01222	0.03456	0.00057	231	86	220	10	219	4	0.5
~~STB2-89~~	~~0.6~~	~~0.07907~~	~~0.00145~~	~~1.32055~~	~~0.0261~~	~~0.12111~~	~~0.00172~~	~~1174~~	~~19~~	~~855~~	~~11~~	~~737~~	~~10~~	~~16~~
STB2-90	0.67	0.05436	0.00202	0.46987	0.01755	0.06268	0.00097	386	56	391	12	392	6	-0.3
STB2-91	0.45	0.0542	0.00114	0.46971	0.0104	0.06284	0.0009	379	26	391	7	393	5	-0.5
STB2-92	0.24	0.0566	0.00321	0.39808	0.02177	0.05101	0.00077	476	129	340	16	321	5	5.9
~~STB2-93~~	~~0.62~~	~~0.05834~~	~~0.00377~~	~~0.28534~~	~~0.01834~~	~~0.03546~~	~~0.00061~~	~~543~~	~~111~~	~~255~~	~~14~~	~~225~~	~~4~~	~~13.3~~
STB2-94	0.24	0.07045	0.00136	1.41271	0.02904	0.14541	0.00207	941	21	894	12	875	12	2.2
~~STB2-95~~	~~0.38~~	~~0.29843~~	~~0.00514~~	~~24.98591~~	~~0.47004~~	~~0.60712~~	~~0.00851~~	~~3462~~	~~14~~	~~3308~~	~~18~~	~~3058~~	~~34~~	~~13.2~~
STB2-96	0.34	0.07115	0.00153	1.42721	0.03208	0.14546	0.00212	962	24	900	13	875	12	2.9
STB2-97	0.48	0.06953	0.00146	1.48241	0.0327	0.15461	0.00224	915	23	923	13	927	13	-0.4
STB2-98	0.39	0.05633	0.00129	0.50549	0.01208	0.06507	0.00095	465	28	415	8	406	6	2.2
STB2-99	0.41	0.0694	0.00153	1.4494	0.03346	0.15144	0.0022	911	25	910	14	909	12	0.1
STB2-100	0.5	0.05583	0.00132	0.51712	0.0127	0.06716	0.00098	446	30	423	8	419	6	1

GS-N														
GS-N-001	0.43	0.06771	0.00174	1.33474	0.0343	0.14295	0.00211	860	30	861	15	861	12	0
GS-N-002	0.67	0.0546	0.00235	0.47878	0.02037	0.06358	0.00103	396	66	397	14	397	6	0
GS-N-003	0.73	0.05168	0.00161	0.30874	0.00949	0.04332	0.00067	271	42	273	7	273	4	0
GS-N-004	0.26	0.06882	0.00164	1.40977	0.03371	0.14854	0.00217	893	26	893	14	893	12	0
GS-N-005	0.63	0.05021	0.00139	0.23105	0.00639	0.03337	0.0005	205	37	211	5	212	3	-0.5
GS-N-006	0.63	0.05039	0.00265	0.2202	0.01144	0.03169	0.00054	213	89	202	10	201	3	0.5
GS-N-007	0.7	0.05047	0.00145	0.23765	0.00679	0.03414	0.00051	217	39	216	6	216	3	0
GS-N-008	0.44	0.05401	0.00132	0.45837	0.01125	0.06154	0.00089	371	30	383	8	385	5	-0.5
GS-N-009	0.68	0.05071	0.00234	0.24963	0.01143	0.0357	0.00058	228	76	226	9	226	4	0
GS-N-010	0.44	0.05747	0.00164	0.47596	0.01353	0.06006	0.0009	510	37	395	9	376	5	5.1
GS-N-011	0.55	0.0507	0.00172	0.24636	0.00823	0.03523	0.00056	227	48	224	7	223	3	0.4
GS-N-012	0.47	0.05033	0.00175	0.2366	0.00815	0.03409	0.00053	210	51	216	7	216	3	0
GS-N-013	0.64	0.05058	0.00189	0.24467	0.00896	0.03508	0.00057	222	55	222	7	222	4	0
GS-N-014	0.35	0.05448	0.00173	0.47326	0.01496	0.06299	0.00096	391	44	393	10	394	6	-0.3
GS-N-015	0.73	0.0535	0.00177	0.41365	0.01351	0.05607	0.00089	350	45	352	10	352	5	0
~~GS-N-016~~	~~0.48~~	~~0.06536~~	~~0.00186~~	~~0.58815~~	~~0.0167~~	~~0.06525~~	~~0.00098~~	~~786~~	~~35~~	~~470~~	~~11~~	~~407~~	~~6~~	~~15.5~~
GS-N-017	0.73	0.05456	0.00224	0.46926	0.01884	0.06237	0.00108	394	59	391	13	390	7	0.3
GS-N-018	0.53	0.0541	0.00161	0.45267	0.01342	0.06067	0.00091	375	40	379	9	380	6	-0.3
GS-N-019	0.52	0.05038	0.00156	0.23154	0.00713	0.03333	0.00051	213	43	211	6	211	3	0
GS-N-020	0.85	0.05432	0.00157	0.47118	0.01348	0.0629	0.00096	384	37	392	9	393	6	-0.3
GS-N-021	0.35	0.05351	0.00204	0.40509	0.01525	0.0549	0.00088	350	56	345	11	345	5	0
GS-N-022	0.4	0.05512	0.00197	0.51422	0.01803	0.06765	0.0011	417	49	421	12	422	7	-0.2
GS-N-023	0.49	0.05072	0.00161	0.24393	0.00765	0.03487	0.00054	228	44	222	6	221	3	0.5
GS-N-024	1.09	0.05497	0.00183	0.50162	0.01648	0.06617	0.00106	411	45	413	11	413	6	0
GS-N-025	0.61	0.05437	0.00209	0.46418	0.01765	0.06191	0.00099	386	57	387	12	387	6	0
GS-N-026	0.59	0.05064	0.00303	0.24374	0.01423	0.03491	0.00069	224	98	221	12	221	4	0
GS-N-027	0.39	0.06628	0.00214	1.23622	0.03946	0.13525	0.00214	815	41	817	18	818	12	-0.1

GS-N-028	0.63	0.05472	0.00326	0.48912	0.02847	0.06481	0.00129	401	95	404	19	405	8	-0.2
GS-N-029	0.43	0.07174	0.00185	1.61467	0.04173	0.16322	0.00242	979	29	976	16	975	13	0.1
GS-N-030	0.59	0.04948	0.00496	0.22173	0.02178	0.0325	0.00065	171	224	203	18	206	4	-1.5
GS-N-031	0.33	0.05901	0.00172	0.51218	0.01483	0.06293	0.00095	567	37	420	10	393	6	6.9
GS-N-032	0.99	0.05119	0.00354	0.27777	0.01896	0.03935	0.00073	249	122	249	15	249	5	0
GS-N-033	0.82	0.05534	0.00273	0.5056	0.02457	0.06625	0.00115	426	77	415	17	414	7	0.2
GS-N-034	0.82	0.05077	0.00563	0.26395	0.02886	0.0377	0.00089	230	203	238	23	239	6	-0.4
~~GS-N-035~~	~~0.29~~	~~0.07187~~	~~0.00193~~	~~0.53729~~	~~0.0144~~	~~0.05421~~	~~0.00081~~	~~982~~	~~31~~	~~437~~	~~10~~	~~340~~	~~5~~	~~28.5~~
GS-N-036	0.34	0.07101	0.00266	1.36298	0.04688	0.13921	0.00209	958	79	873	20	840	12	3.9
GS-N-037	0.61	0.0504	0.00159	0.23974	0.00747	0.03449	0.00053	213	44	218	6	219	3	-0.5
GS-N-038	0.2	0.04842	0.00517	0.13402	0.01419	0.02007	0.00041	120	199	128	13	128	3	0
GS-N-039	0.6	0.12976	0.00337	6.85457	0.17724	0.38306	0.00603	2095	24	2093	23	2091	28	0.2
GS-N-040	0.45	0.06958	0.00203	1.49217	0.04308	0.1555	0.00245	916	34	927	18	932	14	-0.5
GS-N-041	0.75	0.05487	0.00225	0.47804	0.01916	0.06318	0.00109	407	59	397	13	395	7	0.5
GS-N-042	0.4	0.05556	0.00175	0.52959	0.01646	0.06911	0.00109	435	42	432	11	431	7	0.2
GS-N-043	0.53	0.05555	0.00198	0.531	0.01858	0.06932	0.00116	434	48	432	12	432	7	0
GS-N-044	0.65	0.05054	0.00408	0.24769	0.01966	0.03554	0.00077	220	140	225	16	225	5	0
GS-N-045	0.5	0.05081	0.0024	0.25312	0.01172	0.03613	0.00065	232	74	229	9	229	4	0
GS-N-046	0.64	0.05409	0.0023	0.47182	0.01961	0.06325	0.00111	375	62	392	14	395	7	-0.8
GS-N-047	0.88	0.05053	0.00292	0.23992	0.01369	0.03443	0.00061	219	99	218	11	218	4	0
GS-N-048	0.94	0.05028	0.00255	0.23057	0.01146	0.03325	0.0006	208	82	211	9	211	4	0
GS-N-049	0.13	0.06793	0.00194	1.37126	0.03906	0.14637	0.00223	866	34	877	17	881	13	-0.5
GS-N-050	0.57	0.05037	0.00231	0.23812	0.01071	0.03428	0.0006	212	72	217	9	217	4	0
GS-N-051	0.51	0.05073	0.00255	0.23546	0.01165	0.03366	0.00059	229	82	215	10	213	4	0.9
GS-N-052	0.33	0.06898	0.00215	1.42453	0.04373	0.14975	0.0024	898	37	899	18	900	13	-0.1
GS-N-053	0.4	0.05081	0.00165	0.2607	0.00836	0.0372	0.00058	232	46	235	7	235	4	0
GS-N-054	0.53	0.06972	0.00211	1.46291	0.04394	0.15215	0.00238	920	37	915	18	913	13	0.2
GS-N-055	0.73	0.05161	0.00262	0.28639	0.01434	0.04023	0.0007	268	83	256	11	254	4	0.8

GS-N-056	0.44	0.05435	0.00194	0.46245	0.01624	0.0617	0.00101	386	50	386	11	386	6	0
GS-N-057	0.16	0.06913	0.00194	1.4149	0.0396	0.14842	0.00227	903	33	895	17	892	13	0.3
GS-N-058	0.67	0.06963	0.00222	1.44638	0.04569	0.15063	0.00239	917	39	908	19	904	13	0.4
GS-N-059	0.62	0.05565	0.00188	0.53988	0.01792	0.07035	0.00115	438	45	438	12	438	7	0
GS-N-060	0.46	0.05554	0.00204	0.44256	0.01598	0.05778	0.00095	434	51	372	11	362	6	2.8
GS-N-061	0.21	0.05485	0.00173	0.49744	0.01549	0.06577	0.00104	406	42	410	11	411	6	-0.2
GS-N-062	0.67	0.05054	0.00357	0.24643	0.01715	0.03536	0.00069	220	123	224	14	224	4	0
GS-N-063	0.44	0.05054	0.00186	0.24039	0.00869	0.03449	0.00058	220	53	219	7	219	4	0
GS-N-064	0.64	0.05075	0.00257	0.24675	0.01232	0.03525	0.00062	229	83	224	10	223	4	0.4
GS-N-065	0.42	0.05436	0.00172	0.46527	0.01461	0.06207	0.00097	386	43	388	10	388	6	0
GS-N-066	0.67	0.05303	0.00216	0.40693	0.01625	0.05565	0.00097	330	59	347	12	349	6	-0.6
GS-N-067	0.87	0.05114	0.0024	0.27023	0.0124	0.03832	0.0007	247	72	243	10	242	4	0.4
GS-N-068	0.24	0.06813	0.00214	1.364	0.0423	0.14518	0.00234	873	38	874	18	874	13	0
GS-N-069	0.63	0.06904	0.00241	1.40568	0.04832	0.14765	0.00245	900	44	891	20	888	14	0.3
GS-N-070	1.17	0.052	0.00591	0.26834	0.03003	0.03743	0.00073	285	260	241	24	237	5	1.7
GS-N-071	0.57	0.05453	0.00322	0.46203	0.02684	0.06144	0.00113	393	97	386	19	384	7	0.5
GS-N-072	1.06	0.05036	0.00462	0.24545	0.02216	0.03534	0.00079	212	162	223	18	224	5	-0.4
GS-N-073	0.37	0.04932	0.00239	0.18197	0.00862	0.02675	0.00049	163	76	170	7	170	3	0
GS-N-074	0.57	0.05449	0.00218	0.47349	0.01858	0.06301	0.00109	391	57	394	13	394	7	0
GS-N-075	0.5	0.0548	0.00314	0.47976	0.02707	0.06349	0.00118	404	93	398	19	397	7	0.3
GS-N-076	0.34	0.0545	0.00206	0.48326	0.01799	0.0643	0.00107	392	54	400	12	402	6	-0.5
GS-N-077	0.75	0.05045	0.00378	0.22907	0.01689	0.03292	0.00067	216	130	209	14	209	4	0
GS-N-078	0.25	0.05466	0.00221	0.47897	0.01893	0.06354	0.0011	398	58	397	13	397	7	0
GS-N-079	0.45	0.05433	0.00239	0.46546	0.01999	0.06212	0.00113	385	64	388	14	389	7	-0.3
GS-N-080	0.49	0.05455	0.00269	0.47303	0.02277	0.06288	0.0012	394	74	393	16	393	7	0
~~GS-N-081~~	~~0.5~~	~~0.06815~~	~~0.00265~~	~~0.8139~~	~~0.03104~~	~~0.0866~~	~~0.00148~~	~~873~~	~~51~~	~~605~~	~~17~~	~~535~~	~~9~~	~~13.1~~
GS-N-082	0.31	0.05445	0.00199	0.46848	0.01685	0.06239	0.00104	390	51	390	12	390	6	0
GS-N-083	0.19	0.06643	0.00237	1.21456	0.04257	0.13258	0.00223	820	45	807	20	803	13	0.5

GS-N-084	0.22	0.06826	0.00217	1.41246	0.04416	0.15005	0.00244	876	38	894	19	901	14	-0.8
GS-N-085	0.46	0.05052	0.00269	0.24395	0.01275	0.03502	0.00064	219	87	222	10	222	4	0
GS-N-086	0.44	0.0503	0.00219	0.23794	0.01012	0.0343	0.00062	209	65	217	8	217	4	0
GS-N-087	0.7	0.0545	0.00231	0.47901	0.01985	0.06373	0.00114	392	61	397	14	398	7	-0.3
GS-N-088	0.68	0.05002	0.00282	0.23052	0.01269	0.03342	0.00067	196	90	211	10	212	4	-0.5
GS-N-089	0.28	0.05456	0.00198	0.49475	0.01756	0.06576	0.00112	394	49	408	12	411	7	-0.7
GS-N-090	0.82	0.05063	0.00459	0.26172	0.02335	0.03749	0.00085	224	159	236	19	237	5	-0.4
GS-N-091	0.56	0.05044	0.004	0.2312	0.01804	0.03324	0.0007	215	138	211	15	211	4	0
GS-N-092	0.51	0.05056	0.00211	0.23563	0.00961	0.03379	0.0006	221	62	215	8	214	4	0.5
GS-N-093	0.7	0.05459	0.00401	0.46956	0.03394	0.06238	0.00128	395	126	391	23	390	8	0.3
GS-N-094	0.71	0.0506	0.00249	0.25044	0.01199	0.03589	0.0007	223	75	227	10	227	4	0
GS-N-095	0.42	0.04605	0.0053	0.2079	0.02353	0.03275	0.00068		228	192	20	208	4	-7.7
GS-N-096	0.42	0.05434	0.00265	0.46666	0.02226	0.06227	0.00115	385	74	389	15	389	7	0
GS-N-097	0.42	0.0544	0.00221	0.47427	0.01881	0.06322	0.00113	388	57	394	13	395	7	-0.3
GS-N-098	0.42	0.05561	0.0022	0.51248	0.01985	0.06683	0.00117	437	55	420	13	417	7	0.7
GS-N-099	1.57	0.05592	0.00369	0.55416	0.03574	0.07186	0.00153	449	105	448	23	447	9	0.2
GS-N-100	0.18	0.06988	0.00264	1.48617	0.05497	0.15422	0.00269	925	48	925	22	925	15	0
STB3														
STB3-01	0.31	0.05588	0.00133	0.52794	0.01294	0.06852	0.001	448	30	430	9	427	6	0.7
STB3-02	0.45	0.05466	0.00167	0.46421	0.01429	0.06159	0.00094	398	42	387	10	385	6	0.5
STB3-03	0.68	0.05129	0.0014	0.29061	0.00804	0.04109	0.00061	254	37	259	6	260	4	-0.4
STB3-04	0.78	0.07001	0.00153	1.44159	0.03258	0.14933	0.00215	929	24	906	14	897	12	1
STB3-05	0.65	0.05069	0.00312	0.2472	0.01513	0.03537	0.0006	227	110	224	12	224	4	0
STB3-06	0.43	0.05542	0.00139	0.47572	0.0122	0.06225	0.00091	429	32	395	8	389	6	1.5
STB3-07	0.54	0.05598	0.00146	0.53009	0.01409	0.06867	0.00101	452	34	432	9	428	6	0.9
STB3-08	0.36	0.05574	0.00223	0.48391	0.01801	0.06296	0.00092	442	91	401	12	394	6	1.8

STB3-09	0.48	0.05708	0.00279	0.49186	0.02287	0.0625	0.00095	495	111	406	16	391	6	3.8
STB3-10	0.55	0.05122	0.00264	0.24587	0.01255	0.03481	0.00059	251	86	223	10	221	4	0.9
STB3-11	0.69	0.05138	0.00187	0.26475	0.00964	0.03736	0.00058	258	55	238	8	236	4	0.8
STB3-12	0.32	0.0568	0.00218	0.48239	0.0171	0.0616	0.0009	484	87	400	12	385	5	3.9
STB3-13	0.62	0.05453	0.00138	0.47709	0.01228	0.06345	0.00093	393	32	396	8	397	6	-0.3
STB3-14	0.71	0.05031	0.00294	0.23568	0.01368	0.03397	0.00057	209	103	215	11	215	4	0
STB3-15	0.62	0.0509	0.0014	0.2742	0.00763	0.03907	0.00058	236	37	246	6	247	4	-0.4
STB3-16	0.76	0.05358	0.00187	0.44007	0.01536	0.05956	0.00092	353	51	370	11	373	6	-0.8
STB3-17	0.63	0.05069	0.00465	0.23755	0.02164	0.03398	0.00063	227	171	216	18	215	4	0.5
STB3-18	0.48	0.0501	0.00148	0.22089	0.00653	0.03197	0.00048	200	41	203	5	203	3	0
STB3-19	0.5	0.0549	0.00136	0.49249	0.01242	0.06505	0.00095	408	31	407	8	406	6	0.2
STB3-20	0.44	0.05675	0.00126	0.52642	0.01202	0.06727	0.00097	482	26	429	8	420	6	2.1
STB3-21	0.49	0.05414	0.00141	0.45818	0.01204	0.06137	0.0009	377	34	383	8	384	5	-0.3
~~STB3-22~~	~~1.29~~	~~0.05674~~	~~0.0016~~	~~0.26388~~	~~0.00749~~	~~0.03372~~	~~0.00051~~	~~481~~	~~37~~	~~238~~	~~6~~	~~214~~	~~3~~	~~11.2~~
STB3-23	0.69	0.05447	0.00184	0.48705	0.01643	0.06484	0.00101	391	48	403	11	405	6	-0.5
STB3-24	0.44	0.05065	0.00343	0.23063	0.01548	0.03302	0.00058	225	121	211	13	209	4	1
STB3-25	0.46	0.05513	0.00148	0.47164	0.0128	0.06203	0.00091	417	35	392	9	388	6	1
STB3-26	0.29	0.05504	0.00207	0.43098	0.01495	0.05679	0.00081	414	86	364	11	356	5	2.2
STB3-27	0.55	0.05442	0.00108	0.44112	0.00922	0.05878	0.00084	388	23	371	6	368	5	0.8
STB3-28	0.64	0.05674	0.00123	0.57199	0.0129	0.0731	0.00106	481	26	459	8	455	6	0.9
STB3-29	0.8	0.05131	0.00165	0.25503	0.00821	0.03604	0.00057	255	45	231	7	228	4	1.3
STB3-30	0.38	0.06922	0.00131	1.46392	0.02935	0.15336	0.00219	905	20	916	12	920	12	-0.4
~~STB3-31~~	~~0.06~~	~~0.09972~~	~~0.00153~~	~~3.50166~~	~~0.05963~~	~~0.25462~~	~~0.0035~~	~~1619~~	~~14~~	~~1528~~	~~13~~	~~1462~~	~~18~~	~~10.7~~
STB3-32	0.54	0.05507	0.00104	0.47377	0.00952	0.06238	0.00088	415	22	394	7	390	5	1
STB3-33	0.47	0.05227	0.00185	0.23547	0.00828	0.03267	0.00053	297	51	215	7	207	3	3.9
STB3-34	0.82	0.05527	0.00112	0.45776	0.00974	0.06006	0.00086	423	24	383	7	376	5	1.9
STB3-35	0.63	0.05298	0.00115	0.25262	0.00567	0.03458	0.0005	328	26	229	5	219	3	4.6
STB3-36	0.43	0.05352	0.00098	0.38226	0.00749	0.05179	0.00073	351	21	329	6	326	4	0.9

STB3-37	0.93	0.05676	0.00117	0.47449	0.0102	0.06062	0.00087	482	24	394	7	379	5	4
STB3-38	0.41	0.0569	0.00144	0.51961	0.01335	0.06621	0.001	488	31	425	9	413	6	2.9
STB3-39	0.88	0.04895	0.00156	0.23507	0.00751	0.03482	0.00055	145	46	214	6	221	3	-3.2
STB3-40	0.22	0.07093	0.00114	1.52149	0.02688	0.15555	0.00215	955	17	939	11	932	12	0.8
STB3-41	0.91	0.09126	0.00163	2.8967	0.05529	0.23015	0.00327	1452	17	1381	14	1335	17	8.8
~~STB3-42~~	~~0.32~~	~~0.06294~~	~~0.00361~~	~~0.50732~~	~~0.02806~~	~~0.05846~~	~~0.0009~~	~~706~~	~~126~~	~~417~~	~~19~~	~~366~~	~~5~~	~~13.9~~
STB3-43	0.65	0.05683	0.00112	0.51571	0.01072	0.06581	0.00094	485	23	422	7	411	6	2.7
STB3-44	0.5	0.05418	0.00137	0.48377	0.01244	0.06475	0.00097	379	32	401	9	404	6	-0.7
STB3-45	0.54	0.05269	0.00135	0.47544	0.01242	0.06543	0.00098	315	33	395	9	409	6	-3.4
STB3-46	0.46	0.05587	0.00113	0.50333	0.01069	0.06533	0.00093	447	24	414	7	408	6	1.5
STB3-47	0.46	0.05149	0.00116	0.24859	0.00578	0.035	0.00051	263	28	225	5	222	3	1.4
STB3-48	0.21	0.0545	0.00117	0.50139	0.0112	0.0667	0.00096	392	26	413	8	416	6	-0.7
STB3-49	0.22	0.05285	0.00118	0.48478	0.01117	0.06651	0.00097	322	27	401	8	415	6	-3.4
~~STB3-50~~	~~0.9~~	~~0.08548~~	~~0.01049~~	~~0.76555~~	~~0.09241~~	~~0.06495~~	~~0.00144~~	~~1327~~	~~249~~	~~577~~	~~53~~	~~406~~	~~9~~	~~42.1~~
STB3-51	0.61	0.05124	0.0023	0.26965	0.01212	0.03816	0.0006	252	74	242	10	241	4	0.4
~~STB3-52~~	~~1.58~~	~~0.09967~~	~~0.00144~~	~~3.47455~~	~~0.05698~~	~~0.25278~~	~~0.00347~~	~~1618~~	~~14~~	~~1521~~	~~13~~	~~1453~~	~~18~~	~~11.4~~
~~STB3-53~~	~~0.28~~	~~0.06505~~	~~0.00136~~	~~0.57929~~	~~0.01272~~	~~0.06457~~	~~0.00091~~	~~776~~	~~24~~	~~464~~	~~8~~	~~403~~	~~6~~	~~15.1~~
STB3-54	0.57	0.05443	0.0015	0.44557	0.01261	0.05936	0.00086	389	38	374	9	372	5	0.5
~~STB3-55~~	~~0.63~~	~~0.06174~~	~~0.00176~~	~~0.55735~~	~~0.01624~~	~~0.06545~~	~~0.00096~~	~~665~~	~~38~~	~~450~~	~~11~~	~~409~~	~~6~~	~~10~~
STB3-56	0.45	0.06826	0.00148	1.28491	0.02912	0.1365	0.00196	876	25	839	13	825	11	1.7
STB3-57	0.48	0.05433	0.00107	0.46878	0.00984	0.06257	0.00087	385	24	390	7	391	5	-0.3
~~STB3-58~~	~~0.69~~	~~0.06513~~	~~0.00207~~	~~0.57378~~	~~0.01842~~	~~0.06388~~	~~0.00096~~	~~779~~	~~42~~	~~460~~	~~12~~	~~399~~	~~6~~	~~15.3~~
STB3-59	1.19	0.05575	0.00107	0.5353	0.01095	0.06962	0.00097	442	23	435	7	434	6	0.2
STB3-60	0.41	0.05044	0.00166	0.23402	0.00783	0.03364	0.0005	215	50	214	6	213	3	0.5
STB3-61	0.54	0.05255	0.0025	0.24486	0.01108	0.0338	0.00051	309	111	222	9	214	3	3.7
STB3-62	0.5	0.0546	0.00133	0.49611	0.01247	0.06589	0.00095	396	31	409	8	411	6	-0.5
STB3-63	0.95	0.05599	0.00088	0.52043	0.00909	0.0674	0.00092	452	18	425	6	420	6	1.2
STB3-64	0.56	0.05573	0.00133	0.52872	0.01305	0.0688	0.00098	442	30	431	9	429	6	0.5

STB3-65	0.31	0.06121	0.00159	0.86497	0.02297	0.10247	0.00151	647	32	633	13	629	9	0.6
STB3-66	0.76	0.05096	0.00133	0.2776	0.00745	0.0395	0.00057	239	36	249	6	250	4	-0.4
STB3-67	0.92	0.05359	0.00317	0.45208	0.02658	0.06117	0.00106	354	102	379	19	383	6	-1
STB3-68	0.57	0.05672	0.0013	0.51363	0.01227	0.06566	0.00093	481	29	421	8	410	6	2.7
STB3-69	0.51	0.05189	0.00199	0.34699	0.0134	0.04849	0.00074	281	60	302	10	305	5	-1
STB3-70	0.31	0.05472	0.00096	0.47349	0.00903	0.06275	0.00087	401	21	394	6	392	5	0.5
STB3-71	0.89	0.05161	0.00324	0.23815	0.01448	0.03347	0.00053	268	145	217	12	212	3	2.4
STB3-72	0.78	0.05576	0.00131	0.50004	0.01217	0.06502	0.00093	443	30	412	8	406	6	1.5
STB3-73	0.24	0.06933	0.00106	1.33744	0.02286	0.13988	0.00192	909	16	862	10	844	11	2.1
STB3-74	0.33	0.0508	0.00093	0.2426	0.00478	0.03463	0.00048	232	22	221	4	219	3	0.9
STB3-75	1.07	0.05058	0.00137	0.23105	0.00643	0.03312	0.00048	222	38	211	5	210	3	0.5
STB3-76	0.39	0.05099	0.00109	0.24068	0.00544	0.03423	0.00048	240	28	219	4	217	3	0.9
STB3-77	0.43	0.05718	0.00088	0.51934	0.00901	0.06586	0.0009	498	18	425	6	411	5	3.4
STB3-78	0.59	0.05174	0.00188	0.24254	0.0089	0.03399	0.00051	274	57	220	7	215	3	2.3
STB3-79	0.55	0.05571	0.00113	0.53265	0.01148	0.06933	0.00098	441	25	434	8	432	6	0.5
STB3-80	0.62	0.05129	0.00199	0.25039	0.00976	0.0354	0.00055	254	61	227	8	224	3	1.3
STB3-81	0.28	0.05481	0.0009	0.48468	0.00882	0.06412	0.00088	404	19	401	6	401	5	0
STB3-82	0.43	0.05435	0.00139	0.42518	0.01121	0.05673	0.00082	386	34	360	8	356	5	1.1
~~STB3-83~~	~~1.11~~	~~0.06361~~	~~0.0021~~	~~0.57959~~	~~0.01934~~	~~0.06607~~	~~0.00099~~	~~729~~	~~45~~	~~464~~	~~12~~	~~412~~	~~6~~	~~12.6~~
STB3-84	0.45	0.05014	0.00125	0.23241	0.00599	0.03361	0.00049	201	34	212	5	213	3	-0.5
STB3-85	0.82	0.05065	0.00116	0.26872	0.00644	0.03847	0.00055	225	30	242	5	243	3	-0.4
STB3-86	0.37	0.0555	0.00087	0.53262	0.00932	0.06959	0.00095	432	18	434	6	434	6	0
STB3-87	0.73	0.05136	0.00429	0.26694	0.022	0.03769	0.0008	257	148	240	18	238	5	0.8
STB3-88	0.61	0.05005	0.00188	0.23806	0.00899	0.03449	0.00052	197	60	217	7	219	3	-0.9
STB3-89	0.58	0.05489	0.00201	0.48183	0.01779	0.06365	0.00097	408	55	399	12	398	6	0.3
STB3-90	0.31	0.06882	0.00112	1.44129	0.02589	0.15185	0.00211	893	17	906	11	911	12	-0.5
STB3-91	0.29	0.05462	0.00095	0.47525	0.00902	0.06309	0.00087	397	20	395	6	394	5	0.3
STB3-92	0.19	0.06968	0.00112	1.44979	0.02596	0.15088	0.00209	919	17	910	11	906	12	0.4

~~STB3-93~~	~~0.45~~	~~0.07046~~	~~0.00898~~	~~0.4508~~	~~0.05681~~	~~0.0464~~	~~0.0009~~	~~942~~	~~275~~	~~378~~	~~40~~	~~292~~	~~6~~	~~29.5~~
STB3-94	0.42	0.05425	0.00107	0.48945	0.01027	0.06542	0.00092	381	24	405	7	409	6	-1
STB3-95	0.47	0.05469	0.00143	0.4751	0.01282	0.06299	0.00091	400	35	395	9	394	6	0.3
STB3-96	0.58	0.05787	0.0012	0.53695	0.01178	0.06729	0.00095	525	25	436	8	420	6	3.8
STB3-97	0.63	0.05718	0.00125	0.51731	0.0119	0.0656	0.00093	498	27	423	8	410	6	3.2
STB3-98	0.5	0.05074	0.00114	0.23927	0.00562	0.0342	0.00049	229	29	218	5	217	3	0.5
STB3-99	0.64	0.05164	0.00192	0.26011	0.00976	0.03652	0.00055	270	58	235	8	231	3	1.7
~~STB3-100~~	~~0.48~~	~~0.06376~~	~~0.00261~~	~~0.56916~~	~~0.02173~~	~~0.06474~~	~~0.00096~~	~~734~~	~~89~~	~~457~~	~~14~~	~~404~~	~~6~~	~~13.1~~
JS04														
~~JS04-01~~	~~1.16~~	~~0.11028~~	~~0.01751~~	~~0.81104~~	~~0.12536~~	~~0.05334~~	~~0.00194~~	~~1804~~	~~308~~	~~603~~	~~70~~	~~335~~	~~12~~	~~80~~
JS04-02	0.03	0.05488	0.0012	0.46044	0.0081	0.06085	0.00079	408	50	385	6	381	5	1
~~JS04-03~~	~~0.64~~	~~0.06921~~	~~0.00093~~	~~0.6797~~	~~0.01021~~	~~0.07121~~	~~0.00094~~	~~905~~	~~14~~	~~527~~	~~6~~	~~443~~	~~6~~	~~19~~
~~JS04-04~~	~~0.09~~	~~0.07424~~	~~0.00152~~	~~1.1668~~	~~0.01872~~	~~0.11399~~	~~0.00146~~	~~1048~~	~~42~~	~~785~~	~~9~~	~~696~~	~~8~~	~~12.8~~
~~JS04-05~~	~~0.67~~	~~0.10581~~	~~0.00127~~	~~3.56702~~	~~0.04992~~	~~0.24444~~	~~0.00319~~	~~1728~~	~~11~~	~~1542~~	~~11~~	~~1410~~	~~17~~	~~22.6~~
JS04-06	1.06	0.12834	0.00143	6.361	0.08493	0.3594	0.00461	2075	11	2027	12	1979	22	4.9
~~JS04-07~~	~~0.82~~	~~0.04605~~	~~0.02332~~	~~1.02319~~	~~0.51506~~	~~0.16116~~	~~0.00907~~		~~847~~	~~716~~	~~258~~	~~963~~	~~50~~	~~-25.6~~
~~JS04-08~~	~~0.62~~	~~0.06886~~	~~0.00305~~	~~0.8167~~	~~0.03383~~	~~0.08602~~	~~0.00135~~	~~895~~	~~94~~	~~606~~	~~19~~	~~532~~	~~8~~	~~13.9~~
~~JS04-09~~	~~0.9~~	~~0.07048~~	~~0.00442~~	~~0.46015~~	~~0.0278~~	~~0.04735~~	~~0.0008~~	~~942~~	~~132~~	~~384~~	~~19~~	~~298~~	~~5~~	~~28.9~~
JS04-10	0.96	0.06058	0.00074	0.63032	0.00893	0.07545	0.00098	624	14	496	6	469	6	5.8
~~JS04-11~~	~~0.42~~	~~0.14592~~	~~0.0032~~	~~5.97631~~	~~0.10423~~	~~0.29703~~	~~0.00394~~	~~2299~~	~~39~~	~~1972~~	~~15~~	~~1677~~	~~20~~	~~37.1~~
~~JS04-12~~	~~0.21~~	~~0.07882~~	~~0.00168~~	~~1.57504~~	~~0.02667~~	~~0.14494~~	~~0.00186~~	~~1168~~	~~43~~	~~960~~	~~11~~	~~873~~	~~10~~	~~10~~
~~JS04-13~~	~~0.93~~	~~0.07275~~	~~0.0011~~	~~0.80744~~	~~0.0133~~	~~0.08048~~	~~0.00108~~	~~1007~~	~~15~~	~~601~~	~~7~~	~~499~~	~~6~~	~~20.4~~
~~JS04-14~~	~~0.37~~	~~0.0622~~	~~0.00191~~	~~0.39126~~	~~0.01076~~	~~0.04562~~	~~0.00062~~	~~681~~	~~67~~	~~335~~	~~8~~	~~288~~	4	~~16.3~~
JS04-15	0.36	0.06861	0.00181	1.10829	0.02526	0.11716	0.00155	887	56	757	12	714	9	6
JS04-16	0.47	0.06114	0.0008	0.64586	0.00962	0.07659	0.001	644	14	506	6	476	6	6.3
~~JS04-17~~	~~0.63~~	~~0.06696~~	~~0.00229~~	~~0.65212~~	~~0.02038~~	~~0.07064~~	~~0.00099~~	~~836~~	~~73~~	~~510~~	~~13~~	~~440~~	~~6~~	~~15.9~~

JS04-18	0.46	0.05965	0.00179	0.49307	0.01323	0.05995	0.0008	591	67	407	9	375	5	8.5
~~JS04-19~~	~~0.86~~	~~0.06906~~	~~0.00398~~	~~0.40424~~	~~0.02244~~	~~0.04245~~	~~0.00066~~	~~901~~	~~122~~	~~345~~	~~16~~	~~268~~	~~4~~	~~28.7~~
JS04-20	0.11	0.07017	0.00079	1.53849	0.02077	0.15898	0.00205	933	12	946	8	951	11	-0.5
~~JS04-21~~	~~0.39~~	~~0.06378~~	~~0.00085~~	~~0.64474~~	~~0.00969~~	~~0.0733~~	~~0.00096~~	~~734~~	~~14~~	~~505~~	~~6~~	~~456~~	~~6~~	~~10.7~~
JS04-22	0.63	0.06018	0.00081	0.5486	0.00834	0.0661	0.00087	610	15	444	5	413	5	7.5
~~JS04-23~~	~~1.37~~	~~0.09236~~	~~0.00713~~	~~0.42867~~	~~0.03187~~	~~0.03366~~	~~0.00069~~	~~1475~~	~~151~~	~~362~~	~~23~~	~~213~~	4	~~70~~
JS04-24	0.33	0.05311	0.00069	0.25075	0.00372	0.03423	0.00045	333	15	227	3	217	3	4.6
JS04-25	0.34	0.05688	0.00154	0.49062	0.01161	0.06256	0.00083	487	61	405	8	391	5	3.6
~~JS04-26~~	~~0.67~~	~~0.06045~~	~~0.00191~~	~~0.3433~~	~~0.01082~~	~~0.04118~~	~~0.00063~~	~~620~~	~~42~~	~~300~~	~~8~~	~~260~~	4	~~15.4~~
JS04-27	0.68	0.07669	0.00092	1.82141	0.02561	0.17222	0.00224	1113	13	1053	9	1024	12	8.7
JS04-28	0.53	0.05686	0.00075	0.56556	0.00848	0.07213	0.00094	486	15	455	5	449	6	1.3
JS04-29	1.05	0.05843	0.00113	0.38742	0.0078	0.04807	0.00067	546	22	332	6	303	4	9.6
JS04-30	0.48	0.11557	0.00129	4.94541	0.06659	0.31029	0.004	1889	11	1810	11	1742	20	8.4
JS04-31	0.92	0.0579	0.00081	0.52039	0.00819	0.06518	0.00086	526	16	425	5	407	5	4.4
JS04-32	0.41	0.05849	0.00171	0.54179	0.01407	0.06718	0.0009	548	65	440	9	419	5	5
~~JS04-33~~	~~0.79~~	~~0.07527~~	~~0.00346~~	~~0.61146~~	~~0.02646~~	~~0.05892~~	~~0.00091~~	~~1076~~	~~95~~	~~484~~	~~17~~	~~369~~	~~6~~	~~31.2~~
~~JS04-34~~	~~0.81~~	~~0.06106~~	~~0.00261~~	~~0.33602~~	~~0.01351~~	~~0.03991~~	~~0.00058~~	~~641~~	~~94~~	~~294~~	~~10~~	~~252~~	4	~~16.7~~
~~JS04-35~~	~~0.47~~	~~0.06295~~	~~0.00211~~	~~0.59817~~	~~0.01822~~	~~0.06892~~	~~0.00096~~	~~706~~	~~73~~	~~476~~	~~12~~	~~430~~	~~6~~	~~10.7~~
JS04-36	0.94	0.0673	0.00316	0.96035	0.04273	0.1035	0.00156	847	100	683	22	635	9	7.6
JS04-37	0.54	0.05648	0.00189	0.54025	0.01653	0.06937	0.00095	471	76	439	11	432	6	1.6
JS04-38	0.68	0.06233	0.00102	0.60551	0.01069	0.07044	0.00095	685	18	481	7	439	6	9.6
JS04-39	1.03	0.05475	0.0033	0.28836	0.01681	0.0382	0.00059	402	139	257	13	242	4	6.2
~~JS04-40~~	~~0.88~~	~~0.06117~~	~~0.00084~~	~~0.48558~~	~~0.00752~~	~~0.05756~~	~~0.00076~~	~~645~~	~~15~~	~~402~~	~~5~~	~~361~~	~~5~~	~~11.4~~
~~JS04-41~~	~~0.59~~	~~0.0688~~	~~0.0025~~	~~0.57686~~	~~0.01923~~	~~0.06081~~	~~0.00088~~	~~893~~	~~77~~	~~462~~	~~12~~	~~381~~	~~5~~	~~21.3~~
JS04-42	0.83	0.07109	0.00086	1.27288	0.01805	0.12983	0.0017	960	13	834	8	787	10	6
JS04-43	0.88	0.05628	0.00081	0.53938	0.00864	0.0695	0.00092	463	16	438	6	433	6	1.2
JS04-44	0.32	0.07241	0.00084	1.55002	0.02147	0.15522	0.00202	997	13	951	9	930	11	2.3
JS04-45	0.31	0.07565	0.00091	1.40505	0.0199	0.13468	0.00176	1086	13	891	8	815	10	9.3

~~JS04-46~~	~~0.28~~	~~0.12182~~	~~0.00137~~	~~5.36985~~	~~0.07301~~	~~0.31965~~	~~0.00414~~	~~1983~~	~~11~~	~~1880~~	~~12~~	~~1788~~	~~20~~	~~10.9~~
JS04-47	0.53	0.06097	0.00081	0.60822	0.0092	0.07234	0.00095	638	15	482	6	450	6	7.1
~~JS04-48~~	~~0.55~~	~~0.06745~~	~~0.00083~~	~~0.63841~~	~~0.00916~~	~~0.06864~~	~~0.0009~~	~~852~~	~~13~~	~~501~~	~~6~~	~~428~~	~~5~~	~~17.1~~
~~JS04-49~~	~~1.16~~	~~0.0654~~	~~0.00093~~	~~0.63835~~	~~0.0101~~	~~0.07078~~	~~0.00094~~	~~787~~	~~15~~	~~501~~	~~6~~	~~441~~	~~6~~	~~13.6~~
JS04-50	0.12	0.09046	0.00103	2.81139	0.03843	0.22537	0.00293	1435	12	1359	10	1310	15	9.5
JS04-51	0.61	0.05796	0.00073	0.58105	0.00847	0.07269	0.00095	528	14	465	5	452	6	2.9
~~JS04-52~~	~~1.08~~	~~0.06128~~	~~0.00086~~	~~0.51695~~	~~0.0081~~	~~0.06117~~	~~0.00082~~	~~649~~	~~15~~	~~423~~	~~5~~	~~383~~	~~5~~	~~10.4~~
JS04-53	0.07	0.11647	0.00132	5.05021	0.06905	0.31441	0.00409	1903	11	1828	12	1762	20	8
JS04-54	0.42	0.05578	0.00201	0.35303	0.01172	0.0459	0.00064	444	82	307	9	289	4	6.2
JS04-55	0.62	0.0572	0.00075	0.55096	0.0083	0.06984	0.00092	499	15	446	5	435	6	2.5
JS04-56	0.46	0.05957	0.00087	0.54445	0.00883	0.06628	0.00088	588	16	441	6	414	5	6.5
JS04-57	0.54	0.05618	0.00271	0.28298	0.01304	0.03653	0.00053	459	110	253	10	231	3	9.5
~~JS04-58~~	~~0.77~~	~~0.06714~~	~~0.00257~~	~~0.69507~~	~~0.02466~~	~~0.07509~~	~~0.00108~~	~~842~~	~~82~~	~~536~~	~~15~~	~~467~~	~~6~~	~~14.8~~
JS04-59	0.72	0.06034	0.00228	0.60273	0.02117	0.07245	0.00102	616	84	479	13	451	6	6.2
JS04-60	0.2	0.07247	0.00087	1.49129	0.02118	0.14922	0.00196	999	13	927	9	897	11	3.3
JS04-61	0.28	0.05647	0.00067	0.52675	0.00745	0.06764	0.00088	471	14	430	5	422	5	1.9
~~JS04-62~~	~~0.25~~	~~0.08713~~	~~0.00195~~	~~2.16661~~	~~0.039~~	~~0.18036~~	~~0.00238~~	~~1363~~	~~44~~	~~1170~~	~~13~~	~~1069~~	~~13~~	~~27.5~~
~~JS04-63~~	~~0.5~~	~~0.05718~~	~~0.00228~~	~~0.05528~~	~~0.00204~~	~~0.00701~~	~~0.0001~~	~~499~~	~~90~~	~~55~~	~~2~~	~~45~~	~~0.7~~	~~22.2~~
JS04-64	0.19	0.0716	0.00082	1.37233	0.01902	0.13898	0.00181	975	13	877	8	839	10	4.5
~~JS04-65~~	~~0.27~~	~~0.10795~~	~~0.00274~~	~~3.09204~~	~~0.06561~~	~~0.20775~~	~~0.00291~~	~~1765~~	~~48~~	~~1431~~	~~16~~	~~1217~~	~~16~~	~~45~~
~~JS04-66~~	~~1~~	~~0.05976~~	~~0.00105~~	~~0.33483~~	~~0.0063~~	~~0.04063~~	~~0.00055~~	~~595~~	~~20~~	~~293~~	~~5~~	~~257~~	~~3~~	~~14~~
~~JS04-67~~	~~0.38~~	~~0.06407~~	~~0.00094~~	~~0.60241~~	~~0.00979~~	~~0.06818~~	~~0.00092~~	~~744~~	~~16~~	~~479~~	~~6~~	~~425~~	~~6~~	~~12.7~~
~~JS04-68~~	~~0.76~~	~~0.05714~~	~~0.00093~~	~~0.30922~~	~~0.00547~~	~~0.03924~~	~~0.00053~~	~~497~~	~~18~~	~~274~~	~~4~~	~~248~~	~~3~~	~~10.5~~
~~JS04-69~~	~~1.24~~	~~0.09873~~	~~0.00404~~	~~3.06853~~	~~0.11622~~	~~0.22542~~	~~0.00346~~	~~1600~~	~~78~~	~~1425~~	~~29~~	~~1310~~	~~18~~	~~22.1~~
JS04-70	0.48	0.05669	0.0019	0.38743	0.01182	0.04956	0.00068	480	76	332	9	312	4	6.4
~~JS04-71~~	~~0.86~~	~~0.0772~~	~~0.004~~	~~0.4117~~	~~0.02031~~	~~0.03868~~	~~0.00062~~	~~1126~~	~~106~~	~~350~~	~~15~~	~~245~~	~~4~~	~~42.9~~
~~JS04-72~~	~~0.43~~	~~0.06787~~	~~0.00211~~	~~0.61453~~	~~0.01714~~	~~0.06567~~	~~0.0009~~	~~865~~	~~66~~	~~486~~	~~11~~	~~410~~	~~5~~	~~18.5~~
JS04-73	0.57	0.05964	0.00076	0.57965	0.0086	0.07047	0.00093	591	14	464	6	439	6	5.7

JS04-74	0.75	0.05617	0.00072	0.52159	0.00775	0.06733	0.00089	459	15	426	5	420	5	1.4
~~JS04-75~~	~~0.57~~	~~0.07744~~	~~0.00093~~	~~1.46043~~	~~0.02073~~	~~0.13674~~	~~0.0018~~	~~1133~~	~~13~~	~~914~~	~~9~~	~~826~~	~~10~~	~~10.7~~
~~JS04-76~~	~~0.34~~	~~0.10216~~	~~0.00133~~	~~1.53308~~	~~0.02285~~	~~0.10882~~	~~0.00146~~	~~1664~~	~~12~~	~~944~~	~~9~~	~~666~~	~~8~~	~~41.7~~
JS04-77	0.71	0.06034	0.0008	0.64075	0.00975	0.077	0.00103	616	15	503	6	478	6	5.2
~~JS04-78~~	~~0.93~~	~~0.06676~~	~~0.00095~~	~~0.69728~~	~~0.01112~~	~~0.07574~~	~~0.00102~~	~~830~~	~~15~~	~~537~~	~~7~~	~~471~~	~~6~~	~~14~~
JS04-79	0.41	0.07472	0.00202	1.57932	0.03687	0.15329	0.00209	1061	56	962	15	919	12	4.7
~~JS04-80~~	~~1.03~~	~~0.06733~~	~~0.00712~~	~~0.59542~~	~~0.06195~~	~~0.06414~~	~~0.0012~~	~~848~~	~~229~~	~~474~~	~~39~~	~~401~~	~~7~~	~~18.2~~
JS04-81	0.63	0.05191	0.00471	0.30411	0.02696	0.04249	0.00082	281	208	270	21	268	5	0.7
~~JS04-82~~	~~0.77~~	~~0.06405~~	~~0.00174~~	~~0.57325~~	~~0.01574~~	~~0.0649~~	~~0.00096~~	~~743~~	~~34~~	~~460~~	~~10~~	~~405~~	~~6~~	~~13.6~~
JS04-83	0.17	0.05596	0.00166	0.49291	0.01299	0.06388	0.00087	451	67	407	9	399	5	2
JS04-84	1.19	0.06064	0.00089	0.56634	0.00931	0.06773	0.00091	626	16	456	6	422	5	8.1
JS04-85	0.28	0.04605	0.00147	0.05629	0.00161	0.00887	0.00013		66	56	2	56.9	0.8	-1.6
JS04-86	0.96	0.05996	0.00093	0.57525	0.00982	0.06957	0.00094	602	17	461	6	434	6	6.2
~~JS04-87~~	~~0.91~~	~~0.06727~~	~~0.00094~~	~~0.67131~~	~~0.01058~~	~~0.07236~~	~~0.00097~~	~~846~~	~~15~~	~~522~~	~~6~~	~~450~~	~~6~~	~~16~~
JS04-88	0.46	0.0545	0.00086	0.32585	0.00562	0.04336	0.00059	392	18	286	4	274	4	4.4
JS04-89	0.39	0.12466	0.00152	6.29824	0.09089	0.36637	0.00487	2024	11	2018	13	2012	23	0.6
JS04-90	0.71	0.06123	0.00253	0.53103	0.02058	0.0629	0.00091	647	91	432	14	393	6	9.9
JS04-91	0.4	0.05697	0.00078	0.36648	0.00573	0.04665	0.00062	490	15	317	4	294	4	7.8
~~JS04-92~~	~~1.17~~	~~0.07668~~	~~0.00391~~	~~0.41797~~	~~0.02025~~	~~0.03953~~	~~0.00063~~	~~1113~~	~~104~~	~~355~~	~~15~~	~~250~~	~~4~~	~~42~~
JS04-93	0.22	0.0567	0.00156	0.5158	0.01241	0.06597	0.00089	480	62	422	8	412	5	2.4
~~JS04-94~~	~~0.68~~	~~0.06672~~	~~0.00288~~	~~0.62134~~	~~0.02508~~	~~0.06754~~	~~0.00102~~	~~829~~	~~92~~	~~491~~	~~16~~	~~421~~	~~6~~	~~16.6~~
JS04-95	0.96	0.07181	0.00095	1.26947	0.01929	0.12819	0.00172	981	14	832	9	778	10	6.9
JS04-96	0.58	0.14869	0.00183	8.13718	0.11828	0.39683	0.0053	2331	11	2246	13	2154	24	8.2
JS04-97	0.45	0.06001	0.00201	0.53405	0.0163	0.06455	0.0009	604	74	434	11	403	5	7.7
JS04-98	0.18	0.06166	0.00083	0.63411	0.00978	0.07458	0.001	662	15	499	6	464	6	7.5
JS04-99	0.24	0.17678	0.00212	11.18255	0.16013	0.45869	0.00608	2623	11	2538	13	2434	27	7.8
~~JS04-100~~	~~0.74~~	~~0.06187~~	~~0.00085~~	~~0.50636~~	~~0.00788~~	~~0.05935~~	~~0.0008~~	~~670~~	~~15~~	~~416~~	~~5~~	~~372~~	~~5~~	~~11.8~~

STB1														
STB1-01	0.41	0.0547	0.00085	0.50449	0.00883	0.06688	0.00092	400	18	415	6	417	6	-0.5
~~STB1-02~~	~~1.24~~	~~0.10971~~	~~0.00176~~	~~4.18093~~	~~0.07438~~	~~0.27633~~	~~0.00388~~	~~1795~~	~~15~~	~~1670~~	~~15~~	109	~~20~~	~~14.1~~
STB1-03	1.13	0.05582	0.00175	0.57047	0.0182	0.07411	0.00111	445	44	458	12	~~204~~	7	-0.7
~~STB1-04~~	~~0.41~~	~~0.1817~~	~~0.00251~~	~~10.3301~~	~~0.16572~~	~~0.41225~~	~~0.00563~~	~~2668~~	~~12~~	~~2465~~	~~15~~	206	~~26~~	~~19.9~~
STB1-05	0.43	0.05161	0.00261	0.30329	0.01532	0.04261	0.00069	268	86	269	12	206	4	0
STB1-06	0.43	0.05619	0.00394	0.56368	0.03924	0.07275	0.00133	460	122	454	25	210	8	0.2
STB1-07	0.6	0.05536	0.00101	0.51852	0.01023	0.06791	0.00095	427	21	424	7	214	6	0
STB1-08	0.4	0.05548	0.00119	0.55537	0.01259	0.07259	0.00104	432	26	449	8	215	6	-0.7
STB1-09	0.55	0.0619	0.00102	0.92233	0.01681	0.10805	0.0015	671	18	664	9	226	9	0.5
STB1-10	0.69	0.05477	0.00136	0.5092	0.01306	0.06742	0.00099	403	32	418	9	228	6	-0.7
STB1-11	0.31	0.05545	0.00147	0.52944	0.01439	0.06923	0.00102	430	35	431	10	256	6	-0.2
~~STB1-12~~	~~0.25~~	~~0.06148~~	~~0.0011~~	~~0.52425~~	~~0.0102~~	~~0.06183~~	~~0.00087~~	~~656~~	~~20~~	~~428~~	~~7~~	269	~~5~~	~~10.6~~
STB1-13	0.51	0.05508	0.00102	0.51941	0.01043	0.06839	0.00096	415	22	425	7	272	6	-0.2
STB1-14	0.2	0.12219	0.00183	6.40892	0.10873	0.38032	0.00528	1988	14	2033	15	304	25	-4.3
STB1-15	1.5	0.09438	0.00145	3.49578	0.06039	0.26857	0.00373	1516	15	1526	14	359	19	-1.2
STB1-16	0.45	0.05555	0.00134	0.50431	0.01264	0.06584	0.00095	434	31	415	9	364	6	1
STB1-17	0.46	0.05523	0.00096	0.52588	0.01001	0.06905	0.00097	422	20	429	7	386	6	-0.2
STB1-18	0.29	0.05559	0.00108	0.50365	0.01051	0.0657	0.00093	436	23	414	7	386	6	1
STB1-19	0.76	0.05565	0.00117	0.53467	0.01188	0.06967	0.001	438	26	435	8	~~387~~	6	0.2
STB1-20	0.49	0.05698	0.00126	0.49851	0.01161	0.06344	0.00091	491	27	411	8	387	6	3.5
STB1-21	0.88	0.0552	0.00247	0.4933	0.02212	0.0648	0.00104	420	71	407	15	393	6	0.5
~~STB1-22~~	~~0.62~~	~~0.06748~~	~~0.00364~~	~~0.29894~~	~~0.01545~~	~~0.03213~~	~~0.0005~~	~~853~~	~~115~~	~~266~~	~~12~~	397	~~3~~	~~30.4~~
STB1-23	0.73	0.05327	0.0026	0.45492	0.02221	0.06192	0.00101	340	81	381	16	397	6	-1.6
STB1-24	0.46	0.05581	0.00196	0.54879	0.01942	0.07131	0.00111	445	51	444	13	397	7	0
STB1-25	0.14	0.05004	0.00104	0.22414	0.00494	0.03248	0.00046	197	27	205	4	398	3	-0.5
STB1-26	0.49	0.05433	0.00123	0.47064	0.01117	0.06282	0.0009	385	29	392	8	403	5	-0.3

STB1-27	0.44	0.05593	0.00103	0.53594	0.01066	0.06949	0.00098	450	22	436	7	405	6	0.7
STB1-28	0.49	0.06068	0.00158	0.85437	0.02287	0.1021	0.00152	628	33	627	13	408	9	0
STB1-29	1.35	0.05134	0.00268	0.28726	0.01495	0.04057	0.00068	256	89	256	12	410	4	0
STB1-30	0.33	0.05568	0.00097	0.54703	0.01044	0.07124	0.001	440	20	443	7	410	6	-0.2
STB1-31	0.8	0.05012	0.00205	0.2343	0.00959	0.0339	0.00054	201	65	214	8	411	3	-0.5
STB1-32	0.5	0.05656	0.001	0.56948	0.01101	0.07301	0.00102	474	21	458	7	417	6	0.9
STB1-33	0.48	0.07024	0.00122	1.44897	0.0276	0.14958	0.0021	935	19	909	11	421	12	1.1
STB1-34	0.97	0.09148	0.00218	3.20456	0.0787	0.25402	0.00387	1457	25	1458	19	~~422~~	20	-0.1
STB1-35	0.1	0.05449	0.00101	0.46428	0.00931	0.06178	0.00087	391	22	387	6	423	5	0.3
STB1-36	0.47	0.05533	0.00162	0.5406	0.0162	0.07084	0.00106	426	40	439	11	424	6	-0.5
STB1-37	0.38	0.09245	0.00164	3.21879	0.06225	0.25247	0.00359	1477	17	1462	15	426	18	1.8
~~STB1-38~~	~~1.24~~	~~0.06439~~	~~0.00192~~	~~0.62347~~	~~0.01884~~	~~0.07021~~	~~0.00107~~	~~754~~	~~38~~	~~492~~	~~12~~	426	~~6~~	~~12.6~~
STB1-39	0.46	0.05453	0.00131	0.47798	0.01193	0.06356	0.00093	393	31	397	8	427	6	0
STB1-40	0.43	0.05518	0.00317	0.52488	0.02897	0.06899	0.00109	420	132	428	19	429	7	-0.5
STB1-41	2.15	0.05948	0.00126	0.72158	0.01611	0.08797	0.00127	585	25	552	10	430	8	1.5
STB1-42	0.24	0.05507	0.00109	0.49666	0.01048	0.06539	0.00093	415	24	409	7	430	6	0.2
STB1-43	0.39	0.06999	0.00119	1.51548	0.02842	0.15701	0.0022	928	18	937	11	430	12	-0.3
STB1-44	1.08	0.12595	0.00216	6.03621	0.11346	0.34753	0.00494	2042	16	1981	16	432	24	6.2
STB1-45	0.7	0.05703	0.00142	0.57489	0.01481	0.07309	0.00106	493	32	461	10	432	6	1.3
STB1-46	0.66	0.05599	0.00135	0.54661	0.01372	0.07079	0.00103	452	31	443	9	433	6	0.5
STB1-47	0.58	0.13022	0.0022	6.76647	0.12588	0.37679	0.00532	2101	15	2081	16	434	25	1.9
STB1-48	0.64	0.06585	0.00162	1.2206	0.03115	0.1344	0.00198	802	30	810	14	~~437~~	11	-0.4
STB1-49	1.55	0.16565	0.00283	10.78044	0.20205	0.47191	0.00671	2514	15	2504	17	437	29	0.9
STB1-50	0.13	0.07125	0.00128	1.56916	0.0307	0.15969	0.00226	965	19	958	12	441	13	0.3
~~STB1-51~~	~~0.77~~	~~0.1361~~	~~0.0046~~	~~6.40577~~	~~0.19248~~	~~0.34136~~	~~0.00526~~	~~2178~~	~~60~~	~~2033~~	~~26~~	441	~~25~~	~~15.1~~
STB1-52	0.25	0.07623	0.00218	1.82383	0.04506	0.17352	0.00248	1101	58	1054	16	444	14	6.8
STB1-53	0.64	0.04848	0.00369	0.1138	0.00862	0.01702	0.0003	123	136	109	8	444	2	0
STB1-54	0.54	0.05095	0.00116	0.25012	0.00596	0.0356	0.00052	239	29	227	5	452	3	0.4

STB1-55	0.33	0.16697	0.00286	10.78672	0.20321	0.46843	0.00662	2527	15	2505	18	453	29	2
~~STB1-56~~	~~0.1~~	~~0.08148~~	~~0.00149~~	~~1.67286~~	~~0.03315~~	~~0.14888~~	~~0.00212~~	~~1233~~	~~19~~	~~998~~	~~13~~	454	~~12~~	~~11.5~~
STB1-57	1.08	0.05566	0.00146	0.5315	0.01431	0.06924	0.00104	439	34	433	9	455	6	0.2
STB1-58	0.5	0.05068	0.00148	0.23614	0.00707	0.03379	0.0005	226	42	215	6	455	3	0.5
STB1-59	0.49	0.05548	0.0028	0.52282	0.02635	0.06833	0.00114	432	82	427	18	461	7	0.2
STB1-60	0.52	0.05529	0.00158	0.4918	0.01437	0.06449	0.00097	424	39	406	10	544	6	0.7
~~STB1-61~~	~~0.5~~	~~0.06225~~	~~0.00124~~	~~0.58098~~	~~0.01236~~	~~0.06768~~	~~0.00097~~	~~683~~	~~23~~	~~465~~	~~8~~	627	~~6~~	~~10.2~~
STB1-62	0.53	0.05647	0.00137	0.5357	0.01352	0.06879	0.00101	471	31	436	9	661	6	1.6
STB1-63	0.59	0.17121	0.00315	11.01587	0.21934	0.46653	0.00676	2570	16	2524	19	763	30	4.1
STB1-64	0.68	0.07084	0.00162	1.45359	0.03467	0.14878	0.00219	953	26	911	14	764	12	1.9
STB1-65	0.3	0.07625	0.00234	1.55853	0.04218	0.14824	0.00214	1102	63	954	17	807	12	7.1
STB1-66	0.27	0.07266	0.00136	1.58547	0.03205	0.15822	0.00226	1004	20	965	13	813	13	1.9
STB1-67	0.24	0.06843	0.00132	1.3333	0.02756	0.14128	0.00202	882	21	860	12	829	11	0.9
STB1-68	0.15	0.05564	0.00117	0.56088	0.01251	0.07309	0.00106	438	26	452	8	852	6	-0.7
STB1-69	0.34	0.11395	0.00209	4.89113	0.09739	0.31125	0.00444	1863	17	1801	17	889	22	6.6
STB1-70	0.87	0.05442	0.00207	0.43599	0.01666	0.05809	0.00092	388	57	367	12	891	6	0.8
STB1-71	0.33	0.05048	0.00152	0.25081	0.00767	0.03603	0.00054	217	43	227	6	894	3	-0.4
STB1-72	0.44	0.05264	0.00145	0.24033	0.00678	0.03311	0.00049	313	38	219	6	~~895~~	3	4.3
STB1-73	0.32	0.07472	0.00151	1.82576	0.03938	0.17718	0.00257	1061	22	1055	14	899	14	0.9
STB1-74	0.6	0.05554	0.00124	0.51896	0.01218	0.06775	0.00099	434	28	424	8	902	6	0.2
STB1-75	1.91	0.06593	0.00256	1.24721	0.04852	0.13716	0.00225	804	54	822	22	922	13	-0.8
STB1-76	0.24	0.06983	0.0016	1.44633	0.03457	0.15018	0.00222	923	26	908	14	940	12	0.7
STB1-77	0.39	0.04979	0.00238	0.22277	0.01064	0.03244	0.00054	185	80	204	9	947	3	-1
STB1-78	0.08	0.05421	0.00125	0.42855	0.01035	0.05732	0.00084	380	29	362	7	955	5	0.8
STB1-79	0.59	0.05181	0.00233	0.30845	0.01391	0.04316	0.00069	277	74	273	11	1031	4	0.4
STB1-80	0.35	0.05535	0.00204	0.50143	0.01865	0.06569	0.00103	426	55	413	13	1042	6	0.7
STB1-81	0.55	0.07416	0.00158	1.79384	0.04043	0.17539	0.00257	1046	23	1043	15	1052	14	0.4
~~STB1-82~~	~~1.49~~	~~0.10555~~	~~0.00732~~	~~3.9133~~	~~0.26147~~	~~0.26888~~	~~0.00503~~	~~1724~~	~~131~~	~~1616~~	~~54~~	1384	~~26~~	~~12.3~~

STB1-83	0.31	0.19677	0.00376	13.31079	0.27393	0.4905	0.00704	2800	17	2702	19	1451	30	8.8
STB1-84	0.92	0.06687	0.00177	1.1607	0.03152	0.12586	0.0019	834	32	782	15	1459	11	2.4
STB1-85	0.57	0.05702	0.00208	0.53851	0.01982	0.06848	0.00108	492	53	437	13	1534	7	2.3
STB1-86	0.18	0.07131	0.0015	1.45433	0.03239	0.14788	0.00216	966	23	912	13	~~1535~~	12	2.6
STB1-87	0.62	0.05843	0.00177	0.5129	0.0158	0.06365	0.00098	546	41	420	11	1569	6	5.5
STB1-88	0.59	0.05643	0.00131	0.48084	0.01166	0.06178	0.00091	469	29	399	8	~~1573~~	6	3.4
STB1-89	0.83	0.0554	0.00201	0.51021	0.0187	0.06678	0.00105	428	54	419	13	~~1680~~	6	0.5
STB1-90	0.31	0.06638	0.00174	1.14987	0.0309	0.1256	0.00191	818	32	777	15	1747	11	1.8
~~STB1-91~~	~~1.16~~	~~0.15979~~	~~0.00322~~	~~9.06795~~	~~0.19497~~	~~0.41147~~	~~0.006~~	~~2453~~	~~18~~	~~2345~~	~~20~~	~~1893~~	~~27~~	~~10.4~~
STB1-92	0.13	0.10057	0.00272	3.82211	0.08752	0.27562	0.00396	1635	51	1597	18	1923	20	4.2
STB1-93	0.48	0.07149	0.00173	1.51524	0.03803	0.15367	0.0023	971	28	937	15	2061	13	1.6
STB1-94	0.71	0.06735	0.00226	1.23843	0.04202	0.13333	0.00211	849	44	818	19	2078	12	1.4
STB1-95	0.44	0.0547	0.00162	0.47926	0.01448	0.06353	0.00097	400	41	398	10	~~2222~~	6	0.3
STB1-96	0.67	0.05307	0.00202	0.35394	0.01355	0.04836	0.00077	332	58	308	10	~~2225~~	5	1.3
STB1-97	0.51	0.09188	0.00194	3.03522	0.06773	0.23953	0.00351	1465	22	1417	17	2468	18	5.9
~~STB1-98~~	~~0.21~~	~~0.1174~~	~~0.00248~~	~~4.82143~~	~~0.10774~~	~~0.29777~~	~~0.00439~~	~~1917~~	~~20~~	~~1789~~	~~19~~	2477	~~22~~	~~14.1~~
STB1-99	0.5	0.05644	0.00197	0.54593	0.01927	0.07013	0.0011	470	50	442	13	2492	7	1.1
STB1-100	1.03	0.05622	0.00127	0.53473	0.01263	0.06896	0.00102	461	28	435	8	2573	6	1.2
Q403														
~~Q403-01~~	~~0.49~~	~~0.06843~~	~~0.00434~~	~~0.64807~~	~~0.03914~~	~~0.06869~~	~~0.00132~~	~~882~~	~~135~~	~~507~~	~~24~~	~~428~~	~~8~~	~~18.5~~
Q403-02	0.55	0.05685	0.00175	0.60512	0.01894	0.07718	0.00122	486	42	480	12	479	7	0.2
~~Q403-03~~	~~0.52~~	~~0.06584~~	~~0.00384~~	~~0.66653~~	~~0.03726~~	~~0.07343~~	~~0.00122~~	~~801~~	~~126~~	~~519~~	~~23~~	~~457~~	~~7~~	~~13.6~~
Q403-04	0.87	0.0579	0.00191	0.56907	0.01904	0.07127	0.00114	526	46	457	12	444	7	2.9
Q403-05	0.57	0.06187	0.00203	0.61208	0.02022	0.07173	0.00117	670	43	485	13	447	7	8.5
Q403-06	0.6	0.06037	0.0017	0.60268	0.01728	0.07239	0.00114	617	35	479	11	451	7	6.2
~~Q403-07~~	~~1.37~~	~~0.06285~~	~~0.00437~~	~~0.34196~~	~~0.02355~~	~~0.03945~~	~~0.00077~~	~~703~~	~~114~~	~~299~~	~~18~~	~~249~~	~~5~~	~~20.1~~
Q403-08	0.61	0.05629	0.00159	0.59724	0.01723	0.07694	0.00121	464	37	475	11	478	7	-0.6

~~Q403-09~~	~~0.44~~	~~0.06453~~	~~0.00216~~	~~0.68501~~	~~0.02301~~	~~0.07698~~	~~0.00127~~	~~759~~	~~43~~	~~530~~	~~14~~	~~478~~	~~8~~	~~10.9~~
~~Q403-10~~	~~0.49~~	~~0.08273~~	~~0.00211~~	~~0.66928~~	~~0.01757~~	~~0.05866~~	~~0.00092~~	~~1263~~	~~28~~	~~520~~	~~11~~	~~367~~	~~6~~	~~41.7~~
Q403-11	0.83	0.05725	0.0081	0.50473	0.07052	0.06394	0.00142	501	318	415	48	400	9	3.8
~~Q403-12~~	~~0.75~~	~~0.06093~~	~~0.00197~~	~~0.38698~~	~~0.01264~~	~~0.04606~~	~~0.00075~~	~~637~~	~~43~~	~~332~~	~~9~~	~~290~~	~~5~~	~~14.5~~
Q403-13	0.58	0.06126	0.00171	0.61988	0.01774	0.07338	0.00116	648	35	490	11	456	7	7.5
Q403-14	0.41	0.05686	0.00161	0.59418	0.01715	0.07578	0.0012	486	36	474	11	471	7	0.6
~~Q403-15~~	~~0.54~~	~~0.06358~~	~~0.00167~~	~~0.64869~~	~~0.01754~~	~~0.07399~~	~~0.00116~~	~~728~~	~~32~~	~~508~~	~~11~~	~~460~~	~~7~~	~~10.4~~
Q403-16	0.5	0.05496	0.00275	0.49856	0.0249	0.06578	0.00115	411	80	411	17	411	7	0
~~Q403-17~~	~~0.77~~	~~0.06835~~	~~0.00328~~	~~0.37156~~	~~0.01766~~	~~0.03942~~	~~0.00071~~	~~879~~	~~68~~	~~321~~	~~13~~	~~249~~	4	~~28.9~~
Q403-18	0.55	0.05656	0.00174	0.58757	0.01841	0.07533	0.00121	474	41	469	12	468	7	0.2
Q403-19	0.82	0.05622	0.00231	0.55279	0.02278	0.07129	0.00121	461	61	447	15	444	7	0.7
Q403-20	0.5	0.06249	0.00336	0.67328	0.03436	0.07814	0.00131	691	118	523	21	485	8	7.8
~~Q403-21~~	~~0.47~~	~~0.06478~~	~~0.002~~	~~0.63625~~	~~0.01986~~	~~0.07122~~	~~0.00116~~	~~767~~	~~39~~	~~500~~	~~12~~	~~444~~	~~7~~	~~12.6~~
Q403-22	0.61	0.06153	0.00173	0.63293	0.01821	0.07459	0.00119	658	35	498	11	464	7	7.3
Q403-23	0.48	0.06577	0.00366	0.52305	0.0277	0.05768	0.00098	799	120	427	18	362	6	18
Q403-24	0.57	0.05682	0.00154	0.59405	0.01656	0.07582	0.0012	485	35	473	11	471	7	0.4
~~Q403-25~~	~~0.73~~	~~0.06584~~	~~0.00862~~	~~0.51336~~	~~0.06636~~	~~0.05655~~	~~0.00118~~	~~801~~	~~290~~	~~421~~	~~45~~	~~355~~	~~7~~	~~18.6~~
Q403-26	0.55	0.0565	0.00171	0.58668	0.01803	0.0753	0.00122	472	40	469	12	468	7	0.2
Q403-27	0.45	0.05635	0.0015	0.58977	0.01623	0.07589	0.00111	466	36	471	10	472	7	-0.2
Q403-28	0.62	0.06266	0.00137	0.61509	0.0141	0.07118	0.00104	697	25	487	9	443	6	9.9
~~Q403-29~~	~~0.58~~	~~0.06469~~	~~0.00146~~	~~0.62845~~	~~0.01483~~	~~0.07045~~	~~0.00103~~	~~764~~	~~26~~	~~495~~	~~9~~	~~439~~	~~6~~	~~12.8~~
Q403-30	0.53	0.05706	0.00118	0.56547	0.01244	0.07186	0.00103	494	25	455	8	447	6	1.8
Q403-31	0.49	0.05645	0.00144	0.56835	0.01494	0.07301	0.00108	470	33	457	10	454	6	0.7
~~Q403-32~~	~~0.43~~	~~0.06836~~	~~0.00242~~	~~0.56449~~	~~0.01822~~	~~0.05989~~	~~0.00087~~	~~879~~	~~75~~	~~454~~	~~12~~	~~375~~	~~5~~	~~21.1~~
Q403-33	0.57	0.05893	0.00134	0.58816	0.01395	0.07236	0.00106	565	27	470	9	450	6	4.4
Q403-34	0.51	0.0571	0.00106	0.58914	0.01184	0.07481	0.00106	495	22	470	8	465	6	1.1
Q403-35	0.96	0.06064	0.00456	0.20597	0.01505	0.02464	0.00043	626	167	190	13	157	3	21
~~Q403-36~~	~~0.24~~	~~0.07433~~	~~0.00258~~	~~1.1498~~	~~0.04003~~	~~0.11216~~	~~0.00182~~	~~1050~~	~~44~~	~~777~~	~~19~~	~~685~~	~~11~~	~~13.4~~

Q403-37	0.75	0.05794	0.00409	0.55212	0.03891	0.06909	0.00118	527	125	446	25	431	7	3.5
Q403-38	0.65	0.05815	0.00128	0.53778	0.01241	0.06706	0.00098	535	26	437	8	418	6	4.5
Q403-39	0.52	0.05645	0.00141	0.5714	0.01482	0.07339	0.00108	470	32	459	10	457	6	0.4
Q403-40	0.45	0.05756	0.0018	0.59396	0.01891	0.07482	0.00114	513	43	473	12	465	7	1.7
Q403-41	0.48	0.05597	0.00141	0.5781	0.01507	0.0749	0.0011	451	33	463	10	466	7	-0.6
Q403-42	0.4	0.05564	0.00126	0.56477	0.01336	0.0736	0.00107	438	28	455	9	458	6	-0.7
Q403-43	0.41	0.0562	0.00148	0.57617	0.01561	0.07434	0.00111	460	34	462	10	462	7	0
Q403-44	0.45	0.05602	0.00141	0.57964	0.01508	0.07503	0.00111	453	32	464	10	466	7	-0.4
Q403-45	0.51	0.05633	0.00147	0.57414	0.01544	0.07391	0.0011	465	34	461	10	460	7	0.2
Q403-46	0.38	0.05725	0.00132	0.65318	0.01578	0.08274	0.00121	501	29	510	10	512	7	-0.4
Q403-47	0.44	0.05666	0.00192	0.57899	0.01985	0.07409	0.00115	478	48	464	13	461	7	0.7
Q403-48	0.5	0.05545	0.00256	0.52398	0.02416	0.06852	0.00112	430	73	428	16	427	7	0.2
Q403-49	0.51	0.05647	0.00162	0.58504	0.01724	0.07512	0.00112	471	39	468	11	467	7	0.2
Q403-50	0.41	0.0567	0.00127	0.59285	0.01399	0.07582	0.0011	480	28	473	9	471	7	0.4
~~Q403-51~~	~~0.56~~	~~0.06394~~	~~0.0015~~	~~0.65575~~	~~0.01594~~	~~0.07437~~	~~0.00111~~	~~740~~	~~27~~	~~512~~	~~10~~	~~462~~	~~7~~	~~10.8~~
Q403-52	0.47	0.05701	0.00167	0.62888	0.01876	0.07998	0.00121	492	39	495	12	496	7	-0.2
Q403-53	0.47	0.05676	0.00162	0.60627	0.0177	0.07745	0.00117	482	38	481	11	481	7	0
Q403-54	0.37	0.05639	0.00151	0.58547	0.0161	0.07529	0.00112	468	35	468	10	468	7	0
Q403-55	0.44	0.05599	0.00127	0.55434	0.01319	0.07179	0.00105	452	28	448	9	447	6	0.2
Q403-56	0.56	0.06928	0.00161	1.4616	0.03534	0.15298	0.00229	907	26	915	15	918	13	-0.3
Q403-57	0.52	0.05768	0.00137	0.58718	0.01446	0.07381	0.00109	518	29	469	9	459	7	2.2
Q403-58	0.5	0.05549	0.00221	0.54558	0.02179	0.07129	0.00113	432	61	442	14	444	7	-0.5
Q403-59	0.43	0.05648	0.00194	0.56374	0.01953	0.07238	0.00114	471	49	454	13	450	7	0.9
Q403-60	0.48	0.05561	0.0015	0.53042	0.01472	0.06916	0.00104	437	36	432	10	431	6	0.2
Q403-61	0.34	0.05481	0.00412	0.50259	0.0375	0.06649	0.00125	404	134	413	25	415	8	-0.5
Q403-62	0.39	0.0553	0.00145	0.57794	0.01559	0.07578	0.00113	424	34	463	10	471	7	-1.7
Q403-63	0.61	0.05979	0.00585	0.53118	0.05111	0.06443	0.00116	596	220	433	34	403	7	7.4
Q403-64	0.47	0.0561	0.00177	0.56241	0.01806	0.07269	0.00111	456	44	453	12	452	7	0.2

Q403-65	0.4	0.05891	0.00269	0.61049	0.02628	0.07516	0.00116	564	102	484	17	467	7	3.6
Q403-66	0.53	0.05646	0.00147	0.58353	0.01567	0.07494	0.00113	471	34	467	10	466	7	0.2
Q403-67	0.6	0.05667	0.00152	0.60076	0.01651	0.07686	0.00116	479	35	478	10	477	7	0.2
Q403-68	0.76	0.05154	0.00298	0.30641	0.01766	0.0431	0.00073	265	101	271	14	272	5	-0.4
Q403-69	0.54	0.05613	0.00189	0.58332	0.01976	0.07536	0.0012	458	47	467	13	468	7	-0.2
Q403-70	0.34	0.05597	0.00177	0.53914	0.01725	0.06985	0.0011	451	43	438	11	435	7	0.7
~~Q403-71~~	~~0.44~~	~~0.04605~~	~~0.00753~~	~~0.46074~~	~~0.075~~	~~0.07257~~	~~0.00111~~		~~288~~	~~385~~	~~52~~	~~452~~	~~7~~	~~-14.8~~
Q403-72	0.45	0.05792	0.00143	0.60186	0.01542	0.07535	0.00113	527	31	478	10	468	7	2.1
Q403-73	0.96	0.0564	0.00129	0.59157	0.0141	0.07605	0.00113	468	28	472	9	473	7	-0.2
Q403-74	0.54	0.0561	0.00154	0.56246	0.01574	0.07269	0.00112	456	35	453	10	452	7	0.2
Q403-75	0.4	0.05497	0.00224	0.50451	0.02064	0.06655	0.00106	411	63	415	14	415	6	0
Q403-76	0.43	0.05694	0.00156	0.61212	0.01723	0.07795	0.00119	489	36	485	11	484	7	0.2
Q403-77	0.48	0.05518	0.00539	0.5107	0.04951	0.06711	0.00139	420	181	419	33	419	8	0
Q403-78	0.42	0.05628	0.00198	0.60597	0.0215	0.07808	0.00122	463	51	481	14	485	7	-0.8
Q403-79	0.43	0.05659	0.00128	0.59582	0.01411	0.07634	0.00113	476	28	475	9	474	7	0.2
Q403-80	0.38	0.05706	0.00181	0.60111	0.0194	0.07639	0.00118	494	44	478	12	475	7	0.6
Q403-81	0.51	0.05673	0.00167	0.59647	0.0179	0.07624	0.00119	481	39	475	11	474	7	0.2
Q403-82	0.43	0.05683	0.00181	0.59412	0.01916	0.0758	0.00118	485	44	473	12	471	7	0.4
Q403-83	0.7	0.05633	0.00156	0.58063	0.01651	0.07474	0.00114	465	37	465	11	465	7	0
Q403-84	0.45	0.06077	0.00161	0.60342	0.01641	0.072	0.0011	631	33	479	10	448	7	6.9
Q403-85	0.63	0.05829	0.00184	0.58412	0.01868	0.07267	0.00114	541	43	467	12	452	7	3.3
Q403-86	0.49	0.05628	0.00136	0.5859	0.01475	0.07549	0.00113	463	30	468	9	469	7	-0.2
Q403-87	0.44	0.05644	0.0018	0.59256	0.01915	0.07613	0.00118	470	44	473	12	473	7	0
Q403-88	0.64	0.05671	0.00225	0.59956	0.0239	0.07666	0.00124	480	59	477	15	476	7	0.2
Q403-89	0.42	0.05989	0.00184	0.63213	0.01976	0.07653	0.00119	600	41	497	12	475	7	4.6
Q403-90	0.29	0.05657	0.00138	0.59733	0.0151	0.07657	0.00115	475	30	476	10	476	7	0
Q403-91	0.38	0.05572	0.00167	0.56384	0.01726	0.07337	0.00113	441	41	454	11	456	7	-0.4
Q403-92	0.47	0.05701	0.00174	0.60382	0.01871	0.0768	0.0012	492	41	480	12	477	7	0.6

Q403-93	0.47	0.05681	0.00145	0.58483	0.01537	0.07464	0.00113	484	32	468	10	464	7	0.9
Q403-94	0.43	0.05538	0.00181	0.49459	0.01633	0.06475	0.00102	428	46	408	11	404	6	1
Q403-95	0.43	0.15172	0.00306	9.71889	0.20896	0.46448	0.00685	2365	18	2408	20	2459	30	-3.8
Q403-96	0.55	0.06759	0.00328	0.85065	0.03901	0.09128	0.00146	856	103	625	21	563	9	11
Q403-97	0.58	0.05964	0.00279	0.60579	0.02674	0.07367	0.00114	590	104	481	17	458	7	5
Q403-98	0.89	0.0563	0.0014	0.59385	0.01528	0.07648	0.00115	464	31	473	10	475	7	-0.4
Q403-99	0.59	0.0939	0.00198	3.31967	0.07414	0.25633	0.0038	1506	21	1486	17	1471	19	2.4
~~Q403-100~~	~~0.79~~	~~0.11625~~	~~0.00239~~	~~4.15385~~	~~0.09093~~	~~0.25909~~	~~0.00382~~	~~1899~~	~~20~~	~~1665~~	~~18~~	~~1485~~	~~20~~	~~27.9~~
Q1618														
Q1618-001	0.53	0.05506	0.00111	0.51778	0.0113	0.0682	0.001	415	25	424	8	425	6	-0.2
Q1618-002	0.28	0.05486	0.00372	0.4751	0.03211	0.06279	0.00113	407	119	395	22	393	7	0.5
Q1618-003	0.45	0.05527	0.00113	0.518	0.01145	0.06796	0.001	423	25	424	8	424	6	0
Q1618-004	0.41	0.05509	0.00132	0.46525	0.01175	0.06124	0.00091	416	31	388	8	383	6	1.3
Q1618-005	0.24	0.05415	0.00275	0.45398	0.0231	0.06079	0.00103	377	84	380	16	380	6	0
Q1618-006	0.5	0.05397	0.00519	0.45224	0.0432	0.06076	0.00125	370	178	379	30	380	8	-0.3
Q1618-007	0.5	0.05508	0.00109	0.51566	0.01107	0.06789	0.001	415	24	422	7	423	6	-0.2
Q1618-008	0.39	0.05671	0.00114	0.53093	0.01157	0.06789	0.001	480	24	432	8	423	6	2.1
Q1618-009	0.26	0.05403	0.00121	0.47919	0.01142	0.06431	0.00096	372	28	398	8	402	6	-1
Q1618-010	0.39	0.05501	0.00122	0.52444	0.01238	0.06913	0.00103	413	28	428	8	431	6	-0.7
Q1618-011	0.43	0.05552	0.00125	0.51725	0.01243	0.06755	0.001	433	28	423	8	421	6	0.5
Q1618-012	0.49	0.05774	0.00124	0.54041	0.01249	0.06787	0.001	520	26	439	8	423	6	3.8
Q1618-013	0.37	0.06115	0.00135	0.58499	0.01371	0.06937	0.00104	645	26	468	9	432	6	8.3
Q1618-014	0.47	0.05549	0.00122	0.53392	0.01254	0.06977	0.00104	432	27	434	8	435	6	-0.2
Q1618-015	0.54	0.05526	0.00099	0.5205	0.01037	0.0683	0.001	423	21	425	7	426	6	-0.2
Q1618-016	0.37	0.05507	0.00117	0.52209	0.01184	0.06874	0.00102	415	26	427	8	429	6	-0.5
Q1618-017	0.39	0.05539	0.00105	0.54117	0.01122	0.07085	0.00104	428	23	439	7	441	6	-0.5
Q1618-018	0.52	0.05633	0.00103	0.52379	0.01058	0.06743	0.00098	465	22	428	7	421	6	1.7

Q1618-019	0.3	0.05404	0.00108	0.45158	0.00979	0.06059	0.00089	373	24	378	7	379	5	-0.3
Q1618-020	0.37	0.10417	0.00145	4.12592	0.06831	0.28719	0.00414	1700	14	1659	14	1627	21	4.5
Q1618-021	0.36	0.05543	0.00205	0.52509	0.01772	0.0687	0.00103	430	84	429	12	428	6	0.2
Q1618-022	0.36	0.0552	0.00121	0.52596	0.01228	0.06909	0.00102	420	27	429	8	431	6	-0.5
Q1618-023	0.44	0.05518	0.00255	0.53374	0.02325	0.07015	0.00109	420	106	434	15	437	7	-0.7
Q1618-024	0.56	0.05365	0.00147	0.46778	0.01324	0.06323	0.00098	356	37	390	9	395	6	-1.3
Q1618-025	0.42	0.05688	0.00263	0.53023	0.02303	0.06761	0.00106	487	105	432	15	422	6	2.4
Q1618-026	0.33	0.05642	0.00109	0.53252	0.01123	0.06844	0.00101	469	23	433	7	427	6	1.4
Q1618-027	0.31	0.05389	0.00378	0.46642	0.03268	0.06276	0.00111	366	127	389	23	392	7	-0.8
Q1618-028	0.45	0.05427	0.00131	0.48401	0.01234	0.06467	0.00097	382	31	401	8	404	6	-0.7
Q1618-029	0.47	0.05572	0.00126	0.53683	0.01291	0.06987	0.00104	441	28	436	9	435	6	0.2
Q1618-030	0.53	0.05641	0.00109	0.55162	0.0116	0.07091	0.00105	469	23	446	8	442	6	0.9
Q1618-031	0.4	0.05475	0.00273	0.46932	0.02344	0.06216	0.00106	402	81	391	16	389	6	0.5
Q1618-032	0.34	0.05525	0.00199	0.47591	0.01738	0.06246	0.001	422	53	395	12	391	6	1
Q1618-033	0.65	0.05529	0.00122	0.52385	0.01231	0.0687	0.00103	424	27	428	8	428	6	0
Q1618-034	0.39	0.05516	0.00144	0.50279	0.01366	0.06609	0.001	419	34	414	9	413	6	0.2
Q1618-035	0.38	0.05555	0.00126	0.53196	0.01282	0.06944	0.00104	434	28	433	8	433	6	0
Q1618-036	0.47	0.05787	0.0011	0.536	0.01117	0.06716	0.00099	525	22	436	7	419	6	4.1
Q1618-037	0.4	0.05936	0.00135	0.57584	0.01388	0.07034	0.00106	580	28	462	9	438	6	5.5
Q1618-038	0.44	0.05546	0.00108	0.52336	0.01112	0.06842	0.00101	431	23	427	7	427	6	0
Q1618-039	0.35	0.05579	0.00131	0.52303	0.01295	0.06798	0.00102	444	30	427	9	424	6	0.7
Q1618-040	0.28	0.05425	0.00273	0.46428	0.02336	0.06206	0.00106	381	82	387	16	388	6	-0.3
Q1618-041	0.36	0.05679	0.00129	0.52995	0.01281	0.06766	0.00102	483	28	432	9	422	6	2.4
Q1618-042	0.42	0.05521	0.00155	0.53125	0.01547	0.06978	0.00108	421	38	433	10	435	7	-0.5
Q1618-043	0.42	0.05504	0.00126	0.52103	0.01266	0.06864	0.00104	414	29	426	8	428	6	-0.5
Q1618-044	0.38	0.05566	0.00117	0.53527	0.01213	0.06973	0.00104	439	26	435	8	435	6	0
Q1618-045	0.43	0.05642	0.00122	0.53521	0.0124	0.06879	0.00103	469	26	435	8	429	6	1.4
Q1618-046	0.42	0.05566	0.00215	0.51761	0.01837	0.06745	0.00103	439	88	424	12	421	6	0.7

Q1618-047	0.31	0.05426	0.00194	0.47754	0.01736	0.06382	0.00102	382	53	396	12	399	6	-0.8
Q1618-048	0.37	0.05646	0.00114	0.53873	0.01181	0.06919	0.00103	471	24	438	8	431	6	1.6
Q1618-049	0.45	0.05665	0.00121	0.52428	0.01203	0.0671	0.00101	478	26	428	8	419	6	2.1
Q1618-050	0.34	0.05542	0.00099	0.53532	0.0106	0.07004	0.00103	429	21	435	7	436	6	-0.2
Q1618-051	0.59	0.05436	0.00174	0.4707	0.01539	0.06278	0.00098	386	46	392	11	393	6	-0.3
Q1618-052	0.38	0.05485	0.00104	0.47165	0.00985	0.06236	0.00092	406	23	392	7	390	6	0.5
Q1618-053	0.5	0.05504	0.00317	0.54458	0.03138	0.07175	0.00126	414	97	441	21	447	8	-1.3
Q1618-054	0.47	0.0552	0.00123	0.51445	0.01219	0.06758	0.00102	420	28	421	8	422	6	-0.2
Q1618-055	0.41	0.05579	0.00128	0.54406	0.01322	0.07071	0.00107	444	29	441	9	440	6	0.2
Q1618-056	0.46	0.05664	0.00131	0.52548	0.01288	0.06728	0.00102	478	29	429	9	420	6	2.1
Q1618-057	0.36	0.05672	0.00127	0.53275	0.01273	0.06811	0.00103	481	28	434	8	425	6	2.1
Q1618-058	0.99	0.05034	0.00194	0.28626	0.01117	0.04123	0.00067	211	60	256	9	260	4	-1.5
Q1618-059	0.39	0.05615	0.00139	0.51831	0.01347	0.06694	0.00102	458	32	424	9	418	6	1.4
Q1618-060	0.39	0.05502	0.00151	0.52949	0.01504	0.06979	0.00108	413	37	431	10	435	7	-0.9
Q1618-061	0.51	0.07508	0.00151	1.65137	0.03586	0.15949	0.00242	1071	21	990	14	954	13	3.8
Q1618-062	0.4	0.05484	0.00124	0.52633	0.01265	0.06959	0.00106	406	28	429	8	434	6	-1.2
Q1618-063	0.58	0.0574	0.00099	0.51625	0.01002	0.06521	0.00096	507	20	423	7	407	6	3.9
Q1618-064	0.27	0.05071	0.00153	0.24127	0.00748	0.0345	0.00054	228	43	219	6	219	3	0
Q1618-065	0.5	0.05988	0.00123	0.61118	0.0136	0.07402	0.00111	599	24	484	9	460	7	5.2
Q1618-066	0.43	0.05528	0.00135	0.52907	0.01362	0.06941	0.00106	424	31	431	9	433	6	-0.5
Q1618-067	0.5	0.0552	0.00125	0.52754	0.01268	0.0693	0.00105	420	28	430	8	432	6	-0.5
Q1618-068	0.52	0.05685	0.00134	0.54634	0.0136	0.06969	0.00107	486	29	443	9	434	6	2.1
Q1618-069	0.42	0.05482	0.0014	0.52551	0.014	0.06951	0.00108	405	33	429	9	433	7	-0.9
Q1618-070	0.52	0.0543	0.00224	0.47208	0.01953	0.06304	0.00107	384	62	393	13	394	6	-0.3
Q1618-071	0.24	0.05514	0.00115	0.48024	0.0108	0.06316	0.00095	418	25	398	7	395	6	0.8
~~Q1618-072~~	~~0.45~~	~~0.06145~~	~~0.00304~~	~~0.53199~~	~~0.02618~~	~~0.06278~~	~~0.00114~~	~~655~~	~~74~~	~~433~~	~~17~~	~~393~~	~~7~~	~~10.2~~
Q1618-073	0.41	0.05771	0.00234	0.57807	0.02159	0.07265	0.00113	519	91	463	14	452	7	2.4
Q1618-074	0.42	0.05647	0.00115	0.53756	0.01187	0.06903	0.00104	471	24	437	8	430	6	1.6

Q1618-075	0.33	0.05587	0.0037	0.49423	0.03258	0.06415	0.00121	447	113	408	22	401	7	1.7
Q1618-076	0.47	0.05719	0.00127	0.54396	0.01288	0.06897	0.00105	499	27	441	8	430	6	2.6
Q1618-077	0.43	0.0544	0.00121	0.47888	0.0114	0.06383	0.00097	388	28	397	8	399	6	-0.5
Q1618-078	0.17	0.05743	0.0018	0.50176	0.0138	0.06336	0.00095	508	71	413	9	396	6	4.3
Q1618-079	0.46	0.05613	0.00118	0.54091	0.01227	0.06988	0.00106	458	25	439	8	435	6	0.9
Q1618-080	0.42	0.05915	0.00146	0.58915	0.01532	0.07222	0.00111	573	31	470	10	450	7	4.4
Q1618-081	0.4	0.05553	0.00131	0.54851	0.01365	0.07163	0.0011	434	29	444	9	446	7	-0.4
Q1618-082	0.39	0.05668	0.00118	0.54437	0.01223	0.06964	0.00106	479	25	441	8	434	6	1.6
~~Q1618-083~~	~~0.61~~	~~0.06757~~	~~0.00133~~	~~0.62092~~	~~0.01334~~	~~0.06663~~	~~0.00101~~	~~855~~	~~22~~	~~490~~	~~8~~	~~416~~	~~6~~	~~17.8~~
Q1618-084	0.26	0.05509	0.00176	0.50412	0.0165	0.06636	0.00106	416	45	414	11	414	6	0
Q1618-085	0.56	0.05632	0.00132	0.55532	0.01377	0.07149	0.0011	465	29	448	9	445	7	0.7
Q1618-086	0.75	0.13108	0.00224	6.55349	0.12621	0.36253	0.00547	2112	16	2053	17	1994	26	5.9
Q1618-087	0.57	0.05647	0.00114	0.56042	0.01229	0.07197	0.00109	471	24	452	8	448	7	0.9
Q1618-088	0.36	0.05569	0.00118	0.55408	0.01266	0.07214	0.0011	440	26	448	8	449	7	-0.2
Q1618-089	0.46	0.05831	0.00142	0.53819	0.01378	0.06693	0.00104	541	30	437	9	418	6	4.5
Q1618-090	0.43	0.05591	0.00106	0.50027	0.01041	0.06488	0.00098	449	22	412	7	405	6	1.7
Q1618-091	0.42	0.06017	0.00265	0.60375	0.02484	0.07277	0.00115	610	98	480	16	453	7	6
Q1618-092	0.55	0.05797	0.00128	0.55841	0.01317	0.06985	0.00107	529	27	450	9	435	6	3.4
Q1618-093	0.44	0.0595	0.00119	0.55956	0.01221	0.06819	0.00103	585	23	451	8	425	6	6.1
Q1618-094	0.94	0.05959	0.00138	0.5074	0.0125	0.06174	0.00095	589	28	417	8	386	6	8
Q1618-095	0.4	0.05605	0.00128	0.54013	0.01308	0.06987	0.00107	454	28	439	9	435	6	0.9
~~Q1618-096~~	~~0.26~~	~~0.0696~~	~~0.00147~~	~~0.99522~~	~~0.02255~~	~~0.10368~~	~~0.0016~~	~~917~~	~~23~~	~~701~~	~~11~~	~~636~~	~~9~~	~~10.2~~
Q1618-097	0.41	0.05743	0.00168	0.56108	0.01693	0.07084	0.00113	508	39	452	11	441	7	2.5
Q1618-098	0.38	0.05497	0.00156	0.51793	0.01524	0.06833	0.00108	411	38	424	10	426	7	-0.5
Q1618-099	0.28	0.05466	0.00252	0.46852	0.02163	0.06215	0.00107	398	72	390	15	389	6	0.3
~~Q1618-100~~	~~0.86~~	~~0.06224~~	~~0.00304~~	~~0.36116~~	~~0.01762~~	~~0.04208~~	~~0.00074~~	~~682~~	~~74~~	~~313~~	~~13~~	~~266~~	~~5~~	~~17.7~~

Q1643														
Q1643-01	0.62	0.05536	0.00101	0.53568	0.01016	0.07016	0.00094	427	21	436	7	437	6	-0.2
Q1643-02	0.27	0.05457	0.002	0.46851	0.01704	0.06226	0.00095	395	54	390	12	389	6	0.3
Q1643-03	0.56	0.05554	0.00107	0.53391	0.01055	0.0697	0.00095	434	22	434	7	434	6	0
Q1643-04	0.28	0.05411	0.00225	0.45772	0.01885	0.06134	0.00094	376	65	383	13	384	6	-0.3
Q1643-05	0.33	0.0547	0.00443	0.47124	0.03777	0.06246	0.00118	400	147	392	26	391	7	0.3
Q1643-06	0.24	0.05419	0.00103	0.46156	0.00906	0.06176	0.00084	379	22	385	6	386	5	-0.3
Q1643-07	0.48	0.05454	0.00181	0.46622	0.01538	0.06198	0.00092	393	47	389	11	388	6	0.3
Q1643-08	1.11	0.05366	0.00382	0.41893	0.0295	0.05661	0.00104	357	126	355	21	355	6	0
Q1643-09	0.67	0.12614	0.00363	6.42135	0.16066	0.3692	0.00523	2045	52	2035	22	2026	25	0.9
Q1643-10	0.37	0.05553	0.00101	0.55505	0.01044	0.07248	0.00098	434	20	448	7	451	6	-0.7
Q1643-11	0.36	0.05508	0.00104	0.49469	0.00962	0.06513	0.00088	415	21	408	7	407	5	0.2
~~Q1643-12~~	~~0.72~~	~~0.06189~~	~~0.00107~~	~~0.30894~~	~~0.00555~~	~~0.0362~~	~~0.00048~~	~~670~~	~~18~~	~~273~~	~~4~~	~~229~~	~~3~~	~~19.2~~
Q1643-13	0.43	0.05575	0.0011	0.53705	0.01088	0.06985	0.00095	442	23	436	7	435	6	0.2
~~Q1643-14~~	~~0.83~~	~~0.05888~~	~~0.00307~~	~~0.24903~~	~~0.01246~~	~~0.03067~~	~~0.00045~~	~~563~~	~~117~~	~~226~~	~~10~~	~~195~~	~~3~~	~~15.9~~
Q1643-15	0.61	0.05466	0.00216	0.46733	0.01829	0.062	0.00095	398	60	389	13	388	6	0.3
Q1643-16	0.39	0.05514	0.00193	0.46691	0.01622	0.0614	0.00092	418	51	389	11	384	6	1.3
Q1643-17	0.4	0.05486	0.00116	0.52168	0.01123	0.06895	0.00094	407	25	426	7	430	6	-0.9
~~Q1643-18~~	~~0.69~~	~~0.07204~~	~~0.00121~~	~~0.51742~~	~~0.00907~~	~~0.05208~~	~~0.0007~~	~~987~~	~~17~~	~~423~~	~~6~~	~~327~~	~~4~~	~~29.4~~
Q1643-19	0.3	0.05451	0.00193	0.45599	0.01602	0.06066	0.00093	392	51	381	11	380	6	0.3
Q1643-20	0.43	0.05446	0.00188	0.46196	0.01586	0.06151	0.00093	390	50	386	11	385	6	0.3
Q1643-21	0.16	0.06713	0.00112	1.16382	0.02034	0.12572	0.00169	842	17	784	10	763	10	2.8
~~Q1643-22~~	~~0.78~~	~~0.14099~~	~~0.00208~~	~~6.74915~~	~~0.10734~~	~~0.34712~~	~~0.00455~~	~~2239~~	~~12~~	~~2079~~	~~14~~	~~1921~~	~~22~~	~~16.6~~
Q1643-23	0.53	0.05633	0.00095	0.54269	0.00956	0.06986	0.00093	465	18	440	6	435	6	1.1
Q1643-24	0.47	0.05584	0.00109	0.53829	0.01084	0.0699	0.00095	446	22	437	7	436	6	0.2
Q1643-25	0.52	0.05431	0.00225	0.47335	0.01948	0.0632	0.00098	384	64	394	13	395	6	-0.3
~~Q1643-26~~	~~0.69~~	~~0.09045~~	~~0.00323~~	~~0.80558~~	~~0.02813~~	~~0.06458~~	~~0.00106~~	~~1435~~	~~42~~	~~600~~	~~16~~	~~403~~	~~6~~	~~48.9~~
Q1643-27	0.49	0.05692	0.00108	0.5231	0.01018	0.06664	0.00092	488	21	427	7	416	6	2.6

~~Q1643-28~~	~~0.66~~	~~0.14936~~	~~0.00228~~	~~7.57258~~	~~0.12334~~	~~0.36764~~	~~0.00487~~	~~2339~~	~~13~~	~~2182~~	~~15~~	~~2018~~	~~23~~	~~15.9~~
Q1643-29	0.29	0.05957	0.00217	0.55316	0.01846	0.06735	0.00097	588	81	447	12	420	6	6.4
Q1643-30	0.13	0.07005	0.0011	1.60903	0.02682	0.16655	0.00221	930	16	974	10	993	12	-1.9
Q1643-31	0.3	0.05409	0.00245	0.46797	0.02103	0.06274	0.001	375	72	390	15	392	6	-0.5
Q1643-32	0.5	0.07539	0.0013	1.80303	0.03244	0.17342	0.00235	1079	17	1047	12	1031	13	4.7
Q1643-33	0.63	0.05548	0.00092	0.52534	0.00918	0.06867	0.00092	432	18	429	6	428	6	0.2
Q1643-34	0.34	0.05579	0.00122	0.52298	0.01161	0.06797	0.00095	444	26	427	8	424	6	0.7
~~Q1643-35~~	~~0.58~~	~~0.15976~~	~~0.00425~~	~~4.70803~~	~~0.10649~~	~~0.21373~~	~~0.00299~~	~~2453~~	~~46~~	~~1769~~	~~19~~	~~1249~~	~~16~~	~~96.4~~
Q1643-36	0.71	0.05386	0.00264	0.46115	0.02227	0.06208	0.00105	365	78	385	15	388	6	-0.8
Q1643-37	0.4	0.05572	0.00114	0.52942	0.01107	0.0689	0.00096	441	24	431	7	430	6	0.2
Q1643-38	0.37	0.05404	0.00114	0.44523	0.00954	0.05974	0.00083	373	25	374	7	374	5	0
Q1643-39	0.56	0.06123	0.00185	0.59699	0.01798	0.07069	0.00105	647	39	475	11	440	6	8
Q1643-40	0.62	0.05597	0.00188	0.4593	0.01528	0.05951	0.0009	451	47	384	11	373	5	2.9
Q1643-41	0.78	0.09994	0.00169	3.69532	0.06547	0.26811	0.00365	1623	15	1570	14	1531	19	6
~~Q1643-42~~	~~0.87~~	~~0.14845~~	~~0.00602~~	~~2.87454~~	~~0.10803~~	~~0.14041~~	~~0.00314~~	~~2328~~	~~35~~	~~1375~~	~~28~~	~~847~~	~~18~~	~~62.3~~
Q1643-43	0.53	0.07356	0.00135	1.89433	0.03594	0.18674	0.00257	1029	18	1079	13	1104	14	-6.8
Q1643-44	0.59	0.11397	0.00186	5.0156	0.08645	0.31909	0.00428	1864	14	1822	15	1785	21	4.4
Q1643-45	0.44	0.05572	0.00129	0.53599	0.0125	0.06975	0.00099	441	28	436	8	435	6	0.2
Q1643-46	0.64	0.05291	0.00155	0.29308	0.00858	0.04017	0.00059	325	40	261	7	254	4	2.8
~~Q1643-47~~	~~0.89~~	~~0.09787~~	~~0.00171~~	~~3.15917~~	~~0.05732~~	~~0.23407~~	~~0.00322~~	~~1584~~	~~16~~	~~1447~~	~~14~~	~~1356~~	~~17~~	~~16.8~~
Q1643-48	0.23	0.11513	0.0019	5.17563	0.09002	0.32596	0.00438	1882	15	1849	15	1819	21	3.5
Q1643-49	0.93	0.05149	0.00223	0.25058	0.01077	0.03529	0.00055	263	70	227	9	224	3	1.3
Q1643-50	0.42	0.05522	0.0011	0.47592	0.00966	0.0625	0.00087	421	23	395	7	391	5	1
Q1643-51	0.4	0.05753	0.00106	0.54012	0.01032	0.06807	0.00093	512	20	439	7	425	6	3.3
~~Q1643-52~~	~~2.05~~	~~0.07391~~	~~0.00204~~	~~1.19391~~	~~0.03216~~	~~0.11713~~	~~0.00187~~	~~1039~~	~~30~~	~~798~~	~~15~~	~~714~~	~~11~~	~~11.8~~
Q1643-53	0.47	0.05551	0.00162	0.47716	0.01377	0.06232	0.00094	433	38	396	9	390	6	1.5
~~Q1643-54~~	~~1.22~~	~~0.06721~~	~~0.00212~~	~~0.40067~~	~~0.01232~~	~~0.04323~~	~~0.0007~~	~~844~~	~~38~~	~~342~~	~~9~~	~~273~~	~~4~~	~~25.3~~
~~Q1643-55~~	~~0.25~~	~~0.11608~~	~~0.002~~	~~4.81397~~	~~0.08654~~	~~0.3007~~	~~0.00409~~	~~1897~~	~~15~~	~~1787~~	~~15~~	~~1695~~	~~20~~	~~11.9~~

Q1643-56	0.69	0.05595	0.00366	0.36786	0.02382	0.04768	0.00084	450	113	318	18	300	5	6
~~Q1643-57~~	~~0.72~~	~~0.06326~~	~~0.00204~~	~~0.38514~~	~~0.01215~~	~~0.04414~~	~~0.00072~~	~~717~~	~~40~~	~~331~~	~~9~~	~~278~~	~~4~~	~~19.1~~
~~Q1643-58~~	~~0.32~~	~~0.11306~~	~~0.00196~~	~~4.54099~~	~~0.08214~~	~~0.29123~~	~~0.00397~~	~~1849~~	~~15~~	~~1739~~	~~15~~	~~1648~~	~~20~~	~~12.2~~
~~Q1643-59~~	~~0.91~~	~~0.08573~~	~~0.00607~~	~~0.80488~~	~~0.05492~~	~~0.06809~~	~~0.0013~~	~~1332~~	~~141~~	~~600~~	~~31~~	~~425~~	~~8~~	~~41.2~~
Q1643-60	0.56	0.0566	0.00142	0.35814	0.00895	0.04588	0.00068	476	30	311	7	289	4	7.6
Q1643-61	0.46	0.07258	0.00135	1.52049	0.02907	0.15191	0.00211	1002	19	939	12	912	12	3
Q123														
Q123-01	0.44	0.06197	0.00122	0.60628	0.01304	0.07094	0.00107	673	23	481	8	442	6	8.8
Q123-02	0.84	0.06215	0.00192	0.60284	0.01908	0.07034	0.00113	679	41	479	12	438	7	9.4
Q123-03	0.4	0.05766	0.00113	0.56194	0.01209	0.07067	0.00105	517	23	453	8	440	6	3
Q123-04	0.46	0.05487	0.00121	0.5017	0.01185	0.06629	0.00101	407	27	413	8	414	6	-0.2
Q123-05	0.6	0.0611	0.00211	0.63966	0.02248	0.07591	0.00123	643	48	502	14	472	7	6.4
~~Q123-06~~	~~0.47~~	~~0.07418~~	~~0.00418~~	~~0.78477~~	~~0.04192~~	~~0.07673~~	~~0.00137~~	~~1046~~	~~117~~	~~588~~	~~24~~	~~477~~	~~8~~	~~23.3~~
Q123-07	0.6	0.05834	0.00115	0.60131	0.01302	0.07474	0.00112	543	23	478	8	465	7	2.8
~~Q123-08~~	~~1.07~~	~~0.08804~~	~~0.00317~~	~~1.54535~~	~~0.05592~~	~~0.12728~~	~~0.00222~~	~~1383~~	~~43~~	~~949~~	~~22~~	~~772~~	~~13~~	~~22.9~~
Q123-09	0.5	0.05831	0.00094	0.59675	0.01111	0.0742	0.00109	541	19	475	7	461	7	3
Q123-10	0.57	0.05944	0.001	0.5371	0.01032	0.06552	0.00096	583	20	437	7	409	6	6.8
~~Q123-11~~	~~0.42~~	~~0.06694~~	~~0.00313~~	~~0.64582~~	~~0.0283~~	~~0.06998~~	~~0.00115~~	~~836~~	~~100~~	~~506~~	~~17~~	~~436~~	~~7~~	~~16.1~~
Q123-12	0.45	0.05202	0.00229	0.32689	0.0146	0.04556	0.00073	286	73	287	11	287	5	0
Q123-13	0.41	0.06028	0.00111	0.61064	0.01252	0.07346	0.00109	614	21	484	8	457	7	5.9
~~Q123-14~~	~~0.74~~	~~0.08188~~	~~0.00493~~	~~0.8559~~	~~0.04897~~	~~0.07581~~	~~0.00141~~	~~1243~~	~~121~~	~~628~~	~~27~~	~~471~~	~~8~~	~~33.3~~
Q123-15	0.51	0.0558	0.00118	0.54678	0.01251	0.07105	0.00106	444	26	443	8	442	6	0.2
Q123-16	0.48	0.05758	0.00117	0.53519	0.01189	0.0674	0.001	514	25	435	8	420	6	3.6
Q123-17	0.43	0.05583	0.0016	0.52682	0.01569	0.06841	0.00105	446	39	430	10	427	6	0.7
Q123-18	0.66	0.06155	0.0014	0.55875	0.01353	0.06583	0.00101	659	27	451	9	411	6	9.7
Q123-19	0.52	0.05959	0.00098	0.5909	0.01114	0.0719	0.00106	589	19	471	7	448	6	5.1

~~Q123-20~~	~~0.53~~	~~0.06319~~	~~0.00305~~	~~0.61018~~	~~0.02767~~	~~0.07003~~	~~0.00117~~	~~715~~	~~105~~	~~484~~	~~17~~	~~436~~	~~7~~	~~11~~
Q123-21	0.46	0.059	0.0016	0.54701	0.01553	0.06723	0.00104	567	36	443	10	419	6	5.7
Q123-22	0.65	0.05749	0.00091	0.57486	0.01062	0.07251	0.00106	510	19	461	7	451	6	2.2
Q123-23	0.32	0.05607	0.0022	0.57216	0.02264	0.07399	0.00123	455	58	459	15	460	7	-0.2
~~Q123-24~~	~~0.52~~	~~0.06564~~	~~0.00119~~	~~0.5654~~	~~0.01143~~	~~0.06246~~	~~0.00093~~	~~795~~	~~20~~	~~455~~	~~7~~	~~391~~	~~6~~	~~16.4~~
Q123-25	0.46	0.05644	0.00166	0.55157	0.01682	0.07086	0.0011	470	40	446	11	441	7	1.1
Q123-26	0.46	0.05527	0.00119	0.51966	0.01206	0.06817	0.00104	423	26	425	8	425	6	0
Q123-27	0.6	0.0559	0.00172	0.54729	0.01742	0.07098	0.0011	448	43	443	11	442	7	0.2
Q123-28	1.51	0.06255	0.00123	0.61369	0.01325	0.07114	0.00107	693	23	486	8	443	6	9.7
Q123-29	0.55	0.05518	0.00094	0.5076	0.00986	0.0667	0.00098	420	20	417	7	416	6	0.2
Q123-30	0.46	0.05605	0.00137	0.57948	0.01503	0.07496	0.00114	454	32	464	10	466	7	-0.4
Q123-31	0.74	0.055	0.00109	0.55904	0.01211	0.07369	0.00111	412	24	451	8	458	7	-1.5
Q123-32	0.49	0.05697	0.00123	0.52402	0.01221	0.06669	0.001	490	27	428	8	416	6	2.9
Q123-33	0.48	0.05535	0.0013	0.50478	0.01259	0.06613	0.00102	426	30	415	8	413	6	0.5
Q123-34	0.57	0.05642	0.00116	0.59082	0.01316	0.07593	0.00115	469	25	471	8	472	7	-0.2
Q123-35	0.62	0.05794	0.00157	0.49722	0.01405	0.06223	0.00097	527	35	410	10	389	6	5.4
Q123-36	0.56	0.05498	0.00099	0.49645	0.01003	0.06547	0.00098	411	21	409	7	409	6	0
Q123-37	0.59	0.05698	0.00088	0.57281	0.01038	0.07288	0.00107	491	18	460	7	453	6	1.5
Q123-38	0.47	0.05523	0.00135	0.50284	0.01298	0.06602	0.00103	422	31	414	9	412	6	0.5
Q123-39	0.56	0.05499	0.00151	0.50779	0.01437	0.06696	0.00108	412	35	417	10	418	7	-0.2
~~Q123-40~~	~~0.51~~	~~0.06415~~	~~0.00301~~	~~0.57586~~	~~0.02533~~	~~0.0651~~	~~0.00105~~	~~747~~	~~102~~	~~462~~	~~16~~	~~407~~	~~6~~	~~13.5~~
~~Q123-41~~	~~0.47~~	~~0.06044~~	~~0.00228~~	~~0.37117~~	~~0.01417~~	~~0.04453~~	~~0.00074~~	~~619~~	~~54~~	~~321~~	~~10~~	~~281~~	~~5~~	~~14.2~~
Q123-42	0.5	0.05534	0.00166	0.51244	0.01588	0.06714	0.00106	426	41	420	11	419	6	0.2
Q123-43	0.53	0.0554	0.00103	0.54589	0.01125	0.07144	0.00107	428	22	442	7	445	6	-0.7
~~Q123-44~~	~~0.67~~	~~0.06436~~	~~0.00155~~	~~0.68692~~	~~0.01745~~	~~0.07738~~	~~0.0012~~	~~753~~	~~29~~	~~531~~	~~11~~	~~480~~	~~7~~	~~10.6~~
Q123-45	0.66	0.05597	0.00137	0.55886	0.01447	0.07239	0.00112	451	31	451	9	451	7	0
Q123-46	0.7	0.05624	0.00143	0.58575	0.01556	0.07551	0.0012	462	32	468	10	469	7	-0.2
Q123-47	0.71	0.05595	0.00103	0.56972	0.01164	0.07382	0.00111	450	22	458	8	459	7	-0.2

Q123-48	0.43	0.05561	0.00133	0.51475	0.01298	0.06711	0.00104	437	30	422	9	419	6	0.7
Q123-49	0.55	0.05669	0.00158	0.51978	0.01507	0.06648	0.00104	479	37	425	10	415	6	2.4
Q123-50	0.59	0.0558	0.00169	0.5459	0.01704	0.07093	0.00112	444	42	442	11	442	7	0
Q123-51	0.39	0.05206	0.00211	0.32991	0.01351	0.04594	0.00076	288	63	289	10	290	5	-0.3
Q123-52	0.45	0.05206	0.00214	0.31393	0.01306	0.04372	0.00072	288	65	277	10	276	4	0.4
Q123-53	0.67	0.05641	0.00167	0.55537	0.01694	0.07139	0.00114	469	40	449	11	445	7	0.9
Q123-54	0.49	0.05504	0.00114	0.50347	0.0113	0.06633	0.00101	414	25	414	8	414	6	0
Q123-55	0.72	0.05623	0.00091	0.56892	0.01065	0.07336	0.00109	461	19	457	7	456	7	0.2
Q123-56	0.54	0.05564	0.00157	0.51886	0.01516	0.06761	0.00108	438	37	424	10	422	7	0.5
Q123-57	0.71	0.05633	0.00127	0.57265	0.01373	0.07371	0.00115	465	27	460	9	458	7	0.4
Q123-58	0.39	0.05576	0.00144	0.54737	0.01471	0.07118	0.00114	443	32	443	10	443	7	0
Q123-59	0.04	0.05485	0.00127	0.50939	0.01259	0.06734	0.00104	406	29	418	8	420	6	-0.5
Q123-60	0.52	0.06033	0.00152	0.55312	0.01461	0.06647	0.00104	615	31	447	10	415	6	7.7
Q123-61	0.47	0.06029	0.0014	0.5568	0.01371	0.06697	0.00104	614	28	449	9	418	6	7.4
Q123-62	0.55	0.05637	0.00103	0.58682	0.01199	0.07548	0.00114	467	22	469	8	469	7	0
Q123-63	0.4	0.0551	0.00105	0.50463	0.0106	0.0664	0.00101	416	23	415	7	414	6	0.2
Q123-64	0.47	0.05564	0.00227	0.52529	0.02151	0.06845	0.00119	438	60	429	14	427	7	0.5
Q123-65	0.43	0.05676	0.00119	0.52026	0.01184	0.06646	0.00102	482	25	425	8	415	6	2.4
Q123-66	0.46	0.05535	0.00149	0.5164	0.01437	0.06765	0.0011	426	34	423	10	422	7	0.2
Q123-67	0.48	0.05574	0.00175	0.54733	0.01747	0.07119	0.00119	442	42	443	11	443	7	0
Q123-68	0.76	0.05599	0.00103	0.56247	0.01153	0.07285	0.0011	452	22	453	7	453	7	0
Q123-69	0.44	0.05607	0.00182	0.55649	0.01831	0.07197	0.00121	455	44	449	12	448	7	0.2
Q123-70	0.45	0.05538	0.00148	0.51217	0.01428	0.06706	0.00107	428	35	420	10	418	6	0.5
Q123-71	0.32	0.0555	0.00148	0.52973	0.01468	0.0692	0.00112	432	34	432	10	431	7	0.2
Q123-72	0.61	0.05623	0.00103	0.57374	0.01171	0.07398	0.00112	461	21	460	8	460	7	0
Q123-73	0.43	0.05413	0.00107	0.55106	0.01196	0.07381	0.00113	376	24	446	8	459	7	-2.8
Q123-74	0.56	0.05528	0.00111	0.50524	0.01114	0.06627	0.00101	424	24	415	8	414	6	0.2
Q123-75	0.52	0.05519	0.00181	0.51466	0.01732	0.06762	0.00109	420	47	422	12	422	7	0

Q123-76	0.45	0.05554	0.00198	0.50216	0.01822	0.06555	0.00109	434	51	413	12	409	7	1
Q123-77	0.73	0.05883	0.00152	0.56077	0.01524	0.06911	0.00108	561	33	452	10	431	7	4.9
Q123-78	0.39	0.05883	0.00362	0.59655	0.03615	0.07352	0.00155	561	95	475	23	457	9	3.9
Q123-79	0.54	0.05607	0.00103	0.57068	0.01172	0.0738	0.00112	455	22	458	8	459	7	-0.2
Q123-80	0.51	0.05532	0.00132	0.51599	0.01298	0.06763	0.00107	425	29	422	9	422	6	0
Q123-81	1.02	0.05604	0.00168	0.56856	0.0174	0.07357	0.00123	454	39	457	11	458	7	-0.2
Q123-82	0.77	0.059	0.00142	0.58464	0.01485	0.07185	0.00113	567	29	467	10	447	7	4.5
Q123-83	0.38	0.05173	0.00246	0.31173	0.01489	0.04369	0.00075	273	78	276	12	276	5	0
Q123-84	0.48	0.05311	0.00131	0.50028	0.013	0.0683	0.00109	333	31	412	9	426	7	-3.3
Q123-85	0.75	0.05584	0.00104	0.56395	0.01168	0.07323	0.00112	446	22	454	8	456	7	-0.4
Q123-86	0.65	0.06184	0.00148	0.63672	0.01615	0.07466	0.00117	669	29	500	10	464	7	7.8
Q123-87	0.43	0.05562	0.00118	0.54021	0.01235	0.07043	0.0011	437	25	439	8	439	7	0
Q123-88	0.54	0.05535	0.00141	0.51469	0.01373	0.06742	0.00108	426	32	422	9	421	7	0.2
Q123-89	0.52	0.05553	0.00178	0.52559	0.01709	0.06863	0.00116	434	43	429	11	428	7	0.2
Q123-90	0.54	0.05528	0.00116	0.522	0.01185	0.06847	0.00106	424	25	426	8	427	6	-0.2
Q123-91	0.46	0.05516	0.00179	0.51074	0.01691	0.06714	0.00113	419	44	419	11	419	7	0
Q123-92	0.64	0.05995	0.00203	0.59561	0.0205	0.07203	0.0012	602	46	474	13	448	7	5.8
Q123-93	0.43	0.06108	0.00159	0.54998	0.01497	0.06529	0.00105	642	32	445	10	408	6	9.1
Q123-94	0.62	0.05624	0.00164	0.57746	0.01726	0.07445	0.00124	462	38	463	11	463	7	0
Q123-95	0.49	0.05495	0.00139	0.5097	0.01354	0.06725	0.00107	410	32	418	9	420	6	-0.5
Q123-96	1.04	0.05494	0.00113	0.50301	0.01128	0.06638	0.00103	410	25	414	8	414	6	0
Q123-97	0.58	0.05675	0.00129	0.56161	0.01363	0.07176	0.00112	482	28	453	9	447	7	1.3
Q123-98	0.36	0.05489	0.00174	0.50675	0.01639	0.06695	0.00112	408	43	416	11	418	7	-0.5
Q123-99	0.54	0.05611	0.00108	0.57503	0.01226	0.07431	0.00114	457	23	461	8	462	7	-0.2
Q123-100	0.57	0.05758	0.00153	0.5411	0.01501	0.06814	0.00109	514	34	439	10	425	7	3.3
Q7														
Q7-01	0.41	0.08179	0.00136	2.4048	0.04076	0.2132	0.00266	1240	16	1244	12	1246	14	-0.5

Q7-02	1.17	0.07418	0.0014	1.79255	0.03397	0.17523	0.00226	1046	19	1043	12	1041	12	0.5
Q7-03	0.41	0.05949	0.00129	0.54995	0.01178	0.06704	0.00089	585	25	445	8	418	5	6.5
Q7-04	0.77	0.05589	0.00176	0.38503	0.01193	0.04996	0.00069	448	44	331	9	314	4	5.4
~~Q7-05~~	~~0.66~~	~~0.06237~~	~~0.00297~~	~~0.33542~~	~~0.01571~~	~~0.039~~	~~0.00062~~	~~687~~	~~73~~	~~294~~	~~12~~	~~247~~	~~4~~	~~19~~
Q7-06	0.84	0.05326	0.00141	0.24955	0.00648	0.03398	0.00047	340	34	226	5	215	3	5.1
Q7-07	0.42	0.05364	0.00224	0.418	0.01715	0.05651	0.00084	356	66	355	12	354	5	0.3
~~Q7-08~~	~~0.55~~	~~0.11641~~	~~0.00219~~	~~2.7855~~	~~0.05186~~	~~0.17351~~	~~0.00231~~	~~1902~~	~~16~~	~~1352~~	~~14~~	~~1031~~	~~13~~	~~84.5~~
Q7-09	0.78	0.05396	0.00217	0.2899	0.01152	0.03896	0.00056	369	63	258	9	246	3	4.9
Q7-10	0.91	0.11371	0.00215	5.03959	0.09517	0.32138	0.00422	1860	17	1826	16	1796	21	3.6
Q7-11	0.37	0.05181	0.00207	0.27673	0.01079	0.03873	0.0006	277	61	248	9	245	4	1.2
Q7-12	0.55	0.06772	0.00116	1.146	0.01994	0.12271	0.00153	860	17	775	9	746	9	3.9
Q7-13	1.16	0.11339	0.00217	4.98294	0.09508	0.31866	0.00421	1854	17	1816	16	1783	21	4
Q7-14	0.72	0.06124	0.00152	0.6041	0.01482	0.07153	0.00096	648	30	480	9	445	6	7.9
Q7-15	0.88	0.05375	0.00112	0.28156	0.00589	0.03798	0.00048	361	25	252	5	240	3	5
Q7-16	0.5	0.0535	0.0024	0.295	0.01302	0.03999	0.0006	350	72	262	10	253	4	3.6
Q7-17	0.6	0.05299	0.00117	0.28601	0.00626	0.03914	0.00051	328	27	255	5	248	3	2.8
Q7-18	0.19	0.06059	0.0015	0.60083	0.01456	0.0719	0.00099	625	29	478	9	448	6	6.7
~~Q7-19~~	~~0.41~~	~~0.07626~~	~~0.00132~~	~~1.3183~~	~~0.02309~~	~~0.12536~~	~~0.00157~~	~~1102~~	~~17~~	~~854~~	~~10~~	~~761~~	~~9~~	~~12.2~~
~~Q7-20~~	~~0.36~~	~~0.11112~~	~~0.02196~~	~~3.25302~~	~~0.62753~~	~~0.21233~~	~~0.00911~~	~~1818~~	~~395~~	~~1470~~	~~150~~	~~1241~~	~~48~~	~~46.5~~
Q7-21	0.76	0.05216	0.00144	0.25868	0.00706	0.03596	0.00048	292	38	234	6	228	3	2.6
Q7-22	0.72	0.0565	0.00134	0.4881	0.01146	0.06264	0.00083	472	29	404	8	392	5	3.1
Q7-23	0.9	0.05051	0.00358	0.27191	0.01907	0.03904	0.00066	219	129	244	15	247	4	-1.2
Q7-24	1.15	0.11502	0.00202	5.20498	0.09216	0.32815	0.00415	1880	15	1853	15	1829	20	2.8
Q7-25	0.55	0.11792	0.0021	5.84844	0.10482	0.35965	0.00458	1925	16	1954	16	1981	22	-2.8
Q7-26	0.7	0.05518	0.00156	0.30676	0.0085	0.04031	0.00057	420	37	272	7	255	4	6.7
~~Q7-27~~	~~0.62~~	~~0.0582~~	~~0.00536~~	~~0.33404~~	~~0.03012~~	~~0.04163~~	~~0.00078~~	~~537~~	~~209~~	~~293~~	~~23~~	~~263~~	~~5~~	~~11.4~~
Q7-28	0.59	0.11744	0.00207	5.33096	0.09479	0.32918	0.00416	1918	16	1874	15	1834	20	4.6
Q7-29	0.51	0.05864	0.00129	0.56239	0.01228	0.06955	0.00091	554	26	453	8	433	5	4.6

~~Q7-30~~	~~0.19~~	~~0.14519~~	~~0.00269~~	~~4.50643~~	~~0.08317~~	~~0.22507~~	~~0.00293~~	~~2290~~	~~16~~	~~1732~~	~~15~~	~~1309~~	~~15~~	~~74.9~~
Q7-31	0.52	0.0922	0.00173	3.08816	0.058	0.24288	0.00312	1472	18	1430	14	1402	16	5
~~Q7-32~~	~~0.74~~	~~0.06249~~	~~0.00129~~	~~0.55272~~	~~0.01131~~	~~0.06414~~	~~0.00083~~	~~691~~	~~23~~	~~447~~	~~7~~	~~401~~	~~5~~	~~11.5~~
Q7-33	0.08	0.07106	0.00136	1.44415	0.02771	0.14737	0.00189	959	20	907	12	886	11	2.4
~~Q7-34~~	~~0.39~~	~~0.06663~~	~~0.00212~~	~~0.2436~~	~~0.00754~~	~~0.02651~~	~~0.00039~~	~~826~~	~~40~~	~~221~~	~~6~~	~~169~~	~~2~~	~~30.8~~
Q7-35	0.86	0.05283	0.00366	0.3076	0.02098	0.04222	0.00075	322	123	272	16	267	5	1.9
Q7-36	0.47	0.11599	0.00206	5.11064	0.09168	0.31951	0.00401	1895	16	1838	15	1787	20	6
Q7-37	0.73	0.05749	0.00186	0.52297	0.01667	0.06597	0.00094	510	45	427	11	412	6	3.6
Q7-38	0.43	0.06104	0.00173	0.57656	0.016	0.0685	0.00097	641	36	462	10	427	6	8.2
~~Q7-39~~	~~0.57~~	~~0.06766~~	~~0.00343~~	~~0.2865~~	~~0.01389~~	~~0.03071~~	~~0.00046~~	~~858~~	~~108~~	~~256~~	~~11~~	~~195~~	~~3~~	~~31.3~~
Q7-40	0.57	0.05889	0.00124	0.53973	0.01129	0.06646	0.00087	563	24	438	7	415	5	5.5
Q7-41	0.38	0.11607	0.00212	5.05045	0.09263	0.31553	0.00399	1897	16	1828	16	1768	20	7.3
~~Q7-42~~	~~0.72~~	~~0.06841~~	~~0.0013~~	~~0.52227~~	~~0.00994~~	~~0.05536~~	~~0.00071~~	~~881~~	~~20~~	~~427~~	~~7~~	~~347~~	~~4~~	~~23.1~~
Q7-43	0.42	0.07408	0.00142	1.62435	0.03117	0.159	0.00205	1044	19	980	12	951	11	3.1
Q7-44	0.83	0.12584	0.00247	6.01945	0.11743	0.34688	0.00462	2041	17	1979	17	1920	22	6.3
Q7-45	0.5	0.1404	0.0026	7.17266	0.13333	0.37047	0.00473	2232	16	2133	17	2032	22	9.8
Q7-46	0.83	0.05721	0.00189	0.33843	0.0108	0.0429	0.00066	500	43	296	8	271	4	9.2
~~Q7-47~~	~~0.99~~	~~0.06918~~	~~0.00228~~	~~0.4422~~	~~0.01393~~	~~0.04635~~	~~0.00075~~	~~904~~	~~39~~	~~372~~	~~10~~	~~292~~	~~5~~	~~27.4~~
Q7-48	0.51	0.05493	0.00137	0.36773	0.00894	0.04854	0.00067	409	30	318	7	306	4	3.9
Q7-49	0.97	0.05615	0.00138	0.53333	0.01282	0.06888	0.00095	458	30	434	8	429	6	1.2
Q7-50	0.74	0.16934	0.00323	11.26515	0.21459	0.48241	0.00628	2551	16	2545	18	2538	27	0.5
Q7-51	0.33	0.05029	0.00133	0.22764	0.00593	0.03282	0.00048	208	34	208	5	208	3	0
Q7-52	0.52	0.05464	0.00129	0.47164	0.01114	0.06258	0.00086	398	29	392	8	391	5	0.3
Q7-53	0.54	0.05107	0.00137	0.25702	0.00686	0.03649	0.00052	244	36	232	6	231	3	0.4
Q7-54	0.7	0.05231	0.04373	0.31474	0.26013	0.04362	0.00559	299	###	278	201	275	35	1.1
Q7-55	0.63	0.05668	0.0021	0.57588	0.02113	0.07367	0.00109	479	55	462	14	458	7	0.9
Q7-56	0.47	0.05436	0.00136	0.44507	0.01104	0.05936	0.00085	386	31	374	8	372	5	0.5
Q7-57	0.6	0.06945	0.00144	1.44375	0.03017	0.15074	0.00207	912	22	907	13	905	12	0.2

Q7-58	0.48	0.05578	0.00092	0.47873	0.0082	0.06223	0.0008	444	18	397	6	389	5	2.1
Q7-59	0.56	0.10549	0.00157	4.44966	0.07004	0.30585	0.00393	1723	13	1722	13	1720	19	0.2
Q7-60	0.59	0.05478	0.00119	0.49196	0.01075	0.06512	0.00088	403	26	406	7	407	5	-0.2
Q7-61	0.16	0.05167	0.00095	0.28676	0.00541	0.04024	0.00053	271	21	256	4	254	3	0.8
Q7-62	0.51	0.05113	0.00096	0.24155	0.00461	0.03426	0.00045	247	22	220	4	217	3	1.4
Q7-63	0.66	0.14587	0.00244	7.79689	0.13412	0.38757	0.00527	2298	14	2208	15	2112	24	8.8
Q7-64	0.61	0.05473	0.00112	0.50225	0.01034	0.06654	0.0009	401	24	413	7	415	5	-0.5
Q7-65	0.44	0.05014	0.00181	0.22263	0.00798	0.0322	0.00047	201	56	204	7	204	3	0
Q7-66	0.78	0.05082	0.0013	0.26698	0.00682	0.03809	0.00053	233	34	240	5	241	3	-0.4
Q7-67	0.7	0.05156	0.00112	0.31021	0.00677	0.04362	0.00059	266	27	274	5	275	4	-0.4
Q7-68	0.25	0.11411	0.00177	5.02951	0.082	0.31961	0.00414	1866	14	1824	14	1788	20	4.4
Q7-69	0.74	0.05438	0.00122	0.46202	0.0104	0.06161	0.00085	387	27	386	7	385	5	0.3
Q7-70	0.77	0.05473	0.0012	0.44994	0.00991	0.05961	0.00081	401	26	377	7	373	5	1.1
Q7-71	0.89	0.10449	0.00222	3.91557	0.08263	0.27173	0.00398	1705	19	1617	17	1550	20	10
Q7-72	0.68	0.051	0.00127	0.27112	0.00675	0.03855	0.00053	241	33	244	5	244	3	0
Q7-73	0.59	0.05357	0.00124	0.42129	0.00975	0.05702	0.00079	353	28	357	7	357	5	0
Q7-74	1.65	0.05285	0.00137	0.33367	0.00865	0.04578	0.00064	322	34	292	7	289	4	1
Q7-75	0.43	0.05231	0.00181	0.34806	0.0119	0.04825	0.00073	299	50	303	9	304	4	-0.3
Q7-76	1.05	0.05583	0.00199	0.51867	0.01817	0.06737	0.00105	446	50	424	12	420	6	1
Q7-77	0.79	0.05091	0.00112	0.2551	0.00563	0.03633	0.0005	237	27	231	5	230	3	0.4
Q7-78	0.91	0.05348	0.00131	0.40674	0.00992	0.05515	0.00077	349	31	347	7	346	5	0.3
Q7-79	0.59	0.06538	0.00118	1.16354	0.02155	0.12905	0.00172	787	19	784	10	782	10	0.3
Q7-80	0.49	0.05507	0.00172	0.50006	0.01543	0.06585	0.00098	415	43	412	10	411	6	0.2
Q7-81	0.74	0.05453	0.00139	0.46748	0.0118	0.06217	0.00091	393	31	389	8	389	6	0
Q7-82	0.39	0.05493	0.00112	0.49515	0.01019	0.06536	0.00089	409	23	408	7	408	5	0
Q7-83	0.56	0.11035	0.00227	4.66269	0.09629	0.30638	0.00434	1805	19	1761	17	1723	21	4.8
Q7-84	0.7	0.0713	0.00136	1.51664	0.02944	0.15423	0.00209	966	19	937	12	925	12	1.3
Q7-85	0.71	0.05171	0.00175	0.30499	0.01017	0.04277	0.00065	273	49	270	8	270	4	0

Q7-86	1.06	0.19304	0.00345	13.35691	0.24539	0.50172	0.00669	2768	14	2705	17	2621	29	5.6
Q7-87	0.3	0.09085	0.00166	2.88216	0.05404	0.23003	0.00309	1443	17	1377	14	1335	16	8.1
Q7-88	0.57	0.05751	0.0017	0.64261	0.01869	0.08102	0.00122	511	38	504	12	502	7	0.4
Q7-89	0.1	0.05642	0.0012	0.58128	0.01241	0.07471	0.00104	469	24	465	8	464	6	0.2
Q7-90	0.51	0.05147	0.00139	0.29664	0.00792	0.04179	0.0006	262	36	264	6	264	4	0
Q7-91	0.34	0.05408	0.0012	0.41802	0.00931	0.05605	0.00078	374	26	355	7	352	5	0.9
~~Q7-92~~	~~0.47~~	~~0.13409~~	~~0.00391~~	~~6.33518~~	~~0.16147~~	~~0.34265~~	~~0.00483~~	~~2152~~	~~52~~	~~2023~~	~~22~~	~~1899~~	~~23~~	~~13.3~~
Q7-93	0.12	0.05502	0.00119	0.49977	0.01091	0.06586	0.00091	413	26	412	7	411	6	0.2
Q7-94	0.73	0.05632	0.00156	0.53835	0.01478	0.06932	0.00102	465	35	437	10	432	6	1.2
Q7-95	0.97	0.05565	0.00147	0.54358	0.01429	0.07083	0.00103	438	33	441	9	441	6	0
Q7-96	2.25	0.05106	0.0017	0.27224	0.00897	0.03866	0.00058	244	48	244	7	245	4	-0.4
Q7-97	0.82	0.05128	0.0014	0.27948	0.00761	0.03952	0.00057	253	37	250	6	250	4	0
Q7-98	0.84	0.0555	0.00211	0.51967	0.01949	0.06789	0.00107	432	55	425	13	423	6	0.5
Q7-99	0.43	0.05512	0.00129	0.5029	0.01172	0.06616	0.00095	417	28	414	8	413	6	0.2
Q7-100	0.47	0.05189	0.0023	0.32488	0.01415	0.0454	0.00075	281	69	286	11	286	5	0
Q7-101	0.75	0.05032	0.00124	0.22238	0.00547	0.03204	0.00046	210	31	204	5	203	3	0.5
Q7-102	0.47	0.05607	0.0013	0.47942	0.01106	0.062	0.00089	455	27	398	8	388	5	2.6
Q7-103	0.69	0.0508	0.00145	0.25464	0.00719	0.03634	0.00055	232	38	230	6	230	3	0
Q7-104	0.91	0.05069	0.00168	0.24883	0.0081	0.0356	0.00055	227	47	226	7	226	3	0
Q7-105	0.7	0.0546	0.00167	0.47109	0.01422	0.06256	0.00095	396	41	392	10	391	6	0.3
Z2														
~~Z2-01~~	~~0.47~~	~~0.0631~~	~~0.00216~~	~~0.5318~~	~~0.01684~~	~~0.06112~~	~~0.00079~~	~~712~~	~~74~~	~~433~~	~~11~~	~~382~~	~~5~~	~~13.4~~
~~Z2-02~~	~~1.84~~	~~0.07295~~	~~0.00139~~	~~0.71073~~	~~0.01338~~	~~0.07065~~	~~0.00091~~	~~1013~~	~~19~~	~~545~~	~~8~~	~~440~~	~~5~~	~~23.9~~
Z2-03	0.7	0.06013	0.0013	0.4835	0.0104	0.05831	0.00076	608	25	400	7	365	5	9.6
Z2-04	1.23	0.06097	0.0011	0.54274	0.00977	0.06455	0.00081	638	19	440	6	403	5	9.2
Z2-05	0.69	0.07619	0.00115	1.555	0.02398	0.148	0.00179	1100	14	952	10	890	10	7

Z2-06	0.1	0.06486	0.00097	0.85581	0.01312	0.09568	0.00115	770	15	628	7	589	7	6.6
~~Z2-07~~	~~1.56~~	~~0.11619~~	~~0.00963~~	~~0.49604~~	~~0.03974~~	~~0.03096~~	~~0.00066~~	~~1898~~	~~154~~	~~409~~	~~27~~	~~197~~	~~4~~	~~108~~
~~Z2-08~~	~~0.31~~	~~0.06261~~	~~0.00119~~	~~0.51212~~	~~0.00969~~	~~0.05932~~	~~0.00075~~	~~695~~	~~20~~	~~420~~	~~7~~	~~371~~	~~5~~	~~13.2~~
Z2-09	1	0.05587	0.00136	0.49089	0.01187	0.06371	0.00082	447	31	406	8	398	5	2
Z2-10	1.3	0.05973	0.00101	0.54266	0.00924	0.06589	0.00082	594	18	440	6	411	5	7.1
Z2-11	0.26	0.05736	0.00096	0.53061	0.00899	0.06709	0.00082	505	18	432	6	419	5	3.1
Z2-12	0.91	0.05423	0.003	0.28435	0.01525	0.03803	0.00053	381	128	254	12	241	3	5.4
~~Z2-13~~	~~1.05~~	~~0.07702~~	~~0.00157~~	~~1.79005~~	~~0.03621~~	~~0.16854~~	~~0.00218~~	~~1122~~	~~21~~	~~1042~~	~~13~~	~~1004~~	~~12~~	~~11.8~~
Z2-14	0.53	0.05811	0.00104	0.50818	0.00912	0.06342	0.00079	534	19	417	6	396	5	5.3
~~Z2-15~~	~~0.69~~	~~0.05779~~	~~0.00136~~	~~0.30552~~	~~0.00704~~	~~0.03834~~	~~0.00051~~	~~522~~	~~28~~	~~271~~	~~5~~	~~243~~	~~3~~	~~11.5~~
Z2-16	0.48	0.05492	0.0015	0.49264	0.01333	0.06504	0.00085	409	37	407	9	406	5	0.2
Z2-17	0.55	0.0588	0.0012	0.42043	0.00853	0.05185	0.00067	560	23	356	6	326	4	9.2
Z2-18	0.29	0.07133	0.00104	1.43304	0.02156	0.14569	0.00174	967	14	903	9	877	10	3
Z2-19	0.58	0.05094	0.0019	0.22834	0.00841	0.03251	0.00046	238	59	209	7	206	3	1.5
~~Z2-20~~	~~0.3~~	~~0.092~~	~~0.00229~~	~~1.25256~~	~~0.02699~~	~~0.09875~~	~~0.00124~~	~~1467~~	~~48~~	~~825~~	~~12~~	~~607~~	~~7~~	~~35.9~~
Z2-21	0.38	0.07764	0.00219	1.96351	0.04953	0.18343	0.00234	1138	58	1103	17	1086	13	4.8
~~Z2-22~~	~~0.36~~	~~0.0618~~	~~0.00107~~	~~0.54773~~	~~0.00949~~	~~0.06426~~	~~0.0008~~	~~667~~	~~18~~	~~444~~	~~6~~	~~401~~	~~5~~	~~10.7~~
Z2-23	0.64	0.07764	0.00117	1.51556	0.0234	0.14154	0.00171	1138	14	937	9	853	10	9.8
~~Z2-24~~	~~0.1~~	~~0.07338~~	~~0.00173~~	~~1.05634~~	~~0.0213~~	~~0.1044~~	~~0.00126~~	~~1025~~	~~49~~	~~732~~	~~11~~	~~640~~	~~7~~	~~14.4~~
Z2-25	0.72	0.06057	0.00264	0.61907	0.02571	0.07413	0.001	624	96	489	16	461	6	6.1
Z2-26	0.56	0.05617	0.00141	0.494	0.01226	0.06377	0.00084	459	32	408	8	399	5	2.3
~~Z2-27~~	~~1.7~~	~~0.05869~~	~~0.00134~~	~~0.29076~~	~~0.00652~~	~~0.03593~~	~~0.00048~~	~~556~~	~~27~~	~~259~~	~~5~~	~~228~~	~~3~~	~~13.6~~
Z2-28	0.83	0.05409	0.00137	0.24724	0.0062	0.03314	0.00044	375	33	224	5	210	3	6.7
Z2-29	0.71	0.05146	0.0025	0.27642	0.01321	0.03895	0.0006	261	81	248	11	246	4	0.8
Z2-30	0.94	0.05233	0.00195	0.32106	0.01163	0.04449	0.00069	300	54	283	9	281	4	0.7
Z2-31	0.33	0.05812	0.00167	0.55916	0.01451	0.06978	0.00086	534	64	451	9	435	5	3.7
~~Z2-32~~	~~1.03~~	~~0.06281~~	~~0.00109~~	~~0.5582~~	~~0.00977~~	~~0.06444~~	~~0.0008~~	~~702~~	~~18~~	~~450~~	~~6~~	~~403~~	~~5~~	~~11.7~~
~~Z2-33~~	~~0.65~~	~~0.07703~~	~~0.00408~~	~~1.40296~~	~~0.07104~~	~~0.13209~~	~~0.00206~~	~~1122~~	~~108~~	~~890~~	~~30~~	~~800~~	~~12~~	~~11.3~~

Z2-34	0.61	0.05249	0.00391	0.1966	0.01427	0.02716	0.00046	307	172	182	12	173	3	5.2
~~Z2-35~~	~~0.47~~	~~0.06283~~	~~0.00208~~	~~0.46217~~	~~0.01472~~	~~0.05334~~	~~0.00084~~	~~702~~	~~41~~	~~386~~	~~10~~	~~335~~	~~5~~	~~15.2~~
~~Z2-36~~	~~1.67~~	~~0.11609~~	~~0.0018~~	~~4.2966~~	~~0.06755~~	~~0.26837~~	~~0.00332~~	~~1897~~	~~13~~	~~1693~~	~~13~~	~~1533~~	~~17~~	~~23.7~~
Z2-37	0.64	0.05955	0.00271	0.47845	0.02079	0.05828	0.0008	587	101	397	14	365	5	8.8
Z2-38	0.83	0.05975	0.00099	0.53916	0.00902	0.06543	0.0008	595	17	438	6	409	5	7.1
Z2-39	0.58	0.06021	0.001	0.56946	0.00957	0.06858	0.00084	611	17	458	6	428	5	7
Z2-40	0.57	0.0547	0.00101	0.26838	0.00496	0.03557	0.00044	400	21	241	4	225	3	7.1
~~Z2-41~~	~~0.55~~	~~0.05657~~	~~0.00229~~	~~0.2469~~	~~0.00948~~	~~0.03165~~	~~0.00041~~	~~475~~	~~92~~	~~224~~	~~8~~	~~201~~	~~3~~	~~11.4~~
Z2-42	1.16	0.05523	0.0038	0.3628	0.02464	0.04763	0.00079	422	123	314	18	300	5	4.7
~~Z2-43~~	~~1~~	~~0.06956~~	~~0.00173~~	~~0.55522~~	~~0.0136~~	~~0.05788~~	~~0.00077~~	~~915~~	~~29~~	~~448~~	~~9~~	~~363~~	~~5~~	~~23.4~~
Z2-44	0.47	0.05894	0.00288	0.4772	0.02239	0.05872	0.0008	565	109	396	15	368	5	7.6
Z2-45	0.99	0.05868	0.00464	0.48067	0.03718	0.05941	0.00096	555	178	399	25	372	6	7.3
Z2-46	0.38	0.05784	0.00106	0.46136	0.0084	0.05784	0.00073	524	20	385	6	362	4	6.4
Z2-47	0.26	0.05875	0.00175	0.55388	0.01497	0.06838	0.00086	558	67	448	10	426	5	5.2
~~Z2-48~~	~~0.4~~	~~0.06641~~	~~0.00126~~	~~0.51759~~	~~0.00975~~	~~0.05652~~	~~0.00072~~	~~819~~	~~20~~	~~424~~	~~7~~	~~354~~	~~4~~	~~19.8~~
Z2-49	0.85	0.05528	0.00324	0.47022	0.02667	0.06169	0.00091	424	134	391	18	386	6	1.3
Z2-50	0.25	0.05821	0.00109	0.50822	0.00941	0.06331	0.0008	538	20	417	6	396	5	5.3
~~Z2-51~~	~~0.83~~	~~0.12623~~	~~0.00216~~	~~5.03778~~	~~0.08591~~	~~0.28938~~	~~0.0037~~	~~2046~~	~~14~~	~~1826~~	~~14~~	~~1638~~	~~18~~	~~24.9~~
Z2-52	0.62	0.05881	0.00157	0.50063	0.0131	0.06172	0.00085	560	34	412	9	386	5	6.7
Z2-53	0.33	0.05539	0.00183	0.50484	0.01541	0.0661	0.00085	428	76	415	10	413	5	0.5
Z2-54	1.29	0.05372	0.00424	0.37282	0.0288	0.05033	0.00079	359	181	322	21	317	5	1.6
Z2-55	0.5	0.05209	0.00092	0.24761	0.00441	0.03447	0.00042	289	20	225	4	218	3	3.2
Z2-56	0.93	0.05383	0.00142	0.43446	0.0111	0.05852	0.00083	364	33	366	8	367	5	-0.3
~~Z2-57~~	~~0.74~~	~~0.07738~~	~~0.00313~~	~~1.10246~~	~~0.04198~~	~~0.10333~~	~~0.00142~~	~~1131~~	~~83~~	~~755~~	~~20~~	~~634~~	~~8~~	~~19.1~~
Z2-58	0.27	0.05636	0.00177	0.46161	0.0133	0.0594	0.00075	467	71	385	9	372	5	3.5
Z2-59	0.48	0.05375	0.00187	0.22248	0.00753	0.03001	0.00044	361	50	204	6	191	3	6.8
Z2-60	0.77	0.06096	0.00112	0.55669	0.01019	0.06621	0.00083	638	20	449	7	413	5	8.7
~~Z2-61~~	~~1.48~~	~~0.17382~~	~~0.00787~~	~~1.29639~~	~~0.05381~~	~~0.05409~~	~~0.00098~~	~~2595~~	~~77~~	~~844~~	~~24~~	~~340~~	~~6~~	~~148~~

Z2-62	0.39	0.05993	0.00145	0.46751	0.01092	0.05656	0.0008	601	27	389	8	355	5	9.6
Z2-63	0.88	0.05656	0.0011	0.45638	0.0088	0.0585	0.00074	474	22	382	6	366	5	4.4
Z2-64	1.18	0.05824	0.00101	0.54853	0.00952	0.06829	0.00084	539	18	444	6	426	5	4.2
~~Z2-65~~	~~0.85~~	~~0.09502~~	~~0.00154~~	~~2.58027~~	~~0.04217~~	~~0.1969~~	~~0.00242~~	~~1528~~	~~15~~	~~1295~~	~~12~~	~~1159~~	~~13~~	~~31.8~~
~~Z2-66~~	~~0.81~~	~~0.09548~~	~~0.00536~~	~~0.60578~~	~~0.03265~~	~~0.04602~~	~~0.00073~~	~~1538~~	~~108~~	~~481~~	~~21~~	~~290~~	~~4~~	~~65.9~~
Z2-67	0.74	0.0537	0.00233	0.26979	0.01139	0.03643	0.00059	358	66	243	9	231	4	5.2
Z2-68	0.78	0.05451	0.00174	0.42703	0.01335	0.0568	0.0008	392	45	361	9	356	5	1.4
Z2-69	0.98	0.04605	0.00274	0.22565	0.013	0.03554	0.00052		130	207	11	225	3	-8
Z2-70	0.48	0.05444	0.0026	0.32832	0.01504	0.04374	0.0006	389	110	288	11	276	4	4.3
Z2-71	0.69	0.06821	0.00132	1.18918	0.02269	0.12641	0.00162	875	20	796	11	767	9	3.8
~~Z2-72~~	~~0.45~~	~~0.05987~~	~~0.0022~~	~~0.38354~~	~~0.01312~~	~~0.04646~~	~~0.00061~~	~~599~~	~~81~~	~~330~~	~~10~~	~~293~~	~~4~~	~~12.6~~
Z2-73	0.52	0.05826	0.00098	0.55414	0.00933	0.06897	0.00084	540	18	448	6	430	5	4.2
Z2-74	0.51	0.05488	0.00151	0.49639	0.01347	0.06558	0.00087	407	37	409	9	409	5	0
Z2-75	0.28	0.05504	0.00205	0.47439	0.01654	0.06251	0.00083	414	85	394	11	391	5	0.8
Z2-76	0.85	0.05858	0.00132	0.52281	0.01153	0.0647	0.00086	552	26	427	8	404	5	5.7
Z2-77	0.4	0.05535	0.00201	0.24824	0.00843	0.03253	0.00042	426	83	225	7	206	3	9.2
Z2-78	0.59	0.06151	0.00121	0.4858	0.00941	0.05726	0.00073	657	21	402	6	359	4	12
Z2-79	0.77	0.05498	0.00168	0.48659	0.01468	0.06417	0.00087	411	43	403	10	401	5	0.5
Z2-80	0.41	0.0564	0.00115	0.5298	0.01067	0.06811	0.00086	468	23	432	7	425	5	1.6
~~Z2-81~~	~~0.3~~	~~0.06114~~	~~0.00128~~	~~0.48713~~	~~0.00998~~	~~0.05777~~	~~0.00075~~	~~644~~	~~23~~	~~403~~	~~7~~	~~362~~	~~5~~	~~11.3~~
Z2-82	0.7	0.05732	0.00113	0.43282	0.00845	0.05474	0.00069	504	22	365	6	344	4	6.1
~~Z2-83~~	~~0.34~~	~~0.0627~~	~~0.00118~~	~~0.5095~~	~~0.00948~~	~~0.05892~~	~~0.00074~~	~~698~~	~~20~~	~~418~~	~~6~~	~~369~~	~~5~~	~~13.3~~
~~Z2-84~~	~~0.58~~	~~0.06572~~	~~0.00161~~	~~0.59502~~	~~0.01427~~	~~0.06565~~	~~0.00088~~	~~797~~	~~28~~	~~474~~	~~9~~	~~410~~	~~5~~	~~15.6~~
Z2-85	0.46	0.0509	0.00201	0.29026	0.01082	0.04136	0.00054	236	93	259	9	261	3	-0.8
Z2-86	0.6	0.05929	0.0011	0.54443	0.01	0.06658	0.00084	578	20	441	7	416	5	6
~~Z2-87~~	~~0.72~~	~~0.08162~~	~~0.0014~~	~~0.5929~~	~~0.01014~~	~~0.05267~~	~~0.00065~~	~~1236~~	~~16~~	~~473~~	~~6~~	~~331~~	~~4~~	~~42.9~~
Z2-88	0.49	0.06489	0.00173	1.14144	0.02938	0.12755	0.00183	771	31	773	14	774	10	-0.1
Z2-89	0.45	0.05608	0.00118	0.53205	0.01106	0.0688	0.00089	456	24	433	7	429	5	0.9

~~Z2-90~~	~~0.94~~	~~0.05691~~	~~0.00348~~	~~0.30571~~	~~0.01825~~	~~0.03895~~	~~0.0007~~	~~488~~	~~100~~	~~271~~	~~14~~	~~246~~	~~4~~	~~10.2~~
Z2-91	0.56	0.05196	0.00193	0.25452	0.00923	0.03552	0.00052	284	56	230	7	225	3	2.2
Z2-92	0.96	0.05703	0.00105	0.5648	0.01034	0.07181	0.0009	493	20	455	7	447	5	1.8
Z2-93	0.42	0.05648	0.00228	0.47442	0.01812	0.06092	0.00081	471	92	394	12	381	5	3.4
Z2-94	0.31	0.05538	0.00189	0.27418	0.00867	0.03591	0.00046	428	78	246	7	227	3	8.4
Z2-95	0.96	0.0528	0.00128	0.27109	0.00641	0.03723	0.0005	320	30	244	5	236	3	3.4
Z2-96	0.68	0.0589	0.00104	0.51676	0.00905	0.06361	0.00079	563	19	423	6	398	5	6.3
~~Z2-97~~	~~0.81~~	~~0.12264~~	~~0.00732~~	~~0.35643~~	~~0.02032~~	~~0.02108~~	~~0.00037~~	~~1995~~	~~109~~	~~310~~	~~15~~	~~134~~	~~2~~	~~131~~
Z2-98	0.32	0.05966	0.00205	0.53714	0.01703	0.06529	0.00086	591	76	437	11	408	5	7.1
ADT1														
~~ADT1-01~~	~~0.75~~	~~0.16542~~	~~0.0022~~	~~9.20263~~	~~0.14396~~	~~0.40341~~	~~0.00558~~	~~2512~~	~~12~~	~~2358~~	~~14~~	~~2185~~	~~26~~	~~15~~
ADT1-02	0.63	0.05071	0.00295	0.25008	0.01451	0.03576	0.00059	228	103	227	12	226	4	0.4
~~ADT1-03~~	~~0.66~~	~~0.09694~~	~~0.00134~~	~~3.29453~~	~~0.05305~~	~~0.24645~~	~~0.00339~~	~~1566~~	~~14~~	~~1480~~	~~13~~	~~1420~~	~~18~~	~~10.3~~
~~ADT1-04~~	~~0.26~~	~~0.06907~~	~~0.00164~~	~~0.69357~~	~~0.01711~~	~~0.07281~~	~~0.00106~~	~~901~~	~~28~~	~~535~~	~~10~~	~~453~~	~~6~~	~~18.1~~
ADT1-05	0.94	0.05682	0.00169	0.43722	0.01315	0.0558	0.00087	485	39	368	9	350	5	5.1
ADT1-06	0.91	0.05596	0.00206	0.54766	0.02031	0.07096	0.00111	451	55	443	13	442	7	0.2
ADT1-07	0.84	0.05533	0.00219	0.46519	0.01837	0.06097	0.00101	426	58	388	13	382	6	1.6
ADT1-08	0.47	0.05421	0.00333	0.44328	0.02689	0.0593	0.00113	380	102	373	19	371	7	0.5
ADT1-09	0.54	0.05483	0.00271	0.49409	0.02441	0.06535	0.00107	405	81	408	17	408	6	0
ADT1-10	0.49	0.05036	0.00127	0.24084	0.00627	0.03468	0.0005	212	34	219	5	220	3	-0.5
~~ADT1-11~~	~~0.54~~	~~0.08828~~	~~0.00123~~	~~2.49673~~	~~0.0404~~	~~0.20509~~	~~0.00282~~	~~1389~~	~~14~~	~~1271~~	~~12~~	~~1203~~	~~15~~	~~15.5~~
ADT1-12	1.1	0.05554	0.00098	0.51755	0.00995	0.06757	0.00095	434	20	424	7	421	6	0.7
ADT1-13	0.63	0.05026	0.00165	0.23503	0.00783	0.03391	0.0005	207	50	214	6	215	3	-0.5
ADT1-14	0.53	0.05029	0.00214	0.22738	0.00969	0.03279	0.00052	208	69	208	8	208	3	0
ADT1-15	0.75	0.05062	0.00144	0.24168	0.00706	0.03462	0.00051	224	41	220	6	219	3	0.5
ADT1-16	0.45	0.05321	0.00269	0.23815	0.01145	0.03246	0.00051	338	118	217	9	206	3	5.3

ADT1-17	0.51	0.05453	0.00581	0.45097	0.04762	0.05997	0.00131	393	198	378	33	375	8	0.8
ADT1-18	0.57	0.05446	0.00363	0.45725	0.03018	0.06088	0.00114	390	115	382	21	381	7	0.3
ADT1-19	0.43	0.05049	0.0013	0.23612	0.00629	0.03391	0.00049	218	36	215	5	215	3	0
~~ADT1-20~~	~~0.41~~	~~0.09609~~	~~0.00273~~	~~2.78806~~	~~0.06819~~	~~0.21044~~	~~0.00304~~	~~1549~~	~~55~~	~~1352~~	~~18~~	~~1231~~	~~16~~	~~25.8~~
ADT1-21	0.59	0.05525	0.00568	0.49528	0.04993	0.06501	0.00175	422	178	409	34	406	11	0.7
~~ADT1-22~~	~~0.77~~	~~0.06546~~	~~0.00183~~	~~0.53638~~	~~0.0152~~	~~0.05942~~	~~0.00092~~	~~789~~	~~34~~	~~436~~	~~10~~	~~372~~	~~6~~	~~17.2~~
ADT1-23	0.06	0.05924	0.00145	0.56689	0.01158	0.06941	0.00095	576	55	456	8	433	6	5.3
ADT1-24	0.58	0.05538	0.00389	0.47971	0.03342	0.06281	0.00116	428	123	398	23	393	7	1.3
ADT1-25	0.46	0.05042	0.00214	0.23297	0.00986	0.03351	0.00055	214	67	213	8	212	3	0.5
~~ADT1-26~~	~~0.38~~	~~0.06474~~	~~0.00198~~	~~0.49115~~	~~0.01333~~	~~0.05503~~	~~0.00077~~	~~766~~	~~66~~	~~406~~	~~9~~	~~345~~	~~5~~	~~17.7~~
ADT1-27	0.73	0.05491	0.00176	0.49906	0.01617	0.06591	0.00102	409	45	411	11	411	6	0
ADT1-28	0.41	0.05041	0.00194	0.22744	0.00877	0.03272	0.00052	214	60	208	7	208	3	0
~~ADT1-29~~	~~0.79~~	~~0.0714~~	~~0.00228~~	~~0.34692~~	~~0.01113~~	~~0.03524~~	~~0.00056~~	~~969~~	~~40~~	~~302~~	~~8~~	~~223~~	~~3~~	~~35.4~~
ADT1-30	0.66	0.05049	0.00121	0.2308	0.00575	0.03315	0.00048	218	32	211	5	210	3	0.5
ADT1-31	0.82	0.0519	0.00323	0.241	0.01493	0.03367	0.00057	281	111	219	12	213	4	2.8
~~ADT1-32~~	~~0.52~~	~~0.06674~~	~~0.00217~~	~~0.73803~~	~~0.02416~~	~~0.08018~~	~~0.00126~~	~~830~~	~~42~~	~~561~~	~~14~~	~~497~~	~~8~~	~~12.9~~
ADT1-33	0.22	0.0553	0.0014	0.49105	0.01286	0.06439	0.00092	424	34	406	9	402	6	1
~~ADT1-34~~	~~0.82~~	~~0.07423~~	~~0.00618~~	~~0.34772~~	~~0.02804~~	~~0.03397~~	~~0.00071~~	~~1048~~	~~174~~	~~303~~	~~21~~	~~215~~	~~4~~	~~40.9~~
ADT1-35	0.4	0.05066	0.0012	0.23914	0.0059	0.03423	0.00049	225	32	218	5	217	3	0.5
ADT1-36	0.39	0.05589	0.00232	0.50631	0.0211	0.0657	0.00104	448	64	416	14	410	6	1.5
ADT1-37	0.7	0.0553	0.00153	0.50765	0.01432	0.06657	0.00099	424	37	417	10	415	6	0.5
ADT1-38	0.61	0.05042	0.00211	0.24083	0.0101	0.03464	0.00054	214	68	219	8	220	3	-0.5
~~ADT1-39~~	~~0.97~~	~~0.09047~~	~~0.00493~~	~~2.78871~~	~~0.14473~~	~~0.22356~~	~~0.00371~~	~~1435~~	~~107~~	~~1353~~	~~39~~	~~1301~~	~~20~~	~~10.3~~
~~ADT1-40~~	~~0.8~~	~~0.05818~~	~~0.00169~~	~~0.26054~~	~~0.00771~~	~~0.03247~~	~~0.00048~~	~~537~~	~~39~~	~~235~~	~~6~~	~~206~~	~~3~~	~~14.1~~
ADT1-41	0.34	0.05714	0.00307	0.56909	0.03039	0.07223	0.00126	497	87	457	20	450	8	1.6
ADT1-42	0.77	0.08163	0.00114	2.3245	0.03751	0.20649	0.00282	1237	14	1220	11	1210	15	2.2
ADT1-43	0.49	0.09301	0.00142	3.12348	0.0534	0.24352	0.00339	1488	15	1438	13	1405	18	5.9
ADT1-44	0.61	0.05504	0.00325	0.47569	0.0279	0.06268	0.0011	414	100	395	19	392	7	0.8

ADT1-45	0.54	0.0569	0.00098	0.45651	0.00857	0.05818	0.00081	488	20	382	6	365	5	4.7
~~ADT1-46~~	~~0.72~~	~~0.06624~~	~~0.00338~~	~~0.55613~~	~~0.02685~~	~~0.06089~~	~~0.00099~~	~~814~~	~~109~~	~~449~~	~~18~~	~~381~~	~~6~~	~~17.8~~
~~ADT1-47~~	~~0.75~~	~~0.09173~~	~~0.0056~~	~~0.7602~~	~~0.04457~~	~~0.06011~~	~~0.00103~~	~~1462~~	~~119~~	~~574~~	~~26~~	~~376~~	~~6~~	~~52.7~~
~~ADT1-48~~	~~0.25~~	~~0.09414~~	~~0.00131~~	~~2.47008~~	~~0.03971~~	~~0.19026~~	~~0.0026~~	~~1511~~	~~14~~	~~1263~~	~~12~~	~~1123~~	~~14~~	~~34.6~~
ADT1-49	0.57	0.05211	0.00242	0.25039	0.01098	0.03485	0.00053	290	109	227	9	221	3	2.7
ADT1-50	0.56	0.05389	0.00203	0.25408	0.00947	0.03419	0.00057	366	54	230	8	217	4	6
~~ADT1-51~~	~~0.79~~	~~0.05736~~	~~0.00341~~	~~0.25855~~	~~0.01481~~	~~0.03269~~	~~0.00053~~	~~505~~	~~135~~	~~233~~	~~12~~	~~207~~	~~3~~	~~12.6~~
ADT1-52	0.9	0.05562	0.00092	0.50881	0.00923	0.06634	0.00092	437	19	418	6	414	6	1
ADT1-53	2.09	0.09047	0.00129	2.92264	0.04775	0.23428	0.00322	1435	14	1388	12	1357	17	5.7
ADT1-54	0.55	0.0926	0.0013	3.12935	0.05048	0.24507	0.00335	1480	14	1440	12	1413	17	4.7
ADT1-55	0.09	0.05528	0.00231	0.47796	0.01882	0.06271	0.00089	424	96	397	13	392	5	1.3
ADT1-56	0.55	0.05407	0.0028	0.25222	0.01242	0.03383	0.00054	374	120	228	10	214	3	6.5
~~ADT1-57~~	~~0.67~~	~~0.06261~~	~~0.00338~~	~~0.51567~~	~~0.02724~~	~~0.05973~~	~~0.00118~~	~~695~~	~~79~~	~~422~~	~~18~~	~~374~~	~~7~~	~~12.8~~
~~ADT1-58~~	~~0.79~~	~~0.06695~~	~~0.00169~~	~~0.6134~~	~~0.01574~~	~~0.06644~~	~~0.00102~~	~~836~~	~~29~~	~~486~~	~~10~~	~~415~~	~~6~~	~~17.1~~
ADT1-59	0.88	0.05146	0.00139	0.29422	0.00809	0.04146	0.00063	261	36	262	6	262	4	0
~~ADT1-60~~	~~0.95~~	~~0.06344~~	~~0.00158~~	~~0.29742~~	~~0.00755~~	~~0.034~~	~~0.00051~~	~~723~~	~~29~~	~~264~~	~~6~~	~~216~~	~~3~~	~~22.2~~
ADT1-61	0.76	0.06022	0.0049	0.54041	0.04266	0.06508	0.00129	611	182	439	28	406	8	8.1
~~ADT1-62~~	~~0.83~~	~~0.07303~~	~~0.03043~~	~~0.36463~~	~~0.1513~~	~~0.03621~~	~~0.00141~~	~~1015~~	~~893~~	~~316~~	~~113~~	~~229~~	~~9~~	~~38~~
ADT1-63	0.77	0.05324	0.00291	0.2468	0.01291	0.03362	0.00053	339	127	224	11	213	3	5.2
ADT1-64	0.61	0.05512	0.00088	0.53033	0.00937	0.06977	0.00096	417	18	432	6	435	6	-0.7
~~ADT1-65~~	~~0.49~~	~~0.06016~~	~~0.00319~~	~~0.28423~~	~~0.0143~~	~~0.03426~~	~~0.00057~~	~~609~~	~~118~~	~~254~~	~~11~~	~~217~~	~~4~~	~~17.1~~
ADT1-66	0.28	0.06125	0.00187	0.92278	0.02491	0.10928	0.00155	648	67	664	13	669	9	-0.7
ADT1-67	0.45	0.05245	0.00165	0.23827	0.00749	0.03294	0.00052	305	43	217	6	209	3	3.8
ADT1-68	0.24	0.0558	0.00227	0.51361	0.02062	0.06674	0.00115	444	59	421	14	416	7	1.2
~~ADT1-69~~	~~0.61~~	~~0.08948~~	~~0.00149~~	~~2.4616~~	~~0.04476~~	~~0.1995~~	~~0.00282~~	~~1414~~	~~16~~	~~1261~~	~~13~~	~~1173~~	~~15~~	~~20.5~~
ADT1-70	0.75	0.06253	0.00177	0.64032	0.01824	0.07426	0.00116	692	35	503	11	462	7	8.9
ADT1-71	0.74	0.05497	0.00157	0.26368	0.00761	0.03479	0.00054	411	37	238	6	220	3	8.2
ADT1-72	0.66	0.05425	0.00144	0.2643	0.00713	0.03533	0.00053	381	34	238	6	224	3	6.3

ADT1-73	0.9	0.09224	0.00156	3.13441	0.05758	0.24641	0.0035	1472	16	1441	14	1420	18	3.7
ADT1-74	0.51	0.05549	0.00124	0.46956	0.01084	0.06136	0.00089	432	27	391	7	384	5	1.8
ADT1-75	0.6	0.05624	0.00133	0.47535	0.01154	0.0613	0.00091	462	29	395	8	384	6	2.9
ADT1-76	0.38	0.07845	0.00119	1.64091	0.02784	0.15167	0.00209	1158	15	986	11	910	12	8.4
~~ADT1-77~~	~~0.57~~	~~0.0591~~	~~0.00404~~	~~0.27748~~	~~0.01829~~	~~0.03405~~	~~0.00062~~	~~571~~	~~153~~	~~249~~	~~15~~	~~216~~	~~4~~	~~15.3~~
ADT1-78	0.85	0.05425	0.00133	0.43737	0.01097	0.05846	0.00087	381	31	368	8	366	5	0.5
ADT1-79	0.48	0.05603	0.00119	0.46502	0.01033	0.06019	0.00087	454	25	388	7	377	5	2.9
ADT1-80	0.69	0.05054	0.00193	0.24427	0.00923	0.03505	0.00058	220	57	222	8	222	4	0
~~ADT1-81~~	~~0.91~~	~~0.0594~~	~~0.00171~~	~~0.41556~~	~~0.012~~	~~0.05073~~	~~0.00079~~	~~582~~	~~36~~	~~353~~	~~9~~	~~319~~	~~5~~	~~10.7~~
ADT1-82	0.53	0.04947	0.0013	0.24025	0.00641	0.03522	0.00053	170	35	219	5	223	3	-1.8
ADT1-83	1.1	0.0779	0.00152	1.99989	0.04103	0.18617	0.0027	1144	20	1115	14	1101	15	3.9
ADT1-84	0.62	0.05124	0.00179	0.24666	0.00859	0.03491	0.00056	252	51	224	7	221	3	1.4
~~ADT1-85~~	~~0.61~~	~~0.09216~~	~~0.00145~~	~~2.41105~~	~~0.04204~~	~~0.18972~~	~~0.00264~~	~~1471~~	~~15~~	~~1246~~	~~13~~	~~1120~~	~~14~~	~~31.3~~
ADT1-86	0.57	0.05114	0.00239	0.44394	0.02049	0.06295	0.00112	247	73	373	14	394	7	-5.3
ADT1-87	0.55	0.05668	0.00162	0.48327	0.01386	0.06182	0.00096	479	37	400	9	387	6	3.4
ADT1-88	0.63	0.05924	0.00436	0.483	0.03431	0.05913	0.00112	576	165	400	23	370	7	8.1
ADT1-89	0.79	0.07156	0.00366	1.49543	0.07258	0.15156	0.00244	974	107	929	30	910	14	2.1
ADT1-90	1.21	0.05631	0.0011	0.46309	0.00957	0.05964	0.00085	465	23	386	7	373	5	3.5
~~ADT1-91~~	~~0.74~~	~~0.06798~~	~~0.0022~~	~~0.3058~~	~~0.00981~~	~~0.03262~~	~~0.00053~~	~~868~~	~~40~~	~~271~~	~~8~~	~~207~~	~~3~~	~~30.9~~
ADT1-92	0.64	0.08236	0.00132	2.34219	0.04146	0.20623	0.00287	1254	16	1225	13	1209	15	3.7
ADT1-93	0.46	0.05531	0.00106	0.44585	0.00908	0.05845	0.00083	425	22	374	6	366	5	2.2
~~ADT1-94~~	~~0.55~~	~~0.15617~~	~~0.02305~~	~~1.56275~~	~~0.22555~~	~~0.07258~~	~~0.00225~~	~~2415~~	~~265~~	~~956~~	~~89~~	~~452~~	~~13~~	~~112~~
ADT1-95	0.6	0.052	0.00149	0.2389	0.00688	0.03331	0.00051	285	38	218	6	211	3	3.3
ADT1-96	0.48	0.0522	0.00193	0.23398	0.00859	0.0325	0.00054	294	54	213	7	206	3	3.4
ADT1-97	0.52	0.04881	0.00158	0.22963	0.00745	0.03412	0.00054	139	47	210	6	216	3	-2.8
ADT1-98	0.97	0.11119	0.00192	5.01324	0.09328	0.32694	0.00468	1819	16	1822	16	1824	23	-0.3
ADT1-99	0.51	0.07749	0.00266	1.5753	0.04893	0.14744	0.00217	1134	70	961	19	887	12	8.3
ADT1-100	0.29	0.05757	0.00102	0.4916	0.00937	0.06192	0.00087	513	20	406	6	387	5	4.9

ADT4														
ADT4-01	0.02	0.05511	0.00165	0.5458	0.01451	0.07183	0.001	417	69	442	10	447	6	-1.1
~~ADT4-02~~	~~0.7~~	~~0.063~~	~~0.00178~~	~~0.34825~~	~~0.01006~~	~~0.04008~~	~~0.00059~~	~~708~~	~~37~~	~~303~~	~~8~~	~~253~~	~~4~~	~~19.8~~
ADT4-03	0.39	0.04915	0.00375	0.18866	0.01408	0.02784	0.00045	155	173	175	12	177	3	-1.1
ADT4-04	0.65	0.05135	0.00202	0.29443	0.01167	0.04157	0.00063	257	63	262	9	263	4	-0.4
~~ADT4-05~~	~~1.2~~	~~0.08386~~	~~0.00758~~	~~0.08575~~	~~0.00753~~	~~0.00742~~	~~0.00016~~	~~1289~~	~~182~~	~~84~~	~~7~~	~~48~~	~~1~~	~~75~~
ADT4-06	0.61	0.11954	0.00162	5.50456	0.08739	0.33389	0.00461	1949	13	1901	14	1857	22	5
ADT4-07	0.61	0.05858	0.00239	0.50772	0.02079	0.06285	0.00098	552	62	417	14	393	6	6.1
ADT4-08	0.51	0.05096	0.00118	0.23776	0.00576	0.03383	0.00048	239	31	217	5	214	3	1.4
~~ADT4-09~~	~~0.9~~	~~0.0749~~	~~0.00702~~	~~0.54879~~	~~0.05026~~	~~0.05314~~	~~0.00107~~	~~1066~~	~~196~~	~~444~~	~~33~~	~~334~~	~~7~~	~~32.9~~
~~ADT4-10~~	~~0.14~~	~~0.05806~~	~~0.00125~~	~~0.34012~~	~~0.00773~~	~~0.04248~~	~~0.0006~~	~~532~~	~~26~~	~~297~~	~~6~~	~~268~~	~~4~~	~~10.8~~
~~ADT4-11~~	~~0.99~~	~~0.07011~~	~~0.00338~~	~~0.5763~~	~~0.02631~~	~~0.05961~~	~~0.00092~~	~~932~~	~~101~~	~~462~~	~~17~~	~~373~~	~~6~~	~~23.9~~
ADT4-12	0.77	0.06167	0.00155	0.57256	0.01491	0.06732	0.00097	663	32	460	10	420	6	9.5
~~ADT4-13~~	~~0.67~~	~~0.08384~~	~~0.00711~~	~~0.78535~~	~~0.06463~~	~~0.06793~~	~~0.00138~~	~~1289~~	~~171~~	~~589~~	~~37~~	~~424~~	~~8~~	~~38.9~~
ADT4-14	0.58	0.05512	0.00206	0.48972	0.01845	0.06442	0.00097	417	57	405	13	402	6	0.7
ADT4-15	0.42	0.05584	0.00214	0.44629	0.01586	0.05796	0.00084	446	87	375	11	363	5	3.3
~~ADT4-16~~	~~0.41~~	~~0.06268~~	~~0.00311~~	~~0.57326~~	~~0.02695~~	~~0.06633~~	~~0.00105~~	~~697~~	~~108~~	~~460~~	~~17~~	~~414~~	~~6~~	~~11.1~~
ADT4-17	0.26	0.0503	0.00128	0.23697	0.00625	0.03416	0.0005	209	35	216	5	217	3	-0.5
~~ADT4-18~~	~~1.67~~	~~0.07936~~	~~0.00915~~	~~0.79859~~	~~0.09023~~	~~0.07298~~	~~0.00169~~	~~1181~~	~~239~~	~~596~~	~~51~~	~~454~~	~~10~~	~~31.3~~
ADT4-19	0.39	0.06192	0.00255	0.61544	0.02367	0.07209	0.00108	671	90	487	15	449	6	8.5
ADT4-20	0.21	0.07862	0.00209	1.63589	0.03721	0.15091	0.00209	1163	54	984	14	906	12	8.6
ADT4-21	0.22	0.05565	0.00124	0.49887	0.01163	0.065	0.00093	438	28	411	8	406	6	1.2
ADT4-22	0.55	0.05526	0.00128	0.54701	0.01318	0.07178	0.00104	423	29	443	9	447	6	-0.9
~~ADT4-23~~	~~0.79~~	~~0.05697~~	~~0.00232~~	~~0.2957~~	~~0.01212~~	~~0.03763~~	~~0.00057~~	~~490~~	~~64~~	~~263~~	~~9~~	~~238~~	~~4~~	~~10.5~~
~~ADT4-24~~	~~0.88~~	~~0.07001~~	~~0.00617~~	~~0.37455~~	~~0.03271~~	~~0.03879~~	~~0.00077~~	~~929~~	~~148~~	~~323~~	~~24~~	~~245~~	~~5~~	~~31.8~~
~~ADT4-25~~	~~0.7~~	~~0.0753~~	~~0.00212~~	~~0.58544~~	~~0.01679~~	~~0.05637~~	~~0.00085~~	~~1077~~	~~34~~	~~468~~	~~11~~	~~354~~	~~5~~	~~32.2~~

ADT4-26	0.86	0.05643	0.001	0.50362	0.00974	0.06471	0.0009	469	21	414	7	404	5	2.5
~~ADT4-27~~	~~0.81~~	~~0.06881~~	~~0.00349~~	~~0.36356~~	~~0.01753~~	~~0.03832~~	~~0.0006~~	~~893~~	~~107~~	~~315~~	~~13~~	~~242~~	~~4~~	~~30.2~~
ADT4-28	0.24	0.06816	0.00195	1.21619	0.03041	0.1294	0.00181	874	61	808	14	784	10	3.1
ADT4-29	0.86	0.04605	0.00841	0.03633	0.00658	0.00572	0.00013		312	36	6	36.8	0.8	-2.2
~~ADT4-30~~	~~0.64~~	~~0.06555~~	~~0.00358~~	~~0.58107~~	~~0.03039~~	~~0.06429~~	~~0.00102~~	~~792~~	~~118~~	~~465~~	~~20~~	~~402~~	~~6~~	~~15.7~~
~~ADT4-31~~	~~0.98~~	~~0.07807~~	~~0.00435~~	~~0.37922~~	~~0.02016~~	~~0.03523~~	~~0.00059~~	~~1149~~	~~114~~	~~326~~	~~15~~	~~223~~	4	~~46.2~~
ADT4-32	0.6	0.05323	0.00275	0.34175	0.01687	0.04656	0.0007	339	120	298	13	293	4	1.7
ADT4-33	0.18	0.05887	0.00129	0.58111	0.01334	0.07158	0.00102	562	26	465	9	446	6	4.3
~~ADT4-34~~	~~0.56~~	~~0.07955~~	~~0.00139~~	~~1.63027~~	~~0.031~~	~~0.1486~~	~~0.00209~~	~~1186~~	~~18~~	~~982~~	~~12~~	~~893~~	~~12~~	~~10~~
~~ADT4-35~~	~~0.23~~	~~0.07856~~	~~0.00228~~	~~1.35577~~	~~0.03434~~	~~0.12516~~	~~0.00177~~	~~1161~~	~~59~~	~~870~~	~~15~~	~~760~~	~~10~~	~~14.5~~
~~ADT4-36~~	~~0.67~~	~~0.07506~~	~~0.00188~~	~~0.9273~~	~~0.02386~~	~~0.08958~~	~~0.00132~~	~~1070~~	~~29~~	~~666~~	~~13~~	~~553~~	~~8~~	~~20.4~~
~~ADT4-37~~	~~0.08~~	~~0.08958~~	~~0.0034~~	~~0.87132~~	~~0.03052~~	~~0.07054~~	~~0.00103~~	~~1417~~	~~74~~	~~636~~	~~17~~	~~439~~	~~6~~	~~44.9~~
~~ADT4-38~~	~~0.88~~	~~0.07121~~	~~0.0019~~	~~0.64176~~	~~0.01754~~	~~0.06534~~	~~0.00097~~	~~963~~	~~32~~	~~503~~	~~11~~	~~408~~	~~6~~	~~23.3~~
ADT4-39	0.71	0.05271	0.00256	0.34695	0.01689	0.04773	0.00074	316	82	302	13	301	5	0.3
~~ADT4-40~~	~~0.8~~	~~0.09185~~	~~0.00177~~	~~0.65353~~	~~0.01333~~	~~0.05159~~	~~0.00074~~	~~1464~~	~~19~~	~~511~~	~~8~~	~~324~~	~~5~~	~~57.7~~
~~ADT4-41~~	~~0.66~~	~~0.07079~~	~~0.0037~~	~~0.58076~~	~~0.02887~~	~~0.0595~~	~~0.00097~~	~~951~~	~~110~~	~~465~~	~~19~~	~~373~~	~~6~~	~~24.7~~
ADT4-42	0.07	0.07358	0.00159	1.59108	0.02718	0.15683	0.00209	1030	45	967	11	939	12	3
~~ADT4-43~~	~~0.78~~	~~0.05957~~	~~0.00304~~	~~0.37948~~	~~0.01844~~	~~0.0462~~	~~0.00071~~	~~588~~	~~114~~	~~327~~	~~14~~	~~291~~	~~4~~	~~12.4~~
~~ADT4-44~~	~~0.89~~	~~0.07688~~	~~0.00509~~	~~1.22418~~	~~0.07812~~	~~0.11548~~	~~0.00205~~	~~1118~~	~~136~~	~~812~~	~~36~~	~~705~~	~~12~~	~~15.2~~
ADT4-45	0.22	0.05492	0.00142	0.49641	0.01321	0.06554	0.00095	409	34	409	9	409	6	0
~~ADT4-46~~	~~0.77~~	~~0.06783~~	~~0.00198~~	~~0.54956~~	~~0.01631~~	~~0.05875~~	~~0.00088~~	~~863~~	~~37~~	~~445~~	~~11~~	~~368~~	~~5~~	~~20.9~~
~~ADT4-47~~	~~0.45~~	~~0.06202~~	~~0.00249~~	~~0.56821~~	~~0.02123~~	~~0.06645~~	~~0.00098~~	~~675~~	~~88~~	~~457~~	~~14~~	~~415~~	~~6~~	~~10.1~~
~~ADT4-48~~	~~0.6~~	~~0.06797~~	~~0.00121~~	~~0.57474~~	~~0.01113~~	~~0.06131~~	~~0.00085~~	~~868~~	~~19~~	~~461~~	~~7~~	~~384~~	~~5~~	~~20.1~~
ADT4-49	0.67	0.05673	0.00118	0.4329	0.00948	0.05534	0.00079	481	25	365	7	347	5	5.2
~~ADT4-50~~	~~0.56~~	~~0.10729~~	~~0.00342~~	~~3.21002~~	~~0.09077~~	~~0.21699~~	~~0.00319~~	~~1754~~	~~60~~	~~1460~~	~~22~~	~~1266~~	~~17~~	~~38.5~~
~~ADT4-51~~	~~0.89~~	~~0.0766~~	~~0.0068~~	~~0.3294~~	~~0.0285~~	~~0.03119~~	~~0.00063~~	~~1111~~	~~184~~	~~289~~	~~22~~	~~198~~	~~4~~	~~46~~
ADT4-52	0.23	0.05736	0.00123	0.51859	0.01168	0.06555	0.00093	505	26	424	8	409	6	3.7
~~ADT4-53~~	~~1.18~~	~~0.0715~~	~~0.00453~~	~~0.65007~~	~~0.03978~~	~~0.06594~~	~~0.00109~~	~~972~~	~~133~~	~~509~~	~~24~~	~~412~~	~~7~~	~~23.5~~

~~ADT4-54~~	~~1.08~~	~~0.11986~~	~~0.00549~~	~~4.21702~~	~~0.17873~~	~~0.25518~~	~~0.00443~~	~~1954~~	~~84~~	~~1677~~	~~35~~	~~1465~~	~~23~~	~~33.4~~
~~ADT4-55~~	~~0.48~~	~~0.06977~~	~~0.00161~~	~~0.90658~~	~~0.02165~~	~~0.09422~~	~~0.00137~~	~~922~~	~~26~~	~~655~~	~~12~~	~~580~~	~~8~~	~~12.9~~
ADT4-56	1.12	0.05691	0.00121	0.5546	0.01237	0.07066	0.00101	488	26	448	8	440	6	1.8
ADT4-57	0.4	0.07406	0.00272	1.62149	0.05444	0.1588	0.00234	1043	76	979	21	950	13	3.1
ADT4-58	0.43	0.05884	0.00271	0.54051	0.02351	0.06662	0.001	561	103	439	15	416	6	5.5
ADT4-59	0.36	0.05646	0.00223	0.52067	0.01908	0.06689	0.00097	470	89	426	13	417	6	2.2
~~ADT4-60~~	~~0.55~~	~~0.10122~~	~~0.00727~~	~~0.46191~~	~~0.03196~~	~~0.0331~~	~~0.00063~~	~~1647~~	~~137~~	~~386~~	~~22~~	~~210~~	~~4~~	~~83.8~~
~~ADT4-61~~	~~0.56~~	~~0.06385~~	~~0.00155~~	~~0.61457~~	~~0.01542~~	~~0.06979~~	~~0.00101~~	~~737~~	~~29~~	~~486~~	~~10~~	~~435~~	~~6~~	~~11.7~~
ADT4-62	0.57	0.06249	0.00251	0.6155	0.02297	0.07143	0.00105	691	88	487	14	445	6	9.4
ADT4-63	0.88	0.05727	0.0017	0.5321	0.01604	0.06737	0.001	502	41	433	11	420	6	3.1
ADT4-64	0.53	0.0542	0.00178	0.23468	0.00777	0.0314	0.00047	379	48	214	6	199	3	7.5
ADT4-65	1.18	0.06518	0.00145	1.13102	0.02612	0.12583	0.00182	780	26	768	12	764	10	0.5
ADT4-66	0.78	0.05882	0.00281	0.51949	0.02357	0.06406	0.00096	560	107	425	16	400	6	6.3
ADT4-67	0.08	0.0554	0.00144	0.26419	0.00587	0.03459	0.00047	428	59	238	5	219	3	8.7
~~ADT4-68~~	~~0.46~~	~~0.06319~~	~~0.00259~~	~~0.50904~~	~~0.01942~~	~~0.05842~~	~~0.00087~~	~~715~~	~~89~~	~~418~~	~~13~~	~~366~~	~~5~~	~~14.2~~
~~ADT4-69~~	~~0.43~~	~~0.10806~~	~~0.00178~~	~~4.06047~~	~~0.07343~~	~~0.27247~~	~~0.00381~~	~~1767~~	~~15~~	~~1646~~	~~15~~	~~1553~~	~~19~~	~~13.8~~
~~ADT4-70~~	~~0.29~~	~~0.11401~~	~~0.00173~~	~~4.05533~~	~~0.06919~~	~~0.25794~~	~~0.00353~~	~~1864~~	~~14~~	~~1645~~	~~14~~	~~1479~~	~~18~~	~~26~~
ADT4-71	0.4	0.08446	0.00248	2.41585	0.06212	0.20745	0.00295	1303	58	1247	18	1215	16	7.2
~~ADT4-72~~	~~0.35~~	~~0.09481~~	~~0.00198~~	~~0.53836~~	~~0.01168~~	~~0.04117~~	~~0.0006~~	~~1524~~	~~21~~	~~437~~	~~8~~	~~260~~	~~4~~	~~68.1~~
ADT4-73	0.6	0.05773	0.00181	0.46983	0.01496	0.05901	0.00087	520	44	391	10	370	5	5.7
ADT4-74	0.39	0.05977	0.00263	0.51097	0.02109	0.062	0.00094	595	98	419	14	388	6	8
~~ADT4-75~~	~~0.55~~	~~0.08347~~	~~0.00589~~	~~0.46471~~	~~0.03176~~	~~0.04038~~	~~0.00071~~	~~1280~~	~~142~~	~~388~~	~~22~~	~~255~~	~~4~~	~~52.2~~
ADT4-76	1.18	0.09735	0.0022	2.13521	0.04954	0.15905	0.0024	1574	22	1160	16	951	13	22
ADT4-77	0.5	0.06076	0.00115	0.54842	0.01109	0.06545	0.00091	631	22	444	7	409	6	8.6
ADT4-78	0.78	0.06662	0.00274	1.0542	0.04319	0.11475	0.00187	826	58	731	21	700	11	4.4
ADT4-79	0.52	0.05599	0.0014	0.26324	0.00678	0.03409	0.0005	452	32	237	5	216	3	9.7
ADT4-80	0.95	0.057	0.00358	0.48274	0.02932	0.06143	0.00097	491	142	400	20	384	6	4.2
~~ADT4-81~~	~~0.25~~	~~0.14569~~	~~0.00394~~	~~3.62837~~	~~0.08304~~	~~0.18062~~	~~0.00261~~	~~2296~~	~~48~~	~~1556~~	~~18~~	~~1070~~	~~14~~	~~115~~

~~ADT4-82~~	~~0.82~~	~~0.06693~~	~~0.00327~~	~~0.61965~~	~~0.02873~~	~~0.06715~~	~~0.00103~~	~~836~~	~~104~~	~~490~~	~~18~~	~~419~~	~~6~~	~~16.9~~
ADT4-83	0.41	0.05785	0.00125	0.54962	0.01238	0.0689	0.00098	524	26	445	8	430	6	3.5
ADT4-84	0.81	0.05649	0.00153	0.4312	0.01186	0.05535	0.00083	472	35	364	8	347	5	4.9
~~ADT4-85~~	~~0.74~~	~~0.06314~~	~~0.00192~~	~~0.50772~~	~~0.01555~~	~~0.05831~~	~~0.00089~~	~~713~~	~~39~~	~~417~~	~~10~~	~~365~~	~~5~~	~~14.2~~
ADT4-86	0.2	0.05144	0.00273	0.23767	0.01206	0.03351	0.00052	261	125	217	10	212	3	2.4
ADT4-87	2.45	0.07706	0.00147	1.57142	0.03178	0.14786	0.00209	1123	20	959	13	889	12	7.9
~~ADT4-88~~	~~0.67~~	~~0.16884~~	~~0.00283~~	~~8.80975~~	~~0.1609~~	~~0.37837~~	~~0.00529~~	~~2546~~	~~14~~	~~2319~~	~~17~~	~~2069~~	~~25~~	~~23.1~~
~~ADT4-89~~	~~0.59~~	~~0.10421~~	~~0.00182~~	~~3.54958~~	~~0.06698~~	~~0.24698~~	~~0.00346~~	~~1700~~	~~16~~	~~1538~~	~~15~~	~~1423~~	~~18~~	~~19.5~~
~~ADT4-90~~	~~0.73~~	~~0.06481~~	~~0.00593~~	~~0.33636~~	~~0.03011~~	~~0.03764~~	~~0.00071~~	~~768~~	~~200~~	~~294~~	~~23~~	~~238~~	4	~~23.5~~
ADT4-91	1.71	0.06896	0.0014	1.28425	0.02736	0.13503	0.00192	898	22	839	12	816	11	2.8
~~ADT4-92~~	~~0.46~~	~~0.06106~~	~~0.00334~~	~~0.25471~~	~~0.01337~~	~~0.03025~~	~~0.00047~~	~~641~~	~~121~~	~~230~~	~~11~~	~~192~~	~~3~~	~~19.8~~
ADT4-93	0.37	0.07444	0.00145	1.67808	0.03452	0.16347	0.00232	1053	21	1000	13	976	13	2.5
~~ADT4-94~~	~~0.48~~	~~0.0748~~	~~0.00138~~	~~0.7347~~	~~0.01445~~	~~0.07122~~	~~0.001~~	~~1063~~	~~19~~	~~559~~	~~8~~	~~444~~	~~6~~	~~25.9~~
~~ADT4-95~~	~~0.3~~	~~0.11803~~	~~0.00207~~	~~4.87284~~	~~0.09216~~	~~0.29938~~	~~0.0042~~	~~1927~~	~~16~~	~~1798~~	~~16~~	~~1688~~	~~21~~	~~14.2~~
ADT4-96	0.87	0.04605	0.00392	0.22973	0.01918	0.03619	0.00061		188	210	16	229	4	-8.3
~~ADT4-97~~	~~0.57~~	~~0.06382~~	~~0.00785~~	~~0.56779~~	~~0.06892~~	~~0.06453~~	~~0.00126~~	~~736~~	~~274~~	~~457~~	~~45~~	~~403~~	~~8~~	~~13.4~~
ADT4-98	1.39	0.05564	0.00135	0.52641	0.01319	0.0686	0.00099	438	31	429	9	428	6	0.2
~~ADT4-99~~	~~0.53~~	~~0.06602~~	~~0.00308~~	~~0.62182~~	~~0.0274~~	~~0.06831~~	~~0.00105~~	~~807~~	~~100~~	~~491~~	~~17~~	~~426~~	~~6~~	~~15.3~~
ADT4-100	0.61	0.05881	0.00451	0.41353	0.03097	0.051	0.00084	560	173	351	22	321	5	9.3
ADT6														
ADT6-01	0.49	0.05702	0.00272	0.45444	0.02158	0.05779	0.00095	492	76	380	15	362	6	5
ADT6-02	0.68	0.05432	0.00121	0.4467	0.01044	0.05962	0.00084	384	28	375	7	373	5	0.5
ADT6-03	0.46	0.05417	0.0012	0.44636	0.01039	0.05975	0.00084	378	28	375	7	374	5	0.3
ADT6-04	0.59	0.05454	0.00137	0.45767	0.01187	0.06085	0.00087	393	33	383	8	381	5	0.5
ADT6-05	0.55	0.05516	0.00138	0.469	0.01213	0.06165	0.00089	419	33	390	8	386	5	1
ADT6-06	0.39	0.05514	0.00115	0.4628	0.01019	0.06086	0.00086	418	25	386	7	381	5	1.3

ADT6-07	0.52	0.05086	0.0028	0.28407	0.01502	0.04051	0.00063	234	128	254	12	256	4	-0.8
ADT6-08	0.81	0.05706	0.00105	0.48335	0.00962	~~0.06142~~	0.00085	494	22	400	7	384	5	4.2
ADT6-09	0.7	0.05669	0.00098	0.48505	0.00915	0.06204	0.00086	479	20	402	6	388	5	3.6
ADT6-10	0.74	0.05424	0.00319	0.43779	0.02568	0.05852	0.00098	381	102	369	18	367	6	0.5
~~ADT6-11~~	~~0.83~~	~~0.06257~~	~~0.00315~~	~~0.49163~~	~~0.02355~~	~~0.05699~~	~~0.00087~~	~~694~~	~~110~~	~~406~~	~~16~~	~~357~~	~~5~~	~~13.7~~
ADT6-12	0.63	0.05809	0.00269	0.4573	0.02005	0.0571	0.00085	533	104	382	14	358	5	6.7
ADT6-13	0.84	0.05455	0.00125	0.45209	0.01085	0.06009	0.00085	394	29	379	8	376	5	0.8
~~ADT6-14~~	~~0.75~~	~~0.06878~~	~~0.00301~~	~~0.54537~~	~~0.0224~~	~~0.05751~~	~~0.00086~~	~~892~~	~~93~~	~~442~~	~~15~~	~~360~~	~~5~~	~~22.8~~
~~ADT6-15~~	~~1.24~~	~~0.10216~~	~~0.00488~~	~~0.73376~~	~~0.03295~~	~~0.05209~~	~~0.00085~~	~~1664~~	~~91~~	~~559~~	~~19~~	~~327~~	~~5~~	~~70.9~~
ADT6-16	0.87	0.05657	0.0012	0.5145	0.01144	0.06595	0.00094	475	26	421	8	412	6	2.2
ADT6-17	0.4	0.0582	0.00089	0.46884	0.00803	0.05841	0.0008	537	17	390	6	366	5	6.6
ADT6-18	0.58	0.05425	0.00128	0.4538	0.01117	0.06066	0.00086	381	31	380	8	380	5	0
ADT6-19	0.57	0.05433	0.00096	0.45702	0.00879	0.06099	0.00084	385	21	382	6	382	5	0
ADT6-20	0.65	0.05415	0.00113	0.44929	0.0099	0.06017	0.00085	377	26	377	7	377	5	0
ADT6-21	0.7	0.05445	0.00169	0.45751	0.01434	0.06093	0.00092	390	43	383	10	381	6	0.5
ADT6-22	0.64	0.05662	0.00131	0.48472	0.01164	0.06208	0.00089	477	29	401	8	388	5	3.4
ADT6-23	0.8	0.05404	0.00107	0.43611	0.00918	0.05852	0.00082	373	24	368	6	367	5	0.3
ADT6-24	0.65	0.05422	0.00146	0.45858	0.01264	0.06133	0.0009	380	36	383	9	384	5	-0.3
ADT6-25	0.54	0.05417	0.0017	0.45468	0.01448	0.06087	0.00091	378	45	381	10	381	6	0
ADT6-26	0.72	0.05716	0.00147	0.49437	0.01302	0.06271	0.00092	498	33	408	9	392	6	4.1
~~ADT6-27~~	~~0.58~~	~~0.07154~~	~~0.00302~~	~~0.54725~~	~~0.02162~~	~~0.05548~~	~~0.00082~~	~~973~~	~~88~~	~~443~~	~~14~~	~~348~~	~~5~~	~~27.3~~
ADT6-28	0.73	0.05448	0.00127	0.46019	0.01117	0.06125	0.00088	391	30	384	8	383	5	0.3
~~ADT6-29~~	~~0.93~~	~~0.05894~~	~~0.00105~~	~~0.32513~~	~~0.00628~~	~~0.04~~	~~0.00055~~	~~565~~	~~20~~	~~286~~	~~5~~	~~253~~	~~3~~	~~13~~
ADT6-30	1	0.05552	0.00106	0.48087	0.00978	0.0628	0.00088	433	22	399	7	393	5	1.5
ADT6-31	0.39	0.05626	0.00107	0.54075	0.01095	0.0697	0.00098	463	22	439	7	434	6	1.2
ADT6-32	0.53	0.05404	0.00204	0.44666	0.01688	0.05993	0.00093	373	57	375	12	375	6	0
ADT6-33	0.61	0.05465	0.00161	0.45182	0.01362	0.05994	0.00087	398	42	379	10	375	5	1.1
ADT6-34	0.55	0.05449	0.00171	0.45274	0.01446	0.06025	0.00088	391	46	379	10	377	5	0.5

~~ADT6-35~~	~~0.52~~	~~0.07372~~	~~0.00218~~	~~0.5135~~	~~0.01536~~	~~0.05051~~	~~0.00077~~	~~1034~~	~~36~~	~~421~~	~~10~~	~~318~~	~~5~~	~~32.4~~
~~ADT6-36~~	~~0.64~~	~~0.06843~~	~~0.00314~~	~~0.50357~~	~~0.02179~~	~~0.05337~~	~~0.00082~~	~~882~~	~~97~~	~~414~~	~~15~~	~~335~~	~~5~~	~~23.6~~
ADT6-37	0.58	0.05416	0.00154	0.44852	0.01307	0.06005	0.00087	378	40	376	9	376	5	0
~~ADT6-38~~	~~0.68~~	~~0.06168~~	~~0.00137~~	~~0.50807~~	~~0.01178~~	~~0.05973~~	~~0.00085~~	~~663~~	~~27~~	~~417~~	~~8~~	~~374~~	~~5~~	~~11.5~~
ADT6-39	0.51	0.0542	0.00119	0.44716	0.01031	0.05982	0.00084	379	28	375	7	375	5	0
ADT6-40	0.54	0.05542	0.00236	0.4494	0.01799	0.05881	0.00086	429	97	377	13	368	5	2.4
ADT6-41	0.55	0.05438	0.00154	0.45896	0.01324	0.0612	0.0009	387	39	384	9	383	5	0.3
ADT6-42	0.56	0.05438	0.00146	0.45787	0.01254	0.06105	0.00089	387	36	383	9	382	5	0.3
ADT6-43	0.52	0.05572	0.00164	0.48779	0.0146	0.06348	0.00094	441	41	403	10	397	6	1.5
~~ADT6-44~~	~~1.33~~	~~0.05739~~	~~0.00342~~	~~0.31963~~	~~0.0188~~	~~0.04039~~	~~0.00075~~	~~507~~	~~97~~	~~282~~	~~14~~	~~255~~	~~5~~	~~10.6~~
ADT6-45	0.62	0.11501	0.00182	5.42898	0.09517	0.34228	0.00473	1880	15	1889	15	1898	23	-0.9
ADT6-46	0.49	0.05659	0.0029	0.49676	0.02531	0.06365	0.00108	476	83	410	17	398	7	3
ADT6-47	0.62	0.05598	0.00119	0.50726	0.01131	0.06571	0.00093	452	26	417	8	410	6	1.7
ADT6-48	0.63	0.05435	0.00145	0.45935	0.01255	0.06129	0.00089	386	36	384	9	383	5	0.3
ADT6-49	0.41	0.05763	0.0013	0.3915	0.00922	0.04926	0.0007	516	28	335	7	310	4	8.1
ADT6-50	0.41	0.0536	0.00102	0.45371	0.00924	0.06138	0.00086	354	23	380	6	384	5	-1
ADT6-51	0.82	0.05418	0.00132	0.44617	0.01121	0.05971	0.00086	379	31	375	8	374	5	0.3
ADT6-52	0.61	0.05487	0.00109	0.47044	0.00993	0.06217	0.00087	407	24	391	7	389	5	0.5
ADT6-53	0.61	0.05384	0.0012	0.44104	0.01024	0.0594	0.00085	364	28	371	7	372	5	-0.3
ADT6-54	0.6	0.05434	0.00177	0.45615	0.01497	0.06086	0.00092	385	47	382	10	381	6	0.3
~~ADT6-55~~	~~1~~	~~0.07095~~	~~0.00633~~	~~0.40894~~	~~0.03576~~	~~0.04181~~	~~0.00074~~	~~956~~	~~189~~	~~348~~	~~26~~	~~264~~	~~5~~	~~31.8~~
ADT6-56	0.53	0.05443	0.00187	0.45576	0.01573	0.06072	0.00093	389	50	381	11	380	6	0.3
ADT6-57	0.56	0.05432	0.00206	0.44838	0.01708	0.05986	0.00092	384	58	376	12	375	6	0.3
~~ADT6-58~~	~~0.7~~	~~0.06431~~	~~0.00263~~	~~0.39382~~	~~0.01609~~	~~0.04441~~	~~0.0007~~	~~752~~	~~60~~	~~337~~	~~12~~	~~280~~	~~4~~	~~20.4~~
ADT6-59	0.69	0.05438	0.00134	0.45673	0.01161	0.0609	0.00087	387	32	382	8	381	5	0.3
ADT6-60	0.54	0.05425	0.00193	0.4472	0.01601	0.05977	0.00091	381	53	375	11	374	6	0.3
ADT6-61	0.57	0.05456	0.0014	0.46349	0.01216	0.0616	0.0009	394	33	387	8	385	5	0.5
~~ADT6-62~~	~~0.89~~	~~0.06807~~	~~0.00159~~	~~0.53275~~	~~0.01288~~	~~0.05675~~	~~0.00082~~	~~871~~	~~27~~	~~434~~	~~9~~	~~356~~	~~5~~	~~21.9~~

ADT6-63	0.99	0.0541	0.00211	0.44001	0.01713	0.05897	0.00093	375	59	370	12	369	6	0.3
ADT6-64	0.82	0.05696	0.00341	0.42964	0.02486	0.0547	0.00085	490	136	363	18	343	5	5.8
ADT6-65	0.54	0.05413	0.00159	0.44112	0.01317	0.05909	0.00087	376	41	371	9	370	5	0.3
ADT6-66	0.6	0.05435	0.00143	0.46697	0.0126	0.06231	0.00091	386	35	389	9	390	6	-0.3
ADT6-67	0.61	0.05687	0.00132	0.46437	0.01113	0.05921	0.00085	486	29	387	8	371	5	4.3
ADT6-68	0.6	0.05411	0.0016	0.44448	0.01335	0.05956	0.00088	376	41	373	9	373	5	0
ADT6-69	0.7	0.05159	0.00108	0.24943	0.0055	0.03506	0.00049	267	26	226	4	222	3	1.8
ADT6-70	0.53	0.04893	0.00481	0.24146	0.02342	0.03579	0.00058	144	220	220	19	227	4	-3.1
ADT6-71	0.47	0.05416	0.00125	0.45397	0.01087	0.06078	0.00087	378	29	380	8	380	5	0
ADT6-72	0.76	0.05427	0.00148	0.46149	0.01289	0.06166	0.0009	382	37	385	9	386	5	-0.3
ADT6-73	0.14	0.05575	0.001	0.53912	0.01038	0.07012	0.00097	442	21	438	7	437	6	0.2
ADT6-74	0.55	0.05435	0.00136	0.45688	0.01175	0.06096	0.00088	386	33	382	8	381	5	0.3
ADT6-75	0.74	0.06004	0.00164	0.48589	0.01356	0.05868	0.00086	605	36	402	9	368	5	9.2
ADT6-76	0.56	0.05338	0.00282	0.43023	0.02179	0.05846	0.00088	345	123	363	15	366	5	-0.8
ADT6-77	0.46	0.0557	0.00162	0.4798	0.01412	0.06246	0.00093	440	39	398	10	391	6	1.8
ADT6-78	0.71	0.0541	0.00159	0.4413	0.01309	0.05915	0.00089	375	40	371	9	370	5	0.3
ADT6-79	0.56	0.05064	0.00115	0.24958	0.00589	0.03574	0.00051	224	29	226	5	226	3	0
ADT6-80	0.81	0.05608	0.00145	0.44802	0.01186	0.05792	0.00084	456	34	376	8	363	5	3.6
~~ADT6-81~~	~~0.5~~	~~0.04605~~	~~0.00573~~	~~0.37134~~	~~0.04584~~	~~0.05849~~	~~0.00097~~		~~238~~	~~321~~	~~34~~	~~366~~	~~6~~	~~-12.3~~
~~ADT6-82~~	~~0.62~~	~~0.06172~~	~~0.00113~~	~~0.49906~~	~~0.00979~~	~~0.05863~~	~~0.00082~~	~~664~~	~~20~~	~~411~~	~~7~~	~~367~~	~~5~~	~~12~~
ADT6-83	0.61	0.05407	0.00133	0.4512	0.01137	0.06051	0.00088	374	31	378	8	379	5	-0.3
ADT6-84	0.67	0.05467	0.00144	0.45985	0.01238	0.06099	0.00089	399	35	384	9	382	5	0.5
ADT6-85	0.54	0.05666	0.00118	0.44864	0.00976	0.05742	0.00081	478	25	376	7	360	5	4.4
ADT6-86	0.55	0.0565	0.0012	0.57806	0.01283	0.07419	0.00105	472	26	463	8	461	6	0.4
~~ADT6-87~~	~~0.71~~	~~0.07467~~	~~0.00408~~	~~0.55184~~	~~0.02879~~	~~0.0536~~	~~0.00086~~	~~1060~~	~~113~~	~~446~~	~~19~~	~~337~~	~~5~~	~~32.3~~
ADT6-88	0.59	0.05702	0.00141	0.47602	0.0121	0.06053	0.00088	492	31	395	8	379	5	4.2
ADT6-89	0.74	0.05413	0.00171	0.41402	0.01324	0.05546	0.00083	376	45	352	10	348	5	1.1
ADT6-90	0.47	0.05408	0.00155	0.4493	0.01308	0.06024	0.00089	374	39	377	9	377	5	0

ADT6-91	0.75	0.05443	0.00153	0.44522	0.01273	0.05932	0.00087	389	38	374	9	371	5	0.8
ADT6-92	0.96	0.05827	0.00135	0.48892	0.01168	0.06084	0.00088	540	28	404	8	381	5	6
ADT6-93	0.36	0.05408	0.00131	0.44257	0.01107	0.05934	0.00085	374	31	372	8	372	5	0
ADT6-94	0.54	0.05421	0.00191	0.43926	0.01551	0.05876	0.0009	380	52	370	11	368	5	0.5
~~ADT6-95~~	~~0.58~~	~~0.06196~~	~~0.00164~~	~~0.44187~~	~~0.01187~~	~~0.05171~~	~~0.00077~~	~~673~~	~~33~~	~~372~~	~~8~~	~~325~~	~~5~~	~~14.5~~
ADT6-96	0.66	0.05432	0.00206	0.46275	0.01764	0.06177	0.00094	384	58	386	12	386	6	0
ADT6-97	0.83	0.05469	0.00118	0.43841	0.00987	0.05812	0.00083	400	26	369	7	364	5	1.4
~~ADT6-98~~	~~0.47~~	~~0.16614~~	~~0.00323~~	~~0.88079~~	~~0.01792~~	~~0.03844~~	~~0.00055~~	~~2519~~	~~17~~	~~641~~	~~10~~	~~243~~	~~3~~	~~164~~
ADT6-99	0.88	0.14146	0.00285	7.64916	0.1611	0.39209	0.0057	2245	18	2191	19	2133	26	5.3
ADT6-100	0.68	0.05455	0.00144	0.45723	0.01233	0.06078	0.00089	394	35	382	9	380	5	0.5
ADT3														
ADT3-01	0.53	0.05966	0.00198	0.47722	0.01573	0.058	0.0009	591	45	396	11	363	5	9.1
ADT3-02	0.64	0.05487	0.00183	0.4417	0.01464	0.05836	0.00089	407	47	371	10	366	5	1.4
ADT3-03	0.85	0.05315	0.00158	0.42007	0.01246	0.05731	0.00086	335	40	356	9	359	5	-0.8
ADT3-04	0.52	0.05558	0.00138	0.43433	0.01083	0.05666	0.00083	436	30	366	8	355	5	3.1
ADT3-05	0.59	0.05409	0.00161	0.42137	0.01251	0.05648	0.00085	375	40	357	9	354	5	0.8
ADT3-06	0.55	0.05498	0.0029	0.43721	0.02208	0.05767	0.00089	411	121	368	16	361	5	1.9
ADT3-07	0.48	0.05363	0.00168	0.42039	0.01312	0.05683	0.00086	356	43	356	9	356	5	0
ADT3-08	0.93	0.05637	0.00153	0.42075	0.01145	0.05411	0.00081	467	34	357	8	340	5	5
ADT3-09	0.49	0.05347	0.00145	0.41171	0.01115	0.05582	0.00083	349	35	350	8	350	5	0
ADT3-10	0.46	0.05331	0.00273	0.42006	0.02126	0.05713	0.00096	342	84	356	15	358	6	-0.6
ADT3-11	0.56	0.05394	0.00166	0.40571	0.01243	0.05453	0.00082	369	42	346	9	342	5	1.2
ADT3-12	0.69	0.05829	0.0016	0.45174	0.01239	0.05619	0.00084	541	34	378	9	352	5	7.4
ADT3-13	0.59	0.05414	0.0019	0.4242	0.01477	0.05681	0.00089	377	50	359	11	356	5	0.8
ADT3-14	0.4	0.05305	0.00167	0.40489	0.01265	0.05533	0.00085	331	43	345	9	347	5	-0.6
ADT3-15	0.59	0.05349	0.00196	0.41649	0.01513	0.05645	0.00088	350	54	354	11	354	5	0
ADT3-16	0.62	0.0535	0.00198	0.41405	0.01515	0.05611	0.00088	350	54	352	11	352	5	0

ADT3-17	0.54	0.05386	0.00161	0.41392	0.01228	0.05571	0.00084	365	40	352	9	349	5	0.9
ADT3-18	1.11	0.05502	0.00149	0.41832	0.01126	0.05512	0.00082	413	34	355	8	346	5	2.6
ADT3-19	0.65	0.05523	0.00135	0.44855	0.01144	0.05888	0.00087	422	32	376	8	369	5	1.9
ADT3-20	0.7	0.05437	0.00132	0.42948	0.01091	0.05726	0.00084	386	32	363	8	359	5	1.1
ADT3-21	0.78	0.05286	0.00192	0.26027	0.00957	0.03569	0.00055	323	55	235	8	226	3	4
ADT3-22	0.59	0.0564	0.00165	0.46925	0.01415	0.06032	0.00089	468	41	391	10	378	5	3.4
ADT3-23	0.78	0.05463	0.00124	0.44914	0.01077	0.0596	0.00086	397	29	377	8	373	5	1.1
ADT3-24	0.61	0.05427	0.00161	0.43645	0.0133	0.0583	0.00087	382	42	368	9	365	5	0.8
ADT3-25	0.69	0.05666	0.00154	0.46527	0.01313	0.05953	0.00088	478	37	388	9	373	5	4
ADT3-26	0.62	0.05639	0.00194	0.45885	0.01601	0.05899	0.00091	468	50	383	11	369	6	3.8
ADT3-27	0.52	0.05565	0.00145	0.44186	0.01199	0.05756	0.00085	438	35	372	8	361	5	3
ADT3-28	0.55	0.05492	0.00202	0.43634	0.01627	0.05759	0.00088	409	56	368	12	361	5	1.9
ADT3-29	0.55	0.05413	0.00162	0.44058	0.01349	0.05901	0.00089	376	42	371	10	370	5	0.3
ADT3-30	0.49	0.05501	0.00176	0.43676	0.01426	0.05756	0.00087	413	46	368	10	361	5	1.9
ADT3-31	0.68	0.05601	0.0016	0.44645	0.01311	0.05778	0.00087	453	39	375	9	362	5	3.6
ADT3-32	0.63	0.05452	0.00161	0.44331	0.01344	0.05895	0.00088	393	42	373	9	369	5	1.1
ADT3-33	0.73	0.0602	0.00274	0.50575	0.02175	0.06093	0.00092	611	101	416	15	381	6	9.2
ADT3-34	0.67	0.05606	0.0031	0.44958	0.02384	0.05816	0.00092	455	126	377	17	364	6	3.6
ADT3-35	0.46	0.05399	0.00282	0.44269	0.02312	0.05945	0.00097	371	88	372	16	372	6	0
ADT3-36	0.51	0.05456	0.00158	0.44762	0.01327	0.05948	0.00089	394	40	376	9	372	5	1.1
ADT3-37	0.75	0.0543	0.00204	0.45033	0.01711	0.06013	0.00093	384	57	378	12	376	6	0.5
ADT3-38	0.59	0.05543	0.00118	0.44497	0.01005	0.0582	0.00084	430	26	374	7	365	5	2.5
ADT3-39	0.59	0.05666	0.00255	0.45987	0.01948	0.05887	0.00089	478	102	384	14	369	5	4.1
ADT3-40	0.8	0.05426	0.00439	0.44773	0.03599	0.05982	0.00113	382	148	376	25	375	7	0.3
ADT3-41	0.76	0.05405	0.00168	0.44233	0.01404	0.05934	0.00089	373	45	372	10	372	5	0
ADT3-42	0.66	0.05727	0.00116	0.46263	0.01007	0.05857	0.00084	502	24	386	7	367	5	5.2
ADT3-43	0.74	0.05422	0.00199	0.45728	0.01701	0.06115	0.00094	380	56	382	12	383	6	-0.3
ADT3-44	0.74	0.05417	0.00162	0.43166	0.01318	0.05778	0.00087	378	42	364	9	362	5	0.6

ADT3-45	0.64	0.05799	0.00131	0.46038	0.01098	0.05756	0.00084	529	28	385	8	361	5	6.6
ADT3-46	0.8	0.06005	0.00315	0.47655	0.02389	0.05756	0.0009	605	117	396	16	361	5	9.7
ADT3-47	0.6	0.05484	0.00129	0.45302	0.01115	0.0599	0.00087	406	30	379	8	375	5	1.1
ADT3-48	0.58	0.05515	0.00164	0.44912	0.01368	0.05905	0.00088	418	42	377	10	370	5	1.9
ADT3-49	0.68	0.05595	0.00107	0.45729	0.00946	0.05926	0.00084	450	23	382	7	371	5	3
ADT3-50	0.57	0.05409	0.00259	0.42945	0.0206	0.05757	0.00092	375	79	363	15	361	6	0.6
ADT3-51	0.66	0.05619	0.00142	0.4536	0.01185	0.05854	0.00086	460	33	380	8	367	5	3.5
ADT3-52	0.61	0.05619	0.00288	0.44019	0.02151	0.05681	0.00089	460	117	370	15	356	5	3.9
ADT3-53	0.61	0.054	0.00142	0.43883	0.01187	0.05893	0.00088	371	35	369	8	369	5	0
ADT3-54	0.77	0.05568	0.00143	0.44585	0.01185	0.05806	0.00086	440	34	374	8	364	5	2.7
ADT3-55	0.5	0.05388	0.00187	0.42948	0.01511	0.0578	0.00088	366	52	363	11	362	5	0.3
ADT3-56	0.63	0.05387	0.00172	0.43607	0.01411	0.0587	0.0009	366	45	367	10	368	5	-0.3
ADT3-57	0.51	0.05487	0.00174	0.43452	0.01401	0.05743	0.00086	407	45	366	10	360	5	1.7
ADT3-58	0.46	0.05464	0.00148	0.43174	0.01199	0.0573	0.00085	398	36	364	9	359	5	1.4
ADT3-59	0.58	0.05442	0.00264	0.43312	0.02101	0.05771	0.00093	388	80	365	15	362	6	0.8
ADT3-60	0.64	0.05402	0.00214	0.43319	0.01732	0.05815	0.0009	372	62	365	12	364	5	0.3
~~ADT3-61~~	~~0.93~~	~~0.07136~~	~~0.00169~~	~~0.56468~~	~~0.01391~~	~~0.05738~~	~~0.00084~~	~~968~~	~~27~~	~~455~~	~~9~~	~~360~~	~~5~~	~~26.4~~
ADT3-62	0.69	0.05473	0.00162	0.44004	0.01327	0.0583	0.00087	401	41	370	9	365	5	1.4
ADT3-63	0.71	0.05478	0.00141	0.4306	0.01145	0.057	0.00083	403	34	364	8	357	5	2
ADT3-64	0.41	0.05454	0.00274	0.45273	0.02274	0.06019	0.001	393	83	379	16	377	6	0.5
ADT3-65	0.63	0.05715	0.00347	0.46496	0.0272	0.05901	0.00096	497	138	388	19	370	6	4.9
ADT3-66	0.53	0.05529	0.00156	0.43647	0.01261	0.05725	0.00085	424	38	368	9	359	5	2.5
ADT3-67	0.58	0.05355	0.00218	0.43687	0.01787	0.05916	0.00093	352	64	368	13	371	6	-0.8
ADT3-68	0.52	0.05401	0.00187	0.43998	0.01544	0.05908	0.0009	371	52	370	11	370	5	0
ADT3-69	0.58	0.0582	0.0034	0.46993	0.02639	0.05856	0.00094	537	131	391	18	367	6	6.5
ADT3-70	0.53	0.05352	0.00157	0.42342	0.01269	0.05738	0.00085	351	41	358	9	360	5	-0.6
ADT3-71	0.55	0.05693	0.00163	0.45674	0.0134	0.05818	0.00087	489	39	382	9	365	5	4.7
ADT3-72	1	0.05434	0.00168	0.44147	0.01383	0.05891	0.00089	385	43	371	10	369	5	0.5

ADT3-73	0.57	0.0542	0.00153	0.42995	0.01242	0.05753	0.00085	379	39	363	9	361	5	0.6
ADT3-74	0.53	0.05385	0.00152	0.43273	0.0125	0.05827	0.00086	365	39	365	9	365	5	0
ADT3-75	0.49	0.05358	0.00164	0.41613	0.01294	0.05632	0.00084	353	44	353	9	353	5	0
ADT3-76	0.69	0.05354	0.00208	0.42863	0.01676	0.05805	0.0009	352	60	362	12	364	5	-0.5
ADT3-77	0.65	0.05391	0.00192	0.4311	0.01546	0.058	0.00089	367	53	364	11	363	5	0.3
ADT3-78	0.58	0.05442	0.00204	0.43406	0.01638	0.05785	0.0009	388	57	366	12	363	5	0.8
ADT3-79	0.42	0.05436	0.00264	0.43518	0.02116	0.05805	0.00093	386	80	367	15	364	6	0.8
ADT3-80	0.78	0.05424	0.00143	0.43171	0.01171	0.05772	0.00084	381	35	364	8	362	5	0.6
ADT3-81	0.67	0.05428	0.00137	0.45304	0.01182	0.06053	0.00088	383	33	379	8	379	5	0
ADT3-82	0.63	0.05682	0.00352	0.4494	0.02688	0.05736	0.00094	484	141	377	19	360	6	4.7
ADT3-83	0.47	0.05429	0.00153	0.42158	0.01217	0.05631	0.00083	383	39	357	9	353	5	1.1
ADT3-84	0.46	0.05435	0.0022	0.4383	0.01783	0.05848	0.00091	386	63	369	13	366	6	0.8
ADT3-85	0.69	0.05396	0.00151	0.42298	0.01207	0.05684	0.00084	369	38	358	9	356	5	0.6
ADT3-86	0.8	0.05967	0.00152	0.47611	0.01246	0.05787	0.00085	592	32	395	9	363	5	8.8
ADT3-87	0.71	0.05447	0.00157	0.42666	0.01256	0.05681	0.00085	391	40	361	9	356	5	1.4
~~ADT3-88~~	~~0.77~~	~~0.0633~~	~~0.00165~~	~~0.4933~~	~~0.01322~~	~~0.05652~~	~~0.00083~~	~~718~~	~~33~~	~~407~~	~~9~~	~~354~~	~~5~~	~~15~~
ADT3-89	0.7	0.05764	0.00128	0.46353	0.01077	0.05832	0.00084	516	27	387	7	365	5	6
ADT3-90	0.6	0.05354	0.00257	0.42792	0.02047	0.05797	0.00096	352	78	362	15	363	6	-0.3
ADT3-91	0.57	0.05458	0.00162	0.44309	0.01332	0.05887	0.00088	395	41	372	9	369	5	0.8
ADT3-92	0.44	0.0559	0.00142	0.44013	0.01148	0.0571	0.00083	448	33	370	8	358	5	3.4
ADT3-93	0.63	0.0541	0.00172	0.43879	0.01409	0.05882	0.00089	375	45	369	10	368	5	0.3
ADT3-94	0.46	0.05426	0.00266	0.44291	0.0216	0.0592	0.00098	382	80	372	15	371	6	0.3
ADT3-95	0.55	0.05433	0.00198	0.42445	0.01554	0.05666	0.00087	385	55	359	11	355	5	1.1
ADT3-96	0.5	0.05466	0.00124	0.43842	0.01036	0.05817	0.00084	398	28	369	7	364	5	1.4
ADT3-97	0.39	0.06004	0.00276	0.51241	0.02354	0.06189	0.00098	605	72	420	16	387	6	8.5
ADT3-98	0.53	0.05649	0.00164	0.45032	0.0133	0.05781	0.00086	472	39	378	9	362	5	4.4
ADT3-99	0.6	0.05368	0.00213	0.42533	0.0169	0.05746	0.0009	358	61	360	12	360	5	0
ADT3-100	0.62	0.05539	0.00183	0.45804	0.01526	0.05997	0.00092	428	47	383	11	375	6	2.1

Appendix to Chapter 3.1

SUPPLEMENTAL ITEM 1: Description of zircon separation and LA-ICP-MS U–Pb dating of zircon

Detrital heavy minerals were separated following standard procedures (e.g. Liu et al., 2013). A quantity of zircon grains (generally more than 200) were randomly selected, enclosed in epoxy resin and polished to yield a smooth flat internal surface (slice). After being photographed under reflected and transmitted light, the samples were prepared for cathodoluminescence (CL) imaging in order to choose potential internal target sites for U-Pb dating (e.g. Liu et al., 2013; Yang et al., 2013). CL imaging was carried out using a Quanta 200 FEG Scanning Electron Microscope at the SEEC lab, in the School of Earth and Space Science at Peking University. The U-Pb dating was performed on an Agilent 7500a ICP-MS connected to a 193 nm Excimer laser ablation system of American New Wave UP 193 SS at the China University of Geosciences, Beijing, following the method described by Yang et al. (2013). The operating parameters were as follows: Ar plasma gas flow rate was 1.13 l/min, radio frequency (RF) power was 1350 W and elemental integral time was 10 ms for Si and Zr and 50 ms for other elements. Helium with a flow rate of 0.89 l/min was used as the carrier gas to enhance the transport efficiency of the ablated material. The spot diameter was 36 μm with an analytical laser frequency of 10 Hz. Each analysis consisted of 5 s pre-denudation and 45 s signal acquisition. The Glitter 4.4.1 software was used to calculate the U/Pb isotope ratios and element contents. Age calculations, plotting of relative probability and concordia diagrams were made using ISOPLOT (version 3.0) (Ludwig, 2003). Standard zircon TEMORA 1 was used as an external standard for correction of isotopic ratios to

calculate the U/Pb ages, while zircons Qinghu and 91500 were the monitoring standards. For elemental concentration analysis, NIST 610 was the external standard, and 29Si was the internal standard (Wiedenbeck et al., 1995; Black et al., 2003). Meanwhile, NIST 612 and NIST 614 were used as monitoring standards. The common Pb correction was performed following the method described by Andersen (2002). A detailed description of the technical procedure is given in Liu et al. (2013). For ICP-MS analyses, those ages with a discordance degree >10% were excluded from analysis (e.g. Gehrels et al., 2003; Yang et al., 2013).

REFERENCES CITED

Andersen, T., 2002, Correction of common lead in U–Pb analyses that do not report ^{204}Pb: Chemical Geology, v. 192, p. 59-79.

Black, L. P., Kamo, S. L., Allen, C. M., Aleinikoff, J. N., Davis, D. W., Korsch, R. J., and Foudoulis, C., 2003, TEMORA 1: a new zircon standard for Phanerozoic U–Pb geochronology: Chemical Geology, v. 200, no. 1–2, p. 155-170, doi: 10.1016/S0009-2541(03)00165-7.

Gehrels, G. E., Yin, A., and Wang, X. F., 2003, Detrital-zircon geochronology of the northeastern Tibetan plateau: Geological Society of America Bulletin, v. 115, no. 7, p. 881-896, doi: 10.1130/0016-7606(2003)115<0881:DGOTNT>2.0.CO;2.

Liu, D. D., Jolivet, M., Yang, W., Zhang, Z. Y., Feng, C., Zhu, B., and Guo, Z. J., 2013a, Latest Palaeozoic-Early Mesozoic basin-range interactions in South Tian Shan (Northwest China) and their tectonic significance: Constraints from detrital zircon U-Pb ages: Tectonophysics v. 599, 197-213, 10.1016/j.tecto.2013.04.018.

Ludwig, K.R., 2003, User's Manual for Isoplot/Ex, Version 3.00: A Geochronological Toolkit for Microsoft Excel: Berkeley Geochronology Center Special Publication 4, 77 p.

Wiedenbeck, M., Alle, P., Corfu, F., Griffin, W., Meier, M., Oberli, F., Quadt, A. v., Roddick, J., and Spiegel, W., 1995, Three natural zircon standards for U‐Th‐Pb, Lu‐Hf, trace element and REE analyses: Geostandards Newsletter, v. 19, no. 1, p. 1-23, doi: 10.1111/j.1751-908X.1995.tb00147.x.

Yang, W., Jolivet, M., Dupont‐Nivet, G., Guo, Z., Zhang, Z., and Wu, C., 2013, Source to sink relations between the Tian Shan and Junggar Basin (northwest China) from Late Palaeozoic to Quaternary: evidence from detrital U‐Pb zircon geochronology: Basin Research, v. 25, no. 2, p. 219-240, doi: 10.1111/j.1365-2117.2012.00558.x.

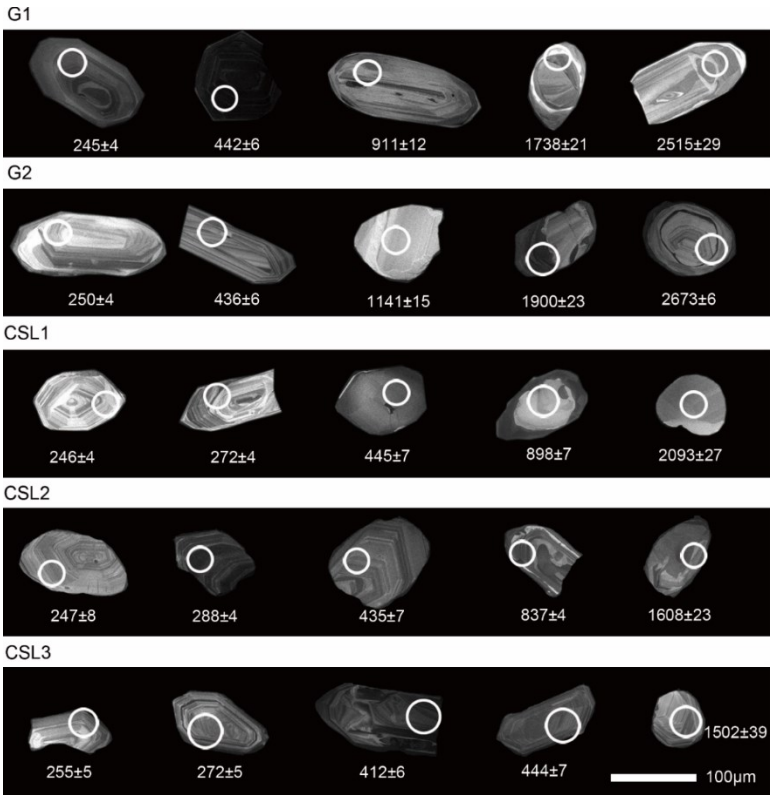

Figure DR1. Representative CL images of zircons from the five sandstone samples. The white circles show the locations of the U-Pb analysis. Numbers are U-Pb ages in Ma.

Table DR1. LA-ICP-MS U-Pb data of detrital zircons from the five sandstone samples.

Analysis number	Th/U	Isotopic ratios and errors						Ages and errors (Ma)						Disc.%
		$^{207}Pb/^{206}Pb$	1σ	$^{207}Pb/^{235}U$	1σ	$^{206}Pb/^{238}U$	1σ	$^{207}Pb/^{206}Pb$	1σ	$^{207}Pb/^{235}U$	1σ	$^{206}Pb/^{238}U$	1σ	
G1														
G1-01	0.63	0.0515	0.0033	0.24542	0.0158	0.03455	0.0007	263	113	223	13	219	4	1.8
G1-02	0.83	0.05187	0.0011	0.29852	0.0066	0.04173	0.0006	280	26	265	5	264	4	0.4
G1-03	1.02	0.10533	0.0019	4.38056	0.0838	0.30157	0.0044	1720	17	1709	16	1699	22	1.2
G1-04	0.56	0.05157	0.0017	0.30509	0.0099	0.0429	0.0007	266	47	270	8	271	4	-0.4
G1-05	1.29	0.05069	0.0018	0.24618	0.009	0.03522	0.0005	227	56	223	7	223	3	0
G1-06	0.83	0.0557	0.0019	0.54558	0.0186	0.07103	0.0011	440	48	442	12	442	7	0
G1-07	0.53	0.05508	0.0025	0.49104	0.0212	0.06465	0.001	416	105	406	14	404	6	0.5
G1-08	0.58	0.05718	0.002	0.63047	0.0218	0.07996	0.0013	498	48	496	14	496	8	0
G1-09	0.38	0.05482	0.0011	0.49534	0.0104	0.06552	0.0009	405	24	409	7	409	6	0
G1-10	0.18	0.1137	0.0026	4.85082	0.0883	0.30941	0.0043	1859	42	1794	15	1738	21	7
G1-11	0.92	0.05097	0.0016	0.26092	0.0081	0.03712	0.0006	239	44	235	7	235	3	0
G1-12	0.34	0.05153	0.0012	0.29683	0.0072	0.04177	0.0006	265	31	264	6	264	4	0
G1-13	0.9	0.05569	0.0014	0.53408	0.0141	0.06954	0.001	440	34	435	9	433	6	0.5
G1-14	0.47	0.14373	0.0021	8.10866	0.1333	0.4091	0.0057	2273	13	2243	15	2211	26	2.8
G1-15	0.45	0.16304	0.0023	9.76594	0.1598	0.43437	0.006	2487	12	2413	15	2325	27	7
G1-16	1.08	0.10442	0.0018	4.38305	0.081	0.30438	0.0044	1704	16	1709	15	1713	22	-0.5
G1-17	0.35	0.16566	0.0024	10.891	0.1808	0.47673	0.0066	2514	13	2514	15	2513	29	0
G1-18	0.52	0.08408	0.0013	2.38023	0.0417	0.20527	0.0029	1294	16	1237	13	1204	15	7.5
G1-19	0.16	0.17233	0.0026	11.3413	0.1917	0.47722	0.0067	2580	13	2552	16	2515	29	2.6
G1-20	0.81	0.05116	0.0017	0.27949	0.0095	0.03961	0.0006	248	51	250	8	250	4	0
G1-21	0.44	0.05066	0.0027	0.25517	0.0138	0.03652	0.0006	225	95	231	11	231	4	0
G1-22	0.52	0.11444	0.0017	5.28953	0.0881	0.33516	0.0046	1871	14	1867	14	1863	22	0.4

G1-23	0.57	0.05122	0.002	0.27755	0.011	0.0393	0.0006	251	62	249	9	248	4	0.4
G1-24	0.54	0.05526	0.0012	0.50941	0.0116	0.06684	0.001	423	27	418	8	417	6	0.2
G1-25	1.14	0.0547	0.0043	0.49384	0.038	0.06547	0.0014	400	136	408	26	409	8	-0.2
~~G1-26~~	0.68	~~0.14597~~	~~0.0042~~	~~6.33588~~	~~0.1552~~	~~0.3148~~	~~0.0047~~	~~2299~~	~~50~~	~~2023~~	~~21~~	~~1764~~	~~23~~	30.3
G1-27	0.8	0.05102	0.0028	0.27828	0.015	0.03955	0.0007	242	92	249	12	250	4	-0.4
G1-28	0.19	0.07063	0.0012	1.54431	0.0295	0.15856	0.0022	947	19	948	12	949	12	-0.1
G1-29	0.65	0.05084	0.0017	0.24375	0.0084	0.03476	0.0005	234	52	221	7	220	3	0.5
G1-30	0.45	0.05584	0.0013	0.5427	0.0128	0.07047	0.001	446	28	440	8	439	6	0.2
~~G1-31~~	0.9	~~0.15784~~	~~0.0024~~	~~8.87929~~	~~0.1531~~	~~0.40793~~	~~0.0058~~	~~2433~~	~~13~~	~~2326~~	~~16~~	~~2205~~	~~26~~	10.3
G1-32	0.85	0.05119	0.0018	0.27434	0.0099	0.03886	0.0006	249	54	246	8	246	4	0
G1-33	1	0.11312	0.0017	4.99015	0.0862	0.31988	0.0045	1850	14	1818	15	1789	22	3.4
G1-34	0.51	0.10895	0.0017	4.68899	0.0823	0.3121	0.0044	1782	15	1765	15	1751	22	1.8
G1-35	0.35	0.05151	0.0016	0.29349	0.0091	0.04132	0.0007	264	43	261	7	261	4	0
G1-36	0.71	0.05039	0.0031	0.2389	0.0145	0.03438	0.0007	213	105	218	12	218	4	0
G1-37	1.13	0.05252	0.0016	0.34415	0.0107	0.04752	0.0007	308	43	300	8	299	4	0.3
G1-38	0.45	0.08533	0.0015	2.8191	0.0532	0.23957	0.0034	1323	17	1361	14	1384	18	-4.4
G1-39	0.93	0.10591	0.0019	4.22105	0.0831	0.28902	0.0042	1730	17	1678	16	1637	21	5.7
G1-40	0.85	0.10884	0.0021	4.72962	0.0975	0.31511	0.0047	1780	18	1773	17	1766	23	0.8
G1-41	0.42	0.05491	0.001	0.50591	0.0102	0.06681	0.001	409	22	416	7	417	6	-0.2
G1-42	0.68	0.11445	0.0018	5.28829	0.0917	0.33507	0.0047	1871	14	1867	15	1863	23	0.4
G1-43	0.92	0.05653	0.001	0.59129	0.0118	0.07585	0.0011	473	21	472	8	471	6	0.2
G1-44	0.39	0.05515	0.0016	0.50229	0.0148	0.06605	0.001	418	39	413	10	412	6	0.2
G1-45	0.53	0.14585	0.0022	8.00285	0.1384	0.39788	0.0056	2298	14	2231	16	2159	26	6.4
~~G1-46~~	0.23	~~0.16008~~	~~0.0024~~	~~7.31502~~	~~0.1265~~	~~0.33136~~	~~0.0046~~	~~2457~~	~~13~~	~~2151~~	~~15~~	~~1845~~	~~22~~	33.2
G1-47	0.6	0.05206	0.0025	0.30914	0.0148	0.04306	0.0007	288	80	274	11	272	4	0.7
G1-48	0.41	0.05107	0.0014	0.277	0.0076	0.03933	0.0006	244	36	248	6	249	4	-0.4
G1-49	0.43	0.08344	0.0016	2.53296	0.0522	0.22014	0.0032	1280	20	1282	15	1283	17	-0.2
G1-50	0.5	0.06668	0.0012	1.24406	0.0245	0.1353	0.0019	828	20	821	11	818	11	0.4

G1-51	0.33	0.09204	0.0015	3.04097	0.0549	0.23957	0.0034	1468	16	1418	14	1384	18	6.1
G1-52	0.66	0.05189	0.0031	0.32212	0.0193	0.04501	0.0008	281	104	284	15	284	5	0
G1-53	0.62	0.05075	0.0021	0.25792	0.0109	0.03685	0.0006	229	68	233	9	233	4	0
G1-54	0.8	0.05077	0.0014	0.26328	0.0073	0.0376	0.0006	230	37	237	6	238	3	-0.4
G1-55	0.59	0.05153	0.0013	0.2961	0.0079	0.04167	0.0006	265	34	263	6	263	4	0
G1-56	1.41	0.05368	0.0012	0.37075	0.0089	0.05008	0.0007	358	29	320	7	315	4	1.6
G1-57	0.33	0.06898	0.0021	1.42189	0.0384	0.14951	0.0022	898	65	898	16	898	12	0
G1-58	0.64	0.05093	0.0012	0.25904	0.0064	0.03688	0.0005	238	31	234	5	233	3	0.4
G1-59	0.17	0.11423	0.0018	5.10596	0.0912	0.32414	0.0046	1868	15	1837	15	1810	22	3.2
G1-60	0.71	0.05077	0.0015	0.26541	0.0079	0.03791	0.0006	230	42	239	6	240	3	-0.4
~~G1-61~~	0.96	~~0.06652~~	~~0.0053~~	~~0.81213~~	~~0.0633~~	~~0.08855~~	~~0.0016~~	~~823~~	~~173~~	~~604~~	~~35~~	~~547~~	~~10~~	10.4
G1-62	0.37	0.0575	0.0011	0.63345	0.0129	0.07989	0.0011	511	22	498	8	495	7	0.6
G1-63	1.26	0.15045	0.0025	8.58319	0.159	0.41369	0.0059	2351	15	2295	17	2232	27	5.3
G1-64	0.65	0.05543	0.0014	0.49439	0.0127	0.06467	0.001	430	32	408	9	404	6	1
G1-65	0.4	0.05612	0.0011	0.5488	0.0118	0.07092	0.001	457	24	444	8	442	6	0.5
G1-66	0.21	0.07078	0.0012	1.48119	0.0277	0.15175	0.0022	951	18	923	11	911	12	1.3
G1-67	0.84	0.11869	0.0023	5.38012	0.1092	0.32871	0.0049	1937	17	1882	17	1832	24	5.7
G1-68	0.14	0.07213	0.0013	1.60154	0.0315	0.161	0.0023	990	19	971	12	962	13	0.9
~~G1-69~~	0.78	~~0.06946~~	~~0.0036~~	~~0.37967~~	~~0.0199~~	~~0.03964~~	~~0.0007~~	~~912~~	~~80~~	~~327~~	~~15~~	~~251~~	~~4~~	30.3
G1-70	0.51	0.05114	0.0014	0.27216	0.0076	0.03859	0.0006	247	37	244	6	244	4	0
G1-71	0.56	0.05472	0.002	0.49634	0.018	0.06578	0.0011	401	52	409	12	411	7	-0.5
G1-72	0.13	0.05626	0.0012	0.52365	0.0114	0.06749	0.001	463	25	428	8	421	6	1.7
G1-73	0.79	0.1766	0.003	11.6643	0.2187	0.47896	0.0069	2621	15	2578	18	2523	30	3.9
G1-74	0.47	0.05452	0.0021	0.47244	0.0179	0.06283	0.0011	393	55	393	12	393	6	0
G1-75	0.79	0.05071	0.0103	0.24626	0.0496	0.03521	0.0011	228	340	224	40	223	7	0.4
G1-76	0.54	0.05112	0.0014	0.27337	0.0078	0.03878	0.0006	246	38	245	6	245	4	0
G1-77	0.73	0.05537	0.0013	0.50816	0.0123	0.06655	0.001	427	29	417	8	415	6	0.5
G1-78	0.47	0.05527	0.0034	0.4982	0.0305	0.06537	0.0011	423	105	410	21	408	7	0.5

G1-79	0.35	0.05087	0.0017	0.25931	0.0086	0.03697	0.0006	235	48	234	7	234	4	0
G1-80	0.84	0.05531	0.0015	0.51813	0.0145	0.06793	0.001	425	36	424	10	424	6	0
G1-81	0.6	0.07042	0.0016	1.48552	0.0343	0.15298	0.0023	941	24	924	14	918	13	0.7
G1-82	1.51	0.05108	0.0015	0.26725	0.0081	0.03794	0.0006	244	42	240	6	240	4	0
G1-83	0.74	0.07602	0.002	1.85895	0.0499	0.17731	0.0028	1096	30	1067	18	1052	15	4.2
~~G1-84~~	0.58	~~0.07162~~	~~0.0015~~	~~1.08971~~	~~0.024~~	~~0.11033~~	~~0.0016~~	~~975~~	~~23~~	~~748~~	~~12~~	~~675~~	~~9~~	10.8
~~G1-85~~	1.19	~~0.0734~~	~~0.0023~~	~~0.32264~~	~~0.0103~~	~~0.03187~~	~~0.0005~~	~~1025~~	~~39~~	~~284~~	~~8~~	~~202~~	~~3~~	40.6
G1-86	0.46	0.15437	0.0027	9.35623	0.1809	0.4395	0.0063	2395	16	2374	18	2348	28	2
G1-87	0.65	0.05088	0.0036	0.25225	0.0178	0.03595	0.0007	235	127	228	14	228	4	0
G1-88	0.66	0.05795	0.0015	0.67309	0.0184	0.08422	0.0013	528	34	523	11	521	8	0.4
G1-89	0.41	0.11923	0.0022	5.46625	0.1079	0.33244	0.0048	1945	17	1895	17	1850	23	5.1
G1-90	0.63	0.05086	0.0022	0.25954	0.011	0.037	0.0006	234	68	234	9	234	4	0
G1-91	0.45	0.10806	0.0024	4.68482	0.1086	0.31437	0.0049	1767	21	1765	19	1762	24	0.3
G1-92	0.4	0.05481	0.0013	0.4883	0.0123	0.06461	0.001	404	31	404	8	404	6	0
G1-93	0.26	0.05167	0.0014	0.31416	0.0086	0.04409	0.0007	271	36	277	7	278	4	-0.4
G1-94	0.54	0.05132	0.004	0.27236	0.0209	0.03849	0.0006	255	180	245	17	243	4	0.8
G1-95	0.33	0.0555	0.0013	0.5231	0.013	0.06835	0.001	432	30	427	9	426	6	0.2
~~G1-96~~	0.62	~~0.06956~~	~~0.0039~~	~~0.28522~~	~~0.0153~~	~~0.02974~~	~~0.0005~~	~~915~~	~~119~~	~~255~~	~~12~~	~~189~~	~~3~~	34.9
G1-97	0.35	0.05547	0.0013	0.52505	0.0125	0.06864	0.001	431	28	429	8	428	6	0.2
~~G1-98~~	0.44	~~0.07538~~	~~0.003~~	~~1.09414~~	~~0.0398~~	~~0.10528~~	~~0.0016~~	~~1079~~	~~81~~	~~751~~	~~19~~	~~645~~	~~9~~	16.4
~~G1-99~~	0.71	~~0.09205~~	~~0.0018~~	~~2.61051~~	~~0.0534~~	~~0.20566~~	~~0.003~~	~~1468~~	~~19~~	~~1304~~	~~15~~	~~1206~~	~~16~~	21.7
~~G1-100~~	0.2	~~0.06036~~	~~0.0016~~	~~0.4407~~	~~0.0118~~	~~0.05295~~	~~0.0008~~	~~617~~	~~32~~	~~371~~	~~8~~	~~333~~	~~5~~	11.4
G2														
G2-01	0.84	0.05626	0.0014	0.5906	0.0155	0.07612	0.0012	463	32	471	10	473	7	-0.4
G2-02	0.53	0.05598	0.0017	0.57068	0.0179	0.07392	0.0012	452	41	458	12	460	7	-0.4
G2-03	0.42	0.09234	0.0024	3.23511	0.0882	0.25406	0.0041	1474	28	1466	21	1459	21	1
~~G2-04~~	~~0.78~~	~~0.08027~~	~~0.0024~~	~~0.81933~~	~~0.0246~~	~~0.07402~~	~~0.0012~~	~~1204~~	~~34~~	~~608~~	~~14~~	~~460~~	~~7~~	~~32.2~~
G2-05	0.6	0.05589	0.0017	0.56596	0.0174	0.07343	0.0012	448	40	455	11	457	7	-0.4

G2-06	1.26	0.12134	0.002	5.88373	0.1081	0.35162	0.005	1976	15	1959	16	1942	24	1.8
G2-07	0.38	0.17154	0.0027	11.0958	0.1987	0.46906	0.0065	2573	14	2531	17	2479	29	3.8
G2-08	0.55	0.1031	0.0019	4.13918	0.0816	0.29112	0.0042	1681	17	1662	16	1647	21	2.1
G2-09	0.68	0.18964	0.0032	13.5033	0.2492	0.51634	0.0074	2739	14	2716	17	2684	31	2
G2-10	0.16	0.12279	0.0021	6.02188	0.1127	0.35564	0.0051	1997	16	1979	16	1961	24	1.8
G2-11	0.31	0.11343	0.0019	5.23371	0.0951	0.33459	0.0047	1855	15	1858	15	1861	23	-0.3
G2-12	0.52	0.056	0.0017	0.56248	0.0177	0.07284	0.0011	452	42	453	11	453	7	0
G2-13	0.55	0.17143	0.0028	11.1497	0.2028	0.47165	0.0066	2572	14	2536	17	2491	29	3.3
G2-14	0.75	0.0909	0.002	2.92728	0.0669	0.23354	0.0035	1445	22	1389	17	1353	18	6.8
G2-15	0.3	0.05808	0.0034	0.68658	0.0403	0.08572	0.0016	533	96	531	24	530	9	0.2
G2-16	0.51	0.13659	0.0023	7.40382	0.1397	0.39307	0.0056	2184	15	2161	17	2137	26	2.2
G2-17	0.66	0.18589	0.0032	12.9027	0.2447	0.50333	0.0073	2706	15	2673	18	2628	31	3
G2-18	0.37	0.17399	0.0029	11.5864	0.2137	0.48289	0.0068	2596	14	2572	17	2540	30	2.2
G2-19	0.46	0.05651	0.002	0.54624	0.0193	0.0701	0.0011	472	51	443	13	437	7	1.4
G2-20	0.71	0.05565	0.0012	0.53938	0.0122	0.07028	0.001	438	26	438	8	438	6	0
G2-21	0.45	0.08983	0.0016	3.19892	0.0622	0.25825	0.0037	1422	18	1457	15	1481	19	-4
G2-22	0.49	0.16659	0.0028	10.883	0.2013	0.47373	0.0067	2524	15	2513	17	2500	29	1
G2-23	1.05	0.11376	0.0019	5.01273	0.0945	0.31954	0.0045	1860	16	1821	16	1787	22	4.1
G2-24	0.73	0.05594	0.0016	0.55434	0.0159	0.07186	0.0011	450	37	448	10	447	7	0.2
G2-25	1.56	0.05652	0.0012	0.57131	0.0127	0.07329	0.0011	473	25	459	8	456	6	0.7
G2-26	0.42	0.07846	0.0019	2.0931	0.0526	0.19346	0.0029	1159	27	1147	17	1140	16	1.7
G2-27	0.16	0.07979	0.0017	2.12992	0.0471	0.19358	0.0028	1192	22	1159	15	1141	15	4.5
G2-28	0.58	0.10339	0.0018	4.10674	0.0791	0.28803	0.0041	1686	17	1656	16	1632	21	3.3
G2-29	0.61	0.0562	0.0011	0.53945	0.0117	0.06961	0.001	460	24	438	8	434	6	0.9
G2-30	0.69	0.0563	0.0011	0.55476	0.0117	0.07145	0.001	464	23	448	8	445	6	0.7
G2-31	0.61	0.05661	0.0012	0.55822	0.0129	0.0715	0.0011	476	27	450	8	445	6	1.1
G2-32	~~0.68~~	0.0563	0.0011	0.57298	0.0117	0.0738	0.0011	~~464~~	~~22~~	~~460~~	~~8~~	~~459~~	~~6~~	~~0.2~~
G2-33	0.96	0.10738	0.0021	4.23401	0.0887	0.28592	0.0042	1755	19	1681	17	1621	21	8.3

G2-34	0.32	0.05543	0.0018	0.5344	0.0179	0.06991	0.0011	430	47	435	12	436	7	-0.2
G2-35	0.32	0.16319	0.0041	10.3325	0.2134	0.45921	0.0066	2489	43	2465	19	2436	29	2.2
G2-36	0.10	0.07019	0.0013	1.4545	0.0291	0.15026	0.0022	934	20	912	12	902	12	1.1
G2-37	0.75	0.05645	0.0014	0.54389	0.0143	0.06986	0.001	470	33	441	9	435	6	1.4
G2-38	0.62	0.05555	0.0012	0.5357	0.0125	0.06994	0.001	434	27	436	8	436	6	0
G2-39	0.12	0.12994	0.0022	6.44196	0.1223	0.3595	0.0051	2097	16	2038	17	1980	24	5.9
G2-40	0.63	0.07344	0.0016	1.84264	0.0423	0.18194	0.0027	1026	24	1061	15	1078	15	-4.8
G2-41	0.51	0.1519	0.0044	8.66058	0.2119	0.4135	0.0062	2367	50	2303	22	2231	28	6.1
G2-42	0.41	0.0693	0.0014	1.38754	0.03	0.1452	0.0021	908	22	884	13	874	12	1.1
G2-43	0.62	0.05625	0.0015	0.56316	0.0154	0.0726	0.0011	462	34	454	10	452	7	0.4
G2-44	0.39	0.16562	0.0029	10.7561	0.2086	0.47095	0.0068	2514	15	2502	18	2488	30	1
G2-45	0.51	0.13215	0.0027	7.28326	0.1575	0.39967	0.006	2127	19	2147	19	2168	28	-1.9
G2-46	0.48	0.0934	0.0019	3.19514	0.069	0.24807	0.0037	1496	20	1456	17	1429	19	4.7
G2-47	0.35	0.05563	0.0012	0.54634	0.0127	0.07122	0.001	438	27	443	8	444	6	-0.2
G2-48	0.32	0.09267	0.0017	3.2087	0.0637	0.25108	0.0036	1481	18	1459	15	1444	19	2.6
G2-49	0.30	0.17529	0.0031	11.8677	0.2316	0.49094	0.007	2609	16	2594	18	2575	30	1.3
G2-50	0.48	0.05621	0.0015	0.55819	0.0152	0.07201	0.0011	461	34	450	10	448	7	0.4
G2-51	0.51	0.0562	0.0011	0.57713	0.0119	0.07447	0.0011	460	23	463	8	463	6	0
G2-52	0.42	0.14868	0.0028	8.7967	0.1787	0.42902	0.0063	2331	17	2317	19	2301	28	1.3
G2-53	0.43	0.10283	0.0019	4.10471	0.0826	0.28947	0.0042	1676	18	1655	16	1639	21	2.3
G2-54	1.98	0.05612	0.0011	0.50006	0.0107	0.06461	0.0009	457	24	412	7	404	6	2
G2-55	0.76	0.0562	0.0012	0.55998	0.0123	0.07226	0.0011	460	25	452	8	450	6	0.4
G2-56	1.23	0.1122	0.0021	5.21027	0.1075	0.33673	0.0049	1835	18	1854	18	1871	24	-1.9
G2-57	0.92	0.10884	0.0021	4.67533	0.0968	0.31149	0.0046	1780	18	1763	17	1748	22	1.8
G2-58	0.15	0.12871	0.0023	6.52646	0.1294	0.36771	0.0053	2080	17	2049	17	2019	25	3
G2-59	0.64	0.1979	0.0043	14.7199	0.3323	0.53937	0.0086	2809	18	2797	21	2781	36	1
G2-60	0.52	0.18485	0.0034	13.3539	0.2689	0.52386	0.0076	2697	16	2705	19	2716	32	-0.7
G2-61	0.67	0.05609	0.0014	0.56348	0.0145	0.07285	0.0011	456	31	454	9	453	7	0.2

G2-62	0.81	0.0564	0.0015	0.57914	0.0155	0.07446	0.0011	468	34	464	10	463	7	0.2
G2-63	0.71	0.05767	0.0022	0.63205	0.0242	0.07947	0.0013	517	55	497	15	493	8	0.8
G2-64	0.11	0.11911	0.003	5.62975	0.1159	0.34279	0.0049	1943	46	1921	18	1900	23	2.3
G2-65	0.58	0.05656	0.0014	0.55247	0.0141	0.07083	0.0011	474	31	447	9	441	6	1.4
G2-66	0.60	0.05609	0.0015	0.56505	0.0156	0.07306	0.0011	456	35	455	10	455	7	0
G2-67	0.61	0.05591	0.0013	0.55606	0.0135	0.07212	0.0011	449	29	449	9	449	6	0
G2-68	0.98	0.05105	0.0029	0.27784	0.0158	0.03947	0.0007	243	100	249	13	250	4	-0.4
G2-69	1.06	0.05627	0.0012	0.55705	0.0122	0.07179	0.0011	463	25	450	8	447	6	0.7
G2-70	0.43	0.0912	0.002	3.19857	0.0742	0.25432	0.0038	1451	23	1457	18	1461	20	-0.7
G2-71	0.73	0.05625	0.0014	0.57203	0.0143	0.07374	0.0011	462	30	459	9	459	7	0
G2-72	1.43	0.15581	0.003	9.27764	0.1955	0.43178	0.0064	2411	18	2366	19	2314	29	4.2
G2-73	0.56	0.05602	0.0013	0.56793	0.014	0.07351	0.0011	453	30	457	9	457	7	0
G2-74	0.46	0.05575	0.0013	0.53869	0.0133	0.07007	0.001	442	30	438	9	437	6	0.2
G2-75	0.24	0.16565	0.0032	10.773	0.2257	0.4716	0.0069	2514	17	2504	19	2491	30	0.9
G2-76	0.09	0.07688	0.0018	2.00678	0.0488	0.18928	0.0029	1118	26	1118	16	1117	16	0.1
G2-77	0.34	0.05566	0.0013	0.53129	0.0132	0.06921	0.001	439	30	433	9	431	6	0.5
G2-78	0.39	0.05601	0.0017	0.55315	0.0173	0.07161	0.0011	453	42	447	11	446	7	0.2
G2-79	0.46	0.05721	0.0013	0.62606	0.0154	0.07935	0.0012	500	29	494	10	492	7	0.4
G2-80	0.45	0.05632	0.0014	0.5674	0.015	0.07305	0.0011	465	33	456	10	455	7	0.2
G2-81	0.22	0.08855	0.0018	2.91119	0.0633	0.2384	0.0035	1394	21	1385	16	1378	18	1.2
G2-82	0.61	0.05974	0.0015	0.63635	0.0169	0.07724	0.0012	594	32	500	10	480	7	4.2
G2-83	0.66	0.05522	0.0014	0.55545	0.0147	0.07295	0.0011	421	33	449	10	454	7	-1.1
G2-84	0.32	0.05593	0.0014	0.54168	0.0137	0.07023	0.0011	450	31	440	9	438	6	0.5
G2-85	0.67	0.05585	0.0014	0.56389	0.0151	0.07321	0.0011	446	33	454	10	455	7	-0.2
G2-86	0.43	0.0555	0.0013	0.55145	0.0139	0.07206	0.0011	432	30	446	9	449	7	-0.7
G2-87	0.37	0.12253	0.0024	6.13432	0.1314	0.36302	0.0053	1993	19	1995	19	1996	25	-0.2
G2-88	0.32	0.05547	0.0014	0.53321	0.0143	0.06971	0.0011	431	33	434	9	434	6	0
G2-89	0.31	0.08161	0.0018	2.38432	0.0552	0.21186	0.0032	1236	23	1238	17	1239	17	-0.2

G2-90	0.55	0.08392	0.0034	2.61628	0.0964	0.22612	0.0035	1291	80	1305	27	1314	19	-1.8
G2-91	0.55	0.0556	0.0015	0.54394	0.0153	0.07094	0.0011	436	36	441	10	442	7	-0.2
G2-92	1.02	0.05739	0.0015	0.58373	0.0157	0.07375	0.0011	507	33	467	10	459	7	1.7
G2-93	0.54	0.05596	0.0016	0.55635	0.0158	0.0721	0.0011	451	37	449	10	449	7	0
G2-94	0.72	0.06365	0.0019	0.66556	0.0203	0.07582	0.0012	730	38	518	12	471	7	10
G2-95	0.12	0.12968	0.0034	6.5453	0.1452	0.36607	0.0053	2094	48	2052	20	2011	25	4.1
G2-96	0.79	0.1017	0.0023	4.11779	0.0993	0.29362	0.0045	1655	23	1658	20	1660	22	-0.3
G2-97	0.70	0.0625	0.0024	0.983	0.0371	0.11406	0.002	691	51	695	19	696	11	-0.1
G2-98	0.41	0.08038	0.0033	2.25637	0.0838	0.2036	0.0033	1206	82	1199	26	1195	18	0.9
G2-99	0.40	0.05614	0.0013	0.5606	0.0138	0.07241	0.0011	458	29	452	9	451	7	0.2
G2-100	0.68	0.10211	0.0026	4.18777	0.1114	0.2974	0.0047	1663	27	1672	22	1678	23	-0.9
CSL1														
CSL1-01	0.47	0.05531	0.001	0.52714	0.0105	0.06911	0.001	425	21	430	7	431	6	-0.2
CSL1-02	0.67	0.05537	0.0013	0.50288	0.0121	0.06585	0.001	427	29	414	8	411	6	0.7
CSL1-03	0.68	0.09502	0.0013	3.41491	0.0555	0.2606	0.0036	1528	14	1508	13	1493	19	2.3
CSL1-04	0.86	0.10431	0.0017	4.63072	0.0821	0.32192	0.0046	1702	15	1755	15	1799	22	-5.4
CSL1-05	0.60	0.05116	0.002	0.28751	0.0114	0.04075	0.0007	248	62	257	9	257	4	0
CSL1-06	0.58	0.07112	0.0021	1.46546	0.0446	0.14941	0.0023	961	37	916	18	898	13	2
CSL1-07	0.76	0.05566	0.0012	0.54107	0.0123	0.07049	0.001	439	26	439	8	439	6	0
CSL1-08	0.58	0.0565	0.0009	0.57685	0.0105	0.07404	0.001	472	19	462	7	460	6	0.4
CSL1-09	1.00	0.12957	0.0025	6.85303	0.1402	0.38354	0.0058	2092	17	2093	18	2093	27	0
CSL1-10	0.57	0.06345	0.001	0.6445	0.0114	0.07366	0.001	723	17	505	7	458	6	10.3
CSL1-11	0.36	0.06618	0.0022	1.27842	0.0378	0.14009	0.002	812	70	836	17	845	12	-1.1
CSL1-12	0.35	0.05634	0.0011	0.56859	0.0119	0.07318	0.001	466	23	457	8	455	6	0.4
CSL1-13	0.88	0.11323	0.0016	5.17647	0.0856	0.33151	0.0047	1852	13	1849	14	1846	23	0.3
~~CSL1-14~~	~~0.33~~	~~0.05156~~	~~0.0027~~	~~0.29478~~	~~0.0154~~	~~0.04146~~	~~0.0007~~	~~266~~	~~90~~	~~262~~	~~12~~	~~262~~	~~4~~	~~0~~
CSL1-15	0.60	0.05696	0.001	0.58621	0.011	0.07463	0.0011	490	20	468	7	464	6	0.9
CSL1-16	0.61	0.05613	0.0011	0.55694	0.0115	0.07195	0.001	458	23	450	8	448	6	0.4

CSL1-17	0.13	0.05635	0.0016	0.58034	0.0172	0.07468	0.0011	466	39	465	11	464	7	0.2
CSL1-18	0.35	0.07033	0.0011	1.42101	0.0254	0.14652	0.0021	938	17	898	11	881	12	1.9
CSL1-19	0.47	0.05431	0.0023	0.45465	0.0192	0.06071	0.001	384	66	381	13	380	6	0.3
CSL1-20	0.14	0.06725	0.007	0.36566	0.0372	0.03944	0.0007	845	224	316	28	249	4	26.9
CSL1-21	0.43	0.11071	0.003	3.66399	0.0826	0.24002	0.0034	1811	50	1564	18	1387	18	30.6
CSL1-22	0.45	0.05634	0.001	0.5627	0.0111	0.07242	0.001	466	21	453	7	451	6	0.4
CSL1-23	0.39	0.14714	0.0021	7.90503	0.132	0.38959	0.0055	2313	13	2220	15	2121	26	9.1
CSL1-24	0.62	0.05744	0.0013	0.64583	0.0157	0.08153	0.0012	508	29	506	10	505	7	0.2
CSL1-25	0.78	0.05586	0.0013	0.5575	0.0137	0.07238	0.0011	447	30	450	9	450	6	0
CSL1-26	1.87	0.05557	0.0015	0.54011	0.0151	0.07048	0.0011	435	36	438	10	439	7	-0.2
CSL1-27	0.10	0.14872	0.0035	1.60787	0.0297	0.07841	0.0011	2331	41	973	12	487	7	99.8
CSL1-28	0.22	0.10589	0.0015	4.35369	0.0729	0.29816	0.0042	1730	14	1704	14	1682	21	2.9
CSL1-29	0.48	0.09789	0.0017	3.58208	0.0696	0.26536	0.0039	1584	17	1546	15	1517	20	4.4
CSL1-30	0.28	0.07024	0.0011	1.11378	0.0197	0.11498	0.0016	935	17	760	9	702	9	8.3
CSL1-31	0.19	0.06896	0.001	1.31719	0.0225	0.13851	0.0019	898	16	853	10	836	11	2
CSL1-32	0.89	0.05729	0.0014	0.56089	0.0148	0.07099	0.001	503	33	452	10	442	6	2.3
CSL1-33	0.73	0.05153	0.0014	0.2996	0.0085	0.04216	0.0006	265	39	266	7	266	4	0
CSL1-34	1.24	0.05119	0.0024	0.2841	0.0131	0.04024	0.0007	249	75	254	10	254	4	0
CSL1-35	2.05	0.05139	0.0016	0.26846	0.0087	0.03788	0.0006	258	46	241	7	240	4	0.4
CSL1-36	0.95	0.0549	0.0018	0.50002	0.0164	0.06604	0.001	408	46	412	11	412	6	0
~~CSL1-37~~	~~0.55~~	~~0.05143~~	~~0.0014~~	~~0.29579~~	~~0.0082~~	~~0.04171~~	~~0.0006~~	~~260~~	~~37~~	~~263~~	~~6~~	~~263~~	~~4~~	~~0~~
~~CSL1-38~~	~~0.25~~	~~0.0525~~	~~0.0012~~	~~0.36486~~	~~0.0088~~	~~0.05039~~	~~0.0007~~	~~307~~	~~29~~	~~316~~	~~7~~	~~317~~	~~5~~	~~-0.3~~
CSL1-39	0.31	0.08718	0.0015	2.79585	0.0538	0.23255	0.0034	1364	17	1354	14	1348	18	1.2
CSL1-40	1.02	0.05606	0.001	0.58253	0.0113	0.07535	0.0011	455	21	466	7	468	6	-0.4
CSL1-41	0.55	0.05636	0.001	0.56719	0.0114	0.07297	0.0011	467	21	456	7	454	6	0.4
CSL1-42	0.87	0.05575	0.0024	0.5671	0.0248	0.07376	0.0012	442	68	456	16	459	7	-0.7
CSL1-43	0.54	0.1501	0.0023	8.94687	0.1586	0.43224	0.0062	2347	14	2333	16	2316	28	1.3
~~CSL1-44~~	~~0.67~~	~~0.06305~~	~~0.0015~~	~~1.08482~~	~~0.0267~~	~~0.12478~~	~~0.0019~~	~~710~~	~~28~~	~~746~~	~~13~~	~~758~~	~~11~~	~~-1.6~~

CSL1-45	0.30	0.06881	0.0012	1.44568	0.0273	0.15236	0.0022	893	18	908	11	914	12	-0.7
CSL1-46	1.55	0.0518	0.0017	0.29859	0.01	0.0418	0.0007	277	48	265	8	264	4	0.4
CSL1-47	0.69	0.05673	0.0012	0.55456	0.0124	0.07089	0.001	481	25	448	8	442	6	1.4
CSL1-48	1.18	0.05485	0.0014	0.49614	0.0133	0.06559	0.001	406	34	409	9	410	6	-0.2
CSL1-49	0.37	0.05652	0.001	0.59282	0.0113	0.07605	0.0011	473	20	473	7	473	7	0
CSL1-50	0.65	0.05587	0.001	0.5562	0.0113	0.07219	0.0011	447	22	449	7	449	6	0
CSL1-51	0.78	0.07849	0.0166	0.72336	0.1521	0.06684	0.0017	1159	463	553	90	417	11	32.6
CSL1-52	0.82	0.05097	0.0015	0.2729	0.0082	0.03883	0.0006	239	41	245	7	246	4	-0.4
CSL1-53	0.29	0.05724	0.0019	0.54847	0.0162	0.06949	0.001	501	74	444	11	433	6	2.5
CSL1-54	0.57	0.06015	0.0011	0.58844	0.0117	0.07095	0.001	609	21	470	7	442	6	6.3
CSL1-55	1.03	0.0564	0.0019	0.55552	0.0193	0.07142	0.0011	468	49	449	13	445	7	0.9
CSL1-56	0.70	0.05115	0.0017	0.27639	0.0091	0.03918	0.0006	248	48	248	7	248	4	0
CSL1-57	0.49	0.05165	0.0013	0.3068	0.0081	0.04307	0.0007	270	34	272	6	272	4	0
CSL1-58	0.16	0.05837	0.0079	0.45477	0.061	0.05651	0.0011	544	309	381	43	354	7	7.6
CSL1-59	0.97	0.05544	0.0017	0.52333	0.0165	0.06846	0.0011	430	42	427	11	427	7	0
CSL1-60	0.48	0.05625	0.0011	0.5426	0.0117	0.06995	0.001	462	24	440	8	436	6	0.9
CSL1-61	0.57	0.05204	0.0019	0.3066	0.0113	0.04272	0.0007	287	56	272	9	270	4	0.7
CSL1-62	0.79	0.05572	0.0013	0.5486	0.013	0.0714	0.0011	441	28	444	9	445	6	-0.2
CSL1-63	0.81	0.05616	0.0011	0.57212	0.0119	0.07387	0.0011	459	23	459	8	459	6	0
CSL1-64	0.38	0.05112	0.0021	0.27008	0.0112	0.03831	0.0006	246	64	243	9	242	4	0.4
CSL1-65	1.06	0.05103	0.0055	0.27967	0.0301	0.03974	0.0008	242	204	250	24	251	5	-0.4
CSL1-66	0.40	0.05653	0.0014	0.58485	0.015	0.07503	0.0011	473	31	468	10	466	7	0.4
CSL1-67	0.54	0.05402	0.0018	0.44134	0.015	0.05925	0.0009	372	48	371	11	371	6	0
CSL1-68	0.68	0.05157	0.0026	0.30688	0.0152	0.04315	0.0007	266	83	272	12	272	4	0
CSL1-69	0.38	0.07633	0.0014	1.92678	0.0381	0.18306	0.0027	1104	19	1090	13	1084	14	1.8
CSL1-70	0.75	0.05612	0.0012	0.60723	0.014	0.07847	0.0012	457	26	482	9	487	7	-1
CSL1-71	0.63	0.05189	0.0021	0.33062	0.0136	0.04621	0.0008	281	64	290	10	291	5	-0.3
CSL1-72	0.53	0.05698	0.0013	0.55174	0.0129	0.07022	0.0011	491	27	446	8	437	6	2.1

CSL1-73	0.45	0.05581	0.0013	0.55599	0.0138	0.07224	0.0011	445	29	449	9	450	7	-0.2
CSL1-74	1.09	0.05706	0.0015	0.5736	0.0152	0.0729	0.0011	494	33	460	10	454	7	1.3
CSL1-75	0.39	0.05669	0.0012	0.6019	0.0132	0.07699	0.0011	479	24	478	8	478	7	0
CSL1-76	0.37	0.09919	0.0018	4.01267	0.0793	0.29335	0.0043	1609	18	1637	16	1658	21	-3
CSL1-77	0.88	0.05832	0.0011	0.58506	0.0121	0.07274	0.0011	542	22	468	8	453	6	3.3
CSL1-78	0.13	0.05774	0.0012	0.60346	0.0133	0.07578	0.0011	520	24	479	8	471	7	1.7
CSL1-79	0.26	0.05549	0.0012	0.52664	0.0117	0.06882	0.001	432	25	430	8	429	6	0.2
CSL1-80	1.41	0.05712	0.0015	0.57355	0.0152	0.07281	0.0011	496	32	460	10	453	7	1.5
CSL1-81	1.44	0.05073	0.0075	0.25196	0.037	0.03602	0.001	229	274	228	30	228	6	0
CSL1-82	0.20	0.05578	0.0019	0.5735	0.0173	0.07457	0.0011	444	77	460	11	464	7	-0.9
CSL1-83	0.82	0.0553	0.0037	0.50891	0.034	0.06673	0.0014	424	113	418	23	416	8	0.5
CSL1-84	0.57	0.07057	0.0014	1.46625	0.031	0.15067	0.0022	945	21	917	13	905	12	1.3
CSL1-85	0.82	0.05635	0.0014	0.57064	0.015	0.07344	0.0011	466	32	458	10	457	7	0.2
CSL1-86	0.90	0.05553	0.0011	0.53494	0.0111	0.06986	0.001	434	23	435	7	435	6	0
CSL1-87	0.13	0.11647	0.0021	5.48676	0.1099	0.34161	0.005	1903	17	1899	17	1894	24	0.5
CSL1-88	1.14	0.05973	0.0012	0.60338	0.0128	0.07325	0.0011	594	23	479	8	456	6	5
CSL1-89	0.48	0.05715	0.0018	0.62184	0.0198	0.07891	0.0013	497	42	491	12	490	8	0.2
CSL1-90	0.37	0.07555	0.0178	0.41927	0.0984	0.04025	0.0011	1083	521	356	70	254	7	40.2
CSL1-91	0.33	0.05692	0.0017	0.6071	0.0187	0.07734	0.0012	488	40	482	12	480	7	0.4
CSL1-92	0.73	0.05623	0.0016	0.57019	0.0168	0.07353	0.0012	461	38	458	11	457	7	0.2
CSL1-93	0.82	0.05137	0.003	0.29007	0.0168	0.04095	0.0008	257	99	259	13	259	5	0
CSL1-94	0.54	0.07355	0.0038	1.58273	0.0774	0.15608	0.0026	1029	107	963	30	935	15	3
CSL1-95	0.57	0.06932	0.0014	1.42772	0.0313	0.14935	0.0022	908	23	901	13	897	13	0.4
CSL1-96	1.10	0.05167	0.0041	0.31241	0.0248	0.04384	0.0008	271	146	276	19	277	5	-0.4
CSL1-97	0.78	0.05601	0.0019	0.54947	0.0193	0.07114	0.0012	453	49	445	13	443	7	0.5
CSL1-98	0.15	0.07128	0.0015	1.49786	0.0347	0.15238	0.0023	965	24	930	14	914	13	1.8
CSL1-99	0.76	0.19485	0.0041	15.3616	0.3482	0.5717	0.0091	2784	18	2838	22	2915	37	-4.5
CSL1-100	0.24	0.09631	0.0019	3.58594	0.0775	0.27	0.004	1554	20	1546	17	1541	20	0.8

CSL2														
CSL2-01	0.65	0.05592	0.0013	0.55508	0.0131	0.07198	0.0011	449	28	448	9	448	6	0
CSL2-02	0.60	0.05196	0.0048	0.31859	0.0295	0.04446	0.0008	284	177	281	23	280	5	0.4
CSL2-03	0.33	0.06987	0.0015	1.41254	0.0317	0.1466	0.0022	925	24	894	13	882	12	1.4
CSL2-04	0.97	0.14565	0.0028	8.45586	0.1738	0.42098	0.0061	2295	17	2281	19	2265	28	1.3
CSL2-05	0.64	0.05547	0.0016	0.53346	0.0154	0.06974	0.0011	431	37	434	10	435	7	-0.2
CSL2-06	0.59	0.0556	0.0017	0.51871	0.0161	0.06766	0.0011	436	42	424	11	422	6	0.5
CSL2-07	0.66	0.0558	0.0016	0.55406	0.0163	0.072	0.0011	444	38	448	11	448	7	0
CSL2-08	0.39	0.05514	0.0014	0.50757	0.0136	0.06675	0.001	418	34	417	9	417	6	0
CSL2-09	0.06	0.06424	0.0014	1.04703	0.0234	0.11819	0.0017	750	24	727	12	720	10	1
CSL2-10	0.79	0.05199	0.0022	0.33322	0.0142	0.04648	0.0008	285	67	292	11	293	5	-0.3
CSL2-11	0.28	0.08981	0.0019	3.05629	0.0679	0.24678	0.0037	1421	21	1422	17	1422	19	-0.1
CSL2-12	0.48	0.05103	0.0022	0.27902	0.0117	0.03964	0.0007	242	66	250	9	251	4	-0.4
CSL2-13	0.16	0.06883	0.0014	1.30188	0.0288	0.13716	0.002	894	23	847	13	829	11	2.2
CSL2-14	1.01	0.05692	0.0017	0.61357	0.0183	0.07817	0.0012	488	39	486	12	485	7	0.2
CSL2-15	0.55	0.05492	0.0019	0.48597	0.0167	0.06416	0.001	409	49	402	11	401	6	0.2
CSL2-16	0.59	0.05102	0.0018	0.27512	0.01	0.0391	0.0006	242	54	247	8	247	4	0
CSL2-17	0.46	0.05548	0.0016	0.52256	0.0151	0.0683	0.0011	432	38	427	10	426	6	0.2
CSL2-18	0.58	0.07085	0.0018	1.54562	0.04	0.1582	0.0024	953	29	949	16	947	14	0.2
CSL2-19	0.69	0.08495	0.0019	2.39368	0.0549	0.20431	0.0031	1314	23	1241	16	1198	16	9.7
CSL2-20	0.45	0.05099	0.0013	0.2736	0.007	0.03891	0.0006	240	32	246	6	246	4	0
CSL2-21	0.65	0.101	0.0041	3.94432	0.1449	0.28322	0.0046	1643	76	1623	30	1608	23	2.2
CSL2-22	1.12	0.05141	0.0015	0.2866	0.0086	0.04043	0.0006	259	41	256	7	255	4	0.4
CSL2-23	1	0.06996	0.0017	1.46857	0.0372	0.15222	0.0023	927	28	918	15	913	13	0.5
CSL2-24	0.65	0.05234	0.0029	0.35254	0.0197	0.04884	0.0008	300	96	307	15	307	5	0
CSL2-25	0.78	0.05304	0.0023	0.38058	0.0162	0.05203	0.0009	331	67	327	12	327	5	0
CSL2-26	0.35	0.05579	0.0014	0.55287	0.0138	0.07186	0.0011	444	30	447	9	447	7	0
CSL2-27	0.87	0.05112	0.0042	0.27564	0.0223	0.0391	0.0007	246	150	247	18	247	4	0

CSL2-28	0.29	0.05265	0.0023	0.35913	0.0159	0.04947	0.0008	314	70	312	12	311	5	0.3
CSL2-29	0.12	0.06985	0.0016	1.47996	0.0346	0.15364	0.0023	924	25	922	14	921	13	0.1
~~CSL2-30~~	~~0.76~~	~~0.05454~~	~~0.0016~~	~~0.47763~~	~~0.0138~~	~~0.06351~~	~~0.001~~	~~393~~	~~37~~	~~396~~	~~9~~	~~397~~	~~6~~	~~-0.3~~
CSL2-31	0.92	0.05582	0.002	0.55234	0.0196	0.07175	0.0012	445	49	447	13	447	7	0
~~CSL2-32~~	~~1.05~~	~~0.0557~~	~~0.0022~~	~~0.53667~~	~~0.0208~~	~~0.06987~~	~~0.0011~~	~~440~~	~~57~~	~~436~~	~~14~~	~~435~~	~~7~~	~~0.2~~
CSL2-33	0.69	0.05503	0.0014	0.49893	0.0132	0.06574	0.001	413	33	411	9	410	6	0.2
CSL2-34	1.46	0.06558	0.002	1.17825	0.0369	0.13027	0.0021	793	39	790	17	789	12	0.1
CSL2-35	0.26	0.073	0.002	1.72455	0.0483	0.17129	0.0027	1014	32	1018	18	1019	15	-0.5
CSL2-36	0.4	0.05162	0.0019	0.30651	0.0112	0.04305	0.0007	269	55	271	9	272	4	-0.4
CSL2-37	0.46	0.05144	0.0014	0.29729	0.0083	0.0419	0.0007	261	36	264	6	265	4	-0.4
CSL2-38	0.81	0.05484	0.0019	0.45335	0.0162	0.05995	0.001	406	51	380	11	375	6	1.3
CSL2-39	0.92	0.05256	0.0022	0.35723	0.0149	0.04928	0.0009	310	64	310	11	310	5	0
CSL2-40	0.47	0.05875	0.0014	0.66081	0.0168	0.08156	0.0012	558	30	515	10	505	7	2
CSL2-41	0.5	0.05216	0.0043	0.33844	0.0278	0.04705	0.0009	292	151	296	21	296	6	0
CSL2-42	0.55	0.0554	0.0019	0.53112	0.0184	0.06951	0.0011	428	49	433	12	433	7	0
CSL2-43	0.99	0.11369	0.0026	5.02233	0.1187	0.32032	0.0049	1859	22	1823	20	1791	24	3.8
CSL2-44	0.58	0.12028	0.0028	5.54722	0.1347	0.33441	0.0052	1960	23	1908	21	1860	25	5.4
CSL2-45	0.65	0.05147	0.0036	0.30196	0.0211	0.04254	0.0008	262	124	268	16	269	5	-0.4
CSL2-46	0.29	0.05619	0.0015	0.5648	0.0157	0.07289	0.0011	460	35	455	10	454	7	0.2
CSL2-47	0.61	0.10511	0.0025	4.46385	0.1114	0.30794	0.0048	1716	24	1724	21	1731	23	-0.9
~~CSL2-48~~	~~0.33~~	~~0.05663~~	~~0.0016~~	~~0.62028~~	~~0.0178~~	~~0.07942~~	~~0.0012~~	~~477~~	~~37~~	~~490~~	~~11~~	~~493~~	~~7~~	~~-0.6~~
CSL2-49	0.15	0.06584	0.0017	1.25947	0.0331	0.13871	0.0022	801	30	828	15	837	12	-1.1
CSL2-50	0.54	0.05527	0.0016	0.52329	0.015	0.06866	0.0011	423	37	427	10	428	7	-0.2
CSL2-51	0.56	0.05571	0.0016	0.54285	0.0156	0.07066	0.001	441	38	440	10	440	6	0
CSL2-52	0.36	0.07689	0.0018	1.91983	0.0458	0.18105	0.0027	1118	25	1088	16	1073	14	4.2
CSL2-53	1.55	0.05134	0.0019	0.2804	0.0102	0.03961	0.0006	256	56	251	8	250	4	0.4
CSL2-54	0.42	0.05499	0.0034	0.51347	0.0312	0.06771	0.0011	412	106	421	21	422	7	-0.2
CSL2-55	0.4	0.06929	0.003	1.09812	0.0447	0.11494	0.0018	907	92	752	22	701	10	7.3

CSL2-56	0.45	0.05169	0.0023	0.30701	0.0135	0.04307	0.0007	272	71	272	11	272	4	0
CSL2-57	0.68	0.12532	0.0021	5.9464	0.108	0.34409	0.0048	2033	15	1968	16	1906	23	6.7
CSL2-58	0.03	0.05845	0.0013	0.67258	0.0153	0.08344	0.0012	547	26	522	9	517	7	1
CSL2-59	0.99	0.0569	0.0014	0.61328	0.0157	0.07816	0.0012	488	31	486	10	485	7	0.2
CSL2-60	0.27	0.07618	0.0014	1.8584	0.0359	0.17691	0.0025	1100	18	1066	13	1050	14	4.8
CSL2-61	0.34	0.05756	0.0011	0.65646	0.0138	0.0827	0.0012	513	23	512	8	512	7	0
CSL2-62	0.49	0.08566	0.0016	2.66194	0.0522	0.22535	0.0032	1331	18	1318	14	1310	17	1.6
CSL2-63	0.18	0.08677	0.0015	2.73884	0.0506	0.22889	0.0032	1355	17	1339	14	1329	17	2
~~CSL2-64~~	~~0.61~~	~~0.05258~~	~~0.0016~~	~~0.35858~~	~~0.011~~	~~0.04945~~	~~0.0007~~	~~311~~	~~43~~	~~311~~	~~8~~	~~311~~	~~5~~	~~0~~
CSL2-65	1.46	0.07206	0.0017	1.66622	0.0414	0.16767	0.0025	988	27	996	16	999	14	-0.3
CSL2-66	0.62	0.0559	0.0015	0.54445	0.0147	0.07062	0.001	448	35	441	10	440	6	0.2
CSL2-67	0.81	0.07618	0.0016	1.76413	0.038	0.16792	0.0024	1100	22	1032	14	1001	13	9.9
CSL2-68	0.69	0.05617	0.0011	0.52498	0.0108	0.06777	0.001	459	23	428	7	423	6	1.2
CSL2-69	0.26	0.05344	0.0011	0.37238	0.0083	0.05053	0.0007	348	26	321	6	318	4	0.9
CSL2-70	0.57	0.07438	0.0031	1.78768	0.0701	0.1743	0.0027	1052	87	1041	26	1036	15	1.5
CSL2-71	0.16	0.06603	0.0018	1.10355	0.0261	0.1212	0.0017	807	59	755	13	737	10	2.4
CSL2-72	0.52	0.05245	0.0013	0.35161	0.0088	0.04861	0.0007	305	31	306	7	306	4	0
CSL2-73	0.68	0.06615	0.0015	1.23256	0.0298	0.13512	0.002	811	27	816	14	817	11	-0.1
CSL2-74	0.62	0.0471	0.0068	0.29254	0.042	0.04505	0.0009	54	269	261	33	284	5	-8.1
CSL2-75	0.44	0.05578	0.0012	0.54872	0.0123	0.07134	0.001	444	26	444	8	444	6	0
~~CSL2-76~~	~~0.96~~	~~0.0528~~	~~0.002~~	~~0.36765~~	~~0.0137~~	~~0.0505~~	~~0.0008~~	~~320~~	~~55~~	~~318~~	~~10~~	~~318~~	~~5~~	~~0~~
CSL2-77	0.51	0.05584	0.0015	0.56255	0.0155	0.07305	0.0011	446	34	453	10	455	7	-0.4
CSL2-78	1	0.05608	0.0015	0.55762	0.0155	0.07211	0.0011	456	35	450	10	449	7	0.2
CSL2-79	0.46	0.05602	0.0015	0.35311	0.0097	0.04571	0.0007	453	34	307	7	288	4	6.6
CSL2-80	0.81	0.05682	0.0017	0.54034	0.0161	0.06896	0.0011	485	38	439	11	430	7	2.1
CSL2-81	0.4	0.06906	0.0017	1.51337	0.0388	0.15891	0.0025	901	29	936	16	951	14	-1.6
CSL2-82	0.4	0.05752	0.0016	0.66337	0.0189	0.08363	0.0013	512	36	517	12	518	8	-0.2
CSL2-83	0.43	0.05743	0.0016	0.60143	0.0168	0.07594	0.0012	508	35	478	11	472	7	1.3

CSL2-84	0.3	0.07185	0.0017	1.5712	0.0395	0.15859	0.0024	982	27	959	16	949	14	1.1
CSL2-85	0.13	0.06888	0.0017	1.46715	0.0384	0.15446	0.0024	895	30	917	16	926	13	-1
CSL2-86	0.65	0.05642	0.0023	0.58027	0.0236	0.07458	0.0013	469	60	465	15	464	8	0.2
CSL2-87	0.21	0.0733	0.0018	1.65061	0.0427	0.1633	0.0025	1022	28	990	16	975	14	1.5
CSL2-88	0.83	0.05144	0.0022	0.29488	0.0127	0.04157	0.0007	261	67	262	10	263	4	-0.4
CSL2-89	0.7	0.19207	0.0049	13.5337	0.3581	0.51097	0.0084	2760	23	2718	25	2661	36	3.7
CSL2-90	0.53	0.05422	0.0023	0.45612	0.0197	0.061	0.001	380	66	382	14	382	6	0
~~CSL2-91~~	~~0.53~~	~~0.05545~~	~~0.0026~~	~~0.51916~~	~~0.0246~~	~~0.06789~~	~~0.0012~~	~~430~~	~~75~~	~~425~~	~~16~~	~~423~~	~~7~~	~~0.5~~
CSL2-92	0.52	0.09124	0.0024	3.09334	0.0834	0.24585	0.0039	1452	28	1431	21	1417	20	2.5
CSL2-93	0.39	0.07239	0.002	1.62315	0.0467	0.16259	0.0026	997	33	979	18	971	14	0.8
CSL2-94	0.21	0.05552	0.0015	0.54068	0.0151	0.07062	0.0011	433	35	439	10	440	7	-0.2
CSL2-95	0.57	0.09055	0.004	3.13844	0.1278	0.25139	0.0041	1437	86	1442	31	1446	21	-0.6
CSL2-96	0.25	0.06849	0.002	1.24203	0.0373	0.1315	0.0021	883	36	820	17	796	12	3
CSL2-97	0.54	0.0567	0.0016	0.6166	0.0182	0.07887	0.0013	480	38	488	11	489	8	-0.2
CSL2-98	0.23	0.05594	0.0014	0.54958	0.0148	0.07124	0.0011	450	33	445	10	444	7	0.2
CSL2-99	0.87	0.05145	0.0024	0.29205	0.0135	0.04117	0.0008	261	72	260	11	260	5	0
CSL2-100	0.35	0.05713	0.0021	0.6434	0.0236	0.08167	0.0014	497	51	504	15	506	8	-0.4
CSL3														
CSL3-01	~~0.13~~	~~0.05517~~	~~0.0013~~	~~0.50171~~	~~0.012~~	~~0.06594~~	~~0.001~~	~~419~~	~~28~~	~~413~~	~~8~~	~~412~~	~~6~~	~~0.2~~
CSL3-02	0.58	0.05553	0.0017	0.54093	0.0172	0.07063	0.0011	434	43	439	11	440	7	-0.2
CSL3-03	0.97	0.05158	0.0023	0.31051	0.0139	0.04365	0.0008	267	71	275	11	275	5	0
CSL3-04	0.45	0.07636	0.0015	1.82299	0.0383	0.17311	0.0026	1105	20	1054	14	1029	14	7.4
CSL3-05	0.51	0.05168	0.0015	0.30315	0.009	0.04254	0.0007	271	40	269	7	269	4	0
CSL3-06	~~0.66~~	~~0.08359~~	~~0.0017~~	~~2.38147~~	~~0.0506~~	~~0.20659~~	~~0.0031~~	~~1283~~	~~20~~	~~1237~~	~~15~~	~~1211~~	~~16~~	~~5.9~~
CSL3-07	~~0.64~~	~~0.05664~~	~~0.002~~	~~0.58377~~	~~0.0206~~	~~0.07473~~	~~0.0012~~	~~478~~	~~49~~	~~467~~	~~13~~	~~465~~	~~7~~	~~0.4~~
CSL3-08	0.61	0.05592	0.0013	0.55642	0.0139	0.07215	0.0011	449	29	449	9	449	7	0
CSL3-09	0.51	0.05039	0.0014	0.24655	0.0072	0.03547	0.0006	213	39	224	6	225	3	-0.4
CSL3-10	0.94	0.0989	0.0018	3.90235	0.0772	0.28609	0.0043	1603	17	1614	16	1622	21	-1.2

CSL3-11	0.46	0.05608	0.0015	0.55141	0.0155	0.07129	0.0011	456	36	446	10	444	7	0.5
CSL3-12	0.73	0.05159	0.0033	0.30602	0.0194	0.04301	0.0008	267	112	271	15	271	5	0
CSL3-13	0.77	0.0521	0.0036	0.29028	0.0197	0.0404	0.0007	290	122	259	16	255	5	1.6
CSL3-14	0.58	0.05159	0.0016	0.29206	0.0094	0.04105	0.0006	267	45	260	7	259	4	0.4
CSL3-15	0.5	0.05646	0.0011	0.5388	0.0115	0.0692	0.001	471	23	438	8	431	6	1.6
CSL3-16	~~0.93~~	~~0.05133~~	~~0.0017~~	~~0.2997~~	~~0.01~~	~~0.04233~~	~~0.0007~~	~~256~~	~~49~~	~~266~~	~~8~~	~~267~~	~~4~~	~~-0.4~~
CSL3-17	0.59	0.056	0.0011	0.55924	0.012	0.07241	0.0011	452	24	451	8	451	6	0
CSL3-18	0.33	0.05569	0.0012	0.54468	0.0122	0.07092	0.0011	440	25	442	8	442	6	0
CSL3-19	0.89	0.05161	0.0018	0.30471	0.0107	0.04281	0.0007	268	51	270	8	270	4	0
CSL3-20	0.73	0.05081	0.0017	0.25666	0.0086	0.03663	0.0006	232	47	232	7	232	4	0
CSL3-21	0.42	0.05556	0.0017	0.54721	0.0165	0.07142	0.0011	435	39	443	11	445	7	-0.4
CSL3-22	~~0.53~~	~~0.0553~~	~~0.0015~~	~~0.52915~~	~~0.015~~	~~0.06938~~	~~0.0011~~	~~424~~	~~36~~	~~431~~	~~10~~	~~432~~	~~7~~	~~-0.2~~
CSL3-23	0.67	0.05749	0.0047	0.34096	0.0271	0.04302	0.0008	510	185	298	21	272	5	9.6
CSL3-24	0.66	0.05469	0.0012	0.48332	0.011	0.06408	0.001	400	26	400	7	400	6	0
CSL3-25	0.51	0.05182	0.0025	0.31577	0.0152	0.04418	0.0008	277	78	279	12	279	5	0
CSL3-26	0.54	0.05517	0.0017	0.51708	0.0157	0.06796	0.0011	419	40	423	10	424	7	-0.2
CSL3-27	0.39	0.05633	0.0012	0.55078	0.012	0.07089	0.0011	465	24	446	8	442	6	0.9
CSL3-28	0.4	0.05498	0.0011	0.49057	0.0108	0.0647	0.001	411	25	405	7	404	6	0.2
CSL3-29	0.78	0.05534	0.0012	0.54647	0.0123	0.0716	0.0011	426	25	443	8	446	6	-0.7
CSL3-30	0.47	0.0516	0.0013	0.29915	0.0077	0.04204	0.0006	268	32	266	6	265	4	0.4
CSL3-31	0.3	0.05561	0.0019	0.53045	0.0179	0.06916	0.0011	437	46	432	12	431	7	0.2
CSL3-32	0.58	0.0508	0.0018	0.25068	0.0092	0.03578	0.0006	232	55	227	7	227	4	0
CSL3-33	0.63	0.05162	0.0017	0.29987	0.0098	0.04212	0.0007	269	46	266	8	266	4	0
CSL3-34	0.5	0.05041	0.0012	0.25617	0.0063	0.03685	0.0006	214	31	232	5	233	3	-0.4
CSL3-35	0.54	0.05477	0.0012	0.48707	0.0113	0.06448	0.001	403	27	403	8	403	6	0
CSL3-36	0.25	0.05507	0.0014	0.52684	0.0133	0.06937	0.0011	415	30	430	9	432	6	-0.5
CSL3-37	0.47	0.05509	0.0014	0.55457	0.014	0.07299	0.0011	416	30	448	9	454	7	-1.3
CSL3-38	0.57	0.11151	0.002	4.87149	0.0944	0.31675	0.0046	1824	17	1797	16	1774	23	2.8

CSL3-39	0.94	0.05119	0.0019	0.28993	0.0108	0.04107	0.0007	249	56	259	8	259	4	0
CSL3-40	0.55	0.05135	0.0031	0.29487	0.0176	0.04163	0.0007	257	105	262	14	263	5	-0.4
CSL3-41	0.4	0.16483	0.0031	10.6646	0.2173	0.46913	0.0071	2506	16	2494	19	2480	31	1
CSL3-42	1.12	0.05156	0.0022	0.30229	0.013	0.04251	0.0007	266	66	268	10	268	5	0
CSL3-43	0.61	0.05584	0.0013	0.55993	0.0133	0.07271	0.0011	446	28	451	9	452	7	-0.2
CSL3-44	0.9	0.05148	0.0014	0.29588	0.0082	0.04168	0.0006	262	37	263	6	263	4	0
CSL3-45	0.32	0.05744	0.0016	0.61627	0.0176	0.0778	0.0012	508	37	488	11	483	7	1
CSL3-46	1.12	0.05248	0.0026	0.34374	0.0167	0.04749	0.0008	306	80	300	13	299	5	0.3
CSL3-47	0.53	0.05116	0.0025	0.2908	0.0143	0.04121	0.0007	248	82	259	11	260	4	-0.4
CSL3-48	0.47	0.05069	0.0024	0.24289	0.0116	0.03475	0.0006	227	78	221	9	220	4	0.5
CSL3-49	0.59	0.05574	0.0019	0.5371	0.0187	0.06987	0.0011	442	49	437	12	435	7	0.5
CSL3-50	0.9	0.05127	0.0019	0.29027	0.011	0.04105	0.0007	253	58	259	9	259	4	0
CSL3-51	0.45	0.0556	0.0011	0.53934	0.0114	0.07034	0.001	436	23	438	8	438	6	0
CSL3-52	0.81	0.05158	0.0018	0.30681	0.0105	0.04313	0.0007	267	50	272	8	272	4	0
CSL3-53	0.59	0.05148	0.0017	0.29343	0.0097	0.04133	0.0007	262	47	261	8	261	4	0
CSL3-54	0.54	0.05613	0.0013	0.32317	0.008	0.04175	0.0006	458	29	284	6	264	4	7.6
CSL3-55	0.38	0.0565	0.0012	0.56451	0.0129	0.07245	0.0011	472	26	454	8	451	6	0.7
CSL3-56	1.03	0.05527	0.0033	0.4838	0.0282	0.06346	0.0012	423	98	401	19	397	7	1
CSL3-57	0.58	0.05179	0.0018	0.30555	0.0104	0.04278	0.0007	276	50	271	8	270	4	0.4
CSL3-58	0.62	0.05151	0.0016	0.29928	0.0093	0.04213	0.0007	264	42	266	7	266	4	0
CSL3-59	0.67	0.10164	0.0021	3.86428	0.0828	0.27568	0.0041	1654	20	1606	17	1570	21	5.4
CSL3-60	0.45	0.05783	0.0021	0.646	0.023	0.08099	0.0013	523	50	506	14	502	8	0.8
CSL3-61	0.49	0.05665	0.0017	0.32486	0.0096	0.04158	0.0006	478	39	286	7	263	4	8.7
CSL3-62	0.48	0.05564	0.0015	0.53916	0.0148	0.07026	0.0011	438	34	438	10	438	7	0
CSL3-63	0.52	0.05567	0.0017	0.52766	0.0164	0.06873	0.0011	439	41	430	11	428	7	0.5
CSL3-64	1.45	0.05803	0.0024	0.70382	0.0295	0.08795	0.0015	531	62	541	18	543	9	-0.4
CSL3-65	0.53	0.09522	0.0036	3.43202	0.1182	0.26142	0.0042	1532	73	1512	27	1497	21	2.3
CSL3-66	0.65	0.05436	0.0017	0.45752	0.0146	0.06103	0.001	386	44	383	10	382	6	0.3

CSL3-67	0.51	0.05542	0.0015	0.52583	0.0141	0.0688	0.0011	429	33	429	9	429	6	0
CSL3-68	0.92	0.05146	0.0024	0.29693	0.0137	0.04184	0.0007	261	75	264	11	264	4	0
CSL3-69	~~0.94~~	0.05152	0.0021	0.29733	0.0123	0.04185	0.0007	264	65	264	10	264	4	0
CSL3-70	1.04	0.05177	0.002	0.31234	0.0119	0.04374	0.0008	275	56	276	9	276	5	0
CSL3-71	0.56	0.05331	0.0019	0.30094	0.0106	0.04093	0.0007	342	51	267	8	259	4	3.1
CSL3-72	0.5	0.05166	0.0027	0.29172	0.0153	0.04094	0.0007	270	87	260	12	259	5	0.4
CSL3-73	0.28	0.05525	0.0013	0.53166	0.0129	0.06978	0.0011	422	29	433	9	435	6	-0.5
CSL3-74	0.57	0.05173	0.0018	0.30412	0.0105	0.04263	0.0007	273	50	270	8	269	4	0.4
~~CSL3-75~~	1.34	0.08126	0.0025	0.43458	0.0132	0.03878	0.0007	1228	34	366	9	245	4	49.4
CSL3-76	3.82	0.05124	0.0023	0.28649	0.0127	0.04054	0.0007	252	69	256	10	256	4	0
CSL3-77	0.71	0.05171	0.0019	0.30653	0.011	0.04299	0.0007	273	53	271	9	271	4	0
~~CSL3-78~~	~~0.51~~	0.06587	0.0017	0.61079	0.0157	0.06724	0.001	802	29	484	10	420	6	15.2
CSL3-79	0.45	~~0.05575~~	~~0.0014~~	~~0.5408~~	~~0.0139~~	~~0.07034~~	~~0.0011~~	~~442~~	~~31~~	~~439~~	~~9~~	~~438~~	~~7~~	~~0.2~~
CSL3-80	1	0.0859	0.0026	2.77293	0.0832	0.23408	0.0038	1336	33	1348	22	1356	20	-1.5
CSL3-81	0.6	0.05147	0.0024	0.30168	0.0141	0.0425	0.0007	262	76	268	11	268	5	0
CSL3-82	0.74	0.05152	0.007	0.28864	0.0388	0.04063	0.0009	264	259	257	31	257	6	0
CSL3-83	0.54	0.0553	0.0014	0.52934	0.0134	0.06941	0.0011	424	30	431	9	433	6	-0.5
CSL3-84	0.6	0.05135	0.0019	0.29861	0.0108	0.04217	0.0007	257	53	265	8	266	4	-0.4
CSL3-85	0.75	0.05119	0.0016	0.2579	0.008	0.03653	0.0006	249	42	233	6	231	4	0.9
CSL3-86	0.66	0.05156	0.0018	0.3026	0.0104	0.04256	0.0007	266	49	268	8	269	4	-0.4
CSL3-87	0.66	0.05536	0.0014	0.52022	0.0137	0.06814	0.0011	427	32	425	9	425	6	0
CSL3-88	0.86	0.05155	0.0022	0.29682	0.0128	0.04175	0.0007	266	66	264	10	264	5	0
CSL3-89	0.64	0.05191	0.0017	0.31777	0.0101	0.04439	0.0007	281	44	280	8	280	4	0
CSL3-90	0.77	0.05526	0.0018	0.50689	0.0168	0.06651	0.0011	423	46	416	11	415	6	0.2
~~CSL3-91~~	0.42	0.08731	0.0022	1.70999	0.0445	0.14202	0.0022	1367	27	1012	17	856	13	18.2
CSL3-92	0.43	0.05546	0.0015	0.5249	0.0141	0.06864	0.0011	431	33	428	9	428	6	0
CSL3-93	~~0.5~~	0.07675	0.002	1.96941	0.0515	0.18607	0.0029	1115	28	1105	18	1100	16	1.4
CSL3-94	0.47	0.05145	0.0016	0.29321	0.0093	0.04132	0.0007	261	43	261	7	261	4	0

CSL3-95	0.43	0.05591	0.002	0.55431	0.0195	0.0719	0.0012	449	50	448	13	448	7	0
CSL3-96	0.62	0.0517	0.0019	0.31532	0.0114	0.04423	0.0007	272	53	278	9	279	4	-0.4
CSL3-97	~~0.52~~	0.06833	0.0019	1.33206	0.0363	0.14138	0.0022	879	31	860	16	852	13	0.9
CSL3-98	1.25	0.0515	0.0018	0.29382	0.0105	0.04138	0.0007	263	52	262	8	261	4	0.4
CSL3-99	0.68	0.05173	0.0044	0.3006	0.0253	0.04214	0.0008	273	155	267	20	266	5	0.4
CSL3-100	0.59	0.10151	0.0025	3.96501	0.0998	0.28327	0.0044	1652	25	1627	20	1608	22	2.7

Table DR2. Zircon U-Pb ages from plutons of the Eastern Kunlun Range, Altyn Tagh Range and Qilian Shan.

Altyn Tagh Range			Qilian Shan			East Kunlun Range		
Author	Year	Age(Ma)	Author	Year	Age(Ma)	Author	Year	Age(Ma)
	2005	413	Yue et al.,	2005	1728	She Hongquan et al.,	2007	215
		482			482	Li Shijin et al.,	2008	224
		1870			424	Wang Song et al.,	2009	237
		1877			472	Li Dongsheng et al.,	2009	206
Yue et al.,		479			480			223
	2003	270			423	Feng Chengyou et al.,	2009	237
		272			406	Huang Limei et al.,	2012	459
		270			425	Guo Lei et al.,	2010	256
Gehrels et al.,		440			366	Gao Yongbao et al.,	2012	228
	2003	922			248			234
		389			434	Liu Chengdong et al.,	2003	242
		2720			441	Liu Yunhua et al.,	2006	204
		442			473	Wu Xiangke et al.,	2011	218
		290			430	Feng Chengyou et al.,	2011	219
		404	Gehrels et al.,	2003	461			235
Cowgill et al.,		457	Cowgill et al.,	2003	459	Chen Danling et al.,	2011	212

		518			922	Ren Erfeng et al.,	2012	403
		475			928			394
		969			442	Feng Chengyou et al.,	2010	227
		444			422			220
		2396	Lu Songnian et al.,	2008	2366	Gao Yongbao et al.,	2011	430
	2008	2582			2412			431
		2604			1939	Feng Chengyou et al.,	2009	417
		2830			2348			468
		3574			1852	Chen Junlu et al.,	2004	405
		3665			1763			2380
		2396			844			816
		1978			740			401
		2670			1050	Cui Meihui et al.,	2011	480
		2830			1020	Wang Bingzhang et al.,	2009	271
		1986			1020			284
		2374			1020			251
		2351			987	Mo xuanxue et al.,	2005	212
		2358			928	Qinghai Geology	2008	214
		2366			917	investigation institute		225
		2412			917	Xiao Aifang et al.,	2005	405
		2426			878	Wang Xiangli et al.,	2010	1090
		1900			953			312
Lu Songnian et al.,		930			875	Gao Yongbao et al.,	2010	430
	2005	474			878			430
Wu Cailai et al.,		446			864			430

		435			855	Qinghai Geology	2003	410
		431			844	investigation institute		419
Yang Jingsui et al.,	2008	479			821	Ma Yongshou et al.,	2010	550
Yang Wenqiang et al.,	2012	453			1776			2046
Hao Jie et al.,	2006	467			740	Wu Shaofeng et al.,	2012	429
Sun Jiming et al.,	2012	497			1793	Tan Shengxiang et al.,	2004	831
	2013	923			1800	Cao Shitai et al.,	2011	429
		910	Wang Chao et al.,	2013	976			430
		927			952	Wang Binzhang	2012	440
		924			941			450
		906			935	Feng Chengyou et al.,	2010	219
		916			953	Xi Rengang et al.,	2011	231
		938			915	Guo Tongzhen et al.,	2011	389
		907			907	Qinghai Geology	2010	224
Wang Chao et al.,						investigation institute		
Xiu Qunye et al.,	2007	449			932	Feng Chengyou et al.,	2012	227
	2012	446			918			220
		477			930	Chang Youying et al.,	2009	223
		477	Liu Liang et al.,	2013	783			214
		514			748			225
		417			847	Liu Xiaokang et al.,	2011	419
		488			847	Chen Bo et al.,	2012	410
		479			457	Gao Xiaofeng et al.,	2011	443
		506			446	Luo Zhaohua et al.,	2002	212
Han Dengbin et al.,		431			909	Mo xuanxue et al.,	2007	471

		443			1005		485
		417			891	Mo xuanxue et al., 2005	387
		431			890		386
		440			516		408
	2007	435	Shi Rendeng et al.,	2004	550		408
		433	Meng Fancong et al.,	2010	505		401
		435	Zeng Jianyuan et al.,	2007	497	Chen Hongwei et al., 2006	403
Wu Cailai et al.,		431	Wu Cailai et al.,	2010	501		394
	2012	750			512	Lu Songnian et al., 2002	522
		763			508		2468
Liu Han et al.,		754			477		1955
Liu Liang et al.,	1999	524			463	Yang Jinsui et al., 1996	518
	2006	776			424	Feng Jianyun et al., 2010	509
Zeng Jianyuan et al.,		774			435	Wang Binzhang 2012	509
	2009	757			429		434
		438	Song Zhongbao et al.,	2004	482		435
Lu Songnian et al.,		425	Song Zhongbao et al.,	2007	458		419
	2009	2679	Huang Chuanjian et al.,	1995	486		421
		856	Wu Cailai et al.,	2007	477		413
		1312			463		409
		1209	Wang Yusheng et al.,	2001	940		1782
		871			1030		2642
		1311			1020		881
		450	Wang Yusheng et al.,	2000	930		923
Wu Yuezhong et al.,		465			930		427

		445			750			451
		452	Guo Jinjing et al.,	1999	920			189
		448			910			290
		327	Mei Hualin et al.,	1998	2670			397
		313	Mei Hualin et al.,	1999	880			683
		397	Xu Wanchun et al.,	2007	891			373
Xiao Peixi et al.,	2003	495	Wang Christina Yan et al.,	2005	445			394
Song Zhongbao et al.,	2004	482	Xu Wangchun et al.,	2007	776			373
	2011	462			774			369
Liu Han et al.,		437	Li Xianhua et al.,	2004	827			370
Zhang Zhicheng et al.,	2008	521	Ayers et al.,	2002	1921			397
Kang Lei et al.,	2011	500	Mattinson et al.,	2006	433			395
Gherels et al.,	1999	480	Xia Xiaohong et al.,	2009	490			370
Chen Xuanhua et al.,	2003	443	He Shiping et al.,	2007	443			357
	2013	450			1782			284
Dong Shunli et al.,		465			385			241
	2012	478			471			250
Zhang Zhanwu et al.,		470	Li Shuguang et al.,	2004	447			217
Dong Zengchan et al.,	2011	445	Zhang Zhaowei et al.,	2012	441			224
Liu Han et al.,	2012	2007	Wei Fanghui et al.,	2012	441	Ma Shengchao et al.,	2012	219
	2012	467	Zhang Zhaowei et al.,	2012	443			235
		462	Mao Jingwen et al.,	2000	460	Cui Meihui et al.,	2012	480
		470	Xiong Ziliang et al.,	2012	424	Zhang Dequan et al.,	2001	438
Ma Zhongping et al.,		464			402	Cheng Nengsong et al.,	2008	517
Yang Qi et al.,	2004	443	Su Jianping et al.,	2004	444			516

		485	Yu Jiyuan et al.,	2012	455			559
Liu Liang et al.,	2007	750	Wu Cailai et al.,	2006	476			482
	2005	846			463			516
Zhangjianxin		844	Wang Yinchuan et al.,	2012	1765			549
zhangjianxin	2004	842	Wu Cailai et al.,	2004	383	Yang Jingsui et al.,	1995	518
	2009	1800	Chen Junlu et al.,	2006	440	Lu Songnian et al.,	2002	522
Liuliang		821	Wang Hongliang et al.,	2007	1192	Yang Jingsui et al.,	1996	579
	2005	482	Qi Ruirong et al.,	2012	463	Li Huaikun et al.,	2006	506
Qixuexiang		404	Huang Zengbao et al.,	2010	414	Guangxi Geology	2003	1209
	2013	754	Xiang Zengqun et al.,	2007	504	investigation institute		871
		752	Yang Jinsui et al.,	2008	479			550
		647	Xiao Lin et al.,	1997	2152			408
		730	Yong Yong et al.,	2008	454			397
		857			846			320
		719			756			381
		867			853			271
		563	Xu Xueyi et al.,	2008	723	Qinghai Geology	2004	831
Liuliang						investigation institute		
Wu Cailai et al.,	2001	446	Zeng Jianyuan et al.,	2006	776	Yang Jinsui et al.,	2005	417
	2003	2926			774			421
		1728	Chen Junlu et al.,	2008	445			250
Chen Xuanhua et al.,		405	Xia Xiaohong et al.,	2010	490			308
Wu Suoping et al.,	2007	385	He Yanhong et al.,	2005	447	Bian Qiantao et al.,	1999	402
Li Weidong et al.,	2012	462	Guo Jinjing et al.,	1999	917	Cheng Nengsong et al.,	2000	447
Cao Yuting et al.,	2013	579	Pei Xianzhi et al.,	2007	440	Gao Xiaofeng et al.,	2010	458

	2010	410			450	Shanxi Geology investigation institute	2003	432
Liu Feng et al.,								
	2013	457	He Yanhong et al.,	2005	1900	Feng Jianyun et al.,	2010	509
		419			2350	Zhang Yafeng et al.,	2010	515
		411			2500	Sun Yu et al.,	2009	255
		503	Wu Cailai et al.,	2008	465	Liu Chengdong et al.,	2004	239
		420			470			242
		419			444	Liu Chengdong et al.,	2000	236
		411			372			235
		420			271	Long Xiaoping et al.,	2006	411
Liu Han et al.,		405			260			396
	2003	418	Li Jianfeng et al.,	2010	415	Zhang Jianxin et al.,	2003	402
		413			435	Liu Zhanqing et al.,	2011	516
Chen Xuanhua et al.,		413	Dong Guoan et al.,	2007	930			332
					918			441
					790	Li Wangye et al.,	2007	493
			Wu Cailai et al.,	2007	446	Lu Lu et al.,	2010	423
					409	Zhang Yaoling et al.,	2010	406
					403	Sun Yu et al.,	2009	254
					375	China University of Geosciences (Wuhan)	2003	205
					372	Ren Junhu et al.,	2009	436
			Wu Peng et al.,	2012	499			413
			Yu Jiyuan et al.,	2012	910			403
			Xue Ning et al.,	2009	829	Xiong Fuhao et al.,	2011	249

		842
Su Jianping et al.,	2004	751
Lu Xinxiang et al.,	2007	440
Xia Xiaohong et al.,	2012	501
		495
Dang Jinhua et al.,	2011	345
Liu Bin et al.,	2012	407
		406
Liu et al.,	2004	242
		239
Cheng Nengsong et al.,	2002	448
		427
		920
Zhang Jianxin et al.,	2003	460
Cheng Nengsong et al.,	1999	500
Li Huaikun et al.,	2006	500
China University of Geosciences (Wuhan)	2003	438
Zhu Yunhai et al.,	2005	419
		401
Li Fudong et al.,	1993	222
		206
		223
Zhan fayu et al.,	2007	230
		222
		215
		228
		219
Zhang Hongfei et al.,	2006	218
Bian Qiantao et al.,	2007	402
Lu Lu et al.,	2010	409

		391
Robbinson et al.,	2003	74
Li wei et al.,	2013	485
Li wei et al.,	2013	439
Li wei et al.,	2013	424
Li wei et al.,	2013	262
Li wei et al.,	2013	462
Li wei et al.,	2013	428
Li wei et al.,	2013	446

Appendix to Chapter 3.2

Appendix S1 U-Pb analysis of detrital zircons from the 11 sandstone samples.

Analysis number	Th/U	Isotopic ratios and errors								Ages and errors (Ma)				Disc. %
		$^{207}Pb/^{206}Pb$	1σ	$^{207}Pb/^{235}U$	1σ	$^{206}Pb/^{238}U$	1σ	$^{207}Pb/^{206}Pb$	1σ	$^{207}Pb/^{235}U$	1σ	$^{206}Pb/^{238}U$	1σ	
Eboliang Section														
E122														
E122-01	0.52	0.0554	0.00116	0.49806	0.01086	0.0652	0.00089	428	26	410	7	407	5	0.74
~~E122-02~~	~~0.09~~	~~0.10225~~	~~0.0017~~	~~3.17139~~	~~0.05659~~	~~0.2249~~	~~0.00305~~	~~1665~~	~~15~~	~~1450~~	~~14~~	~~1308~~	~~16~~	~~27.29~~
E122-03	0.12	0.05628	0.00709	0.31113	0.03871	0.04009	0.0008	464	287	275	30	253	5	8.70
E122-04	0.16	0.05481	0.00117	0.4915	0.01088	0.06503	0.00089	404	26	406	7	406	5	0.00

E122-05	0.18	0.05521	0.00114	0.5273	0.01134	0.06926	0.00096	421	25	430	8	432	6	-0.46
E122-06	0.18	0.05579	0.0015	0.52337	0.01427	0.06803	0.00097	444	36	427	10	424	6	0.71
E122-07	0.19	0.0672	0.00118	1.27243	0.02387	0.1373	0.00184	844	19	833	11	829	10	0.48
E122-08	0.19	0.05133	0.00316	0.28735	0.01749	0.04059	0.00073	256	107	256	14	256	5	0.00
E122-09	0.19	0.05678	0.00466	0.31603	0.02584	0.04036	0.00069	483	152	279	20	255	4	9.41
E122-10	0.24	0.0513	0.00162	0.29954	0.00953	0.04234	0.00062	254	46	266	7	267	4	-0.37
E122-11	0.25	0.05551	0.00121	0.49239	0.01108	0.06432	0.00088	433	27	407	8	402	5	1.24
E122-12	0.25	0.05504	0.00127	0.49814	0.01182	0.06563	0.00091	414	29	410	8	410	6	0.00
E122-13	0.27	0.05629	0.00146	0.55426	0.01466	0.0714	0.00101	464	34	448	10	445	6	0.67
~~E122-14~~	~~0.28~~	~~0.07471~~	~~0.00135~~	~~1.18126~~	~~0.02263~~	~~0.11465~~	~~0.00156~~	~~1061~~	~~19~~	~~792~~	~~11~~	~~700~~	~~9~~	~~13.14~~
E122-15	0.29	0.05495	0.00212	0.50292	0.01937	0.06637	0.00103	410	58	414	13	414	6	0.00
E122-16	0.29	0.05454	0.00109	0.44195	0.00919	0.05876	0.0008	393	24	372	6	368	5	1.09
~~E122-17~~	~~0.30~~	~~0.08134~~	~~0.00178~~	~~1.97992~~	~~0.04471~~	~~0.1765~~	~~0.00248~~	~~1230~~	~~23~~	~~1109~~	~~15~~	~~1048~~	~~14~~	~~17.37~~
E122-18	0.31	0.09088	0.00153	2.84816	0.05136	0.22725	0.00308	1444	16	1368	14	1320	16	9.39
E122-19	0.32	0.0553	0.0016	0.50138	0.0147	0.06575	0.00094	424	40	413	10	410	6	0.73
E122-20	0.33	0.06351	0.00113	1.01438	0.01925	0.11582	0.00157	725	20	711	10	706	9	0.71
E122-21	0.34	0.0513	0.00253	0.28041	0.01376	0.03964	0.00062	254	84	251	11	251	4	0.00
~~E122-22~~	~~0.35~~	~~0.09845~~	~~0.00489~~	~~0.56439~~	~~0.02652~~	~~0.04158~~	~~0.00067~~	~~1595~~	~~95~~	~~454~~	~~17~~	~~263~~	~~4~~	~~72.62~~
E122-23	0.35	0.05372	0.00244	0.40019	0.01802	0.05401	0.00088	359	72	342	13	339	5	0.88
~~E122-24~~	~~0.38~~	~~0.09506~~	~~0.00745~~	~~0.46102~~	~~0.03503~~	~~0.03517~~	~~0.00068~~	~~1529~~	~~152~~	~~385~~	~~24~~	~~223~~	~~4~~	~~72.65~~
E122-25	0.39	0.05507	0.00122	0.51675	0.01183	0.06804	0.00095	415	27	423	8	424	6	-0.24
E122-26	0.41	0.05507	0.00176	0.52356	0.01692	0.06894	0.00099	415	47	428	11	430	6	-0.47
E122-27	0.41	0.11964	0.00289	5.55451	0.13611	0.33665	0.00504	1951	23	1909	21	1871	24	4.28
E122-28	0.42	0.05454	0.00104	0.45579	0.00913	0.0606	0.00083	393	22	381	6	379	5	0.53
~~E122-29~~	~~0.43~~	~~0.16137~~	~~0.00292~~	~~8.3304~~	~~0.15825~~	~~0.37434~~	~~0.0053~~	~~2470~~	~~15~~	~~2268~~	~~17~~	~~2050~~	~~25~~	~~20.49~~
E122-30	0.43	0.05508	0.00147	0.50454	0.0137	0.06643	0.00095	415	36	415	9	415	6	0.00
E122-31	0.44	0.05561	0.0017	0.54981	0.0169	0.07169	0.00104	437	43	445	11	446	6	-0.22
E122-32	0.45	0.05523	0.00123	0.50988	0.01169	0.06694	0.00093	422	28	418	8	418	6	0.00

E122-33	0.45	0.05518	0.00151	0.5081	0.01407	0.06677	0.00098	420	36	417	9	417	6	0.00
~~E122-34~~	~~0.45~~	~~0.0697~~	~~0.00222~~	~~0.8972~~	~~0.02559~~	~~0.09336~~	~~0.00131~~	~~919~~	~~67~~	~~650~~	~~14~~	~~575~~	~~8~~	~~13.04~~
E122-35	0.45	0.05097	0.00256	0.27525	0.01381	0.03916	0.00061	239	87	247	11	248	4	-0.40
E122-36	0.47	0.10084	0.00221	3.94729	0.08912	0.28383	0.00409	1640	22	1623	18	1611	21	1.80
E122-37	0.48	0.05502	0.00133	0.51592	0.01277	0.068	0.00096	413	31	422	9	424	6	-0.47
E122-38	0.49	0.05141	0.00198	0.28248	0.0108	0.03985	0.00062	259	59	253	9	252	4	0.40
~~E122-39~~	~~0.50~~	~~0.06467~~	~~0.00209~~	~~0.568~~	~~0.01841~~	~~0.06369~~	~~0.00094~~	~~764~~	~~44~~	~~457~~	~~12~~	~~398~~	~~6~~	~~14.82~~
E122-40	0.50	0.05297	0.00156	0.3766	0.01117	0.05156	0.00075	328	41	325	8	324	5	0.31
E122-41	0.51	0.05126	0.00194	0.2897	0.01089	0.04098	0.00064	253	58	258	9	259	4	-0.39
E122-42	0.51	0.05618	0.00154	0.57044	0.01584	0.07362	0.00107	459	36	458	10	458	6	0.00
E122-43	0.51	0.05501	0.00152	0.50342	0.01404	0.06636	0.00098	413	36	414	9	414	6	0.00
E122-44	0.52	0.05507	0.00129	0.51751	0.01242	0.06814	0.00097	415	29	423	8	425	6	-0.47
E122-45	0.52	0.0556	0.00173	0.52994	0.01657	0.06912	0.00104	436	43	432	11	431	6	0.23
E122-46	0.53	0.05334	0.00145	0.37283	0.01026	0.05069	0.00074	343	36	322	8	319	5	0.94
E122-47	0.54	0.05533	0.00128	0.52147	0.01242	0.06833	0.00097	426	29	426	8	426	6	0.00
~~E122-48~~	~~0.55~~	~~0.13115~~	~~0.00775~~	~~0.68322~~	~~0.03829~~	~~0.03778~~	~~0.00071~~	~~2113~~	~~106~~	~~529~~	~~23~~	~~239~~	~~4~~	~~121.34~~
E122-49	0.57	0.055	0.00242	0.51077	0.02238	0.06734	0.00108	412	69	419	15	420	7	-0.24
E122-50	0.57	0.05541	0.00138	0.5364	0.01363	0.07019	0.00101	429	32	436	9	437	6	-0.23
E122-51	0.57	0.05666	0.00166	0.55631	0.01635	0.0712	0.00106	478	39	449	11	443	6	1.35
E122-52	0.58	0.05523	0.002	0.52011	0.01886	0.06829	0.00102	422	54	425	13	426	6	-0.23
E122-53	0.58	0.05501	0.00157	0.50499	0.01456	0.06657	0.00097	413	39	415	10	415	6	0.00
E122-54	0.58	0.07188	0.00161	1.64689	0.03795	0.16613	0.00238	983	25	988	15	991	13	-0.30
E122-55	0.59	0.04605	0.00345	0.2773	0.02022	0.04368	0.00074		166	249	16	276	5	-9.78
E122-56	0.59	0.0591	0.00166	0.53659	0.01514	0.06583	0.00098	571	36	436	10	411	6	6.08
~~E122-57~~	~~0.60~~	~~0.06445~~	~~0.00268~~	~~0.39721~~	~~0.01639~~	~~0.04469~~	~~0.00072~~	~~756~~	~~60~~	~~340~~	~~12~~	~~282~~	~~4~~	~~20.57~~
E122-58	0.61	0.05561	0.00152	0.52775	0.01456	0.06882	0.001	437	36	430	10	429	6	0.23
~~E122-59~~	~~0.62~~	~~0.09041~~	~~0.00283~~	~~2.28277~~	~~0.06365~~	~~0.18312~~	~~0.00262~~	~~1434~~	~~61~~	~~1207~~	~~20~~	~~1084~~	~~14~~	~~32.29~~

E122-60	0.62	0.05407	0.00151	0.44631	0.01261	0.05985	0.00088	374	38	375	9	375	5	0.00
E122-61	0.63	0.05343	0.00786	0.43342	0.06326	0.05882	0.00141	347	282	366	45	368	9	-0.54
E122-62	0.65	0.05118	0.00209	0.27503	0.01117	0.03897	0.00063	249	64	247	9	246	4	0.41
~~E122-63~~	~~0.65~~	~~0.0837~~	~~0.00219~~	~~2.01817~~	~~0.05349~~	~~0.17484~~	~~0.00258~~	~~1286~~	~~29~~	~~1122~~	~~18~~	~~1039~~	~~14~~	~~23.77~~
E122-64	0.66	0.09948	0.00219	3.725	0.08429	0.27151	0.00392	1614	22	1577	18	1548	20	4.26
E122-65	0.67	0.05106	0.00209	0.28513	0.01163	0.04049	0.00064	244	65	255	9	256	4	-0.39
E122-66	0.68	0.05556	0.0018	0.54149	0.01764	0.07067	0.00106	435	46	439	12	440	6	-0.23
E122-67	0.68	0.05635	0.0014	0.58911	0.01491	0.07581	0.0011	466	31	470	10	471	7	-0.21
~~E122-68~~	~~0.68~~	~~0.07969~~	~~0.00195~~	~~1.58734~~	~~0.03961~~	~~0.14444~~	~~0.00211~~	~~1189~~	~~27~~	~~965~~	~~16~~	~~870~~	~~12~~	~~10.92~~
E122-69	0.70	0.05562	0.00187	0.52307	0.01753	0.06819	0.00105	437	47	427	12	425	6	0.47
E122-70	0.70	0.05524	0.00295	0.51502	0.02697	0.06761	0.00128	422	83	422	18	422	8	0.00
E122-71	0.70	0.05647	0.00143	0.58703	0.01512	0.07538	0.0011	471	32	469	10	468	7	0.21
E122-72	0.70	0.05211	0.00238	0.33275	0.01515	0.04631	0.00074	290	75	292	12	292	5	0.00
E122-73	0.74	0.05485	0.00231	0.48992	0.02046	0.06477	0.00104	406	65	405	14	405	6	0.00
E122-74	0.76	0.06537	0.00168	1.10357	0.02876	0.12242	0.00181	786	31	755	14	744	10	1.48
E122-75	0.77	0.05685	0.00226	0.29848	0.01178	0.03807	0.00061	486	59	265	9	241	4	9.96
~~E122-76~~	~~0.80~~	~~0.0975~~	~~0.00224~~	~~2.60489~~	~~0.06112~~	~~0.19372~~	~~0.00282~~	~~1577~~	~~23~~	~~1302~~	~~17~~	~~1141~~	~~15~~	~~38.21~~
E122-77	0.81	0.06175	0.00236	0.77124	0.02943	0.09057	0.00143	665	55	580	17	559	8	3.76
E122-78	0.83	0.05534	0.00141	0.52063	0.01342	0.06822	0.00101	426	32	426	9	425	6	0.24
~~E122-79~~	~~0.84~~	~~0.07033~~	~~0.00162~~	~~0.89965~~	~~0.02117~~	~~0.09276~~	~~0.00134~~	~~938~~	~~26~~	~~652~~	~~11~~	~~572~~	~~8~~	~~13.99~~
E122-80	0.84	0.05573	0.00147	0.48095	0.01284	0.06258	0.00093	442	34	399	9	391	6	2.05
E122-81	0.84	0.05449	0.00135	0.49646	0.01249	0.06607	0.00097	391	31	409	8	412	6	-0.73
E122-82	0.86	0.0556	0.0017	0.52104	0.01595	0.06795	0.00103	436	41	426	11	424	6	0.47
E122-83	0.89	0.07142	0.0018	1.49145	0.03811	0.15142	0.00225	969	29	927	16	909	13	1.98
E122-84	0.90	0.0546	0.00145	0.407	0.01088	0.05405	0.00081	396	34	347	8	339	5	2.36
E122-85	0.93	0.05119	0.00257	0.29461	0.01465	0.04173	0.0007	249	83	262	11	264	4	-0.76
E122-86	0.94	0.0557	0.00189	0.54539	0.01853	0.071	0.00109	440	48	442	12	442	7	0.00
E122-87	0.94	0.0552	0.00166	0.523	0.01579	0.0687	0.00103	420	41	427	11	428	6	-0.23

~~E122-88~~	~~0.96~~	~~0.09752~~	~~0.00238~~	~~3.23386~~	~~0.0803~~	~~0.24046~~	~~0.00357~~	~~1577~~	~~25~~	~~1465~~	~~19~~	~~1389~~	~~19~~	~~13.53~~
E122-89	1.01	0.05121	0.00142	0.28193	0.00787	0.03992	0.00061	250	37	252	6	252	4	0.00
E122-90	1.02	0.06166	0.00154	0.59592	0.01513	0.07008	0.00103	662	30	475	10	437	6	8.70
E122-91	1.06	0.05508	0.00184	0.51205	0.01705	0.06741	0.00106	415	46	420	11	421	6	-0.24
E122-92	1.10	0.05699	0.00202	0.62179	0.02192	0.07912	0.00125	491	50	491	14	491	7	0.00
E122-93	1.11	0.05629	0.00314	0.34594	0.01915	0.04457	0.00075	464	93	302	14	281	5	7.47
E122-94	1.12	0.05637	0.00215	0.60428	0.02298	0.07773	0.00123	467	56	480	15	483	7	-0.62
E122-95	1.17	0.0533	0.00164	0.41201	0.01269	0.05605	0.00086	342	42	350	9	352	5	-0.57
E122-96	1.24	0.05529	0.00226	0.51791	0.02096	0.06792	0.00113	424	61	424	14	424	7	0.00
E122-97	1.27	0.05657	0.00382	0.61391	0.04095	0.07868	0.00151	475	114	486	26	488	9	-0.41
E122-98	1.32	0.05663	0.00182	0.55621	0.01781	0.07123	0.00112	477	43	449	12	444	7	1.13
E122-99	1.36	0.06638	0.00331	0.89959	0.04256	0.09828	0.00152	819	107	652	23	604	9	7.95
E122-100	1.50	0.07139	0.00189	1.53676	0.04099	0.15608	0.00235	969	31	945	16	935	13	1.07
E122-101	1.58	0.05153	0.00188	0.2918	0.01062	0.04106	0.00065	265	54	260	8	259	4	0.39
~~E122-102~~	~~1.74~~	~~0.11687~~	~~0.00301~~	~~3.01009~~	~~0.07827~~	~~0.18676~~	~~0.00283~~	~~1909~~	~~26~~	~~1410~~	~~20~~	~~1104~~	~~15~~	~~72.92~~
~~E122-103~~	~~1.79~~	~~0.05947~~	~~0.01845~~	~~0.20007~~	~~0.06186~~	~~0.0244~~	~~0.00064~~	~~584~~	~~602~~	~~185~~	~~52~~	~~155~~	~~4~~	~~19.35~~
E122-104	1.80	0.05372	0.00165	0.42462	0.01306	0.05732	0.00089	359	42	359	9	359	5	0.00
E122-105	2.51	0.0705	0.00188	1.43784	0.03868	0.14788	0.00224	943	31	905	16	889	13	1.80
E123														
E123-01	0.83	0.05097	0.00166	0.27264	0.00884	0.03879	0.0006	239	46	245	7	245	4	0.00
E123-02	0.70	0.05628	0.002	0.58143	0.02066	0.07492	0.00113	463	52	465	13	466	7	-0.21
E123-03	0.36	0.05547	0.00175	0.53115	0.01682	0.06944	0.00103	431	44	433	11	433	6	0.00
E123-04	0.66	0.05529	0.00125	0.51648	0.01201	0.06774	0.00095	424	28	423	8	423	6	0.00
E123-05	1.03	0.0513	0.00208	0.28237	0.0114	0.03992	0.00062	254	64	253	9	252	4	0.40
E123-06	0.12	0.0703	0.00142	1.47643	0.03105	0.1523	0.0021	937	22	921	13	914	12	0.77
E123-07	0.78	0.05064	0.00159	0.24322	0.00765	0.03483	0.00052	224	45	221	6	221	3	0.00
E123-08	0.63	0.05531	0.00153	0.52283	0.01466	0.06854	0.00098	425	37	427	10	427	6	0.00

E123-09	0.62	0.05533	0.00148	0.52074	0.01408	0.06825	0.00099	426	35	426	9	426	6	0.00
E123-10	0.62	0.05152	0.00304	0.29557	0.01726	0.0416	0.00074	264	101	263	14	263	5	0.00
E123-11	0.71	0.05576	0.00268	0.54452	0.02594	0.07082	0.00116	443	77	441	17	441	7	0.00
E123-12	0.52	0.07203	0.00162	1.52594	0.03533	0.15363	0.00216	987	25	941	14	921	12	2.17
E123-13	0.55	0.05139	0.00238	0.28751	0.0132	0.04057	0.00066	258	75	257	10	256	4	0.39
E123-14	0.13	0.07048	0.00142	1.4688	0.03084	0.15113	0.00208	942	22	918	13	907	12	1.21
E123-15	0.64	0.05518	0.00135	0.51406	0.01287	0.06756	0.00096	420	31	421	9	421	6	0.00
E123-16	0.59	0.06948	0.00156	1.45273	0.03344	0.15162	0.00215	913	25	911	14	910	12	0.11
E123-17	0.76	0.05089	0.00226	0.26417	0.01166	0.03764	0.0006	236	72	238	9	238	4	0.00
E123-18	0.12	0.06917	0.00141	1.42494	0.03016	0.14938	0.00207	904	22	899	13	897	12	0.22
E123-19	0.77	0.05102	0.00172	0.26664	0.00902	0.0379	0.00057	242	50	240	7	240	4	0.00
E123-20	0.35	0.05391	0.00194	0.45125	0.01497	0.06071	0.00085	367	83	378	10	380	5	-0.53
E123-21	0.10	0.07142	0.00142	1.45737	0.03036	0.14798	0.00203	969	22	913	13	890	11	2.58
E123-22	0.54	0.05527	0.00153	0.51887	0.01453	0.06807	0.00098	423	37	424	10	425	6	-0.24
E123-23	0.14	0.07088	0.00142	1.46728	0.03071	0.15011	0.00207	954	22	917	13	902	12	1.66
E123-24	0.12	0.0692	0.00141	1.46157	0.03099	0.15316	0.00212	905	22	915	13	919	12	-0.44
E123-25	0.80	0.05104	0.00168	0.27668	0.00915	0.03931	0.00058	243	49	248	7	249	4	-0.40
E123-26	0.65	0.05108	0.00205	0.27479	0.01101	0.03901	0.0006	244	64	247	9	247	4	0.00
E123-27	0.69	0.05714	0.0013	0.58866	0.01374	0.0747	0.00105	497	28	470	9	464	6	1.29
E123-28	0.63	0.05523	0.00144	0.5166	0.01363	0.06783	0.00098	422	34	423	9	423	6	0.00
E123-29	0.84	0.0561	0.00148	0.51941	0.01389	0.06714	0.00096	456	35	425	9	419	6	1.43
~~E123-30~~	~~0.59~~	~~0.06137~~	~~0.00201~~	~~0.32562~~	~~0.01071~~	~~0.03847~~	~~0.00057~~	~~652~~	~~45~~	~~286~~	~~8~~	~~243~~	4	~~17.70~~
E123-31	0.45	0.05632	0.00152	0.58867	0.01611	0.07579	0.00109	465	36	470	10	471	7	-0.21
E123-32	0.59	0.05144	0.00318	0.28371	0.01738	0.04	0.00068	261	109	254	14	253	4	0.40
E123-33	0.78	0.05086	0.00182	0.26311	0.00941	0.03751	0.00057	234	54	237	8	237	4	0.00
E123-34	0.18	0.05564	0.00125	0.49308	0.01142	0.06426	0.0009	438	28	407	8	401	5	1.50
E123-35	0.60	0.05502	0.0015	0.50697	0.01403	0.06681	0.00095	413	37	416	9	417	6	-0.24
E123-36	0.64	0.05579	0.00159	0.52287	0.01508	0.06797	0.00098	444	39	427	10	424	6	0.71

E123-37	0.63	0.05135	0.00338	0.28958	0.01893	0.04089	0.0007	257	119	258	15	258	4	0.00
E123-38	0.73	0.06904	0.00146	1.43813	0.03158	0.15104	0.0021	900	24	905	13	907	12	-0.22
E123-39	0.53	0.05526	0.00169	0.51676	0.01598	0.06781	0.00098	423	43	423	11	423	6	0.00
E123-40	0.56	0.05576	0.00161	0.54797	0.01593	0.07126	0.00104	443	39	444	10	444	6	0.00
E123-41	0.51	0.05489	0.00152	0.50169	0.01413	0.06627	0.00095	408	38	413	10	414	6	-0.24
~~E123-42~~	~~0.27~~	~~0.0871~~	~~0.00191~~	~~1.26754~~	~~0.02858~~	~~0.10553~~	~~0.00148~~	~~1363~~	~~23~~	~~831~~	~~13~~	~~647~~	~~9~~	~~28.44~~
E123-43	1.28	0.0508	0.00198	0.25868	0.01003	0.03693	0.00058	232	60	234	8	234	4	0.00
E123-44	0.56	0.05571	0.00229	0.52089	0.02129	0.0678	0.00109	441	62	426	14	423	7	0.71
~~E123-45~~	~~0.72~~	~~0.07834~~	~~0.00199~~	~~1.87648~~	~~0.04827~~	~~0.1737~~	~~0.00256~~	~~1156~~	~~28~~	~~1073~~	~~17~~	~~1032~~	~~14~~	~~12.02~~
E123-46	0.22	0.06928	0.00159	1.5055	0.03533	0.15759	0.00223	907	26	933	14	943	12	-1.06
E123-47	0.24	0.07269	0.00251	1.815	0.06263	0.18106	0.00279	1005	45	1051	23	1073	15	-6.34
E123-48	0.82	0.05511	0.00153	0.48839	0.01374	0.06427	0.00093	417	37	404	9	402	6	0.50
E123-49	0.39	0.06985	0.00143	1.4017	0.02987	0.14552	0.00201	924	23	890	13	876	11	1.60
~~E123-50~~	~~0.73~~	~~0.06627~~	~~0.00237~~	~~0.35375~~	~~0.01263~~	~~0.03871~~	~~0.00059~~	~~815~~	~~49~~	~~308~~	~~9~~	~~245~~	~~4~~	~~25.71~~
E123-51	1.40	0.05264	0.00211	0.37941	0.0152	0.05226	0.00079	313	63	327	11	328	5	-0.30
E123-52	1.11	0.05088	0.00486	0.26747	0.02536	0.03812	0.00072	235	179	241	20	241	4	0.00
E123-53	0.45	0.07113	0.00157	1.49981	0.03415	0.15289	0.00214	961	25	930	14	917	12	1.42
E123-54	0.50	0.05521	0.00163	0.52659	0.01561	0.06917	0.00102	421	40	430	10	431	6	-0.23
E123-55	0.59	0.05122	0.00205	0.28835	0.01144	0.04082	0.00065	251	62	257	9	258	4	-0.39
E123-56	0.63	0.05541	0.00159	0.52393	0.01514	0.06856	0.00099	429	39	428	10	427	6	0.23
E123-57	0.79	0.05366	0.00248	0.28451	0.01309	0.03845	0.0006	357	76	254	10	243	4	4.53
E123-59	0.10	0.06964	0.00191	1.3939	0.03297	0.14517	0.002	918	58	886	14	874	11	1.37
E123-60	0.71	0.0963	0.00223	3.29517	0.07781	0.24812	0.00358	1554	24	1480	18	1429	18	8.75
E123-61	0.51	0.0556	0.00176	0.53196	0.01692	0.06937	0.00102	436	45	433	11	432	6	0.23
E123-62	0.24	0.07365	0.0018	1.52621	0.03787	0.15026	0.00217	1032	28	941	15	902	12	4.32
E123-63	1.08	0.05214	0.00858	0.34281	0.05605	0.04768	0.00115	292	304	299	42	300	7	-0.33
E123-64	0.40	0.05588	0.00222	0.57166	0.02265	0.07418	0.00114	448	61	459	15	461	7	-0.43
E123-65	0.70	0.05069	0.00141	0.25851	0.00728	0.03698	0.00053	227	39	233	6	234	3	-0.43

E123-66	0.54	0.05556	0.00169	0.52553	0.01606	0.06859	0.00101	435	42	429	11	428	6	0.23
E123-67	0.85	0.05074	0.00286	0.26611	0.01483	0.03803	0.00066	229	97	240	12	241	4	-0.41
~~E123-68~~	~~0.20~~	~~0.09592~~	~~0.00204~~	~~2.57881~~	~~0.05687~~	~~0.19496~~	~~0.00271~~	~~1546~~	~~22~~	~~1295~~	~~16~~	~~1148~~	~~15~~	~~34.67~~
E123-69	0.13	0.07016	0.00162	1.44615	0.03424	0.14945	0.00211	933	26	908	14	898	12	1.11
E123-70	0.78	0.05119	0.00296	0.27501	0.01585	0.03896	0.00062	249	104	247	13	246	4	0.41
E123-71	0.80	0.05555	0.00145	0.5316	0.0141	0.06939	0.001	434	34	433	9	432	6	0.23
E123-72	0.65	0.0558	0.0021	0.54425	0.02039	0.07073	0.0011	444	56	441	13	441	7	0.00
E123-73	0.75	0.06901	0.0019	1.44684	0.04016	0.15202	0.00225	899	33	909	17	912	13	-0.33
E123-74	0.86	0.05131	0.00263	0.27103	0.01368	0.0383	0.00068	255	83	244	11	242	4	0.83
E123-75	0.57	0.05151	0.00294	0.2841	0.01604	0.03999	0.0007	264	97	254	13	253	4	0.40
E123-76	0.80	0.05116	0.00229	0.27836	0.01232	0.03945	0.00065	248	71	249	10	249	4	0.00
E123-77	0.15	0.07006	0.00172	1.46182	0.03654	0.15129	0.00218	930	28	915	15	908	12	0.77
E123-78	0.80	0.05085	0.00563	0.26438	0.02904	0.0377	0.00076	234	210	238	23	239	5	-0.42
E123-79	0.60	0.05109	0.00275	0.27516	0.01471	0.03905	0.00063	245	93	247	12	247	4	0.00
E123-80	0.09	0.06919	0.00193	1.34945	0.03279	0.14146	0.00196	904	59	867	14	853	11	1.64
E123-81	0.77	0.05391	0.00344	0.44454	0.02802	0.05979	0.0011	367	109	373	20	374	7	-0.27
E123-82	0.55	0.05545	0.0019	0.52855	0.01806	0.06912	0.00106	430	49	431	12	431	6	0.00
E123-83	0.92	0.05107	0.00315	0.27385	0.01675	0.03889	0.00067	244	109	246	13	246	4	0.00
E123-84	0.69	0.05182	0.00209	0.31246	0.01255	0.04372	0.00068	277	63	276	10	276	4	0.00
E123-85	0.57	0.05476	0.00145	0.48306	0.01291	0.06397	0.00093	402	34	400	9	400	6	0.00
E123-86	0.79	0.05449	0.00189	0.47864	0.01653	0.06369	0.00099	391	50	397	11	398	6	-0.25
E123-87	0.82	0.05824	0.00187	0.533	0.01706	0.06636	0.00101	539	44	434	11	414	6	4.83
~~E123-88~~	~~0.57~~	~~0.06186~~	~~0.00182~~	~~0.54314~~	~~0.01609~~	~~0.06367~~	~~0.00093~~	~~669~~	~~39~~	~~440~~	~~11~~	~~398~~	~~6~~	~~10.55~~
E123-89	1.55	0.05089	0.00813	0.26653	0.04218	0.03798	0.001	236	288	240	34	240	6	0.00
E123-90	0.60	0.05511	0.00147	0.46725	0.01263	0.06148	0.00089	417	35	389	9	385	5	1.04
E123-91	0.49	0.05527	0.0016	0.52338	0.01525	0.06866	0.00102	423	39	427	10	428	6	-0.23
E123-92	0.61	0.05121	0.00245	0.27861	0.01316	0.03945	0.00066	250	78	250	10	249	4	0.40
E123-93	0.72	0.05127	0.00317	0.27865	0.01706	0.03941	0.00067	253	109	250	14	249	4	0.40

E123-94	1.57	0.05124	0.00241	0.25985	0.01218	0.03677	0.00058	252	79	235	10	233	4	0.86
E123-95	0.47	0.05628	0.00146	0.55503	0.01462	0.07151	0.00104	463	33	448	10	445	6	0.67
E123-96	0.59	0.05669	0.00179	0.51996	0.01642	0.06651	0.00101	479	43	425	11	415	6	2.41
E123-97	0.10	0.05522	0.00154	0.50066	0.01404	0.06574	0.00096	421	37	412	9	410	6	0.49
E123-98	0.54	0.05563	0.00156	0.53956	0.01517	0.07033	0.00104	438	37	438	10	438	6	0.00
E123-99	0.76	0.07141	0.00179	1.4484	0.03683	0.14708	0.00212	969	29	909	15	885	12	2.71
E123-100	0.42	0.05525	0.00182	0.51855	0.01704	0.06806	0.00103	422	46	424	11	424	6	0.00
EBLE														
~~EBLE-01~~	~~0.16~~	~~0.15424~~	~~0.00377~~	~~6.23369~~	~~0.12741~~	~~0.29312~~	~~0.00394~~	~~2393~~	~~43~~	~~2009~~	~~18~~	~~1657~~	~~20~~	~~44.42~~
EBLE-02	0.66	0.05655	0.00138	0.59554	0.0145	0.07637	0.0011	474	29	474	9	474	7	0.00
EBLE-03	0.61	0.05611	0.00175	0.56966	0.01766	0.07362	0.0011	457	43	458	11	458	7	0.00
EBLE-04	1.22	0.05142	0.00172	0.28997	0.00954	0.0409	0.00063	260	47	259	8	258	4	0.39
EBLE-05	1.02	0.05459	0.00158	0.43733	0.01253	0.05809	0.00086	395	38	368	9	364	5	1.10
EBLE-06	0.77	0.05152	0.0023	0.29882	0.01315	0.04206	0.00068	264	71	265	10	266	4	-0.38
EBLE-07	0.79	0.05199	0.00161	0.25137	0.00774	0.03506	0.00052	285	44	228	6	222	3	2.70
EBLE-08	0.49	0.05613	0.00215	0.56663	0.02137	0.07321	0.00117	458	55	456	14	455	7	0.22
EBLE-09	1.04	0.05748	0.00203	0.64321	0.0223	0.08115	0.00129	510	48	504	14	503	8	0.20
EBLE-10	0.93	0.09888	0.00226	3.84768	0.08806	0.28217	0.00411	1603	22	1603	18	1602	21	0.06
EBLE-11	0.76	0.06946	0.00365	1.08281	0.05569	0.11304	0.0021	912	75	745	27	690	12	7.97
~~EBLE-12~~	~~0.52~~	~~0.07558~~	~~0.00217~~	~~0.89493~~	~~0.02522~~	~~0.08587~~	~~0.00134~~	~~1084~~	~~32~~	~~649~~	~~14~~	~~531~~	~~8~~	~~22.22~~
EBLE-13	0.87	0.05153	0.00162	0.29376	0.00911	0.04134	0.00062	265	44	262	7	261	4	0.38
EBLE-14	1.66	0.05151	0.00129	0.29378	0.00736	0.04136	0.00059	264	32	262	6	261	4	0.38
EBLE-15	0.54	0.05543	0.0021	0.52765	0.01952	0.06904	0.00116	430	53	430	13	430	7	0.00
EBLE-16	0.45	0.05461	0.00469	0.47171	0.04012	0.06264	0.00119	396	158	392	28	392	7	0.00
EBLE-17	1.21	0.05733	0.00714	0.42361	0.05209	0.05358	0.00131	504	231	359	37	336	8	6.85
EBLE-18	0.66	0.05117	0.00271	0.28811	0.01506	0.04083	0.00068	248	90	257	12	258	4	-0.39
EBLE-19	0.49	0.05496	0.0029	0.49362	0.02561	0.06513	0.00112	411	85	407	17	407	7	0.00

EBLE-20	0.02	0.05981	0.00154	0.80069	0.02047	0.09709	0.00142	597	31	597	12	597	8	0.00
EBLE-21	0.58	0.05153	0.00491	0.28883	0.02718	0.04065	0.00085	265	174	258	21	257	5	0.39
EBLE-22	0.33	0.05575	0.00278	0.53508	0.02617	0.0696	0.0012	442	78	435	17	434	7	0.23
EBLE-23	0.51	0.05534	0.00185	0.5201	0.01712	0.06815	0.00106	426	46	425	11	425	6	0.00
EBLE-24	0.37	0.05564	0.00149	0.53907	0.01427	0.07026	0.00104	438	33	438	9	438	6	0.00
EBLE-25	0.06	0.05711	0.00274	0.65143	0.02948	0.08273	0.00131	496	108	509	18	512	8	-0.59
EBLE-26	0.08	0.05879	0.00178	0.72548	0.02162	0.08949	0.00136	559	39	554	13	553	8	0.18
EBLE-27	0.91	0.06884	0.002	1.40042	0.03985	0.14753	0.00231	894	34	889	17	887	13	0.23
EBLE-28	0.09	0.05935	0.00154	0.76731	0.01976	0.09376	0.00138	580	31	578	11	578	8	0.00
EBLE-29	1.06	0.16123	0.00359	10.09879	0.22524	0.45426	0.00645	2469	20	2444	21	2414	29	2.28
EBLE-30	0.25	0.06857	0.00176	1.14444	0.02908	0.12104	0.00178	886	29	775	14	737	10	5.16
EBLE-31	0.33	0.05068	0.00193	0.24711	0.00925	0.03536	0.00057	226	57	224	8	224	4	0.00
EBLE-32	0.20	0.0704	0.0019	1.50219	0.03982	0.15474	0.00238	940	30	931	16	927	13	0.43
EBLE-33	0.59	0.05571	0.00196	0.53588	0.01831	0.06975	0.00115	441	47	436	12	435	7	0.23
EBLE-34	0.66	0.05761	0.00389	0.52862	0.03517	0.06655	0.00125	515	113	431	23	415	8	3.86
EBLE-35	0.56	0.05597	0.00159	0.5553	0.01561	0.07195	0.00107	451	37	448	10	448	6	0.00
EBLE-36	0.29	0.05655	0.00164	0.58635	0.01679	0.0752	0.00113	474	37	469	11	467	7	0.43
EBLE-37	0.59	0.05242	0.00148	0.34686	0.00966	0.04799	0.00072	304	37	302	7	302	4	0.00
EBLE-38	0.25	0.05605	0.00167	0.5598	0.01637	0.07244	0.00112	454	38	451	11	451	7	0.00
EBLE-39	0.75	0.05518	0.00263	0.54808	0.02545	0.07204	0.00129	420	72	444	17	448	8	-0.89
EBLE-40	1.01	0.05719	0.00249	0.62889	0.02686	0.07975	0.00134	499	64	495	17	495	8	0.00
EBLE-41	0.80	0.09172	0.00218	3.4319	0.08107	0.27136	0.00392	1462	24	1512	19	1548	20	-5.56
EBLE-42	0.16	0.05536	0.00184	0.55179	0.01799	0.07229	0.00114	427	45	446	12	450	7	-0.89
EBLE-43	0.93	0.05243	0.00272	0.34913	0.0177	0.04829	0.00088	304	82	304	13	304	5	0.00
EBLE-44	0.15	0.06883	0.00181	1.49285	0.03855	0.15729	0.00236	894	29	927	16	942	13	-1.59
EBLE-45	0.40	0.05634	0.00157	0.51194	0.01402	0.06589	0.00099	466	35	420	9	411	6	2.19
EBLE-46	0.90	0.05714	0.00166	0.63091	0.0179	0.08008	0.00124	497	36	497	11	497	7	0.00
EBLE-47	0.55	0.07175	0.00218	1.20748	0.03585	0.12204	0.00189	979	36	804	16	742	11	8.36

EBLE-48	0.86	0.07153	0.0021	1.64366	0.04696	0.16664	0.00263	973	33	987	18	994	15	-0.70
EBLE-49	1.38	0.05141	0.00321	0.28512	0.01746	0.04022	0.00076	259	106	255	14	254	5	0.39
EBLE-50	1.13	0.05663	0.00214	0.59569	0.02185	0.07628	0.00129	477	51	474	14	474	8	0.00
EBLE-51	0.66	0.08232	0.00462	2.46304	0.13194	0.21699	0.00362	1253	113	1261	39	1266	19	-1.03
EBLE-52	0.43	0.05582	0.00159	0.5423	0.01515	0.07045	0.00106	445	36	440	10	439	6	0.23
~~EBLE-53~~	~~0.75~~	~~0.06064~~	~~0.00425~~	~~0.47741~~	~~0.03255~~	~~0.0571~~	~~0.00091~~	~~627~~	~~156~~	~~396~~	~~22~~	~~358~~	~~6~~	~~10.61~~
EBLE-54	0.46	0.05474	0.00181	0.48047	0.01552	0.06365	0.001	402	44	398	11	398	6	0.00
EBLE-55	0.47	0.05152	0.00175	0.29305	0.00975	0.04125	0.00065	264	48	261	8	261	4	0.00
EBLE-56	0.46	0.05205	0.00171	0.3259	0.01042	0.04541	0.00073	288	44	286	8	286	5	0.00
EBLE-57	0.25	0.05948	0.00207	0.76845	0.02605	0.09369	0.0015	585	46	579	15	577	9	0.35
EBLE-58	0.21	0.0564	0.00178	0.5748	0.01765	0.0739	0.00117	468	40	461	11	460	7	0.22
EBLE-59	0.54	0.05466	0.00317	0.4748	0.02692	0.063	0.00118	398	93	394	19	394	7	0.00
EBLE-60	0.40	0.1006	0.00257	4.30114	0.10791	0.31004	0.00459	1635	26	1694	21	1741	23	-6.09
EBLE-61	0.71	0.05422	0.00395	0.45022	0.03222	0.06021	0.00118	380	126	377	23	377	7	0.00
EBLE-62	0.45	0.05419	0.00215	0.45406	0.01751	0.06076	0.00102	379	57	380	12	380	6	0.00
EBLE-63	0.34	0.05627	0.00172	0.57623	0.01721	0.07426	0.00115	463	39	462	11	462	7	0.00
EBLE-64	0.49	0.0545	0.00308	0.46071	0.02561	0.06131	0.00108	392	93	385	18	384	7	0.26
EBLE-65	0.90	0.06721	0.00208	1.32604	0.03986	0.14308	0.00226	844	37	857	17	862	13	-0.58
EBLE-66	0.57	0.05119	0.00229	0.27419	0.01193	0.03884	0.00068	249	68	246	10	246	4	0.00
EBLE-67	0.42	0.07787	0.00209	2.0848	0.05468	0.19415	0.00294	1144	29	1144	18	1144	16	0.00
EBLE-68	0.71	0.05457	0.00166	0.46962	0.01395	0.06241	0.00097	395	39	391	10	390	6	0.26
EBLE-69	1.09	0.07142	0.00235	1.6305	0.05191	0.16555	0.00272	969	39	982	20	988	15	-0.61
EBLE-70	0.49	0.05319	0.00247	0.39244	0.01775	0.0535	0.00094	337	71	336	13	336	6	0.00
EBLE-71	0.92	0.05476	0.00177	0.49783	0.01564	0.06592	0.00104	402	42	410	11	412	6	-0.49
EBLE-72	0.63	0.05453	0.00245	0.47014	0.02048	0.06253	0.00111	393	66	391	14	391	7	0.00
EBLE-73	0.41	0.05055	0.00206	0.24042	0.00952	0.03449	0.00058	220	60	219	8	219	4	0.00
EBLE-74	0.72	0.05641	0.00244	0.58364	0.02447	0.07503	0.00133	469	61	467	16	466	8	0.21
EBLE-75	0.96	0.05903	0.00204	0.74616	0.02504	0.09166	0.00148	568	45	566	15	565	9	0.18

EBLE-76	0.92	0.05124	0.0041	0.2815	0.02202	0.03984	0.00087	252	138	252	17	252	5	0.00
EBLE-77	1.29	0.08695	0.00284	2.78739	0.08802	0.23248	0.00387	1359	36	1352	24	1347	20	0.89
~~EBLE-78~~	~~0.17~~	~~0.08563~~	~~0.00264~~	~~2.3541~~	~~0.07017~~	~~0.19936~~	~~0.0032~~	~~1330~~	~~33~~	~~1229~~	~~21~~	~~1172~~	~~17~~	~~13.48~~
EBLE-79	0.79	0.05622	0.00189	0.57563	0.01869	0.07425	0.00121	461	43	462	12	462	7	0.00
EBLE-80	1.10	0.0929	0.00258	3.31686	0.08948	0.25889	0.00396	1486	29	1485	21	1484	20	0.13
EBLE-81	0.88	0.06238	0.00196	1.12047	0.03413	0.13026	0.00209	687	38	763	16	789	12	-3.30
EBLE-82	0.59	0.05037	0.00179	0.22709	0.00781	0.03269	0.00054	212	49	208	6	207	3	0.48
EBLE-83	0.86	0.05536	0.00194	0.53636	0.01822	0.07025	0.00116	427	47	436	12	438	7	-0.46
EBLE-85	0.20	0.07019	0.0023	1.44418	0.04575	0.14919	0.00244	934	39	907	19	896	14	1.23
EBLE-86	0.74	0.05601	0.002	0.57207	0.01978	0.07406	0.00122	453	48	459	13	461	7	-0.43
EBLE-87	4.04	0.16052	0.00503	10.55132	0.31749	0.47663	0.00828	2461	28	2484	28	2513	36	-2.07
EBLE-88	0.15	0.11569	0.00339	5.62295	0.15916	0.35242	0.0056	1891	29	1920	24	1946	27	-2.83
EBLE-89	0.31	0.05062	0.00198	0.24858	0.00943	0.03561	0.0006	224	57	225	8	226	4	-0.44
EBLE-90	1.05	0.05095	0.0028	0.26785	0.01433	0.03812	0.00071	239	89	241	11	241	4	0.00
EBLE-91	0.23	0.05802	0.00215	0.68511	0.02452	0.08561	0.00145	531	49	530	15	530	9	0.00
EBLE-92	0.48	0.0601	0.00202	0.5798	0.01879	0.06995	0.00113	607	42	464	12	436	7	6.42
EBLE-93	0.16	0.05607	0.00173	0.56103	0.01673	0.07255	0.00115	455	39	452	11	452	7	0.00
EBLE-94	0.92	0.05141	0.00264	0.2757	0.01378	0.03889	0.00071	259	81	247	11	246	4	0.41
EBLE-95	0.64	0.056	0.00206	0.55528	0.01964	0.0719	0.00124	452	48	448	13	448	7	0.00
EBLE-96	0.69	0.05548	0.00221	0.52408	0.02015	0.06849	0.00117	432	55	428	13	427	7	0.23
EBLE-97	0.54	0.05561	0.00202	0.53078	0.0186	0.0692	0.00114	437	49	432	12	431	7	0.23
EBLE-98	0.94	0.0472	0.00177	0.05785	0.0021	0.00889	0.00015	59	51	57	2	57.1	1	-0.18
EBLE-99	0.69	0.05505	0.00195	0.56694	0.01932	0.07466	0.00124	414	47	456	13	464	7	-1.72
EBLE-100	0.94	0.05112	0.00241	0.27577	0.01251	0.03911	0.00074	246	70	247	10	247	5	0.00
E2-2														
E22-01	0.89	0.05566	0.00119	0.52896	0.01161	0.06891	0.00091	439	26	431	8	430	5	0.23
~~E22-02~~	~~1.02~~	~~0.10325~~	~~0.00154~~	~~3.29917~~	~~0.05315~~	~~0.2317~~	~~0.003~~	~~1683~~	~~14~~	~~1481~~	~~13~~	~~1343~~	~~16~~	~~25.32~~

~~E22-03~~	~~0.33~~	~~0.16039~~	~~0.00204~~	~~7.82901~~	~~0.11221~~	~~0.35395~~	~~0.00445~~	~~2460~~	~~11~~	~~2212~~	~~13~~	~~1953~~	~~21~~	~~25.96~~
~~E22-04~~	~~1.52~~	~~0.0795~~	~~0.01369~~	~~0.51848~~	~~0.0883~~	~~0.04729~~	~~0.00141~~	~~1185~~	~~303~~	~~424~~	~~59~~	~~298~~	~~9~~	~~42.28~~
E22-05	0.56	0.11572	0.00157	5.23075	0.07844	0.32777	0.00417	1891	12	1858	13	1828	20	3.45
E22-06	3.28	0.05132	0.00344	0.28455	0.01894	0.0402	0.00065	255	123	254	15	254	4	0.00
E22-07	0.87	0.05879	0.00103	0.69497	0.01284	0.08571	0.0011	559	20	536	8	530	7	1.13
~~E22-08~~	~~0.50~~	~~0.05792~~	~~0.00147~~	~~0.23948~~	~~0.00617~~	~~0.02998~~	~~0.00041~~	~~527~~	~~33~~	~~218~~	~~5~~	~~190~~	~~3~~	~~14.74~~
E22-09	0.65	0.05131	0.00104	0.26443	0.00555	0.03737	0.00049	255	25	238	4	237	3	0.42
E22-10	1.36	0.05347	0.00102	0.37303	0.00741	0.05058	0.00066	349	23	322	5	318	4	1.26
E22-11	0.57	0.05268	0.00253	0.35708	0.01705	0.04915	0.00075	315	81	310	13	309	5	0.32
E22-12	0.22	0.05542	0.00097	0.50153	0.00929	0.06562	0.00085	429	20	413	6	410	5	0.73
E22-13	0.80	0.05137	0.00348	0.26788	0.01795	0.03781	0.00067	257	121	241	14	239	4	0.84
E22-14	0.89	0.18641	0.00243	12.81803	0.18745	0.4986	0.0063	2711	11	2666	14	2608	27	3.95
E22-15	0.34	0.07112	0.00101	1.57562	0.02455	0.16065	0.00204	961	14	961	10	960	11	0.10
~~E22-16~~	~~0.48~~	~~0.10491~~	~~0.00142~~	~~2.84101~~	~~0.04255~~	~~0.19636~~	~~0.00248~~	~~1713~~	~~12~~	~~1366~~	~~11~~	~~1156~~	~~13~~	~~48.18~~
E22-17	0.87	0.05116	0.00165	0.26799	0.00867	0.03798	0.00053	248	49	241	7	240	3	0.42
E22-18	0.74	0.08918	0.00124	2.71598	0.04156	0.22084	0.00279	1408	13	1333	11	1286	15	9.49
E22-19	0.88	0.0527	0.00658	0.34792	0.04317	0.04787	0.00097	316	243	303	33	301	6	0.66
E22-20	0.57	0.05644	0.00096	0.53814	0.00969	0.06914	0.00089	470	19	437	6	431	5	1.39
~~E22-21~~	~~0.55~~	~~0.06243~~	~~0.00247~~	~~0.57045~~	~~0.02262~~	~~0.06626~~	~~0.00095~~	~~689~~	~~60~~	~~458~~	~~15~~	~~414~~	~~6~~	~~10.63~~
E22-22	0.35	0.0705	0.00175	1.37737	0.0346	0.14167	0.00196	943	29	879	15	854	11	2.93
E22-23	0.63	0.05618	0.00124	0.52173	0.01189	0.06733	0.00089	459	28	426	8	420	5	1.43
E22-24	0.39	0.05512	0.00144	0.50051	0.01327	0.06585	0.00088	417	36	412	9	411	5	0.24
E22-25	0.78	0.053	0.00134	0.37332	0.00963	0.05107	0.00068	329	35	322	7	321	4	0.31
E22-26	1.28	0.05112	0.00231	0.27186	0.01227	0.03856	0.00056	246	77	244	10	244	3	0.00
E22-27	0.84	0.05031	0.0016	0.23245	0.00741	0.0335	0.00047	209	48	212	6	212	3	0.00
E22-28	0.69	0.05473	0.00168	0.49692	0.01536	0.06583	0.00091	401	45	410	10	411	6	-0.24
E22-29	0.80	0.05177	0.00292	0.29264	0.01648	0.04099	0.0006	275	102	261	13	259	4	0.77
E22-30	0.34	0.08355	0.00216	2.29683	0.06024	0.19932	0.00278	1282	30	1211	19	1172	15	9.39

~~E22-31~~	~~0.27~~	~~0.09608~~	~~0.00238~~	~~2.60666~~	~~0.05482~~	~~0.19677~~	~~0.00256~~	~~1549~~	~~48~~	~~1303~~	~~15~~	~~1158~~	~~14~~	~~33.77~~
~~E22-32~~	~~0.30~~	~~0.09227~~	~~0.00134~~	~~2.09444~~	~~0.03324~~	~~0.16458~~	~~0.00209~~	~~1473~~	~~14~~	~~1147~~	~~11~~	~~982~~	~~12~~	~~16.80~~
E22-33	1.20	0.0497	0.00562	0.28883	0.0322	0.04215	0.00078	181	251	258	25	266	5	-3.01
E22-34	0.13	0.12283	0.00176	5.56008	0.08732	0.32822	0.00417	1998	13	1910	14	1830	20	9.18
E22-35	0.78	0.05697	0.00116	0.62408	0.0132	0.07944	0.00104	490	25	492	8	493	6	-0.20
E22-36	0.86	0.05336	0.00204	0.29991	0.01143	0.04075	0.0006	344	59	266	9	257	4	3.50
E22-37	0.72	0.05705	0.00135	0.42163	0.01022	0.05359	0.00071	493	31	357	7	337	4	5.93
E22-38	1.02	0.05229	0.00312	0.31085	0.01842	0.04311	0.00068	298	107	275	14	272	4	1.10
~~E22-39~~	~~1.66~~	~~0.08419~~	~~0.00168~~	~~1.6013~~	~~0.03302~~	~~0.13791~~	~~0.00184~~	~~1297~~	~~21~~	~~971~~	~~13~~	~~833~~	~~10~~	~~16.57~~
E22-40	0.82	0.0597	0.00188	0.54264	0.01715	0.0659	0.00092	593	44	440	11	411	6	7.06
E22-41	0.57	0.05148	0.0012	0.27932	0.00665	0.03934	0.00053	262	31	250	5	249	3	0.40
E22-42	2.57	0.11623	0.00203	5.21804	0.09583	0.3255	0.00433	1899	16	1856	16	1817	21	4.51
~~E22-43~~	~~0.68~~	~~0.08309~~	~~0.00288~~	~~1.55524~~	~~0.04938~~	~~0.13575~~	~~0.00188~~	~~1271~~	~~69~~	~~953~~	~~20~~	~~821~~	~~11~~	~~16.08~~
E22-44	0.18	0.07517	0.00123	1.8158	0.03168	0.17515	0.00226	1073	17	1051	11	1040	12	3.17
~~E22-45~~	~~1.22~~	~~0.05786~~	~~0.0027~~	~~0.30007~~	~~0.01392~~	~~0.0376~~	~~0.00056~~	~~524~~	~~75~~	~~266~~	~~11~~	~~238~~	~~3~~	~~11.76~~
E22-46	0.24	0.05655	0.0014	0.59007	0.01487	0.07566	0.00102	474	32	471	9	470	6	0.21
E22-47	0.89	0.05585	0.00151	0.53315	0.01457	0.06922	0.00096	446	36	434	10	431	6	0.70
E22-48	0.77	0.05204	0.0014	0.31321	0.00857	0.04364	0.00059	287	38	277	7	275	4	0.73
E22-49	0.56	0.05226	0.0015	0.35633	0.01033	0.04944	0.00068	297	41	309	8	311	4	-0.64
E22-50	1.07	0.06562	0.00438	1.14162	0.07546	0.12614	0.00221	794	110	773	36	766	13	0.91
E22-51	0.48	0.05196	0.00147	0.29366	0.00838	0.04098	0.00056	284	40	261	7	259	3	0.77
~~E22-52~~	~~0.65~~	~~0.08509~~	~~0.00276~~	~~0.56702~~	~~0.01834~~	~~0.04832~~	~~0.0007~~	~~1318~~	~~40~~	~~456~~	~~12~~	~~304~~	~~4~~	~~50.00~~
E22-53	0.35	0.1145	0.00182	4.88675	0.08337	0.30946	0.00399	1872	14	1800	14	1738	20	7.71
E22-54	0.45	0.05761	0.00127	0.65053	0.01476	0.08187	0.00108	515	28	509	9	507	6	0.39
~~E22-55~~	~~1.05~~	~~0.17136~~	~~0.00283~~	~~10.31985~~	~~0.18069~~	~~0.43667~~	~~0.00575~~	~~2571~~	~~14~~	~~2464~~	~~16~~	~~2336~~	~~26~~	~~10.06~~
E22-56	0.28	0.0947	0.00151	3.27258	0.05587	0.25057	0.00322	1522	15	1475	13	1441	17	5.62
E22-57	0.56	0.05515	0.00343	0.51281	0.03169	0.06742	0.00107	418	110	420	21	421	6	-0.24
~~E22-58~~	~~0.81~~	~~0.07723~~	~~0.00131~~	~~0.97307~~	~~0.0175~~	~~0.09136~~	~~0.00118~~	~~1127~~	~~17~~	~~690~~	~~9~~	~~564~~	~~7~~	~~22.34~~

E22-59	0.21	0.06601	0.00148	1.11053	0.02543	0.12199	0.00166	807	26	758	12	742	10	2.16
E22-60	0.62	0.07577	0.00142	2.03301	0.03971	0.19455	0.00257	1089	20	1127	13	1146	14	-4.97
E22-61	0.36	0.05066	0.00166	0.23824	0.00784	0.0341	0.00048	225	50	217	6	216	3	0.46
E22-62	0.55	0.05684	0.00125	0.58231	0.01316	0.07429	0.00099	485	27	466	8	462	6	0.87
E22-63	1.01	0.05346	0.0015	0.36609	0.01034	0.04965	0.00069	348	39	317	8	312	4	1.60
E22-64	0.95	0.05985	0.002	0.55753	0.01867	0.06754	0.00095	598	48	450	12	421	6	6.89
E22-65	0.45	0.12825	0.00223	6.44501	0.11805	0.36438	0.0048	2074	16	2038	16	2003	23	3.54
~~E22-66~~	~~0.76~~	~~0.06626~~	~~0.00207~~	~~0.29214~~	~~0.00911~~	~~0.03197~~	~~0.00046~~	~~815~~	~~41~~	~~260~~	~~7~~	~~203~~	~~3~~	~~28.08~~
~~E22-67~~	~~0.63~~	~~0.11456~~	~~0.0023~~	~~4.77476~~	~~0.09853~~	~~0.30221~~	~~0.00416~~	~~1873~~	~~19~~	~~1780~~	~~17~~	~~1702~~	~~21~~	~~10.05~~
E22-68	0.70	0.14652	0.00287	8.01644	0.162	0.3967	0.00544	2306	17	2233	18	2154	25	7.06
E22-69	0.61	0.0519	0.0014	0.31906	0.0087	0.04457	0.00061	281	38	281	7	281	4	0.00
E22-70	0.55	0.08278	0.00151	2.31807	0.04415	0.20305	0.00267	1264	18	1218	14	1192	14	6.04
E22-71	1.18	0.05174	0.00821	0.31185	0.04916	0.0437	0.001	274	294	276	38	276	6	0.00
E22-72	0.44	0.0688	0.00141	1.27643	0.02708	0.13453	0.00179	893	23	835	12	814	10	2.58
E22-73	0.81	0.05587	0.00169	0.51072	0.01551	0.06628	0.00092	447	43	419	10	414	6	1.21
E22-74	1.70	0.11633	0.00226	5.15504	0.1035	0.32132	0.00434	1901	18	1845	17	1796	21	5.85
~~E22-75~~	~~0.69~~	~~0.1172~~	~~0.00207~~	~~4.66314~~	~~0.08648~~	~~0.28848~~	~~0.00377~~	~~1914~~	~~16~~	~~1761~~	~~16~~	~~1634~~	~~19~~	~~17.14~~
E22-76	0.72	0.05476	0.00119	0.48828	0.01093	0.06465	0.00086	402	27	404	7	404	5	0.00
E22-77	0.24	0.07076	0.00153	1.42787	0.0316	0.14631	0.00197	950	24	901	13	880	11	2.39
E22-78	0.27	0.1172	0.0021	5.13918	0.0967	0.31793	0.00416	1914	17	1843	16	1780	20	7.53
E22-79	0.82	0.05952	0.00118	0.48898	0.01005	0.05956	0.00079	586	23	404	7	373	5	8.31
E22-80	0.47	0.14732	0.00271	8.69286	0.1668	0.42784	0.00568	2315	16	2306	17	2296	26	0.83
E22-81	0.83	0.05921	0.00241	0.55329	0.02248	0.06776	0.001	575	63	447	15	423	6	5.67
E22-82	0.92	0.17139	0.00307	11.32017	0.21268	0.4789	0.00626	2571	15	2550	18	2522	27	1.94
~~E22-83~~	~~0.60~~	~~0.12296~~	~~0.00221~~	~~4.62564~~	~~0.08716~~	~~0.27276~~	~~0.00355~~	~~2000~~	~~17~~	~~1754~~	~~16~~	~~1555~~	~~18~~	~~28.62~~
E22-84	0.91	0.05358	0.00264	0.42537	0.0209	0.05757	0.00084	353	85	360	15	361	5	-0.28
~~E22-85~~	~~0.41~~	~~0.1495~~	~~0.00271~~	~~6.94671~~	~~0.132~~	~~0.33691~~	~~0.00441~~	~~2340~~	~~16~~	~~2105~~	~~17~~	~~1872~~	~~21~~	~~25.00~~
E22-86	0.63	0.05703	0.00145	0.555	0.0142	0.07056	0.00098	493	33	448	9	440	6	1.82

E22-87	1.26	0.06583	0.00196	1.11102	0.03303	0.12237	0.00176	801	38	759	16	744	10	2.02
~~E22-88~~	~~0.39~~	~~0.0607~~	~~0.00166~~	~~0.48816~~	~~0.01341~~	~~0.05831~~	~~0.00081~~	~~629~~	~~36~~	~~404~~	~~9~~	~~365~~	~~5~~	~~10.68~~
E22-89	0.38	0.07755	0.00157	1.86711	0.03895	0.17457	0.00234	1135	22	1070	14	1037	13	9.45
E22-90	0.70	0.05223	0.00195	0.27744	0.01029	0.03851	0.00057	295	58	249	8	244	4	2.05
E22-91	1.03	0.05111	0.00294	0.28054	0.01606	0.0398	0.00062	246	103	251	13	252	4	-0.40
E22-92	0.59	0.05116	0.0063	0.2757	0.03371	0.03908	0.00081	248	238	247	27	247	5	0.00
E22-93	0.77	0.05478	0.00241	0.49398	0.02162	0.06539	0.00098	403	71	408	15	408	6	0.00
E22-94	0.26	0.07047	0.00222	1.45284	0.04135	0.14952	0.00204	942	66	911	17	898	11	1.45
E22-95	0.51	0.05916	0.00146	0.64416	0.01615	0.07894	0.00108	573	31	505	10	490	6	3.06
~~E22-96~~	~~1.43~~	~~0.05563~~	~~0.00146~~	~~0.24113~~	~~0.0064~~	~~0.03143~~	~~0.00043~~	~~438~~	~~35~~	~~219~~	~~5~~	~~199~~	~~3~~	~~10.05~~
E22-97	0.47	0.07585	0.00178	1.77315	0.04228	0.16949	0.00234	1091	26	1036	15	1009	13	8.13
E22-98	0.23	0.11971	0.00236	5.55536	0.11326	0.33648	0.00448	1952	19	1909	18	1870	22	4.39
E22-99	0.83	0.05282	0.00259	0.35776	0.0174	0.04911	0.00076	321	82	311	13	309	5	0.65
E22-100	0.47	0.05185	0.00203	0.31347	0.01222	0.04384	0.00065	279	62	277	9	277	4	0.00
E22-101	0.21	0.18104	0.00359	12.30849	0.2523	0.49297	0.00658	2662	17	2628	19	2584	28	3.02
E22-102	0.31	0.06139	0.00131	0.55013	0.01206	0.06498	0.00087	653	25	445	8	406	5	9.61
E22-103	0.36	0.07292	0.00155	1.39473	0.03042	0.13869	0.00187	1012	23	887	13	837	11	5.97
E22-104	0.82	0.05127	0.00196	0.27486	0.01049	0.03887	0.00057	253	61	247	8	246	4	0.41
E22-105	0.44	0.17388	0.00347	10.90171	0.22485	0.45459	0.00604	2595	18	2515	19	2416	27	7.41
EBLN														
EBLN-01	1.35	0.05144	0.00237	0.28787	0.01318	0.04058	0.00067	261	75	257	10	256	4	0.39
EBLN-02	0.86	0.05112	0.00295	0.28109	0.01612	0.03987	0.00068	246	101	252	13	252	4	0.00
EBLN-03	0.08	0.05586	0.0011	0.54894	0.01138	0.07126	0.00101	447	23	444	7	444	6	0.00
EBLN-04	0.91	0.05586	0.00168	0.51618	0.01569	0.06701	0.00101	447	41	423	11	418	6	1.20
EBLN-05	0.45	0.05481	0.00265	0.48829	0.02344	0.0646	0.00109	404	77	404	16	404	7	0.00
EBLN-06	0.66	0.05204	0.00158	0.32566	0.00994	0.04538	0.00069	287	42	286	8	286	4	0.00
EBLN-07	0.68	0.05605	0.00124	0.5642	0.01293	0.07299	0.00106	454	27	454	8	454	6	0.00

EBLN-08	0.44	0.05472	0.00235	0.48563	0.02075	0.06435	0.00104	401	67	402	14	402	6	0.00
EBLN-09	0.48	0.05161	0.0027	0.29671	0.0153	0.04169	0.00076	268	85	264	12	263	5	0.38
EBLN-10	0.35	0.06323	0.00165	0.67688	0.01796	0.07763	0.00116	716	32	525	11	482	7	8.92
EBLN-11	0.81	0.05487	0.00124	0.51794	0.01209	0.06845	0.001	407	28	424	8	427	6	-0.70
EBLN-12	1.08	0.05571	0.00133	0.54648	0.01337	0.07114	0.00104	441	30	443	9	443	6	0.00
EBLN-13	0.21	0.05156	0.00296	0.29386	0.01652	0.04133	0.00081	266	93	262	13	261	5	0.38
EBLN-14	0.48	0.05547	0.00151	0.5278	0.01453	0.069	0.00104	431	35	430	10	430	6	0.00
EBLN-15	1.34	0.05147	0.0024	0.29241	0.0134	0.0412	0.00074	262	72	260	11	260	5	0.00
EBLN-16	0.79	0.0517	0.0018	0.31526	0.01093	0.04422	0.0007	272	51	278	8	279	4	-0.36
EBLN-17	0.43	0.05089	0.00333	0.271	0.0175	0.03862	0.00074	236	113	243	14	244	5	-0.41
EBLN-18	0.51	0.05118	0.00361	0.28333	0.01979	0.04014	0.00074	249	125	253	16	254	5	-0.39
EBLN-19	0.64	0.05169	0.00328	0.31258	0.01959	0.04385	0.00083	272	109	276	15	277	5	-0.36
EBLN-20	0.54	0.05511	0.00184	0.50601	0.01687	0.06658	0.00106	417	46	416	11	416	6	0.00
EBLN-21	0.66	0.05586	0.00162	0.55548	0.01618	0.07211	0.00112	447	38	449	11	449	7	0.00
EBLN-22	0.44	0.0514	0.00267	0.29288	0.01501	0.04132	0.00075	259	84	261	12	261	5	0.00
EBLN-23	0.63	0.05564	0.00141	0.54149	0.01395	0.07057	0.00105	438	32	439	9	440	6	-0.23
EBLN-24	0.59	0.05573	0.00158	0.54205	0.0155	0.07053	0.00107	442	37	440	10	439	6	0.23
EBLN-25	0.87	0.05591	0.00207	0.55139	0.02031	0.07152	0.00115	449	53	446	13	445	7	0.22
EBLN-26	0.45	0.05126	0.00218	0.27782	0.01171	0.03931	0.00065	253	66	249	9	249	4	0.00
EBLN-27	0.69	0.05555	0.00121	0.56249	0.01271	0.07343	0.00106	434	26	453	8	457	6	-0.88
EBLN-28	0.93	0.05222	0.00184	0.31887	0.01117	0.04428	0.00071	295	51	281	9	279	4	0.72
EBLN-29	0.54	0.05517	0.00177	0.51239	0.01651	0.06734	0.00103	419	45	420	11	420	6	0.00
EBLN-30	0.73	0.05578	0.00135	0.54356	0.01346	0.07066	0.00105	444	30	441	9	440	6	0.23
EBLN-31	0.75	0.05151	0.00209	0.29439	0.0119	0.04144	0.00067	264	63	262	9	262	4	0.00
EBLN-32	0.61	0.05179	0.00189	0.31338	0.01133	0.04387	0.00073	276	52	277	9	277	5	0.00
EBLN-33	0.22	0.07893	0.00168	1.98443	0.04375	0.18233	0.00266	1170	22	1110	15	1080	15	8.33
EBLN-34	0.60	0.05096	0.00279	0.26475	0.01421	0.03767	0.00072	239	88	238	11	238	4	0.00
EBLN-35	0.15	0.05659	0.00126	0.59577	0.01372	0.07634	0.00111	476	27	475	9	474	7	0.21

EBLN-36	0.01	0.05521	0.0012	0.56046	0.01265	0.07361	0.00106	421	26	452	8	458	6	-1.31
EBLN-37	0.43	0.05544	0.00229	0.51852	0.02112	0.06783	0.00116	430	60	424	14	423	7	0.24
EBLN-38	0.64	0.05175	0.00191	0.30859	0.01131	0.04324	0.0007	274	54	273	9	273	4	0.00
EBLN-39	0.14	0.05579	0.00138	0.56681	0.01432	0.07367	0.0011	444	31	456	9	458	7	-0.44
EBLN-40	0.93	0.05193	0.00216	0.31905	0.01324	0.04456	0.00072	282	65	281	10	281	4	0.00
EBLN-41	1.00	0.05095	0.00261	0.26465	0.01345	0.03767	0.00063	239	86	238	11	238	4	0.00
EBLN-42	0.58	0.05176	0.00381	0.31273	0.02269	0.04382	0.00088	275	129	276	18	276	5	0.00
EBLN-43	0.52	0.05529	0.00159	0.51913	0.015	0.06809	0.00106	424	37	425	10	425	6	0.00
EBLN-44	0.51	0.06866	0.0017	1.36188	0.0343	0.14384	0.00215	889	28	873	15	866	12	0.81
EBLN-45	0.70	0.05592	0.002	0.48676	0.01728	0.06312	0.00103	449	50	403	12	395	6	2.03
EBLN-46	0.40	0.07454	0.00166	1.83209	0.04207	0.17823	0.00262	1056	24	1057	15	1057	14	-0.09
EBLN-47	0.73	0.05553	0.00195	0.54243	0.01887	0.07083	0.00116	434	49	440	12	441	7	-0.23
EBLN-48	0.69	0.0515	0.00255	0.29336	0.01436	0.04131	0.00073	263	80	261	11	261	5	0.00
EBLN-49	0.64	0.05191	0.00381	0.32092	0.02315	0.04483	0.00093	281	127	283	18	283	6	0.00
EBLN-50	0.48	0.05539	0.00135	0.52848	0.01317	0.06918	0.00103	428	30	431	9	431	6	0.00
EBLN-51	0.43	0.05394	0.0023	0.4411	0.01868	0.05927	0.00091	369	68	371	13	371	6	0.00
EBLN-52	0.72	0.05492	0.00316	0.48739	0.02783	0.06432	0.00106	409	98	403	19	402	6	0.25
EBLN-53	0.75	0.05547	0.00216	0.53313	0.02071	0.06966	0.00103	431	60	434	14	434	6	0.00
EBLN-54	0.65	0.05441	0.00223	0.46704	0.01906	0.06221	0.00096	388	64	389	13	389	6	0.00
EBLN-55	0.55	0.05165	0.00954	0.31528	0.05772	0.04425	0.00129	270	325	278	45	279	8	-0.36
EBLN-56	0.63	0.05527	0.00201	0.51427	0.01862	0.06745	0.00102	423	54	421	12	421	6	0.00
EBLN-57	0.65	0.05174	0.00309	0.31854	0.01881	0.04462	0.00078	274	103	281	14	281	5	0.00
EBLN-58	0.68	0.05133	0.00506	0.28224	0.02759	0.03986	0.0008	256	183	252	22	252	5	0.00
EBLN-59	0.37	0.05619	0.00247	0.56948	0.02483	0.07347	0.00117	460	68	458	16	457	7	0.22
EBLN-60	0.86	0.05158	0.0032	0.30106	0.01853	0.04231	0.00071	267	110	267	14	267	4	0.00
EBLN-61	0.15	0.07201	0.00202	1.59043	0.04508	0.1601	0.00229	986	35	966	18	957	13	0.94
EBLN-62	1.14	0.10737	0.00335	4.6069	0.14259	0.31101	0.00492	1755	34	1751	26	1746	24	0.52
EBLN-63	0.24	0.05183	0.0033	0.2948	0.01862	0.04123	0.00068	278	114	262	15	260	4	0.77

EBLN-64	0.08	0.05601	0.0014	0.56846	0.01449	0.07357	0.00101	453	33	457	9	458	6	-0.22
EBLN-65	0.79	0.05156	0.00986	0.29819	0.05662	0.04193	0.00112	266	338	265	44	265	7	0.00
EBLN-66	1.28	0.05108	0.00323	0.26458	0.01666	0.03755	0.0006	244	115	238	13	238	4	0.00
EBLN-67	0.71	0.05132	0.00431	0.29114	0.02422	0.04112	0.00077	255	154	259	19	260	5	-0.38
EBLN-68	0.45	0.05229	0.00634	0.3421	0.04113	0.04743	0.00102	298	232	299	31	299	6	0.00
EBLN-69	0.67	0.05554	0.00174	0.52777	0.01655	0.06889	0.00101	434	44	430	11	429	6	0.23
EBLN-70	0.57	0.05533	0.00237	0.522	0.02211	0.0684	0.00109	426	66	426	15	427	7	-0.23
EBLN-71	0.45	0.05538	0.00144	0.52335	0.01367	0.0685	0.00098	428	33	427	9	427	6	0.00
EBLN-72	0.36	0.05232	0.00411	0.34094	0.02647	0.04725	0.00089	299	143	298	20	298	5	0.00
EBLN-73	0.41	0.05507	0.00543	0.50325	0.04907	0.06625	0.00138	415	182	414	33	414	8	0.00
EBLN-74	0.63	0.0516	0.00544	0.29688	0.03094	0.04171	0.0009	268	195	264	24	263	6	0.38
EBLN-75	0.87	0.05128	0.00357	0.27974	0.01926	0.03954	0.0007	253	125	250	15	250	4	0.00
EBLN-76	0.29	0.05661	0.00185	0.5933	0.01934	0.07599	0.00111	476	46	473	12	472	7	0.21
EBLN-77	0.51	0.05577	0.00145	0.54215	0.01421	0.07048	0.001	443	34	440	9	439	6	0.23
EBLN-78	0.64	0.08575	0.00184	2.71854	0.05948	0.22985	0.00321	1333	22	1334	16	1334	17	-0.07
EBLN-79	0.54	0.05171	0.00807	0.29944	0.04636	0.04198	0.00104	273	290	266	36	265	6	0.38
EBLN-80	0.75	0.05137	0.00324	0.28477	0.01769	0.04019	0.00072	257	110	254	14	254	4	0.00
EBLN-81	0.52	0.05487	0.00302	0.4951	0.0268	0.06541	0.00118	407	89	408	18	408	7	0.00
EBLN-82	0.86	0.05073	0.00465	0.25487	0.02307	0.03643	0.00074	229	167	231	19	231	5	0.00
EBLN-83	0.48	0.05146	0.0034	0.28276	0.0184	0.03984	0.00074	261	115	253	15	252	5	0.40
EBLN-84	0.47	0.05358	0.00302	0.4213	0.02347	0.05701	0.00096	353	95	357	17	357	6	0.00
EBLN-85	0.58	0.05162	0.00459	0.29869	0.02625	0.04195	0.00083	269	163	265	21	265	5	0.00
EBLN-86	0.76	0.05081	0.0168	0.27349	0.08988	0.03903	0.00157	232	512	245	72	247	10	-0.81
EBLN-87	1.46	0.0511	0.01761	0.26198	0.08962	0.03717	0.00166	245	530	236	72	235	10	0.43
EBLN-88	0.54	0.05173	0.00678	0.30156	0.03914	0.04226	0.00098	273	251	268	31	267	6	0.37
EBLN-89	0.67	0.05185	0.00395	0.31374	0.02359	0.04387	0.00083	279	137	277	18	277	5	0.00
EBLN-90	0.52	0.05584	0.00208	0.5526	0.02021	0.07175	0.00115	446	53	447	13	447	7	0.00
EBLN-91	0.25	0.05178	0.01638	0.30507	0.09576	0.04272	0.00178	276	497	270	75	270	11	0.00

EBLN-92	0.44	0.05516	0.00157	0.50094	0.01433	0.06584	0.00094	419	39	412	10	411	6	0.24
EBLN-93	0.72	0.05538	0.00311	0.50947	0.0283	0.0667	0.00112	428	94	418	19	416	7	0.48
EBLN-94	0.52	0.05529	0.00129	0.51686	0.01219	0.06778	0.00095	424	29	423	8	423	6	0.00
EBLN-95	0.45	0.05584	0.00159	0.55045	0.01558	0.07148	0.00106	446	37	445	10	445	6	0.00
EBLN-96	0.65	0.05588	0.00156	0.55064	0.01528	0.07145	0.00107	448	36	445	10	445	6	0.00
EBLN-97	0.01	0.05131	0.0016	0.28145	0.00872	0.03977	0.00059	255	44	252	7	251	4	0.40
EBLN-98	1.06	0.05124	0.00417	0.27894	0.02246	0.03948	0.00073	252	149	250	18	250	5	0.00
EBLN-99	0.35	0.05605	0.00122	0.55821	0.01234	0.07221	0.001	454	26	450	8	449	6	0.22
EBLN-100	0.35	0.05571	0.00159	0.53992	0.01529	0.07028	0.00104	441	37	438	10	438	6	0.00
E-E1														
EE1-01	0.44	0.0569	0.00146	0.61574	0.01599	0.07847	0.00109	488	33	487	10	487	7	0.00
EE1-02	1.01	0.05245	0.00817	0.29482	0.0456	0.04077	0.00077	305	325	262	36	258	5	1.55
EE1-03	0.31	0.05581	0.00136	0.5447	0.01343	0.07077	0.00099	445	31	442	9	441	6	0.23
~~EE1-04~~	~~0.11~~	~~0.06787~~	~~0.00136~~	~~0.72157~~	~~0.01495~~	~~0.07709~~	~~0.00104~~	~~865~~	~~22~~	~~552~~	~~9~~	~~479~~	~~6~~	~~15.24~~
EE1-05	0.41	0.05637	0.00121	0.55323	0.01222	0.07115	0.00096	467	26	447	8	443	6	0.90
EE1-06	1.26	0.05479	0.00241	0.48706	0.02138	0.06446	0.00096	404	71	403	15	403	6	0.00
EE1-07	0.57	0.05906	0.00112	0.54782	0.01085	0.06725	0.00089	569	22	444	7	420	5	5.71
EE1-08	0.68	0.05179	0.00543	0.31219	0.03251	0.04371	0.00084	276	200	276	25	276	5	0.00
EE1-09	1.09	0.0535	0.00413	0.28259	0.02129	0.03831	0.00063	350	177	253	17	242	4	4.55
EE1-10	1.23	0.05936	0.0047	0.56417	0.0436	0.06894	0.00116	580	178	454	28	430	7	5.58
EE1-11	0.68	0.05511	0.00114	0.50726	0.01078	0.06674	0.00089	417	25	417	7	416	5	0.24
EE1-12	0.23	0.07607	0.00215	1.80375	0.04495	0.17198	0.00231	1097	58	1047	16	1023	13	7.23
EE1-13	1.02	0.05525	0.0034	0.51547	0.03151	0.06765	0.00108	422	108	422	21	422	7	0.00
EE1-14	1.11	0.05141	0.00287	0.28311	0.01537	0.03993	0.00078	259	89	253	12	252	5	0.40
EE1-15	0.75	0.0524	0.00168	0.35442	0.01137	0.04904	0.00071	303	47	308	9	309	4	-0.32
EE1-16	0.82	0.05518	0.00107	0.51245	0.0103	0.06734	0.00089	420	23	420	7	420	5	0.00

EE1-17	1.02	0.05126	0.00434	0.2787	0.02335	0.03943	0.00077	253	154	250	19	249	5	0.40
EE1-18	1.18	0.05112	0.00229	0.27054	0.0121	0.03837	0.00057	246	75	243	10	243	4	0.00
EE1-19	0.98	0.05547	0.00216	0.5242	0.02043	0.06852	0.00099	431	61	428	14	427	6	0.23
EE1-20	0.54	0.07945	0.0034	2.29407	0.09207	0.20941	0.00312	1183	87	1210	28	1226	17	-3.51
EE1-21	1.52	0.05137	0.00422	0.28247	0.02307	0.03987	0.00067	257	155	253	18	252	4	0.40
EE1-22	1.24	0.05108	0.00235	0.27636	0.0126	0.03923	0.00061	244	76	248	10	248	4	0.00
EE1-23	0.60	0.14649	0.00265	7.8407	0.14796	0.3881	0.00525	2305	16	2213	17	2114	24	9.04
EE1-24	0.38	0.05638	0.00153	0.56821	0.01554	0.07307	0.00102	467	36	457	10	455	6	0.44
~~EE1-25~~	~~1.16~~	~~0.07506~~	~~0.00705~~	~~0.41524~~	~~0.03825~~	~~0.04013~~	~~0.00073~~	~~1070~~	~~196~~	~~353~~	~~27~~	~~254~~	~~5~~	~~38.98~~
~~EE1-26~~	~~0.42~~	~~0.08003~~	~~0.00166~~	~~1.36764~~	~~0.0292~~	~~0.12391~~	~~0.00168~~	~~1198~~	~~22~~	~~875~~	~~13~~	~~753~~	~~10~~	~~16.20~~
EE1-27	0.58	0.05135	0.0017	0.28336	0.00939	0.04001	0.00057	257	50	253	7	253	4	0.00
EE1-28	0.73	0.05931	0.0091	0.58311	0.08838	0.07131	0.00167	578	344	466	57	444	10	4.95
EE1-29	0.68	0.06167	0.00146	0.57812	0.01383	0.06797	0.00094	663	28	463	9	424	6	9.20
~~EE1-30~~	~~0.86~~	~~0.06249~~	~~0.00411~~	~~0.35218~~	~~0.02299~~	~~0.04087~~	~~0.00067~~	~~691~~	~~112~~	~~306~~	~~17~~	~~258~~	~~4~~	~~18.60~~
EE1-31	0.63	0.05118	0.00212	0.27812	0.01144	0.0394	0.00061	249	66	249	9	249	4	0.00
EE1-32	0.04	0.05645	0.00116	0.58872	0.01245	0.07563	0.00101	470	25	470	8	470	6	0.00
EE1-33	0.69	0.05806	0.00718	0.52513	0.06423	0.0656	0.00116	532	280	429	43	410	7	4.63
EE1-34	0.84	0.05145	0.00474	0.29393	0.02681	0.04142	0.00082	261	170	262	21	262	5	0.00
~~EE1-35~~	~~0.85~~	~~0.08146~~	~~0.00992~~	~~0.46531~~	~~0.05578~~	~~0.04143~~	~~0.0009~~	~~1232~~	~~251~~	~~388~~	~~39~~	~~262~~	~~6~~	~~48.09~~
EE1-36	0.54	0.11479	0.00245	4.88045	0.10658	0.30829	0.00432	1877	20	1799	18	1732	21	8.37
EE1-37	0.62	0.05502	0.0053	0.2982	0.02828	0.03931	0.00064	413	220	265	22	249	4	6.43
EE1-38	0.54	0.05504	0.00127	0.5093	0.01192	0.0671	0.00092	414	29	418	8	419	6	-0.24
~~EE1-39~~	~~0.47~~	~~0.07022~~	~~0.00447~~	~~0.70124~~	~~0.04329~~	~~0.07243~~	~~0.0011~~	~~935~~	~~134~~	~~540~~	~~26~~	~~451~~	~~7~~	~~19.73~~
EE1-40	0.77	0.05622	0.00369	0.28454	0.01822	0.0367	0.00075	461	106	254	14	232	5	9.48
EE1-41	0.99	0.05359	0.00716	0.41991	0.0556	0.05681	0.0013	354	257	356	40	356	8	0.00
EE1-42	0.49	0.05467	0.00264	0.44252	0.02129	0.05869	0.00088	399	81	372	15	368	5	1.09
EE1-43	0.75	0.05134	0.00231	0.29386	0.01315	0.0415	0.00064	256	74	262	10	262	4	0.00
~~EE1-44~~	~~1.09~~	~~0.08277~~	~~0.00568~~	~~0.84326~~	~~0.05609~~	~~0.07389~~	~~0.00124~~	~~1264~~	~~138~~	~~621~~	~~31~~	~~460~~	~~7~~	~~35.00~~

~~EE1-45~~	~~0.19~~	~~0.09751~~	~~0.0026~~	~~2.51088~~	~~0.05782~~	~~0.18675~~	~~0.0025~~	~~1577~~	~~51~~	~~1275~~	~~17~~	~~1104~~	~~14~~	~~42.84~~
EE1-46	0.14	0.05643	0.00225	0.54484	0.02164	0.07001	0.00106	469	61	442	14	436	6	1.38
EE1-47	0.43	0.07492	0.00281	1.78188	0.06204	0.1725	0.00242	1066	77	1039	23	1026	13	3.90
EE1-48	1.02	0.05158	0.00213	0.28841	0.01184	0.04054	0.00062	267	66	257	9	256	4	0.39
EE1-49	0.13	0.05618	0.00128	0.56809	0.01315	0.07332	0.001	459	28	457	9	456	6	0.22
EE1-50	0.23	0.05543	0.00155	0.51614	0.01454	0.06751	0.00094	430	38	423	10	421	6	0.48
~~EE1-51~~	~~0.32~~	~~0.05883~~	~~0.00629~~	~~0.32639~~	~~0.0344~~	~~0.04024~~	~~0.00073~~	~~561~~	~~242~~	~~287~~	~~26~~	~~254~~	~~5~~	~~12.99~~
EE1-52	0.70	0.10871	0.0022	4.30469	0.08942	0.28713	0.00393	1778	19	1694	17	1627	20	9.28
EE1-53	0.86	0.05165	0.00169	0.28655	0.0094	0.04023	0.00058	270	49	256	7	254	4	0.79
EE1-54	0.53	0.05504	0.0023	0.4542	0.01887	0.05984	0.00091	414	66	380	13	375	6	1.33
EE1-55	0.65	0.05619	0.00174	0.53329	0.01646	0.06882	0.001	460	43	434	11	429	6	1.17
~~EE1-56~~	~~1.05~~	~~0.08~~	~~0.01759~~	~~0.43808~~	~~0.09563~~	~~0.03972~~	~~0.00105~~	~~1197~~	~~481~~	~~369~~	~~68~~	~~251~~	~~6~~	~~47.01~~
~~EE1-57~~	~~0.48~~	~~0.06557~~	~~0.00565~~	~~0.64505~~	~~0.05439~~	~~0.07135~~	~~0.00126~~	~~793~~	~~187~~	~~505~~	~~34~~	~~444~~	~~8~~	~~13.74~~
~~EE1-58~~	~~0.26~~	~~0.07072~~	~~0.00216~~	~~0.98416~~	~~0.02695~~	~~0.10093~~	~~0.00137~~	~~949~~	~~64~~	~~696~~	~~14~~	~~620~~	~~8~~	~~12.26~~
EE1-59	1.12	0.05129	0.00259	0.28048	0.01405	0.03966	0.00062	254	86	251	11	251	4	0.00
EE1-60	0.66	0.05141	0.00622	0.29192	0.03514	0.04117	0.0008	259	236	260	28	260	5	0.00
EE1-61	0.47	0.05554	0.00255	0.53329	0.02328	0.06964	0.00099	434	105	434	15	434	6	0.00
EE1-62	0.65	0.05525	0.00117	0.51939	0.01125	0.06816	0.00092	422	26	425	8	425	6	0.00
EE1-63	0.58	0.05206	0.00209	0.32769	0.01305	0.04564	0.00071	288	62	288	10	288	4	0.00
EE1-64	1.15	0.05194	0.00396	0.32109	0.02432	0.04483	0.00076	283	141	283	19	283	5	0.00
EE1-65	0.38	0.05554	0.00133	0.51703	0.01251	0.06751	0.00093	434	30	423	8	421	6	0.48
EE1-66	0.25	0.0515	0.00213	0.29397	0.01206	0.04139	0.00063	263	66	262	9	261	4	0.38
EE1-67	1.06	0.05537	0.00321	0.51409	0.02961	0.06732	0.00108	427	100	421	20	420	7	0.24
EE1-68	0.80	0.05128	0.0025	0.28186	0.01366	0.03986	0.00062	253	83	252	11	252	4	0.00
EE1-69	0.57	0.05417	0.00156	0.44323	0.01279	0.05933	0.00085	378	39	373	9	372	5	0.27
EE1-70	0.73	0.05592	0.00245	0.51688	0.02215	0.06703	0.00115	449	65	423	15	418	7	1.20
~~EE1-71~~	~~0.83~~	~~0.05739~~	~~0.00376~~	~~0.31222~~	~~0.01989~~	~~0.03945~~	~~0.00061~~	~~507~~	~~148~~	~~276~~	~~15~~	~~249~~	4	~~10.84~~
~~EE1-72~~	~~0.41~~	~~0.06321~~	~~0.01992~~	~~0.36456~~	~~0.11446~~	~~0.04183~~	~~0.00114~~	~~715~~	~~631~~	~~316~~	~~85~~	~~264~~	~~7~~	~~19.70~~

EE1-73	0.84	0.05273	0.01311	0.27028	0.06696	0.03718	0.0008	317	457	243	54	235	5	3.40
EE1-74	0.65	0.05616	0.00223	0.56783	0.02206	0.07331	0.00122	459	57	457	14	456	7	0.22
EE1-75	1.02	0.05115	0.00198	0.27746	0.01067	0.03934	0.00059	248	61	249	8	249	4	0.00
~~EE1-76~~	~~0.65~~	~~0.05807~~	~~0.01015~~	~~0.3196~~	~~0.0554~~	~~0.03992~~	~~0.00091~~	~~532~~	~~376~~	~~282~~	~~43~~	~~252~~	~~6~~	~~11.90~~
EE1-77	0.05	0.0547	0.00123	0.49529	0.01134	0.06566	0.0009	400	28	409	8	410	5	-0.24
EE1-78	0.52	0.05129	0.00158	0.28952	0.00887	0.04093	0.0006	254	44	258	7	259	4	-0.39
EE1-79	0.59	0.05681	0.00156	0.5871	0.01613	0.07493	0.00107	484	36	469	10	466	6	0.64
EE1-80	0.96	0.05577	0.00444	0.52901	0.04152	0.06879	0.00139	443	139	431	28	429	8	0.47
EE1-81	0.39	0.05134	0.002	0.29126	0.01128	0.04113	0.00062	256	61	260	9	260	4	0.00
EE1-82	0.90	0.05259	0.00274	0.32594	0.01672	0.04494	0.00078	311	85	286	13	283	5	1.06
~~EE1-83~~	~~1.18~~	~~0.06156~~	~~0.01089~~	~~0.36438~~	~~0.06395~~	~~0.04293~~	~~0.00093~~	~~659~~	~~394~~	~~315~~	~~48~~	~~271~~	~~6~~	~~16.24~~
EE1-84	0.55	0.05476	0.00138	0.48863	0.01245	0.06471	0.0009	402	33	404	8	404	5	0.00
EE1-85	0.67	0.051	0.00369	0.27791	0.01993	0.03951	0.00069	241	131	249	16	250	4	-0.40
EE1-86	0.50	0.05775	0.00291	0.52297	0.02528	0.06568	0.00095	520	114	427	17	410	6	4.15
~~EE1-87~~	~~1.09~~	~~0.07289~~	~~0.01318~~	~~0.3872~~	~~0.0694~~	~~0.03853~~	~~0.00091~~	~~1011~~	~~398~~	~~332~~	~~51~~	~~244~~	~~6~~	~~36.07~~
EE1-88	0.78	0.05162	0.00266	0.28127	0.01435	0.03951	0.00064	269	87	252	11	250	4	0.80
~~EE1-89~~	~~0.16~~	~~0.09003~~	~~0.00204~~	~~0.60252~~	~~0.0138~~	~~0.04853~~	~~0.00067~~	~~1426~~	~~24~~	~~479~~	~~9~~	~~305~~	~~4~~	~~57.05~~
EE1-90	0.84	0.05113	0.00286	0.28041	0.01553	0.03977	0.00066	247	97	251	12	251	4	0.00
EE1-91	0.61	0.05497	0.00232	0.49612	0.02061	0.06545	0.00106	411	64	409	14	409	6	0.00
EE1-92	1.15	0.05161	0.00419	0.27288	0.02172	0.03835	0.0006	268	186	245	17	243	4	0.82
EE1-93	0.75	0.05119	0.0018	0.27705	0.00964	0.03924	0.00059	249	52	248	8	248	4	0.00
EE1-94	0.51	0.05566	0.00317	0.56632	0.03204	0.07378	0.00117	439	98	456	21	459	7	-0.65
EE1-95	0.66	0.1259	0.00434	5.99185	0.18689	0.34517	0.00507	2041	62	1975	27	1912	24	6.75
EE1-96	0.45	0.05531	0.00206	0.49841	0.01844	0.06534	0.001	425	55	411	12	408	6	0.74
EE1-97	1.37	0.05508	0.00189	0.49653	0.01691	0.06537	0.00098	415	49	409	11	408	6	0.25
EE1-98	0.70	0.05547	0.00398	0.53677	0.03806	0.07016	0.0013	431	126	436	25	437	8	-0.23
EE1-99	0.03	0.08212	0.00203	2.19029	0.04584	0.19344	0.00256	1248	50	1178	15	1140	14	9.47
EE1-100	0.72	0.05552	0.00158	0.53572	0.01514	0.06997	0.00102	433	37	436	10	436	6	0.00

EE1-101	0.50	0.05877	0.00415	0.54693	0.03765	0.0675	0.00104	559	159	443	25	421	6	5.23
EE1-102	0.26	0.0571	0.00155	0.58653	0.01597	0.07449	0.00106	495	35	469	10	463	6	1.30
EE1-103	0.52	0.05116	0.00198	0.27015	0.01033	0.03829	0.0006	248	59	243	8	242	4	0.41
EE1-104	0.77	0.05139	0.0022	0.28962	0.01219	0.04087	0.00067	258	66	258	10	258	4	0.00
EE1-105	0.07	0.06049	0.00173	0.71953	0.01808	0.08628	0.00117	621	63	550	11	533	7	3.19
E-D1														
ED1-01	0.39	0.05475	0.00123	0.50946	0.01176	0.06747	0.00093	402	28	418	8	421	6	-0.71
ED1-02	0.84	0.05114	0.00216	0.27443	0.01154	0.03891	0.0006	247	68	246	9	246	4	0.00
ED1-03	0.26	0.05491	0.00163	0.49656	0.01493	0.06557	0.00092	409	42	409	10	409	6	0.00
ED1-04	0.35	0.05672	0.00097	0.49287	0.00899	0.06301	0.00084	481	19	407	6	394	5	3.30
ED1-05	1.17	0.05113	0.00408	0.27318	0.02174	0.03874	0.00063	247	151	245	17	245	4	0.00
ED1-06	1.08	0.05119	0.00175	0.26778	0.00915	0.03793	0.00057	249	51	241	7	240	4	0.42
ED1-07	0.65	0.05475	0.00403	0.48362	0.03534	0.06405	0.0011	402	134	401	24	400	7	0.25
ED1-08	0.67	0.05386	0.00152	0.41917	0.01197	0.05643	0.0008	365	39	355	9	354	5	0.28
ED1-09	0.77	0.0514	0.00244	0.27544	0.01298	0.03886	0.00061	259	79	247	10	246	4	0.41
ED1-10	0.31	0.05474	0.00112	0.4878	0.01043	0.06462	0.00086	402	25	403	7	404	5	-0.25
ED1-11	0.12	0.05682	0.00165	0.53504	0.01381	0.06829	0.00091	485	66	435	9	426	6	2.11
ED1-12	0.46	0.05124	0.00196	0.28278	0.01087	0.04002	0.00058	252	62	253	9	253	4	0.00
ED1-13	0.77	0.05533	0.00137	0.48903	0.01239	0.06408	0.00089	426	32	404	8	400	5	1.00
ED1-14	0.25	0.05528	0.00174	0.49229	0.01564	0.06458	0.00092	424	46	406	11	403	6	0.74
ED1-15	0.91	0.0556	0.00121	0.51409	0.01157	0.06705	0.00091	436	27	421	8	418	5	0.72
ED1-16	0.37	0.0563	0.00187	0.48413	0.01463	0.06236	0.00085	464	75	401	10	390	5	2.82
ED1-17	0.65	0.05565	0.0027	0.54884	0.02641	0.07152	0.00115	438	78	444	17	445	7	-0.22
ED1-18	0.52	0.05091	0.00196	0.26564	0.01024	0.03784	0.00057	237	61	239	8	239	4	0.00
ED1-19	0.29	0.05519	0.0014	0.49735	0.01285	0.06535	0.00092	420	33	410	9	408	6	0.49
ED1-20	1.07	0.05507	0.01022	0.48515	0.08916	0.06388	0.00193	415	342	402	61	399	12	0.75
ED1-21	1.27	0.05159	0.0055	0.27447	0.02913	0.03858	0.00071	267	206	246	23	244	4	0.82

ED1-22	0.73	0.05109	0.00327	0.27369	0.01744	0.03884	0.00062	245	117	246	14	246	4	0.00
~~ED1-23~~	~~0.26~~	~~0.08291~~	~~0.00244~~	~~1.82484~~	~~0.04733~~	~~0.15962~~	~~0.00221~~	~~1267~~	~~59~~	~~1054~~	~~17~~	~~955~~	~~12~~	~~10.37~~
ED1-24	0.74	0.05094	0.00287	0.26982	0.01513	0.03841	0.00062	238	100	243	12	243	4	0.00
ED1-25	0.38	0.05472	0.00172	0.48447	0.01532	0.0642	0.00093	401	45	401	10	401	6	0.00
ED1-26	0.10	0.06348	0.00173	0.67007	0.01593	0.07656	0.00103	724	59	521	10	476	6	9.45
ED1-27	0.40	0.05565	0.0018	0.5103	0.0166	0.06649	0.00095	438	47	419	11	415	6	0.96
ED1-28	0.67	0.05477	0.00176	0.49528	0.01602	0.06557	0.00095	403	47	409	11	409	6	0.00
ED1-29	0.48	0.07029	0.00136	1.42365	0.02887	0.14688	0.002	937	21	899	12	883	11	1.81
ED1-30	0.70	0.05147	0.00354	0.27145	0.01855	0.03824	0.00066	262	125	244	15	242	4	0.83
ED1-31	1.17	0.05499	0.00784	0.51041	0.07226	0.06731	0.00156	412	277	419	49	420	9	-0.24
ED1-32	0.30	0.0551	0.00112	0.52068	0.01101	0.06853	0.00093	416	24	426	7	427	6	-0.23
ED1-33	0.40	0.0648	0.00123	0.9182	0.01831	0.10275	0.00138	768	21	661	10	631	8	4.75
ED1-34	0.91	0.05561	0.0022	0.51228	0.02018	0.0668	0.00102	437	60	420	14	417	6	0.72
ED1-35	0.52	0.05125	0.00153	0.28183	0.00853	0.03988	0.00056	252	44	252	7	252	3	0.00
ED1-36	0.59	0.05544	0.00174	0.49712	0.0157	0.06502	0.00095	430	44	410	11	406	6	0.99
ED1-37	0.76	0.05106	0.00219	0.28396	0.01205	0.04033	0.00064	244	68	254	10	255	4	-0.39
ED1-38	0.75	0.0515	0.00342	0.29532	0.01946	0.04158	0.00071	263	120	263	15	263	4	0.00
ED1-39	0.55	0.0514	0.00199	0.2845	0.01098	0.04013	0.0006	259	61	254	9	254	4	0.00
ED1-40	0.67	0.05713	0.00144	0.56479	0.01434	0.07168	0.00104	497	31	455	9	446	6	2.02
ED1-41	1.33	0.0543	0.00249	0.2769	0.01259	0.03697	0.0006	384	73	248	10	234	4	5.98
ED1-42	0.53	0.05422	0.00124	0.47802	0.01123	0.06392	0.00088	380	29	397	8	399	5	-0.50
ED1-43	0.93	0.05531	0.0048	0.50151	0.04316	0.06575	0.00125	425	160	413	29	410	8	0.73
ED1-44	0.68	0.05105	0.00317	0.28278	0.01746	0.04016	0.00066	243	112	253	14	254	4	-0.39
ED1-45	0.75	0.05493	0.00119	0.4977	0.01114	0.0657	0.0009	409	27	410	8	410	5	0.00
ED1-46	0.61	0.0513	0.00227	0.2873	0.01271	0.04061	0.00062	254	73	256	10	257	4	-0.39
ED1-47	0.65	0.05094	0.00328	0.26622	0.01695	0.0379	0.00069	238	113	240	14	240	4	0.00
ED1-48	0.65	0.05477	0.00142	0.48674	0.01277	0.06444	0.00091	403	34	403	9	403	6	0.00
ED1-49	0.17	0.0551	0.0012	0.48003	0.01082	0.06317	0.00086	416	27	398	7	395	5	0.76

ED1-50	0.46	0.0551	0.00123	0.51407	0.0118	0.06765	0.00093	416	28	421	8	422	6	-0.24
ED1-51	0.67	0.05091	0.00417	0.26407	0.02153	0.03761	0.00064	237	154	238	17	238	4	0.00
ED1-52	1.10	0.05468	0.006	0.46719	0.05088	0.06196	0.0013	399	207	389	35	388	8	0.26
ED1-53	1.34	0.05118	0.00959	0.28735	0.05341	0.04071	0.00114	249	327	256	42	257	7	-0.39
ED1-54	0.99	0.05114	0.00143	0.26845	0.00761	0.03807	0.00054	247	39	241	6	241	3	0.00
ED1-55	0.34	0.05791	0.00175	0.52191	0.01594	0.06535	0.00093	526	42	426	11	408	6	4.41
ED1-56	0.37	0.05141	0.00363	0.2876	0.02004	0.04056	0.00076	259	125	257	16	256	5	0.39
ED1-57	0.49	0.055	0.0016	0.50152	0.01479	0.06612	0.00093	412	41	413	10	413	6	0.00
ED1-58	0.81	0.05112	0.00345	0.26872	0.01802	0.03811	0.00063	246	123	242	14	241	4	0.41
ED1-59	0.84	0.08684	0.00231	2.5669	0.06896	0.21432	0.00319	1357	29	1291	20	1252	17	8.39
ED1-60	0.63	0.05157	0.00218	0.26441	0.01121	0.03718	0.00055	266	70	238	9	235	3	1.28
ED1-61	2.43	0.04605	0.00451	0.2355	0.02272	0.03709	0.00061		205	215	19	235	4	-8.51
ED1-62	0.41	0.05112	0.00256	0.26577	0.01319	0.0377	0.00062	246	84	239	11	239	4	0.00
ED1-63	0.72	0.05099	0.00306	0.27765	0.01646	0.03948	0.0007	240	104	249	13	250	4	-0.40
ED1-64	0.85	0.05118	0.00601	0.27246	0.03178	0.0386	0.0008	249	225	245	25	244	5	0.41
ED1-65	1.03	0.05477	0.00495	0.49421	0.04423	0.06543	0.00132	403	166	408	30	409	8	-0.24
ED1-66	0.46	0.05097	0.0021	0.2622	0.01079	0.0373	0.00056	239	67	236	9	236	3	0.00
ED1-67	0.57	0.05555	0.0042	0.52225	0.03902	0.06818	0.00133	434	132	427	26	425	8	0.47
ED1-68	0.61	0.05541	0.00189	0.52565	0.01797	0.06879	0.00103	429	50	429	12	429	6	0.00
ED1-69	0.84	0.05112	0.00469	0.27753	0.02535	0.03937	0.0007	246	173	249	20	249	4	0.00
ED1-70	0.41	0.05534	0.00151	0.51461	0.01425	0.06742	0.00097	426	37	422	10	421	6	0.24
ED1-71	0.41	0.05603	0.00166	0.52498	0.01558	0.06794	0.00101	454	40	428	10	424	6	0.94
ED1-72	0.59	0.05099	0.00221	0.26692	0.01151	0.03796	0.00059	240	71	240	9	240	4	0.00
ED1-73	0.49	0.05516	0.00131	0.50699	0.0123	0.06665	0.00093	419	30	416	8	416	6	0.00
ED1-74	0.33	0.05098	0.0015	0.2661	0.00791	0.03785	0.00055	240	42	240	6	239	3	0.42
ED1-75	0.78	0.05144	0.00285	0.27297	0.01497	0.03847	0.00065	261	95	245	12	243	4	0.82
ED1-76	1.28	0.05085	0.00496	0.27255	0.02641	0.03887	0.00075	234	183	245	21	246	5	-0.41
ED1-77	0.50	0.05123	0.00278	0.28354	0.01525	0.04013	0.00067	251	93	253	12	254	4	-0.39

ED1-78	0.28	0.06976	0.00154	1.36816	0.03111	0.14222	0.00198	921	25	875	13	857	11	2.10
~~ED1-79~~	~~0.55~~	~~0.06234~~	~~0.00213~~	~~0.55365~~	~~0.01897~~	~~0.06439~~	~~0.00095~~	~~686~~	~~48~~	~~447~~	~~12~~	~~402~~	~~6~~	~~11.19~~
ED1-80	0.65	0.05106	0.0036	0.27021	0.0188	0.03837	0.00071	244	125	243	15	243	4	0.00
ED1-81	0.51	0.05495	0.00153	0.49226	0.01391	0.06495	0.00093	410	38	406	9	406	6	0.00
~~ED1-82~~	~~0.12~~	~~0.07406~~	~~0.00163~~	~~0.89628~~	~~0.0203~~	~~0.08775~~	~~0.00122~~	~~1043~~	~~24~~	~~650~~	~~11~~	~~542~~	~~7~~	~~19.93~~
ED1-83	1.69	0.05145	0.00154	0.27783	0.0084	0.03915	0.00056	261	43	249	7	248	3	0.40
ED1-84	0.94	0.05112	0.00421	0.27862	0.02281	0.03952	0.0007	246	153	250	18	250	4	0.00
~~ED1-85~~	~~0.87~~	~~0.11326~~	~~0.00264~~	~~2.35281~~	~~0.05587~~	~~0.15063~~	~~0.00217~~	~~1852~~	~~23~~	~~1228~~	~~17~~	~~904~~	~~12~~	~~35.84~~
ED1-86	1.02	0.05131	0.00197	0.27634	0.01055	0.03905	0.0006	255	59	248	8	247	4	0.40
ED1-87	0.88	0.05102	0.0041	0.26961	0.02151	0.03832	0.00068	242	149	242	17	242	4	0.00
ED1-88	0.39	0.05422	0.00718	0.46994	0.06186	0.06284	0.00134	380	258	391	43	393	8	-0.51
ED1-89	0.77	0.05102	0.00198	0.26847	0.01038	0.03815	0.00058	242	61	241	8	241	4	0.00
~~ED1-90~~	~~1.07~~	~~0.08609~~	~~0.00352~~	~~0.49617~~	~~0.02002~~	~~0.04179~~	~~0.00069~~	~~1340~~	~~52~~	~~409~~	~~14~~	~~264~~	~~4~~	~~54.92~~
ED1-91	1.09	0.05124	0.00245	0.27192	0.0129	0.03848	0.00062	252	79	244	10	243	4	0.41
ED1-92	0.61	0.05485	0.00173	0.49103	0.01564	0.06491	0.00094	406	45	406	11	405	6	0.25
ED1-93	0.64	0.05465	0.01365	0.48843	0.12138	0.0648	0.00197	398	430	404	83	405	12	-0.25
ED1-94	1.12	0.05088	0.00511	0.27698	0.02721	0.03947	0.00102	235	173	248	22	250	6	-0.80
ED1-95	0.71	0.05158	0.00346	0.2786	0.01851	0.03917	0.00069	267	120	250	15	248	4	0.81
ED1-96	0.39	0.05088	0.00279	0.28755	0.01562	0.04098	0.00069	235	94	257	12	259	4	-0.77
ED1-97	0.41	0.0562	0.00168	0.5221	0.01573	0.06736	0.00099	460	41	427	10	420	6	1.67
~~ED1-98~~	~~0.50~~	~~0.07315~~	~~0.00322~~	~~0.53757~~	~~0.02337~~	~~0.05328~~	~~0.00089~~	~~1018~~	~~61~~	~~437~~	~~15~~	~~335~~	~~5~~	~~30.45~~
ED1-99	0.31	0.05145	0.00155	0.27687	0.0084	0.03902	0.00057	261	43	248	7	247	4	0.40
ED1-100	1.02	0.05624	0.00302	0.31235	0.01661	0.04027	0.00069	462	87	276	13	255	4	8.24
EB1														
EB1-01	1.06	0.05102	0.00149	0.27416	0.00816	0.03897	0.00059	242	41	246	7	246	4	0.00
EB1-02	0.89	0.05633	0.00163	0.53744	0.01598	0.06919	0.00103	465	40	437	11	431	6	1.39
EB1-03	0.83	0.05428	0.00549	0.46	0.04603	0.06145	0.00135	383	186	384	32	384	8	0.00

EB1-04	0.51	0.05536	0.00589	0.51156	0.05386	0.06701	0.0015	427	196	419	36	418	9	0.24
EB1-05	0.35	0.05547	0.00139	0.53677	0.01389	0.07016	0.00104	431	32	436	9	437	6	-0.23
EB1-06	0.87	0.05544	0.00185	0.51585	0.01736	0.06747	0.00107	430	47	422	12	421	6	0.24
EB1-07	0.65	0.05142	0.0023	0.28967	0.01289	0.04085	0.00069	260	71	258	10	258	4	0.00
EB1-08	1.09	0.05106	0.00216	0.27844	0.01177	0.03954	0.00065	244	67	249	9	250	4	-0.40
EB1-09	0.96	0.05123	0.00192	0.28524	0.01076	0.04037	0.00064	251	58	255	9	255	4	0.00
EB1-10	0.98	0.05443	0.0014	0.42485	0.01127	0.0566	0.00083	389	34	360	8	355	5	1.41
EB1-11	0.60	0.05135	0.0014	0.27505	0.00772	0.03884	0.00057	257	38	247	6	246	4	0.41
EB1-12	0.96	0.05581	0.00312	0.51746	0.02884	0.06723	0.00113	445	94	423	19	419	7	0.95
EB1-13	0.35	0.05132	0.00225	0.29056	0.01273	0.04105	0.00068	255	70	259	10	259	4	0.00
EB1-14	1.15	0.05161	0.00221	0.29376	0.01264	0.04128	0.00065	268	70	262	10	261	4	0.38
EB1-15	0.81	0.05524	0.00353	0.50834	0.03231	0.06672	0.00116	422	111	417	22	416	7	0.24
EB1-16	0.53	0.07648	0.00182	1.87134	0.04623	0.17741	0.00264	1108	27	1071	16	1053	14	5.22
EB1-17	0.85	0.05641	0.00593	0.57698	0.06003	0.07416	0.00166	469	193	463	39	461	10	0.43
EB1-18	0.08	0.0553	0.00105	0.4187	0.00858	0.0549	0.00077	424	23	355	6	345	5	2.90
EB1-19	0.63	0.05128	0.00226	0.28075	0.01236	0.0397	0.00065	253	71	251	10	251	4	0.00
EB1-20	1.04	0.05163	0.0022	0.30553	0.01301	0.04291	0.00069	269	68	271	10	271	4	0.00
EB1-21	1.20	0.05392	0.00126	0.41156	0.01004	0.05534	0.0008	368	30	350	7	347	5	0.86
EB1-22	0.09	0.05545	0.00122	0.50554	0.01165	0.0661	0.00095	430	27	415	8	413	6	0.48
EB1-23	1.20	0.05114	0.00378	0.27516	0.02015	0.03901	0.00074	247	132	247	16	247	5	0.00
EB1-24	0.75	0.05347	0.00171	0.29884	0.00973	0.04052	0.0006	349	47	265	8	256	4	3.52
EB1-25	0.33	0.05546	0.00147	0.53106	0.01441	0.06944	0.00104	431	35	433	10	433	6	0.00
EB1-26	0.59	0.0551	0.00144	0.50762	0.0136	0.0668	0.001	416	34	417	9	417	6	0.00
EB1-27	0.44	0.05156	0.00363	0.30116	0.02112	0.04235	0.00074	266	128	267	16	267	5	0.00
EB1-28	0.33	0.05557	0.00172	0.52186	0.01633	0.0681	0.00104	435	43	426	11	425	6	0.24
EB1-29	0.42	0.05499	0.00118	0.50021	0.0113	0.06596	0.00095	412	26	412	8	412	6	0.00
EB1-30	0.24	0.0515	0.00148	0.29673	0.00869	0.04178	0.00063	263	40	264	7	264	4	0.00
EB1-31	0.72	0.05153	0.00191	0.29471	0.01091	0.04147	0.00066	265	56	262	9	262	4	0.00

EB1-32	0.40	0.05529	0.00165	0.51374	0.01562	0.06737	0.001	424	42	421	10	420	6	0.24
EB1-33	2.19	0.05173	0.00207	0.3143	0.01262	0.04405	0.00069	273	63	278	10	278	4	0.00
EB1-34	1.47	0.05124	0.00157	0.28583	0.00886	0.04045	0.00061	252	44	255	7	256	4	-0.39
EB1-35	0.52	0.0556	0.00129	0.49882	0.01206	0.06505	0.00094	436	29	411	8	406	6	1.23
EB1-36	0.74	0.0515	0.00196	0.29334	0.01126	0.0413	0.00063	263	60	261	9	261	4	0.00
EB1-37	1.14	0.05132	0.00266	0.27903	0.01438	0.03942	0.00067	255	87	250	11	249	4	0.40
EB1-38	0.32	0.05643	0.00131	0.54546	0.01315	0.07009	0.00102	469	29	442	9	437	6	1.14
EB1-39	0.40	0.05381	0.00299	0.43111	0.02385	0.05809	0.00098	363	94	364	17	364	6	0.00
EB1-40	0.71	0.05553	0.00149	0.5338	0.01467	0.0697	0.00103	434	35	434	10	434	6	0.00
~~EB1-41~~	~~0.98~~	~~0.05818~~	~~0.00316~~	~~0.33051~~	~~0.01788~~	~~0.04119~~	~~0.00068~~	~~537~~	~~89~~	~~290~~	~~14~~	~~260~~	~~4~~	~~11.54~~
EB1-42	0.62	0.05511	0.00133	0.50901	0.01267	0.06697	0.00097	417	31	418	9	418	6	0.00
EB1-43	0.33	0.05119	0.00141	0.28865	0.00811	0.04089	0.0006	249	38	257	6	258	4	-0.39
EB1-44	0.47	0.05399	0.00154	0.30365	0.00883	0.04078	0.0006	371	39	269	7	258	4	4.26
~~EB1-45~~	~~0.42~~	~~0.09304~~	~~0.00362~~	~~1.68923~~	~~0.06055~~	~~0.13167~~	~~0.00198~~	~~1489~~	~~75~~	~~1004~~	~~23~~	~~797~~	~~11~~	~~25.97~~
EB1-46	0.92	0.05124	0.00243	0.28245	0.01331	0.03997	0.00066	252	78	253	11	253	4	0.00
EB1-47	1.02	0.05543	0.0011	0.48486	0.01023	0.06342	0.00089	430	24	401	7	396	5	1.26
EB1-48	0.68	0.06068	0.00226	0.57806	0.02158	0.06908	0.00107	628	54	463	14	431	6	7.42
~~EB1-49~~	~~0.10~~	~~0.07772~~	~~0.00206~~	~~1.15~~	~~0.02596~~	~~0.10732~~	~~0.00149~~	~~1140~~	~~54~~	~~777~~	~~12~~	~~657~~	~~9~~	~~18.26~~
EB1-50	0.51	0.05626	0.00135	0.50747	0.01259	0.0654	0.00095	463	30	417	8	408	6	2.21
EB1-51	0.41	0.05452	0.00138	0.47452	0.0123	0.06311	0.00089	393	33	394	8	395	5	-0.25
EB1-51	0.72	0.05596	0.00123	0.56379	0.01293	0.07305	0.00105	451	27	454	8	455	6	-0.22
EB1-52	0.70	0.05094	0.00238	0.26478	0.01221	0.0377	0.00064	238	75	239	10	239	4	0.00
EB1-52	0.44	0.05577	0.00126	0.51319	0.01204	0.06672	0.00095	443	28	421	8	416	6	1.20
EB1-53	0.74	0.05485	0.00369	0.49237	0.03294	0.0651	0.00109	406	120	407	22	407	7	0.00
EB1-53	0.88	0.05528	0.00519	0.53557	0.04981	0.07025	0.00145	424	172	435	33	438	9	-0.68
EB1-54	0.62	0.05535	0.00199	0.50825	0.01839	0.06659	0.00098	426	54	417	12	416	6	0.24
EB1-55	0.30	0.05497	0.00142	0.50122	0.01312	0.06612	0.00095	411	34	413	9	413	6	0.00
EB1-56	1.65	0.05083	0.00448	0.25675	0.02248	0.03663	0.00068	233	163	232	18	232	4	0.00

EB1-57	0.99	0.05444	0.00602	0.47493	0.05209	0.06326	0.00131	389	210	395	36	395	8	0.00
EB1-58	0.64	0.05156	0.00282	0.28445	0.01548	0.04	0.00065	266	95	254	12	253	4	0.40
EB1-59	1.31	0.05107	0.00135	0.26992	0.00726	0.03833	0.00055	244	36	243	6	242	3	0.41
EB1-60	0.90	0.05102	0.003	0.26326	0.01541	0.03742	0.00061	242	105	237	12	237	4	0.00
EB1-61	0.56	0.05088	0.00129	0.25839	0.00671	0.03683	0.00052	235	35	233	5	233	3	0.00
EB1-62	0.35	0.05528	0.00144	0.51227	0.01352	0.0672	0.00096	424	34	420	9	419	6	0.24
EB1-63	0.18	0.05089	0.00171	0.26111	0.00878	0.0372	0.00056	236	50	236	7	235	3	0.43
EB1-64	0.81	0.05112	0.00348	0.27155	0.01831	0.03852	0.00069	246	121	244	15	244	4	0.00
EB1-65	0.57	0.05148	0.00255	0.29586	0.01451	0.04167	0.0007	262	82	263	11	263	4	0.00
EB1-66	0.58	0.05135	0.00363	0.26867	0.01889	0.03794	0.00065	257	129	242	15	240	4	0.83
EB1-67	0.59	0.05131	0.00184	0.28135	0.00999	0.03976	0.00063	255	53	252	8	251	4	0.40
EB1-68	0.36	0.0571	0.00157	0.47403	0.01312	0.0602	0.00088	495	36	394	9	377	5	4.51
EB1-69	0.23	0.05554	0.00182	0.52263	0.01708	0.06823	0.00105	434	46	427	11	425	6	0.47
EB1-70	0.53	0.05569	0.00175	0.5146	0.01612	0.06701	0.00102	440	43	422	11	418	6	0.96
EB1-71	0.38	0.05511	0.00185	0.51166	0.01709	0.06732	0.00104	417	47	420	11	420	6	0.00
EB1-72	0.47	0.05517	0.00181	0.51003	0.01667	0.06704	0.00103	419	46	418	11	418	6	0.00
EB1-73	1.40	0.05102	0.00335	0.2662	0.01727	0.03783	0.00069	242	115	240	14	239	4	0.42
EB1-74	0.33	0.06749	0.00273	1.24492	0.04672	0.13379	0.00201	853	86	821	21	809	11	1.48
EB1-75	0.47	0.05507	0.00387	0.31138	0.02163	0.041	0.00077	415	122	275	17	259	5	6.18
EB1-76	0.62	0.05628	0.00143	0.52246	0.01349	0.06731	0.00096	463	33	427	9	420	6	1.67
EB1-77	0.95	0.05513	0.0039	0.51014	0.03587	0.06709	0.00115	417	127	419	24	419	7	0.00
EB1-78	0.51	0.05625	0.00215	0.56564	0.02165	0.07292	0.00111	462	58	455	14	454	7	0.22
EB1-79	1.32	0.05096	0.00418	0.27512	0.02224	0.03914	0.00082	239	145	247	18	248	5	-0.40
EB1-80	0.47	0.05541	0.00201	0.51439	0.01863	0.06731	0.00102	429	54	421	12	420	6	0.24
EB1-81	0.80	0.05088	0.00229	0.2709	0.01212	0.0386	0.0006	235	74	243	10	244	4	-0.41
EB1-82	1.27	0.05106	0.00329	0.26441	0.01687	0.03755	0.00067	244	114	238	14	238	4	0.00
EB1-83	0.66	0.0516	0.00218	0.30781	0.0129	0.04325	0.0007	268	66	272	10	273	4	-0.37
EB1-84	0.40	0.05544	0.00186	0.51043	0.01714	0.06675	0.00102	430	48	419	12	417	6	0.48

EB1-85	1.12	0.05151	0.00281	0.29128	0.01563	0.041	0.00073	264	90	260	12	259	5	0.39
EB1-86	0.18	0.06044	0.00202	0.86545	0.02619	0.10386	0.00147	619	74	633	14	637	9	-0.63
EB1-87	0.68	0.05627	0.00162	0.5448	0.01574	0.07019	0.00104	463	38	442	10	437	6	1.14
EB1-88	0.89	0.05542	0.00177	0.49601	0.01592	0.06489	0.00096	429	45	409	11	405	6	0.99
EB1-89	0.75	0.05552	0.00263	0.50851	0.02389	0.06641	0.0011	433	75	417	16	414	7	0.72
EB1-90	0.67	0.05087	0.00263	0.27148	0.01391	0.0387	0.00065	235	87	244	11	245	4	-0.41
EB1-91	0.57	0.06092	0.0017	0.55548	0.01567	0.06612	0.00097	636	36	449	10	413	6	8.72
EB1-92	0.82	0.05096	0.00184	0.27481	0.00992	0.0391	0.00059	239	55	247	8	247	4	0.00
EB1-93	1.11	0.05148	0.0041	0.28826	0.02275	0.0406	0.00076	262	145	257	18	257	5	0.00
EB1-94	0.14	0.05858	0.00141	0.50696	0.01252	0.06275	0.00089	552	30	416	8	392	5	6.12
EB1-95	0.82	0.05504	0.00422	0.51057	0.03891	0.06727	0.00118	414	140	419	26	420	7	-0.24
EB1-96	1.12	0.05133	0.00377	0.28244	0.02067	~~0.0399~~	0.00064	256	137	253	16	252	4	0.40
EB1-97	0.55	0.05161	0.00291	0.29801	0.01676	0.04187	0.00065	268	101	265	13	264	4	0.38
EB1-98	0.31	0.05114	0.0011	0.27954	0.00621	0.03963	0.00053	247	28	250	5	251	3	-0.40
EB1-99	0.62	0.05163	0.00364	0.28309	0.01984	0.03976	0.00066	269	130	253	16	251	4	0.80
EB1-100	0.58	0.05581	0.0025	0.53246	0.02375	0.06918	0.00109	445	71	433	16	431	7	0.46
Huatugou Section **S23**														
S23-01	0.90	0.05982	0.00111	0.58324	0.01128	0.07069	0.00092	597	21	467	7	440	6	6.14
~~S23-02~~	~~0.40~~	~~0.28214~~	~~0.00383~~	~~16.27658~~	~~0.24462~~	~~0.41832~~	~~0.00527~~	~~3375~~	~~11~~	~~2893~~	~~14~~	~~2253~~	~~24~~	~~49.80~~
S23-03	0.57	0.07536	0.00113	1.66574	0.02707	0.16027	0.00204	1078	15	996	10	958	11	3.97
S23-04	1.04	0.05776	0.00136	0.64895	0.01562	0.08147	0.00109	521	30	508	10	505	6	0.59
S23-05	0.42	0.05107	0.00193	0.27371	0.01037	0.03887	0.00054	244	62	246	8	246	3	0.00
~~S23-06~~	~~0.72~~	~~0.07544~~	~~0.00256~~	~~1.24423~~	~~0.04222~~	~~0.11959~~	~~0.00173~~	~~1080~~	~~45~~	~~821~~	~~19~~	~~728~~	~~10~~	~~12.77~~
~~S23-07~~	~~0.25~~	~~0.09551~~	~~0.00251~~	~~0.96832~~	~~0.02199~~	~~0.07353~~	~~0.00097~~	~~1538~~	~~51~~	~~688~~	~~11~~	~~457~~	~~6~~	~~50.55~~
S23-08	0.52	0.07119	0.00114	1.31571	0.02256	0.13401	0.00172	963	17	853	10	811	10	5.18

~~S23-09~~	~~0.77~~	~~0.09241~~	~~0.00136~~	~~2.15715~~	~~0.03452~~	~~0.16927~~	~~0.00215~~	~~1476~~	~~14~~	~~1167~~	~~11~~	~~1008~~	~~12~~	~~46.43~~
S23-10	0.91	0.05709	0.0023	0.4597	0.0185	0.05839	0.00083	495	63	384	13	366	5	4.92
~~S23-11~~	~~0.62~~	~~0.06271~~	~~0.00102~~	~~0.49215~~	~~0.00856~~	~~0.05691~~	~~0.00073~~	~~698~~	~~18~~	~~406~~	~~6~~	~~357~~	~~4~~	~~13.73~~
~~S23-12~~	~~1.37~~	~~0.09164~~	~~0.003~~	~~0.82553~~	~~0.02674~~	~~0.06532~~	~~0.00098~~	~~1460~~	~~39~~	~~611~~	~~15~~	~~408~~	~~6~~	~~49.75~~
~~S23-13~~	~~0.71~~	~~0.05959~~	~~0.00215~~	~~0.29976~~	~~0.01082~~	~~0.03648~~	~~0.00052~~	~~589~~	~~53~~	~~266~~	~~8~~	~~231~~	~~3~~	~~15.15~~
S23-14	0.80	0.05617	0.00191	0.50875	0.01741	0.06567	0.0009	459	51	418	12	410	5	1.95
S23-15	1.50	0.05563	0.00162	0.50568	0.01483	0.06591	0.00091	438	41	416	10	411	6	1.22
S23-16	0.18	0.11457	0.00163	4.9073	0.07669	0.31059	0.00392	1873	13	1804	13	1744	19	7.40
S23-17	0.29	0.05358	0.0018	0.39153	0.01319	0.05299	0.00076	353	50	335	10	333	5	0.60
~~S23-18~~	~~1.03~~	~~0.06568~~	~~0.00384~~	~~0.31858~~	~~0.01848~~	~~0.03517~~	~~0.00057~~	~~796~~	~~95~~	~~281~~	~~14~~	~~223~~	~~4~~	~~26.01~~
S23-19	0.90	0.05108	0.00224	0.26581	0.01165	0.03773	0.00053	244	75	239	9	239	3	0.00
S23-20	0.69	0.052	0.00155	0.29968	0.00902	0.04179	0.00056	285	44	266	7	264	3	0.76
S23-21	0.52	0.05879	0.00153	0.59425	0.01576	0.0733	0.00098	559	35	474	10	456	6	3.95
S23-22	0.54	0.05744	0.00115	0.63505	0.01318	0.08017	0.00105	508	24	499	8	497	6	0.40
S23-23	0.92	0.05922	0.00149	0.5921	0.01512	0.07249	0.001	575	32	472	10	451	6	4.66
~~S23-24~~	~~0.59~~	~~0.11824~~	~~0.00178~~	~~3.46697~~	~~0.05646~~	~~0.21261~~	~~0.00271~~	~~1930~~	~~13~~	~~1520~~	~~13~~	~~1243~~	~~14~~	~~55.27~~
S23-25	0.84	0.05272	0.00118	0.26428	0.00607	0.03635	0.00048	317	29	238	5	230	3	3.48
S23-26	0.50	0.05183	0.00193	0.28998	0.01082	0.04057	0.00057	278	60	259	9	256	4	1.17
S23-27	0.39	0.06869	0.00142	1.31071	0.02794	0.13838	0.00185	889	23	850	12	835	10	1.80
~~S23-28~~	~~0.50~~	~~0.13723~~	~~0.00207~~	~~6.6602~~	~~0.10875~~	~~0.35192~~	~~0.0045~~	~~2193~~	~~13~~	~~2067~~	~~14~~	~~1944~~	~~21~~	~~12.81~~
S23-29	0.19	0.05802	0.00148	0.64309	0.01655	0.08037	0.00111	531	33	504	10	498	7	1.20
S23-30	0.68	0.05659	0.0015	0.54797	0.01469	0.07022	0.00097	476	35	444	10	437	6	1.60
S23-31	0.27	0.05706	0.00122	0.42005	0.00924	0.05339	0.00071	494	26	356	7	335	4	6.27
S23-32	0.52	0.05283	0.00296	0.38118	0.0213	0.05232	0.00079	322	100	328	16	329	5	-0.30
~~S23-33~~	~~0.58~~	~~0.09534~~	~~0.00174~~	~~2.65888~~	~~0.05058~~	~~0.20223~~	~~0.0027~~	~~1535~~	~~18~~	~~1317~~	~~14~~	~~1187~~	~~14~~	~~29.32~~
S23-34	0.28	0.05849	0.00155	0.65082	0.01745	0.08069	0.00111	548	35	509	11	500	7	1.80
~~S23-35~~	~~0.84~~	~~0.06678~~	~~0.00152~~	~~0.58491~~	~~0.01363~~	~~0.06352~~	~~0.00086~~	~~831~~	~~27~~	~~468~~	~~9~~	~~397~~	~~5~~	~~17.88~~
~~S23-36~~	~~0.90~~	~~0.07486~~	~~0.00211~~	~~1.10063~~	~~0.03122~~	~~0.10662~~	~~0.00151~~	~~1065~~	~~35~~	~~754~~	~~15~~	~~653~~	~~9~~	~~15.47~~

S23-37	0.30	0.05444	0.00253	0.44363	0.02052	0.05909	0.00089	389	77	373	14	370	5	0.81
~~S23-38~~	~~1.84~~	~~0.0865~~	~~0.01437~~	~~0.49774~~	~~0.08151~~	~~0.04173~~	~~0.00116~~	~~1349~~	~~345~~	~~410~~	~~55~~	~~264~~	~~7~~	~~55.30~~
~~S23-39~~	~~0.30~~	~~0.11819~~	~~0.00197~~	~~4.88162~~	~~0.08646~~	~~0.29951~~	~~0.00391~~	~~1929~~	~~15~~	~~1799~~	~~15~~	~~1689~~	~~19~~	~~14.21~~
~~S23-40~~	~~0.55~~	~~0.06573~~	~~0.00153~~	~~0.69384~~	~~0.01643~~	~~0.07655~~	~~0.00104~~	~~798~~	~~28~~	~~535~~	~~10~~	~~475~~	~~6~~	~~12.63~~
~~S23-41~~	~~0.78~~	~~0.06953~~	~~0.0014~~	~~0.63775~~	~~0.01329~~	~~0.06651~~	~~0.00088~~	~~915~~	~~22~~	~~501~~	~~8~~	~~415~~	~~5~~	~~20.72~~
~~S23-42~~	~~0.37~~	~~0.06436~~	~~0.00132~~	~~0.67922~~	~~0.01442~~	~~0.07653~~	~~0.00102~~	~~753~~	~~24~~	~~526~~	~~9~~	~~475~~	~~6~~	~~10.74~~
~~S23-43~~	~~0.26~~	~~0.116~~	~~0.00192~~	~~4.40414~~	~~0.07773~~	~~0.27532~~	~~0.00358~~	~~1895~~	~~15~~	~~1713~~	~~15~~	~~1568~~	~~18~~	~~20.85~~
~~S23-44~~	~~1.66~~	~~0.12684~~	~~0.00272~~	~~4.02296~~	~~0.08773~~	~~0.22998~~	~~0.00325~~	~~2055~~	~~20~~	~~1639~~	~~18~~	~~1334~~	~~17~~	~~54.05~~
~~S23-45~~	~~0.52~~	~~0.07301~~	~~0.00199~~	~~0.70317~~	~~0.01905~~	~~0.06984~~	~~0.00103~~	~~1014~~	~~32~~	~~541~~	~~11~~	~~435~~	~~6~~	~~24.37~~
S23-46	0.72	0.05709	0.00111	0.53841	0.01085	0.06839	0.0009	495	23	437	7	426	5	2.58
S23-47	0.34	0.056	0.00133	0.31324	0.00756	0.04056	0.00055	452	30	277	6	256	3	8.20
S23-48	0.51	0.07226	0.00124	1.41492	0.0258	0.14199	0.00184	993	18	895	11	856	10	4.56
~~S23-49~~	~~0.77~~	~~0.11574~~	~~0.00216~~	~~3.24577~~	~~0.06313~~	~~0.20336~~	~~0.00272~~	~~1891~~	~~17~~	~~1468~~	~~15~~	~~1193~~	~~15~~	~~58.51~~
S23-50	0.48	0.05651	0.00138	0.52018	0.01287	0.06675	0.00091	472	31	425	9	417	5	1.92
S23-51	1.15	0.05521	0.00441	0.33102	0.02623	0.04348	0.00077	421	147	290	20	274	5	5.84
~~S23-52~~	~~0.38~~	~~0.10268~~	~~0.0028~~	~~3.5135~~	~~0.08335~~	~~0.24818~~	~~0.00332~~	~~1673~~	~~52~~	~~1530~~	~~19~~	~~1429~~	~~17~~	~~17.07~~
S23-53	0.14	0.05745	0.00119	0.58464	0.01255	0.0738	0.00098	509	25	467	8	459	6	1.74
~~S23-54~~	~~0.46~~	~~0.0621~~	~~0.00229~~	~~0.33745~~	~~0.01232~~	~~0.0394~~	~~0.0006~~	~~678~~	~~52~~	~~295~~	~~9~~	~~249~~	~~4~~	~~18.47~~
S23-55	1.02	0.05203	0.00199	0.32044	0.01222	0.04466	0.00066	287	60	282	9	282	4	0.00
~~S23-56~~	~~0.61~~	~~0.08221~~	~~0.00346~~	~~0.43717~~	~~0.01719~~	~~0.03857~~	~~0.00058~~	~~1250~~	~~84~~	~~368~~	~~12~~	~~244~~	~~4~~	~~50.82~~
S23-57	0.89	0.05833	0.00129	0.49542	0.01123	0.06159	0.00083	542	27	409	8	385	5	6.23
~~S23-58~~	~~0.92~~	~~0.06049~~	~~0.00154~~	~~0.43169~~	~~0.0112~~	~~0.05175~~	~~0.0007~~	~~621~~	~~33~~	~~364~~	~~8~~	~~325~~	~~4~~	~~12.00~~
S23-59	0.42	0.05114	0.00166	0.27261	0.00888	0.03865	0.00054	247	49	245	7	244	3	0.41
~~S23-60~~	~~0.21~~	~~0.06801~~	~~0.00126~~	~~0.86006~~	~~0.0167~~	~~0.0917~~	~~0.0012~~	~~869~~	~~20~~	~~630~~	~~9~~	~~566~~	~~7~~	~~11.31~~
S23-61	0.66	0.05647	0.00141	0.563	0.01426	0.0723	0.00099	471	32	453	9	450	6	0.67
~~S23-62~~	~~1.20~~	~~0.07977~~	~~0.00342~~	~~0.26333~~	~~0.01112~~	~~0.02394~~	~~0.00039~~	~~1191~~	~~58~~	~~237~~	~~9~~	~~153~~	~~2~~	~~54.90~~
S23-63	0.61	0.05702	0.00151	0.44945	0.01208	0.05715	0.00078	492	36	377	8	358	5	5.31
~~S23-64~~	~~0.44~~	~~0.06968~~	~~0.00141~~	~~0.83841~~	~~0.01763~~	~~0.08725~~	~~0.00116~~	~~919~~	~~23~~	~~618~~	~~10~~	~~539~~	~~7~~	~~14.66~~

S23-65	0.30	0.06744	0.00206	1.05614	0.02903	0.11359	0.00153	851	65	732	14	694	9	5.48
~~S23-66~~	~~0.47~~	~~0.10688~~	~~0.0021~~	~~2.18495~~	~~0.04437~~	~~0.14824~~	~~0.00199~~	~~1747~~	~~19~~	~~1176~~	~~14~~	~~891~~	~~11~~	~~31.99~~
~~S23-67~~	~~1.39~~	~~0.09779~~	~~0.00306~~	~~0.41085~~	~~0.01283~~	~~0.03047~~	~~0.00044~~	~~1582~~	~~37~~	~~349~~	~~9~~	~~193~~	~~3~~	~~80.83~~
~~S23-68~~	~~0.46~~	~~0.0626~~	~~0.00242~~	~~0.30222~~	~~0.01161~~	~~0.03501~~	~~0.00053~~	~~695~~	~~56~~	~~268~~	~~9~~	~~222~~	~~3~~	~~20.72~~
S23-69	0.93	0.05644	0.00275	0.50189	0.02438	0.06448	0.00095	470	81	413	16	403	6	2.48
~~S23-70~~	~~0.95~~	~~0.15705~~	~~0.00292~~	~~7.1459~~	~~0.13915~~	~~0.32995~~	~~0.00437~~	~~2424~~	~~17~~	~~2130~~	~~17~~	~~1838~~	~~21~~	~~31.88~~
S23-71	0.49	0.0585	0.00128	0.47121	0.01061	0.05841	0.00079	549	27	392	7	366	5	7.10
~~S23-72~~	~~0.90~~	~~0.07804~~	~~0.00353~~	~~0.38954~~	~~0.01752~~	~~0.0362~~	~~0.00055~~	~~1148~~	~~65~~	~~334~~	~~13~~	~~229~~	~~3~~	~~45.85~~
S23-73	0.84	0.07472	0.00276	1.67624	0.06171	0.16267	0.00244	1061	50	1000	23	972	14	2.88
S23-74	1.09	0.07257	0.0016	1.65798	0.03749	0.16567	0.00225	1002	25	993	14	988	12	0.51
S23-75	0.48	0.05951	0.00172	0.56859	0.01656	0.06928	0.00097	586	39	457	11	432	6	5.79
S23-76	0.57	0.0531	0.00235	0.36647	0.01618	0.05005	0.00075	333	73	317	12	315	5	0.63
~~S23-77~~	~~0.59~~	~~0.11243~~	~~0.00748~~	~~4.14382~~	~~0.27242~~	~~0.26727~~	~~0.00518~~	~~1839~~	~~91~~	~~1663~~	~~54~~	~~1527~~	~~26~~	~~20.43~~
S23-78	0.48	0.05647	0.00139	0.52322	0.01309	0.06718	0.00093	471	32	427	9	419	6	1.91
S23-79	0.93	0.0563	0.00149	0.54066	0.01445	0.06963	0.00097	464	35	439	10	434	6	1.15
~~S23-80~~	~~0.83~~	~~0.07164~~	~~0.00192~~	~~0.54993~~	~~0.01488~~	~~0.05566~~	~~0.00078~~	~~976~~	~~33~~	~~445~~	~~10~~	~~349~~	~~5~~	~~27.51~~
S23-81	1.00	0.05454	0.00163	0.46337	0.01387	0.06161	0.00089	393	41	387	10	385	5	0.52
S23-82	1.04	0.05622	0.00172	0.26853	0.00826	0.03464	0.00049	461	43	242	7	220	3	10.00
~~S23-83~~	~~0.52~~	~~0.158~~	~~0.00318~~	~~6.63991~~	~~0.13842~~	~~0.30475~~	~~0.00412~~	~~2434~~	~~18~~	~~2065~~	~~18~~	~~1715~~	~~20~~	~~41.92~~
S23-84	0.53	0.07549	0.00189	1.51616	0.03833	0.14565	0.00207	1082	29	937	15	877	12	6.84
~~S23-85~~	~~0.62~~	~~0.06274~~	~~0.00299~~	~~0.30336~~	~~0.01438~~	~~0.03506~~	~~0.00053~~	~~699~~	~~75~~	~~269~~	~~11~~	~~222~~	~~3~~	~~21.17~~
S23-86	0.61	0.06149	0.00328	0.74273	0.03806	0.08761	0.00129	656	117	564	22	541	8	4.25
S23-87	0.70	0.06905	0.00145	1.08881	0.02364	0.11435	0.00154	900	24	748	11	698	9	7.16
S23-88	0.78	0.05774	0.00145	0.58246	0.01483	0.07315	0.00102	520	32	466	10	455	6	2.42
~~S23-89~~	~~0.23~~	~~0.10682~~	~~0.00217~~	~~2.89306~~	~~0.06097~~	~~0.1964~~	~~0.00263~~	~~1746~~	~~20~~	~~1380~~	~~16~~	~~1156~~	~~14~~	~~51.04~~
S23-90	0.30	0.05557	0.00339	0.50205	0.03035	0.06551	0.00109	435	105	413	21	409	7	0.98
~~S23-91~~	~~0.68~~	~~0.0673~~	~~0.00218~~	~~0.76152~~	~~0.02472~~	~~0.08205~~	~~0.00119~~	~~847~~	~~43~~	~~575~~	~~14~~	~~508~~	~~7~~	~~13.19~~
S23-92	0.66	0.06629	0.00335	0.85555	0.04291	0.09359	0.0015	816	78	628	23	577	9	8.84

S23-93	0.48	0.05824	0.00152	0.51203	0.01351	0.06375	0.00089	539	34	420	9	398	5	5.53
S23-94	0.64	0.07896	0.0021	2.09477	0.05617	0.19237	0.00275	1171	31	1147	18	1134	15	3.26
S23-95	0.59	0.07104	0.00181	1.14503	0.02961	0.11687	0.00164	959	30	775	14	713	9	8.70
~~S23-96~~	~~0.59~~	~~0.07591~~	~~0.00219~~	~~0.91575~~	~~0.0264~~	~~0.08748~~	~~0.00128~~	~~1093~~	~~35~~	~~660~~	~~14~~	~~541~~	~~8~~	~~22.00~~
~~S23-97~~	~~0.90~~	~~0.07554~~	~~0.00221~~	~~1.05384~~	~~0.031~~	~~0.10117~~	~~0.00145~~	~~1083~~	~~36~~	~~731~~	~~15~~	~~621~~	~~8~~	~~17.71~~
S23-98	1.59	0.05432	0.00422	0.29322	0.02264	0.03914	0.00067	384	144	261	18	248	4	5.24
S23-99	0.52	0.05085	0.00132	0.20762	0.00546	0.02961	0.00041	234	36	192	5	188	3	2.13
~~S23-100~~	~~0.53~~	~~0.07504~~	~~0.002~~	~~1.28609~~	~~0.03464~~	~~0.12428~~	~~0.00176~~	~~1070~~	~~32~~	~~840~~	~~15~~	~~755~~	~~10~~	~~11.26~~
~~S23-101~~	~~0.80~~	~~0.16182~~	~~0.00363~~	~~6.39452~~	~~0.14657~~	~~0.28655~~	~~0.004~~	~~2475~~	~~21~~	~~2032~~	~~20~~	~~1624~~	~~20~~	~~52.40~~
S23-102	0.51	0.07223	0.00179	1.37014	0.03447	0.13756	0.00191	992	29	876	15	831	11	5.42
QX1-2														
QX12-01	0.98	0.16544	0.00258	10.87573	0.18187	0.47671	0.00627	2512	13	2513	16	2513	27	-0.04
QX12-02	0.39	0.09239	0.00183	3.2869	0.06704	0.25799	0.00352	1475	20	1478	16	1480	18	-0.34
QX12-03	1.08	0.05616	0.00121	0.57956	0.01285	0.07484	0.001	459	27	464	8	465	6	-0.22
QX12-04	0.64	0.05436	0.00255	0.46272	0.02162	0.06173	0.00093	386	78	386	15	386	6	0.00
~~QX12-05~~	~~0.51~~	~~0.07223~~	~~0.00279~~	~~0.79208~~	~~0.02839~~	~~0.07954~~	~~0.00116~~	~~992~~	~~81~~	~~592~~	~~16~~	~~493~~	~~7~~	~~20.08~~
QX12-06	0.88	0.0515	0.00298	0.30001	0.01723	0.04225	0.00067	263	103	266	13	267	4	-0.37
QX12-07	0.32	0.05724	0.00099	0.66779	0.01225	0.0846	0.0011	501	20	519	7	524	7	-0.95
QX12-08	0.72	0.07573	0.00175	1.86887	0.04396	0.17896	0.00249	1088	26	1070	16	1061	14	2.54
QX12-09	0.91	0.05711	0.00123	0.57663	0.01278	0.07323	0.00098	496	26	462	8	456	6	1.32
QX12-10	0.54	0.11013	0.00171	4.83599	0.08081	0.31845	0.00413	1802	14	1791	14	1782	20	1.12
QX12-11	0.98	0.05598	0.00226	0.56441	0.02271	0.07311	0.00109	452	63	454	15	455	7	-0.22
QX12-12	1.57	0.08027	0.002	2.25843	0.05667	0.20403	0.00291	1204	28	1199	18	1197	16	0.58
~~QX12-13~~	~~0.70~~	~~0.09105~~	~~0.00322~~	~~1.99752~~	~~0.06479~~	~~0.15912~~	~~0.00226~~	~~1448~~	~~69~~	~~1115~~	~~22~~	~~952~~	~~13~~	~~17.12~~
QX12-14	0.64	0.05686	0.00191	0.58285	0.01962	0.07433	0.00107	486	49	466	13	462	6	0.87
QX12-15	0.75	0.05462	0.00165	0.47799	0.01453	0.06346	0.00088	397	43	397	10	397	5	0.00
QX12-16	0.15	0.05701	0.00104	0.60077	0.01147	0.07642	0.00099	492	21	478	7	475	6	0.63

QX12-17	4.87	0.06529	0.00131	1.17088	0.02421	0.13004	0.00174	784	22	787	11	788	10	-0.13
QX12-18	1.10	0.05598	0.00196	0.57328	0.02007	0.07426	0.00106	452	52	460	13	462	6	-0.43
QX12-19	0.77	0.05675	0.00182	0.59943	0.01929	0.07659	0.00109	482	46	477	12	476	7	0.21
QX12-20	0.62	0.05629	0.00233	0.58256	0.02388	0.07505	0.00116	464	63	466	15	467	7	-0.21
QX12-21	0.75	0.05632	0.00178	0.58417	0.01845	0.07522	0.00108	465	45	467	12	468	6	-0.21
~~QX12-22~~	~~0.59~~	~~0.13856~~	~~0.00218~~	~~6.71233~~	~~0.11333~~	~~0.35129~~	~~0.00458~~	~~2209~~	~~14~~	~~2074~~	~~15~~	~~1941~~	~~22~~	~~13.81~~
QX12-23	0.53	0.06129	0.00181	0.83931	0.02497	0.0993	0.00138	649	40	619	14	610	8	1.48
QX12-24	0.98	0.10752	0.00239	4.52605	0.10229	0.30524	0.00435	1758	22	1736	19	1717	21	2.39
QX12-25	0.96	0.05172	0.00256	0.30546	0.01506	0.04283	0.00065	273	85	271	12	270	4	0.37
QX12-26	0.68	0.05663	0.00145	0.58717	0.01529	0.07519	0.00103	477	34	469	10	467	6	0.43
QX12-27	0.38	0.07005	0.00134	1.48045	0.02944	0.15325	0.00203	930	21	922	12	919	11	0.33
QX12-28	0.69	0.05622	0.00216	0.58505	0.02247	0.07546	0.0011	461	59	468	14	469	7	-0.21
QX12-29	0.76	0.05653	0.00155	0.56013	0.01543	0.07186	0.001	473	37	452	10	447	6	1.12
QX12-30	1.12	0.05573	0.00095	0.54749	0.00989	0.07123	0.00092	442	19	443	6	444	6	-0.23
QX12-31	0.34	0.06106	0.00139	0.89185	0.02061	0.10591	0.00145	641	27	647	11	649	8	-0.31
QX12-32	0.66	0.05564	0.0016	0.54968	0.01583	0.07164	0.00102	438	39	445	10	446	6	-0.22
QX12-33	1.48	0.07623	0.00268	1.90419	0.06686	0.18113	0.00271	1101	46	1083	23	1073	15	2.61
QX12-34	0.82	0.08791	0.00201	2.87374	0.06686	0.23704	0.00328	1381	24	1375	18	1371	17	0.73
QX12-35	1.89	0.06417	0.00214	1.06299	0.03555	0.12011	0.00171	747	47	735	17	731	10	0.55
QX12-36	0.62	0.05213	0.00594	0.32721	0.03698	0.04552	0.00094	291	217	287	28	287	6	0.00
QX12-37	0.95	0.05627	0.00398	0.55184	0.03871	0.07111	0.0012	463	126	446	25	443	7	0.68
QX12-38	0.48	0.05042	0.00312	0.23573	0.0145	0.0339	0.00055	214	111	215	12	215	3	0.00
QX12-39	0.26	0.07032	0.00126	1.42486	0.02683	0.14693	0.00193	938	19	899	11	884	11	1.70
QX12-40	0.32	0.0569	0.0015	0.56991	0.01522	0.07263	0.001	488	35	458	10	452	6	1.33
QX12-41	0.65	0.06442	0.00179	1.10746	0.03099	0.12466	0.00176	755	36	757	15	757	10	0.00
QX12-42	0.66	0.05635	0.00168	0.57562	0.01729	0.07407	0.00104	466	42	462	11	461	6	0.22
QX12-43	0.47	0.09583	0.00163	3.26367	0.05852	0.24694	0.00324	1544	16	1472	14	1423	17	8.50
QX12-44	0.14	0.06729	0.00161	1.15268	0.02321	0.12424	0.0016	847	51	779	11	755	9	3.18

QX12-45	0.15	0.05149	0.00154	0.29294	0.00879	0.04125	0.00058	263	43	261	7	261	4	0.00
QX12-46	0.54	0.05662	0.00131	0.60318	0.01427	0.07724	0.00104	477	29	479	9	480	6	-0.21
QX12-47	1.02	0.05204	0.00308	0.32845	0.01932	0.04576	0.00071	287	106	288	15	288	4	0.00
QX12-48	0.54	0.05691	0.00135	0.57156	0.01377	0.07283	0.00099	488	30	459	9	453	6	1.32
QX12-49	1.24	0.16762	0.00408	10.90377	0.26622	0.47166	0.00729	2534	21	2515	23	2491	32	1.73
QX12-50	0.60	0.08904	0.00154	3.04165	0.05547	0.24769	0.00326	1405	17	1418	14	1427	17	-1.54
QX12-51	0.47	0.05622	0.00135	0.58389	0.01429	0.07531	0.00102	461	31	467	9	468	6	-0.21
QX12-52	0.58	0.05644	0.00146	0.57695	0.01515	0.07412	0.00101	470	34	462	10	461	6	0.22
QX12-53	0.08	0.05607	0.00135	0.52638	0.01288	0.06806	0.00093	455	31	429	9	424	6	1.18
QX12-54	0.47	0.05674	0.00139	0.61004	0.01524	0.07795	0.00106	481	32	484	10	484	6	0.00
QX12-55	0.12	0.05548	0.00162	0.52374	0.01359	0.06847	0.0009	431	66	428	9	427	5	0.23
QX12-56	0.74	0.05569	0.00123	0.53634	0.01207	0.06983	0.00094	440	27	436	8	435	6	0.23
QX12-57	1.01	0.05686	0.00208	0.583	0.02133	0.07434	0.00107	486	55	466	14	462	6	0.87
~~QX12-58~~	~~0.87~~	~~0.07349~~	~~0.00188~~	~~0.6113~~	~~0.01576~~	~~0.06031~~	~~0.00084~~	~~1027~~	~~30~~	~~484~~	~~10~~	~~378~~	~~5~~	~~28.04~~
QX12-59	0.76	0.05608	0.00552	0.54045	0.05285	0.06987	0.00131	456	186	439	35	435	8	0.92
~~QX12-60~~	~~1.18~~	~~0.06658~~	~~0.00163~~	~~0.66821~~	~~0.01661~~	~~0.07277~~	~~0.00099~~	~~825~~	~~30~~	~~520~~	~~10~~	~~453~~	~~6~~	~~14.79~~
QX12-61	0.63	0.05669	0.00156	0.58424	0.01616	0.07472	0.00104	479	37	467	10	465	6	0.43
QX12-62	0.83	0.10127	0.00198	4.14488	0.08358	0.29677	0.00404	1648	19	1663	16	1675	20	-1.61
QX12-63	0.52	0.05647	0.00135	0.57567	0.014	0.07392	0.00101	471	30	462	9	460	6	0.43
QX12-64	1.05	0.05986	0.00183	0.80308	0.02449	0.09727	0.0014	599	41	599	14	598	8	0.17
QX12-65	0.94	0.05612	0.00141	0.58171	0.01485	0.07515	0.00103	457	33	466	10	467	6	-0.21
QX12-66	0.54	0.07914	0.00148	2.10921	0.04105	0.19323	0.00257	1176	19	1152	13	1139	14	3.25
QX12-67	0.94	0.05612	0.0017	0.56207	0.01714	0.07262	0.00102	457	43	453	11	452	6	0.22
QX12-68	0.85	0.05589	0.00163	0.56009	0.0164	0.07265	0.00104	448	40	452	11	452	6	0.00
QX12-69	0.48	0.06966	0.00141	1.44058	0.03009	0.14993	0.00201	918	22	906	13	901	11	0.55
QX12-70	0.59	0.05641	0.00148	0.58013	0.0154	0.07456	0.00103	469	35	465	10	464	6	0.22
QX12-71	0.49	0.05523	0.00203	0.53376	0.01952	0.07007	0.00102	422	56	434	13	437	6	-0.69
QX12-72	1.05	0.0517	0.00142	0.31741	0.00882	0.04451	0.00061	272	39	280	7	281	4	-0.36

QX12-73	0.61	0.05623	0.00134	0.57607	0.01392	0.07428	0.00102	461	30	462	9	462	6	0.00
QX12-74	0.38	0.0556	0.00135	0.52692	0.01296	0.06871	0.00094	436	31	430	9	428	6	0.47
QX12-75	0.53	0.05089	0.00197	0.27132	0.01045	0.03866	0.00056	236	62	244	8	245	3	-0.41
QX12-76	0.17	0.05802	0.00126	0.67936	0.01508	0.08489	0.00115	531	26	526	9	525	7	0.19
QX12-77	0.69	0.05732	0.00131	0.63599	0.01483	0.08045	0.0011	504	28	500	9	499	7	0.20
QX12-78	0.88	0.08273	0.00232	2.491	0.06993	0.2183	0.00322	1263	32	1269	20	1273	17	-0.79
QX12-79	0.92	0.05659	0.00165	0.58228	0.01696	0.0746	0.00106	476	40	466	11	464	6	0.43
QX12-80	0.75	0.05643	0.00147	0.58574	0.01539	0.07526	0.00104	469	34	468	10	468	6	0.00
QX12-81	0.54	0.05622	0.00123	0.57271	0.01281	0.07386	0.001	461	27	460	8	459	6	0.22
QX12-82	0.45	0.05672	0.00121	0.59679	0.01305	0.07628	0.00102	481	26	475	8	474	6	0.21
QX12-83	0.39	0.05637	0.0013	0.55414	0.013	0.07127	0.00097	467	29	448	8	444	6	0.90
QX12-84	0.13	0.07604	0.00229	1.4311	0.03869	0.13651	0.00183	1096	62	902	16	825	10	9.33
QX12-85	0.29	0.07007	0.00141	1.47637	0.03063	0.15276	0.00205	930	22	921	13	916	11	0.55
QX12-86	0.61	0.05728	0.00125	0.57293	0.01277	0.07252	0.00098	502	26	460	8	451	6	2.00
QX12-87	0.55	0.05585	0.00152	0.56251	0.01543	0.07302	0.00103	446	36	453	10	454	6	-0.22
QX12-88	0.87	0.05601	0.00138	0.56669	0.01414	0.07336	0.00101	453	32	456	9	456	6	0.00
QX12-89	0.47	0.05206	0.00154	0.32345	0.0096	0.04504	0.00064	288	42	285	7	284	4	0.35
QX12-90	1.88	0.05612	0.00161	0.57916	0.0166	0.07481	0.00107	457	39	464	11	465	6	-0.22
QX12-91	0.22	0.10798	0.00198	4.61033	0.08808	0.30954	0.00409	1766	17	1751	16	1738	20	1.61
QX12-92	0.76	0.05692	0.00145	0.5887	0.01513	0.07499	0.00104	488	33	470	10	466	6	0.86
QX12-93	0.77	0.05666	0.00184	0.58596	0.01899	0.07497	0.0011	478	46	468	12	466	7	0.43
QX12-94	0.46	0.05484	0.00131	0.49459	0.01198	0.06538	0.0009	406	30	408	8	408	5	0.00
QX12-95	0.65	0.05607	0.00132	0.56714	0.0135	0.07333	0.00101	455	29	456	9	456	6	0.00
QX12-96	0.72	0.05191	0.00207	0.3286	0.0129	0.04589	0.00074	281	60	288	10	289	5	-0.35
QX12-97	0.63	0.0573	0.00178	0.59506	0.01839	0.07529	0.00111	503	42	474	12	468	7	1.28
QX12-98	0.42	0.06986	0.00135	1.48761	0.02983	0.15437	0.00205	924	21	925	12	925	11	0.00
QX12-99	0.72	0.0566	0.0017	0.53984	0.01609	0.06914	0.00102	476	40	438	11	431	6	1.62
~~QX12-100~~	~~0.27~~	~~0.07158~~	~~0.00225~~	~~0.89404~~	~~0.02533~~	~~0.09058~~	~~0.00122~~	~~974~~	~~65~~	~~649~~	~~14~~	~~559~~	~~7~~	~~16.10~~

QX12-101	0.76	0.05309	0.00161	0.3525	0.0106	0.04813	0.00071	333	42	307	8	303	4	1.32
QX12-102	4.95	0.05688	0.00163	0.60994	0.01753	0.07774	0.00111	487	39	484	11	483	7	0.21
QX12-103	2.22	0.08821	0.00193	2.80568	0.06258	0.2306	0.00318	1387	23	1357	17	1338	17	3.66
~~QX12-104~~	~~1.18~~	~~0.08321~~	~~0.00192~~	~~0.75961~~	~~0.01762~~	~~0.06618~~	~~0.00093~~	~~1274~~	~~24~~	~~574~~	~~10~~	~~413~~	~~6~~	~~38.98~~
QX12-105	0.61	0.05736	0.00144	0.62582	0.01585	0.07909	0.00111	505	32	493	10	491	7	0.41
QX1-1														
QX11-01	0.43	0.12106	0.00237	5.75521	0.11939	0.3447	0.00494	1972	18	1940	18	1909	24	3.30
QX11-02	0.87	0.05115	0.00162	0.26807	0.00855	0.038	0.00058	248	46	241	7	240	4	0.42
QX11-03	0.20	0.06854	0.00141	1.26705	0.02748	0.13403	0.0019	885	23	831	12	811	11	2.47
QX11-04	0.27	0.0517	0.00231	0.28611	0.01275	0.04013	0.00064	272	73	255	10	254	4	0.39
QX11-05	0.53	0.05456	0.00146	0.31714	0.00867	0.04215	0.00062	394	36	280	7	266	4	5.26
QX11-06	0.70	0.16508	0.00317	10.88889	0.22156	0.47827	0.00682	2508	17	2514	19	2520	30	-0.48
QX11-07	0.61	0.05147	0.0015	0.29769	0.00881	0.04194	0.00062	262	41	265	7	265	4	0.00
~~QX11-08~~	~~0.84~~	~~0.07476~~	~~0.00215~~	~~0.59077~~	~~0.01721~~	~~0.05729~~	~~0.00087~~	~~1062~~	~~35~~	~~471~~	~~11~~	~~359~~	~~5~~	~~31.20~~
QX11-09	0.46	0.05057	0.00171	0.24406	0.00826	0.035	0.00055	221	49	222	7	222	3	0.00
QX11-10	0.73	0.10903	0.00416	4.71724	0.16453	0.31378	0.00487	1783	71	1770	29	1759	24	1.36
QX11-11	0.36	0.05758	0.00136	0.65895	0.01598	0.08298	0.00121	514	29	514	10	514	7	0.00
~~QX11-12~~	~~0.53~~	~~0.0843~~	~~0.00312~~	~~2.18569~~	~~0.07398~~	~~0.18805~~	~~0.0028~~	~~1299~~	~~74~~	~~1176~~	~~24~~	~~1111~~	~~15~~	~~16.92~~
QX11-13	0.51	0.0816	0.00193	2.34736	0.05678	0.20858	0.0031	1236	25	1227	17	1221	17	1.23
QX11-14	0.63	0.05556	0.00212	0.53579	0.02046	0.06993	0.00109	435	57	436	14	436	7	0.00
QX11-15	0.49	0.05208	0.00207	0.33304	0.01317	0.04637	0.00074	289	61	292	10	292	5	0.00
QX11-16	0.63	0.05379	0.0022	0.41682	0.01707	0.05619	0.00087	362	64	354	12	352	5	0.57
QX11-17	0.84	0.05169	0.00245	0.31615	0.01489	0.04435	0.00074	272	77	279	11	280	5	-0.36
QX11-18	0.54	0.05174	0.00317	0.30696	0.01865	0.04302	0.00075	274	107	272	14	272	5	0.00
QX11-19	0.24	0.06966	0.00165	1.44573	0.03512	0.15048	0.00219	918	27	908	15	904	12	0.44
QX11-20	0.45	0.05336	0.00205	0.38208	0.01472	0.05192	0.00079	344	60	329	11	326	5	0.92
QX11-21	0.90	0.05721	0.00163	0.64131	0.01857	0.08128	0.00119	500	38	503	11	504	7	-0.20

QX11-22	0.00	0.05593	0.00198	0.55102	0.0196	0.07143	0.00109	450	52	446	13	445	7	0.22
QX11-23	0.46	0.07281	0.00175	1.55307	0.03813	0.15467	0.00227	1009	27	952	15	927	13	2.70
QX11-24	0.53	0.05551	0.00219	0.52815	0.02079	0.06899	0.0011	433	59	431	14	430	7	0.23
QX11-25	1.06	0.05813	0.00293	0.68403	0.03417	0.08533	0.00146	535	79	529	21	528	9	0.19
QX11-26	0.40	0.07511	0.00192	1.87304	0.0485	0.18082	0.00273	1071	29	1072	17	1071	15	0.00
QX11-27	0.74	0.05671	0.00177	0.58088	0.01813	0.07427	0.00115	480	42	465	12	462	7	0.65
~~QX11-28~~	~~0.31~~	~~0.12816~~	~~0.00375~~	~~4.5386~~	~~0.11543~~	~~0.25684~~	~~0.00373~~	~~2073~~	~~53~~	~~1738~~	~~21~~	~~1474~~	~~19~~	~~40.64~~
QX11-29	0.48	0.05913	0.00692	0.75485	0.08755	0.09256	0.00209	572	217	571	51	571	12	0.00
QX11-30	0.78	0.0556	0.00132	0.53901	0.01311	0.07029	0.00102	436	29	438	9	438	6	0.00
QX11-31	0.50	0.05708	0.00178	0.62736	0.0196	0.0797	0.00122	495	42	494	12	494	7	0.00
QX11-32	0.61	0.05456	0.00123	0.46464	0.01077	0.06175	0.00088	394	28	387	7	386	5	0.26
QX11-33	0.38	0.06058	0.0013	0.57402	0.01279	0.0687	0.00097	624	25	461	8	428	6	7.71
QX11-34	1.11	0.05577	0.00152	0.55238	0.01523	0.07181	0.00106	443	36	447	10	447	6	0.00
QX11-35	0.55	0.05466	0.00197	0.45791	0.0165	0.06074	0.00094	398	53	383	11	380	6	0.79
QX11-36	0.36	0.05234	0.00252	0.38486	0.01755	0.05333	0.00081	300	112	331	13	335	5	-1.19
QX11-37	0.42	0.05505	0.0015	0.50172	0.01379	0.06608	0.00097	414	36	413	9	412	6	0.24
QX11-38	0.48	0.07132	0.00169	1.51879	0.03682	0.15441	0.00223	967	27	938	15	926	12	1.30
QX11-39	0.21	0.0546	0.00175	0.44958	0.01442	0.05971	0.0009	396	45	377	10	374	5	0.80
QX11-40	1.25	0.0556	0.00151	0.54291	0.01487	0.07081	0.00105	436	35	440	10	441	6	-0.23
QX11-41	0.94	0.05658	0.00279	0.5946	0.02916	0.07621	0.00124	475	80	474	19	473	7	0.21
QX11-42	0.83	0.05516	0.00219	0.50986	0.02012	0.06702	0.00106	419	60	418	14	418	6	0.00
QX11-43	0.58	0.05564	0.0016	0.54424	0.01576	0.07093	0.00105	438	39	441	10	442	6	-0.23
QX11-44	0.39	0.05623	0.00137	0.50123	0.01245	0.06464	0.00092	461	31	413	8	404	6	2.23
QX11-45	0.32	0.05513	0.00199	0.50622	0.01829	0.06658	0.00102	417	53	416	12	416	6	0.00
QX11-46	0.43	0.0554	0.00143	0.50109	0.01313	0.06559	0.00095	428	33	412	9	410	6	0.49
QX11-47	0.63	0.05211	0.00363	0.33315	0.02294	0.04636	0.00086	290	123	292	17	292	5	0.00
QX11-48	0.66	0.11523	0.00256	5.24332	0.11947	0.32995	0.00476	1883	21	1860	19	1838	23	2.45
QX11-49	0.14	0.25577	0.0054	22.09347	0.48131	0.62634	0.00891	3221	18	3188	21	3135	35	2.74

QX11-50	0.68	0.09747	0.00241	3.60613	0.09039	0.26828	0.00395	1576	26	1551	20	1532	20	2.87
QX11-51	0.53	0.05478	0.00145	0.48321	0.01292	0.06396	0.00093	403	34	400	9	400	6	0.00
QX11-52	0.29	0.0563	0.00276	0.50126	0.02345	0.06457	0.00096	464	112	413	16	403	6	2.48
QX11-53	0.97	0.05624	0.00147	0.55803	0.01469	0.07195	0.00105	462	33	450	10	448	6	0.45
QX11-54	0.89	0.05493	0.00209	0.49639	0.0188	0.06553	0.00102	409	57	409	13	409	6	0.00
QX11-55	0.96	0.05484	0.00267	0.49216	0.02373	0.06507	0.00107	406	78	406	16	406	6	0.00
QX11-56	0.49	0.05148	0.00205	0.30348	0.01208	0.04275	0.00065	262	63	269	9	270	4	-0.37
QX11-57	1.00	0.05963	0.00164	0.56532	0.01564	0.06875	0.00101	590	35	455	10	429	6	6.06
QX11-58	0.45	0.05091	0.00241	0.21292	0.00955	0.03033	0.00045	237	111	196	8	193	3	1.55
QX11-59	0.36	0.05575	0.0017	0.52278	0.01593	0.068	0.00101	442	42	427	11	424	6	0.71
QX11-60	0.48	0.1137	0.00253	4.86928	0.11044	0.31053	0.00441	1859	22	1797	19	1743	22	6.66
QX11-61	0.75	0.05539	0.00188	0.51466	0.01749	0.06738	0.00101	428	49	422	12	420	6	0.48
QX11-62	0.80	0.05497	0.00185	0.50338	0.01683	0.0664	0.00103	411	47	414	11	414	6	0.00
QX11-63	0.18	0.124	0.00275	6.1883	0.14022	0.36188	0.00513	2015	21	2003	20	1991	24	1.21
QX11-64	0.19	0.05848	0.00209	0.65378	0.02321	0.08107	0.00124	548	51	511	14	503	7	1.59
QX11-65	0.08	0.06092	0.0017	0.63955	0.01546	0.07613	0.00106	637	61	502	10	473	6	6.13
~~QX11-66~~	~~1.79~~	~~0.07212~~	~~0.00273~~	~~0.60598~~	~~0.0227~~	~~0.06093~~	~~0.00097~~	~~989~~	~~50~~	~~481~~	~~14~~	~~381~~	~~6~~	~~26.25~~
~~QX11-67~~	~~0.23~~	~~0.06097~~	~~0.00147~~	~~0.48682~~	~~0.01187~~	~~0.0579~~	~~0.00083~~	~~638~~	~~29~~	~~403~~	~~8~~	~~363~~	~~5~~	~~11.02~~
QX11-68	0.24	0.06963	0.00163	1.40082	0.03323	0.14587	0.00208	917	26	889	14	878	12	1.25
QX11-69	0.44	0.05686	0.0017	0.60669	0.0181	0.07737	0.00115	486	40	481	11	480	7	0.21
~~QX11-70~~	~~0.55~~	~~0.0789~~	~~0.00247~~	~~1.94063~~	~~0.06048~~	~~0.17836~~	~~0.00274~~	~~1170~~	~~38~~	~~1095~~	~~21~~	~~1058~~	~~15~~	~~10.59~~
QX11-71	0.47	0.06788	0.00173	1.24972	0.03206	0.13351	0.00194	865	30	823	14	808	11	1.86
QX11-72	0.49	0.1089	0.00285	4.6494	0.12144	0.30958	0.00466	1781	26	1758	22	1739	23	2.42
QX11-73	0.96	0.0559	0.00352	0.55795	0.03473	0.07237	0.00126	448	108	450	23	450	8	0.00
QX11-74	0.66	0.0559	0.00154	0.54079	0.0149	0.07016	0.00103	448	36	439	10	437	6	0.46
QX11-75	0.74	0.0552	0.00182	0.51267	0.01673	0.06735	0.00104	420	45	420	11	420	6	0.00
QX11-76	0.90	0.06666	0.00274	1.15326	0.04693	0.12546	0.00202	827	58	779	22	762	12	2.23
QX11-77	0.46	0.05595	0.00159	0.56792	0.0161	0.0736	0.00109	450	37	457	10	458	7	-0.22

QX11-78	0.44	0.05752	0.00983	0.65239	0.11068	0.08224	0.00213	512	330	510	68	509	13	0.20
QX11-79	0.76	0.07296	0.00186	1.56337	0.03982	0.15539	0.00225	1013	29	956	16	931	13	2.69
QX11-80	0.18	0.05745	0.00165	0.65301	0.01862	0.08242	0.00123	509	37	510	11	511	7	-0.20
QX11-81	1.20	0.05536	0.00199	0.52338	0.01863	0.06856	0.00104	427	52	427	12	427	6	0.00
QX11-82	0.72	0.0553	0.00181	0.52169	0.01687	0.06841	0.00104	424	45	426	11	427	6	-0.23
QX11-83	0.74	0.05537	0.00239	0.50967	0.02186	0.06674	0.00104	427	68	418	15	416	6	0.48
QX11-84	0.39	0.05491	0.00162	0.48263	0.01417	0.06374	0.00094	409	40	400	10	398	6	0.50
QX11-85	1.53	0.07638	0.00312	1.89066	0.07597	0.17949	0.00302	1105	53	1078	27	1064	17	3.85
QX11-86	0.68	0.05392	0.00254	0.43298	0.02019	0.05823	0.00092	368	76	365	14	365	6	0.00
QX11-87	1.07	0.05562	0.00162	0.5298	0.01531	0.06908	0.00102	437	38	432	10	431	6	0.23
QX11-88	0.40	0.05325	0.00438	0.39734	0.03238	0.05411	0.001	339	152	340	24	340	6	0.00
QX11-89	0.72	0.05577	0.00154	0.55348	0.01521	0.07196	0.00106	443	36	447	10	448	6	-0.22
QX11-90	0.88	0.05616	0.00179	0.56209	0.01769	0.07257	0.0011	459	43	453	11	452	7	0.22
~~QX11-91~~	~~0.96~~	~~0.06482~~	~~0.00231~~	~~0.56111~~	~~0.01975~~	~~0.06278~~	~~0.00097~~	~~768~~	~~48~~	~~452~~	~~13~~	~~393~~	~~6~~	~~15.01~~
QX11-92	0.26	0.07055	0.00185	1.45582	0.03787	0.14965	0.00218	944	30	912	16	899	12	1.45
QX11-93	0.70	0.05418	0.00227	0.4544	0.01872	0.06082	0.00098	379	64	380	13	381	6	-0.26
QX11-94	0.63	0.09011	0.00232	2.98386	0.07625	0.24014	0.00351	1428	27	1404	19	1387	18	2.96
QX11-95	0.41	0.05438	0.00151	0.42693	0.01176	0.05693	0.00084	387	36	361	8	357	5	1.12
QX11-96	0.84	0.16262	0.00426	10.49347	0.27218	0.46793	0.0071	2483	24	2479	24	2474	31	0.36
QX11-97	0.53	0.05443	0.00244	0.45236	0.01994	0.06027	0.00099	389	69	379	14	377	6	0.53
QX11-98	0.57	0.05411	0.00205	0.44568	0.01662	0.05973	0.00094	376	56	374	12	374	6	0.00
QX11-99	0.46	0.05498	0.00179	0.50368	0.01619	0.06644	0.00101	411	45	414	11	415	6	-0.24
QX11-100	0.31	0.05312	0.00186	0.38975	0.01343	0.05321	0.00082	334	50	334	10	334	5	0.00

Appendix to Chapter 4

Detailed parameter constraints

1. Northeastward migration of the Qaidam Basin along the Altyn Tagh Fault.

Guo et al. (1998) first reported that geochemical fingerprints (e.g. carbon isotopic composition) in the Jurassic oil-bearing sandstone of the Tula Basin were similar to that of the geochemical fingerprints in the Jurassic oil-bearing sandstone oil in the Qaidam Basin. Based on sedimentology along the western Qaidam Basin and low temperature thermochronology studies, Wang et al. (2006) suggested that the Qaidam Basin should derive from the Tula area and be largely northwards transported. By correlating stratigraphic contacts and lithologies with the U-Pb age spectra of Mesozoic samples within sections along the western Qaidam Basin and Tula Basin, Cheng (2015a) also revealed hundreds of kilometers of northeastward migration of the Qaidam Basin along the Altyn Tagh Fault (ATF) since its Eocene initiation.

2. 360 ± 40 km offset along the Altyn Tagh Fault

By matching Late Paleozoic magmatic belts in the western and eastern Kunlun Shan, ranges of 300 to 550 km of displacement have been estimated (Tapponnier et al., 1986; Peltzer and Tapponnier, 1988; Cowgill et al., 2003). By correlating the geological features with the magmatic histories in the Altyn Tagh Range, Qilian Shan and Nan Shan, Gehrels et al. (2003) suggest a 370 to 400 km offsets along the ATF. By reconstructing the crustal shortening of the Qilian Shan region, Yin and Harrison (2000) inferred 360 ± 50 km of displacement along the fault. Based on integrated analysis of the geologic features along the north margin of the Tibetan Plateau, Molnar and Tapponnier (1975) proposed ~400 km of offset along the ATF. In addition, a 400 ± 60 km offset has also been suggested based on the reconstruction of a Jurassic facies boundary across the ATF (Ritts and Biffi, 2000). Collectively, previous estimations of the offset along the ATF generally vary from 300~400 km. Alternatively, based on a detailed analysis of the stratigraphy and geochronology of three key lithologic sections along the ATF, we recently identify two key piercing points which suggest 360 ± 40 km offset along the ATF (Cheng et al., 2015a). Taking into account

all these estimations we define the Cenozoic offset along the ATF to be 360 ± 40 km (Fig. 3A).

2. Simultaneous deformation along the Altyn Tagh Fault and within the Qilian Shan since their Eocene initiation

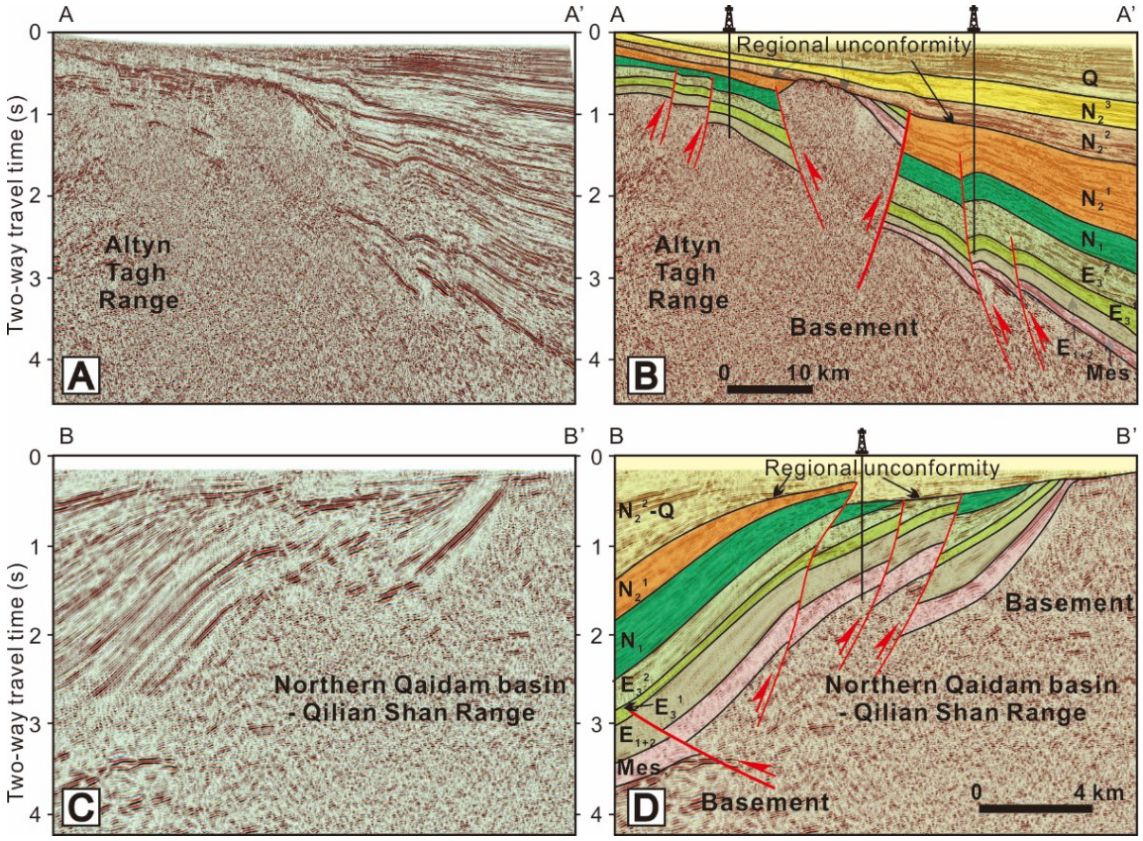

Fig. S1 Seismic profiles in the western Qaidam Basin. (A) Interpreted and (B) non-interpreted seismic profile AA'. (C) Interpreted and (D) non-interpreted seismic profile BB'. See Fig. 1B for location. Note the offset of the Paleogene strata in seismic profiles AA' and BB' indicates the long-term deformation along the ATF and within the Qilian Shan, respectively, since Eocene initiation. Q_1 (Pleistocene strata); N_2^3 (Late Miocene to Pliocene strata); N_2^2 (Middle Miocene strata); N_2^1 (Early Miocene strata); N_1 (Oligocene strata); E_3^2 (Late Eocene strata); E_3^1 (Middle Eocene strata); E_{1+2} (Paleocene to Early Eocene strata); Mes. (Mesozoic strata).

Proposed Cenozoic initiation of the ATF generally varies from Eocene to Miocene. Based on magnetostratigraphy and sedimentological analysis, Yin et al (2002) suggested that the ATF has been active since ca. 49 Ma (Yin et al., 2002). Thermochronological data from the Altyn Tagh Range in conjunction with sedimentological evidence suggests that left-

lateral strike-slip faulting occurred from late Eocene to early Oligocene time (Chen et al., 2001; Jolivet et al., 2001; Meng et al., 2001; Yue et al., 2001; Ritts et al., 2004). By identifying Eocene deformed strata in the western segment of ATF, we recently suggested an Eocene initiation of the left-lateral strike-slip motion along the ATF (Cheng et al., 2015a). In addition, on the seismic profile AA' (trending perpendicular to the strike of the ATF), several basement-involved thrust faults offset the Mesozoic strata and die out in the Eocene and Oligocene strata, which probably indicates the Eocene initiation of the ATF (Fig. S1-B).

With regards to the initiation of the NE-SW crustal shortening in the Qilian Shan, recent finding that the Paleocene to early Eocene initiation of the Cenozoic deformation in the Qilian Shan, shortly after the India-Asia collision, indicating initiation of crustal thickening since then (Jolivet et al. 2001; Yin et al., 2008a; Clark et al., 2010; Duvall et al., 2011; Zhuang et al., 2011; Yuan et al., 2013), challenges the post-Pliocene initial deformation in the northern Tibetan Plateau (Bovet et al., 2009) inferred from northward progressive plateau growth hypothesis (Métivier et al., 1998; Tapponnier et al., 2001). In addition, on the seismic profile BB'' (trending perpendicular to the strike of the Qilian Shan), several basement-involved thrust faults offset the Mesozoic strata and die out in the Eocene and Oligocene strata, which probably indicates the Eocene initiation of the NE-SW crustal shortening (Fig. S1-D).

More importantly, all the faults on the seismic profile AA' and BB' is characterized by long-term activity since Eocene initiation, indicative of simultaneous deformation along the ATF and within the Qilian Shan since Eocene initiation (Fig. S1). The simultaneous deformation of the ATF and the Qilian Shan since the Eocene calls for the possibility that deformation in these two regions are controlled by the same kinematical mechanism (e.g. Yin and Harrison, 2000; Zhang et al., 2014)

4. No integral rotation of Qaidam block since the Eocene.

Based on paleomagnetic data which was obtained from the middle to late Eocene strata and the early to middle Miocene strata from the entire Qaidam Basin, Dupont-Nivet et al. (2002) and Yu et al. (2014) demonstrated that the relatively rigid Qaidam block has been transported northeastward along the ATF during the Cenozoic (Wang et al., 2006), without

obvious basin-scale vertical axis rotation with respect to the Eurasia Plate since the early Eocene.

5. Relative rigid Qaidam block

Effective elastic thickness calculation indicate that the mechanical strength of the Qaidam crust is exceptionally strong compared to that of the Qilian Shan, or even to the rest of the Tibetan Plateau (Braitenberg et al., 2003). In addition, Global anisotropic and isotropic 2D modelling of the Tibetan Plateau crust also reveal the relative Qaidam block comparing with the surrounding mountains, such as Qilian Shan (Le Pape et al., 2009).

Although fold and faults are well developed in the Qaidam Basin, the balanced cross-section within the Qaidam Basin suggest only less than 20 km (10%) NE-SW crustal shortening within the basin (Zhou et al., 2006). Yin et al. (2008b) conducted the balanced cross-section restoration within the Qaidam Basin and give an average of ~35% NE-SW crustal shortening within the basin, but the interpreted deep faults in his model are suspicious duo to the poor quality of the 2D seismic profiles. Based on newly acquired high-quality 3D seismic profile, Cheng et al. (2014, 2015b) suggested that the southwestern Qaidam Basin is governed by a series of strike-slip faults rather than south- or north-directed thrusts which rejects large amounts of NE-SW crustal shortening the southwestern Qaidam Basin. Moreover, based on basin-scale paleomagnetic sampling, Yu et al. (2014) also suggest that the crustal shortening of the Qaidam block have been minimal since Eocene.

We thus consider that post-Early Eocene crustal shortening as well as vertical axis rotation of the Qaidam Block have been minimal. The amount of northeastward migration of that block along the ATF (Wang et al., 2006) must thus have been largely transferred into the Qilian Shan where it can be vertically partitioned into crustal shortening and eastward extrusion (Fig. 2). In other words, the amount of crustal shortening and lateral movement in the Qilian Shan would be largely equivalent to the amount of contemporaneous northeastward migration of the Qaidam Block along the ATF.

6. Mass balance or Volume balance

As shown by Yakovlev and Clark (2014), neglecting the density contrast between the upper and lower crust hardly changes the resulting estimates of the modern orogenic mass.

The occurrence of lower crustal flow in the northeastern Tibetan Plateau has recently been rejected (Lease et al., 2012). From this conclusion and the lack of Cenozoic magmatism in the Qaidam Basin and Qilian Shan (Yin and Harrison, 2000), we consider the Cenozoic crust-mantle interaction and transition as sufficiently week to be neglected in our model. We thus simplified the mass balance to volume balance, and use the term “mass” and “volume” interchangeably.

7. Definition of the “Extrusion” in this study

Due to the northeastward migration of the relative rigid Qaidam block along the ATF, hundreds of kilometers of offset were totally absorbed within the Qilian Shan, which led to the N20E-directed crustal shortening as well as the N110E-directed elongated of the Qilian Shan crust. We thus define the N110E-directed elongation of the Qilian Shan crust as the “eastward extrusion”.

8. The Altyn Tagh Fault terminates within the Qilian Shan.

In this study, we define the ATF terminates within the Qilian Shan rather than bypassing the northern margin of Qilian Shan. In recent years, based on the remote sensing image interpretation, field geological mapping, sedimentology studies, seismic profile interpretation, most researchers suggest that the ATF ends in the Qilian Shan region (e.g. Burchfiel et al., 1989; Meyer et al., 1998; Wittlinger et al., 1998; Tapponnier et al., 2001; Yin and Harrison, 2000; Jolivet et al., 2001; Yin et al., 2002; Cowgill et al., 2003; Dupont-Nivet et al., 2004; Wang et al., 2006; Cheng et al., 2015a). On the contrary, Yue and Liou (1999) and Darby et al. (2005) asserted that the ATF extend beyond the Qilian Shan region and could link to the faults in the Alxa block, the East Mongolia, or even related to the subduction of the subduction in the Sea of Okhotsk. However, their estimation are generally petrotectonic assembles and those strike-slip faults within the Alxa block are far away from the ATF, which would likely to be individual strike-slip fault system. More importantly, based on recent magnetotelluric survey in the northern Tibetan Plateau, the northward expanding of the Altyn Tagh Fault (bypassing the Qilian Shan and expanding to the Alxa block) is completely rejected (Xiao et al., 2015). (Profiles are located in the foreland of the Qilian Shan Ranges and are oriented perpendicular to the inferred fault zone that could be

the continuation of Altyn Tagh Fault). Please check details in the paper of Xiao et al. (2015) JGR, Eastern termination of the Altyn Tagh Fault, western China: Constraints from a magnetotelluric survey Journal of Geophysical Research: Solid Earth.

9. Initial crustal thickness within the Qilian Shan

The initial crustal thickness within the Qilian Shan is poorly constrained. The thick Jurassic and Cretaceous clastic packages and synorogenic conglomerates enable Wang and Coward (1993) to suggest flexural loading of crust around the Qilian Shan during the Jurassic to Cretaceous. Based on comprehensive analysis of geological data in the northern Tibetan Plateau, Meyer et al. (1998) suggested ~47.5 ± 5 km initial crustal thickness of the northern Tibetan Plateau. By conducting low temperature thermochronological study integrated with balance cross-section restoration, Lease et al. (2012) recently estimated a 45 ± 5 km initial crustal thickness. In order to account for this uncertainty we calculated solutions for multiple values of H_0 (35, 40, 45, 50 and 55 km; with a probable value around 45 km).

References

Bovet, P.M., Ritts, B.D., Gehrels, G., et al., 2009. Evidence of Miocene crustal shortening in the north Qilian Shan from Cenozoic stratigraphy of the western Hexi Corridor, Gansu Province, China. *American Journal of Science*, **309**, 290-329.

Braitenberg, C., Wang, Y., Fang, J. and Hsu, H., 2003. Spatial variations of flexure parameters over the Tibet–Quinghai plateau. *Earth and Planetary Science Letters*, **205**, 211-224.

Burchfiel, B.C., Quidong, D., Molnar, P., et al., 1989. Intracrustal detachment within zones of continental deformation. *Geology*, **17**, 748-752.

Cheng, F., Jolivet, M., Fu, S., et al., 2014. Northward growth of the Qimen Tagh Range: A new model accounting for the Late Neogene strike-slip deformation of the SW Qaidam Basin. *Tectonophysics*, **632**, 32-47.

Chen, Z.L., Zhang, Y.Q., Wang, X.F. and Chen, X.H., 2001. Fission Track Dating of Apatite Constrains on the Cenozoic Uplift of the Altyn Tagh Mountain. *Acta Geoscientia Sinica*, **22**, 413-418 (in Chinese with English abstract).

Cheng, F., Guo, Z., Jenkins, H.S., et al., 2015a. Initial rupture and displacement on the Altyn

Tagh fault, northern Tibetan Plateau: Constraints based on residual Mesozoic to Cenozoic strata in the western Qaidam Basin. *Geosphere*, **11**, 921-942.

Cheng, X., Fu, S., Wang, H., et al., 2015b. Geometry and kinematics of the Arlar strike-slip fault, SW Qaidam basin, China: New insights from 3-D seismic data. *Journal of Asian Earth Sciences*, **98**, 198-208.

Clark, M.K., Farley, K.A., Zheng, D., et al., 2010. Early Cenozoic faulting of the northern Tibetan Plateau margin from apatite (U–Th)/He ages. *Earth and Planetary Science Letters*, **296**, 78-88.

Cowgill, E., Yin, A., Harrison, T.M. and Xiao-Feng, W., 2003. Reconstruction of the Altyn Tagh fault based on U-Pb geochronology: Role of back thrusts, mantle sutures, and heterogeneous crustal strength in forming the Tibetan Plateau. Journal of *Geophysical Research*, **108**, 2346.

Darby, B.J., Ritts, B.D., Yue, Y. and Meng, Q., 2005. Did the Altyn Tagh fault extend beyond the Tibetan Plateau? *Earth and Planetary Science Letters*, **240**, 425-435.

Dupont-Nivet, G., Butler, R.F., Yin, A. and Chen, X., 2002. Paleomagnetism indicates no Neogene rotation of the Qaidam Basin in northern Tibet during Indo-Asian collision. *Geology*, **30**, 263-266.

Dupont-Nivet, G., Robinson, D., Butler, R.F., et al., 2004. Concentration of crustal displacement along a weak Altyn Tagh fault: Evidence from paleomagnetism of the northern Tibetan Plateau. *Tectonics*, **23**, TC1020.

Duvall, A.R., Clark, M.K., van der Pluijm, B.A. and Li, C., 2011. Direct dating of Eocene reverse faulting in northeastern Tibet using Ar-dating of fault clays and low-temperature thermochronometry. *Earth and Planetary Science Letters*, **304**, 520-526.

Duvall, A.R., Clark, M.K., Kirby, E., et al., 2013. Low-temperature thermochronometry along the Kunlun and Haiyuan Faults, NE Tibetan Plateau: Evidence for kinematic change during late-stage orogenesis. *Tectonics*, **32**, 1190-1211.

Gehrels, G.E., Yin, A. and Wang, X.F., 2003. Magmatic history of the northeastern Tibetan Plateau. *Journal of Geophysical Research*, **108**, 2423.

Guo, Z.J., Zhang, Z.C. and Zeng, F.G., 1998. Discovery of mega-thick oil sandstone and

asphalt in the Jurassic System in the Tula Basin and its significance. *Chinese Science Bulletin*, **43**, 1898-1901.

Jolivet, M., Brunel, M., Seward, D., et al., 2001. Mesozoic and Cenozoic tectonics of the northern edge of the Tibetan plateau: fission-track constraints. *Tectonophysics*, **343**, 111-134.

Lease, R.O., Burbank, D.W., Zhang, H., et al., 2012. Cenozoic shortening budget for the northeastern edge of the Tibetan Plateau: Is lower crustal flow necessary? *Tectonics*, **31**, TC3011.

Le Pape, F., Jones, A.G., Vozar, J. and Wenbo, W., 2012. Penetration of crustal melt beyond the Kunlun Fault into northern Tibet. *Nature Geoscience*, **5**, 330-335.

Meng, Q.R., Hu, J.M. and Yang, F.Z., 2001. Timing and magnitude of displacement on the Altyn Tagh fault: constraints from stratigraphic correlation of adjoining Tarim and Qaidam basins, NW China. *Terra Nova*, **13**, 86-91.

Métivier, F., Gaudemer, Y., Tapponnier, P. and Meyer, B., 1998. Northeastward growth of the Tibet plateau deduced from balanced reconstruction of two depositional areas: The Qaidam and Hexi Corridor basins, China. *Tectonics*, **17**, 823-842.

Meyer, B., Tapponnier, P., Bourjot, L., et al., 1998. Crustal thickening in Gansu-Qinghai, lithospheric mantle subduction, and oblique, strike-slip controlled growth of the Tibet plateau. *Geophysical Journal International*, **135**, 1-47.

Molnar, P. and Tapponnier, P., 1975. Cenozoic tectonics of Asia: Effects of a continental collision. *Science*, **189**, 419-426.

Peltzer, G. and Tapponnier, P., 1988. Formation and evolution of strike-slip faults, rifts, and basins during the India-Asia collision: An experimental approach. *Journal of Geophysical Research: Solid Earth (1978–2012)*, **93**, 15085-15117.

Ritts, B.D. and Biffi, U., 2000. Magnitude of post-Middle Jurassic (Bajocian) displacement on the central Altyn Tagh fault system, northwest China. *Geological Society of America Bulletin*, **112**, 61-74.

Ritts, B.D., Yue, Y. and Graham, S.A., 2004. Oligocene-Miocene Tectonics and Sedimentation along the Altyn Tagh Fault, Northern Tibetan Plateau: Analysis of the Xorkol, Subei, and Aksay Basins. *The Journal of geology*, **112**, 207-229.

Searle, M., Elliott, J., Phillips, R. and Chung, S.-L., 2011. Crustal–lithospheric structure and continental extrusion of Tibet. *Journal of the Geological Society*, **168**, 633-672.

Tapponnier, P., Peltzer, G. and Armijo, R., 1986. On the mechanics of the collision between India and Asia. *Geological Society, London, Special Publications*, **19**, 113-157.

Tapponnier, P., Xu, Z.Q., Roger, F., et al., 2001. Oblique stepwise rise and growth of the Tibet Plateau. *Science*, **294**, 1671-1677.

Wang, Q. and Coward, M., 1993. The Jiuxi basin, Hexi corridor, NW China: Foreland structural features and hydrocarbon potential. *Journal of Petroleum Geology*, **16**, 169-182.

Wang, E., Xu, F.Y., Zhou, J.X., et al., 2006. Eastward migration of the Qaidam basin and its implications for Cenozoic evolution of the Altyn Tagh fault and associated river systems. *Geological Society of America Bulletin*, **118**, 349-365.

Wittlinger, G., Tapponnier, P., Poupinet, G., et al., 1998. Tomographic evidence for localized lithospheric shear along the Altyn Tagh fault. *Science*, **282**, 74-76.

Wu, L., Xiao, A.C., Yang, S.F., et al., 2012. Two-stage evolution of the Altyn Tagh Fault during the Cenozoic: new insight from provenance analysis of a geological section in NW Qaidam Basin, NW China. *Terra Nova*, **24**, 387-395.

Xiao, Q., Shao G., Liu-Zeng J., et al., 2015. Eastern termination of the Altyn Tagh Fault, western China: Constraints from a magnetotelluric survey, *J. Geophys. Res. Solid Earth*, **120**, doi: 10.1002/2014JB011363.

Yakovlev, P.V. and Clark, M.K., 2014. Conservation and redistribution of crust during the Indo-Asian collision .*Tectonics*, **33**, 1016-1027.

Yin, A. and Harrison, T.M., 2000. Geologic evolution of the Himalayan-Tibetan orogen. *Annual Review of Earth and Planetary Sciences*, **28**, 211-280.

Yin, A., Rumelhart, P., Butler, R., et al., 2002. Tectonic history of the Altyn Tagh fault system in northern Tibet inferred from Cenozoic sedimentation. *Geological Society of America Bulletin*, **114**, 1257-1295.

Yin, A., Dang, Y.Q., Wang, L.C., et al., 2008a. Cenozoic tectonic evolution of Qaidam basin and its surrounding regions (Part 1): The southern Qilian Shan-Nan Shan thrust belt and northern Qaidam basin. *Geological Society of America Bulletin*, **120**, 813-846.

Yin, A., Dang, Y.Q., Zhang, M., et al., 2008b. Cenozoic tectonic evolution of the Qaidam basin and its surrounding regions (Part 3): Structural geology, sedimentation, and regional tectonic reconstruction. *Geological Society of America Bulletin*, **120**, 847-876.

Yu, X.J., Fu, S.T., Guan, S.W., et al., 2014. Paleomagnetism of Eocene and Miocene sediments from the Qaidam basin: Implication for no integral rotation since the Eocene and a rigid Qaidam block. *Geochemistry, Geophysics, Geosystems*, **15**, 2109-2127.

Yue, Y.J. and Liou, J.G., 1999. Two-stage evolution model for the Altyn Tagh fault, China. *Geology*, **27**, 227-230.

Yue, Y.J., Ritts, B.D. and Graham, S.A., 2001. Initiation and long-term slip history of the Altyn Tagh Fault. *International Geology Review*, **43**, 1087-1093.

Yuan, D.Y., Ge, W.P., Chen, Z.W., et al., 2013. The growth of northeastern Tibet and its relevance to large-scale continental geodynamics: A review of recent studies. *Tectonics*, **32**, 2013TC003348.

Yue, Y.J., Graham, S.A., Ritts, B.D. and Wooden, J.L., 2005. Detrital zircon provenance evidence for large-scale extrusion along the Altyn Tagh fault. *Tectonophysics*, **406**, 165-178.

Zhang, H.P., Zhang, P.Z., Zheng, D.W., et al., 2014. Transforming the Miocene Altyn Tagh fault slip into shortening of the north-western Qilian Shan: insights from the drainage basin geometry. *Terra Nova*, **26**, 216-221.

Zhou, J.X., Xu, F.Y., Wang, T.C., et al., 2006. Cenozoic deformation history of the Qaidam Basin, NW China: Results from cross-section restoration and implications for Qinghai–Tibet Plateau tectonics. *Earth and Planetary Science Letters*, **243**, 195-210.

Zhuang, G., Hourigan, J.K., Ritts, B.D. and Kent-Corson, M.L., 2011. Cenozoic multiple-phase tectonic evolution of the northern Tibetan Plateau: Constraints from sedimentary records from Qaidam basin, Hexi Corridor, and Subei basin, northwest China. *American Journal of Science*, **311**, 116-152.

List of Figures and Tables

Figures to Chapter 1

Figure 1. Cenozoic structures and distribution of volcanic rocks in Asia, modified from Yin, 2010.

Figure 2. Digital topographic map of the Tibetan Plateau, Active fault kinematics and suture zones are mainly based on Yin et al. (2007), Taylor and Yin (2009), and Cheng et al. (2014).

Figure 3. Geological map of the Qaidam basin, northern Tibetan plateau, modified from Chen et al. (2015). Seismic profile interpretations of the dip of the basement faults in the southwestern Qaidam basin are debated. Yin et al. (2007) proposed a series of south thrusting faults, whereas Cheng et al. (2014) and Wu et al. (2014) suggested that those are south-dipping faults. We adopted this second point of view in this study. Q-N_2^3—Quaternary to Late Miocene strata; N_2^2—Middle Miocene strata; N_2^1—Early Miocene strata; N_1—Oligocene strata; E_3^2—Late Eocene strata; E_3^1—Middle Eocene strata; E_{1+2}—Paleocene to Early Eocene strata.

Figure 4. Northward propagation model, modified from Meyer et al. (1998). Note the south-dipping fault in the southern Qaidam basin.

Figure 5. Southward propagation model, modified from Yin et al. (2008a). Note the south-thrusting fault in the southern Qaidam basin.

Figure 6. Paleo-Qaidam basin model, cited from Yin et al. (2008a). Note that during the Paleogene, the Paleo-Qaidam basin lies between the elevated Lhasa block and the Fenghuo Shan thrust belt in the south and the elevated Qilian Shan in the north. The region north of the Tibetan plateau was a large topographic depression that links Tarim and Junggar basins across the Tian Shan, as the Tian Shan was not uplifted until the early Miocene. The initiation of the

Eastern Kunlun left-slip transpressional system caused the uplift of the Eastern Kunlun Range, which has partitioned the PaleoQaidam basin into the Hoh Xil basin to the south and the Qaidam basin to the north.

Figure 7. Simplified tectonic map of northern Tibet showing major tectonic terranes, sutures, and faults (modified from Yin et al., 2002). Cenozoic stratigraphic sections (locations shown by turquoise blue squares) were measured by this study at Aertashi, Puska, Jianglisai, and Xishuigou in the southern Tarim Basin. Other relevant stratigraphic sections are Mangnai, Lenghu, Lulehe, Xorkoli, and Jiuxi (Hexi Corridor). Map symbols: N-Q—Neogene–Quaternary sediments, Ts—Tert iary sedimentary rocks, THS—Tethyan Himalayan sequences (Proterozoic to Upper Cretaceous passive-continental-margin strata of northern India), GHC—Greater High Himalayan Crystalline Complex, LHS—Lesser Himalayan metasedimentary series. Major plutonic rocks: Czgr—Cenozoic granites, K-Tgr—plutonic rocks belongi ng to the Gangdese batholith, Ladakh batholith, and Kohistan arc, gr(Q)—plutonic rocks in the Qiangtang terrane (mostly Jurassic–Cretaceous), gr(SP)—plutonic roc ks in the Songpan–Ganzi–Hoh Xil terrane (mostly Late Triassic), gr(KQ)—Ordovician–Silurian and Permian–Triassic plutonic rocks in the Kunlun and Qilian terranes. Major sutures: IYS—Indus-Yalu suture, BNS—Bangong-Nujiang suture, JS—Jinsha suture, AKMS—Ayimaqin-Kunlun-Mutztagh suture, KS—Kudi suture, MCT—Main Centra l thrust, MKT—Main Karakoram thrust, STDS—South Tibet detachment system.

Figure 8. Digital topographic map of northern Tibet showing major tectonic terranes, sutures, and faults within the Qilian Shan.

Figures to Chapter 2.1

Figure 1. Digital topographic map of the western Qaidam Basin and surrounding area. Topography from SRTM data.

Figure 2. Geological map of the Qimen Tagh Range and SW Qaidam Basin. See Fig. 1 for

location and the text for discussion. Modified after the Kulangmiqiti J46C003001 1:250,000 geological map (IGSQP, 2004).

Figure 3. General topographic map of the Qaidam Basin and Eastern Kunlun Mountains with background seismicity from the China Earthquake Networks Center (CENC) from 1st January 1970 to 1st January 2011 (M>3).

Figure 4. Depth-frequency distribution of earthquakes within the study area. Data from the China Earthquakes Networks Center (CENC), 1st January 1970 to 1st January 2011 with M>3. Two seismic profiles (AA' (a) and BB'. (b) (see location on Fig. 3)) are investigated with (left) depth distribution of earthquakes and (right) depth – frequency distribution of seismic events. See text for discussion.

Figure 5. Remote sensing image from Landsat 5 on December 5, 2008 (USGS) (a) and SRTM digital topography map (b) of the Qimen Tagh Range. The red solid lines show the main tectonic structures. See the location in Fig. 1.

Figure 6. Un-interpreted (a) and interpreted SPOT-5 image (b) (Google Earth) centered on the western part of the Middle Qimen Tagh fault (MQF). See the location in Fig. 5. The red solid lines indicate the fault segments imaged by fault scarps on the surface. The dashed line represents the blind fault covered by the Quaternary sediments. The fault scarps in en-échelon arrangement indicates a left-lateral strike-slip movement on the MQF.

Figure 7. Un-interpreted (a) and interpreted SPOT-5 image (b) (Google Earth) centered on the eastern part of the Middle Qimen Tagh fault. See the location in Fig. 5. The red dashline indicates the linear fault linking the Qimen Tagh fault system in the west with the Eastern Kunlun fault system in the east.

Figure 8. Cenozoic formations within the Adatan Valley. (a) General view of the Qimen Tagh

Range. The picture, taken from ~10 km south of the Atantihan River checkpoint, shows the strong relief between the Adatan Valley and the mountains bordered by a series of triangular facets and fault scarps belonging to the MQF. The foothill domain is represented by Cenozoic strata which are deformed and pushed into gentle folds. See the location in Fig. 9. (b) Uplifted Pleistocene series covered by Holocene tillites (left) and general stratigraphic column (right). See the photographs' location in Fig. 9.

Figure 9. Geological sketch of the Qimen Tagh Range showing the distribution of the Cenozoic series. Modified after the Kulangmiqiti J46C003001 1:250,000 geological map (IGSQP, 2004) and the Ayakekumu J45C003004 1:250,000 geological map (IGSSP, 2003). See the location in Fig. 2.

Figure 10. Isopach map of the Upper Xiaganchaigou Formation (E_3^2xg). Three major faults (the Kunbei fault, the Arlar fault and the Hongliuquan fault) are also marked on the isopach map based on seismic data. These data were acquired by the Qinghai Oilfield Company (China) who compiled information from thousands of drill holes and a dense network of seismic profiles in recent years. Note the offset of the 400 isopach line controlled by the faults and indicating the left-lateral strike-slip faulting of these faults.

Figure 11. Seismic profile C-C'in the SW Qaidam Basin. See the location in Figs. 2 and 10. Note that the thickness of the Paleocene to Eocene strata shows a sharp difference between both sides of the Arlar fault. The growth strata associated to the positiveflower structure started to develop during the initial deposition of the Early Miocene unit (N_2^1xy), which suggests that the strike-slip movement on the Arlar fault initiated during the deposition of this unit.

Figure 12. Seismic section D-D'in the SW Qaidam Basin. See Figs. 2 and 10 for location. Note that the strata below the Shangyoushashan Fm. (N_2^1xy) keep a constant thickness in the section, while the strata above it are thinning northward. The thickness of the Paleocene to Eocene strata shows a sharp difference between both sides of the Arlar fault. Meanwhile, Early

Miocene growth strata above the Arlar and Hongliuquan faults indicate the onset of left-lateral strike-slip faulting during the Early Miocene.

Figure 13. Seismic profile E-E' in the SW Qaidam Basin. See the location in Figs. 2 and 10. Note that the thickness of the Paleocene to Eocene strata shows a sharp difference between both sides of the Kunbei fault. Meanwhile, Early Miocene growth strata again indicate an onset of left-lateral strike-slip faulting during the Early Miocene.

Figure 14. Tectonic evolution of the Qimen Tagh Range and the SW Qaidam Basin since the Early Neogene. See the text for discussion

Figures and tables to Chapter 2.2

Figure 1. Digital topographic map of the Tibetan Plateau modified after Taylor and Yin (2009). Active fault kinematics and suture zones are based on Yin et al. (2007), Taylor and Yin (2009), and Cheng et al. (2014). Note that the Hoh Xil Basin has been diced up by the Neogene uplift phase. The yellow stars refer to the location of sampling sites. IYS—Indus Yalu suture zone; AMS—Anyimagen-Kunlun-Muztagh suture zone; JS—Jinsha suture zone; BNS—Bangong Nujiang suture zone.

Figure 2. Geological map of the southwestern Qaidam Basin and surrounding area, modified after the 1:250,000 geologic map (SIGS, 2003; QIGS, 2004). See Figure 1 for location. Active fault kinematics are based on Cheng et al. (2014), SIGS (2003), and QIGS (2004).

Figure 3. Original (A) and interpreted (B) NE-SW–oriented seismic profile 1 in SW Qaidam Basin. See the location in Figure 2. Note that stratigraphic overlaps between the Paleocene to early Eocene (E_{1+2}) and middle to late Eocene (E_3) strata, the middle to late Eocene (E_3) and Oligocene (N_1) strata, and the Oligocene (N_1) and early Miocene (N_2^1) strata, indicating the gradually enlarging basin from Paleocene to middle Miocene. The growth strata within the middle to late Miocene (N_2^2) strata, late Miocene to Pliocene (N_2^3) strata, and Pleistocene (Q_1) strata demonstrate the shrinking of the basin since the Miocene.

Figure 4. Original (A) and interpreted (B) NE-SW–oriented seismic profile 2 in the South Qaidam Basin. See the location in Figure 2. Note that growth strata near the Kunbei and Arlar faults indicate the uplifting of the Eastern Kunlun Range and shrinking of the basin since the Miocene.

Figure 5. Relative probability plots of granitoid pluton ages in (A) the Eastern Kunlun Range, (B) the Altyn Tagh Range, (C) the Qilian Shan, and U-Pb ages of detrital zircons from (D) the Qiangtang and Lhasa blocks as well as (E) the Hoh Xil Basin. The age data were obtained from: J.S. Yang et al. (1996, 2002, 2006); J.X. Zhang et al. (1997, 2001, 2011); Chen et al. (2003); Gehrels et al. (2003a, 2003b); Yue et al. (2005); L. Liu et al. (2007, 2009); Lu et al. (2008); Chen et al. (2012); Dai et al. (2012); L. Liu et al. (2013b); C. Wang et al. (2013); Staisch et al. (2014); L.Y. Zhang et al. (2014). See also Figure DR1 and Table DR1 for more information on the data (see text footnote 1). Double-headed arrow within the figure refers to the few early Cenozoic and late Mesozoic $^{40}Ar/^{39}Ar$ and U-Pb zircon ages found with each range. Age distributions are marked by different shades according to age groups.

Figure 6. Generalized stratigraphic column of the studied Cenozoic series. Paleocurrent directions were obtained from Meng and Fang (2008) and Zhuang et al. (2011). Envir. Cycle and Sed. Rate in the figure refer to the environment cycle and average sedimentary rate in the South Qaidam Basin, respectively. The average sedimentary rate is generally calculated based on the Cenozoic sequence thickness data from three-dimensional seismic profiles (F. Cheng et al., 2014; X. Cheng et al., 2015) and the age ranges of each sequence (F. Yang et al., 1992; Fang et al., 2007; Zhang, 2006; Sun et al., 2005; Lu and Xiong, 2009; Pei et al., 2009; Ke et al., 2013).

Figure 7. (A) Gray-yellow sandstones interbedded with conglomerates of the middle Eocene Lower Xiaganchaigou Formation (E_3^1) in the Huatugou section. (B) Gray-yellow sandstones interbedded with mudstones of the middle Miocene Xiayoushashan Formation (N21) in the

Huatugou section. (C) Core sample of grayish white conglomerates of the middle Miocene Lower Xiaganchaigou Formation (E_3^1) in the Kunbei section. (D–E) Microscopic characteristics (crossed polarized light) of the middle Eocene to Oligocene sandstone core samples from the Kunbei section. Note the large number of lithic fragments, the fining of the grain size, and the increasing textural maturity from middle Eocene to Oligocene. (F) Core sample of conglomerates of the Paleocene Lulehe Formation (E_{1+2}) in the Kunbei section. (G) Carbonate debris included in conglomerates of the Paleocene Lulehe Formation (E_{1+2}) in the Kunbei section (core sample, crossed polarized light microphotograph). (H) Foraminifera in carbonate debris within conglomerates of the Paleocene Lulehe Formation (E_{1+2}) in the Kunbei section (core sample, plane polarized light microphotograph). (I) Angular unconformity between the early Miocene to Pleistocene sediments and the Ordovician basement rocks of the Tanjianshan Group in the Adatan valley.

Figure 8. Representative cathodoluminescence (CL) images of detrital zircons from the 22 sandstone samples. The white circles show the location of the U-Pb analysis spots. Numbers are U-Pb ages in Ma.

Figure 9. U-Pb concordia diagrams for zircon grains of the samples in the Huatugou and Dongchaishan-Gansen sections.

Figure 10. Relative probability plot histograms of U-Pb ages of detrital zircons from the Cenozoic samples in the Huatugou section. The number of zircons is given on the vertical axis (note the change in scale from one sample to the other); the ages, in Ma, are indicated on the horizontal axis.

Figure 11. Relative probability plot histograms of U-Pb ages of detrital zircons from the Cenozoic samples in the DongchaishanGansen section (note the change in scale from one sample to the other); the ages, in Ma, are indicated on the horizontal axis.

Figure 12. U-Pb concordia diagrams for zircon grains of the samples from the Kunbei and Adatan sections.

Figure 13. Relative probability plot histograms of U-Pb ages of detrital zircons from the Cenozoic samples in the Kunbei section. The number of zircons is given on the vertical axis (note the change in scale from one sample to the other); the ages, in Ma, are indicated on the horizontal axis.

Figure 14. Relative probability plot histograms of U-Pb ages of detrital zircons from the Cenozoic samples in the Adatan section. The number of zircons is given on the vertical axis (note the change in scale from one sample to the other); the ages, in Ma, are indicated on the horizontal axis.

Figure 15. (A) Relative probability plot histograms of U-Pb ages of detrital zircons of the 22 samples. The insert diagram to the right corresponds to the black box in the first diagram. (B) Relative probability plots of granitoid pluton ages in the Eastern Kunlun Range.

Figure 16. (A) Paleocene to early Eocene tectonic configuration of the Qaidam Basin. The Eastern Kunlun Range had already uplifted, separating the paleo–Qaidam Basin in the north from the North Qiangtang and Bayan Har terranes to the south. The Qaidam Basin is characterized by small lakes with limited extent during this period. (B) Middle Eocene to Oligocene tectonic configuration of the Qaidam Basin. During this period, the scope of the Qaidam Basin expanded southward with water getting deeper. The southward-expanding Qaidam Basin may have locally inundated the Eastern Kunlun Range and connected with the Kumukol Basin or even the Hoh Xil Basin to the south. (C–D) Miocene to present tectonic configuration of the Qaidam Basin. The scope of the basin narrowed, with water getting gradually shallower during this period. Note that intense Miocene uplifting of the Eastern Kunlun Range separated the Qaidam Basin and Hoh Xil Basin. The Eastern Kunlun Range and the Altyn Tagh Range had already been largely denudated, forming the major two

provenance areas for the sediments deposited in the South Qaidam Basin.

Table 1 Summary of major characteristics and the corresponding statistical data for of the samples

Figures and tables to Chapter 3.1

Figure 1. Digital topographic map of the central segment of the Altyn Tagh fault and surrounding area. Topography is from Shuttle Radar Topography Mission (SRTM) data.

Figure 2. Geologic map of the center segment of the Altyn Tagh fault and the surrounding area, adapted from the Geologic Map of the Tibetan Plateau and Adjacent Areas compiled by Chengdu Institute of Geology and Mineral Resources and Chinese Geological Survey (map scale 1:1,500,000). Ages (zircon U-Pb) of plutons are mainly compiled from: 1—Cowgill et al. (2003); 2—Gehrels et al. (2003a); 3—HGSI (2003); 4—Chen et al. (2004); 5—Li et al. (2013); 6—Wang et al. (2013). See provenance analysis of Jurassic to Cretaceous strata sections for details.

Figure 3. Stratigraphy and lithologic unit descriptions of the Qaidam Basin. The Cenozoic stratigraphy of the basin has been defined and dated in detail using magnetostratigraphy, palynology, and paleontology studies within the entire basin (Fang et al., 2007; Gao et al., 2009; Huang et al., 1996; Huo, 1990; Lu and Xiong, 2009; QBGMR, 1991; Qiu, 2002; Z.M. Sun et al., 2005; Xia et al., 2001; Yang et al., 1992; Zhao et al., 2006). See Figure 2 for seismic profile location. Note the growth strata above the Xiayoushashan Formation (N_2^1xy).

Figure 4. Geologic map (after Qiemo J45C003002 geologic map, scale 1:250,000) and geologic cross section of the study area, compiled from HGSI (2003), Robinson et al. (2003), and XBGMR (1993). Red stars denote locations of U-Pb detrital zircon samples. Ages (zircon U-Pb) of plutons are mainly compiled from HGSI (2003). The western half and eastern half of the Eocene strata are based on the division of Dupont-Nivet et al. (2004).

Figure 5. Typical photomicrographs and field photographs. (A) Lithic sandstone in early

Jurassic strata (J_{1+2}d) of the Tula section, rich in lithic fragments, under plane polarized light. (B) Lithic sandstone in Early Jurassic strata (J_{1+2}d) of the Caishiling section, rich in various lithic fragments, under crossed polarized light. (C) Conglomerate and (D) cross-bedding in Late Jurassic (J_3c) strata of the Tula section. (E) Oil sand and (F) asphalt developed in Late Jurassic (J_3c) strata. Abbreviations: Sch—schist, Pl—plagioclase, Kp—potash feldspar, Q—quartz, Bt—biotite.

Figure 6. Geologic map (after the Washixia J45C002003 geologic map, scale 1:250,000) and geologic cross section of the study area, compiled from GGSI (2003) and XBGMR (1993).

Figure 7. Chronostratigraphic correlation of the relic Mesozoic to Cenozoic strata along the Altyn Tagh fault. GPTS—geomagnetic polarity time scale of Cande and Kent (1995). Observed polarity was compiled from Yin et al. (2002), Z.M. Sun et al. (2005), Zhang (2006), Fang et al. (2007), and Lu and Xiong (2009). Paleocurrents are from Ritts and Biffi (2000). Chronostratigraphic correlation is based on field observation and previous studies (XBGMR, 1993; Guo et al., 1998; Ritts and Biffi, 2000; GGSI, 2003; HGSI, 2003; Robinson et al., 2003). ATF—Altyn Tagh fault.

Figure 8. U-Pb concordia diagrams for zircon grains from the five sandstone samples.

Figure 9. Relative probability histogram plots of U-Pb ages of detrital zircons from the five Jurassic and Cretaceous sandstone samples and relative probability histogram plots of pluton ages in the Altyn Tagh and Eastern Kunlun Ranges. Age data are from Yang et al. (2006), Zhang et al. (2001), Chen et al. (2003), Gehrels et al. (2003a, 2003b), Yue et al. (2005), Yang et al. (2006), L. Liu et al. (2007, 2013), Lu et al. (2008), Liu et al. (2009), Zhang et al. (2011), Li et al. (2013), and Wang et al. (2013). More information on dating and ages is provided in Table DR2.

Figure 10. Seismic profiles in the southwestern Qaidam Basin; see Figure 2 for location. (A)

Uninterpreted and (B) interpreted seismic profiles in the SW–NE direction; (C) uninterpreted and (D) interpreted seismic profiles in NW–SE direction. Note that the growth strata since the Xiayoushashan Formation (N_2^1xy) indicate the intense tectonic movement of the Altyn Tagh fault during middle Miocene time.

Figure 11. Proposed accelerated motion model for the Cenozoic Altyn Tagh fault (ATF). Note the piercing points along the Altyn Tagh fault. (A) Before early Eocene time, the Caishiling section was originally located where the Tula section is situated today. During early Eocene time (ca. 49 Ma), the left-lateral strike-slip faulting along the Altyn Tagh fault initiated, transporting the Qaidam Basin northeastward. Since then, the Tula unit remained stationary and was separated from the Qaidam Basin (B) during middle Miocene time (ca. 15 Ma), when the Caishiling section migrated northeastward to where the Anxi section is situated today. During this period, an intense left-lateral strike-slip faulting along the Altyn Tagh fault occurred and deformed the pre-Miocene strata in the Anxi section. Since then, the Anxi unit was left and separated from the Qaidam Basin (C) during continuous left-lateral strike-slip faulting along the Altyn Tagh fault that transported the Caishiling section to its present position. Consequently, ~360 km total Cenozoic offset is constrained along the Altyn Tagh fault, which is divided into ~170 km of offset between early Eocene and middle Miocene time and ~190 km of offset from the late Miocene until present.

Table 1. Summary of the major characteristics and corresponding statistical data for each of the samples.

Figures and tables to Chapter 3.2

Figure 1. (A) SRTM based digital topographic map of the Tibetan plateau. (B) Digital elevation model (DEM) and major tectonic elements of the Altyn Tagh Range, the Qaidam basin and the surrounding regions. The location of Fig. 2 is identified by the solid box. The DEM map was generated from the 90 m SRTM data. Note that the yellow solid line refers to the location of seismic profile AA'. (C) Interpreted and (D) non-interpreted seismic profile AA'. Note that the succession of Cenozoic depo-centers is marked along the long axis of the

basin. These depo-centers gradually migrated eastward since the Eocene.

Figure 2. Simplified geological map of the northwestern Qaidam basin and eastern segment of the Altyn Tagh Range, adapted from the Geologic Map of the Tibetan plateau and adjacent areas compiled by the Chengdu Institute of Geology and Mineral Resources and Chinese Geological Survey (map scale, 1:1,500,000).

Figure 3. Generalized stratigraphic column of the studied Mesozoic to Cenozoic series. Paleocurrent directions in the Huatugou section were obtained from Meng and Fang, (2008), Wu et al. (2012b) and Zhuang, et al. (2011). Paleocurrent directions in the Eboliang section were obtained from Zhuang, et al. (2011), Wu et al. (2012b) and Heermance et al. (2013). Note that sample CSL3 is cited from Cheng et al. (2015a), and samples HTG-E, HTG-N, CSL4, SZG1 and CSL5 are cited from Cheng et al. (2016). Red arrows refer to the general paleocurrent directions.

Figure 4. Typical photomicrographs and field photographs of the various analyzed sediments. (A) Drill core sample of early to middle Jurassic (J_{1+2}) lithic sandstone obtained from drill well in the Eboliang section; (B) Thin section image of lithic sandstone from the Paleocene to early Eocene strata (E_{1+2}) in the Eboliang section, under crossed polarized light. (C) Horizontally stratified sandstone interbedded with mudstones of the Xiaganchaigou Formation (E_3^1) in the Eboliang section. (D) Thin section image of siltstone from the Oligocene strata (N_1), under crossed polarized light, obtained from drill well in the Eboliang section. (E) Thick-bedded sandstone in the early Miocene strata, Xiayoushashan Formation (N_2^1), Eboliang section. (F) Thin section image of siltstone from the Pliocene strata (N_2^3), in the Eboliang section, under crossed polarized light. (G) Greenish white sandstone intercalated with mudstone in the middle Eocene strata (E_3^1), Huatugou section. (H) Greenish white sandstone intercalated with brownish red mudstone in the late Eocene strata (E_3^1), Huatugou section. (I) Thin section image of sandstone in the Oligocene strata (N_1), Huatugou section, under crossed polarized light.

Figure 5. Representative CL images of zircons from the 11 sandstone samples. The yellow circles show the location of the U-Pb analysis. Numbers are U-Pb ages in Ma.

Figure 6. U-Pb concordia diagrams for zircon grains of the 11 sandstone samples.

Figure 7. Combined probability density functions (lines) and histogram plots (bars) depicting detrital zircon U-Pb ages of samples from the Eboliang section, arranged in stratigraphic order. Age distributions are colored according to age groups, and the pie diagrams show percentages of grains in those age categories. Paleocurrents rose diagrams in black are compiled from Heermance et al. (2013) and rose diagrams in gray are compiled from Wu et al. (2012b) and Ritts and Biffi (2000).

Figure 8. Combined probability density functions (lines) and histogram plots (bars) depicting detrital zircon U-Pb ages of samples from the Huatugou section, arranged in stratigraphic order. Two distinctive age groups, indicative of separate sources, are colored. Paleocurrents rose diagrams are compiled from Meng and Fang, (2008), Wu et al. (2012b) and Zhuang, et al. (2011).

Figure 9. (A) Sketched geological map of the Altyn Tagh Range and surrounding areas, showing the distribution of zircon U–Pb ages for granitoids. The numbers denote ages in Ma. Relative probability plots of zircon U-Pb ages from basement rocks and intrusives in: (B) the Altyn Tagh Range, (C) the Qilian Shan, and (D) the Eastern Kunlun Range. Age data are mainly cited from: Guo and Li, (1999), Sobel and Arnaud, (1999), Yang et al. (2001), Zhang et al. (2001), Yang and Song, (2002), Cowgill et al. (2003), Gehrels et al. (2003a, 2003b), Jolivet et al. (2003), Lu and Yuan, (2003), Robinson et al. 2003, Roger et al. (2003), Chen et al. (2004), IGSQP, (2004), Yue et al. (2004, 2005), Liu et al. (2006), Shi et al. (2006), Song et al. (2006), Wang et al. (2006b), Yang et al. (2006), Lu et al. (2008), Roger et al. (2008), Bovet et al. (2009), Liu et al. (2009), Wu et al. (2009), Xiao et al. (2009), Roger et al. (2010), Zhang

et al. (2011), Dai et al. (2013), Li et al. (2013), Wang et al. (2013), Long et al. (2014), Song et al (2014), Wang et al.(2014b) , Zhang et al. (2014a), Dong et al. (2014, 2015), Chen et al. (2015) and references therein. The blue arrow refers to the northeastward migration of the Huatugou and Eboliang sections from their origins.

Figure 10. (A) Frequency histograms for restricted early Neoproterzoic ages groups of detrital zircons from the Paleocene to early Eocene Lulehe Fm. (E_{1+2}) and the Th/U ratio for those zircon ages. (B) CL images of zircons for all early Neoproterzoic ages zircons from the Paleocene to early Eocene Lulehe Fm. The yellow circles show the location of the U-Pb analysis. Numbers are U-Pb ages in Ma. Note that the ~911 Ma peak age for the Neoproterozoic ages groups coincides with the mean crystallization age of ~910 Ma for the basement rocks in the western segment of the Altyn Tagh Range (Fig. 9A; Wang et al., 2013). The distinctive Th/U ratio and oscillatory zones for those zircons indicate magmatic sources.

Figure 11. Seismic profiles in the southwestern Qaidam basin. See Fig. 2A for location. Note the fold and thrusts in seismic profile BB', indicating the deformation in the northwestern Qaidam basin since the early Miocene. Offset of the Paleogene strata in seismic profiles CC' and DD' indicates the Eocene to Oligocene deformation in the northwestern Qaidam basin which would be associated with deformation along the ATF. Growth strata of the post-Oligocene strata in seismic profiles BB' and CC' indicate intense tectonic movements along the ATF since the Miocene.

Figure 12. Cenozoic kinematic model of the Altyn Tagh Fault and source to sink relation between the western Qaidam basin and the surrounding regions. (A) during the Paleocene to early Eocene, the basement rocks in the Altyn Tagh Range served as the major source for the clastic material deposited in the Eboliang section, while sediments in the Huatugou section were derived from the Eastern Kunlun Range; (B) during the early Eocene to the Oligocene, the Qaidam basin migrated northeastward due to left-lateral strike-slip faulting along the ATF; (3) since the Miocene, intense left-lateral faulting along the ATF continuously offset the

Qaidam basin towards the northeast and triggered post-Oligocene crustal deformation within the Altyn Tagh Range and western Qaidam basin. See text for detailed discussion.

Table 1. Summary of the major characteristics and corresponding U-Pb age data for each sample

Figures and tables to Chapter 4

Figure 1. (A) SRTM-based digital topographic map of the Tibetan Plateau and the surrounding region. (B) SRTM-based digital topographic map of the northern Tibetan Plateau. NQSF, Northern Qilian Shan Fault system; NQF, Northern Qaidam Fault; SDF, Saisitengshang-Dakendaban Fault; DF, Danghe-Nanshan Fault; DTF, Daxueshan Yuole-Nanshan Fault; SF, ShuleNanshan Fault; EF, Elashan Fault; RF, Riyueshan Fault; CF, Changma Fault; ZTF, Zhongwei-Tongxing Fault. Solid lines A–A' and B–B' represent the locations of the seismic profiles presented in Appendix S1. Dash-lined right trapezoid represents the studied Qilian Shan region. (C) SRTM-based present-day crustal-thickness map of the northern Tibetan Plateau and the surrounding region, modified from Li et al. (2014). The white solid triangles represent the locations of seismic stations, and numbers refer to the corresponding crustal thickness.

Figure 2. General model for balanced 3D crustal deformation in the Qilian Shan during the Cenozoic. (A) Perspective view of the Qilian Shan region before deformation. (B) Top view of the Qilian Shan region before deformation. (C) Perspective view of the Qilian Shan region after deformation. (D) Top view of the Qilian Shan region after deformation. (E) Sketch of the main active structures in the northern Tibetan plateau, modified from Duvallet al. (2013). To simplify the model, we consider the shape of the Qilian Shan to be an approximately right-angled trapezoid in plan view. The initiation ages are mainly compiled from previous work (e.g. Mocket al., 1999; Yin et al., 2002, 2007, 2008a,b; Jolivet et al., 2003; Lease et al., 2007; Bovet et al., 2009;Clarket al., 2010; Zheng et al., 2010; Craddock et al., 2011; Duvall et al., 2011, 2013; Hough et al., 2011; Yuan et al., 2011).

Figure 3. (A) Offset estimation along the Altyn Tagh Fault. Data were mainly compiled from Ritts and Biffi (2000), Yin et al. (2002), Gehrels et al. (2003), Yue et al. (2005); Searle et al. (2011) and Cheng et al. (2015). The grey rectangle represents the probable offset along the ATF and its probable time of initiation. In this study, we consider an offset of 360 ± 40 km along the ATF since its Eocene initiation based both on newly found piercing points in the western Qaidam Basin (Cheng et al., 2015) and on a summary of previous estimates, which is represented by the yellow circle. (B) Balanced calculation results. The black lines relate the amount of extrusion within the Qilian Shan (L_e) to the amount of offset along the ATF (L_d), while the blue line relates the amount of N20E directed crustal shortening within the Qilian Shan (L_s) to the amount of offset along the ATF (L_d). Considering the probable 360 km offset along the ATF (represented by the yellow circle in the figure) and an initial crustal thickness of 45 km in the Qilian Shan, there has been 309 km of eastward extrusion and 250 km of N20E directed crustal shortening in the Qilian Shan range, represented by the red circle and the green circle respectively. The pink region represents the possible range of L_e and L_s. In this study, we define the N110E-directed elongation of the Qilian Shan as the eastward extrusion.

Figure 4. (A) Global Positioning System (GPS) velocities relative to stable Eurasia, modified from Zhang et al. (2004). The yellow arrows show the changes in orientation of the displacement vectors, clearly implying ongoing eastward crustal extrusion within the Qilian Shan region. (B) Strike-parallel and strike-perpendicular velocity (N110E) vs. distance. Solid-lined right trapezoid in the Fig. 4A represents the studied Qilian Shan region. GPS data from Gan et al. (2007). Details of the analytical method of geodetic velocities are given in Appendix S2. The sharp decrease in N20E directed GPS velocities from the northern Qaidam Basin to the Hexi Corridor and the large increase in N110E directed GPS velocities from the Altyn Tagh Range to the eastern Qilian Shan imply large amounts of crustal shortening and eastward extrusion within the Qilian Shan region at present.

Figure 5. North-eastward migration model of the Qaidam block, corresponding to crustal

shortening and eastward extrusion inthe Qilian Shan. (A) Pre-deformation phase. (B) Post-deformation phase. Note that hundreds of kilometres of offset along theATF have been absorbed within the Qilian Shan region and partly accommodated by N20E directed crustal shortening (250 ± 18 km). A large amount of this displacement was transferred further east through crustal transpression within the Qilian Shan. This eastward extrusion (~250–370 km) of crustal material from the north-eastern Tibetan Plateau is responsible for strike-slip faulting in the Qilian Shan region, crustal thickening in the Qinling region, anticlockwise rotation of the Ordos block, and extension in the Weihe Graben.

Table 1. Relevant parameter estimates used in this study.

Table 2. N20E crustal shortening, shortening strain, and eastward extrusion estimates.

Table 3. Potential structures that accommodate the eastward crustal extrusion in the Qilian Shan.

Figures and tables to Chapter 5

Figure 1. Topography and distribution of the main faults of the Qaidam Basin and its periphery (Topographic data adopts the SRTM data in 90 m resolution[17]).

Figure 2. Composite stratigraphic column of the Cenozoic strata in the western Qaidam Basin.

Figure 3. Main fault distribution and the Paleogene and Neogene principal stress orientation in the Qaidam Basin and its periphery.

Figure 4. Northward migration model of the strike-slip fault in the western segment of the East Kunlun Mountain, Southwest Qaidam (topography adopts the SRTM data with 90 m resolution[17]).

Figure 5. Formation thickness and fault distribution of the upper member of the Lower Ganchaigou Formation in the Southwestern Qaidam Basin (Modified from reference [58]).

Figure 6. Arlar fault structural profile in the Southwestern Qaidam Basin (Profile location is shown in Fig. 5).

Figure 7. Northward migration model of strike-slip faults in the Southwestern Qaidam Basin (Modified from reference [58]).

Figure 8. Distribution of source rocks and oil and gas in the Qaidam Basin (Modified from reference [27]).

Figure 9. Typical oil reservoir profile in Southwestern Qaidam Basin (Profile location is shown in Figure 8).

Figure 10. Schematic Cenozoic tectonic - sedimentary evolution of the Qaidam Basin and its periphery.

Table 1. Summary of the initial strike-slip time limit of the Altyn Tagh fault.

List of publications during the PhD. thesis work

Papers in preparation:

Cheng F., Jolivet M., Fu S., Zhang C., Zhang, Q., Guo Z., Reconstructing the Cenozoic tectonics in the northern Tibetan plateau: insight from apatite fission track study of deep-drill-core samples from the basement of Qaidam basin. In Prep for Tectonics.

Cheng F., Han B., Jolivet M., Fu S., Zhang C., Guo Z., Tectono-magmatic rejuvenation of the Qaidam craton (northern Tibet): insight from geochronological and geochemical constraints on borehole basement samples. In Prep for EPSL.

Papers in review and revision:

16 **Cheng F.,** Jolivet M., Fu S., Zhang C., Zhang, Q., Guo Z., Large-scale displacement along the Altyn Tagh Fault (North Tibet) since its Eocene initiation: insight from detrital zircon U-Pb geochronology and subsurface data: ***Tectonophysics***, accepted with minor revision.

Published papers:

15 **Cheng, F.**, Fu, S., Jolivet, M., Zhang, C., and Guo, Z., 2016, Source to sink relation between the Eastern Kunlun Range and the Qaidam Basin, northern Tibetan Plateau, during the Cenozoic: ***Geological Society of America Bulletin***, v. 128, no. 1-2, p. 258-283, doi: 10.1130/B31260.1.

14 **Cheng F.**, Jolivet M., Dupont-Nivet G., Wang L., Yu X., Guo Z., Lateral extrusion along the Altyn Tagh Fault, Qilian Shan (NE Tibet): insight from a 3D crustal budget: ***Terra Nova***, v. 27, no. 6, p. 416-425, doi: 10.1111/ter.12173.

13 Wang L. and **Cheng F.**, 2015. DEM and GIS analysis of the stream gradient index for evaluating effects of active tectonics: Tula basin, north Tibet, China, Geoscience and Remote Sensing Symposium (IGARSS), 2015 IEEE International, Milan, 2015, 4680-4683, doi: 10.1109/IGARSS.2015.7326873.

12 Fu S., Ma D., Guo Z., **Cheng F.**, 2015. Strike-slip superimposed Qaidam basin and control on oil and gas accumulation: ***Petroleum Exploration and Development***, v. 42, no. 6, 712-722, doi: 10.11698/PED.2015.06.03.

11 **Cheng, F.,** Guo Z., Jenkins, H., Fu S., and Cheng X., 2015.Initial Rupture and Displacement on the strike-slip Altyn Tagh Fault, Northern Tibetan Plateau: Constraints based on residual Mesozoic to Cenozoic deposits in the western Qaidam Basin: ***Geosphere***, v. 11, no. 3, 921-942, doi: 10.1130/GES01070.1.

10 Liu, D., **Cheng, F.**, Guo, Z., Jolivet, M., Song, Y., 2015. Lahar facies of the Latest Paleozoic Arbasay Formation: Geomorphological characters and paleoenvironment reconstruction of Northern Tian Shan, NW China. ***Journal of Asian Earth Sciences***, v. 113, Part 1, p. 282-292, doi: 10.1016/j.jseaes.2015.01.024.

9 Cheng, X., Fu, S., Wang, H., Yu, X., **Cheng, F.**, Liu, R., Du, W., Guo, Z., 2015. Geometry and kinematics of the Arlar strike-slip fault, SW Qaidam basin, China: New insights from 3-D seismic data. ***Journal of Asian Earth Sciences*** v. 98, 198-208, doi: 10.1016/j.jseaes.2014.09.039.

8 **Cheng, F.,** Jolivet, M., Fu, S., Zhang, Q., Guan, S., Yu, X., and Guo, Z., 2014, Northward

growth of the Qimen Tagh Range: A new model accounting for the Late Neogene strike-slip deformation of the SW Qaidam Basin: ***Tectonophysics***, v. 632, p. 32-47, doi: 10.1016/j.tecto.2014.05.034.

7 Liu, D., Guo, Z., Jolivet, M., **Cheng, F.**, Song, Y., Zhang, Z., 2014. Petrology and geochemistry of Early Permian volcanic rocks in South Tian Shan, NW China: implications for the tectonic evolution and Phanerozoic continental growth. ***International Journal of Earth Sciences*** 103, 737-756, doi: 10.1007/s00531-013-0994-1.

6 Zhu, B., Guo, Z., Zhang, Z., **Cheng, F.**, 2014. Peperites in the Permian Tarim large igneous province in Northwest China and their constraints on the local eruption environments. ***Science China Earth Sciences*** 57, 2914-2921. doi: 10.1007/s11430-014-4966-5.

5 Yu, X.J., Fu, S.T., Guan, S.W., Huang, B., **Cheng, F.**, Cheng, X., Zhang, T., Guo, Z.J., 2014. Paleomagnetism of Eocene and Miocene sediments from the Qaidam basin: Implication for no integral rotation since the Eocene and a rigid Qaidam block. ***Geochemistry, Geophysics, Geosystems*** 15, 2109-2127., doi: 10.1002/2014GC005230.

4 Yu, X., Huang, B., Guan, S., Fu, S., **Cheng, F.**, Cheng, X., Zhang, T., Guo, Z., 2014. Anisotropy of magnetic susceptibility of Eocene and Miocene sediments in the Qaidam Basin, Northwest China: Implication for Cenozoic tectonic transition and depocenter migration. ***Geochemistry, Geophysics, Geosystems*** 15, 2095-2108, doi: 10.1002/2014GC005231.

3 **Cheng F.,** and Guo Z., 2013. Northward Migration of the Western Segment of Eastern Kunlun Strike-slip Fault: Implications for Late Cenozoic Evolution of the Qimen Tagh Range and Southwestern Qaidam Basin, North Tibet, China. ***Acta Geologica Sinica (English Edition)***, v. 87(supp.), p. 205.

2 Zhang C., **Cheng F.**, Huang G., Huang Y., Xing C., Guan B., Zhang Q., Xu G.,. 2013. Sediment and reservoir characteristics with reservoir evaluation of Lunlehe Formation in Qie16 block of Kunlun oilfield in Qaidam Basin: ***Acta Petrologica Sinica***, v. 29, no. 8, p. 2883-2894 (in Chinese with English abstract).

1 Liu, D., Jolivet, M., Yang, W., Zhang, Z., **Cheng, F.**, Zhu, B., Guo, Z., 2013. Latest Paleozoic–Early Mesozoic basin–range interactions in South Tian Shan (northwest China) and their tectonic significance: Constraints from detrital zircon U–Pb ages. ***Tectonophysics*** 599, 197-213, doi: 10.1016/j.tecto.2013.04.018.